FINAL REPORT N84-25128

APPLICATION OF MAGSAT TO LITHOSPHERIC MODELING IN SOUTH AMERICA: PART II-SYNTHESIS OF GEOLOGIC AND SEISMIC DATA FOR DEVELOPMENT OF INTEGRATED CRUSTAL MODELS

(Contract No. NAS 5-26326)

By

G. R. Keller; University of Texas at El Paso
E. G. Lidiak; University of Pittsburgh

(in conjunction with W. J. Hinze, L. W. Braile, and R. R. B. von Frese, Purdue University)

Final Report

submitted to

Goddard Space Flight Center
National Aeronautics & Space Administration
Greenbelt Road
Greenbelt, MD 20771

on

APPLICATION OF MAGSAT TO LITHOSPHERIC MODELING IN SOUTH AMERICA: PART II- SYNTHESIS OF GEOLOGIC AND SEISMIC DATA FOR DEVELOPMENT OF INTEGRATED CRUSTAL MODELS

(Contract No. NAS 5-26326)
by

G. R. Keller and E. G. Lidiak
(in conjunction with W. J. Hinze,
L. W. Braile, and R. R. B. von Frese,
Purdue University)

Department of Geological Sciences
University of Texas at El Paso
El Paso, TX 79968

and

Department of Earth and Planetary Sciences
University of Pittsburgh
Pittsburgh, PA 15260

January, 1984

ABSTRACT

MAGSAT scalar magnetic anomaly data reduced to vertical polarization and long-wavelength-pass filtered free-air gravity anomaly data of South America and the Caribbean are compared to major crustal features. Many interesting relationships are observed. The continental shields generally are more magnetic than adjacent basins, oceans and orogenic belts. In contrast, the major aulacogens are characterized by negative anomalies. Spherical-earth magnetic modeling of the Amazon River and Takatu aulacogens in northeastern South America indicates a less magnetic crust associated with the aulacogens which is compatible with previous studies over the Mississippi River aulacogen and the Rio Grande rift in North America. Spherical-earth modeling of both positive gravity and negative magnetic anomalies observed over the Mississippi Embayment indicate the presence of a non-magnetic zone of high density material within the lower crust associated with the aulacogen.

MAGSAT scalar magnetic anomaly data and available free-air gravity anomalies over Euro-Africa indicate several similar relationships and some important differences. Rift zones and aulacogens tend to be magnetically negative. The Precambrian shields of Africa and Europe exhibit varied magnetic signatures. The reduced to vertical polarization magnetic anomaly map shows a marked tendency for northeasterly striking anomalies in the eastern south Atlantic and adjacent Africa, which are coincident to the tracks of several hotspots for the past 100 million years. Comparison of the radially polarized anomalies of Africa and Europe with similar satellite magnetic anomaly maps of the Western Hemisphere show correlative anomalies across the (closed) Atlantic Ocean adding support to the Mesozoic reconstruction of the continents.

INTRODUCTION

This report summarizes research activities performed on MAGSAT scalar data over South America, Central America and adjacent marine areas under grants provided to Purdue University and the University of Texas at El Paso. Research at Purdue University was conducted by L.W. Braile, W.J. Hinze and R.R.B. von Frese and their students. In the later stages of the project, they were joined by R. Olivier of the Institute of Geophysics of the University of Lausanne, Switzerland. Master of Science theses at Purdue University were prepared by Mark B. Longacre and Jeffrey R. Ridgway. Research at the University of Texas at El Paso was conducted by G.R. Keller working with E.G. Lidiak of the University of Pittsburgh. Master of Science theses were written by D.W. Yuan and K. Scott Remberger respectively at the University of Pittsburgh and the University of Texas at El Paso. A no-cost extension to the original contracts was provided to January 1, 1984 to expand our studies into the Euro-African region.

As of this date, research involved with these grants has resulted in the publication of three papers (Hinze et al., 1982; Longacre et al., 1982; von Frese et al., 1982), three expanded abstracts (Olivier et al., 1982; von Frese, 1982; Yuan et al., 1982) and eight published abstracts (Longacre et al., 1981; von Frese et al., 1981; von Frese and Hinze, 1982; von Frese, 1983; Hinze et al., 1983; Lidiak et al., 1983; Olivier et al., 1983; von Frese et al., 1983). In addition, several presentations regarding the research results were presented at MAGSAT investigator meetings and academic seminars. Master of Science theses were prepared with the support of these grants by D.W. Yuan, "Relation of MAGSAT and Gravity Anomalies to the Main Tectonic Provinces of South America", at the University of Pittsburgh under the supervision of Prof.

E.G. Lidiak, by K. Scott Remberger, "A Crustal Structure Study of South America", at the University of Texas at El Paso under the supervision of Prof. G.R. Keller, by Mark B. Longacre, "Satellite Magnetic Investigation of South America" at Purdue University under the supervision of Prof. W.J. Hinze, and a M.S. thesis is currently in the final stages of preparation by Jeffrey R. Ridgway, "The MAGSAT Scalar Magnetic Anomaly Map of South America", under the supervision of Prof. W.J. Hinze at Purdue University.

DISCUSSION OF RESULTS

Detailed discussions of the research results are presented in the three published papers, three expanded abstracts, and eight abstracts which are provided in Appendix A. Additional information is provided in four graduate theses and new research results will be presented in publications which are currently being prepared.

South America, Central America and adjacent marine areas include some of the most geologically significant regions of the Earth. A primary objective of this research program was to demonstrate the geologic utility of magnetic satellite anomalies by focusing on the spherical-earth interpretation of scalar MAGSAT data, in combination with ancillary geological and geophysical (free-air gravity, seismic, etc.) data, to obtain lithospheric models for these regions related to their contemporary crustal dynamic processes, geologic history, current volcanism and seismicity, and natural resources. Purdue University (L.W. Braile, W.J. Hinze and R.R.B. von Frese) was responsible for processing of the MAGSAT data and preparation of the magnetic and gravity anomaly maps, the University of Texas at El Paso (G.R. Keller) provided the data on seismic investigations of the crust, and the University of Pittsburgh (E.G. Lidiak) assembled the data and prepared the tectonic/geologic maps of South America. All these data were used by the investigators in an integrated interpretation.

As the investigator tapes were made available nearly a year later than originally scheduled, a substantial amount of effort performed under the auspices of this research program was based on an analysis of the preliminary <2°> MAGSAT anomaly data.

Tectonic, gravity anomaly and crustal structure data have been gathered, synthesized, and interpreted for comparison to magnetic anomalies mapped by the MAGSAT satellite over South America. The correlation of reduced-to-pole magnetic and gravity anomalies (Longacre et al., 1981; Hinze et al., 1982) at 350 km elevation with tectonic provinces are shown in Figures 1 and 2 respectively. A map of crustal thickness (Remberger, 1983) is shown as Figure 3. This map represents a compilation of previous results as well as a major effort analyzing Rayleigh wave dispersion data. The non-satellite data have numerous limitations because of the sparse data available in the many remote areas of the continent. The magnetic anomalies mapped as part of the MAGSAT project provide more uniform coverage of the South American continent, but these data are also of an averaged nature. Furthermore, magnetic and gravitational field measurements are sensitive to lithological variations in the crust (and upper mantle) which are not necessarily related to either the crustal thickness or the tectonic features of South America. Nevertheless, numerous interesting relationships exist between the variations in crustal thickness and average crustal shear velocity, the magnetic and free-air gravity anomalies, and the major tectonic features of South America.

The South American Platform (Yuan et al., 1982) is the oldest tectonic province and contains the only known Archean rocks of the continent. The basement of the platform is exposed in three major shields-Guyana, Central Brazilian, and Atlantic. All of these shields contain thick Precambrian metamorphic sequences and a wide variety of volcanic and

intrusive rocks and are characterized by positive magnetic (Figure 1) and free-air gravity anomalies (Figure 2). Exceptions are the eastern part of the Guyana Shield which corresponds to a negative free-air gravity anomaly and the central Atlantic Shield which corresponds to a negative magnetic anomaly.

The sedimentary cover and associated volcanics of the platform, which are of Silurian or younger age, are well developed in four great synclines - Amazon, Parnaiba, Parana, and Chaco basins. These basins are filled with a thick sequence of non-magnetic and Bouguer gravity anomalies. An exception is the Parana basin in which positive magnetic anomalies occur which are associated with a thick sequence of Parana basalts. In general, grabens or aulacogens, underlying the large basins (Amazon and the southern part of Chaco basins) or in the shield (Takatu rift valley), are characterized by magnetic minima and gravity maxima (Figures 1 and 2).

The central and southern portion of the South American platform is undistinguished by any notable variations in crustal thickness. The average thickness of the crust throughout this region is approximately 42 km, which is typical of stable platform and shield areas; the crust may thicken slightly to the north. (The crust beneath the Chaco basin and surrounding areas has not been sampled adequately, however.) The average regional crustal shear wave velocity falls within a range of 3.65 to 3.70 km/s. The pattern of filtered free-air gravity anomalies across the central and southern platform indicate that the entire region is broadly in isostatic equilibrium, as would be expected in a large area of uniformly thick crust. Strongly positive magnetic anomalies occur over the Central Brazilian shield and over the northern and southern Atlantic shield; an intense negative magnetic anomaly occurs over the

Central Atlantic shield. The southern portion of the platform is characterized by an irregular pattern of slightly negative magnetic anomalies. The pattern of magnetic anomalies over the southern and central South American platform does not seem to be associated with variations in crustal thickness, but appears to be related to lithological variations within the crust of the platform. The intense magnetic anomaly over the central Atlantic shield may, for instance, be attributable to thermotectonic reactivation of the crust prior to or during the rifting of South America from Africa.

Two major trends in crustal thickness dominate the crustal structure of the northern South American platform (Figure 3). An east-west trending zone of thickened crust (slightly thicker than 50 km) exists beneath nearly all of northern Brazil. This crustal zone is characterized by average crustal shear wave velocities of at least 3.81 to 3.95 km/s, which implies that in addition to being thick, the crust is more dense than average. The northwestern lobe of the South American platform is underlain by a hook-shaped zone of thinned crust (slightly thinner than 35 km) that roughly parallels the curve of the Andean Cordillera. The average crustal shear wave velocity in this region is poorly defined, but probably falls within the range of 3.70 to 3.77 km/s. The pattern of filtered free-air gravity anomalies over the northeastern platform is very similar to that of the central and southern platform. However, unlike the other intracratonic basins of the South American platform, the Amazon basin is not characterized by a distinct free-air low, although it correlates with a negative Bouguer anomaly where data are available. The slight negative anomaly which lies over the eastern lobe of the Guyana shield is also unusual. A distinctive pair of interconnected magnetic lows covers part of the northeastern platform. One of these

anomalies is centered over the eastern Amazon basin and extends out into the Atlantic Ocean; the other is centered over the intersection of the trend of the Takatu aulacogen with the central Amazon basin and cuts across much of the southern Guyana shield (particularly the eastern lobe). The area covered by these negative magnetic anomalies corresponds with the zone of thickened crust beneath northern Brazil, suggesting that a relationship exists between the two features. Perhaps the zone of thickened crust (and low elevation) represents a subsided rift cushion.

. A ridge-like free-air gravity high (greater than 40 mGals) covers much of the low-lying, sedimentary rock-covered transition zone between the Andean Cordillera and the Amazon basin and Guyana shield, over the northwestern South American platform. The western lobe of the Guyana shield is also characterized by a slight free-air gravity high. These anomalies could be a reflection of the zone of thinned crust mapped beneath the area. A distinctive negative magnetic anomaly lies over the central part of the transition zone, at the intersection of the trend of the Amazon basin with the Andean Cordillera. The relationship of this anomaly to the zone of thinned crust is not clear. The magnetic anomaly could be due to the extensive sedimentary cover of the region, to a fundamental lithological difference in the crust, or to remnant thermal activity.

The Andean Cordillera constitutes the entire western margin of South America with rocks dating from the Precambrian to recent time. It is a region of strong seismicity and volcanism. A relatively narrow belt of thick crust is present beneath the trend of the Andean Cordillera along the western coast of South America. This belt thins gradually southward beneath the Central Andes, and rather abruptly northward beneath the Northern Andes. The crust thickens dramatically beneath the bend in

the mid-Central Andes at latitude 18° South, reaching thicknesses greater than 70 km. The crust also thickens beneath the Northern Andes of western Colombia. Positive free-air gravity anomalies are related to the Andean Cordillera. The most intense of these anomalies is correlative with the sharp bend in the Central Andes. The relationship of the MAGSAT scalar anomalies to the Andes is much less definitive, but a major magnetic minimum is associated with the above mentioned positive anomaly. This is the portion of the Andes with the maximum regional uplift of the surface, the greatest Moho depths and steepest dip of the Benioff zone associated with subduction of the Nazca plate. It also coincides with the location of major recent volcanism. The smaller free-air gravity high over the mid-Northern Andes does not seem to be related either to the elevation of the cordillera or the presence of a crustal root. The anomaly may, however, be caused by the zone of dense, shallow oceanic crust that lies between the Central Cordillera and the Pacific coast of Colombia.

Longacre et al. (1981) and Hinze et al. (1982) show statistically that the magnetic data over the continental areas of South and Central America are more magnetic and magnetically more variable than the adjacent marine areas. The former observation is compatible with evidence that suggests that the seismic Moho is a magnetic boundary and that the upper mantle is only weakly magnetic. The more variable magnetization of the continents reflects their long and complex geologic history which has led to strong horizontal magnetic polarization variations in the crust.

The Caribbean Sea and the Gulf of Mexico are underlain by prominent magnetic minima (Lidiak et al., 1983). Within these oceanic areas, linear magnetic highs correlate with topographic ridges which separate the Gulf of Mexico, the Colombian Basin, and the Venezuelan basin. The

boundaries of the Caribbean plate occur along magnetic gradients. The gradients are particularly sharp along the northern and western margins of the plate, but are gradational along the southern margin where they merge with anomalies associated with the Andean Cordillera.

To obtain further insight concerning the relationships between regional South American tectonic features and geopotential field satellite anomalies, the Euro-African MAGSAT data were investigated. Specifically, satellite (MAGSAT) scalar magnetic anomaly data were compiled and differentially reduced to radial polarization (Figure 4) for comparison with tectonic data of Africa, Europe and adjacent marine areas (Olivier et al., 1982 and 1983; Hinze et al., 1983; von Frese et al., 1983). These studies demonstrated a number of associations to constrain analyses of the tectonic features and geologic history of the region. Rift zones and aulacogens, for example, tend to be magnetically negative. The most intense positive anomaly of the region is the Bangui anomaly which has been interpreted as due to a deep crustal positive magnetization source. There are no near-surface sources which will explain this anomaly. By contrast, the next most intense positive anomaly is over the Kursk region in the Russian Ukraine. This anomaly extends 450 km in a northeasterly direction and is roughly 150 km wide, and is caused according to aeromagnetic anomaly interpretations by near-surface, intensely magnetic ferruginous quartzites. Apparently, there is sufficient long-wavelength energy in the superimposed near-surface anomalies for them to be observed at satellite elevations. The Precambrian shields of Africa and Europe exhibit varied magnetic signatures. All shields are not magnetic highs and, in fact, the Baltic shield is a marked minimum. The reduced to the pole magnetic map shows a marked tendency for northeasterly striking anomalies in the eastern Atlantic and adjacent Africa, which is coincident

to the track of several hot spots for the past 100 million years. However, there is little consistency in the sign of the magnetic anomalies and the track of the hot spots. Comparison of the radially polarized anomalies of Africa and Europe with other reduced to the pole magnetic satellite anomaly maps of the Western Hemisphere (Figure 5) support the reconstruction of the continents prior to the origin of the present-day Atlantic Ocean in the Mesozoic Era.

To illustrate the utility of satellite magnetic data in characterizing the properties and structure of the lithosphere, magnetic modeling of the Amazon River and Takatu aulacogens in northeastern South America (Longacre et al., 1982) and the Mississippi Embayment (von Frese, 1982 and 1983) were undertaken. For the Amazon River and Takatu aulacogens, reduction of MAGSAT scalar magnetic anomaly data to an equivalent condition of vertical polarization shows these tectonic features generally correlated with magnetic anomaly minima. Surface gravity data demonstrate a correlative positive anomaly. Spherical earth modeling of the magnetic data indicates a less magnetic crust associated with the aulacogens which is compatible with previous studies over the Mississippi River aulacogen and Rio Grande rift in North America.

For the Mississippi River aulacogen, spherical earth inversion analysis of free-air gravity, U.S. Naval Oceanographic Office aeromagnetic, and satellite (POGO, MAGSAT) magnetometer data show the Embayment to be characterized by regionally positive gravity and negative magnetic anomalies. Incorporating constraints developed from seismic refraction and surface-wave dispersion studies of the region with Gauss-Legendre quadrature potential field modeling suggests that the regional gravity and magnetic anomalies may be related to a rift zone along the axis of the Embayment which defines a non-magnetic block of high density

material within the lower crust. The decreased magnetization of this component may be due to reversed magnetic remanence, an intra-lithologic variation, or an upwarp of the Curie isotherm.

To assess the crustal component in satellite data, POGO and preliminary MAGSAT magnetometer data were compared with the scalar aeromagnetic data obtained by the U.S. Naval Oceanographic Office (NOO)--Vector Magnetic Survey of the conterminous U.S.A. (von Frese et al., 1982; von Frese and Hinze, 1982). POGO and preliminary MAGSAT data demonstrate remarkable consistency, but the NOO data spherically upward continued by equivalent point source inversion are dominated by long-wavelength ($\cong$ 1000-3000 km) anomalies which are not present in the satellite anomaly data. However, upon removal of these long-wavelength anomalies from the upward continued NOO data, a close comparison observed between the anomalies verifies that satellite magnetic anomalies do portray the crustal component within a range of wavelengths from roughly 1000 km down to the resolution limit of the observations.

Finally, to avoid potential problems and smoothing of the MAGSAT scalar anomaly data by using the 2° averaged data, a scalar anomaly data set of South America has been prepared directly from the investigator tapes. The procedure used which was developed with resources independent of this contract involved selecting orbital profiles observed when K_p values were 3 or less. In addition, the magnetic effect of the equatorial electrojet was minimized by screening profiles for a large "y" component and using only dawn profiles. Furthermore, the NASA ring current correction was applied to the data. Finally, all data were wavenumber filtered between 0.25 deg^{-1} and 0.02 deg^{-1} with a Butterworth filter. Analyses of 25 sets of 3 essentially coincident profiles showed that maximum correlation of coincident, redundant, profiles was obtained using a

minimum low-cutoff of 0.02 deg^{-1}. The resulting data set minimizes geologic anomalies which have dimensions exceeding roughly 2900 km, but it also has minimum disturbance from temporal variations in the geomagnetic field. The data set has been processed by equivalent point source inversion (Longacre et al., 1981; Hinze et al., 1982) taking into account the variable elevation of the data points. The resultant map is shown in Figure 6. This map will be used in subsequent analysis of MAGSAT scalar magnetic anomalies over South America, Central America and associated marine areas.

REFERENCES CITED

Hinze, W.J., R.R.B. von Frese, M.B. Longacre, L.W. Braile, E.G. Lidiak and G.R. Keller, 1982, Regional magnetic and gravity anomalies of South America, Geophys. Res. Lett., v. 9, pp. 314-317.

Hinze, W.J., R. Olivier and R.R.B. von Frese, 1983, Euro-African MAGSAT anomaly-tectonic observations, IAGA Bulletin, v. 47.

Lidiak, E.G., D.W. Yuan, W.J. Hinze, M.B. Longacre and G.R. Keller, 1983, Correlation of tectonic provinces of South America and the Caribbean region with MAGSAT anomalies, Presented at the 10th Caribbean Geological Conference, Cartagena, Colombia.

Longacre, M.B., W.J. Hinze, R.R.B. von Frese, L.W. Braile, E.G. Lidiak and G.R. Keller, 1981, Satellite elevation magnetic and gravity models of major South American plate tectonic features, IAGA Bulletin 45, p. 109.

Longacre, M.B., W.J. Hinze and R.R.B. von Frese, 1982, A satellite magnetic model of northeastern South American aulacogens, Geophys. Res. Lett., v. 9, pp. 318-321.

Olivier, R., W.J. Hinze and R.R.B. von Frese, 1982, Satellite magnetic anomalies of Africa and Europe, SEG 52nd Annual International meeting and Exposition, Technical Program (Abstracts & Biographies), pp. 413-415. See also: Geophysics, v. 48 (1983), p. 468.

Olivier, R., W.J. Hinze and R.R.B. von Frese, 1983, Reduced to pole long-wavelength magnetic anomalies of Africa and Europe, EOS (Am. Geophys. Union Trans.), v. 64.

Remberger, K. Scott, 1983, A crustal structure study of South America, Unpublished M.S. Thesis, Univ. of Texas at El Paso, El Paso, Texas.

von Frese, R.R.B., 1982, Regional anomalies of the Mississippi River aulacogen, SEG 52nd Annual International Meeting and Exposition, Technical Program (Abstracts & Biographies), pp. 295-297. See also: Geophysics, v. 48 (1983), p. 453.

von Frese, R.R.B., 1983, Regional geophysical analysis of Mississippi embayment crustal structure, 112th Annual Meeting of the Society of Mining Engineers of the American Institute of Mining Engineers (SME-AIME), Technical Program & Abstracts, p. 94.

von Frese, R.R.B. and W.J. Hinze, 1982, Do satellite magnetic anomaly data accurately portray the crustal component?, EOS (Am. Geophys. Union Trans.), v. 63, p. 655.

von Frese, R.R.B., R. Olivier and W.J. Hinze, 1983, Long-wavelength magnetic and gravity anomaly correlations of Africa and Europe, IAGA Bulletin 47.

von Frese, R.R.B., W.J. Hinze, J.L. Sexton and L.W. Braile, 1982, Verification of the crustal component in satellite magnetic data, Geophys. Res. Lett., v. 9, pp. 293-295.

von Frese, R.R.B., W.J. Hinze, J.L. Sexton and L.W. Braile, 1981, U.S. aeromagnetic and satellite magnetic anomaly comparisons, IAGA Bulletin 45, p. 107.

Yuan, D.W., E.G. Lidiak, M.B. Longacre and G.R. Keller, 1982, Relation of MAGSAT anomalies to the main tectonic provinces of South America, SEG 52nd Annual International Meeting and Exposition, Technical Program (Abstracts & Biographies), pp. 274-276. See also: Geophysics, 48 (1983).

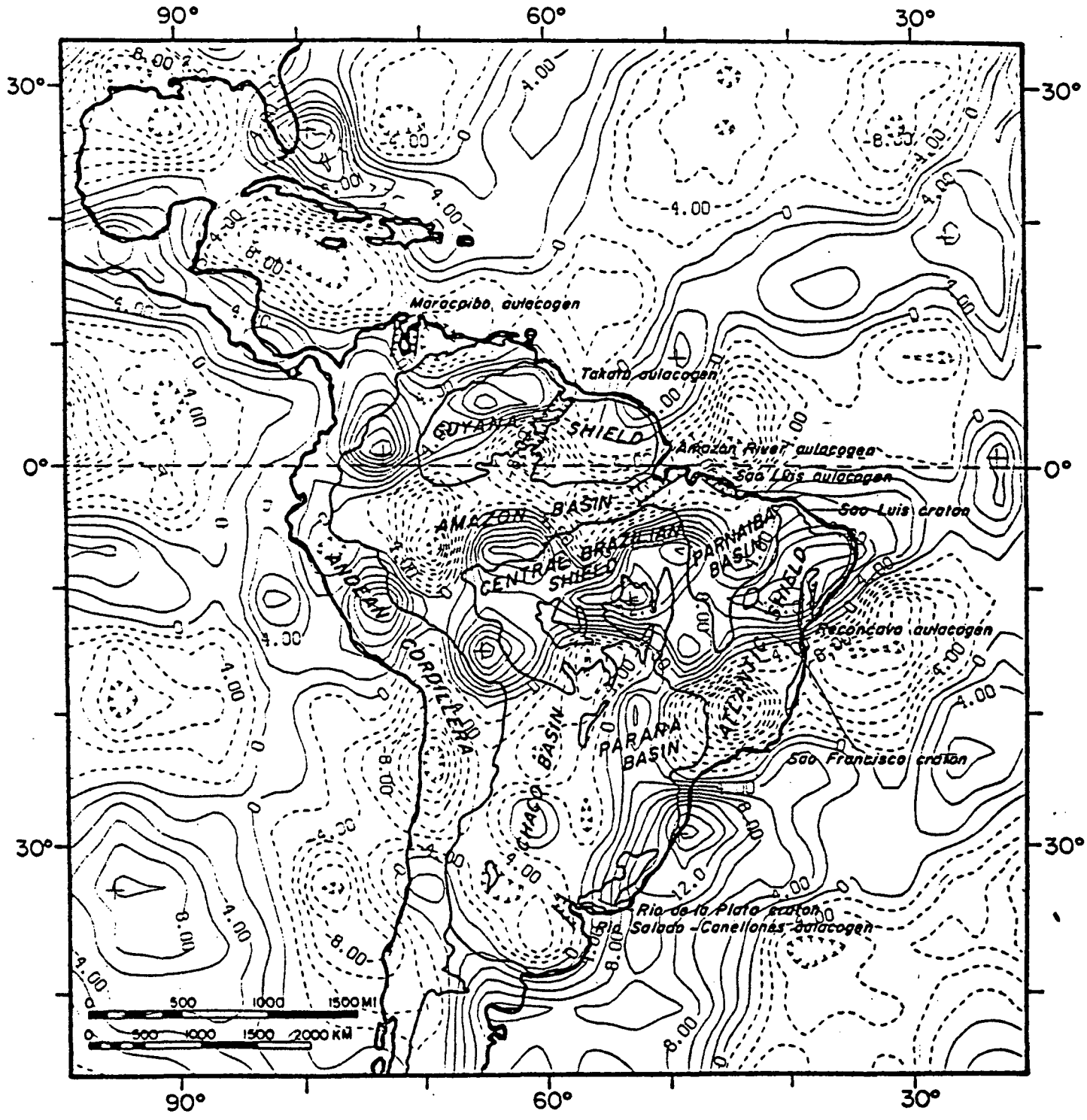

Figure 1. Reduced-to-pole MAGSAT scalar magnetic anomalies at 350 km over South America with major tectonic features. Contour interval is 2 nT.

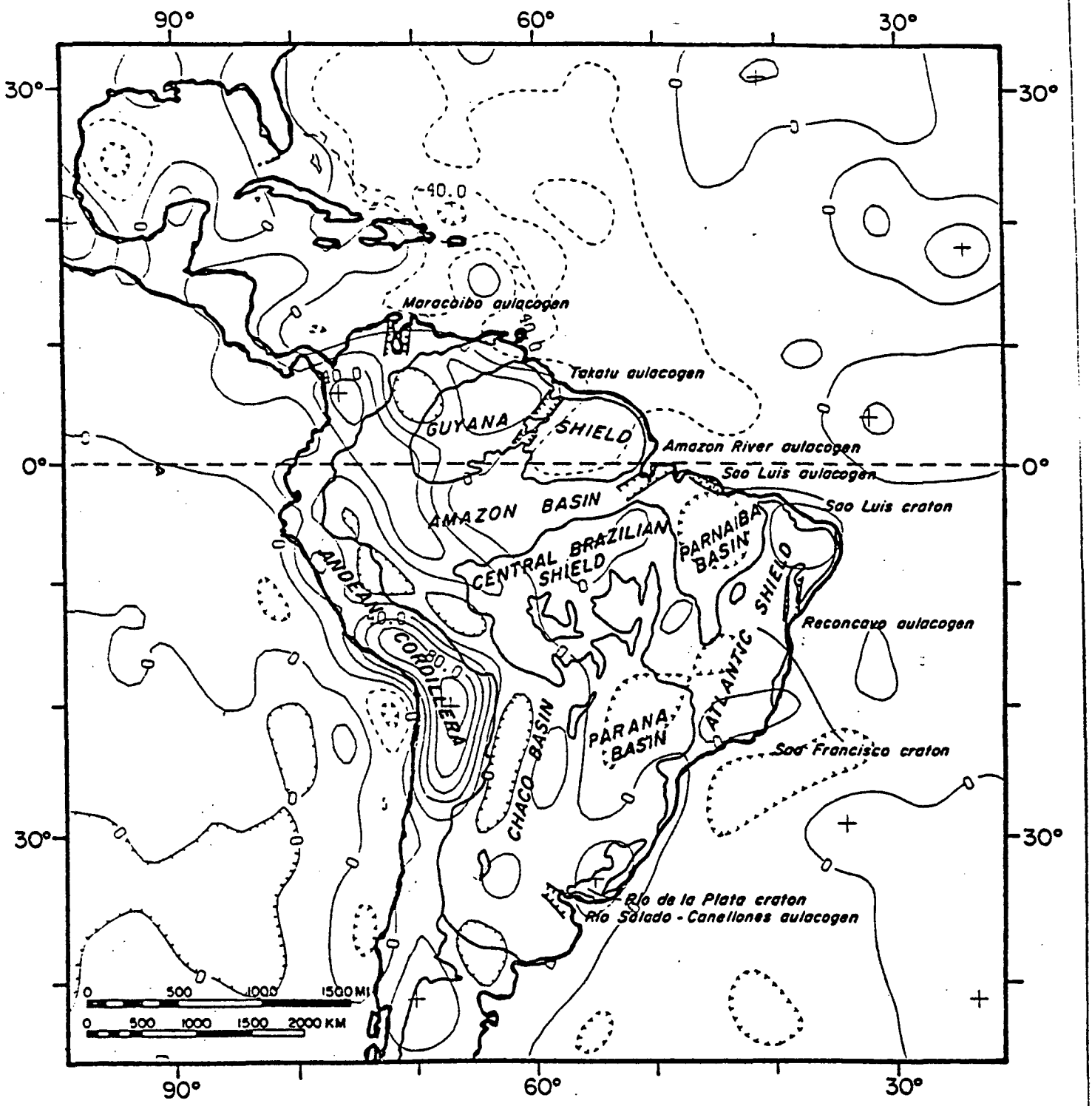

Figure 2. Free-air gravity anomaly at 350 km over South America with major tectonic features. Contour interval is 20 mGal.

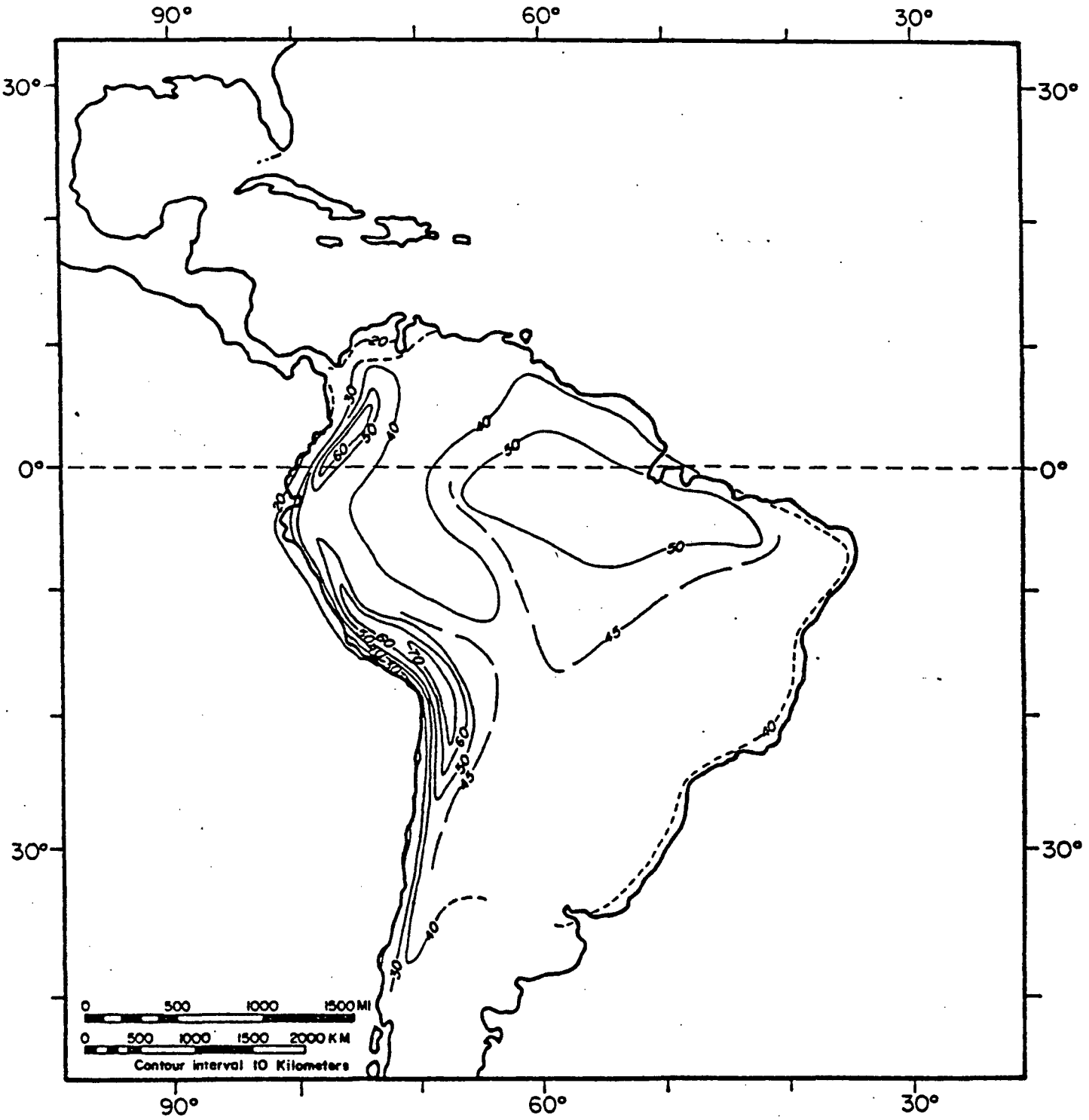

Figure 3. Depth to Moho from published data and surface-wave analysis. Contour interval is 5 and 10 km.

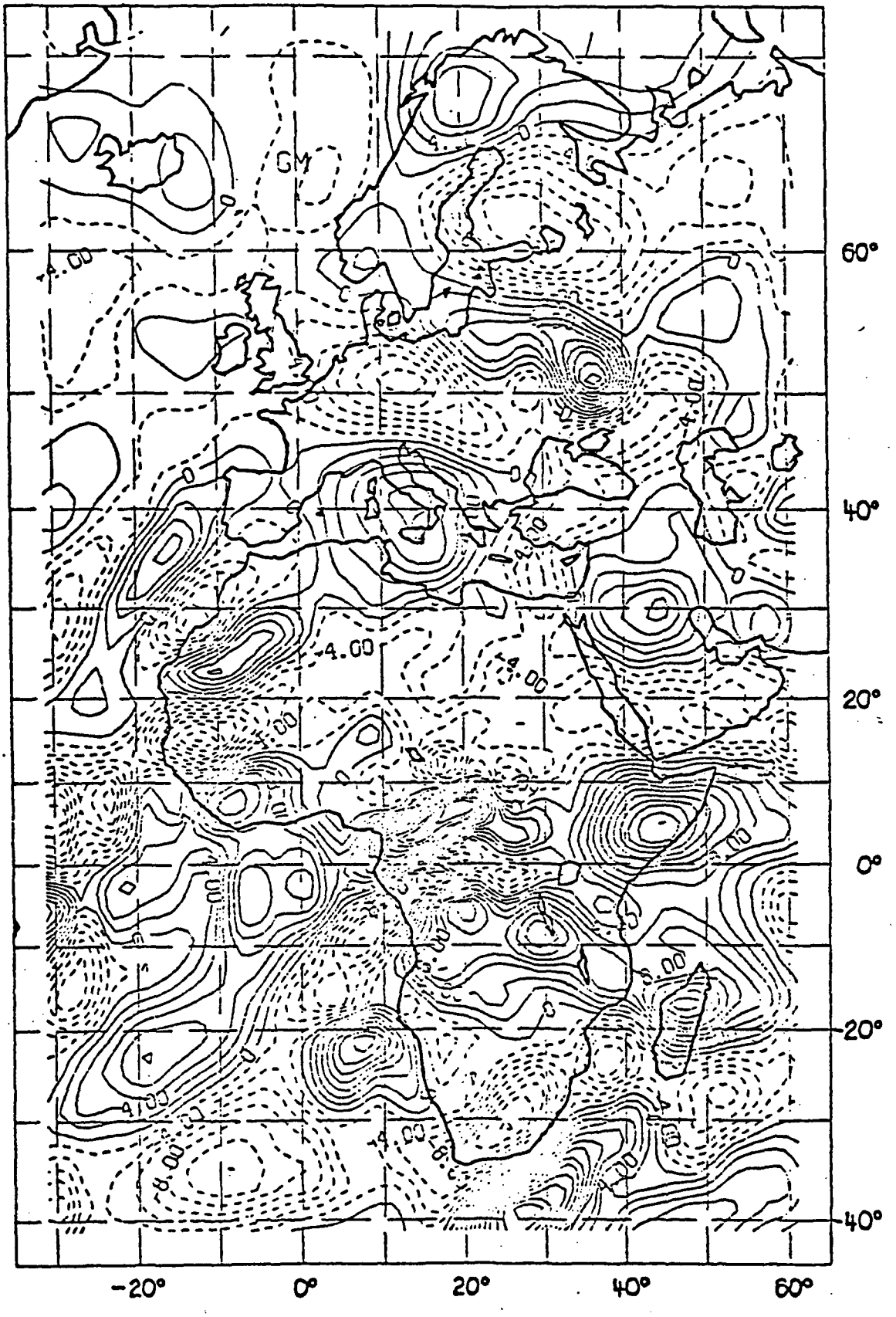

Figure 4. Reduced-to-pole MAGSAT scalar magnetic anomalies at 400 km elevation over Euro-Africa. Contour interval is 2 nT.

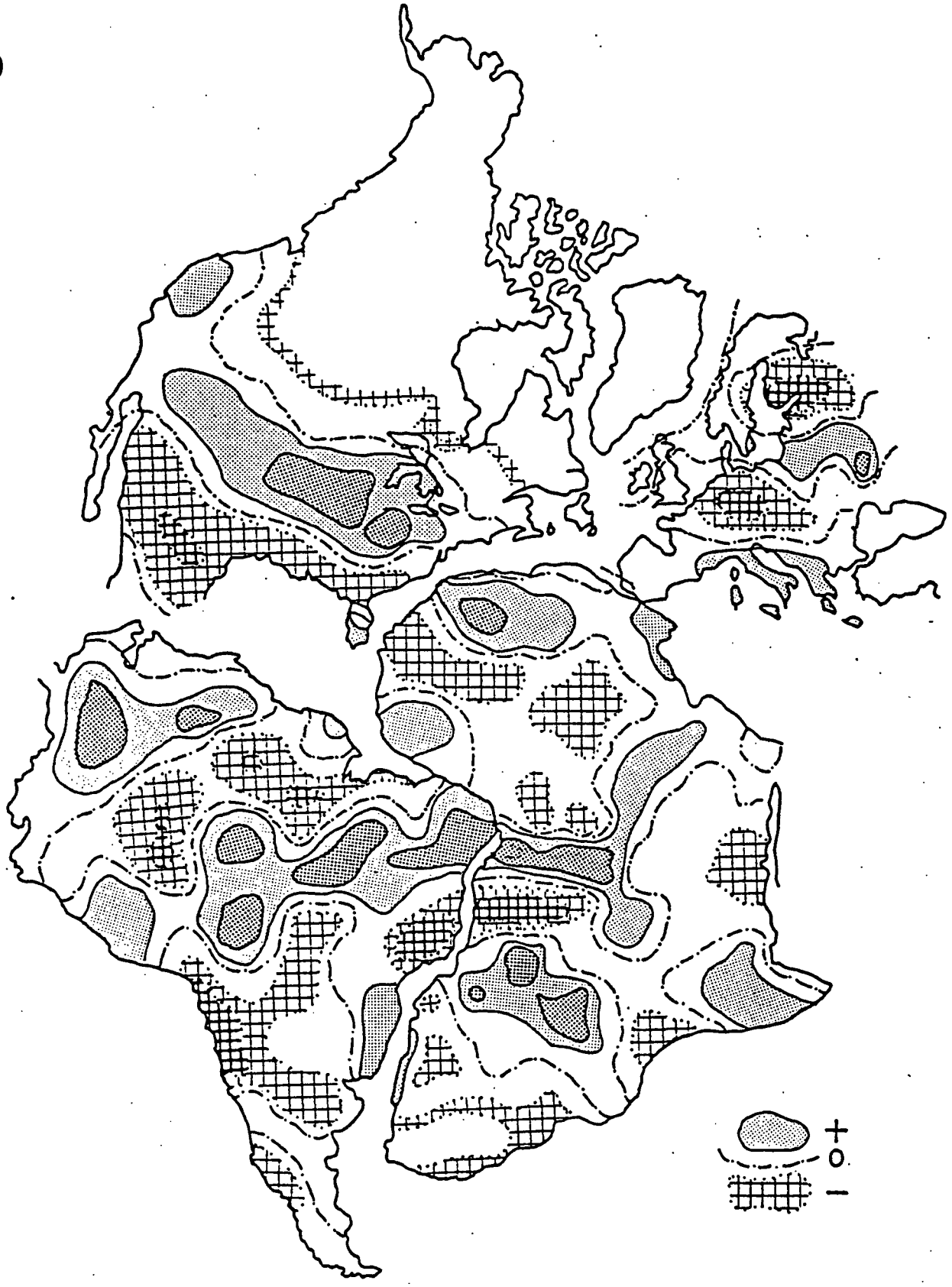

Figure 5. Partial reconstruction of the continents using reduced-to-pole satellite scalar magnetic anomalies.

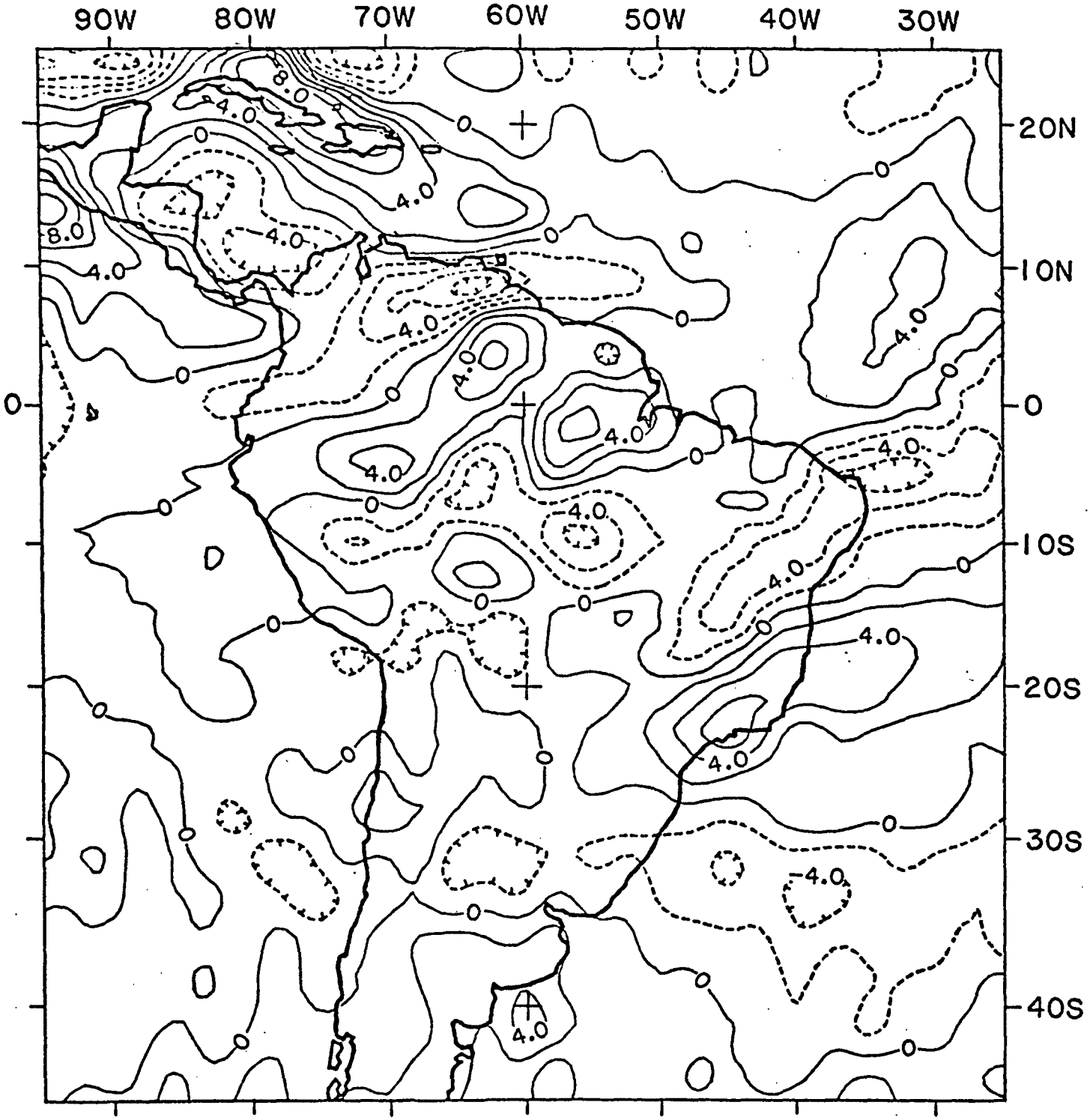

Figure 6. Bandpassed filtered ($4° < \lambda < 50°$) MAGSAT scalar magnetic anomalies at 350 km over South America. Contour interval is 2 nT.

APPENDIX A

Reprints of published articles,
expanded abstracts and abstracts.

REGIONAL MAGNETIC AND GRAVITY ANOMALIES OF SOUTH AMERICA

W.J. Hinze, R.R.B. von Frese, M.B. Longacre[1], and L.W. Braile

Department of Geosciences, Purdue University, West Lafayette, IN 47907

E.G. Lidiak

Department of Earth and Planetary Sciences, University of Pittsburgh, Pittsburgh, PA 15260

G.R. Keller

Department of Geological Sciences, University of Texas at El Paso, El Paso, TX 79968

Abstract. Preliminary satellite scalar magnetic anomaly data (MAGSAT) reduced to vertical polarization and long-wavelength-pass filtered free-air gravity anomaly data of South and Central America are compared to major tectonic features. A number of correlations are observed, but these must be generalized because of the preliminary nature of the geophysical data and the inherent petrophysical variations within tectonic features. Statistical analysis of the magnetic data reveals that South and Central America are more magnetic and magnetically more variable than adjacent marine areas. More obvious correlations exist between magnetic anomalies and tectonic elements of the continents than in the case of oceanic areas. No obvious correlations occur between the tectonic features of the Atlantic Ocean, including the Mid-Atlantic Ridge, and magnetic anomalies. The continental shields generally are more magnetic than adjacent basins, oceans and orogenic belts. In contrast, the major aulacogens are characterized by negative magnetic anomalies. Positive free-air gravity anomalies are related to the Andean Foldbelt, but the relationship of this feature to magnetic anomalies is much less obvious. However, along the west coast of South America, the magnetic anomalies of the Pacific Ocean are separated from those of the eastern platforms by north to northwest trending anomalies. South of the equator along the Foldbelt, gravity maxima are related to magnetic minima, a relationship analogous to the situation observed in the Rocky Mountain Cordillera. North of the equator in Columbia, gravity and magnetic maxima roughly correlate along the Foldbelt.

Introduction

A wide variety of significant geologic problems are represented by the complex geological-geophysical setting of South and Central America and adjacent marine areas. This region includes tectonically active areas, a number of lithospheric plates, advancing and trailing plate margins, hotspots, aulacogens, strong contemporary seismicity and volcanism, well-delineated metallogenic zones in the Cordillera, and a complex mineral-rich Precambrian shield.

Long-wavelength magnetic and gravity anomalies and their correlations provide the opportunity to investigate the regional relations of these features. For the South America region, potential field anomaly compilations are especially important to megatectonic investigations because of access problems which limit surface geologic and geophysical mapping.

Accordingly, preliminary 2°-averaged satellite magnetic anomaly values derived from the recent MAGSAT mission are compiled for South America. These data are differentially reduced to the pole (vertical magnetic polarization) for comparison with tectonic data and surface free-air gravity anomalies upward continued to satellite elevations. Finally, visual spatial correlations between the regional magnetic and gravity anomalies and tectonic data are considered in the context of their potential geological significance.

Data Sources and Preprocessing

The satellite magnetic anomalies used in this investigation are compiled from a preliminary scalar MAGSAT data set from observations made during "quiet day" periods of low temporal magnetic variations. The data set is based upon the average areal value of data taken below 400 km with an average elevation of approximately 350 km. An average of 12 data points with a range from 3 to 32 points per 2° area were used to calculate the average values. The preliminary geomagnetic reference field model MG680982 developed by NASA-GSFC was used to remove the geomagnetic core field component of the data. Comparison of this preliminary MAGSAT data set with POGO magnetic anomalies [Langel, 1979] shows excellent consistency over South America. A subset of these preliminary global MAGSAT data was compiled for the region (99°W-21°W), (45°S-33°N) and differentially reduced to the pole by least squares matrix inversion [von Frese et al., 1981a] on a spherical earth using the IGS-75 field updated to 1980 and an inducing field of 60,000 nT (Fig. 1).

Surface 1°-gridded free-air gravity anomalies for the South America region were compiled from measured and predicted continental data, satellite derived oceanic values, shipborne measurements and interpolated values. Continental values were obtained from the free-air gravity map of South America provided by the Defense Mapping Agency Aerospace Center which includes observed

[1]Now at Sohio Petroleum Company, 100 Pine St., San Francisco, CA 94111

Paper number 2L0344.
0094-8276/82/002L-0344$3.00

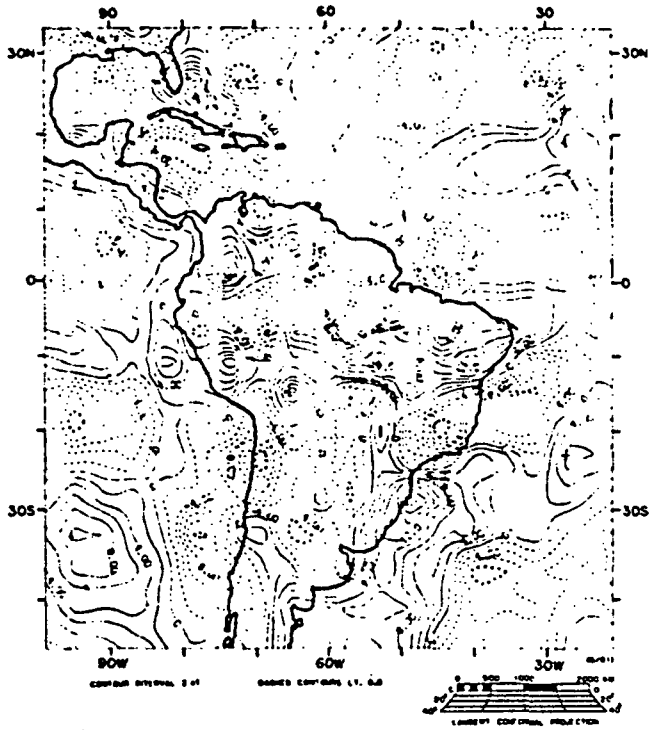

Fig. 1. Equivalent point source field approximation of 2°-averaged scalar MAGSAT magnetic anomaly data differentially reduced to radial polarization at 350 km elevation. The normalized amplitude for the polarizing induction field is 60,000 nT. Contour interval is 2 nT.

values, as well as some predicted values [Woollard and Strange, 1966] largely based on geologic and topographic considerations. Oceanic free-air gravity values were derived principally from GEOS-3 geodetic satellite altimetry data converted to gravity values [Rapp, 1979].

To enhance the longer wavelength components of the 1°-gridded free-air gravity anomalies, as well as to facilitate subsequent inversion processing, the data set was long-wavelength-pass filtered for wavelengths greater than roughly 8° (Fig. 2). For comparison with the satellite magnetic anomalies, the filtered gravity data set was upward continued to 350 km elevation (Fig. 3) by equivalent point source inversion.

To facilitate comparisons between potential field anomalies and tectonic features, a regional tectonic map of Latin America is presented in Figure 4 which emphasizes features with wavelengths of the order of 200 km or greater [Longacre, 1981]. The South American Platform, the largest and geologically oldest of the major tectonic subdivisions, includes continental terrain east of the Andean Foldbelt and north of about 35°S latitude. It consists of Precambrian basement rocks which in places are overlain unconformably with sedimentary and volcanic rocks of Silurian and younger age. The Patagonian Platform with basement rocks of Middle Paleozoic age includes the continental region of South America south of roughly 35°S and east of the Andes. These basement rocks are largely masked by a volcanic-sedimentary rock cover that developed after the Carboniferous. The Andean Cordillera constitute the entire western margin of South America with the northern portion merging into the Caribbean tectonic complexes. This foldbelt consists of rocks dating from the Precambrian to recent time and contains areas of strong seismicity and volcanism, as well as some of the richest metallogenic zones in the world.

Magnetic and Gravity Anomaly - Tectonic Observations

A number of interesting associations between regional tectonic features and magnetic and free-air gravity anomalies are evident by comparing Figures 1 through 4. However, the correlations are seldom exact and are not universal because of the limited resolution and potential imprecision of the averaged and preliminary nature of the magnetic data set, the limited gravity observation coverage and the inherent petrophysical variations within the tectonic elements. In the most regional sense there appears to be a relationship between satellite magnetic anomalies and continental areas (Fig. 1). The magnetic anomalies of the continent are observed to be more positive and more variable than the oceanic anomalies. This is particularly evident in Central America. In an attempt to quantify this subjective observation, the continental and oceanic magnetic data sets were separated and statistically analyzed. The frequency distribution of the oceanic and continental magnetic anomaly amplitudes (Fig. 5) reveals the mean of the oceanic anomalies is -0.9 nT and that of the continents, including the continental shelf, is +0.7 nT, with the continents having a higher standard deviation. A variance test (F test) and a mean test indicate that the oceanic and continental anomalies represent two signifi-

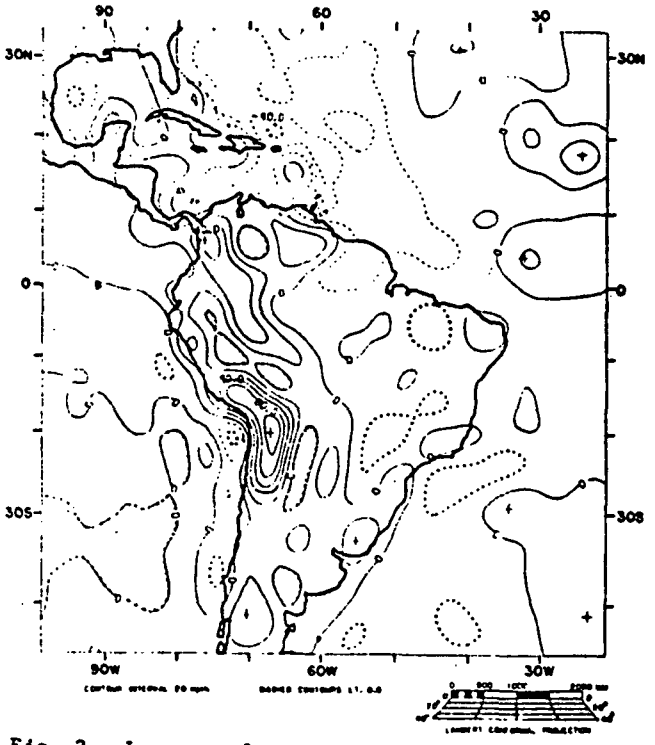

Fig. 2. Long-wavelength-pass ($\lambda \geq 8°$) filtered, surface free-air gravity anomaly map of South America and adjacent areas. Contour interval is 20 mgals.

cantly different populations at the 99% and 99.9% level of significance respectively. Thus, these preliminary results suggest that the continents are more magnetic and variable in their magnetization than the oceans. The former is compatible with the conclusions reached by Wasilewski et al. [1979] that the seismic Moho can be a magnetic boundary and the upper mantle only weakly magnetic. The more variable magnetization of the continents presumably reflects their long and complex geologic history which has led to strong horizontal magnetic polarization variations in the crust.

The strikes of the smoothed surface free-air gravity anomalies (Fig. 2) generally are consistent with tectonic trends. However, at 350 km elevation the gravity data (Fig. 3) have a decidedly north to northwest trend which reflects the dominating effects of the Andean Foldbelt and the features of the eastern margin of the Caribbean Plate at the longer wavelengths. The satellite magnetic data (Fig. 1) by contrast exhibit prominent east-west trends which, although consistent with tectonic features, may also be related to processing noise derived from data reduction efforts to correct for external magnetic field effects, especially in equatorial latitudes [Regan et al., 1981]. In both geophysical data sets, the leading edge of the South American Plate marks an effective boundary between Pacific anomalies of the Nazca Plate and continental anomalies of South America. The trailing edge, by contrast, is characterized by gravity and magnetic anomalies which commonly extend across the eastern continental margin of South America into the Atlantic Ocean.

The major shield areas of South America - Guiana, Central Brazilian, Sao Luiz Craton, Sao Fransicso Craton and the Patagonian Platform (Fig. 4) - are associated with positive magnetic anomalies and no definitive gravity anomalies. In contrast, many of the intra-cratonic basins - Amazon River, Parana, Parnaiba and Chaco (Fig. 4) - are related to negative magnetic anomalies. The Takatu, Amazon River, and Sao Luiz aulacogens also are associated with negative magnetic anomalies that correlate with local positive gravity anomalies. This inverse correlation of anomalies also is observed for the Mississippi Embayment aulacogen where the source of these anomalies has been attributed to either an intra-layer lithologic variation or upwarp of the Curie isotherm in the lower crust [von Frese et al., 1981b]. The major tectonic break between the Chaco Basin and the Patagonian Platform to the south appears as a linear magnetic high which extends into the Andean Foldbelt.

The Andean Foldbelt is dominated by positive gravity anomalies (Figs. 2 and 3). The correlation of magnetic anomalies (Fig. 1) with this tectonic zone is much less obvious and more variable. However, in a general way the magnetic anomalies of the eastern Pacific Ocean are separated from those of the eastern platforms by north to northwest anomaly trends. South of the equator an inverse relationship exists between positive gravity and negative magnetic anomalies. This relationship is consistent with observations by von Frese et al. [1982] for the North American Cordillera, where this inverse correlation may result from regionally higher temperature associated with geodynamic processes which produce thinned crust, mantle intrusives and an inflated elevation that

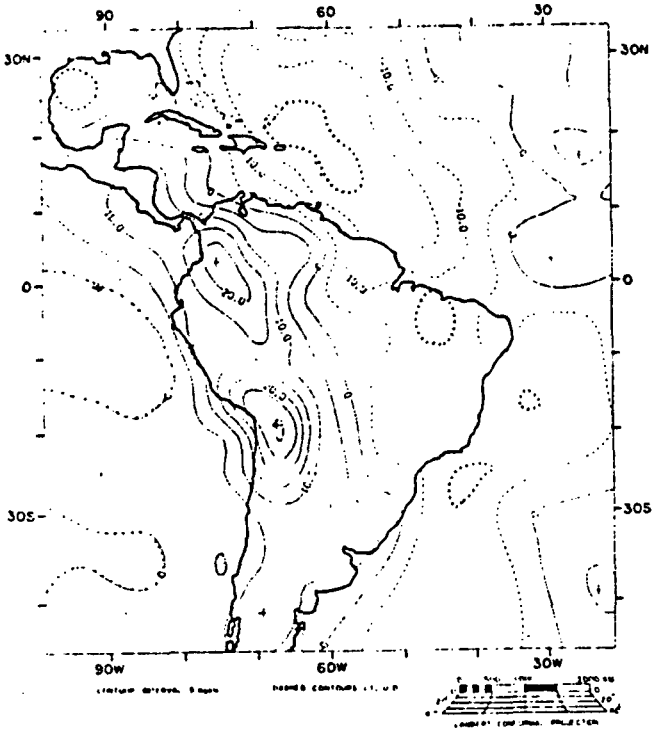

Fig. 3. Free-air gravity anomaly map of South America (Fig. 2) upward continued to 350 km elevation by equivalent point source inversion. Contour interval is 5 mgals.

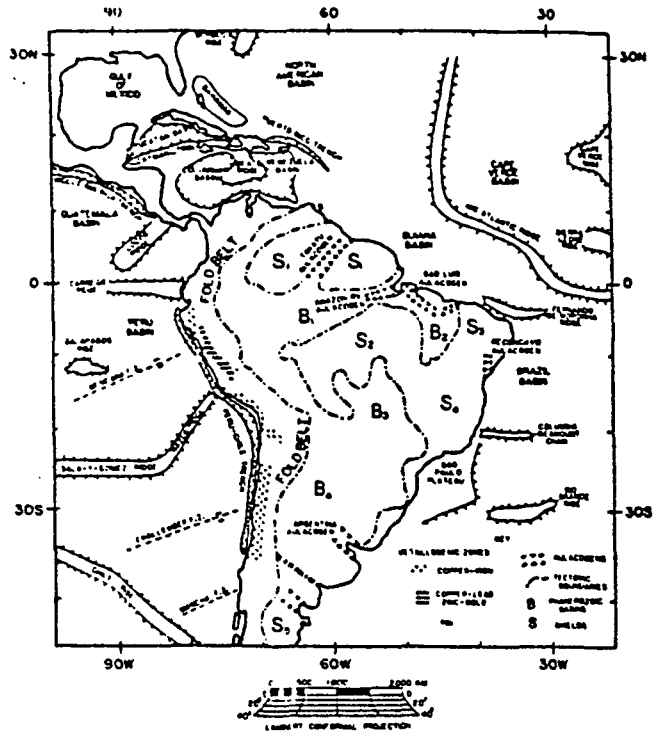

Fig. 4. Generalized tectonic divisions of South America and adjacent areas. S_1 - Guiana Shield, S_2 - Central Brazilian Shield, S_3 - Sao Luiz Craton, S_4 - Sao Francisco Craton, S_5 - Patagonian Platform, B_1 - Amazon River Basin, B_2 - Parnaiba Basin, B_3 - Parana Basin, and B_4 - Chaco Basin.

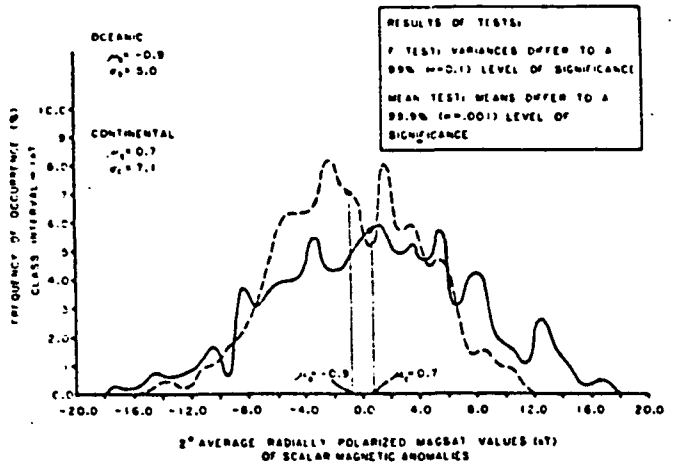

Fig. 5. Frequency distributions for oceanic and continental radially polarized MAGSAT magnetic anomaly data at 350 km elevation for South America and adjacent areas.

may not be isostatically compensated. A parallel zone of negative gravity and positive magnetic anomalies occurs along the eastern flank of the Andean Foldbelt. Similar inverse relationships, observed for continental regions east of the North American Cordillera are shown by seismic evidence to be characterized by thickened crust [von Frese et al., 1982]. This zone is bordered farther eastward by a less obvious linear trend of positive gravity and negative magnetic anomalies that includes the western flank of the Central Brazilian Shield.

Potential field anomalies along the Andean Foldbelt and Central America roughly north of the equator, in general, show direct correlation between positive gravity and magnetic anomalies. The large positive free-air gravity anomaly over Columbia correlates with a linear ophiolite (greenstone) sequence. Seismic refraction measurements in western Colombia indicate higher velocities and density for the rocks associated with this gravity anomaly [Meyer et al., 1973]. Further evidence for the mafic character of these rocks is suggested by the corresponding positive satellite magnetic anomaly which characterizes the region as a zone of enhanced magnetization.

The adjacent marine areas also demonstrate a variety of associations between potential field anomalies and tectonic features that can be useful for understanding the geologic characteristics and history of the area. The Pacific Ocean region, for example, generally exhibits a pattern of inverse correlations between the potential field anomalies with ridges and rises occurring along the flanks of the regional anomalies. The Gulf of Mexico and the Caribbean Sea are gravity and magnetic minima, although the correlation is inexact particularly because of a gravity ridge which separates the Columbian and Yucatan Basins. Potential field anomalies over the Atlantic Ocean adjacent to South America are inconsistent and lack correlation to trends of tectonic features including the Mid-Atlantic Ridge.

Although these complicated anomaly patterns mirror a complex assortment of crustal structures and lithological variations, they also undoubtedly reflect the preliminary character of the data sets used in this study. Efforts currently are underway to develop an improved set of MAGSAT scalar and vector magnetic anomaly data for geologic analysis and modeling. In consideration of the correlations demonstrated by this preliminary investigation, these efforts are anticipated to significantly enhance our understanding of the structure, dynamics and geologic history of the crust and upper mantle of South America.

Acknowledgments. Financial support for this study was provided by the Goddard Space Flight Center under NASA contracts NAS5-25030 and NAS5-26326.

References

Langel, R.A., Near-earth satellite magnetic field measurements: A prelude to MAGSAT, EOS (Am. Geophys. Union Trans.), 60, 667-668, 1979.

Longacre, M.B., Satellite magnetic investigation of South America, Unpubl. M.S. Thesis (Purdue Univ.), 1981.

Meyer, R.P., W.D. Mooney, A.L. Hales, C.E. Helsley, C.P. Woollard, D.M. Hussong, L.W. Kroenke and J.E. Ramirez, Project Navino III: Refraction observations across a leading edge, Malpelo Islands to the Colombian Cordillera Occidental, Am. Geophys. Union Monogr. 19, 105, 1973.

Rapp, R.H., Global anomaly and undulation recovery using GEOS-3 altimeter data, NASA-Final Rept., The Ohio State University Research Foundation, Columbus, 1979.

Regan, R.D., D.W. Handschumacher and M. Sugiura, A closer examination of the reduction of satellite magnetometer data for geological studies, J. Geophys. Res., 86, 9567-9573, 1981.

von Frese, R.R.B., W.J. Hinze, and L.W. Braile, Spherical earth gravity and magnetic anomaly analysis by equivalent point source inversion, Earth Planet. Sci. Lett., 53, 69-83, 1981a.

von Frese, R.R.B., W.J. Hinze, L.W. Braile, and A.J. Luca, Spherical earth gravity and magnetic anomaly modeling by Gauss-Legendre quadrature integration, J. Geophys., 49, 234-242, 1981b.

von Frese, R.R.B., W.J. Hinze and L.W. Braile, Regional North American gravity and magnetic anomaly correlations, Geophys. J.R. Astr. Soc. (in press), 1982.

Wasilewski, P.J., H.H. Thomas and M.A. Mayhew, The Moho as a magnetic boundary, Geophys. Res. Lett., 6, 541-544, 1979.

Woollard, G.P., and W.E. Strange, The prediction of gravity, in Gravity Anomalies: Unsurveyed Areas, Am. Geophys. Union Monogr. 9, 96, 1966.

(Received November 23, 1981;
accepted March 1, 1982.)

EURO-AFRICAN MAGSAT ANOMALY-TECTONIC OBSERVATIONS

W.J. Hinze - Purdue University; R. Olivier - University of Lausanne; and R.R.B. von Frese - Ohio State University

Preliminary satellite (MAGSAT) scalar magnetic anomaly data are compiled and differentially reduced to radial polarization by equivalent point source inversion for comparison with tectonic data of Africa, Europe and adjacent marine areas. A number of associations are evident to constrain analyses of the tectonic features and history of the region. Rift zones and aulacogens, for example, tend to be magnetically negative. The most intense positive anomaly of the region is the Bangui anomaly which has been interpreted as due to a deep crustal positive magnetization source. There are no near-surface sources which will explain this anomaly. By contrast, the next most intense positive anomaly is over the Kursk region in the Russian Ukraine. This anomaly extends 450 km in a northeasterly direction and is roughly 150 km wide, and is caused according to aeromagnetic anomaly interpretations by near-surface, intensely magnetic ferruginous quartzites. Apparently there is sufficient long-wavelength energy in these near-surface anomalies for them to be observed at satellite elevations. The Precambrian shields of Africa and Europe exhibit varied magnetic signatures. All shields are not magnetic highs and, in fact, the Baltic shield is a marked minimum. The reduced to the pole magnetic map shows a marked tendency for northeasterly striking anomalies in the eastern Atlantic and adjacent Africa, which is coincident to the track of several hot spots for the past 100 million years. However, there is little consistency in the sign of the magnetic anomalies and the track of the hot spots. Comparison of the radially polarized anomalies of

Africa and Europe with other reduced to the pole magnetic satellite anomaly maps of the western Hemisphere support the reconstruction of the continents prior to the origin of the present-day Atlantic Ocean in the Mesozoic Era.

Presented at the XVIII IUGG General Assembly, Hamburg, Germany, 1983.

CORRELATION OF TECTONIC PROVINCES OF SOUTH AMERICA AND THE CARIBBEAN REGION WITH MAGSAT ANOMALIES

E.G. Lidiak, D.W. Yuan - University of Pittsburgh; W.J. Hinze, M.B. Longacre - Purdue University; and G.R. Keller - University of Texas at El Paso

Intensities of satellite scalar magnetic anomaly data (MAGSAT) correlate with the main tectonic provinces of South America and the Caribbean region. Magnetic anomalies of the continents generally have higher amplitudes than oceanic anomalies. This is particularly evident in Central America and in the shield areas of South America. The Caribbean Sea and Gulf of Mexico are underlain by prominent magnetic minima. Within these oceanic areas, linear magnetic highs correlate with topographic ridges which separate the Gulf of Mexico, the Colombian Basin, and the Venezuelan Basin.

South America is divisible into a broad craton of Precambrian shields and platforms separated by Phanerozoic basins, grabens and aulacogens to the east, the Phanerozoic Patagonian platform to the south, and the Mesozoic to Cenozoic Andean foldbelt and Caribbean Mountain system to the west and north. The continental shields are mainly more magnetic than continental basins and orogenic belts. This is particularly true of the Guyana shield, the Central Brazilian shield, and parts of the Atlantic shield, all of which are coincident with magnetic highs. The Amazon basin (aulacogen) in contrast is associated with large magnetic lows. Other basins coincide either with magnetic lows or magnetic gradients. Platforms, mainly covered by younger sedimentary rocks, are generally associated with magnetic gradients. Most of the anomalies associated with the Patagonian platform are positive and the gradients have higher amplitudes east of the Andean foldbelt. The northern Andes are

coincident with positive magnetic anomalies, whereas the central and southern Andes are associated mainly with negative anomalies.

The boundaries of the Caribbean plate occur along magnetic gradients. The gradients are particularly sharp along the northern and western margins of the plate, but are gradational along the southern margin where they merge with anomalies associated with the Andean Cordillera. The anomalies along the western margin of the South American plate are also distinct and appear to be separate from those of the adjacent ocean basin. In contrast, eastern South America is characterized by magnetic anomalies which commonly extend into the Atlantic Ocean.

Presented at the 10th Caribbean Geological Conference, Cartagena, Colombia, August, 1983.

A SATELLITE MAGNETIC MODEL OF NORTHEASTERN SOUTH AMERICAN AULACOGENS

M.B. Longacre[1], W.J. Hinze and R.R.B. von Frese

Department of Geosciences, Purdue University, West Lafayette, IN 47907

Abstract. Magnetic modeling of the Amazon River and Takatu Aulacogens in northeastern South America illustrate the utility of satellite magnetic data in characterizing the properties and structure of the lithosphere. Specifically, reduction of preliminary MAGSAT scalar magnetic anomaly data to an equivalent condition of vertical polarization shows a general correlation between magnetic anomaly minima and the Amazon River and Takatu Aulacogens. Surface gravity data demonstrate a correlative positive anomaly. Spherical earth modeling of the magnetic data indicates a less magnetic crust associated with the aulacogens which is compatible with previous studies over the Mississippi River Aulacogen and Rio Grande Rift in North America.

Introduction

South America is particularly significant to regional geophysical investigations because it affords opportunities for integrated analysis of a broad range of geologically interesting tectonic features. However, surface acquisition of the necessary data for these studies frequently is inhibited due to the vast areas involved and problems of access. Hence, satellite geophysical data, such as the magnetic anomaly values obtained from MAGSAT, are especially useful in providing information for developing lithospheric models of major South American tectonic features.

A preliminary set of scalar MAGSAT data is utilized to investigate the magnetic structure and properties of the Takatu and Amazon River Aulacogens in northeastern South America previously recognized by Burke [1978]. The magnetic data are derived from preliminary 2°-averaged scalar MAGSAT magnetic anomaly values which Hinze et al. [1982] have reduced to the pole (equivalent vertical polarization) by equivalent point source inversion [von Frese et al., 1981a]. This radially polarized form of the anomaly data eliminates uncertainties in interpretation caused by the inclination and intensity of the earth's magnetic field which induces magnetization in the lithosphere at depths shallower than the Curie point isotherm of magnetic minerals. This procedure assumes the anomalous magnetic field is caused only by magnetization in the direction of the earth's magnetic field and the inducing field strength is 60,000 nT.

Hinze et al. [1982] present a description of the reduced to radial polarization MAGSAT scalar magnetic anomaly map and its qualitative correlation with regional gravity anomalies and tectonic features. A number of interesting correlations are observed, but they are generalized due to the preliminary nature of the geophysical data and the inherent variations of the petrophysical properties of the tectonic features. One of the more interesting correlations is the approximate spatial coincidence between the Amazon River and Takatu Aulacogens and magnetic anomaly minima shown in Figure 1. In the original 2°-averaged MAGSAT data set, prior to reduction to radial polarization, these correlative anomalies were positive and complicated by their location near the magnetic equator and the spatially rapidly varying magnetic field.

Relationship of Aulacogens to Geophysical Data

The aulacogens (failed-rifts), which originated in late Permian-early Jurassic time during the breakup of the continent of Pangea, are characterized by deep sedimentary troughs with near vertical faulting and associated basaltic intrusions. The troughs occur roughly perpendicular to the South American platform margin. They are associated with relative positive Bouguer gravity anomalies (Fig. 2) presumably related to the basaltic intrusions.

A similar anomaly relationship is observed over the younger, still active, Rio Grande Rift. Mayhew and Majer [1980] have discussed the satellite magnetic anomaly minimum associated with this rift. They suggest that the rift, which has a correlative free-air gravity positive anomaly over the southern extent of its length, is related to a decrease in the relative thickness of the magnetic crust caused by an upwarped Curie isotherm. However, this origin for the magnetic minima in northeast South America seems unlikely because of the great length of time since the formation of the aulacogens.

A similar inverse relationship between the magnetic anomaly minimum observed at satellite elevations by the Polar Orbiting Geophysical Observatory (POGO) and positive surface free-air gravity data has been observed over the Mississippi Embayment by von Frese et al. [1981a]. The embayment is a broad, spoon-shaped basin of Mesozoic and Cenozoic sedimentary rocks which extends into the North American craton from the Gulf Coast. Ervin and McGinnis [1975] suggest on the basis of gravity, crustal seismic, and geologic data that the embayment is the site of a late Precambrian aulacogen which was reactivated in late Cretaceous time by tensional forces initiated during the formation of the present Atlantic Ocean. von Frese et al. [1981b; 1981c] present a quantitative crustal model which duplicates the observed magnetic and gravity anomalies. Several origins are postulated [von Frese et al., 1981c] for satisfying the negative magnetic anomaly including: 1) Strong reversed magnetization of intrusives into the lower crust which were emplaced during the rifting process, 2) petrologic variations be-

[1]Now at Sohio Petroleum Company, 100 Pine St., San Francisco, CA 94111

Paper number 21.0343.
0094-8276/82/002L-0343$3.00

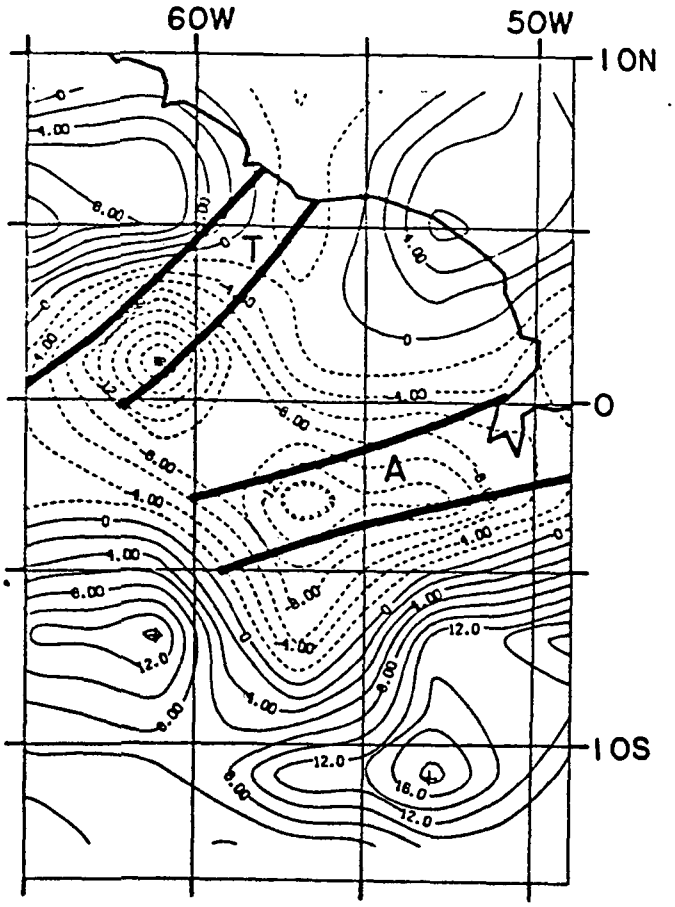

Fig. 1. Radially polarized magnetic anomaly map of northeastern South America derived from MAGSAT scalar data at an average elevation of 350 km. An inducing field of 60,000 nT is assumed. Contour interval is 2 nT. The locations of the Amazon River (A) and Takatu (T) Aulacogens are generalized from Burke [1978], de Almeida [1975] and Potter [1978].

tween the normal lower crustal rock, which is generally highly magnetic, and the intrusions into the crust from the mantle, and 3) increased temperatures in the embayment region which raises the Curie point isotherm from a normal position near the base of the crust to within the crust, thereby decreasing the overall magnetization of the crust.

In general, little evidence currently is available to support or discriminate between these hypotheses for the crustal structure of the embayment. Furthermore, other studies by Mayhew et al. [1980] in Australia and globally by Frey [1979] indicate the rifts and aulacogens are not universally represented by negative satellite magnetic anomalies. Hence, it appears that aulacogens and rifts are manifested in a variety of ways within the magnetic crust, where their variable geophysical signatures may provide clues for understanding their origin and subsequent geologic evolution.

Spherical-Earth Modeling of Aulacogens

A three-dimensional, spherical earth model of the aulacogens was developed using a Gauss-Legendre quadrature integration technique [von Frese et al., 1981b] and radially polarized scalar magnetic anomaly data. The magnetic model (Fig. 3) consists of simplified spherical prisms which produce an anomaly comparable to the observed data at 350 km elevation.

The three positive anomalies, A, D, and E, of Figure 3 represent the Guiana and Central Brazilian Shields by the prisms illustrated which have a relative anomalous magnetization of 2 A/m between depths of 10 to 50 km. These model parameters are consistent with the arguments of Wasilewski et al. [1979] that suggest sources of long-wavelength magnetic anomalies are concentrated in the lower crust which, in general, is substantially more magnetic than the upper crust. Typical estimates of deep crustal magnetization are on the order of 5 A/m [e.g., Hall, 1974; Shuey et al., 1973].

The magnetic anomaly minima associated with the aulacogens are modeled approximately by prisms B and C which respectively have relative anomalous magnetizations of -4 A/m from 20 to 40 km and -3 A/m from 25 to 40 km. However, the resolution of sources by modeling is limited, thus anomalous magnetization may be decreased with an increased prism thickness and vice versa. The same limita-

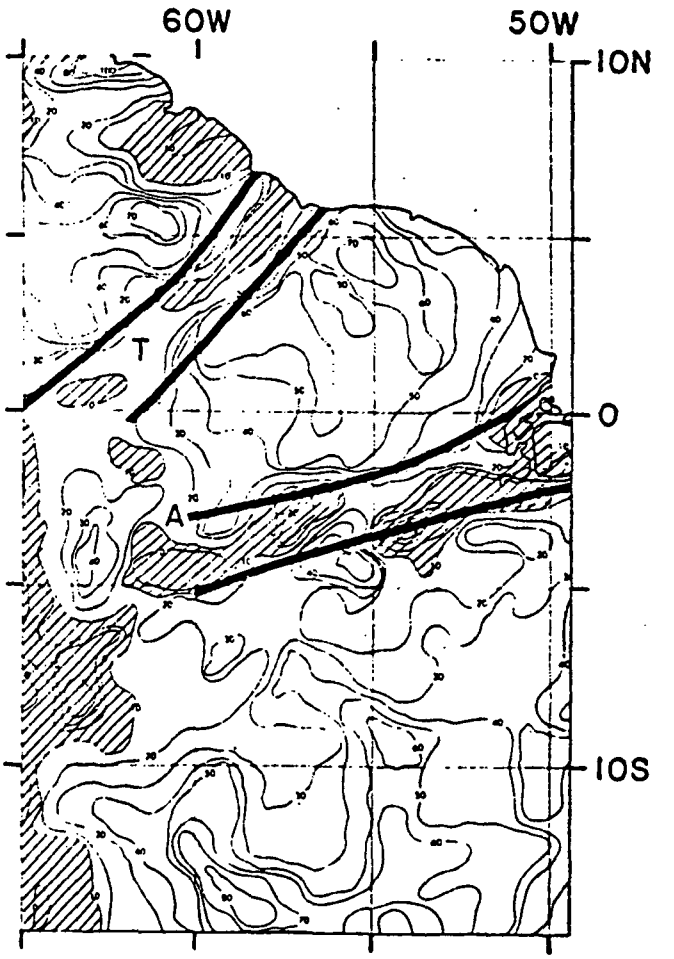

Fig. 2. Bouguer gravity anomaly map of northeastern South America [Wilcox, 1981]. Contour interval is 10 mgal, where shading indicates anomaly values ≥ -10 mgals. The locations of the Amazon River (A) and Takatu (T) Aulacogens are generalized from Burke [1978], de Almeida [1978] and Potter [1978].

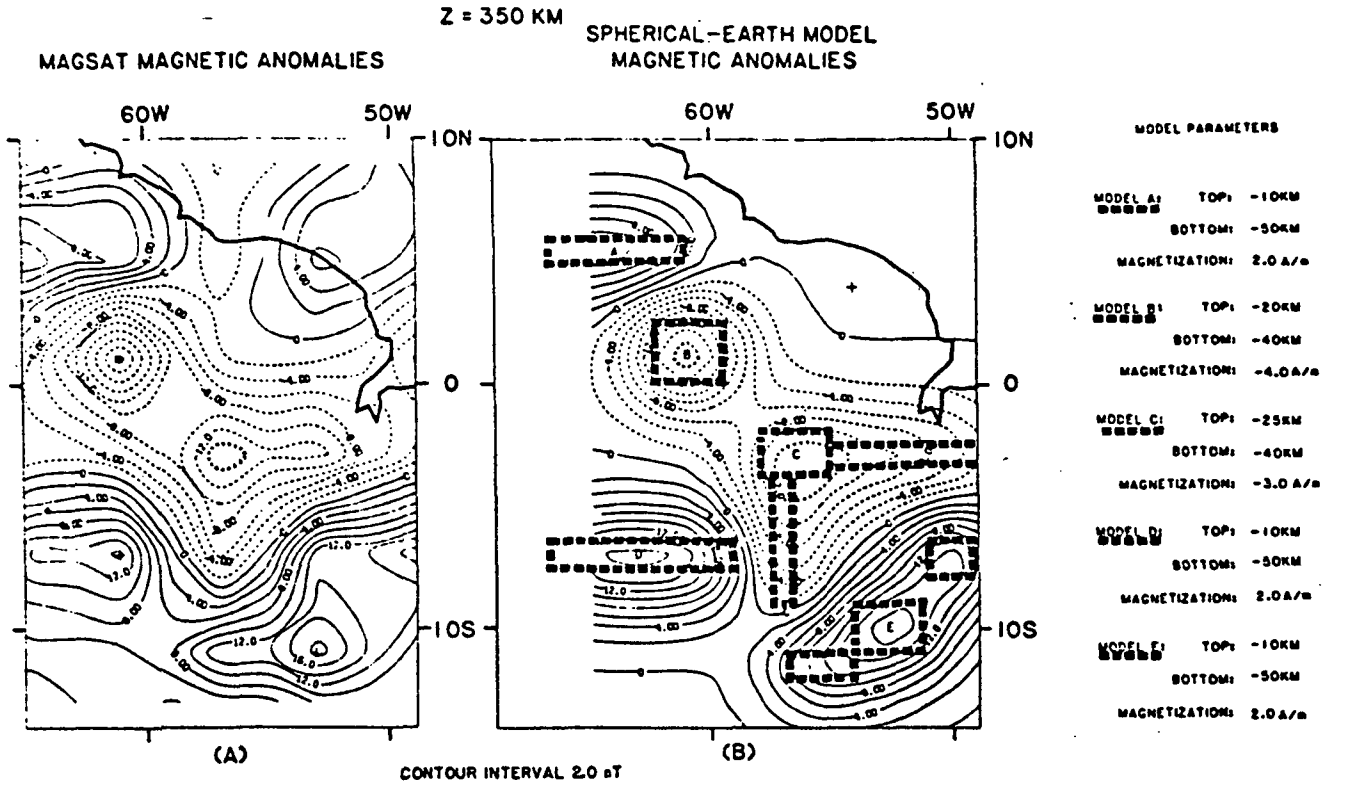

Fig. 3. Comparison at 350 km elevation of radially polarized magnetic anomalies derived from scalar MAGSAT data over northeastern South America (A) and modeled magnetic anomalies (B) which includes location and characteristics of anomaly source models. Contour interval is 2 nT.

tion is present in considering the prism sources of the positive magnetic anomalies. The sources of the anomaly minima have been modeled with prisms which approximate deficiencies in magnetization in the lower crust associated with the aulacogens similar to the model developed by von Frese et al. [1981c] for the Mississippi Embayment Aulacogen. The prism associated with the Takatu Aulacogen does not have the linear character of the aulacogen as delineated by Burke [1978] and the Amazon River Aulacogen model includes a low magnetization arm extending to the south from the Amazon River. No correlative gravity anomaly (Fig. 2) is observed with this south striking arm, suggesting that its source is probably not related to the aulacogen.

Conclusions

Modeling procedures are used with MAGSAT anomalies to investigate the Takatu and Amazon River Aulacogens of South America. Positive gravity and negative magnetic anomalies characterize these features analogous to the regional inverse correlations observed for the Mississippi River and Rio Grande Rift. Indeed, a synthesis of the preliminary 2°-averaged MAGSAT data and deep crustal magnetization information leads to a model that compares favorably with Mississippi Embayment Aulacogen model characteristics derived from POGO anomaly considerations by von Frese et al. [1981b; 1981c].

In general, the models presented here are consistent with the aulacogen hypothesis for the tectonic origins of the anomalies. These results suggest that an aulacogen may be characterized at satellite elevations by observable negative magnetic anomalies related to the rift component that defines a nonmagnetic block of material within the lower crust. It should be emphasized, however, that these models lead to a variety of interpretations which can only be discriminated on the basis of auxiliary geological and geophysical information.

Finally, although the preliminary character of the 2°-averaged MAGSAT data set used in this study obviously limits the geological implications of the models, these results clearly do indicate that the MAGSAT data provide geologically reasonable constraints for investigating the structure and properties of regional lithospheric features.

Acknowledgments. Financial support for this study was provided by the Goddard Space Flight Center under NASA contract NAS5-25030.

References

Burke, K., Evolution of continental rift systems in the light of plate tectonics, in Tectonics and Geophysics of Continental Rifts, ed. by R.B. Ramberg and E.R. Neuman, D. Reidel, Boston, 1978.

de Almeida, F.F.M., Tectonic Map of South America, 1:5,000,000; Explanatory Note, Ministry of Mines

and Energy, National Dept. of Mineral Production, Brasilia: Brazil, 1978.
Ervin, C.P. and L.B. McGinnis, Reelfoot rift: reactivated precursor to the Mississippi Embayment, Geol. Soc. Am. Bull., 86, 1287-1295, 1975.
Frey, H., Global geophysics and geology: correlations of satellite-derived gravity and magnetic anomalies with rifts and sutures, EOS (Am. Geophys. Union Trans.), 60, 398, 1979.
Hall, D.H., Long-wavelength aeromagnetic anomalies and deep crustal magnetization in Manitoba and Northwestern Ontario, Canada, Pageoph., 40, 403-430, 1974.
Hinze, W.J., R.R.B. von Frese, M.B. Longacre, J.L. Sexton, L.W. Braile, E.G. Lidiak and G.R. Keller, Regional magnetic and gravity anomalies of South America, Geophys. Res. Lett., (this issue), 1982.
Mayhew, M.A. and V. Majer, Application of Satellite Magnetic Anomaly Data to Curie Isotherm Mapping, NASA Rept. (NAS5-25720), 1980.
Mayhew, M.A., B.D. Johnson and R.A. Langel, An equivalent source model of the satellite-altitude magnetic anomaly field over Australia, Earth Planet Sci. Lett., 51, 189-198, 1980.
Potter, P.E., Significance and origin of big rivers, J. Geology, 86, 13-33, 1978.
Shuey, T.R., D.K. Schellinger, E.H. Johnson and L.B. Alley, Aeromagnetics and the transition between the Colorado Plateau and the Basin and Range Provinces, Geology, 1, 107-110, 1973.
von Frese, R.R.B., W.J. Hinze and L.W. Braile, Spherical earth gravity and magnetic anomaly analysis by equivalent point source inversion, Earth Planet. Sci. Lett., 53, 69-83, 1981a.
von Frese, R.R.B., W.J. Hinze, L.W. Braile and A.J. Luca, Spherical earth gravity and magnetic modeling by Gauss-Legendre quadrature integration, J. Geophys., 49, 234-242, 1981b.
von Frese, R.R.B., W.J. Hinze, J.L. Sexton and L.W. Braile, Regional magnetic model of the Mississippi Embayment, EOS (Am. Geophys. Union Trans), 62, 1981c.
Wasilewski, P.J., H.H. Thomas and M.A. Mayhew, The Moho as a magnetic boundary, Geophys. Res. Lett., 6, 541-544, 1979.
Wilcox, L., Personal communication, 1981.

(Received November 24, 1981;
accepted March 1, 1982.)

SATELLITE ELEVATION MAGNETIC AND GRAVITY MODELS OF MAJOR SOUTH AMERICAN PLATE TECTONIC FEATURES

M.B. Longacre - Sohio Petroleum Company; R.R.B. von Frese - Ohio State University; W.J. Hinze, L.W. Braile - Purdue University; E.G. Lidiak - University of Pittsburgh; and G.R. Keller - University of Texas, El Paso

Magsat scalar and vector magnetic anomaly data together with regional gravity anomaly data are being used to investigate the regional tectonic features of the South American Plate. An initial step in this analysis is three-dimensional modeling of magnetic and gravity anomalies of major structures such as the Andean subduction zone and the Amazon River Aulacogen at satellite elevations over an appropriate range of physical properties using Gauss-Legendre quadrature integration method. In addition, one degree average free-air gravity anomalies of South America and adjacent marine areas are projected to satellite elevations assuming a spherical earth and available Magsat data are processed to obtain compatible data sets for correlation. Correlation of these data sets is enhanced by reduction of the Magsat data to radial polarization because of the profound effect of the variation of the magnetic inclination over South America. The results of the modeling and correlation of magnetic and gravity anomalies are used with other regional geophysical data and geologic information to illustrate the utility of satellite magnetic data in characterizing the properties and structure of the South American Plate.

Presented at the 4th IAGA Scientific Assembly, Edinburgh, August 3-15, 1981

REDUCED TO POLE LONG-WAVELENGTH MAGNETIC ANOMALIES OF AFRICA AND EUROPE

R. Olivier - University of Lausanne; W.J. Hinze - Purdue University; and R.R.B. von Frese - Ohio State University

To facilitate analysis of the tectonic framework for Africa, Europe and adjacent marine areas, magnetic satellite (MAGSAT) scalar anomaly data are differentially reduced to the pole and compared to regional geologic information and geophysical data including surface free-air gravity anomaly data upward continued to satellite elevation (350 km) on a spherical earth. Comparative analysis shows magnetic anomalies correspond with both ancient as well as more recent Cenozoic structural features. Anomalies associated with ancient structures are primarily caused by intra-crustal lithologic variations such as the crustal disturbance associated with the Bangui anomaly in west-central Africa. In contrast, anomalies correlative with Cenozoic tectonic elements appear to be related to Curie isotherm perturbations. A possible example of the latter is the well-defined trend of magnetic minima that characterize the Alpine orogenic belt from the Atlas mountains to Eurasia. In contrast, a well-defined magnetic satellite minimum extends across the stable craton from Finland to the Ural mountains. Prominent magnetic maxima characterize the Arabian plate, Iceland, the Kursk region of the central Russian uplift, and generally the Precambrian shields of Africa.

Presented at the American Geophysical Union Annual Meeting, Baltimore, Maryland, 1983.

SATELLITE MAGNETIC ANOMALIES OF AFRICA AND EUROPE

R. Olivier - University of Lausanne; W.J. Hinze - Purdue University; and R.R.B. von Frese - Ohio State University

Preliminary satellite (MAGSAT) scalar magnetic anomaly data of Africa, Europe, and adjacent marine areas have been reduced to the pole assuming a constant inducing earth's magnetic field of 60,000 nT. This process leads to a consistent anomaly data set free from marked variations in directional and intensity effects of the earth's magnetic field over this extensive region. The resulting data are correlated with long wavelength-pass filtered free-air gravity anomalies; regional heat flow, and tectonic data to investigate megatectonic elements and the region's geologic history. Magnetic anomalies are related to both ancient as well as more recent Cenozoic structural features. The anomalies associated with ancient structure primarily are caused by intracrustal lithologic variations such as the crustal disturbance associated with the Bangui anomaly in west-central Africa. In contrast, anomalies correlative with Cenozoic tectonic elements appear to be primarily related to Curie isotherm perturbations. A possible example of the latter is the well defined trend of magnetic minima that characterize the Alpine orogenic belt from the Atlas Mountains to Eurasia. Western Europe particularly is dominated by the Alpine (?) magnetic minimum. Prominent magnetic maxima characterize the Arabian plate, Scandinavia, Iceland, and the Kursk region of the central Russian uplift. A well-defined satellite magnetic minima extends from Finland across Russia to the Ural Mountains which correlates with a heat flow minimum and increased crustal thickness.

Processed preliminary satellite (MAGSAT) scalar magnetic anomaly data are useful in studying and providing constraints for the investigation of the megatectonic features and geologic history of Africa, Europe, and

adjacent marine areas. These studies are facilitated by the integration of long wavelength-pass filtered free-air gravity anomalies, regional heat flow, and tectonic data with the magnetic anomalies. The scalar magnetic anomaly map shown in Figure 1 was derived from satellite observations acquired during "quiet day" periods of low temporal magnetic variations. This data set, which was provided by NASA-GSFC, is based on average 2° x 2° areal measurements obtained at an average elevation of about 400 km. The anomalous component was calculated by removing from the observed data the core field magnetic effect, as defined by the preliminary reference field model MG680982 developed by NASA-GSFC.

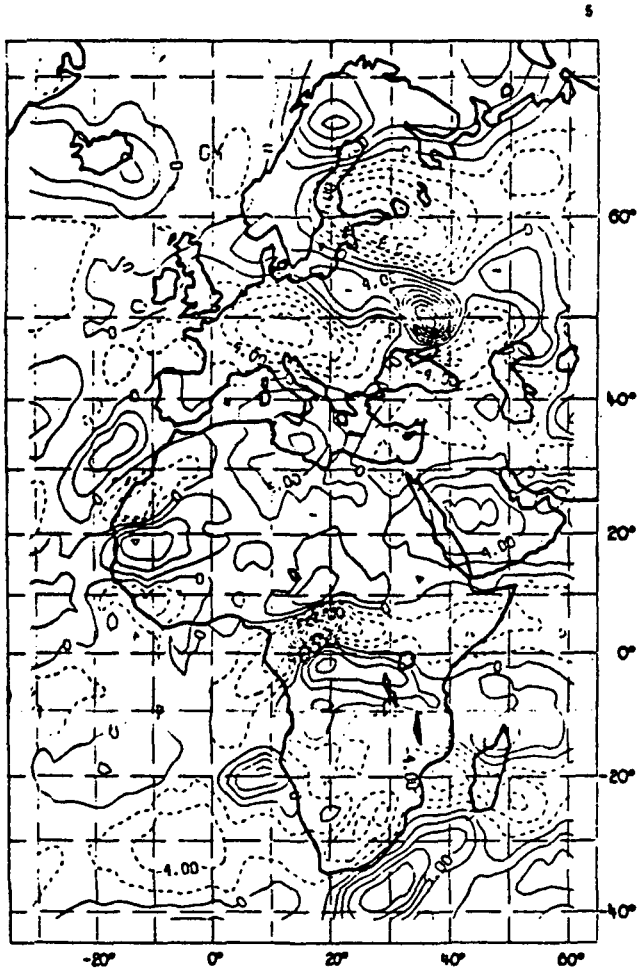

FIG. 1. Total magnetic intensity anomaly map of Africa and Europe derived from Magsat satellite 2°-mean values at an average elevation of about 400 km. Contour interval is 2 nT.

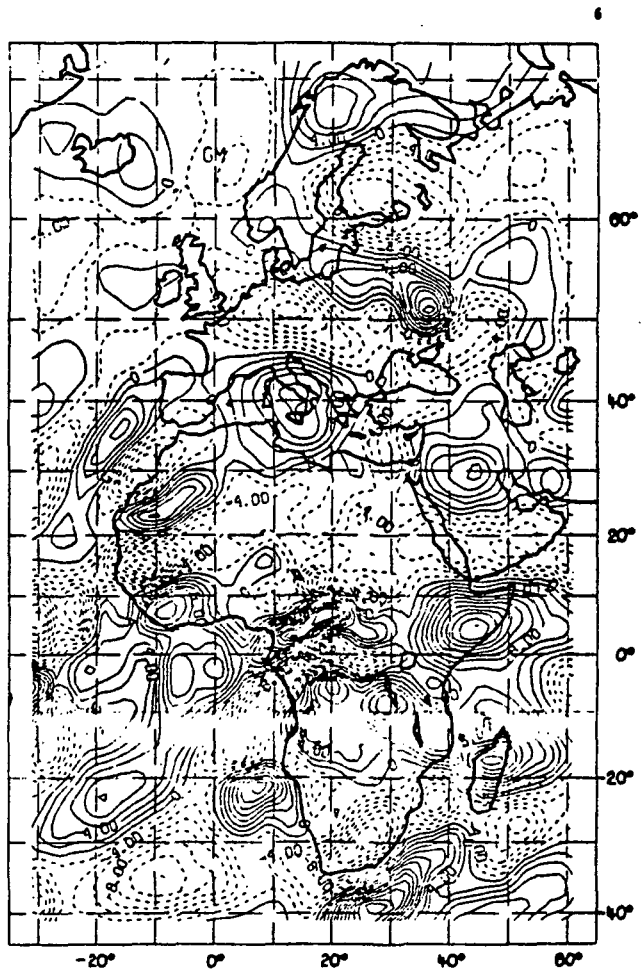

FIG. 2. Equivalent point source field approximation of 2°-averaged scalar Magsat magnetic anomaly data differentially reduced to radial polarization at 400 km elevation. The normalized amplitude for the polarizing field is 60,000 nT. Contour interval is 2 nT.

The region under investigation extends from mid-southern to high northern latitudes and thus shows a wide range of geomagnetic field strength, inclination, and declination. Hence, magnetic anomalies caused by induction in the earth's magnetic field will have signatures considerably different from the same source characteristics. To remove the effect of the highly variable magnetic field, the data used to prepare Figure 1 were differentially reduced to vertical (radial) polarization by equivalent point source inversion.

Least-squares matrix inversion was used to determine the magnetizations of a spherically orthogonal array of dipoles, oriented in the magnetic field defined by the updated IGS 1975 geomagnetic field model, that will duplicate the observed scalar magnetic anomalies. The dipoles were located on a 4 degree grid over the entire study region. To process this large array and make the problem more tractable, the inversion was performed on two independent sets of equivalent point sources. The process, which may be termed boot-strap inversion, was initiated with inversion of point sources over the southern half of the study area. The residual magnetic field obtained by subtracting the model field from the anomaly field was then inverted over a distribution of point dipoles in the remaining half of the data set. This procedure yielded 744 point dipole sources that model the anomalies of Figure 1 with negligible error. To achieve a least squares estimate of Figure 1 reduced to the pole, fields of the point dipoles were recomputed at 400 km elevation assuming an inducing field of 60,000 nT and radial inclination at all sources and observation points (Figure 2).

Comparison of Figures 1 and 2 shows a progressive shift of anomalies toward the poles in Figure 2 relative to Figure 1, with decreasing magnetic inclination and an inversion of the anomaly polarities near the magnetic equator.

Accordingly, assuming magnetizations directed along the current earth's magnetic field, the anomalies of Figure 2 may be used in analysis and modeling, as well as for spatial comparison with other geophysical and tectonic data. A number of interesting correlations are observed. The most prominent anomaly in Africa is the Bangui anomaly of west-central Africa. The magnetic anomaly maxima which correlates with regional heat flow and gravity anomaly minima was interpreted by Regan and Marsh (1982) as originating from a major ancient intracrustal lithologic feature. No profound magnetic anomaly appears to characterize the Tertiary East African rift zone. The Alpine orogenic belt from the Atlas Mountains in northwestern Africa through the Alps of south-central Europe to the orogenic elements of Eurasia is associated with a trend of magnetic minima and heat flow maxima that is especially pronounced in the European Alps. This Alpine trend of magnetic minima appears to ring the northern margin of a positive anomaly centered over the toe of the Italian peninsula. Pronounced magnetic positive anomalies also are located over the northern Arabian Plate, Scandinavia, and Iceland and its associated oceanic plateaus. In contrast, central Europe is dominated by the Alpine (?) magnetic minimum. The most intense maximum of the satellite magnetic data of Europe is found over the Kursk region of the central Russian highland and its well-known high-amplitude positive aeromagnetic anomalies. Finally, a prominent magnetic trend of minima projects westward from the Rifean Timan uplift near the north-central Ural Mountains to the Gulf of Finalnd. The large western minimum is associated with a well-defined heat flow minimum and zone of enhanced crustal thickness.

Reference

Regan, R.D. and March, B.D., 1982, The Bangui magnetic anomaly: Its geological origin, J. Geophys. Res., 87, p. 1107-1120.

Presented at the 52 Annual International Meeting and Exposition of the Society of Exploration Geophysicists, Dallas, TX, 1982.

REGIONAL ANOMALIES OF THE MISSISSIPPI RIVER AULACOGEN

R.R.B. von Frese - Ohio State University

Knowlege of Mississippi embayment crustal structure is particularly important because it is one of the more generally recognized and better known aulacogens and is related to a zone of intense seismicity in a highly urbanized portion of the midcontinent. The embayment is characterized by regionally positive gravity and negative magnetic anomalies that are observable in surface, aerosurvey, and satellite data. Regional, spherical earth modeling using Gauss-Legendre quadrature integration indicates that the long-wavelength gravity and magnetic anomalies of the embayment may be related to a rift zone along the axis of the embayment that defines a nonmagnetic block of high density material within the lower crust. The decreased magnetization of this component may be related to reversed magnetic remanence, or an intralithologic variation, or an upwarp of the Curie isotherm.

The Mississippi embayment is a structural trough of Mesozoic and Cenozoic sedimentary rocks that projects into the North American craton from the Gulf Coast province. The axis of this feature lies along the Mississippi River, tapering northward into the tectonically active New Madrid seismic zone (Figure 1c). A popular tectonic model for the origin of the embayment is that it represents a late Precambrian aulacogen which was reactivated most recently in the late Cretaceous by forces related to the formation of the present Atlantic Ocean basin.

Surface, 1 degree-averaged free-air gravity anomaly data low-pass filtered for wavelengths greater than about 8 degrees characterize the embayment by a regional anomaly of nearly 10 mgal in amplitude (Figure 1a). These data were upward continued on a spherical earth to 450 km

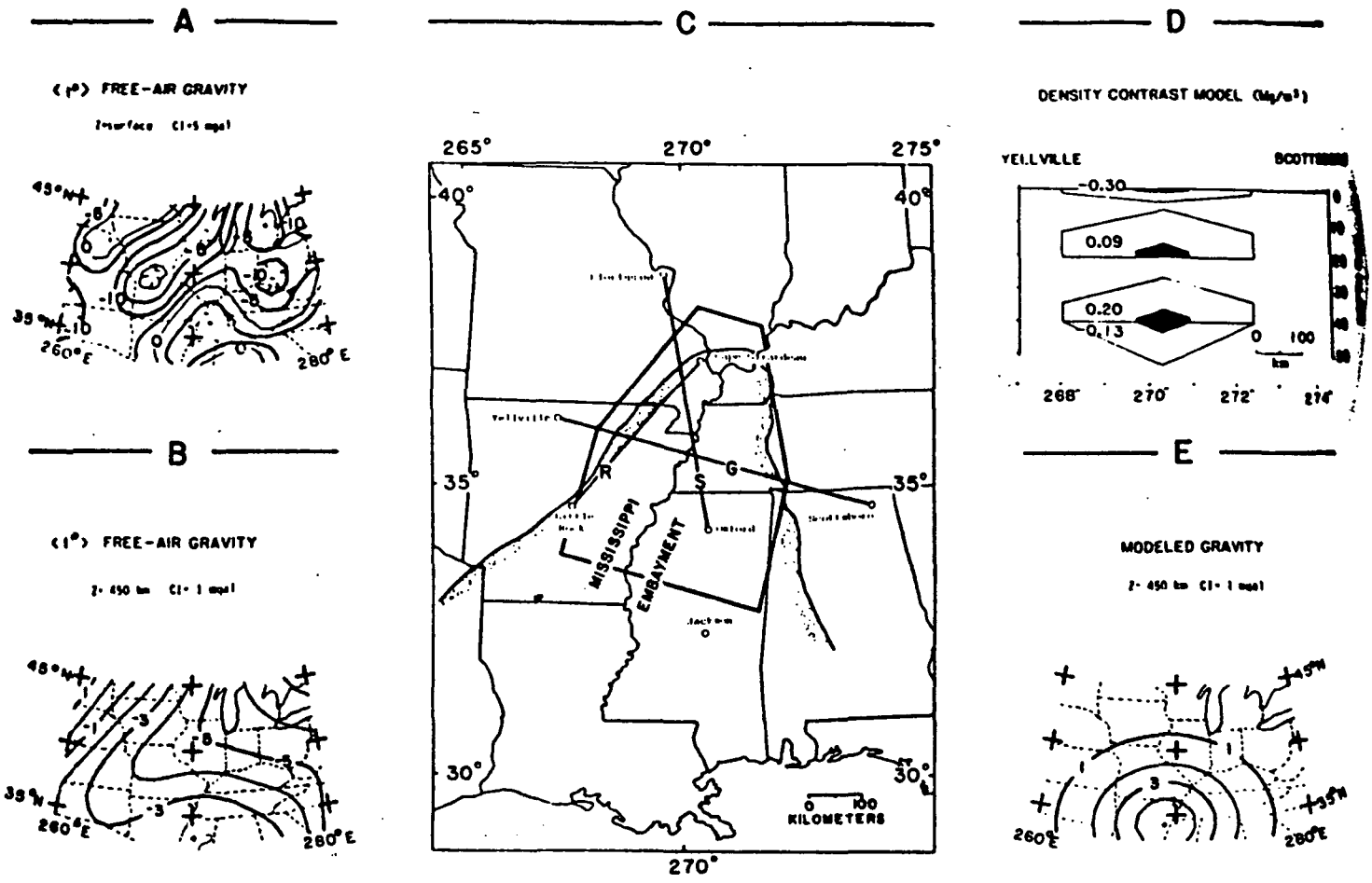

FIG. 1. Regional gravity anomalies and gravity modeling of Mississippi embayment crustal structure.

elevation by equivalent point source inversion (Figure 1b) to enhance the long-wavelength anomaly characteristics, as well as to facilitate comparison with satellite magnetic data and, hence, demonstrate the utility of satellite elevation potential field data for regional modeling applications.

A geologic density contrast model for the crustal structure of the embayment was generalized from published regional Bouguer gravity anomaly, seismic refraction, and surface wave dispersion studies. The configuration of this three-dimensional model is given in Figure 1c and the cross-section along profile G is shown in Figure 1d, where shading represents the projections of the northern ends of the model into the profile. The gravity effect of this spherical model was computed by integrating the effects of Gauss-Legendre quadrature distributed point masses within the model. The modeled positive gravity anomaly (Figure 1e) compares

favorably with the upward continued gravity data (Figure 1b) suggesting the generalized model is representative of the crustal structure of the embayment.

The regional magnetic minimum of the embayment was first observed in POGO satellite magnetometer data (Figure 2a), and subsequently confirmed by the NOO aeromagnetic survey of the conterminous U.S.A. To facilitate modeling, the data of Figure 2a were differentially reduced to the pole (Figure 2b) by equivalent point source inversion using a normalized polarizing field of 60,000 nT and high-pass filtered wavelengths smaller than about 10 degrees (Figure 2d).

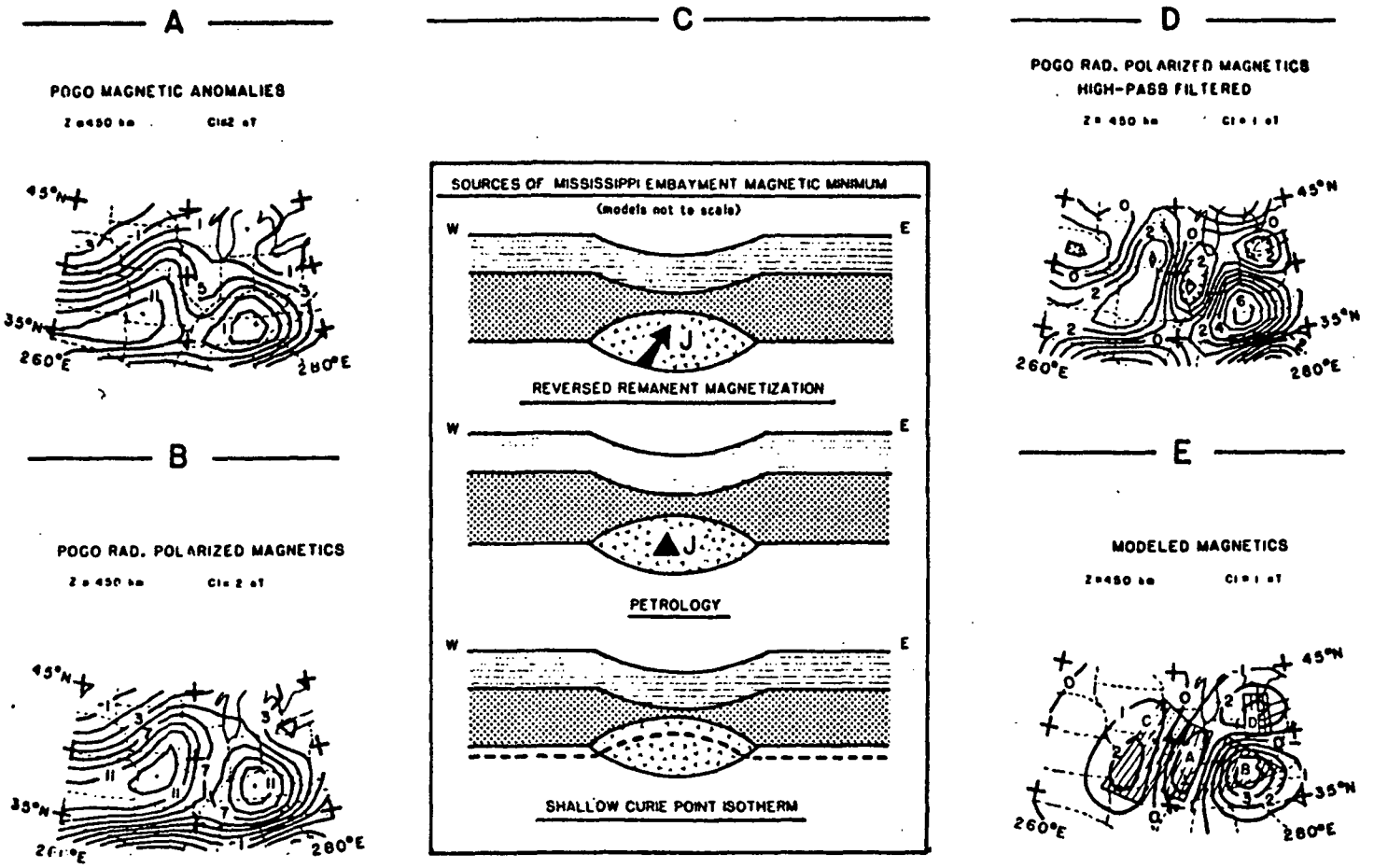

FIG. 2. Regional magnetic anomalies and magnetic modeling of Mississippi embayment crustal structure.

The filtered data (Figure 2d) roughly reveal a -3 nT anomaly for the embayment that can be modeled using results derived from gravity modeling considerations. Analysis of the inverse gravity and magnetic anomaly correlation using Poisson's theorem, and other published arguments favoring deep crustal magnetization variations as the origin of long-wavelength magnetic anomalies, focus on the body located at the base of the crust with density contrast 0.20 Mg/m^2 (Figure 1d) as a primary candidate for the source of the embayment's magnetic minimum. The correlation analysis indicates a magnetization contrast of -2.2 A/m for this body that compares favorably with typcial estimates of deep crustal magnetization. Previous studies have suggested that this body is a manifestation of a mantle upward beneath the embayment consisting of a mixture of crust and intruded upper mantle material that subsequently cooled to form a high density block.

Accordingly, a 3-D, spherical earth model was developed for the radially polarized magnetic data (Figure 2d) using Gauss-Legendre quadrature integration of simplified spherical prismatic bodies (Figure 2e). The modeled anomalies A, B, C, and D are represented by the deep crustal prisms shaded in Figure 2e which all range between depths of 25 to 40 km. The magnetic anomaly minima are approximately modeled by prisms A and D which have magnetizations of -3.9 and -2.7 A/m, respectively, whereas the positive anomalies are modeled by prisms B and C with respective magnetizations 2.7 and 1.2 A/m. These magnetic maxima also correspond inversely to regional free-air gravity minima that may be related to regions of enhanced crustal thickness.

Several origins may be postulated for satisfying the regional magnetic minimum (Figure 2c), which in general can only be discriminated on the basis of auxiliary geologic and geophysical information. These include:

(1) reversed magnetization of intrusives into the lower crust which were emplaced during the rifting process, (2) petrologic variations between the normal lower crustal rocks which are generally highly magnetic and mantle intrusives, and (3) high temperatures in the embayment that raise the Curie point isotherm from a normal position near the base of the crust to within the crust, thereby effectively removing magnetization of the lower crust beneath the position of the isotherm.

Presented at the 52nd Annual International Meeting and Exposition of the Society of Exploration Geophysicists, Dallas, TX, 1982.

REGIONAL GEOPHYSICAL ANALYSIS OF MISSISSIPPI EMBAYMENT CRUSTAL STRUCTURE

R.R.B. von Frese - Ohio State University

Information concerning the crustal structure of the Mississippi Embayment is important for deciphering the mineralization and seismicity of a highly urbanized portion of the midcontinent. Spherical earth inversion analysis of free-air gravity, U.S. Naval Oceanographic Office aeromagnetic, and satellite magnetometer data show the embayment to be characterized by regionally positive gravity and negative magnetic anomalies. Incorporating constraints developed from seismic refraction and surface-wave dispersion studies of the region with Gauss-Legendre quadrature potential field modeling suggests that the regional gravity and magnetic anomalies may be related to a rift zone along the axis of the embayment which defines a non-magnetic block of high density material within the lower crust. The decreased magnetization of this component may be due to reversed magnetic remanence, or an intra-lithologic variation, or an upwarp of the Curie isotherm.

Presented at the 112th Annual Meeting of the Society of Mining Engineers of the American Institute of Mining Engineers (SME-AIME)

DO SATELLITE MAGNETIC ANOMALY DATA ACCURATELY PORTRAY THE CRUSTAL COMPONENT?

R.R.B. von Frese - Ohio State University; and W.J. Hinze - Purdue University

Scalar aeromagnetic data obtained during the U.S. Naval Oceanographic Office (NOO)-Vector Magnetic Survey of the conterminous United States have been upward continued by equivalent point source inversion and compared with POGO satellite magnetic anomaly and preliminary scalar MAGSAT data. Initial comparisons indicate that the upward continued NOO data is dominated by long wavelength (≅ 1000–3000 km) anomalies which are not present in the satellite anomaly data. Thus, the comparison of the data sets is poor. Several possible sources for these differences are present in the data analysis chain. However, upon removal of these long wavelengths from the upward continued NOO data, a close comparison observed between the anomalies verifies that satellite magnetic anomaly data do portray the crustal component within a range of wavelengths from roughly 1000 km down to the resolution limit of the observations.

Presented at the Geomagnetic Conference, Denver, Colorado, 1982.

LONG-WAVELENGTH MAGNETIC AND GRAVITY ANOMALY CORRELATIONS OF AFRICA AND EUROPE

R.R.B. von Frese - Ohio State University; R. Olivier - University of Lausanne; and W.J. Hinze - Purdue University

Regional geopotential anomalies and their correlations provide important constraints for investigating the megatectonic framework of Africa and Europe. Accordingly, preliminary satellite (MAGSAT) scalar magnetic anomaly data are compiled for comparison with long-wavelength-pass filtered free-air gravity anomalies and regional heat-flow and tectonic data. To facilitate the correlation analysis at satellite elevations over a spherical-earth, equivalent point source inversion is used to differentially reduce the magnetic satellite anomalies to the radial pole at 350 km elevation, and to upward continue the first radial derivative of the free-air gravity anomalies. Correlation patterns between these regional geopotential anomaly fields are quantitatively established by moving-window linear regression based on Poisson's theorem. Prominent correlations include direct correspondences for the Baltic Shield, where both anomalies are negative, and the central Mediterranean and Zaire Basin where both anomalies are positive. Inverse relationships are generally common over the Precambrian Shield in northwest Africa, the Basins and Shields in southern Africa, and the Alpine Orogenic Belt. Inverse correlations also presist over the North Sea Rifts, the Benue Rift, and more generally over the East African Rifts. The results of this quantitative correlation analysis support the general inverse relationships of gravity and magnetic anomalies observed for North American continental terrane which may be broadly related to magnetic crustal thickness variations.

Presented at the XVII IUGG General Assembly, Hamburg, Germany, 1983.

GEOPHYSICAL RESEARCH LETTERS, VOL. 9, NO. 4, PAGES 293-295, APRIL 1982

VERIFICATION OF THE CRUSTAL COMPONENT IN SATELLITE MAGNETIC DATA

R.R.B. von Frese, W.J. Hinze, J.L. Sexton and L.W. Braile

Department of Geosciences, Purdue University, West Lafayette, IN 47907

Abstract. To investigate the utility of satellites for mapping crustal magnetic anomalies, POGO (Polar Orbiting Geophysical Observatory) and preliminary MAGSAT magnetometer data are compared with scalar aeromagnetic data obtained by the U.S. Naval Oceanographic Office (NOO)-Vector Magnetic Survey of the conterminous U.S.A. POGO and available MAGSAT data demonstrate remarkable consistency over the study region. The NOO aeromagnetic data are low-pass filtered for wavelengths larger than about 4° and spherically upward continued to 450 km elevation by equivalent point source inversion for direct comparison with POGO satellite magnetometer observations. The upward continued NOO data show that most of the energy is in the long wavelength (≈ 1000-3000 km) anomalies. Removal of these wavelengths by suitable filtering reveals a residual anomaly field that corresponds well with the satellite anomalies, thus demonstrating that the satellite data are useful for mapping crustal magnetic anomalies. A number of correlations between the NOO, POGO and preliminary MAGSAT data are evident at satellite elevations, including a prominent transcontinental magnetic high which extends from the Anadarko Basin of the eastern Texas panhandle to the Cincinnati Arch. The transcontinental magnetic high is breached by negative anomalies located over the Rio Grande Rift and Mississippi River Aulacogen.

Introduction

Satellite magnetometer observations permit the characterization of magnetic signatures for lithospheric regions measured in hundreds or even thousands of kilometers which are not readily obtained from conventional aeromagnetic surveys. These regions, identified and characterized on a global basis, provide useful information for deciphering earth history including paleo and contemporary geodynamics, delineation of segments of the lithosphere into resource provinces, and for numerical modeling of lithospheric processes.

Although highly precise satellite magnetic vector and scalar measurements are becoming increasingly available for lithospheric analysis, few studies have attempted to verify the satellite data directly by comparison with aeromagnetic anomalies. In general, this reflects problems related to measuring and compiling regional-scale aeromagnetic anomaly data sets, as well as difficulties in processing lithospheric potential field anomalies in the spherical domain. A notable exception is the investigation by Langel et al. [1980] in which aeromagnetic and POGO satellite magnetic anomalies over western Canada were compared at satellite elevations. The good spatial and amplitude agreement observed between the data sets provides strong evidence for the utilization of the POGO satellite magnetic anomalies in lithospheric studies.

To further investigate the use of satellites for mapping crustal magnetic anomalies, the present study compares POGO and MAGSAT magnetometer data with scalar aeromagnetic data obtained by the U.S. Naval Oceanographic Office - Vector Magnetic Survey of the conterminous U.S.A.

Data Sets and Processing

The NOO scalar aeromagnetic data, which are available from the National Geophysical and Solar-Terrestrial Data Center at 0.1 km intervals along 1° meridians, were screened for periods of intense diurnal magnetic activity and reduced to anomaly form using the IGS-75 geomagnetic field model updated to the nearest tenth of the survey year (1976.8). The resultant aeromagnetic anomaly profiles were low-pass filtered utilizing a 50% cutoff at 200 km wavelength and contoured [Sexton et al., 1982].

To facilitate inversion processing for comparison with satellite magnetometer observations, the contoured NOO data were gridded at 1° intervals, the mean value (-176 nT) removed, and then high-cut filtered for wavelengths less than about 4°. These data (Figure 1) were spherically upward continued to 450 km elevation (Figure 2) by equivalent point source inversion [von Frese et al., 1981] using the updated IGS-75 geomagnetic field model for direct comparison with POGO satellite magnetic anomalies.

POGO satellite magnetometer observations, obtained during 1968, were processed according to procedures described by Mayhew [1979] to yield the magnetic anomaly map for the study area (Figure 3) at an elevation of 450 km. Briefly, data processing consisted of removal of the POGO 13th degree geomagnetic field from the original orbital profiled data. Next, data profiles were selected in the elevation range (240-700 km) and a least

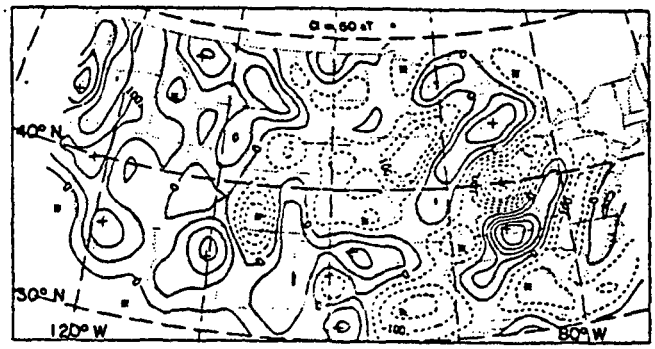

Fig. 1. Low-pass ($\lambda \geq 4°$) filtered NOO aeromagnetic anomaly data for the conterminous U.S. A mean value equal to -176 nT was removed from the data prior to filtering. Contour interval is 50 nT.

Paper number 2L0155.
0094-8276/82/002L-0155$3.00

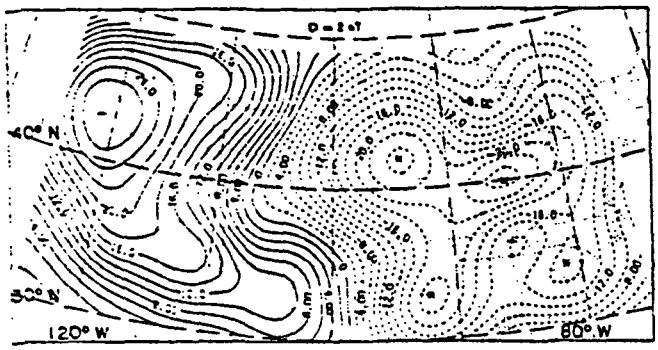

Fig. 2. NOO aeromagnetic anomaly map of the conterminous U.S. (Fig. 1) upward continued to 450 km elevation by equivalent point source inversion. Contour interval is 2 nT.

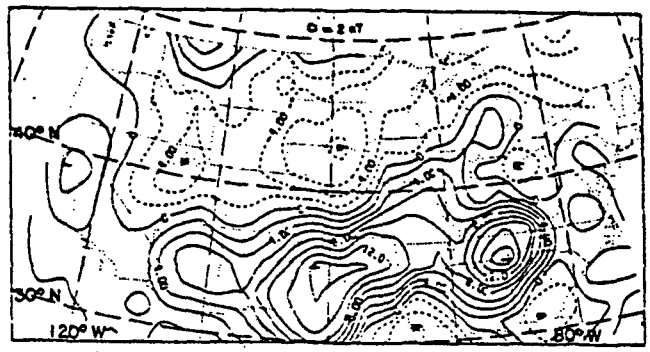

Fig. 4. 2°-averaged MAGSAT magnetic anomaly map for the conterminous U.S. at an average elevation of about 350 km. Contour interval is 2 nT.

squares quadratic function was fitted to the profiles and removed to account for Dst variation arising from ring current flow in the magnetosphere during storm time. An inversion then was performed on a spherical surface grid of prismatic dipolar moments which were oriented in the local direction of the IGRF-1965 updated to 1968. The field of these dipolar moments was recomputed at 450 km elevation in the local direction of the IGRF-1965 updated to 1968 to obtain the total magnetic intensity anomaly map for the U.S. (Figure 3).

Preliminary MAGSAT data for the study area, obtained from NASA's Goddard Space Flight Center, are presented in Figure 4. This map was prepared by averaging quiet-time MAGSAT orbital profile data over 2° x 2° areas for orbits with elevations of 400 km or less. The anomaly reduction was achieved using the preliminary geomagnetic reference field model MG680982 derived from early orbits of the MAGSAT satellite. In Figure 4, the mean number of observations per 2° x 2° area is 12 and the average elevation of the observations is 347 km.

Correlation Analysis and Results

Consideration of POGO data (Figure 3) and MAGSAT data (Figure 4) show that the satellite magnetic anomaly fields are remarkably consistent, in spite of the preliminary nature of the processing used to develop the MAGSAT magnetic anomaly map. However, correlations between the upward continued NOO magnetic anomaly (Figure 2) and satellite magnetic anomaly data are not immediately obvious.

Comparison of Figures 2 and 3 reveals a long wavelength anomaly component in the NOO data that is clearly not evident in the satellite magnetic anomaly data. This feature is characterized in Figure 2 by a long wavelength anomaly with a maximum of about 21 nT over the western third of the U.S. which decreases to a broad minimum of about -21 nT over the eastern half of the U.S. Although this long wavelength feature may be a vestige of the updated IGS-75 reference field used to derive the NOO aeromagnetic anomalies, a crustal origin for this feature cannot at present be excluded. Should the latter alternative hold, then the POGO satellite data would appear to be limited to wavelengths shorter than about 1000 km due, possibly, to errors in the updated IGRF-65 reference field and/or elimination of long wavelength crustal anomaly components by removal of quadratic functions from the orbital profile data prior to the inversion processing.

In any event, this result suggests that the longer wavelength components of Figures 2 and

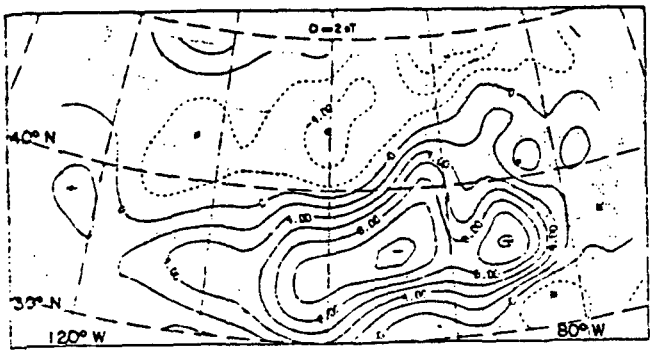

Fig. 3. POGO satellite magnetic anomaly map for the conterminous U.S. at 450 km elevation. Contour interval is 2 nT.

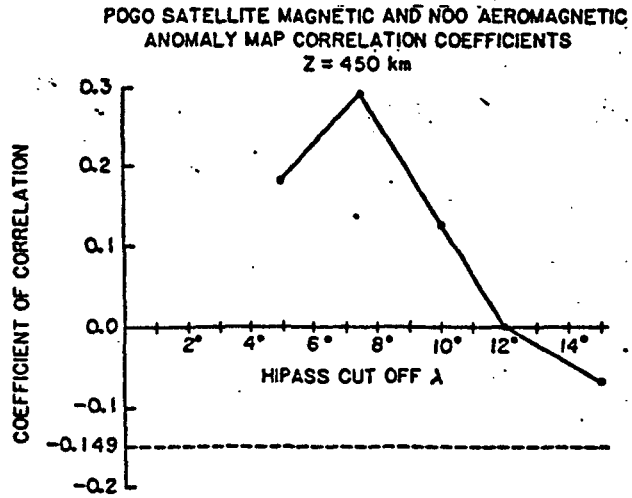

Fig. 5. Distribution of coefficients of linear correlation computed between POGO satellite magnetic and NOO aeromagnetic anomalies high-pass filtered for a number of cutoff wavelengths, λ, at 450 km elevation. The dashed line marks the value of the correlation coefficient between the unfiltered data sets (Figs. 2 and 3).

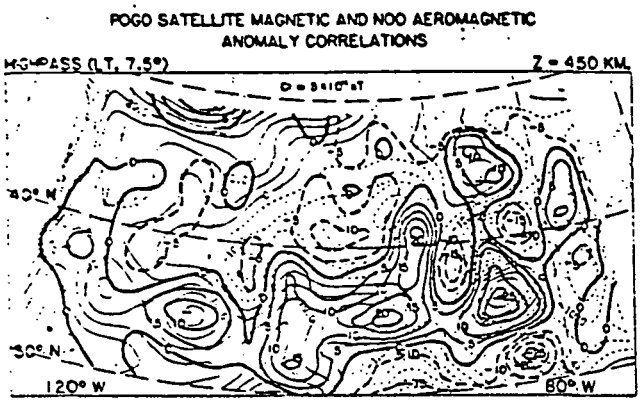

Fig. 6. POGO satellite magnetic (heavy contours) and NOO aeromagnetic (thin contours) anomaly correlations for the conterminous U.S. at 450 km elevation. Both data sets are normalized to a zero mean and high-pass ($\lambda \leq 7.5°$) filtered. Contour values for both data sets are given in multiples of 10^{-1} nT where the contour interval is 0.5 nT.

3 should be removed to facilitate the correlation analysis. Accordingly, these data sets were high-pass filtered for a number of cutoff wavelengths and the correlation coefficient was computed between the filtered maps to assess the anomaly wavelengths most consistently represented in the POGO satellite magnetic anomaly (Figure 3) and upward continued NOO aeromagnetic anomaly (Figure 2) data. The results are shown in Figure 5 where a well defined maximum correlation is observed between the data sets high-pass filtered for anomaly wavelengths smaller than about 800-1000 km ($\simeq 7.5°$). The resultant upward continued NOO and POGO satellite data sets, high-pass filtered for wavelengths smaller than about 7.5°, are plotted together in Figure 6 to facilitate the correlation analysis.

Consideration of Figure 6 shows excellent correspondence between anomalies in the high-passed POGO and upward continued NOO data. Prominent correlations include, for example, a nearly peak-for-peak correspondence related to the transcontinental magnetic high that extends from Kentucky westward to Arizona and then turns northward along California to Oregon. A well defined trend of negative magnetic anomalies are observed in both data sets along the northern margin of the transcontinental magnetic high.

Negative anomalies over the Rio Grande Rift breach the transcontinental magnetic high in both data sets. An additional breach of this anomaly is observed over the northern extension of the Mississippi River Aulacogen, although here the correspondence between the two data sets is perhaps less clear than observed for the Rio Grande Rift. This is because the NOO data in the vicinity of the Mississippi Embayment are strongly influenced by the large magnetic low over Indiana which is poorly defined due to limited NOO magnetic anomaly data in this region [Sexton et al., 1982]. Prominent anomaly maxima over the Michigan Basin centered in Michigan and the Colorado Plateau in Arizona are quite comparable in both data sets as are intense negative anomalies over southern Georgia and the Central Rocky Mountains in Colorado.

Taken together, the results of this analysis indicate that the filtered NOO and POGO data sets correlate remarkably well with respect to the spatial location, sign and general amplitude of their relative anomalies at 450 km elevation. Dissimilarities, in general, are associated with anomalies located near the boundaries of the data sets where edge effects related to the data processing are difficult to avoid.

Conclusions

Upward continued NOO aeromagnetic and POGO satellite magnetic anomaly data for the conterminous U.S. show good correlations for wavelengths shorter than about 7.5° at 450 km elevation. For longer wavelengths the correspondence between the two data sets deteriorates and becomes slightly inverse, due probably to anomaly reduction errors related to inconsistent updated geomagnetic reference field models and/or the removal of quadratic functions from the satellite data that also contain significant long wavelength crustal anomaly components. However, the good overall correspondence between the data sets for anomaly wavelengths smaller than about 800-1000 km ($\simeq 7.5°$) provides strong evidence for the utility of satellites to map crustal magnetic anomalies. Accordingly, MAGSAT data offer considerable promise for studying crustal magnetic anomalies, because of the close morphological similarity observed between POGO and available MAGSAT magnetic anomalies.

Acknowledgments. Financial support for this study was provided in part by the Goddard Space Flight Center under NASA contract NAS5-25030. The cooperation and assistance of George R. Lorentzen and Roger E. Young of the U.S. Naval Oceanographic Office are greatly appreciated.

References

Langel, R.A., R.C. Coles, and M.A. Mayhew, Comparisons of magnetic anomalies of lithospheric origin measured by satellite and airborne magnetometers over western Canada, Can. J. Earth Sci., 17, 876-887, 1980.

Mayhew, M.A., Inversion of satellite magnetic anomaly data, J. Geophys., 45, 119-128, 1979.

Sexton, J.L., W.J. Hinze, R.R.B. von Frese, and L.W. Braile, Long-wavelength aeromagnetic anomaly map of the conterminous U.S.A., Geology, (in press), 1982.

von Frese, R.R.B., W.J. Hinze, and L.W. Braile, Spherical earth gravity and magnetic anomaly analysis by equivalent point source inversion, Earth Planet. Sci. Lett., 53, 69-83, 1981.

(Received November 23, 1981;
accepted January 19, 1982.)

U.S. AEROMAGNETIC AND SATELLITE MAGNETIC ANOMALY COMPARISONS

R.R.B. von Frese - Ohio State University; W.J. Hinze - Purdue University, J.L. Sexton - ARCO; and L.W. Braile - Purdue University

To investigate the utility of satellites for mapping crustal magnetic anomalies, POGO and preliminary MAGSAT magnetometer data are compared with scalar aeromagnetic data obtained by the U.S. Naval Oceanographic Office - Vector Magnetic Survey of the conterminous U.S. The NOO aeromagnetic data, which are available at 0.1 km intervals along 1° meridians, were screened for periods of intense diurnal magnetic activity and reduced to anomaly form using the updated IGS-75 geomagnetic field model. The resultant aeromagnetic anomaly profiles were high-cut filtered utilizing a cutoff at 200 km wavelength, and contoured and gridded at 1° intervals. For comparison with satellite magnetometer observations, these data were low-pass filtered for wavelengths larger than about 4° and spherically upward continued to satellite elevations by equivalent source inversion. The upward continued NOO data show that most of the energy is in the long-wavelength (≅ 1000-3000 km) anomalies. Removal of these wavelengths by suitable filtering reveals a residual anomaly field that compares well with the morphology of the satellite measured anomalies, thus, demonstrating that the satellite data are useful for mapping crustal magnetic anomalies. A number of correlations between the NOO, POGO and preliminary MAGSAT data are evident at satellite elevations, including a prominent transcontinental magnetic high which extends from the Anadarko Basin to the Cincinnati Arch. The transcontinental magnetic high is breached by negative anomalies located over the Rio Grande Rift and Mississippi River Aulacogen. Differentially reduced-to-pole NOO and

POGO magnetic anomaly data show that the transcontinental magnetic high corresponds to a well-defined regional trend of negative free-air gravity and enhanced crustal thickness anomalies.

Presented at the 4th IAGA Scientific Assembly, Edinburgh, August 3-15, 1981

RELATION OF MAGSAT ANOMALIES TO THE MAIN TECTONIC PROVINCES OF SOUTH AMERICA

by

D.W. Yuan[1], E.G. Lidiak[1], M.B. Longacre[2], and G.R. Keller[3]

Comparison of satellite scalar magnetic anomaly data (MAGSAT) to the main tectonic provinces and boundaries of South America reveals a number of geologic correlations. South America is divisible into a broad platform of Precambrian shields and cratons separated by Phanerozoic basins, grabens and aulacogens to the east, the Phanerozoic Patagonian Platform to the south, and the Mesozoic to Cenozoic Andean Fold Belt and Caribbean Mountain System to the west and north. The continental shields are mainly more magnetic than continental basins and orogenic belts. This is particularly true of the Guyana Shield, the Central Brazilian Shield, and parts of the Atlantic Shield, all of which are coincident with magnetic highs. In contrast, the prominent Amazon Basin (aulacogen) is associated with large magnetic lows. Other basins coincide either with magnetic lows or magnetic gradients. Cratons, mainly covered by younger sedimentary rocks, are generally associated with magnetic gradients. Most of the anomalies associated with the Patagonian Platform are positive and have higher amplitudes eastward away from the Andean Fold Belt. The northern Andes are coincident with positive magnetic anomalies, whereas the central and southern Andes are associated mainly with negative anomalies. The trend of the Andean anomalies generally does not follow the trend of the fold belt, but instead has a general east-west trend which is probably related to noise derived from data processing. The anomalies of western South America along the margin of the South American Plate appear to be distinct from those of the adjacent ocean basin. In contrast, eastern South America is characterized by magnetic anomalies which commonly extend into the Atlantic Ocean.

DETAILED DISCUSSION

More detailed assessment of the relation of the magnetic anomalies (Fig. 1) to the main tectonic provinces of South America (Fig. 2) can be made by consideration of the individual provinces and subprovinces. Three extensive provinces can be recognized based on origin, age, and structural development:

South American Platform (Region A, Fig. 2)

Shields and Cratons

This is the oldest province and includes most of eastern South America. The basement of this old platform consolidated between the end of the Precambrian and the Cambrian and contains the only known Archean rocks of the continent. Although partly covered by Phanerozoic rocks, the basement of the South American Platform is well exposed in three major shields and forms the basement of three major cratons:

1. Guyana Shield (A1a, Fig. 2) This entire region is underlain by Precambrian rocks. A magnetic high overlies this region, and the general east-northeast trend of the anomalies coincides with Precambrian structural trends.

2. Central-Brazilian Shield (A1b, Fig. 2) This old cratonic region consolidated prior to 1,800 m.y., and was partially remobilized in the Trans Amazonian orogenic cycle (1,800-2,200 m.y.). Magnetic anomalies are very high in most areas, especially in the eastern region.

3. Atlantic Shield (A4, Fig. 2) This shield lies along the coastal margin of Brazil and Uruguay. A large magnetic anomaly high occurs in the area of the Caririan-Propria Fold Belt (A4a) and is apparently associated with metamorphic and volcanic intrusive rocks of that old belt. The positive anomaly appears to extend eastward into the ocean basin. The Riberira Fold Belt to the south (A4b) is associated with a magnetic low having an east-west trend along the northern part of the belt and with a magnetic high having a north-south trend in the southern part of the belt.

4. Sao Luiz Craton (A5, Fig. 2) The Sao Luiz Craton is a narrow feature along the northeast Atlantic coast. As the main part of the craton is covered by Paleozoic or younger sedimentary rocks, the older crystalline rocks are very poorly known. The magnetic anomaly pattern shows a broad gradient over this area which decreases from south to north. This gradient continues northeastward into the adjacent Atlantic Ocean Basin.

5. Sao Francisco Craton (A2, Fig. 2) The Sao Francisco Craton acted as the foreland to the Brazilian Fold Belt which developed along its borders. The basement of the craton is made up of Lower Precambrian sialic rocks which are partially covered by Mesozoic sedimentary rocks and Cenozoic volcanics. A large magnetic anomaly low occurs along the southern border of the craton and a positive magnetic anomaly occurs at the northern part of the craton. The magnetic low appears to be part of a larger anomaly that extends eastward into the adjacent ocean basin.

6. Rio de La Plata Craton (A6, Fig. 2) This craton is mostly covered by Phanerozoic sediments. The basement of this ancient area consolidated in the Upper Precambrian and probably represents the southernmost extent of Precambrian rocks in the Atlantic coastal region of South America. The craton lies along a strong magnetic gradient between negative magnetic anomalies in the continental areas of eastern Argentina and positive anomalies in coastal Uruguay and southern Brazil. These positive anomalies are part of a larger series of north-to-northeast-trending magnetic highs that occur along the southeastern continental shelf of South America and extend into the Atlantic Ocean Basin.

Basins

The Guyana, Central Brazilian, and Atlantic Shields are separated from one another by large basins which probably are underlain in part by major synclines or grabens. The sedimentary and associated volcanic rocks which occur in these basins are of Silurian or younger age.

1. Amazon Basin (A1c, Fig. 2) The Amazon Basin is the most prominent and the largest basin in South America. It is widely regarded as being an intercratonic basin, and has been variously interpreted as an autogeosyncline, an extensive and complex graben system, a rift basin, and most recently as an aulacogen. The basin contains a thick sequence of Paleozoic, Mesozoic, and Cenozoic sediments and lesser basaltic volcanic rocks. Prominent magnetic lows occur in most of the basin, especially in the eastern part and to the west in the area of the Upper Amazon.

2. Parnaiba Basin (A3, Fig. 2) The Parnaiba Basin is also an intercratonic basin and contains Paleozoic and Mesozoic sedimentary and volcanic rocks. It is separated from the small coastal basins on the north by the Ferrer Arch and from the old craton by younger Precambrian metamorphic and sedimentary rocks. The magnetic signature in this basin is not definitive and appears to occur along an irregular gradient that increases from north to south.

3. Parana Basin (A6b, Fig. 2) Cretaceous basalt (Parana Basalt), covering an area of 1,200,000 km^2, and associated sediments of mainly Mesozoic age fill most of the Parana Basin. Much of the basin is underlain by a magnetic low and a magnetic gradient which is high in the southeast and low in the northwest.

4. Chaco Basin (A6a, Fig. 2) Cenozoic sedimentary and minor volcanic rocks cover most of the Chaco Basin. The magnetic anomaly values are negative in the most of the area, but most anomalies are broad and the negative values are small.

Patagonian Platform (Region B, Fig. 2)

The Patagonian Platform occupies the broad southeast continental margin of South America. It is a young platform with a basement that stabilized from the Middle Paleozoic onwards, developing a volcano-sedimentary cover after the Carboniferous; this cover almost completely masks the platform basement.

The magnetic anomaly pattern in this platform is elongate in shape with a north-south trend that essentially parallels the coast line. The anomalies are positive in most areas and become higher from west to east away from the Andean Fold Belt. A northwest-trending arm of the positive anomalies extends into the Andean Fold Belt.

Andean Fold Belt and Caribbean Mountain System (Region C and C1, Fig. 2)

The Andean Fold Belt, which forms the western margin of South America is part of the Circum-Pacific Mountain System of great seismic and volcanic activity. The enormous quantity and size of the intrusive bodies (Andean batholithic rocks) have contributed to the Andes being referred to as a "magmatic mountain range". The Andes are widely regarded as a classic example of a mountain system formed at a convergent plate margin.

A large magnetic anomaly high occurs along the Cordillera of Colombia, and positive anomalies occupy most areas of the northern part of the Andes (north of lat 16°S). In contrast, a large magnetic anomaly low occurs in the central part of the Andes, and negative anomalies occupy most regions of the central and southern Andes. The trend of these anomalies does not, in general, parallel the north-south structural trend of the fold belt, but in-

stead has a general east-west pattern. This pattern which is common over most of the MAGSAT map is probably related to processing noise derived from data reduction procedures to correct for external magnetic field effects. However, the pattern over the Andes is sufficiently distinct from the generally north-trending magnetic anomalies occurring in the adjacent Pacific Ocean to reflect the boundary between the leading edge of the South America Plate and the oceanic Nazca Plate.

The Caribbean Mountain System, which extends along the northern boundary of the South American Platform, is part of an island arc complex of the eastern Caribbean. The basement of this region consists of Paleozoic rocks with metamorphosed igneous complexes. Sedimentary rocks of Lower Cretaceous or possibly Upper Jurassic age overlie these older rocks. Negative magnetic anomalies appear throughout the system, and they are clearly different from the positive anomaly pattern that occurs along the northern Andes and the Guyana Shield.

---

1. Department of Geology and Planetary Science, University of Pittsburgh, Pittsburgh, PA 15260
2. Department of Geosciences, Purdue University, West Lafayette, IN 47907
3. Department of Geological Sciences, University of Texas at El Paso, El Paso, TX 79968

Presented at the 52nd Annual International Meeting and Exposition of the Society of Exploration Geophysicists, Dallas, TX, 1982

Figure 1. Equivalent point source field approximation of 2^{o}-averaged scalar MAGSAT magnetic anomaly data differentially reduced to radial polarization at 350 km elevation. The normalized amplitude for the polarizing induction field is 60,000 nT. Contour interval is 2 nT.

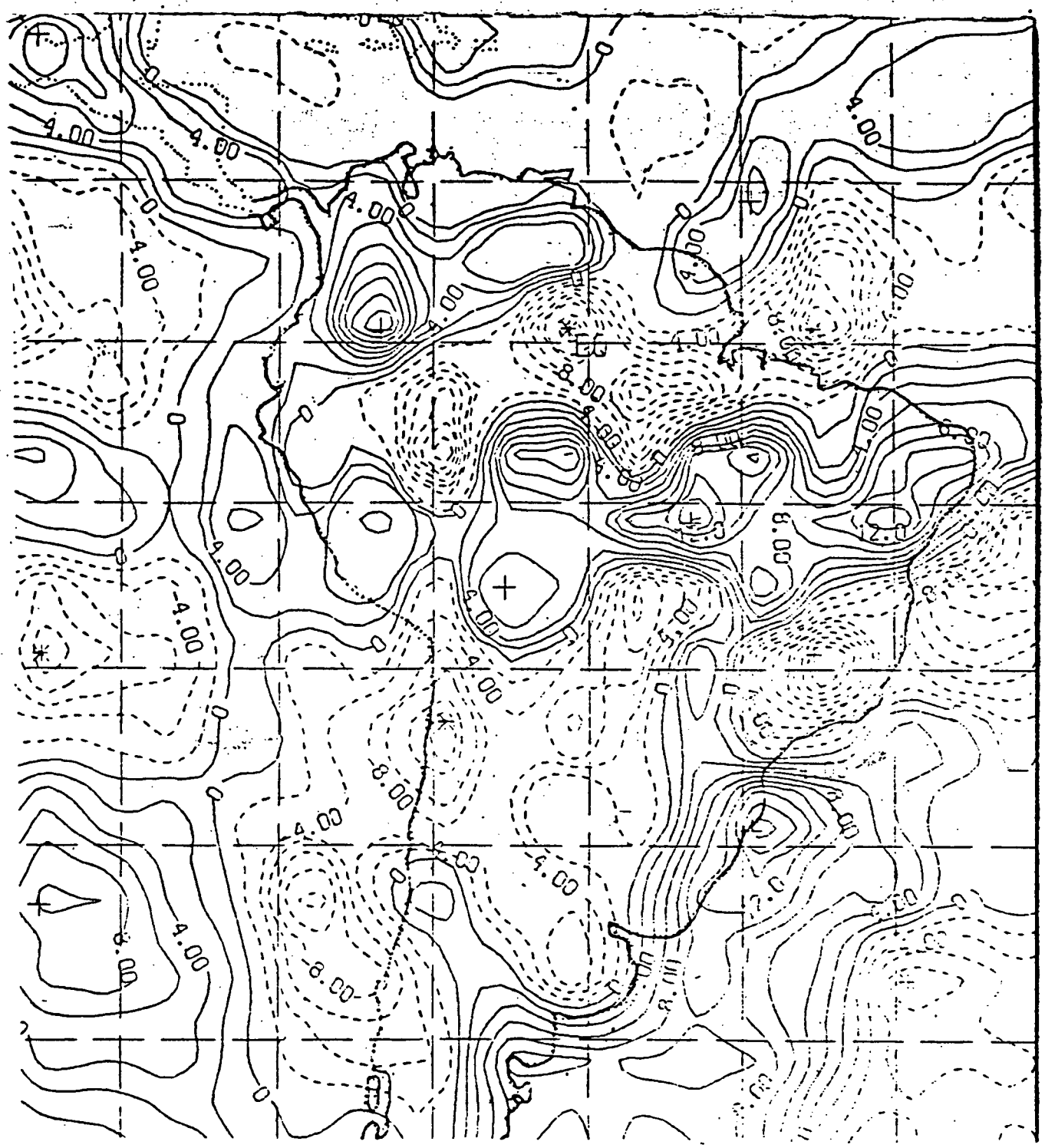

. Figure 2. Tectonic Provinces of South America

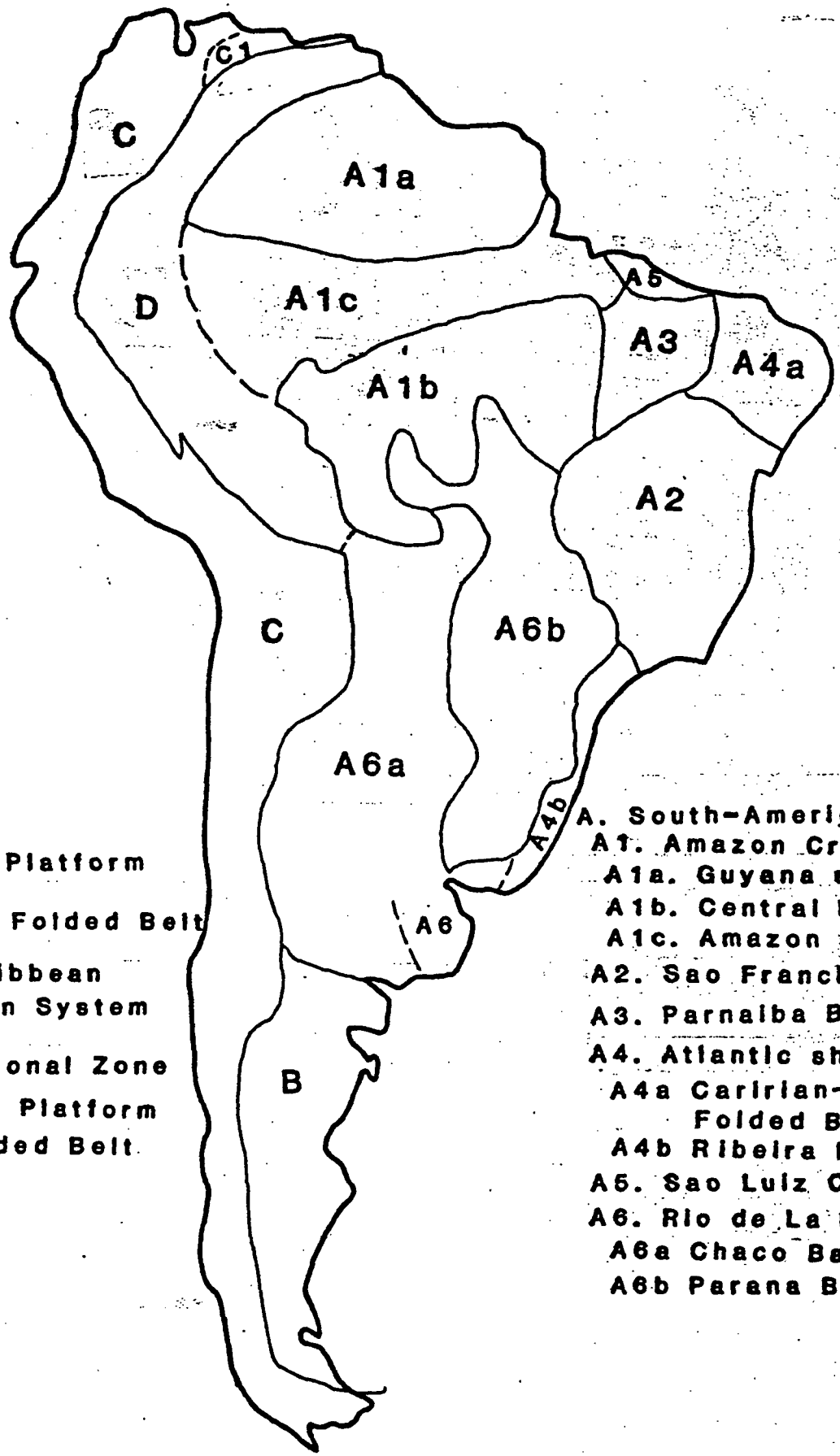

Patagonian Platform

The Andean Folded Belt

C1 The Caribbean Mountain System

The Transitional Zone between the Platform and the Folded Belt

A. South-American Platform
A1. Amazon Craton
A1a. Guyana shield
A1b. Central Brazil shield
A1c. Amazon Basin
A2. Sao Francisco Craton
A3. Parnaiba Basin
A4. Atlantic shield
A4a Caririan-Propria Folded Belt
A4b Ribeira Folded Belt
A5. Sao Luiz Craton
A6. Rio de La Plata Craton
A6a Chaco Basin
A6b Parana Basin

In addition to the preceeding Summary, the University of Texas at El Paso - University of Pittsburg portion of the study concentrated on tectonic and crustal structure studies and resulted in two theses which are included as appendices.

Yuan, Ding-Wen, 1983, Relation of MAGSAT and gravity anomalies to the main tectonic provinces of South America: M.S. Thesis, University of Pittsburgh, 168 p.

Renbarger, K. S., 1984, A crustal structure study of South America: M.S. Thesis, University of Texas at El Paso, 243 p.

APPENDIX A

Relation of Magsat and Gravity Anomalies to the Main Tectonic Provinces of South America

RELATION OF MAGSAT AND GRAVITY ANOMALIES TO THE MAIN TECTONIC PROVINCES OF SOUTH AMERICA

By
Ding-Wen Yuan
B.S., National Taiwan University, 1978

Submitted to the Graduate Faculty of
Art and Sciences in partial fulfillment
of the requirement for the degree of
Master of Science

University of Pittsburgh

1983

ABSTRACT

Comparison of satellite scalar magnetic anomaly data (MAGSAT) to the main tectonic provinces of South America reveals a number of geologic correlations. The magnetic anomalies of the South American continent are generally more positive and variable than the oceanic anomalies. Furthermore, there is better correlation between the magnetic anomalies and the major tectonic elements of the continents than between the anomalies and the main tectonic elements of the adjacent oceanic areas. The oceanic areas generally show no direct correlation to the magnetic anomalies.

The Precambrian continental shields are mainly more magnetic than continental basins and orogenic belts. The shields differ markedly from major aulacogens which are generally charactarized by negative magnetic anomalies and positive gravity anomalies. The Andean orogenic belt shows rather poor correlation with the magnetic anomalies. The magnetic data exhibit instead prominent east-west trends, which although consistent with some tectonic features, may be related to processing noise derived from data reduction procedures to correct for external magnetic field effects. However, the pattern over the Andes is sufficiently distinct from the generally north-trending magnetic anomalies occurring in the adjacent Pacific Ocean to separate effectively the leading edge of the South American Plate from the Nazca Plate. In contrast, eastern South America is characterized by magnetic anomalies which commonly extend across the continental margin into the Atlantic Ocean.

ACKNOWLEDGEMENT

I wish to express my sincere appreciation to my major advisor, Dr. Edward G. Lidiak, for his suggestion of this problem and his constant guidance during all course of this research.

I also wish to express my gratitude to the members of my committee - Dr. Tom Anderson and Dr. Victor A. Schmidt, for their review of the text and constructive criticism.

Many thanks are also due to all teachers from whom I have learned various aspects of earth sciences.

Lately I like to express my deep thanks to my wife, Yi-Ping, for her understanding and patience during the course of this work and typing the final copy.

Financial support for this research was provided by Goddard Space Flight Center under NASA contract NAS5-26326 and is gratefully acknowledged.

TABLE OF CONTENTS

LIST OF FIGURES

LIST OF TABLES

CHAPTER 1

INTRODUCTION

The continent of South America is characterized by a variety of diverse and significant geological features, which includes (1) complex mineral-rich Precambrian shields, (2) contemporary seismicity and volcanism, (3) Precambrian and Phanerozoic orogenic belts, and tectonically active areas, (4) well-delineated Phanerozoic metallogenic zone, (5) subduction zones, (6) hot spots, and (7) grabens and aulacogens. These features, some of which are among the best developed on earth, have in general not been studied in detail.

The purpose of this investigation is to summarize and interpret the previously published geological and geophysical data on South America and to characterize its main tectonic elements. These elements will then be correlated with satellite scalar magnetic (MAGSAT) data and Bouguer and Free-Air gravity anomaly data for the purpose of gaining new insight on the major tectonic features of South America.

The satellite scalar magnetic data used in this investigation are compiled from project MAGSAT; a National Aeronautics and Space Administration-Goddard Space Flight Center (NASA-GSFC) and a U.S. Geological Survey (USGS) magnetic satellite program. MAGSAT measured the near-earth geomagnetic field from October 1979 to June 1980 in a nearly polar orbit at an average elevation of approximately 400 km. A preliminary global data set prepared by NASA-GAFC is based upon an average of 12 data points per 2^{o} area with a range of 3 to 32 points at an average elevation of approximately 350 km. In order to eliminate the problems caused by strong spatial

gradients and low inclinations of the field, the preliminary data set was reduced to the radial polarization by Longacre (1981). The radially polarized map (Fig. 9) was then produced by computing the anomaly field from the equivalent dipoles on a spherical earth assuming radial polarization in a total intensity field of 60,000 nT (Longacre, 1981).

Both the Bouguer and Free-Air gravity anomaly data of the South American continent were provided by the Defense Mapping Agency Aerospace Center (DMAAC) and both of the maps (Fig. 10 and 11) have a contour interval of 10 and 50 mgals. Predicted values (Woollard, 1969) were used in preparing the DMAAC map because many areas of South America, particularly the jungle and mountainous areas, have no gravity control.

It is very difficult to filter auroral external fields from the MAGSAT data and to isolate the crustal magnetic anomaly field because both field-aligned currents at high latitudes and magnetospheric ring-currents in equatorial regions contaminate the MAGSAT data (Ritzwoller and Bentley, 1982). In addition, because of the preliminary nature of the data and the numerous lithologic variations within provinces, correlation between geological characteristics and geophysical characteristics and geophysical data can only be generalized.

CHAPTER 2

GENERAL OUTLINE OF THE GEOTECTONICS OF SOUTH AMERICA

Based on different origins, ages and structural development, three extensive tectonic provinces can be recognized in South America (Fig. 1). The South American Platform (region A, Fig. 1) is the oldest and includes the entire eastern part of South America, between the Orinoco River, in Venezuela, and Baia Blanca, in Argentina. It entirely encompasses the territories of Brazil, Paraguay, Uruguay, Guyana, French Guyana, Surinam, as well as the center and south of Venezuela, and the eastern part of Colombia, Ecuador, Peru and Bolivia, together with the north of Argentina. The basement of this old platform consolidated between the end of the Precambrian and the Cambrian, and contains the only known Archean rocks of the continent. The boundary between the western limit of the platform and the Andean orogenic belt is covered by extensive Cenozoic sediments. The South American Platform is bounded on the south by the Patagonian Platform, in Argentina, and the boundary probably corresponds with the valley of the Rio Colorado.

The Patagonian Platform (region B, fig. 1) encompasses the remaining southeastern part of the continent and is located entirely in Argentinian territory; it also extends over the broad southeast continental margin. It is a young platform, the basement of which stabilized from the Middle Paleozoic onwards, developing a volcano-sedimentary cover after the Carboniferous; this cover almost completely masks the basement of the platform.

The Andean Fold Belt (region C, fig. 1), which lies along the western margin of these two platforms (South American and Patagonian Platforms), is part of the Circum-Pacific mountain system. The enormous quantity and size of the intrusive bodies (Andean batholith or Andean plutonic rock) has contributed to the Andes being referred to as a "magmatic mountain range", and this magmatic activity is an integral part of the Andean subduction zone model. The relation between the magmatic and structural development are discussed in more detail in a later section.

The Caribbean Mountain System (region C1, fig. 1), which extends along the northern boundary of the South American Platform, is part of an island arc of the eastern Caribbean. The basement of this region contains Paleozoic rocks. Sedimentation started in the lower Cretaceous, or possibly in the upper Jurassic.

The South American Platform is limited to the north by the Caribbean Mountain System and to the west by the Central and Northern Andes. These boundaries are not as yet precisely defined. The great sub-Andean foredeep (region D, fig. 1) between Ecuador and the north of Argentina, constitutes a transitional zone between the platform and the fold belt.

2.1. The South American Platform

Although partly covered by Phanerozoic sedimentary formations, the basement of the South American Platform is exposed in three major shields and in smaller massifs isolated by Phanerozoic cover. The Guyana Shield (region A1a, fig. 2) includes the entire region of Precambrian rocks lying north of the Amazon River. The Central-Brazilian Shield (region A1b, fig. 2) lies in the interior of Brazil, south of the Amazon River, and continues into eastern Bolivia. The Atlantic Shield (A4, fig. 2) lies along the coastal margin in Brazil and Uruguay. These three shields are separated from each other by large synclines (or grabens). The sedimentary rocks and associated volcanics that fill the depressions accumulated from Silurian onwards, and are particularly

extensive in the following four great synclines (or grabens): Amazon (A1c, fig. 2), Parnaiba,(A3, fig. 2), Parana (A6b, fig. 2), and Chaco (A6a, fig.2).

According to radiometric data two principal age intervals can be recognized (Almeida, 1970). The older ages are between 1800 and 2200 m.y. (Early Proterozoic), and the younger between 450 and 700 m.y. (Late Proterozoic to Early Paleozoic). These ages are thought to represent events related, respectively, to the Trans-Amazonian and Brazilian orogenic cycles, which are the most important for the Precambrian of South America. Rocks 2700 m.y. or older occur sporadically as highly deformed granulitic gneisses and probably represent the Archean sialic basement on which the rocks of the two main younger cycles developed. Events of intermediate age, 900-1300 m.y. (Middle Proterozoic), can also be recognized in restricted areas, and may be related to the Minas Orogeny, which is well defined in the region of the "Quadrilatero Ferrifero" (Minas Gerais). Table 1 gives the summary of the main Precambrian orogenic cycles, and the principal geotectonic units which are associated with them in the South American Platform (see fig. 3 also).

Four old cratonic regions are defined for South America: (1) Amazon Craton (A1, fig. 2), which includes the Guyana Shield, the Guapore Craton (the Central-Brazilian Shield) and the Apa and Missiones massifs; (2) the Sao Luiz cratonic area (A5,fig. 2), a narrow feature near the northern coast between Belem and Sao Luiz; (3) the Sao Francisco Craton (A2, fig. 2), located southeast of the Parnaiba basin, and reaching the Atlantic coast in the state of Bahia; and (4) the Rio de La Plata Craton (A6, fig. 2), a possible extension of the Amazon Craton, which includes the southeast of Uruguay and the province of Buenos Aires. Fig. 2 shows the approximate boundaries of these geotectonic units.

The idea that the Guyana and Guapore (Central-Brazil) cratonic areas have been a single stable unit during late Precambrian time cannot be definitely proven, as the

basement of the Amazon basin is very poorly known. However, the few radiometric ages thus far obtained in this area, support this thesis (Amaral, 1970). Consolidation of the Amazon craton post-data the 2000-m.y.-old Trans-Amazonian cycle. The Amazon Craton underwent a period of tectonic instability and abundant magmatic activity about 1800 to 1000 m.y. ago. This was followed by a much quieter period which continued until the Phanerozoic, during which time the craton was separated into two shields (Guyana and Guapore Craton) by the development of the Amazon Syncline. The western limits of the craton are hidden and probably do not coincide with those of the South American Platform; the eastern limit constitutes one of the major structural lines of the continent. This eastern boundary is delineated by a series major structures such as deep faults associated with basic and ultrabasic igneous rocks and marginal sedimentary basins. Furthermore, the boundary corresponds to a major fold belt at the end of the Precambrian.

The best-known structures of the Trans-Amazonian Cycle in South America occur along the northern edge of the Guyana Shield between the central and southern regions of Venezuela and Amapa in Brazil. Their rocks vary in lithology and in degree of metamorphism from greenschist to amphibolite facies and include many volcanic rocks and granites formed during and since the main period of tectonism.

The Guapore (Central Brazilian) and Sao Francisco Cratons (A1b, A2, fig. 2) are separated by a large region affected by a major tectonic and magmatic event, the 450-700 m.y. Brazilian orogenic cycle. Numerous basic and ultra-basic intrusions of alpine character are also present, and some of these rocks were dated with results close to 1000 m.y. (Hasui and Almeida, 1970). The Brazilian orogeny also affected the western and southeastern margins of the Sao Francisco Craton (fig. 2 and 3) where reactivation of the craton and development of younger folds occurred. Along the southeastern border of the craton, northwest of the Riberian Fold Belt (fig. 2), an older metamorphic belt of 1100-1400 m.y. age occurs. These ages may be related to the orogeny of the Minas Group near Belo Horizonte.

The Sao Luiz Craton (A5,fig. 2) is very poorly known as the main part is covered by Paleozoic or younger sedimentary rocks. This area is usually considered as a single unit. The Ferrer arch separates the craton from the adjacent Parnaiba Basin. The Sao Luiz Craton extends eastward to the mouth of the Parnaiba River, where structures related to the Brazilian orogenic cycle occur.

The Rio de La Plata Craton is mainly covered by Phanerozoic sediments, which make it difficult to establish its limit and its relation to the Guapore Craton to the northwest. This ancient cratonic area consolidated in the late Precambrian. The basement, where exposed, consists of a gneissic complex, associated with amphibolites, mica schists, phyllites, and quartzites. They probably represent the southern-most occurrence of Precambrian rocks in the Atlantic coastal region as the basement rocks of northern Patagonia previously considered to be Precambrian are mainly Paleozoic accordingly to recent geochronologic studies (Stipanicic et al., 1968; Halpern, 1968). This indicates that the South American Platform does not continue beyond the Colorado River in Argentina.

In summary, most of the South American Platform was consolidated about 1800 m.y. ago, after the Trans-Amazonian orogenic cycle. Ages of 2700 m.y. or older are encountered in granite-gneiss complexes and in migmatites, which are commonly metamorphosed to the granulite facies. Mafic and ultra-mafic intrusions occur sporadically in the rocks. Widespread regions of the South American Platform were re-worked during Late Proterozoic time, less than 1000 m.y. ago, and show a complicated structure. Rocks affected by events of the Minas and Uruacuano cycles, between 900 and 1300 m.y. are restricted in area, but are locally of importance. Systems of folding which were developed in sediments deposited during the Brazilian Cycle (450-700 m.y.) are observed together with more-or-less extensively re-worked pre-Brazilian basement, and some median massifs which are also generally affected by this cycle. Older structures in this basement are well represented in the interior of the state of Goias as

well as in the north-east and south-east of Brazil. Finally, areas remobilized or rejuvenated during the events of the Brazilian orogenic cycle are widespread and cover nearly 40% of the shields, especially in eastern Brazil where they may be confused with older formations, or with Brazilian formations that have been more intensively modified by metamorphism and magmatization.

2.2. Patagonian Platform

The Patagonian Platform is contiguous with the South American Platform, but the limits are hidden by Cenozoic cover. The western boundary is poorly-defined but appears to be transitional with the Andean chain (fig. 1).

The Patagonian Platform is a young platform with a basement that stabilized from the Middle Paleozoic onwards, developing a volcano-sedimentary cover after the Carboniferous; this cover almost completely masks the platform basement. Minor outcrops of the basement occur mainly in the Somun Cura Massif in the north of the platform. Rocks with low to medium degrees of metamorphism and granitoid igneous rocks have been noted in this basement. Elsewhere, in the Malvinas Islands, the basement crops out locally, at Cape Meredith,as metamorphic and eruptive rocks of the Late Proterozoic.

Rocks of Carboniferous to Triassic age are poorly exposed on the Patagonian Platform. However, granitoid intrusive rocks of Carboniferous and Permian age are exposed. These intrusive rocks represent an important period in the evolution of the platform as they may comprise a major part of the basement.

From the Sinemurian (Lower Jurassic) to the Bajocian (Middle Jurassic), marine transgressions flooded the larger part of the Patagonian Platform. Withdrawal of the sea was followed by intense acid volcanism during the Bathonian (Middle Jurassic, above the Bajocian) which is well represented throughout the platform south of latitude 40°S

(Tectonic map of South America, 1978). Important tectonic movements during the Upper Jurassic correspond to the movements (araucanan Phase) of the Andean region. The formation of the dense network of large faults led to the creation of many basins, which are nearly contemporaneous with those along the margins of the South American Platform (Tectonic map of South America, 1978). These basins underwent maximum subsidence during the Cretaceous (fig. 4).

Two main evolutionary stages of geologic development in the Patagonian Platform can be recognized (Harrington, 1970; Zambrano and Urien, 1970):

Stage (1) Pre-Upper Jurassic evolution--this stage refers to the evolution of the basement. Harrington (1970) indicates that a strong Paleozoic deformation (the Southern Hills "aulacogen") with a NW-SE-trending fold belt can be recognized in the hills to the north of Buenos Aires. Elsewhere the pre-Cretaceous trends are predominantly E-W with local deflections. The true Precambrian basement has been found as far south as the Northern Hills of Buenos Aires (lat. 38° S in fig. 5). In other words, no early or middle Precambrian metamorphics have been found in the Patagonian Platform. The schists and phyllites exposed in the Rio Negro and Chubut provinces (San Jorge basin) (fig. 4 and 5) are now considered to be late Precambrian or early Paleozoic in age. The folded low-grade metamorphics cropping out in southern and western Santa Cruz are probably middle Paleozoic, and there is a tendency to ascribe them to the Devonian. The gentle folding and the subhorizontal position of the rock units observed in the basement throughout the Patagonian Platform indicate a predominantly cratonic or neocratonic type of structural deformation, up to Late Jurassic or Early Cretaceous times. An extensive cover of silicic and mesosilicic extrusives spread over northern Patagonia during Triassic times, and over central and southern Patagonia in Jurassic times, and has to a great extent obscured this pre-Mesozoic tectonic feature.

Stage (2) Post-Early Cretaceous evolution- This stage is closely related to the

creation of the basins. The post-Cretaceous tectonic pattern of the Salado, Colorado, Valdes and San Jorge basins (fig. 4) is very similar. Several tectonic episodes are recorded in rocks of the basins (Lesta, 1968). These episodes, which correlate with the Andean movements are mainly due to vertical movements of a predominantly negative type (subsidence). The basins were formed as a result of normal faulting, generally along ESE-WNW or ENE-WSW directions. The inception of faulting probably occurred between middle and younger Jurassic time. The faults were intermittently reactivated throughout Cretaceous time. Basins created by this tectonic reactivation underwent maximum subsidence during the Cretaceous, and are nearly contemporaneous with those of the South American Platform. From Upper-most Cretaceous (Maestrichtian) times onwards, only a few faults have fractured the Tertiary cover. However, subsidence continued during Cenozoic time.

A different tectonic style characterizes the Magallanes and Malvinas basins (fig. 4 and 5). The eastern part of the former and the northern part of the latter show a fault pattern similar to the one described above. However, the western part of the Magallanes basin and the southern part of the Malvinas make up a folded orogenic belt that is a true geosyncline. These regions contain a great thickness of sediments along a belt parallel to the Andean axis, along with ophiolites, and metamorphosed Cretaceous units. A thrust fault parallel to the eastern margin of the Andes in southern Patagonia, which is deflected towards the east in Tierra del Fuego and probably continuing along the Burdwood bank, and the Scotia Arc, is the southern and western boundary of both these basins (Urien and Zambrano, 1973) (fig. 5).

Thus, in summary, three broad areas can be distinguished in the Patagonian Platform:

(1) The eastern part: mostly submerged under the continental shelf. Basins created by the post-Early Cretaceous tectono-magmatic evolution are mainly due to

fracturing. The tectonic features of the Atlantic basins are controlled by vertical movements of the basement blocks along normal faults; major transcurrent faults may also occur here, with a predominant E-W trend, which represent the interaction between a metamorphic and/or igneous basement and oceanic crust.

(2) The central area: including southern part of the Pampean Ranges Massif together with eastern and central Patagonia, with a basement block pattern and E-W, ESE-WNW, or ENE-WSW tensional faults. Towards the west the basement blocks tend to crop out and the fault pattern becomes predominantly N-S; these faults are of compressional type with E-W-trending tensional faults.

(3) The pre-Andean area: the basement blocks become elongate. The basins within the continent become longer and narrower and the axes tend to follow a N-S direction (Nirihuau, the western part of the Magallanes basin fig. 5). The Cretaceous-Cenozoic cover is gently folded along an axis running parallel to the basement blocks. The basins closer to the Andes proper are bounded to the west by thrust fault with a N-S direction.

2.3. Andes Cordillera and the Caribbean Mountain System

2.3.1. The Andes

The Andes, (region c, fig. 1), which form the Pacific boundary of South America, extend for about 7500 km and represent the backbone of the continent. As part of the Circum pacific mountain system, the Andes are a region of great seismic and volcanic activity. From the Mesozoic to the present, most sections of Andes are either characterized by violent volcanism or by widespread plutonism.

Examination of a general geological map of the Andes immediately gives an impression of the enormous quantity and size of the intrusive bodies. Andean plutonic

rocks extend over a distance or more than 4000 km from southern Chile to northern Peru, and have contributed to the Andes being referred to as a magmatic mountain range.

The Andes are situated on the boundary between large and small lithospheric plates. According to the plate tectonic model. orogeny should form at those regions where oceanic crust is subducted beneath continental margins. The Andes are regarded as a typical example of this type of continental/oceanic interface. Cenozoic volcanism is thus probably associated with the subduction of lithosphere plates. It is also possible that frictional heat or the production of radio-active heat are factors determining the formation and rise of these magmas.

The tectonic structure of the Andes is characterized in particular by significant normal faulting (recent extension processes); there are fewer near-surface overthrusts or deformations caused by folding, especially in the overlying rocks (Zeil, 1979). However, the majority of the deep-focus earthquakes and most of the recent volcanic activity are apparently associated with large subduction zones that dip eastward beneath the continent. The normal faults occur as large graben structures that apparently extend deep into the crust. These grabens parallel the strike of the Andes and coincide with the main volcanic regions (fig. 6). The grabens may thus have served in part as conduits for the volcanoes. The age of the inner-Andean tectonic grabens can be approximately determined on the basis of the material with which they are filled: more than 10,000 m of sediments. They are certainly recent and their main development took place in the Cenozoic times. The enormous thickness indicates considerable vertical fracture tectonics during the Tertiary.

Central and Southern Andes

This region is regarded by many geoscientists as a typical model of the subduction of an oceanic plate under a continental plate and of corresponding obduction. The

regional distribution of earthquake hypocentres in Peru and Chile is on the whole clearly patterned in such a way that shallow-focus earthquakes occur in the Pacific coastal zone, most intermediate-focus earthquakes are recorded in the region of minimum gravity values below the Andes, and the majority of deep-focus quakes occur in the boundary zone between the orogen and the eastern foreland. It is thus possible to reconstruct a definite east-dipping Benioff zone. This reconstruction also indicates that the Benioff zone clearly shows lower dip-angles and shallower subduction in northern and central Peru (average 10° to 15° from west to east) than in southern Peru and Chile (average 30°). Hanus and Vanek (1978) suggest that the variation of dip-angles of the Benioff zone implies a non-uniform rate of subduction in the Peru-Chile trench.

Another remarkable characteristic of the Benioff zone is the existence of an aseismic gap at variable depths between 100 and 200 km (depending on the different Benioff dip-angle). The aseismic gap exactly corresponds, in its normal projection toward the surface, with recent volcanic activity. Hanus and Vanek (1978) suggest that this gap would be a partially melted zone, which is supposed to be the source of primary magma for active andesite volcanoes. It is interesting to note that the only Andean zone with a shoshonitic magmatic belt corresponds exactly to the altiplanic zone (region 1, fig. 7) of thickest crust in the central Andes, in which the deepest Benioff zone has developed (Frutos, 1980).

Northern Andes

Thick tholeiitic volcanics dating from the Late Mesozoic, which are associated with equally thick pelitic, in part slightly metamorphic, sediments, occur in the Western Cordillera of Colombia and Ecuador (8A in fig. 7). This "Basic Igneous Complex" was interpreted by various authors (Case, Duran, 1971, Barnes, Paris, 1973, Goossens and Rose, 1973) as a Late Mesozoic island arc or as an oceanic element that became welded to the overall orogen during the Tertiary. In contrast, the Central and Eastern

Cordilleras (1A and 2A in fig. 7) are regarded as sections of continental crust. The boundary between these two units is indistinct (approximately at the Cauca and the Romeral faults). The geophysical data indicate that the crustal and mantle structure in the northern Andes are quite different from that in the south. As the regional distribution and intensity of earthquakes in Colombia follow a statistically confusing pattern, it has not so far been possible to distinguish a uniform Benioff zone, although such a zone is typical in Peru and Chile. Furthermore, deep-focus earthquakes are almost completely lacking in Colombia. This too contrasts with the situation in the central section of the Andes.

Stauder (1975), using geophysical data, proposes separate tongues and various subduction epochs. He justifies this by pointing to the differing spatial locations, the non-uniform dip and the lack of intermediate quakes in southern Peru. Thus, they are no longer based on the subduction of a uniform oceanic plate but instead require that several subduction episodes occur with varying intensity in time and space.

2.3.2. The Caribbean Mountain System

The Caribbean Mountain System (region C1, fig. 1) is part of an island arc of the eastern Caribbean. It formed in a geosynclinal environment to the north of Venezuela. The basement of this area contains Paleozoic rocks with metamorphosed igneous complexes of Paleozoic age. Three main stages of sedimentation can be recognized. The first starts with the upper Jurassic to lower Cretaceous (Caracas Group) and shows characteristic platform features. The second stage occurred from lower to middle Cretaceous. It was followed by the Paleocene-to-lower Eocene stage which was synorogenic and was accompanied by severe submarine ophiolitic volcanism (Tectonic map of South America, 1978). The upper Cretaceous was a period of metamorphism in greenschist to epidote amphibolite facies which increases in intensity northwards and eastwards. Faulting and gravitational sliding toward the south occurred from the upper

Cretaceous onwards and make it difficult to interpret the tectonic development of the chain.

Paleocene and Eocene sedimentation was flysch and wild flysch in the southern and the western part of the fold belt. Subsequent to this uplift and sliding, compression oriented NNW–SSE took place at the end of the Eocene and was followed by Miocene and Pliocene molasse deposition in intra–montane basins. Mesozoic magmatic activity, synchronous with the evolution of the fold belt, is shown mainly by granite plutons and basic and ultrabasic, sometimes submarine, volcanism which included serpentinized peridotites (Tectonic map of South America, 1978).

CHAPTER 3

GEOLOGY OF THE SOUTH AMERICAN PLATFORM AND ITS RELATION TO MAGNETIC AND GRAVITY ANOMALIES

3.1. Amazon Craton

The Amazon Craton (region A1 in fig. 2), includes the Guyana Shield (A1a in fig. 2), the western past of the Central Brazilian Shield (A1b in fig. 2), and the Apa and Missioned massifs (northern part of A6a in fig. 2). The craton comprises an extensive region consolidated since the end of the Trans-Amazonian Cycle (1800-2200 m.y. Middle Precambrian, see Table 1) and evolved subsequently as a cratonic area with unusual characteristics. Its western margin is not defined because of a large transitional zone (region D in fig. 2). The Chaco basin (A6a in fig. 2) overlies the craton along its southern margin. The eastern margin of the Amazon Craton constitutes one of the major structural lines of the continent. This structural line widely exposed in central Brazil and continues from there, under cover, northwards into the area of the mouth of the Amazon. To the south, it extends at least as far as eastern Paraguay, probably continuing beneath the Parana Basin (region A6b in fig. 2), and re-appearing in the south of Uruguay, near the Rio de la Plata (region A6 in fig. 2). This boundary is delineated by a series of major structures including deep faults filled with basic and ultrabasic igneous rocks, marginal sedimentary basins (including a foredeep), and volcanism; furthermore, it corresponds to a major fold belt at the end of the Precambrian (Brazilian Orogenic Cycle, 550-600 m.y.) (D in fig. 3).

The Amazon Craton is characterized by tectonic instability and abundant magmatic activity during the Upper Precambrian (about 1800 to 1000 m.y.). This was followed by a much quieter period which continued until the beginning of the Phanerozoic, during which the craton was separated into two shields (Guyana and Central Brazilian Shields) bordering the Amazon Syncline.

A succession of tectono-magmatic events affected different parts of the craton at different times during upper Precambrian time. All are characterized by large-scale faulting and the formation of tectonic basins in which continental or marine sediments were deposited, some being of molasse type. These events were accompanied by widespread acid-to-intermediate, locally basic, volcanism and by intrusion of granites (including some of rapakivi type), granodiorites, diorites, gabbros, syenites and nepheline syenites. These tectono-magmatic sequences have received various local names. The oldest, which includes the metasedimentary rocks of the Uatuma Group (see Amazon Basin) lies on both sides of the Amazon Syncline, in Brazil, and developed between 1,730 and 1,450 m.y. The metasediments of the Roraima Group also formed at about this time on the Guyana Shield (see Guyana Shield and fig. 8). A third sequence, the Beneficente Group, appeared at about 1,700 m.y. in the south-central part of the craton.

About 1,200±100 m.y. ago the Guyana Shield was the site of another intense tectono-thermal event with major faulting and metamorphism. Granites and alkaline syenites are related to these events in Brazil. Magmatic activity continued until about 1,000 m.y. in Rondonia where abundant granites (many of which show ring structures) and associated volcanism occurs. An important tin mineralization is associated with this magmatic activity.

3.1.1. The Guyana Shield

3.1.1.1. Geology

The Guyana Shield (region A1a, fig. 2) is a famous old cratonic area which encompassed the entire region of French Guyana, Surinam, Guyana, southern part of Venezuela, eastern part of Colombia, and northern part of Brazil (region 21, fig. 7). The whole area consists of Precambrian rocks lying to the north of the Amazon Syncline. The basement of the shield underwent an orogenic cycle, the Trans-Amazonian orogeny (Table 1), around 2,000 m.y.-1,800 m.y. age.

Stratigraphy

The distribution of rock formations of the Guyana Shield are shown on fig. 8. The individual units are described in the following paragraphs.

(1) The Imataca Complex (1 in fig. 8)

The oldest rocks found so far in South America occur in the Imataca complex. This high-grade metamorphic sequence consists of quartz-feldspar gneisses, amphibolite, amphibole-pyroxene gneisses, iron formation, and migmatite. The granulite facies is common. The age range as indicated by whole-rock Rb-Sr isochron plots is 2,700-3,400 m.y. (Hurley, 1970). No name has been given as yet to the thermo-tectonic events that antedate 2,700 m.y., but in keeping with the type locality the term Imataca has been suggested (Hurley and Rand, 1973). In addition, this east-northeast-striking belt as described by Bellizzia (1956), Short and Steenken (1962), and Kalliokoski (1965) also includes younger granitic rocks dated at about 2,100 m.y. (Posadas and Kalliokoski, 1967), which should be grouped with a later thermotectonic episode.

(2) The El Pao and Cuidad Piar-Guri fault systems (fig. 8)

These faults form the southern boundary of the Imataca complex, Short and

Steenken (1962) designated this structural zone as the Bolivar fault system (fig. 8). This zone forms a large shear belt that is a kilometer or more in width and contains mylonite zones between strongly sheared gneisses. McConnell (1969) has suggested that the extension of this fault system to the northeast extends into the line of the presumed ancestral north Atlantic rift.

(3) Pastora–Cariachapo assemblage (Kalliokoski, 1965) (3 in fig. 8)

This assemblage is part of an extensive geosynclinal basin to the south and east of the Imataca region and its bounding fault zone (fig. 8). This assemblage is composed of metasediments and metavolcanics which were folded, metamorphosed, and granitized during the Trans–Amazonian orogeny at about 2,000–1,800 m.y. in Venezuela.

(4) In Guyana, McConnell (1958) and Williams et al. (1967) described the continuation of these geosynclinal sequences as the Barama–Mazaruni assemblage (4 in fig. 8).

1. The underlying Barama Group consists chiefly of pelitic metasediments and metamorphosed lavas and pyroclastics, locally containing manganiferous phyllites.

2. The Mazaruni Group, which conformably lie over the Barama Group, contains pebbly sandstone and conglomerates of the greywacke suite and some volcanics.

This assemblage was metamorphosed to the greenschist facies, except in the more northern part where granites and gneisses (Younger Granite Group) of the locally designated Bartica assemblage contain migmatite complexes. The thermotectonic episode responsible for the development of the granites and gneisses and metamorphism of the Barama–Mazaruni assemblage has been described and dated in the range 1,900–1,800 m.y. by Williams et al. (1967), Snelling (1965, 1969), and McConnell (1969).

The large Guyana–Venezuela basin of sediments, which includes the Pastora–Carichapo assemblage of Venezuela and the Barama–Mazaruni assemblage of northern

Guyana is part of a synclinal facies that is bordered on the south by the Takutu Rift Valley (fig. 8). A major fault occurs along the southern edge of the Takutu Vally. South of this fault is a range of mountains 60 km across underlain by rocks of the Kanuku Group.

(5) The Kanuku Group (2 in fig. 8) (Barron, 1962; Singh, 1966)

It consists chiefly of banded biotite and biotite-garnet gneisses in the amphibolite facies, and hypersthene gneisses, and charnockites of the granulite facies. A relatively poor Rb-Sr whole-rock isochron by Spooner et al. (1971) indicates that the Kanuku Group is at least 2,000 m.y. and distinctly older than the typical trans-Amazonian thermotectonic event (2,000±200 m.y.) which affected most of the rocks of the Guyana Shield. Previously, some geologists (Williams et al., 1967, McConnell, 1969) have assumed that the Kanuku Group was comparable in age to the Imataca, namely older than 2,500 m.y., thus forming part of an Archean basement that rimmed the eugeosynclinal basin of northern Guyana.

(6) The Coeroeni and Falawatra groups (5 in fig. 8)

These gneissic and granulitic rocks of western Surinam may be an extension of the Kanuku Group. These rocks occur along the great fault system of the Takutu Rift Valley.

Priem et al. (1966, 1968) have dated numerous granites in Surinam at 1,900-1,800 m.y. and indicated that the thermotectonic episode is an extension of the Trans-Amazonian event, similar to the case in Guyana. The dating at 2,200-1,800 m.y. of the Guyana is Granites and the Caraibes Granites in French Guyana by Choubert (1964) has tied together the rocks of Surinam and French Guyana into a possible French Guyana-Surinam basin (fig. 8). This basin is elongate from east to west and bounded on the west by the Coeroeni-Falawatra belt of high grade rocks. Thus, western Surinam

appears to represent the uplifted basement on which the sediments of the Surinam-French Guyana basin were deposited. The great fault system outlining the Takutu Rift Valley thus represents a physical separation of the remnant geosynclinal rocks of this eastern basin from those of the Venezuela-Guyana basin to the west (fig. 8).

The stratigraphy of this basin has been established by Choubert (1965), Barruol (1961), and others in Surinam-French Guyana. The correlations between the Venezuela-Guyana basin and the Surinam-French Guyana basin are listing below:

Venezuela-Guyana basin	Surinam-French Guyana
Mazaruni Group	Serie de L'Orapu
Barama Group	Serie de Bonidoro
	Serie de paramaca
Imataca Complex	Coeroeni-Falawatra (Kanuku Group) Ile de Cayenne basement

All of these geosynclinal rocks were metamorphosed and invaded by granites during the Trans-Amazonian orogenic episode (Hurley et al., 1967, 1968) which was the equivalent of the Akawaian episode in Guyana, the Surinam in Surinam, and the Caraibes episode in French Guyana. The tectonic map of South America shows two Guyana structural stages (lower and upper) in the area of the Guyana during this cycle. The rocks vary in lithology and in the degree of metamorphism from greenschist to amphibolite facies and include many volcanic rocks and granite formed during and since the main tectonogenetic processes.

(a) The lower Guyana stage corresponds to more severely metamorphosed and granitized rocks which yield radiometric dates generally more than 1,900 m.y. old.

(b) The upper stage contains the less metamorphosed formations and sedimentary

rocks of molasse character along with abundant acid-to-intermediate volcanics which occurred around 1,900-1,800 m.y.

(7) Roraima Formation

The flat-lying Roraima Formation, which consisting of quartzitic sandstones and quartzites with some conglomerates and shales, unconformably overlies a large region of the Guyana Shield. The mafic dikes of the Roraima intrusive suite were dated at about 1,600 m.y. It is therefore commonly concluded that the Roraima was deposited between 1,600 and 1,700 m.y. after the uplift and erosion of the metamorphic rocks and granites beneath it. The absence of metamorphism and folding on the Roraima sequence indicates that the area has been tectonically stable at least since that time.

3.1.1.2. Magnetic Anomalies

The magnetic anomaly pattern (fig. 9) in the Guyana Shield may be divided into three different portions. One of these portions is in the central and southern part of the shield (C1, fig. 9) where the magnetic anomalies are negative and have magnitudes less than -12 nT. This magnetic low extends southeastward and connects with a large anomaly low of the Amazon Basin. A second anomaly occurs along the north-west part of the shield (B1, fig. 9). A magnetic high overlies this region with a general east-northeast trend. It appears to be part of a larger anomaly that extends southwestward into the Andean fold belt. The third anomaly is in the northeastern part of the shield (B2, fig. 9). It is also a magnetic high with a north-northeast trend and extends northeastward into the adjacent Atlantic ocean basin.

3.1.1.3. Gravity Anomalies

The Bouguer gravity anomaly pattern shows a double low in the Guyana Shield (fig. 10). Both of these anomaly lows have a minimum magnitude around -50 to -80 mgals. One of these peaks is in the eastern part (A1 in fig. 10) and the other is in the western part of the shield (A2 in fig. 10). They are separated by a NE-trending saddle having a magnitude of around 0 to -20 mgals (T1 in fig. 10).

3.1.1.4. Correlation

Generally, the magnetic anomaly and Bouguer gravity anomaly pattern, correlate fairly well with the large geologic features of the Guyana Shield.

The shape of the northwestern magnetic anomaly high (B1 in fig. 9) is elliptical and approximately coincides with the Venezuela-Guyana basin. The long axis of the ellipse has an ENE direction which is the same direction as the Precambrian structural trends (fig. 8). Similarly, the northeastern magnetic high (B2 in fig. 9) is located along the Surinam-French Guyana basin. Its magnetic trend extends northeastward to the Atlantic Ocean basin. The areas between these two magnetic highs show negative values. The large magnetic anomaly low (minimum value less than -12 nT) occurs near the southern center of the shield (C1 in fig. 9) where it is very close to the Takutu rift valley. The Takutu Formation, believed to be of Jurassic-Cretaceous age, along with other non-Precambrian sedimentary rocks in this area may correlate with this magnetic anomaly low. Therefore, there is reason to suggest that the non-metamorphosed Phanerozoic sediment of the rift valley contributes to the magnetic low.

On the Bouguer gravity anomaly map, the double-peaked gravity anomaly lows are separated by a NE-trending saddle. This saddle coincides approximately with the Takutu rift valley and may reflect that structure. Presumably dense rocks are associated with the rift structure.

In general, Precambrian terranes are associated with lower gravity anomalies (less than −30 mgals) than areas that contain non-Precambrian sediments (between 0 to −20 mgals). It is also apparent that the distribution of volcanic rocks on the Guyana Shield (fig.18) shows a relation to the magnetic and gravity anomalies. Areas that contain volcanic rocks generally have positive magnetic anomalies and lower magnitude (−50 to −90 mgals) Bouguer gravity anomalies. In contrast, areas where volcanic rocks are not present are areas of negative magnetic anomalies and higher Bouguer gravity anomalies (0 to −30 mgals). The only exception occurs in the southeastern part of the shield where cratonic granitoids, both acid and intermediate effusive and sub-volcanic rocks (1,000 to 1,800 m.y.). are underlain by negative magnetic anomalies (−4 to −12 nT) and higher Bouguer gravity anomalies (−20 to −50 mgals). Thus, the distribution of volcanic rocks in the Guyana Shield is apparently an important element that influences the magnetic anomaly and Bouguer gravity anomaly patterns.

Finally, there is an apparent correlation based on the thickness of the crust. The western part and the eastern part of the shield with positive magnetic highs and relative Bouguer gravity anomaly lows probably reflect a relative thicker crust than the southern center (Takutu rift valley). The Takutu rift valley with magnetic lows and relative higher Bouguer gravity anomalies are underlain by a relatively thinner crust which may extend northeastward to the coastline or even to the Atlantic ocean

3.1.2. Central Brazilian Shield

3.1.2.1. Geology

The Central Brazilian Shield (region A1b in fig. 2), which is also called the Guapore Craton, is one of the old cratonic regions of the South-American Platform. The eastern border of this region can be observed along the Itacaiunas River, where iron formations were recently discovered. To the north, the Central Brazilian Shield is separated from the Guyana Shield by the Amazon basin. To the southeast, the Central

Brazilian Shield is separated from the Sao Francisco Craton by a large region affected by a major upper Precambrian tectono-magmatic event, in which numerous basic and ultrabasic intrusions of alpine character occur. Some of these rocks were dated with results close to 1,000 m.y. (Hasui and Almeida, 1970).

Geotectonic and Structural Pattern

The oldest known rocks in the Central Brazilian Shield are dated at 2,700±200 m.y. (the Jequie thermotectonic events) and are part of an extensive granite-gneiss terrain (Haralyi and Hasui, 1982). Both the Central Brazilian and Guyana Shields were consolidated prior to 1,800 m.y., and both were partially remobilized in the Trans-Amazonian orogenic cycle (Table 1, 1,800-2,200 m.y.) as defined by Hurley et al. (1967). Several radiometric ages, obtained by K-Ar and Rb-Sr methods (Almaraz, 1967; Hurley et al., 1967), also indicate that the area of the Central Brazilian Shield was affected by the events of the Trans-Amazonian Orogenic Cycle. The thick iron formations of the Serra dos Carajas (Table 2) probably belong to this geotectonic cycle. Neither the Guyana and Central Brazilian Shields were affected by the events of the late Precambrian to early Paleozoic Brazilian orogenic cycle (Table 1). The only younger tectonic events in this region are apparently an intense N-S fracturing, and some Paleozoic-Mesozoic diabase dike intrusions. Remnants of a sedimentary platform cover with associated volcanic rocks of upper Precambrian age are found in several places, overlying this old cratonic area.

Stratigraphy (Table 2)

The stratigraphy still remains obscure, and gneisses, migmatites, amphibolites, schists, quartzites, phyllites, and itabirites (iron formation) have been described from this region.

3.1.2.2. Magnetic Anomalies

The Central Brazilian Shield is characterized by large magnetic anomaly highs (fig. 9). A large high occurs in the eastern region (A1 in fig. 9) near the area of Rio Araguaia and Rio Itacaiunas. The maximum value of this anomaly is more than +12 nT and covers a very large area. A magnetic anomaly high occurs in the western region of the shield (B3 in fig. 9). It is of relatively low magnitude (maximum value is less than +8 nT). Another magnetic high occurs along the northeastern boundary between the Central Brazilian Shield and the Amazon Basin (A5 in fig. 9) but it covers a relatively small area. All these anomalies may be connected and extend east-northeastward through the area of the Caririan-Propria Fold Belt into the Atlantic ocean basin.

3.1.2.3. Gravity Anomalies

The Bouguer gravity anomalies of the Central Brazilian Shield are moderately low (fig. 10). The variations range from -50 mgals to -10 mgals. The Free-Air gravity anomalies of this area show a very smooth pattern, and the variations range between +10 mgals and -10 mgals (fig. 11).

Two linear gravity lows occur in the southern part of the shield on both the Bouguer and Free-Air anomaly maps (A3 and A4 in fig. 10, 11) and have a north-to-northwest-trend. The values range on Bouguer anomaly map is from -90 mgals to -50 mgals and on Free-Air anomaly map is between -40 mgals and -10 mgals. These two linear anomalies are part of a larger series of gravity lows that occur along the northeastern part of South-American Platform (A in fig. 10 and fig. 11).

3.1.2.4. Correlation

As mentioned previously, Precambrian gneisses, migmatites, amphibolites, and itabirites are widespread in the Central Brazilian Shield. The wide distribution of these thick magmatic and magnetic rocks suggest that they are important contributors to the positive magnetic anomalies of the Central Brazilian Shield.

In the eastern area of the shield, thick iron formations were recently discovered along the Itacaiunas River, and a large region was affected by a major upper Precambrian tectono-magmatic event, in which numerous basic and ultra-basic intrusions were emplaced. These rocks may contribute to the magnetic high (A1 in fig. 9) which occurs in the area. Similarly, the presence of a large volume of intrusive rocks in the northwestern part of the shield could contribute to the magnetic high along the northwestern boundary (A5 in fig. 9) between the Central Brazilian Shield and the Amazon basin.

Both the Bouguer and Free-Air gravity anomaly patterns match well with the distribution of rocks of different age in Central Brazilian Shield (Tectonic map of South America). The areas which contain Precambrian rocks show relatively higher gravity anomalies than areas which contain Mesozoic and Cenozoic sedimentary rocks. One reason for this match is that the magmatic and metamorphic rocks of Precambrian age have higher density than the sedimentary rocks of Mesozoic and Cenozoic age. Another reason may be the thickness of the crust. Areas underlain by Precambrian rocks may have a thinner crust than areas Underlain by Mesozoic and Cenozoic rocks. However, it should be emphasized that there is no appreciable difference in elevation between the Precambrian and the Phanerozoic area (fig. 12).

3.1.3. The Amazon Basin

3.1.3.1. Geology

The Amazon Basin (region A1c, fig. 2) is one of the major basins in the South-American Platform. The basin lies between the Central Brazilian Shield and the Guyana Shield and occupies an area of about 1,250,000sq. km. The basin is elongated in shape (about 3,000 km long and 300 km wide in the eastern part and 600-800 km wide in the western region), trending in an almost east-northeast direction from the Peruvian and Colombian borders to the mouth of the Amazon River. The basin contains a thick sequence of Paleozoic, Mesozoic and Cenozoic sediments.

Geotectonic and Structural Pattern

The Amazon basin, regarded as an intercratonic basin by most geologists, has been variously considered to be an autogeosyncline (Morales, 1960), an extensive and complex graben (De Loczy, 1966), a rift basin (De Boer, 1966) and an aulacogen (Burke and Wilson, 1976). According to Harrington (1962) the substable, undeformed nature of the Amazon basin is characteristic of intercratonic basins. The adjacent extensive cratonic areas of the Guyana and Central Brazilian Shields represent stable, positive areas. The last compressional orogenic event to affect the Amazon basin area is indicated by the locally slightly metamorphosed and folded pre-Silurian Uatuma Formation (Precambrian, Table 3). This sequence overlies the crystalline Precambrian basement with an angular unconformity. The entire region can be considered to be the site of major sedimentation, extensional tectonism, basaltic volcanism, fault reactivation, and epeirogenic uplift since Silurian time.

The Amazon basin may be divided into four subunits or subbasins as a result of transverse structures or arches (fig. 3). These subbasins and arches are as follows:

(1) Marajo Subbasin. The Marajo subbasin lies to the east of the Gurupa horst

(region 1, fig. 3) and is basically a graben bounded by a system of normal faults of Cretaceous and early Tertiary age (Bouman et al., 1960). A great thickness of continental Cretaceous deposits and both continental and marine Tertiary sediments occur in the Marajo basin. Paleozoic sediments are preserved in the graben under a cover of these Cretaceous and/or Tertiary sediments (De Boer, 1964).

(2) Gurupa Horst. The Gurupa Horst is bounded by high-angle normal faults on the western side and a steplike fault system on the eastern side. The faults are oriented N-S. Displacement is greater on the eastern than on the western side of the structure. The horst block is narrow and slightly convex westward.

(3) Middle Amazon Subbasin (region3, fig. 3). This area extends from the Purus arch to the Gurupa horst (fig. 3). The axis of the basin is oriented approximately WSW-ENE and the subbasin is slightly asymmetric with southern flanks somewhat steeper than the northern. Within this subbasin is the most complete succession of Paleozoic sediments in the whole of the Amazon area. Outcrops of Paleozoic sediments occur in two narrow bands along the northern and southern edges of the basin.

(4) Coari and Purus Arches (region 4, fig. 3). During the Devonian, the Upper and Middle Amazon Subbasin was separated by the Coari arch. This arch was eroded during lower Carboniferous (De Boer, 1964) and migrated eastward into the present position of the Purus arch. The Purus arch was active in the middle and upper Carboniferous.

(5) Upper Amazon Subbasin (region 5, fig. 3). This subbasin is located between the Iquitos and Purus arches or, more precisely, between the Iquitos and Coari arches. It contains a Silurian to Carboniferous sequence considered to have been deposited in an embayment of the Andean basin, which extended eastward into the lower Amazon area in Devonian and upper Carboniferous time (Harrington, 1962; De Boer, 1964). The

basin has an E-W orientation and is also slightly asymmetric. The Paleozoic sediments do not crop out; around the edges of the basin Tertiary sediments lie directly on the basement

(6) Iquitos Arch (region 6, fig. 3). The Iquitos Arch is a wide structure that separates the Acre pericratonic basin from the Upper Amazon basin. It probably originated during Devonian time and reached its maximum development in the Permian (Norales, 1960).

(7) Arce Subbasin (region 7, fig. 3). Within this subbasin, the folded and faulted sequences of Carboniferous and Cretaceous sediments are overlain by Tertiary deposits. Folds and overthrust faults are related to compressional forces associated with the orogenic cycles of the Andean belt which developed during Cretaceous and Tertiary times. The Acre subbasin was probably formed during Carboniferous times.

Stratigraphy (see Table 3)

Upper Paleozoic strata are well represented in the Amazon basin as are rocks of Cretaceous age. Triassic and Jurassic strata are apparently absent. The upper Paleozoic rocks crop out along both flanks of the middle-lower Amazon basin forming two belts, each about 30-50 km wide and oriented in an east-west direction. The belts are roughly parallel to both the Amazon River and the axis of the basin (fig. 12). The sequences apparently are thick in the middle Amazon basin (up to 7,000 m), while in the upper Amazon basin the total succession is only about 3,000 m (Melo, 1960). They range in age from the Silurian (Trombetas Formation) to the Permian (Sucurundi Formation) (Table 3). The two most important sequences are the Silurian-Devonian and the upper Carboniferous. The oldest Paleozoic rocks (Silurian Trombetas Formation) are separated by an angular unconformity from the underlying Precambrian basement.

Traditionally the Uatuma Formation which underlies the Trombetas Formation in

the upper Amazon was regarded as Cambro-Ordovician. However, recent geochronological work has established that it is Precambrian with an age of 1,100±100 m.y. It must have been deposited before the Amazon intercratonic basin was established. It is therefore comparable with the Jaibara Formation of the Ceara Group (Kegel 1956) in the Parnaiba basin (Table 8). Both are relatively unmetamorphosed sequences, and both are separated by angular unconformities from older and much more highly metamorphosed Precambrian rocks.

An erosional unconformity separates the Silurian Trombetas Formation from the Devonian Maecuru Formation in the Amazon basin. In the central part of the Middle Amazon basin there is no important break in the sedimentary pattern between the Devonian Curua Formation and the Monte Alegre Formation of upper Carboniferous age, however, towards the margins of the basin unconformable relations indicate one or more periods of erosion or nondeposition.

The surface on which these Paleozoic rocks rest in the Amazon is a well-defined erosional surface interpreted by most authors as a peneplane or pediplane (Bigareila, 1964; et al. 1965). In other words, after Permian time there is a big gap in the Amazon succession until Cretaceous beds form. Then, the upper part of the Paleozoic and Mesozoic (Cretaceous only) sequences are truncated by an extensive erosional surface on which rest Cenozoic beds.

Volcanism

Three large South American sedimentary basins (Amazon, Parnaiba, and Parana basins) were subjected to one of the largest volcanic events in the earth's history during Mesozoic-late Paleozoic time. In terms of distribution, the area of the Amazon basin affected by the intrusion and extrusion of basic magma is far larger than that covered by the sedimentary rocks themselves (fig. 13). The Paleozoic and Mesozoic sequences are intruded by diabase which formed dikes and sills, and the number of dikes increase with depth (Rezende, 1966).

In the Amazon basin. the number of dikes cutting the crystalline basement and Silurian-Devonian sequence is greater than those penetrating the Carboniferous Monte Alegre Formation (Rezende, 1966).

The orientation of the diabase dikes are N25°-35°E, N10°-30°W, N55°-65°W, and N75°-85°E (Bischoff, 1963) and follow faults and tensional fractures. The mean total thickness of the intrusions in the prevolcanic sediments is about 260 m and in some places may exceed 600 m. The individual intrusions range from a few meters to several hundred meters in thickness (Vollbrecht, 1964). In the middle Amazon basin are two zones of sill intrusion corresponding to two distinct periods of magmatic activity--one period is of Carboniferous age and the other is of lower Jurassic age (Rezende, 1966), whereas in the upper Amazon basin there is only one age group of sills.

Four basaltic core samples from the Amazon basin were dated by K-Ar methods. The age dates obtained range from 170 to 293 m.y. old. The oldest pre-Mesozoic lava flows occur in an area where 14 flows with a total thickness of 265 m occur (Rezende, 1966). A K-Ar age of 293 m.y. was obtained on this sample. This age is considerably older than that of the extrusive basaltic rocks of the Parnaiba and Parana basins (120-130 m.y.). The remaining three samples from a depth of about 600 m have an average age of about 181 m.y. (upper Triassic or lower Jurassic) (Bigarella, 1973). In a general way, samples from below about 1,000 m are assumed to be Late Carboniferous or Early Permian, while samples above this depth are regarded as upper Triassic or lower Triassic age. No extrusive basaltic rocks are known from the younger period of intrusion.

One earlier period of volcanism is suggested by the occurrence of tuffites in the lower Devonian sequence in the Amazon basin (Ludwig, 1964, p.31). However, no other information is available.

Geologic Development of the Amazon Basin

Two main periods of tectonic activity, represented by epeirogenic disturbances, are recognized in the Amazon basin (Petrobras, internal reports, Bigarella, 1973).

(1) Silurian–Devonian time. Subsidence occurred generally everywhere within the Amazon basin during Silurian–Devonian time. Field evidence indicates that the sea transgressed from two directions and retreated in those same directions during this time interval (De Boer, 1964). In the middle Amazon basin, the thickness of the Silurian–Devonian sequence increases eastwards, reaching a maximum of 5,000 m (De Boer, 1964). In this basin the marine incursion came from the east (Melo, 1960) and transgressed as far west as the Coari arch (West of Purus Arch, fig. 3). In contrast, in the upper Amazon basin the marine incursion was from the west (De Boer, 1964).

(2) Carboniferous time. The pattern of epeirogenic movement during the Carboniferous followed the same pattern as in the Silurian and Devonian. Local uplift occurred while continuous subsidence took place in the middle Amazon basin. It appears that some of the areas which were uplifted and eroded subsequently sank considerably. The thickest Carboniferous sequence (De Boer, 1964, 1966) is in the central part of the middle Amazon basin. In addition, the central part of this subbasin shows continuous sedimentation during the Paleozoic, while in the marginal areas interruption of deposition (unconformities) indicate tectonic movement or, more correctly, deep-seated folding. In general, the rate of subsidence seems to have been greater in Silurian–Devonian times than during the Carboniferous and the Permian. Moreover, the subsidence of the central and eastern part of the basin increased eastwards in the direction of transgression during the Devonian. This situation persisted until the deposition of the Monte Alegre Formation (lower–upper Carboniferous, Table 3). Then, the pattern of subsidence changed and possibly reversed with the Amazon basin being isolated from the sea. The Purus arch and the northern and southern edges of the Middle Amazon subbasin was uplifted after the Devonian regression. Much of the Silurian and Devonian sediment were then eroded.

The information on the tectonic history of the Amazon basin is still elementary. A careful revision of surface and sub-surface data is therefore necessary. Two main periods of faulting are known - one prior to and the other postdating the Mesozoic phase of diabase intrusion. Large-scale faulting of Cretaceous to Tertiary age is restricted to the coastal basins. The faulting predated the Mesozoic intrusive phase and consisted mainly of adjustments resulting from epeirogenic movement. The Gurupa horst (region 2, fig. 3), where Paleozoic sediments to the west are brought against Cretaceous and/or Tertiary rocks, was formed in this way. The maximum intensity of faulting seems to be directly related to the igneous activity, and the large faults follow the same trends as the dykes. These trends are controlled by Precambrian basement structures. Thus many features of the lower and middle Amazon basin, rivers, waterfalls, and rapids (Sternberg, 1950; Bischoff, 1963; Leinz, 1949), are controlled by a Mesozoic NE-SW or N-S fault pattern which in turn reflects a reactivation of Precambrian structural trends. In the upper Amazon the principal fault roughly parallel the axis of the axis of the basin.

3.1.3.2. Magnetic Anomalies

Magnetic anomaly lows occur in most areas of the Amazon Basin (fig. 9). The magnitude of two magnetic minima, one at the east of the middle subbasin (C2 in fig. 9) and the other at the west of the upper subbasin (C3 in fig. 9), is less than -12 nT. Anomaly C2 may go through the mouth of the Amazon river and extend east-to-northeastward into the adjacent Atlantic ocean basin where another large magnetic low occurs. Positive magnetic anomalies occur only in a small area between the middle subbasin and the upper subbasin (northern part of A5 in fig. 9), around the southern border of the Amazon Basin.

3.1.3.3. Gravity Anomalies

In the upper subbasin of the Amazon river and the western region of this basin (the transitional zone between the Platform and the Fold Belt), a large gravity high (B in fig. 10, 11) occurs on both the Bouguer and Free-Air gravity anomaly maps. The maximum value of this gravity high is larger than +40 mgals for the Bouguer and larger than +60 mgals for the Free-Air. Both of these gravity maxima (Bouguer and Free-Air) are located at the central part of the transitional zone.

In the middle subbasin (B1 in fig. 10, 11) and the Marajo subbasin (B2 in fig. 10, 11), i.e. the middle and the lower course of the Amazon river, positive gravity anomalies also occur along with the more local negative anomalies.

3.1.3.4. Correlation

The Amazon Basin contains a thick sequence of Cenozoic, Mesozoic (including numerous diabase dikes and sills), and Paleozoic sediments.No extrusive basaltic rocks are known in the basin. Sedimentary rocks, including sandstone, shale and siltstone, are the main rock type of the Amazon basin. A thick sequence of Permo-Carboniferous evaporites is also present. All of these sedimentary rocks would be expected to have low magnetic susceptibility and thus cause the negative magnetic anomalies. The positive magnetic anomalies in the small area between the upper and the middle subbasin (northern portion of A5 in fig. 9) probably is influenced by the adjacent central Brazilian Shield or could be caused by high heat flow.

Negative gravity anomalies occur locally in the middle and lower course of the Amazon river, perhaps reflecting the thick infilling of low density sedimentary material. Positive gravity highs, however, cover most areas of the Amazon basin and the transitional zone. Compared to the surrounding areas (the Guyana Shield, the Central Brazilian Shield and the Andes), the Amazon Basin and the transitional zone are located along gravity maxima. This suggests that the thickness of the crust underlying the

Amazon basin and the transitional zone is relatively thinner than in the surrounding areas.

The large gravity high that occurs in the transitional zone (B in fig. 10, 11) between the platform and the fold belt is poorly understood. The maximum value of this Bouguer gravity high is the highest in all of South America (even higher than the one associated with the Argentina aulacogen, C in fig. 10, see Sec. 3.6). It may indicate that the thinnest continental crust of South America underlies the area of the transitional zone between the platform and the fold belt.

3.2. Sao Francisco Craton

3.2.1. General Geology

The Sao Francisco Craton (fig. 14 and region A2 in fig. 2), covers about 650,000 km^2. It is located southeast of the Parnaiba basin and is separated from it by the Sao Francisco Arch (fig. 3). On the eastern and southeastern border of the Sao Francisco craton, a metamorphic belt of 1,100–1,400 m.y. age is recognized. These age may be related to the orogeny of the Minas Group, near Belo Horizonte (fig. 14). To the northwest, the Sao Francisco nuclei and the ancient Central Brazil Shield are separated by a large region affected by a major upper Precambrian tectono-magmatic event, in which numerous basic and ultrabasic intrusions of alpine character occur. Some of these rocks were dated with results close to 1,000 m.y. (Hasui and Almeida, 1970). To the southwest, the Brazilian Fold Belt developed along the borders of the Sao Francisco Craton which acted as a foreland to the belt.

In general, the basement of Sao Francisco Craton is comprised of Lower Precambrian formations (Jequie and older) which are radiometrically well-dated (2,700 m.y. or older) although locally re-worked during the Trans-Amazonian Cycle. During the first half of the upper Precambrian, thick detrital sediments covered the craton,

forming the Nova Lima Group and its equivalents. Later on, a more extensive cover was formed on the craton during the Brazilian Cycle (Bambui group 600 m.y.).

Stratigraphy (detail lithology shown on Tables 4, 5 and 6)

(1) The basement of northern part of the Sao Francisco (location 1 in fig. 14) is composed of three metasedimentary units, older than upper Precambrian (1,800 m.y.), all of which have trends oriented close to north-south (Table 4). The Caraiba Group (Barbosa, 1966) is the oldest (minimum age close to 2,000 m.y.). It underwent strong metamorphism that reached the granulite facies. The Uaua Group was affected by a tectonomagmatic event which may have been the Trans-Amazonian orogenic cycle. Migmatites are rare in this unit. The third unit, the Jacobina Group, of great thickness (possibly more than 8,000 m) is composed of epizonal to mesozonal metamorphic rocks (Table 4). Locally, the Jacobina Group is intruded by granites.

The basement of the Sao Francisco craton is covered by sedimentary sequences named the Lavras and Bambui groups (Table 4). Both groups are weakly deformed with faulting and folding typical of platform cover. In some places the general tectonic transition from the unfolded Bambui cover to the fold belts of the Brazilian cycle are presented.

(2) The eastern part of Sao Francisco Craton (region 2 in fig. 14) reaches the coast, north of the Pardo River. In this area, the principal rocks of the basement are metamorphic rocks of amphibolite grade. This complex, not yet studied in detail, is intensely granitized and migmatized, and its structural trends are north-south to NNE-SSW. Some radiometric ages obtained on acid granulites near Salvador (fig. 14) by different methods, are close to 2,000 m.y., and are therefore characteristic of the Trans-Amazonian orogenic cycle.

In the region of the Pardo and Jequitinhonha rivers (fig.14) in southern Bahia, a

late Precambrian basin, formed near the eastern border of the Sao Francisco Craton, can be recognized. It contains sedimentary rocks metamorphosed to the greenschist facies. The original sequence is shown on Table 5. The rocks are only gently folded, but are intensely deformed by faulting. The sequence was recently named Rio Pardo Group (Table 5) (Pedreira et al., 1969), and it shows many similarities to other deposits along the borders of the Sao Francisco Craton.

(3) The southern border of the Sao Francisco craton near Belo Horizonte (fig. 14), in the region known as Quadrilatero Ferrifero (region 3 in fig. 14), is the most intensively studied of all Brazilian Precambrian areas because of the existence of large iron deposits. Dorr (1969) has described the regional stratigraphy and structure of that area (Table 6). An ancient basal complex, composed of granitized and migmatized rocks, was intruded by a granitic body (Engenheiro Correa) with a minimum age of about 2,800 m.y. (Herz, 1970). This complex is covered by Precambrian rocks representing tectonic events older than Brazilian (450–700 m.y.). The older unit, named the Rio das Velhas Series, is composed of two groups (Dorr et al., 1957) separated by an unconformity. The lower, Nova Lima Group, is about 4,000 m thick and composed of fine detrited sediments (Table 6). The upper, Maquine Group, is 1,800 m thick. In the northeastern part of the Quadrilatero Ferrifero the series is composed mainly of gneisses (Reeves, 1966). The Rio das Velhas Series was metamorphosed to the greenschist–amphibolite facies and extensively granitized. It was intruded by granite and granodiorite bodies as well as basic and ultrabasic rocks now metamorphosed. A rich gold mineralization is found associated with the series. Rb-Sr age determinations (Aldrich et al., 1964; Herz, 1970) yield 2,760 and 2,675 m.y. for muscovites from metamorphic rocks of the Rio das Velhas Series.

The Rio das Velhas Series is overlain unconformably by the Minas Series (Table 6), which seems to be younger than the Trans-Amazonian cycle (1,800–2,200 m.y.) but older than 1,300 m.y. (age of the Borrachudo granite which cuts it; herz, 1970). In the

Quadrilatero Ferrifero, where the grade of metamorphism is lower, three groups can be recognized: the lower, Caraca Group, is composed of detritic sediments accumulated during transgressive events; the intermediate, Itabira Group, is composed of mainly chemical sediments, with which are associated large iron deposits (banded ironstone type); and the upper, Piracicaba Group, is of a detrital nature. The total thickness of the Minas Series reaches about 6,000 m. It was intensively deformed, with large-scale folding followed by several type of faulting. These structures indicate northwestward tectonic transport (see Tectonic Studies in Sao Francisco Craton for detail), which occurred in two main compressional events. In the Quadrilatero Ferrifero the metamorphism of the Minas Series is generally that of greenschist facies, but at the northeast corner (Reeves 1966) this series is composed mainly of gneisses and amphibolites. Several granitic and granodioritic bodies, as well as metamorphosed basic and ultrabasic rocks, also intrude the Minas Series.

The Italcolomi Group (Table 6), which overlies the Minas Series with a sharp angular unconformity, has a very restricted occurrence in the Quadrilatero Ferrifero region. The total thickness of the Italcolomi Group exceeds 1,000 m. Its age is unknown, but it probably represents a late episode of the event which deformed and metamorphosed the Minas Series.

3.2.2. Tectonic Studies in Sao Francisco Craton

3.2.2.1. The Serra de Caldas Window, Goias

The Serra de Caldas is a large topographic and structural high in southern Goias (fig. 15). The area discussed here is within the Araxa Fold Belt, which lies between the miogeosyclinal deposits of the Paraguay-Araguria Fold Belt to the west and similar rocks of the Brazilian Fold Belt to the east (Almeida and others, 1973) (fig. 3). This belt is underlain by the Araxa Group (Barbosa, 1955) (Table 7), a eugeosynclinal sequence of 900-1,300 m.y. age (Brazil Dept. Nac. Producao Mineral, 1971). The

Araxa is overlain to the east by the Canastra Group (Barbosa 1955). This group has a flyschlike character and is considered to be 620-900 m.y. old (Brazil Dept. Nac. Producao Mineral, 1971). These rocks pass upward (to the east again) into the molasse and shelf deposits of the Bambui Group of Eocambrian age.

The rocks of the Araxa Fold Belt have a strong tectonic convergence toward the Sao Francisco Craton to the east (Ferreira, 1972). Rocks of the Araxa Group have been thrust over both the Canastra and Bambui Group, and Canastra rocks have been thrust over rocks of the Bambui Group, marking strong west to east tectonic transport during the Eocambrian or earliest Paleozoic.

Stratigraphy (see Table 7 for details of lithology)

The geology of the Serra de Caldas area is known mostly from the work of Braun (1970 b). Three rock groups can be recognized: the Araxa group, the Canastra group, and a sequence of quartzite, siltstone, and lesser shale that can probably be correlated with the Bambui Group.

The Araxa group in Serra Caldas was divided into three units by Braun (1970): (1) the lowermost unit is in amphibolite facies and at several places is gneissic; (2) the middle unit is more psammitic, bedding in this unit is transposed, and the primary planar element is flow cleavage; and (3) the upper unit of the Araxa which surrounds the Serra de Caldas. This third unit was metamorphosed to at least the high greenschist facies, but at places it contains megascopic kyanite and andalusite, suggesting higher rank metamorphism. This unit contains abundant small bodies of ultramafic and related mafic rocks in the form of serpentinite, actinolite schist (probably metapyroxenite), talc schist, and chlorite schist (Braun, 1970a). This part of the Araxa, then, can be considered an ophiolitic melange. (Gansser, 1974; Williams, 1977).

The Canastra Group (Braun 1970b), though strongly deformed, is less so than the

Araxa and bedding can be been in many exposures. The unit is metamorphosed to the biotite grade.

A sequence of orthoquartzite and siltstone containing interbeds of shale underlies the Serra de Calds. These rocks were once confused with the middle unit of the Araxa Group because of their quartzose nature and their position beneath the upper part of the Araxa. However,these rocks, probably deposited in a transitional (continental marine) environment, have nothing in common with the deep marine rocks of the middle part of the Araxa. In the Brasilia area, Dyer(1970) described a sequence of quartzite, siltstone, and "slaty phyllites" at the base of the Bambui Group. The description of these rocks matches closely the rocks at the Serra de Caldas, which, therefore, are tentatively correlated with the Bambui Group.

Tectonic Interpretation

The contacts between these different rock suites mentioned above are marked by a zone of cataclastically deformed rock and a metamorphic discontinuity. These relations show that the rocks are in fault contact and that the Serra is a large antiformal window about 250 km in extent, trending just west of north. Transport of the thrust sheet was probably from west to east, perhaps for a distance of as much as 200 km (A.A. Drake Jr.). Rocks of the Araxa and Canastra Groups were metamorphosed and deformed prior to their emplacement, as shown by the folded early foliations in these rocks and by the low ranks of metamorphism in the Bambui Group.

The thrusting of ophiolite melange onto shelf deposits is of great importance because such occurrences commonly are the result of the obduction of oceanic rocks across a continental margin. The zone of thrusting described here marks the western margin of the Sao Francisco Craton. This obduction must date from the Eocambrian to earliest'Paleozoic.

3.2.2.2. Quadrilatero Ferrifero, Minas Gerais

Quadrilatero Ferrifero, about 7.000 km^2 in central Minas Gerais (fig. 15), is one of the great mining areas in the world. The area is underlain by gneisses and foliated granitoid rocks and three major series of sedimentary and subordinate volcanic rocks set off from each other by angular unconformities (see Table 6 for detailed stratigraphy). Rocks of the Rio das Velhas Series, considered by Dorr (1969) to be the oldest in the Quadrilatero, is a eugeosynclinal suite that is interpreted to grade upward into a molasse, at least locally. These rocks are overlain by the Minas Series of largely shallow-water sediments, including great deposits of iron-formations (oxide facies). The uppermost rocks of this sequence are thought to be flysch. The youngest series, the Itacolomi, consists of rocks thought to represent molasse deposits. The sedimentary and lesser volcanic rocks of these three series have been regionally metamorphosed, primarily to the greenschist facies, although staurolite-bearing schists of the amphibolite facies are present in some places.

All the gneisses and foliated granitoid rocks are interpreted to be intrusive into the sedimentary-volcanic pile and to be post-Rio das Velhas in age. The rocks of the amphibolite facies are thought to result from contact metamorphism and to be in thermal aureoles around granitoid intrusions. The Quadrilatero has, therefore, been interpreted as an island of metasedimentary rock floating in a sea of granite (Dorr, 1969).

The Precambrian pre-Minas rocks of the Quadrilatero Ferrifero in Minas Gerais have been restudied and reinterpreted using a simplified plate-tectonic model by A.A Drake and B.A. Morgan (1980). The principal elements of this interpretation are as follows: (1) Many of the granitoid rocks and gneisses of the area are part of an ancient cratonic massif (the Sao Francisco Craton) and are not later intrusions into metasedimentary and metavolcanic rocks of the region. (2) The cratonic rocks are

overthrust by a sequence of flyschoid rocks of the Nova Lima Group. The sequence includes ultramafic and related mafic rocks that are parts of a disrupted ophiolite assemblage. Metamorphic muscovite from the cratonic basement and from schists of the Nova Lima Group has an age of 2.6 to 2.7 b.y.; therefore, the allochthon was in place by that time. The Nova Lima allochthon, which includes this ophiolitic material, is therefore a very early example of plate tectonics, and was obducted perhaps from the southeast onto the Sao Francisco Craton during Archean time.

3.2.3. Magnetic Anomalies

Two different magnetic anomaly patterns occur in the Sao Francisco Craton (fig. 9). In the southern part of the craton, a large magnetic low occurs (C4 in fig. 9), the minimum value of which is less than -12nT. This magnetic low appears to be part of a larger anomaly that extends eastward into the adjacent ocean basin. To the north is a positive magnetic anomaly that occurs at the northern part of the craton (B4 in fig. 9). The magnitude of this magnetic high is about 10nT.

3.2.4. Gravity Anomalies

A large negative Bouguer gravity anomaly occurs in the area of Sao Francisco Craton (A in fig. 10). This low extends northward into the Parnaiba basin and southwestward into the Parana basin. The magnitude of anomalies increases toward the interior of the craton and reaches a minimum value of less than -130 mgals in the central part of the craton. This minimum value is the lowest Bouguer gravity anomaly in South-America except for the Andes.

The Free-Air gravity anomalies are also low over the Sao Francisco Craton (fig. 11), although not as low is the Bouguer gravity anomaly values. The minimum Free-Air anomaly is about -50 mgals and it occurs in the central part of the craton.

3.2.5. Correlation

Based on the magnetic anomaly map, the Sao Francisco Craton can be divided into two parts.

In the northern part of the craton, the basement is composed of three metasedimentary units (Caraiba, Uaua and Jacobina group, Table 4). Most of the units underwent strong metamorphism, especially the Caraiba group which reached the granulite facies. These metasediments are associated with eruptive rocks of basic and ultrabasic composition. The positive magnetic anomalies (B4, fig. 9) may in part reflect the presence of these rocks. Furthermore, the center of the main magnetic high occurs on the northwestern border of the Sao Francisco Craton in which numerous basic and ultrabasic intrusions of alpine character occur.

In the southern part of the craton, in the region known as Quadrilatero Ferrifero (region 3 in fig. 14), is a major magnetic low (C4, fig. 9). A large iron deposit (banded ironstone type) occurs in this area (in the Minas Series mainly). A large magnetic high should be associated with the iron deposits. Instead the presence of a prominent magnetic low suggests that either the direction of the magnetic field is reversed or the anomaly is caused by other tectonic elements. The fact that the anomaly extends eastward into the Atlantic suggests that large crustal elements are involved.

The mean elevation map of South America indicates that the Sao Francisco Craton (A in fig. 12) contains the highest elevation in South America except for the Andes. Thus, the depth of compensation beneath the Sao Francisco Craton should be very deep in view of isostatic theory. In other words, continental crust under the Sao Francisco Craton must be very thick. The large Bouguer gravity low that occurs here (A in fig. 10) also indicates that a thick continental crust underlies the Sao Francisco Craton. The crust underlying this craton is probably the thickest crust in South America except for the Andes.

Attention is called to the small region of positive Free-Air gravity anomalies that occur at the southern border of the craton (A5 in fig. 11). Rocks of the Nova Lima group (Table 6) occur in this region and include ultramafic and related mafic rocks that are parts of a disrupted ophiolite assemblage. The presence of the Free-Air gravity high and the ophiolite assemblage in this area suggests an association.

3.3. Parnaiba Basin

3.3.1. General Geology

The Parnaiba basin (region A3 in fig. 2) is separated from the Amazon basin by the Tocantins arch (fig. 3). This basin is roughly oval in shape with an area of over 600,000 km^2 (Almeida, 1964) and contains Paleozoic and Mesozoic rocks. To the north are two smaller coastal basins (Sao Luiz and the Barreirinha basins, see Sec. 3.4) which are separated from the Parnaiba basin by the Ferrer arch (fig. 3). The eastern and western margins are delimited by the eastern and central Braziiian Shield, and the southern limit is defined by the Sao Francisco arch.

3.3.2. Geotectonic and Structural Pattern

The Parnaiba basin is an intercratonic basin surrounded by cratonic areas (Sao Luiz, Sao Francisco and Amazon Cratons, fig. 2) of different ages. This basin is usually considered as a single unit. The adjacent small coastal basins are grabens separated from it by the Ferrer arch. It is not yet known with certainty whether Paleozoic sequences occur within all of these coastal basin (see Sec. 3.4). The Sao Luiz area and the Sao Francisco Craton underwent a well defined geologic event at about 2.000 m.y., the Trans-Amazonian orogenic cycle (Snelling and McConnell, 1966; Cordani et al., 1968). These older areas are separated from each other by metamorphic belts which underwent orogenies or were reactivated in late Proterozoic to early Paleozoic 650-450 m.y., Brazilian orogenic cycle (Table 1) (Cordani et al., 1968). Thus, the

margins of the intercratonic basin (i.e. Parnaiba basin) are generally formed by younger Precambrian metamorphic and sedimentary rocks. As in the Amazon area, the Parnaiba basin and its surrounding region may be considered as tectonically undisturbed since the Silurian, except for epeirogenic movement and the reactivation of pre-existing faulting.

The Parnaiba basin has not been subjected to compressional forces except in the south-western part, where the strata are tilted to a maximum of about 25°(Mesner and Wooldridge, 1964). The basin is asymmetrical towards the northwest, so that in the eastern part the sequences dip toward the center at 0.5° -2.0° , whereas in the northwestern part the regional dip of the margin is 4° -5° . Within the basin are shallow anticlinal structures developed with an approximate NE-SW orientation (Kegel, 1953). Locally, more intensive folding may occur in narrow bands associated either with diabase intrusions or faults.

3.3.3. Stratigraphy (see Table 8)

In the Parnaiba basin, the maximum sedimentary thickness is slightly in excess of 3,000 m, of which 2,500 m are of Paleozoic age and the remainer Mesczoic (Kegel, 1956; Mesner and Wooldridge, 1964). According to Almeida (1964) the total sedimentary accumulation locally is in excess of 3,700 m. Thus, Upper Paleozoic rocks are well represented in the Parnaiba basin, as are Mesozoic rocks despite the presence of several unconformities. Cenozoic rocks, on the other hand, are not represented in the Parnaiba basin. The stratigraphic units are usually very uniform and only minor facies changes are found. It might reasonably be expected that the successions are more complete in the central parts of the basin than in the present marginal regions.

The Silurian (or Ordovician ?) Serra Grande Formation (Table 8) is the oldest Paleozoic unit in the Parnaiba basin, and it is separated by an angular unconformity from the underlying Precambrian basement. According to Kegel (1953), the Serra Grande Formation rests on a surface of accentuated relief with elevation differences of

more than 300 m. Recent field work fails to support this contention, and Bigarella et al. (1965) have suggested that the apparent relief was the result of deep-seated folding or warping contemporaneous with deposition and that the original surface was a pediplane as in the Amazon basin.

Within the Devonian succession of the Parnaiba basin are no visible unconformities other than diastems, and the continuous sedimentary cycle which began with the Serra Grande sequence terminates only with the lower Carboniferous. From then onwards hiatus and unconformities are more conspicuous (Table 8).

3.3.4. Geologic Development

The present day shape of the Paleozoic basins found on the South-American Platform is not the same as at the time of deposition. The directions of sedimentary transportation changed and were occasionally even reversed so that the previous area of deposition within the basin became the principal source as a result of uplift (Bigarella and Salamuni, 1967b). The major changes occurred in post-Cretaceous time and were controlled primarily by deep-seated folding (Salamuni and Bigarella, 1967). Paleocurrent analyses seem to indicate that all the intercratonic basins (Amazon, Parnaiba and Parana basin etc.) of the South-American Platform were interconnected at some time during the Devonian, forming a continuous sedimentation area (Bigarella and Salamuni, 1967).

The Parnaiba basin began to subside in Silurian time (Ordovician ?) with the deposition of the Serra Grande Formation. According to Mesner and Wooldridge (1964), the sea entered the Parnaiba basin from the northeast transgressing southwestwards. However, this does not agree with paleocurrent analysis (fig. 17). Bigarella et al. (1965) suggest that the Serra Grande Formation sediments were derived from a northeastern and southeastern source area. It is not clear whether the Amazon and Parnaiba basins were connected during Silurian time. But epeirogenic subsidence continued during the Devonian, at which time the sea reached its maximum extent

connecting all the intercratonic basins. During the lower Carboniferous a gradual uplift of the Parnaiba basin began, and in late lower Carboniferous or early upper Carboniferous time the uplift reached its maximum, exposing the entire basin to erosion (Mesner and Wooldridge 1964). Early in the upper Carboniferous, subsidence occurred and deposition of upper Carboniferous was followed by Permian sedimention.

Something in the Early Triassic the subsidence ceased, only to begin again in later Triassic time. During the Jurassic large volumes of basaltic lavas were erupted (fig. 18), and after the formation of the lavas, the uplift of the basin continued. At the beginning of the Cretaceous the northern margin of the basin began to subside, and large-scale normal faulting began along the northern edge forming the coastal basins (Barreieinhas and Sao Luiz basin, see Sec.3.4 and fig. 19) which contain thick successions of Cretaceous sediments. In Aption (Lower Cretaceous) time the sea submerged the Ferrer arch (fig. 3) transgressing as far west as the Tocantin River (The western boundary of Parnaiba basin) (Mesner and Wooldridge, 1964).

The magnetic and gravity anomalies for this area are discussed in section 3.4.

3.4. Sao Luiz Craton

The Sao Luiz Craton is located along the coastal areas of Para and Maranhao, Brazil (fig. 19). It may be divided into two basins, Sao Luiz Basin on the west and Barreirinha Basin on the east, by the city of Sao Luiz. The Ferrer arch separates these small coastal basins (or grabens) from the adjacent Parnaiba Basin to the south.

3.4.1. Geology

The Sao Luiz cratonic area is still very poorly known, as the main part is covered by Paleozoic or younger sedimentary rocks. Gneisses, schists, and amphibolites occur, intruded by granites, diorites, and other intrusive rocks (Moura, 1936). Age dating yields results close to 2,000 m.y. (Hurley et al., 1967; Almaraz and Cordani, 1969). This cratonic area extends eastwards to the mouth of the Parnaiba River, where structures related to the Brazilian Orogenic Cycle occur.

The Sao Luiz Basin, between the city of Sao Luiz on the east and Para on the west, contains a maximum thickness of about 4,000 m of Devonian–Mississippian (?), Mesozoic, and Cenozoic deposits. A metamorphic belt of late Precambrian–Cambrian age is found along the southern border of the Sao Luiz Craton. This belt, which is largely covered by sediments, can be followed for at least 200 km, and may even extend to 400 km, as correlatable rocks occur near the bay of Sao Jose. It apparently represents part of a fold belt which surrounds the southern borders of the Sao Luiz Craton and which, at the end of the Precambrian, constituted its foreland. Radiometric ages by Rb–Sr and K–Ar methods (Hurley et al., 1967; Almaraz and Cordani, 1969) confirm the Brazilian age for these rocks. Whole–rock Rb–Sr ages close to 600 m.y. indicate that the events are not related to simple isotopic rejuvenation of older rocks (Almeida, et al.). Clastic nonfolded rocks, estimated to be Cambro–Ordovician in age, may represent the molasse of the final stage of the Brazilian cycle in this area. The stratigraphical succession of the Sao Luiz Basin is shown in Table 9.

The Barreirinhas marginal basin, lying between the cities of Sao Luiz and Parnaiba, has a total area of about 85,000 sq. km. The onshore portion of the basin covers 13,000 sq. km in a narrow belt about 300 km long and 2,080 km wide which is entirely covered by Tertiary and Recent sands. As a structural unit, the Barreirinhas basin is superimposed on the northern part of the Paleozoic Maranhao basin as a result of

Wealdian (Lowermost Cretaceous) deformation which produced a series of horsts, grabens, and step blocks through normal faulting. Toward the south, the Ferrer-Urbano Santos-Parnaiba arch separates the Barreirinhas basin from the main part of the Maranhao basin and Parnaiba Basin. To the west lies the shallow intracratonic Sao Luiz basin which connects with the Barreirinhas basin through the narrow Ilha Nova graben (fig. 19). Toward the north and east, the basin appears to open toward the Atlantic Ocean. Positive structures within the basin such as the Atlantic high and the Ilha de Santana, Sobradinho, and Parnaiba platform are relatively shallow, having a sedimentary cover of less than 2,000 m. In the deeper depressions and in the Piaui graben, sedimentary thickness may exceed 12,000 m. The stratigraphical succession of the Barreirinhas basin in shown on the Table 10.

3.4.2. Magnetic Anomalies

The magnetic anomaly pattern over the Sao Luiz Craton shows a broad gradient which decreases from south to north (fig. 9). The anomalies in most parts of the craton are negative. However, the magnetic signature in the Parnaiba basin is not definitive and appears to occur along an irregular gradient that also decreases toward the north (fig. 9). Positive anomalies occur in some areas especially in the southern part of the Parnaiba basin. This magnetic gradient continues northeastward into the adjacent Atlantic Ocean basin.

3.4.3. Gravity Anomalies

On the Free-Air gravity anomaly map (fig. 11), the Sao Luiz Craton and Parnaiba basins may be considered together as a single unit which has a negative gravity anomaly signature with a minimum value in the central part (C in fig. 11). The pattern of this gravity low is roughly oval in shape and opens on the northern side into the Atlantic Ocean.

The Bouguer gravity anomalies in Sao Luiz Craton and Parnaiba basins also are negative (fig. 10), but there are two different patterns in each of these two areas. In the Sao Luiz Craton, the Bouguer anomaly forms an irregular gradient pattern (B3 in fig. 10) and decreases from south to north. In the Parnaiba basin, the anomaly forms a concentrated pattern (A5 in fig. 10). Furthermore, these negative anomalies are part of a larger series of gravity lows that occur in the whole eastern part of the South-American platform.

3.4.4. Correlation

The Sao Luiz Craton is a narrow feature along the northeast Atlantic coast. The Ferrer arch separates this craton from the adjacent Parnaiba basin to the south.

Based on the Bouguer gravity anomaly map, it is suggested that thick continental crust underlies the whole eastern part of South-American Platform as this entire region coincides with a large gravity low (A in fig. 10). This area of thick crust includes the Sao Francisco Craton, most of the Parana basin and even part of the Parnaiba basin. However, crustal thickness decreases northward from the central part of the Parnaiba basin through the Sao Luiz basin into the Atlantic ocean. The same trend of decreasing anomalies also occur on the magnetic anomaly map. This correspondence suggests that the variation of magnetic anomalies may be associated with the variation of the thickness of crust in Sao Luiz Craton and Parnaiba basin. Furthermore, the Sao Luiz Craton is covered by Paleozoic or younger sedimentary rocks in most areas. Magmatic and magnetic rocks are rare. Thus, the Sao Luiz Craton is influenced by the large magnetic low that occurs on the adjacent Atlantic ocean and show moderately negative anomalies. In contrast, the Parnaiba basin contains a large amount of volcanic rock. Large volumes of basaltic lavas were erupted during the Jurassic in the southern center of the basin (fig. 18). Thus, the Parnaiba basin show moderately positive anomalies in most areas.

Basically, Bouguer gravity anomalies are associated with the thickness of continental crust. The anomalies increase whereas the thickness of crust decreases from south to north in the Sao Luiz Craton. A gravity minimum (A5 in fig. 10) occurs at the center of the Parnaiba basin where the thickness of crust reach the maximum of this basin.

Both the Parnaiba basin and the Free-Air gravity anomalies are roughly oval in shape. The thickness of the sediments in the basin increase toward the interior of the basin (Basin 2 in fig. 4). Similarly, the Free-Air anomalies also decrease toward the interior. This indicates that the greater the thickness of low density sediments the more negative are the values of the anomalies.

3.5. The Atlantic Shield

3.5.1. Caririan-Propria Fold Belt

Widespread regions of the South American Platform were re-worked during the upper Precambrian, less than 1,000 m.y. ago, and show a complicated structure. This period of deformation is known as the Brazilian orogenic cycle (Table 1). The Caririan-Propria Fold Belt is part of this cycle. Fold systems that are part of the Brazilian Orogenic cycle are developed in both sediments deposited during the cycle and in re-worked pre-Brazilian basement. Some massifs were also generally affected by this cycle. Older structures in this basement are well represented in the interior of the State of Goias (fig. 15) as well as in the north-and south-east of Brazil. Ages of more than 2,600 m.y. are commonly encountered in granite-gniss complexes and in migmatites, which are commonly metamorphosed to the granulite facies. Mafic and ultramafic intrustions are commonly associated. Structures of the Trans-Amazonian Cycle, re-worked by the Brazilian Cycle, are common, especially in eastern Brazil where they may often be confused with older formations, or with Brazilian formations that have been more intensively modified by metamorphism and migmatization.

In general, the Atlantic coast of South America is parallel to the structure of the Precambrian rocks. A notable exception is the Caririan-Propria Fold Belt in northeastern Brazil (fig. 20), where the ancient structures exhibit a fanshaped pattern. In that region the trends are normal to the coastline, and they end abruptly against the border of the continental shelf. The continental shelf in northeast Brazil is the narrowest of the entire Atlantic seaboard. Moreover, in this region, the continental slope is the longest in the world, characterized by rather persistently steep slopes (Shepard, 1963). Several sedimentary basin were formed in the coastal region and along the continental shelf, during the Mesozoic era, as a result of tectonic activity (fig. 4). These basins, which are grabens or semigrabens, are not controlled by the underlying Precambrian structures, and their principal fault zones are parallel to the coast. The most important exception is the Reconcavo-Tucano basin in northern Bahia (fig. 4 and 20). It is not located along the coast, and its main fault zones are parallel to the Precambrian structures. The faults belong probably to the same system that delimits the continental margin in Southern Bahia.

3.5.1.1. Caririan Fold Belt

The Caririan orogenic area (region A in fig. 20) is exposed to the north of the Pernambuco lineament and to the east of the Parnaiba sedimentary basin. It covers the northeastern corner of Brazil, and probably extends below the sediments of the Parnaiba basin, separating the Sao Luiz from the Sao Francisco Craton (fig. 2). The Caririan orogenic area was affected by intense granitization and migmatization (fig. 18) which is considered to have occurred during the Brazilian orogenic cycle (Almeida et al., 1968); however, Choubert (1970) regards the plutonism to have occurred earlier. K-Ar and Rb-Sr age determinations on rocks of the Ceara Group (Table 11) yield values corresponding to the Brazilian cycle (Hurley et al., 1967; Almeida et al., 1968; Ebert and Brochini, 1968). A particularly significant 650 m.y. reference isochron was obtained for six whole-rock samples, which represents the main metamorphic event in the Caririan area.

Stratigraphy (Table 11)

The older rocks exposed in the Caririan orogenic area are gneisses, migmatites, schists, quartzites, marbles, and amphibolites with radiometric ages ranging from 500 to 2,000 m.y. (Almeida et al., 1968). Such age variation indicates an isotopic rejuvenation process which affected a basement older than upper Precambrian. No clear unconformities have been found at the base of the metasedimentary rocks of the Ceara Group, which represents the Brazilian cycle in that region and overlies the basement.

The Ceara Group (Table 11) is composed of a thick association of micaschists, metaarkoses, metagraywackes, phyllites, marbles, and gneisses. Its stratigraphy is still obscure (Meunier, 1964; Ebert, 1966, 1967, 1970). The lithology is constant over large distances along the strike of the folds but changes noticeably normal to the strike. The rocks of the Ceara Group generally exhibit an amphibolite facies metamorphism, but locally pass to the greenschist facies. Fold axes strike N 10°–50° E and show evidence of drag near the transcurrent faults, especially those trending east-west (fig. 20).

Iron hastingsite-bearing alkaline granites, syenites, and quartz syenites are the post-kinematic rocks of the region. A large number of pegmatites, important for their mineralization in Ta, Ba, Nb, Sn, and Li, also occur. Radiometric ages suggest that the final episodes of the granitization process occurred during the Cambro-Ordovician. At that time the molasse basins marking the final stages of the Brazilian cycle were formed. One such basin, the Taibaras, was affected by granodioritic plutonic intrusions, with associated rhyolites, andesites, and basalts, representing the final magmatic pulse of the Brazilian cycle. K-Ar determinations indicate a minimum age of about 440 m.y. for this magmatic activity.

3.5.1.2. Propria Fold Belt

The Propria Fold Belt (region B in fig. 20) is located at the northeastern border of the Sao Francisco cratonic area. Northwestward from the Propria Fold Belt, and apparently including the northern part of Bahia (fig. 15), is an important system of transcurrent faults (fig. 20). The main faults form to the south the Pernambuco lineament (Ebert, 1962) and to the north the Patos (Kegel, 1965) lineament. Both strike generally east-west and have an extension of hundreds of kilometers, probably extending to the continental shelf. They are dextral with a net slip still unknown but presumably on the order of several tens of kilometers. Alkaline granitic intrusions are known along both lineament. Syenites and quartz syenites are known to occur along the Patos lineament (Vandoros and Coutinho, 1966; Almeida et al., 1971, Santos, 1971). Santos (1971), analyzing the mechanism of that transcurrent faulting, suggested that they originated by NNE-SSW compressional forces accompanied by rotational deformation. This fault system is at least as old as upper Precambrian, as indicated by age determinations (K-Ar amphiboles) on quartz syenites of the Patos lineament (Vandoros and Coutinho, 1966). However, at the end of the Jurassic the main faults were reactivated by vertical movements giving rise to some Mesozoic sedimentary basin. The Cabo cratonic alkaline granite, located along the southern coast of the state of Pernambuco (fig. 15) and having a Cretaceous (±100 m.y.) age (Vandoros, in Almeida et al. 1971), seems to have been intruded along the eastern part of the Pernambuco lineament.

Stratigraphy (Table 12)

During the Brazilian Cycle (Table 1) an orthogeosyncline, designated the Propria geosyncline by Humphrey and Allard (1968), developed along the northeastern border of the Sao Francisco Craton. The basement of this geosyncline is exposed in the internal zones, as indicated by radiometric ages of up to 2,530 m.y. (Hurley et al., 1967). The miogeosynclinal zone in Bahia and Sergipe states (fig. 15) is represented by the Canudos

and Miaba formations (Table 12), respectively. In the eugeosynclinal zone basic volcanic products are associated with pelites, metagraywackes, in part conglomeratic, sandstones, and limestones (Vaza Barris Group). These rocks were metamorphosed to the greenschist facies and locally to the amphibolite facies in the internal zones of the geosynclinal. In some places these rocks were migmatized and granitized, being transformed into syntectonic granodiorite rock bodies (fig. 18). Relicts of red clastic deposits are found both within the geosyncline (Jua Formation) and over the platform (Estancia Group).

Large thrust faults occur at the contact between the geotectonic units. Intense linear folding, inverse faulting, cleavage, and schistosity indicate tectonic transport from the internal zones of the Propria geosyncline toward the Sao Francisco platform, which acted as a foreland during the orogenesis.

The structures of the Propria geosyncline, more than 450 km long, are partially covered by Mesozoic sedimentary basins. These structures trend perpendicularly to the coastline and continue under the narrow continental shelf.

3.5.1.3. Magnetic Anomalies

A large magnetic anomaly high occurs in the area of the Caririan–Propria Fold Belt (A2 in fig. 9). The maximum value of this high is over +12 nT and occurs in the center of the area. No negative anomalies occur in this entire area. The magnetic anomaly pattern has an E–W trend that extends eastward into the adjacent Atlantic ocean basin.

3.5.1.4. Gravity Anomalies

Bouguer gravity anomalies are very low in the Caririan-Propria Fold Belt, especially in the center of the area (A6 in fig. 10). The minimum value of these anomalies is less than -90 mgals and is located in the south-central part of the area. Except along the coast where positive Bouguer anomalies occur, the fold belt is underlain by negative gravity anomalies. The Free-Air anomaly map of the Caririan-Propria Fold Belt (fig. 11), shows a gravity low over the south-central part of the area (A6 in fig. 11) which has a minimum value less than -40 mgals. However, the rest of the region shows a very smooth gravity field (between -10 mgals and -10 mgals in most area). Positive Free-Air anomalies also occur along the coastal areas and increase from the continent toward the ocean (from +10 mgals to over +40 mgals).

3.5.1.5. Correlation

The large magnetic anomaly high (A2 in fig. 9) of the Caririan-Propria Fold Belt is apparently associated with metamorphic and intrusive igneous rocks of Precambrian age (Table 11 and 12). The Ceara group (650 m.y.) is composed of a thick association of micaschists, metaarkoses, phyllites, marbles and gneisses (Table 11); iron hastingsite-bearing alkaline granites is the post-kinematic rock of this region. A large number of pegmatites with Ta, Ba, Nb, Sn and Li mineralization also occur and contribute to the magnetic high.

Both the Bouguer and Free-Air gravity maps show an anomaly low (A6, fig. 10 and 11) in the south-central part of the Caririan-Propria Fold Belt and positive anomalies along the coastal areas. This apparently reflects the fact that the thickness of the continental crust underlying the central part of fold belt is thicker than the crust underlying the coastal area. In addition, the high density oceanic crust may also contribute to the positive anomalies of the coast area. The Reconcavo-Tucano basin (C, fig. 20) with undivided Phanerozoic sediments is associated with the minimum gravity

low at the southern center of the fold belt. This belt contains low density non-metamorphosed sediments as well as Precambrian metamorphic rocks and Tertiary to Precambrian intrusive rocks.

3.5.2. Ribeira Fold Belt

At the extreme south of Minas Gerais and extending towards Sao Paulo, Rio de Janeiro, and Espirito Santo (fig. 21), an important fold belt of the Trans-Amazonian Cycle developed during the middle Precambrian (1,800-2,200 m.y.). This belt probably continues into the southernmost Brazilian states (Parana, Santa Catarina, and Rio Grande do Sul) (fig. 21) as well as to the south of Bahia. Some geologists propose to designate it as the "Paraiba do Sul Fold Belt". Since the former "Paraiba Fold Belt" includes rocks belonging to two different tectonic cycles, the adoption of a new nomenclature for both is justified: the older one, "Paraiba do Sul Fold Belt", corresponding to the Trans-Amazonian cycle, and the younger one, the "Ribeira Fold Belt", corresponding to the Brazilian Cycle (450-700 m.y.).

The Ribeira Fold Belt, in southern Brazil and Uruguay, displays materials of the Brazilian cycle that accumulated in an internal zone of a geosyncline. At least two tectonic sequences can be recognized. The lower, equivalent to the geosynclinal subsidence phase, exhibits typical sedimentation, metamorphism, and granitic to granodioritic magmatism. Ophiolitic magmatism occurs locally. The higher sequence, equivalent to the molasse stage, exhibits sediments with little or no metamorphism, but is associated with granite plutons, rhyolitic-andesitic volcanic rocks, and mineralization.

The infrastructures of the Ribeira Belt include older rocks formed during the Trans-Amazonian cycle, or even earlier. This shows that the Ribeira Fold Belt was formed by regeneration of a previously cratonic area, and not formed on oceanic crust. Consequently, it is characterized by the extreme abundance of granitic plutonism, acid volcanism, and rarity of ophiolitic magmatism and basic volcanism. Incidentally, this

pattern is valid for all of the units of the Brazilian cycle, a fact which indicates that the basement for the late Precambrian geosynclines of South America was of sialic "continental" character.

3.5.2.1. Paraiba de Sul and Ribeira Fold Belt near Rio de Janeiro

The Paraiba do Sul Fold Belt is represented in the state of Rio de Janeiro by the Paraiba-Desengano Series (Ebert, 1957; Rosier, 1965) (Table 13). The Series is composed mainly of paragneisses, metagraywackes, and metaarkoses with subordinate quartzites and mica schists. The metamorphism reaches the amphibolite facies and commonly the granulite facies, when typical charnockites occur (Ebert, 1968). Granitization is widespread and occurred during two cycles. These rocks are best exposed along the coastal region from Bahia to Sao Paulo (fig. 21). The Paraiba-Desengano Series is intruded by several granite, granodiorite, and other rock bodies of different ages. Ebert (1957) and Barbosa et al. (1966) assume that the age of the Paraiba-Desengano Series is late Precambrian. Recent geochronologic studies carried out by Delhal et al. (1969) show that the granulitic rocks of this series are 1,923±66 m.y. old, as indicated by Rb-Sr whole-rock isochrons. U-Pb determinations on zircons from the same rocks yield an age of 2,070 m.y., confirming the presence of the Trans-Amazonian cycle in this belt.

The Ribeira Fold Belt (Brazilian Orogenic Cycle) in the state of Rio de Janeiro is represented by the Serra dos Orgaos Series (Table 13), whose age of 620±20 m.y. is indicated by an Rb-Sr reference isochron (Delhal et la., 1969). It is mainly composed by migmatites and granitic gneisses within the Paraiba do Sul Fold Belt. In this region post-tectonic granites (fig. 18) of the Brazilian cycle were dated by Ledent and Pasteels (1968) by the Rb-Sr method and U-Pb determinations on zircons. The rocks yield ages of about 540±60 m.y., which agree with many other results obtained to the south, from rocks of the Ribeira Fold Belt.

The rocks of the Paraiba do Sul Belt form the escarpments of the Serra do Mar and Mantiqueira and form the Paraiba do Sul Valley (fig. 22), which is part of a large graben. It folds and main faults strike ENE in Sao Paulo, but to the north the trend gradually changes to NE and NNE, parallel to the present coastline (fig. 22).

3.5.2.2. The Ribeira Fold Belt in Sao Paulo, Parana, and Santa Catarina States

In the states of Sao Paulo, Parana, and Santa Catarina (fig. 21), the Ribeira Fold Belt is represented by sediments deposited in a late Precambrian geosyncline. These sediments are assigned to the Sao Roque Acungui and Brusque groups (Table 14). These sequences are composed of phyllites, schists, quartzites dolomites, and limestones with subordinate metaconglomerates, metaarkoses, metagraywackes, and itabirites (Hasui et al., 1969; Marini et al., 1967). The rocks exhibit a greenschist metamorphic facies rising locally to the amphibolite facies, particularly near the coast. Although transitions from the migmatitic-gneissic complex to the epimetamorphic rocks of the Sao Roque and Acungui groups have been described (Melif et al., 1965), it is very difficult to distinguish in this complex the younger rocks from those that probably belong to the trans-Amazonian cycle.

A large number of granitoid bodies are found along the Ribeira Fold Belt (fig. 18). Some are adamellitic granites or granodiorites often porphyroblastic of synkinematic origin. Other are post-tectonic bodies with a subalkaline character as the Serra da Graciosa granites in the state of Parana (Fuck et al., 1967), or are orthoclase-bearing pink granites as the Itu Granite (Hasui et al., 1969). The granitization process is associated with Pb, Ag, Au, Zn, Sn, W, Cu, mineralization.

Cordani and Bittencourt (1967), in a K-Ar geochronologic study, concluded that the sedimentation of the Acungui Group is older than 650 m.y., the metamorphism occurring between 650 and 600 m.y. The post-tectonic granites intruded into the group have ages ranging from 580 to 500 m.y. These ages coincide with those obtained for the Caririan area in northeastern Brazil (Almeida et al., 1968).

The final events in the evolution of the Ribeira Fold Belt consisted in the development of intermontane basins located within fault depressions which were then filled with molassic red detritic sediments and andesitic-rhyolitic volcanic rocks. Such basins, which characterize the transition stage of the consolidation process of the fold belt (Almeida, 1967), are represented by the Castro Group (Trein and Fuck, 1967) (Table 13) and the Camainha (Muratori et al., 1967) and Guaratubinha (Trein and Fuck, 1967) formations at Parana, as well by the Itajai Group and volcanic rocks from Campo Alegre in Santa Catarina. The beds lie unconformably over the Ribeira Fold Belt and are generally not folded, but deformed by faulting. The rocks are unmetamorphosed, and radiometric dating indicates a Cambro-Ordovician age for the associated volcanism at the Ribeira Belt and in other belts of the same cycle.

The metasedimentary and metavolcanic rocks of the Ribeira Belt in this region exhibit an intense linear folding, generally northeast trending. Faulting is conspicuous, and large transcurrent faults have been recognized (fig. 3), such as the Texaquara fault in Sao Paulo (Hennies et al., 1967) (fig. 22). The deformation does not present a clear polarity and the position of the foreland is not known. Some geologists assume it to be hidden under the Paleozoic sediments of the Parana basin (region A6b in fig. 2), whereas others believe that it was located in the region now submerged by the Atlantic Ocean.

3.5.2.3. The Ribeira Fold Belt in State of Rio Grande do Sul

In the state of Rio Grande do Sul (fig. 21), the sediments that accumulated in the Ribeira Belt are represented by the Porongos Group and younger volcanic and detrital rocks. The Porongos Group (Table 15) is composed of a large variety of phyllites, schists, quartzites, limestones, metaconglomerates, metagraywackes, metaarkoses, and rhyolitic, andesitic or pyroclastic metavolcanics. Greenschist facies metamorphism is common in those rocks, but locally the metamorphic grade rises to the amphibolite facies with the formation of gneisses, amphibolites, and marbles with associated

migmatization and granitization. These rocks constitute the Cambai Formation of the Porongos Group (Ribeiro et al., 1966) in the eastern part of that state. Basic and ultrabasic intrusives of ophiolitic character (Goni, 1962; Issler et al., 1967) are associated with the metasediments of the Porongos Group. It is important to notice that ophiolites are exceptional in the Brazilian cycle geosynclines, whereas synorogeanic granite and granodiorite bodies are common.

The Precambrian rocks of Rio Grande do Sul state are cut by large fault systems (Picada, 1968). The Vigia-Roque lineament (fig. 3) with a N 40°E orientation is a normal fault which separates the Cambai Formation to the east from other rocks of the Porongos Group to the west. In turn, the Porongos belt is cut by large left-lateral transcurrent faults (approximately N-S strike), N 30°E-trending large normal faults, and N 70° W-trending minor normal faults. Such fault systems partially determine the location of molasse basins, subsequent volcanism, and mineralization in the region.

The Bom Jardim and Camaqua groups (Table 15) represent the molasse deposits of the final events of the Brazilian cycle in Rio Grande do Sul State (Ribeiro et al., 1966; Tessari and Picada, 1966). They are composed of continental detritic sediments, some of which are polymitic conglomerate. These rocks are weakly or nonmetamorphosed and affected only by fault deformation. Lavas and pyroclastic rocks of andesitic, rhyolitic, and dacitic composition are associated with the sediments, which are also intruded by later granite and granodiorite bodies, one of which is a rapakivi-type granite (Goni, 1961). Age determinations on the eruptive rocks indicate that these events occurred during the Cambro-Ordovician.

The basement of the Brazilian geosyncline in the state of Rio Grande do Sul is represented by the Eucantadas Formation (Table 15) (Tessari and Picada, 1966; Ribeiro et al., 1966). In the southeast of Uruguay this basement is probably locally exposed, but on the basis of present information it is difficult to separate such rocks from similar ones which originated at the end of the Precambrian.

3.5.2.4. Magnetic Anomalies

The magnetic anomaly pattern in the Ribeira fold belt may be divided into two different portions (fig. 9). The northern portion which includes the state of Espirito Santo and Rio de Janeiro (fig. 21), is associated with a magnetic anomaly low (the southern portion of C4 in fig. 9) having a ENE-WSW trend. This trend extends east-northeastward into the Atlantic Ocean. The southern portion, which includes the state of Rio Grande do Sul, Santo Catarina, Parana, and southern part of state of Sao Paulo (fig. 21), is associated with a magnetic high (A3 in fig. 9) having a NNE-SSW trend, and this positive anomaly extends along the southeastern continental shelf of South-America into the Atlantic Ocean basin.

3.5.2.5. Gravity Anomalies

On both the Bouguer and Free-Air gravity maps (fig. 10, 11), the Ribeira Fold Belt is located at the southeastern boundary of a large gravity low (A in fig. 10, 11) that includes the Sao Francisco Craton, Central and Northern part of Parana basin and even extends into the southern part of Parnaiba basin.

On the Bouguer gravity map, the negative anomaly trend extends from the Propria Fold Belt (A6 in fig. 10) along coast into the central part of the Ribeira Fold Belt. The magnitudes of anomalies decrease from the coast into the continent. In contrast, the gravity anomaly trend (C1 in fig. 10) is perpendicular to the coastal line in the southern part of the Ribeira Fold Belt and the magnitudes of the anomalies increase from north to south. Positive gravity anomalies appear in Uruguay.

On the Free-Air gravity map, however, most areas of the Ribeira Fold Belt show positive gravity anomalies especially in the state of Parana (A7 in fig. 11).

3.5.2.6. Correlation

Basically, most areas of Ribeira Fold Belt are similar to the Caririan-Propria Fold Belt to the north which shows high positive magnetic anomalies. These positive anomalies are apparently associated with metamorphic and volcanic intrusive rocks (Table 13, 14, 15 and fig. 18). We may divide the Ribeira Fold Belt into three portions from north to south:

(1) The northern portion (including the state of Rio de Janeiro and southern part of state of Espirito Santo) (fig. 21, 22): Negative magnetic anomalies (south portion of C4 in fig.9) and negative Bouguer gravity anomalies occur in this area. Metasedimentary rocks and volcanic intrusives are the main formation and they are apparently non-magnetic. The existence of magnetic lows is probably influenced by the large anomaly low (C4 in fig. 9) that occurs at the southern part of Sao Francisco Craton (Quadrilatero Ferrifero, in central Minas Gerais, fig. 15) and extends east-northeastward into the adjacent ocean basin (more details in Sec. 3.2).

(2) The central portion (including the state of Sao Paulo, Parana and Santo Catarina) (fig. 21): A high positive magnetic anomaly (A3 in fig. 9) and moderately low Bouguer gravity anomalies occur in this area. Metamorphic, metasedimentary and volcanic rocks are the main formations of the fold belt. However, a large number of granitoid bodies (fig. 18) and itabirites (hematite ore) have been found that may be the major contributor to the high positive anomalies. Positive Free-Air gravity anomalies along with negative Bouguer gravity suggest a fairly thick crust with low density rocks.

(3) The southern portion (including the state of Rio Grande do Sul and northeastern part of Uruguay) (fig. 21, 23): A high positive magnetic anomaly (A3, fig. 9) occurs along the coast line at about latitude 30°S. A NNE-trending gradient of this anomaly extends through the central part of the fold belt. This gradient matches well the geological structural trend (fig. 23). Both Bouguer and Free-Air gravity anomalies

have positive values in this regions. Basic and ultra-basic eruptives of ophiolitic character (Goni, 1962; Issler et al., 1967) may be associated with these high magnetic and gravity anomalies. The total anomalies probably reflect a larger crustal feature.

3.6. Rio de La Plata Craton

3.6.1. General Geology

The Rio de La Plata Craton (region A6, in fig. 2) is mainly covered by Phanerozoic sediments. It includes the southeastern region of Uruguay, the La Plata River region, the basement of the Province of Buenos Aires, northeast Argentina, and the small areas of Sierras Tandil, Azul, and Bayas (fig. 23). The Rio de La Plata Craton is possibly an extension of the Amazon Craton (region A1 in fig. 2), but the Phanerozoic cover makes it difficult to establish its limits and its relation to the Central Braziiian Shield (region A16 in fig. 2) to the northwest. This craton, was consolidated by upper Precambrian time, and probably represents the southmost Precambrian occurrences in the Atlantic coastal region. Basement rocks of northern Patagonia, previously considered to be Precambrian, are mainly Paleozoic accordingly to recent geochronologic studies (Stipanicic et al., 1968; Halperu, 1968). It indicates that the South-America Platform (region A in fig. 1) does not continue beyond the Colorado River in Argentina.

3.6.2. The Rio de La Plata Craton in Uruguay

The Rio de La Plata Craton in Uruguay is shown on fig. 23 (location A1). In this area, the Lavalleja Group (Caorsi and Goni, 1958; Bossi et al., 1965) (Table 16) seems to be equivalent to the Porongos Group of the Ribeira Fold Belt in the state of Rio Grande do Sul (Table 15). It is composed of phyllites, schists, quartzites, marbles, and basic metavolcanic rocks. The metamorphism is of the greenschist facies, locally rising to the amphibolite facies when gneisses and migmatization and granitization

phenomena appear. This group was strongly folded and faulted with a generally north-northeast orientation (but near Maldonado the trend changes to a north-south direction).

In southern Uruguay the Piedras de Afilar and Sierra de Animas Formations (Table 16) seem to represent molassic deposits and subsequent volcanic rocks of a late Brazilian cycle. The radiometric age of 500±30 m.y. (Bossi, 1966) is essentially the same as that obtained for rocks in similar geotectonic position in Southern Brazil. This confirms the suggestion that the late tectonomagmatic events of the Brazilian cycle occurred during the Cambro-Ordovician interval. The Piedras de Afilar Formation lies unconformably over the Lavalleja Group and is composed of sandstones, quartzites, and limestones slightly deformed but unmetamorphosed (Walther, 1927; Jones, 1956). The Sierra de Animas Formation is composed of trachytes, syenites, and rhyolites (Bossi and Fernandes, 1963).

It is possible that the structures formed during the Brazilian cycle surround the Rio de La Plata craton and underlie the continental shelf, emerging again at the Sierras Pampeanas in Argentina. This suggestion is supported by a 650 m.y. age determination (Cazeneuve, 1967) for the Pan de Azucar (Aguas Blancas) granite which forms the basement of folded Devonian beds in the Sierra de la Ventana region in southern Buenos Aires Province.

3.6.3. The Rio de La Plata Craton in the Province of Buenos Aires, Argentina

The basement of the Rio de La Plata Craton in the Province of Buenos Aires (region A2 in fig. 23) is composed of a gneisses complex of metasedimentary origin, associated with amphibolites, mica schists, phyllites, and quartzites. It was affected by migmatization and granitization during at least one tectonic cycle. This resulted in the formation of several types of migmatites, granites, granodiorites, tonalites, and diorites (Walther, 1948; Bonorino, 1950, 1954; Bossi et al., 1965; Quartino and Fabre, 1967). The planar features of this complex generally trend ENE-ESE, in contrast to the dominantly

NNE-ENE trending structures that are typical for the upper Precambrian of the continent (region B in fig. 23). Thick E-W and ESE mylonite and cataclastic rock belts indicate the presence of large faults, probably transcurrent, in the Sierra Azul in Argentina. Geochronologic studies (Cazeneuve, 1967; Hart et al., 1965; Stipanicic and Linares, 1969; Umpierre and Halpern, 1971) yield radiometric ages of around 2,000 m.y. indicating that the Rio de La Plata Craton consolidated at the end of the Trans-Amazonian cycle as did the other ancient cratonic areas of the South-American Platform.

Near Sierras Bayas the basement of the Rio de La Plata Craton is partially covered by the La Tinta Group (Table 17). This group consists of unmetamorphosed and weakly deformed sediments which are about 100 m thick and composed of sandstones, quartzites, limestones, dolomites, and fine-grained detrital sediments. These rocks have been assigned a Paleozoic age and are believed by several geologists (Amos, Almeida, Amaral, and Cordani) possibly to represent an Eocambrian cover similar to those occurring in Brazil and Paraguay.

3.6.4. Parana Basin and Chaco Basin

The Parana basin (A6b, fig. 2) and Chaco basin (A6a, fig. 2) are two of the great synclines in the South American Platform. The Parana basin is an intercratonic basin with substable, subnegative, and undeformed units interposed between the cratonic areas and superimposed on a former Precambrian geosyncline. However, the Chaco basin is a pericratonic basin with sub-mobile, subnegative, and sub-deformed units located along the western border of the cratonic and intercratonic areas (Harrington, 1962).

The sedimentary cover of the South American Platform dates from the Silurian. It is well developed in the Parana and Chaco basins, where the thickness of sediments and associated basalts may reach 5,000 m (fig. 4). The first stage in the evolution of the sedimentary cover started with almost exclusively marine sedimentation during the

Silurian and Devonian, with mixed character during the Carboniferous, followed by continental sedimentation during the Permian and Triassic. This third stage indicates the period of greatest stability of the platform. There were enormous volcanic outpourings of predominantly quartz-tholeiite basalt lava in Gondwanaland during the Jurassic and Cretaceous. The Cretaceous lavas are located along or near separated continental margins and are well-preserved in the great Parana basin (fig. 18). The Parana basalts of Brazil cover an area of 1,200,000 sq km. Some alkaline and alkaline-ultrabasic volcanic rocks, dating from the end of the Jurassic to the Eocene, are known in Brazil and in eastern Paraguay. Carbonatites and kimberlites are associated with them (Tectonic map of South America, 1978), the latter being the source of important diamond deposits. Sediments formed between the Jurassic and the Quaternary almost entirely mask the western limit of the platform, therefore, very little is known. Similar sedimentary cover also obscures the relation in the Chaco basin.

3.6.5. Magnetic Anomalies

The Rio de La Plata Craton in Uruguay and the southern part of the Parana Basin lie along strong positive magnetic gradient (western part of A3 in fig.9), which has a north-to-northeast trend and increases in magnetic intensity from continental areas to coastal regions. The area of the Parana Basin also shows positive magnetic anomalies, but the magnitude is not as high. Another magnetic maximum (B5 in fig. 9), having an intensity of less than 8 nT, occurs at the central part of the basin.

In contrast, the region of the Rio de La Plata Craton in the Province of Buenos Aires, Argentina, and the entire area of the Chaco Basin shows moderately low negative magnetic anomalies. Two different magnetic trends occur, one having a north-to-northeast direction in the northern part of the Chaco Basin (D1 in fig. 9); the other having a southeast trend in the province of Buenos Aires (D2 in fig.9). Both of these trends extend toward the central part of the Andes where a large magnetic anomaly low occurs (C5 in fig. 9).

3.6.6. Gravity Anomalies

Both the Bouguer and Free-Air gravity anomaly maps show that negative gravity anomalies occur in the central and northern part of the Parana Basin (fig. 10, 11). The minimum Bouguer value is less than -120 mgals (A7 in fig. 10) and the minimum Free-Air anomaly is less than -40 mgals (A8 in fig. 11). These negative anomalies are also part of a larger series of gravity lows that occur along the whole eastern part of the South-American Platform (A in fig. 10, 11).

Positive Bouguer (C in fig. 10) and Free-Air (D in fig. 11) gravity anomalies occur in most areas of the Chaco basin and in Rio de La Plata Craton. This positive gravity anomalies start at the mouth of Rio de La Plata and extend north-to-northeastward into the northern part of the Chaco basin. The width of the anomalies becomes narrower from southeast to northwest.

3.6.7. Correlation

The basement of the Rio de La Plata craton in Uruguay is composed of metamorphic and basic metavolcanic rocks. Syntectonic granitoids, including migmatites, and Cretaceous baslt also occur in large volume (fig.18). These areas coincide with strong positive magnetic anomalies. In addition, the basement group of Rio de La Plata craton is strongly folded and faulted with a generally north-northeast orientation which is the same trend as the positive magnetic anomaly gradient. These positive magnetic anomalies along with the anomalies of Ribeira fold belt are part of a larger series of north-to-northeast-trending magnetic highs (A3 in fig. 9) that occur along the southeastern continental shelf of South America and extend into the Atlantic Ocean Basin.

The Parana basalts of Cretaceous age (fig. 18) cover most regions of the Parana basin (around 1,200,000 sq km) and are associated with positive magnetic anomalies.

The magnetic maximum of these anomalies (B5 in fig. 9) occur at the center of the basin which is probably associated with the ultrabasic volcanic rocks in nearby eastern Paraguay.

A large Bouguer gravity anomaly low (A7 in fig. 10) occurs at the central and northern part of Parana Basin. It indicates that a considerable thickness of continental crust covers most of the eastern South-American Platform.

Basically, the negative magnetic anomalies and the positive gravity anomalies that occur in the Chaco Basin and the Rio de La Plata Craton in the Province of Buenos Aires are associated with the Argentina aulacogen, which extend from the area between the Rio de La Plata and Rio Colorado to the central part of Chaco basin. Cenozoic sedimentary rocks cover most regions of these areas. The big rivers of Parana and Salado follow the trend of the aulacogen (fig. 23), as does the Amazon River in the Amazon Basin.

Also worthy of mention is the fact that the Corumba-Cuiba basin (Basin 19 in fig. 4), is located at the magnetic minimum (D1 in fig. 9) (less than -12 nT) and Bouguer gravity maximum (C2 in fig. 10). The Corumba-Cuiba basin contains a maximum thickness of 500 meters of Cenozoic sediments and is surrounded by Paleozoic and Precambrian deposits. It should be one of the areas of thinnest continental crust in South America especially between the great thickness of the Andes and the large eastern part of South-American Platform.

CHAPTER 4

GEOLOGY OF THE PATAGONIAN PLATFORM AND ITS RELATION TO MAGNETIC AND GRAVITY ANOMALIES

4.1. General Geology (also see Sec. 2.2)

The Patagonian Platform (fig. 5 and 24) occupies the broad southeast continental margin of South America. The eastern or Atlantic portion of the platform forms a broad continental shelf (fig. 24) that is the largest in South America, ranging in width from 240 km at the latitude of the Rio de La Plata (lat. 40°S) up to 500 km at the latitude of the Malvinas Islands (Falkland Islands, lat. 50°S). The continental platform has no marked topographic form, and the change from continental platform to continent slope and continental rise is gradual.

The basement of the Patagonian Platform is almost entirely covered by younger sediments and is, therefore, little known. The radiometric data within the Northern Patagonian and Deseado massifs (Southern Patagonian, fig. 5) indicate upper Paleozoic and lower Mesozoic ages only; no Precambrian dates have been obtained (Urien and Zambrano, 1973). Igneous plutons, dikes, and sills (both acid and basic) of Paleozoic to Quaternary age are present in the basement, and they may be the cause of the marked velocity differences and seismic layering which has been observed from the so-called technical basement (Ewing et al., 1963; Ludwig et al., 1968). The structural trend of this "technical" basement differs from those observed in the post-late Jurassic sedimentary fill. A striking example of this is seen in the Lago San Martin area (fig.

5), in southwest Patagonia, near the Andes, where basement structures trend east-west, and those observed in the Cretaceous sedimentary cover are directed north-south.

The eastern continental margin of Argentina is of Atlantic type, characterized by stable continental blocks (without seismic activity). It has been subjected to little or no tectonic deformation since at least upper Paleozoic or lower Mesozoic times (Zambrano and Urien, 1970), except for the tectonic activity and change in structural trends which took place in Late Jurassic or Early Cretaceous times. South of latitude 35° S the elongated marginal-type basins change from parallel to the shore line (north of basin 13, fig. 4) to a new basin type that is perpendicular to the continental margin (fig. 24); south of basin 14, fig. 4).

From the Sinemurian (lower Jurassic) to the Bajocian (middle Jurassic), marine transgressions flooded the larger part of the Patagonian Platform and gave rise to sedimentary cover. The withdrawal of the sea was followed by intense acid volcanism during the Bathonian (middle Jurassic, above Bajocian). Important tectonic activity during the upper Jurassic corresponds to the inter-Malm movements (Araucane Phase) of the Andean region. The formation of a dense network of large faults led to the creation of the basins. In other words, the basins of Patagonian Platform originated as a result of post-Jurassic tectonic processes. Basins created by this tectono-magmatic reactivation are nearly contemporaneous with those basins of the South American Platform and underwent maximum subsidence during the Cretaceous.

Pre-upper Jurassic units crop out in the area, or are present in the subsurface, and are composed of igneous and metamorphic rocks together with indurated sediments which, due to consolidation, have acquired the accoustic properties of true basement rocks.

The basins developed in the continental margin of Southern Brazil and Argentina can be divided into four main types (fig. 24):

(1) Marginal basins which include the Santos, Pelotas basins of southern margin of Brazil (12, 13, fig. 4). The main depositional axes trend to be parallel to the continental margin and the basins are totally or almost totally submerged.

(2) Basins transversal to the craton (such as the Salado basin, fig. 24) or pericratonic types (such as the Colorado basin, fig. 24). These basins are open at the continental edge but have their western part within the continent itself. The main depositional axes seem to be perpendicular to the continental margin.

(3) Intracratonic (such as the Canelones basin, fig. 3) or interneo–cratonic basins (such as the Valdes and SAn Jorge basins, fig. 5, 24) together with scattered "pocket" basins. These basins are not open at the continental edge and occur either within the continent or lie totally within the submerged continental platform.

(4) True geosynclines (such as the Magallanes and Malvinas basin IV, V, fig. 24) where the depositional axes parallel the Andean cordillera and its submerged prolongation.

The basins are filled with Cretaceous, Tertiary, and Quaternary sediments. Except in the Magallanes and probably in the Malvinas basins, the Cretaceous units are generally nonmarine. The oldest marine sediments found up to the present time are of Masestrichtian (Upper Cretaceous) age.

During the Cenozoic, and at a distance from the Andes, the platform tectonics were less severe than during the Cretaceous. In the Paleocene, subsidence in many areas of the platform enabled Atlantic waters to invade as far as the south–east border of the Somun Cura Massif (fig. 5).

At a distance from the Andean chain, the tectonic stability of the Patagonian Platform, from the Miocene onward, is evidenced by marine deposits covering wide

areas and by continental deposits. Severe volcanism, mainly basaltic, took place over the greater part of the platform from the Miocene to the Quaternary. The entire platform is at present undergoing epeirogenic uplift as shown by terraces of Pliocene-Quaternary age which exists along coastal areas of the Patagonian Platform.

4.2. Magnetic Anomalies

The magnetic anomaly pattern over the northern Patagonian Platform shows a positive gradient (B6, fig. 9) which increases from the continent (west) to the coastal area (east) away from the Andean Fold Belt. In addition, a northwest-trending arm (T1, fig. 9) of the positive anomalies extends from the Colorado basin into the Andean Fold Belt. No magnetic anomaly data is available in the southern part of the platform.

4.3. Gravity Anomalies

The Bouguer gravity anomaly pattern (fig. 10) in the Patagonian Platform is elongate in shape with a north-south trend that essentially parallels the coast line and the Andean Fold Belt. These anomalies are moderately low (between 0 and -50 mgals) in most areas and increase the magnitude from west to east away from the Andean Fold Belt. The positive anomalies occur locally in the eastern coastal area.

The Free-Air gravity anomalies are moderately positive and between 0 to +30 mgals (fig. 11). A large gravity maximum (E in fig. 11) with magnitude higher than +60 mgals occurs at the northern part of the platform. Two other small gravity maxima with magnitudes less than +40 mgals are located at the central part (E1 in fig. 11) and southern coastal areas (E2 in fig. 11), respectively. A negative Free-Air gravity anomaly with a northwest trend (T1 in fig. 11) occurs at the northern border of the Patagonian Platform and separates this platform from the South-America Platform to the north.

4.4. Correlation

The Patagonian Platform includes the continental region of South America south of roughly 40° S and east of the Andes. The elevation of this Platform (fig. 16), influenced by the Andes on the west, is lower from west to east away from the Andean Fold Belt. According to isostasy, the thickness of the continental crust should decrease from west to east away from the Andes. The Bouguer gravity anomalies of the platform, which decrease westward, indicate that isostatic compensation does exist under the Patagonian Platform, and that these anomalies are a function of crustal thickness.

At the same time, a consideration must be made of the low positive Free-Air anomalies that occur in the eastern part and high positive Free-Air anomalies that occur in the western part of the platform. One possible interpretation is that the crust under the eastern platform has better compensation than the western part. As regards the gravity maxima, some of these anomalies which occur at the northern (E, fig. 11) and central (E1, fig. 11) part of the platform may be associated with high density volcanic rocks of Mesozoic and Cenozoic age (fig. 18). In other words, both of the positive anomaly maxima (E and E1, fig. 11) occur in areas where thick Mesozoic and Cenozoic volcanics deposits are present. The last of these gravity maxima (E2, fig. 11) occurs in the southern coastal area (Tierra del Fuego, fig. 5). This positive anomaly suggests that appreciable mafic igneous rocks may be present in the deeper parts of this area or that a very thin continental crust may underlie this gravity maximum.

Both magnetic and Free-Air gravity maps show a second set of anomalies; these trend northwestward (T1, fig. 9 and 11) in the northern part of the Patagonian Platform. The magnetic anomalies are positive (0 to +10 nT) and the Free-Air anomalies are negative (0 to -10 mgals). This anomaly trend does not occur on the Bouguer gravity map. It may reflect a buried geological structural trend which is covered by younger sediments.

Because of lack of magnetic data in the southern part of the Patagonian Platform, correlation between the geologic features and the magnetic data is restricted.

CHAPTER 5

GEOLOGY OF THE ANDEAN FOLD BELT AND ITS RELATION TO MAGNETIC AND GRAVITY ANOMALIES

5.1. Geology

1. Northern Section

The northern section includes the Andes of Venezuela, Colombia and Ecuador. A longitudinal graben-like fault (the Cauca and the Romeral faults, fig. 3 and 25) divides the Northern Andes into two domains in Colombia and Ecuador: the Occidental Cordillera in the west, and the Central and Oriental Cordillera in the east. The Western Cordillera is characterized by thick tholeiitic volcanics dating from the Late Mesozoic which are associated with equally thick pelitic, in part slightly metamorphic, sediments. The "Basic Igneous Complex" has been interpreted as a Late Mesozoic island arc or as an oceanic element that welded to the overall orogeny during the Tertiary. In contrast, the Central and Oriental Cordillera are regarded as sections of continental crust. Gabbro and serpentinite as well as greenstone, diabase and pillow-basalt of the "Diabase Formation" occur at the boundary of these two units (the Cauca and the Romeral faults).

The Andean metamorphic basement in Colombia crops out in the Sierra Nevada de Santa Marta (Central Cordillera), Santander Massif (Oriental Cordillera), Guajira peninsula, as well as in the Central and Oriental Cordillera. These amphibolite to granulite grade metamorphic rocks, dating from 700 m.y. to 1,300 m.y., confirm the

existence of Pre-Brazilian elements in the basement of the Andean Cordillera in this region.

In Ecuador, the metamorphic basement of greenschist to amphibolite facies is migmatized and granitized. These rocks are known to occur only in the Oriental Cordillera, where they are regarded as the southern extension of the Central Cordillera of Colombia. According to Herbert (1977) locally highly metamorphic to ultrametamorphic rocks are also Present in the region.

In summary, Precambrian rocks of the northern Andes are rarely present and those that are all belong to the upper Precambrian. The main volume of metamorphic basement rocks are probably Paleozoic in age. These rocks are generally characterized by low-grade metamorphism which possibly occurred during the pre-Devonian "Caledonian" orogeny. This orogeny affected the basement of the Central and Oriental Cordilleras as well as their northern and northeastern continuation in Venezuela and the Oriental Cordillera in Ecuador. It is uncertain whether any links exist with non-Andean upper Precambrian shield rocks, but such links are possible. However, the Occidental Cordillera chains do not contain any of these old substructures. As Mesozoic and Cenozoic intrusive bodies have extensively penetrated into all of the main structural units of the region, it is not yet possible to determine whether relict Precambrian terranes are present or to what extent they have been modified by metamorphism.

2. The Central and Southern Section

The northern segment of this section lies in Peru, Bolivia and northern Chile; the Chile-Argentinian chain constitutes the southern segment. The NW structural trend of the northern segment changes to N-S near latitude 18°S. The southern segment strike NNE-SSW along Pliocene-Quaternary faults and transverse to the NNE-SSE paleographic grain.

The Andean sedimentary cycle started in the northern segment during the upper Triassic and continued until the upper Cretaceous, filling troughs parallel to the general trend of the chain. The sediments are mainly detrital. with no flysch, and extend into the eastern Andean area of Peru. From the Triassic onwards, intense volcanic activity, mainly andesitic, with subordinate rhyolites, dacites and basalts, were associated with the sedimentation.

The Andes have a geosynclinal character from roughly south of latitude 40°or 42° S. They strike N-S in the Patagonian Cordillera, changing gradually to E-W in the Magellan Cordillera and Tierra del Fuego (fig. 21). There is little information available on the eugeosynclinal domain, where marine sediments of upper Jurassic age are associated with basaltic pillow lavas. The formation is particularly well developed in Tierra del Fuego. Deformation took place in the upper Jurassic but is poorly characterized and appears to be associated with intrusive granites. Middle to upper Cretaceous movements are very important, especially in Tierra del Fuego, causing folds and reverse faults. Within the miogeosynclinal domain, sedimentation started in the Oxfordian (upper Jurassic) and includes thick flysch deposits of Aptian (lower Cretaceous) to macestrichtian (upper Cretaceous) age. This was followed, in stratigraphic continuity, by marine molasse deposits which extend, with minor continental interbeds. until the Miocene.

The metamorphic basement in the Coastal and Oriental Cordilleras of the Peruvian Andes, has been described by Steinmann (1929). They are an old group of gneisses, mica schists and granites and a young group of phyllites and quartzites. The age dates are between 679 ± 12 and 642 ± 16 m.y.

In the Bolivian Andes weakly metamorphosed rocks are mentioned from the southern part of the Oriental Cordillera (Zeil, 1979). No ages and rock types are available.

In Chile the Coastal Cordillera is composed largely of metamorphic basement rocks which have been described by Miller (1970), Gonzalez Bonorino (1970,1971), Corvalan and Munizaga (1972) and Munizaga, Aguirre and Herve (1973). Only isolated small amounts of the pre-Andean basement crop out in the area of the High Cordillera. Regionally metamorphosed crystalline schist and phyllites of greenschist facies are the main rock types of the Coastal Cordillera. The age of these rocks and of the regional metamorphism is between 273 and 342 m.y. (Munizaga, Aguirre and Herve, 1973).

In the Argentinian portion of the Andes the metamorphic basement rock is exposed mainly in the northern section and in the eastern chain. Whereas old complexes are almost entirely missing from the Cordillera Principal, metamorphic series are distributed to varying degrees in the Precordillera and the Puna (fig. 7). The metamorphic series in Precordillera are composed mainly of mica schists, gneisses, marbles and amphibolites. While granite and migmatites are rare, large bodies of basic and ultrabasic intrusive rocks occur (Caminos, 1972). As in the Puna, granodioritic intrusions occur with a radiometric age of 530±20 m.y. (Turner, 1972). Turner (1972) also mentions a thick Precambrian metamorphic basement rock in the Cordillera Oriental between 22° and 25° S. This is the only definite Precambrian material in Argentina because it is clearly overlain by Cambrian sediments. The degree of metamorphism is in greenschist facies and no rock types are available.

5.2. Gravity Anomalies and Correlation

In general, the Bouguer gravity anomalies of the Andes form a tremendous low that reflects the great thickness of the continental crust under the fold belt (fig. 10). In contrast, the Free-Air gravity anomalies (fig. 11) are generally positive, forming a very high positive pattern in the highest parts of the Andes (fig. 16). Both the Bouguer and Free-Air gravity anomalies show a distinct trend that parallels the western coast of South America and the Andes Fold Belt.

In the northern Andes, a Bouguer maximum (D1, fig. 10) is developed in the coastal zone west of the Occidental Cordillera. This gravity high extends from Panama to Ecuador and indicates a thin crust or a significant substructure made up of low-silica igneous rocks. On the other hand, in the Central Cordillera negative gravity values down to -220 mgals occur (D2 in fig. 10). This reflects a crustal thickness of approximately 45 km in the area along the Ecuador border (Zeil, 1979). Compared with the 70 km-thick crust at the bend of the Andes to the south (D in fig. 10), it must be assumed here that the substructure in the northern Andes underwent a different tectonic development.

According to Case, Duran, Lopez and Moore (1971), Gonzalez and Vina (1973), and Case and McDonald (1973) the northern part of Colombia down to about the Cauca depression (fig. 3) is underlain by a relatively thin crust between 20 and 30 km thick. This apparently contributes to the positive gravity values. The thickness of the crust increases, but not significantly, from there on towards the east in the region of the Central Cordillera and the Oriental Cordillera. In the area of the border between Colombia and Ecuador positive gravity values indicate that an oceanic crust probably exists from the coast towards the east up to the western slope of the Occidental Cordillera (150 km away from the coast). From there on, however, as far as the region of the Central Cordillera, a continental crust up to about 45 km thick exists (Zeil, 1979).

In the central Andes, along the bend of the fold belt at the approximate latitude of 15^{o}-25^{o}S in the area of the Altiplano (fig. 25), extremely low Bouguer gravity anomalies of down to -400 mgals exist (D in fig. 10). The continental crust in this region is estimated to be about 70 km (Zeil, 1979). In this same central section of the Andes hypocentres of recent earthquakes are distributed statistically on a distinct plane (Benioff zone) dipping eastward from the Pacific under the continent. From this bend in the Andes, lines of high negative gravity values extend south to about latitude 35

S. These values correspond to a large extent to the topography of the range. A −250 mgal anomaly extends as far south as latitude 34°S (San Tiago) (D3 in fig. 10). The thickness of the crust decreases to about 55 km farther south, and to the east at the point where the Andes merge with their eastern foreland normal continental crustal thickness of 30–35 km is present (Dragicevic, 1970).

5.3. Magnetic Anomalies and Correlation

A large magnetic anomaly high of over +12 nT occurs along the Cordilliera of Colombia (A4 in fig. 9), and positive anomalies occupy most areas of the northern part of the Andes (north of latitude 16 S). The only exception occurs in the northern portion of Peru where a low (D3, fig. 9) is present. In contrast, a large magnetic anomaly low (C5 in fig. 9) of less than −12 nT occurs in the central part of the Andes, and negative anomalies occupy most regions of the central and southern Andes.

The trends of these magnetic anomalies do not, in general, parallel the gravity anomalies and follow the north–south structural trend of the fold belt, but instead have a general east–west pattern. This pattern is common over most of the MAGSAT map and is probably related to procession noise derived from data reduction procedures to correct for external magnetic field effects. However, the pattern over the Andes is sufficiently distinct from the generally north-trending magnetic anomalies occurring in the adjacent Pacific Ocean to reflect the boundary between the leading edge of the South America Plate and the oceanic Nazca Plate.

The metamorphic basement plays a very important role in the large anomaly high that occurs in the Cordillera of Colombia. The basement crops out mainly in the Central and Oriental Cordilleras. Exposed are metasediments and metavolcanites of high metamorphic grade (granulite facies is common) which are locally migmatized and intruded by granite, ultrabasic and other intrusives. Furthermore, the Occidental Cordillera of Colombia is associated with a "Basin Igneous Complex", and the intra-

Andean ridge contains very thick submarine basic Cretaceous lavas which are associated with the ultrabasic intrusions. These geologic complexes may in total be an important factor in causing the large magnetic anomaly high in Colombia (A4 in fig. 8). On the other hand, no metamorphic basement and few volcanic rocks occur at the northern portion of Peru. This may be the reason why a magnetic minimum (D3 in fig. 9) occurs in this portion of the northern Andes.

As regards the region of the central and southern Andes (south of latitude 16 S), with the exception of the Coastal Cordillera of Peru and Chile and excluding also the chains of the Oriental Cordillera in the northern part of Argentina, metamorphic basement rocks are rarely present. Negative magnetic anomalies occur in most areas of this region. A large volume of Cenozoic sedimentary rocks characterizes the central part of the Andes where the continental crust reaches its maximum thickness. Granodioritic to dioritic rocks of Cenozoic age are also abundant. Thus, a large magnetic anomaly low (C5 in fig. 9) is associated with these Cenozoic formations. Attention is called to the fact that a deep-sea trench is well-developed along the Pacific margin in this region of the central Andes. According to the plate tectonic theory deep-sea trenches form as a result of the subduction of lithospheric plates at the margins of continents. These trenches, having maximum depths of 8,055±10 m (Fisher, 1974), are characterized by seismically active zones and minimum Bouguer gravity anomalies. These trenches along with two large Cenozoic continental grabens (fig. 6) may significantly influence the magnetic anomalies that occur at the central section of the Andes.

CHAPTER 6

GRABENS AND AULACOGENS

Several types of grabens and aulacogens (or aulacogen-like) structures exist in South America (fig. 3). Each has its own characteristics, and the origin and development of most of them can be tied to plate-tectonic movements. These structures are thus important and interesting features.

The grabens in the Andes are true grabens. They are bounded by normal faults on both sides and are probably caused by deep fractures associated with geanticlinal uplift. In contrast, the Rio Orinoco structure (fig. 3), which is located between the Guyana Shield and the Caribbean Mountain System, is not a true or well-developed graben but is better classified as a trough in which up to 5,000 m of sediments accumulated along an E-W trend. Most of these sediments were deposited in post-Triassic time. Data is insufficient to establish whether or not this is an incipient rift system. The Takutu rift valley (fig. 3) is located at the inner-Guyana shield and is bounded by great faults on both sides. It contains sediments that are several kilometers thick and are believed to be the only Jurassic-Cretaceous formations in the shield. The Takutu rift is a probable aulacogen. A very similar structure occurs in the Amazon basin. The structure underlying the Amazon basin is regarded as a failed arm of a triple junction-the one that does not become a trailing edge of a continent. This basin has also been regarded as being an intercratonic basin and as an extensive and complex graben. In the uplifted cratonic area between the Amazon and Parnaiba basins, there are also several relicts of formerly connected basins. They are called cratonic fault

basins. Remnants are preserved as graben. For example, the Agua Bonita Graben and the Braganca-Jacunda Graben (state of Para) are structures of this type.

In the southern part of the South-America Platform and northern part of Patagonian Platform, two aulacogen-like structures are developed. Each has a large basin associated with it. These are the Salado basin and the Colorado basin (fig. 3). Both are marginal-type basins elongated perpendicular to the continental margin and were formed as a result of fracturing in the post-Cretaceous time.

6.1. The Grabens of the Andean Fold Belt

Large sections of the Andean Fold Belt are intersected by deep fractures that developed approximately at the same time as and parallel to the Cenozoic volcanic zones. Most of these faults can be described as "tectonic grabens". Such structures include the large longitudinal faults which are structural depressions between the individual Cordilleran chains in Colombia/Ecuador, in Bolivia, and in northern and central Chile (fig. 6). Their internal structural characteristics are largely unknown. However, the age of these inner-Andean longitudinal fractures can be approximately determined on the basin of material with which they are filled. They are certainly recent and their main development took place in the Cenozoic; they contain sediments that are between 5 and 15 km thick. It is necessary to use geophysical methods to study in detail the boundaries between these Andean macrostructures because they definitely extend deep into the crust, perhaps even as far as the mantle.

The recent volcanic regions of the Andes are located precisely along areas where the Andes are intersected by the graben-depressions. Both run parallel to the strike of the range (fig. 6). There is thus an apparent connection between recent fracture tectonics, strong uplift, and recent volcanic activity. In the northern Andes the volcanoes are situated in the Central Cordillera (fig. 6 and fig. 25), the basement of which is uplifted most strongly in block-like form. West of the intra-Andean ridge,

i.e. west of the Central Cordillera in Colombia (fig. 25), including its western flank, is a region of linear pericratonic troughs which developed on an oceanic crust. Gabbros and serpentinites as well as greenstones, diabases and pillow-basalts of the "Diabase Formation" have been found in this area. The region lying to the east of the intra-Andean ridge, i.e. the region between the Central and Oriental Cordillera, developed linear intracratonic troughs which are more or less clearly separated by massifs with pre-Cretaceous structures and which show a tendency to be uplifted.

The same connection between recent fracture tectonics, strong uplift and recent volcanic activity also holds true in the central section of the Andes (over a high-altitude plain at 3,500-4,000 m, the Altiplano, fig. 7, 25). In the southern section, despite the gradual decline in height, striking volcanic peaks are still present. As the thick volcanic products frequently do not permit exact identification of the conduits along which they were transported and as the age of the recent grabens is unknown, it is not possible to make any clear statement about the exact correlation between the volcanic activity and the recent tectonic events. However, it is inferred that the large volume of magma and the development of the linear large tectonic grabens are associated with the eastward subduction of oceanic crust along the continental margin and the concomitant geanticlinal Andean Mountain Range.

6.2. Takutu Rift Valley

The Takutu rift valley (fig. 3 and fig. 8) forms the southern boundary of the wide Guyana-Venezuela basin. The rift valley is about 65 km wide, trending east-northeast and containing sediments of several kilometers thickness of the Takutu Formation believed to be of Jurassic-Cretaceous age. South of the great fault bounding the southern edge of the Takutu rift valley is a range of mountains 60 km across that are underlain by rocks of the Kanuku Group (Barron, 1962; Singh, 1966). These rocks consist chiefly of banded biotite and biotite-garnet gneisses in the amphibolite and granulite facies, hypersthene gneisses, and charnockites (fig. 8).

An Rb-Sr isochron by Spooner et al. (1971) indicates that the Kanuku Group is at least 2,000 m.y. old and distinctly older than the typical Trans-Amazonian thermotectonic event that affected most of the rocks of the Guyana Shield. Thus it is possible that the foreland surrounding the great basin of northern Guyana and southern Venezuela may be the Imataca complex on the north and the Kanuku and correlated high-grade rocks on the south (fig. 8). Previously, some geologists have assumed that the Kanuku group was comparable in age to the Imataca (2,700-3,400 m.y.), namely older than 2,500 m.y., thus forming part of an Archean basement that rimmed the eugeosynclinal basin of northern Guyana. But, the younger date (at least 2,000 m.y.) by Spooner et al. (1971) has made the picture more complicated.

The great fault system outlining the Takutu rift valley can be traced to the east and northeast for some 400 km based on the correlation of pyroxene granulites and gneisses of the Bakhuys Mountains in Surinam, with associated charnockites of the Kanuku Group. These gneissic and granulitic rocks in western Surinam have been called the Coeroeni and Falawatra group. They appear to represent the uplifted basement on which the sediments of the Surinam-French Guyana basin were deposited. The faulted uplift of Falawatra basement has resulted in a physical separation of the remnant geosynclinal rocks of this eastern basin from those of the Venezuela-Guyana basin to the west.

The Takutu rift valley is clearly a major rift structure in the South American Platform. The rift is regarded as being an aulacogen (Burke and Wilson, 1976; Burke, 1980; Braile et. al., 1982) associated with continental breakup during Mesozoic time. The rift is remarkable similar in age, size, shape, and configuration to other continental rifts that formed during the opening of the central Atlantic Ocean.

6.3. Amazon Basin (Aulacogen)

A general description of the stratigraphy, geotectonic and structural pattern, volcanism and geologic history of the Amazon basin has already been given in Section 3.1.4. In this section, the different theories of origin are discussed. Three different theories have been proposed to explain the origin and present position of the Amazon.

The current most widely accepted theory for the origin of the Amazon basin is as a triple junction-aulacogen-rift structure (Burke and Dewey, 1973a). Figure 26 shows a developmental sequential model of early doming caused by a mantle plume and deep-seated axial dikes, followed by development of a triple junction rift network (rrr junction), development of an open ocean or a geosyncline and an aulacogen (the failed arm), and finally the formation of a mountain range during compression and the continued development of the aulacogen. Spreading may take place on any of the three arms. If it develops on all three, then three plates are formed, but if only on two, then the failed arm of the triple junction-the one that does not become a trailing edge of a continent-is a zone of weakness, that becomes a rift system. Consequently, it may localize a major river with a delta at its mouth. The typical example is the Niger River and its delta. This rifting is believed to be the cause of most aulacogens, which are long, narrow and deeply filled troughs that extend into cratons.

The structures shown on figure 27 are two Cretaceous triple junctions (Junction A shares one of its three arms with junction B) that joined South America and Africa. Two arms of each junction separate to form the South Atlantic. The third arm of each was abandoned and remains as the Benue Trough (Burke et al. 1971; Grant, 1971; Nwachukwu, 1972; Olade, 1975) and Amazon Basin, respectively. In addition, the same kind of structure is a Tertiary triple junction centered around the Afar Depression. Two arms (the Gulf of Aden and the Red Sea) have begun to separate, while the third (the Ethiopian Rift) failed to move.

A second theory on the origin of the Amazon basin was proposed by Grabert (1971). The Amazon and Parana drainage systems flow over a widespread lateritic cover that is up to 40 m thick. Grabert assumed that since the Triassic or even since the late Paleozoic most of this shield has been uplifted and exposed to weathering. He inferred that its paleodrainage was chiefly radial toward the surrounding seas and oceans. Thus its western rivers should have flowed into the Andean geosyncline. Uplift of the Andes during mid-Tertiary time reversed this patter, causing the Amazon to flow eastward (occupying the position of a structural low) and the Parana to flow southward subparallel to the strike of the Andes. Most probably a widespread inland lake developed during the early stages of this major drainage reorganization.

A third interpretation of the present position of the Amazon and the Parana rivers was suggested by de Rezende (1972). He has emphasized that tectonic control of two gigantic geofracture systems related to the separation of South America and Africa (fig. 28) localized the main drainage systems. Throughout much of its lower course the Amazon does occupy a combined graben and/or linear structural low which preserves lower Paleozoic sediments as a long, narrow belt extending across the Brazilian Precambrian shield with notable parallelism of rivers and lineaments within it. It has also been suggested that the Parana in far south-western Brazil and adjacent Uruguay and Paraguay follows the axis of greatest thickness of Cretaceous basalts (fig. 18) simply because the crust is depressed by their extra weight (Cordani and Vandoros 1967).

Structural control

There is a general consensus that old sutures or vertical mobile belts are zones of weakness extending deep into the lithosphere. They are subject to easy rejuvenation and are more susceptible to fracturing than normal continental lithosphere. The high thermal gradients associated with the old mobile belts become the site of renewed thermal activity, a rift generates giving rise to a spreading ridge, and thus the continent is split and plate separation take place (Windley, 1977).

The Amazon River derives most of its debris from the Andes which are the leading edge of the South American plate. The trailing continental edge (coast) will normally receive more sediment than the collision edge (coast), because they have larger drainage areas. Thus, in the broadest view, rivers respond to the megageomorphology of continents, which is relatable to plate tectonics. If, in addition to rifting and downfaulting parallel to a coastline, there is also a fault or rift system at some angle to the coast, it tends to collect and focus major paleodrainage. The Amazon river is a typical example, and figure 29 shows this rift control on the lower part of the Amazon River.

6.4. Salado and Colorado Basins

There are several marginal geologic basins along the south-eastern border of South America (fig. 4). Two of these marginal basins are the Salado and Colorado basins which are located in the northern part of Argentina. Although it has been suggested that the continental margin of southern Brazil and Argentina has not been deformed since at least upper Paleozoic or lower Mesozoic time (Zambrano and Urien, 1970), major structures and changes in structural trends have occurred in Late Jurassic or Early Cretaceous time. These represent formation of basins and changes in basin trend from parallel to the shore to a new basin type perpendicular to the continental margin which also enter the continent. The Salado and Colorado basins are typical examples for these perpendicular types of basins. The predominant trends are NW-SE, E-W, or WSE-ENE (fig. 24) and the major part of the basins extend into the continental shelf.

Table 18 shows the stratigraphic succession of the post-upper Jurassic sedimentary rocks in Salado and Colorado basins. Figure 30 and figure 31 are cross sections of these two basins illustrating the Cretaceous and Tertiary formations found there.

The presence of lower Cretaceous sediments in the Salado and Colorado basins has not been proven, as no fossil remains older than Cenomanian (lowermost upper

Cretaceous) have been found. However, it should not be forgotten that the basement in the deeper parts of the Salado basin has not yet been reached by wells.

The younger Cretaceous formations in the Salado and Colorado basins are represented by red beds (Zambrano and Urien, 1970). The scarcity of organic remains points to a nonmarine origin. The only possibility for a lateral transition to marine conditions lies in the easternmost part of the basin, close to the continental slope.

Malumian (1968, 1970) made a micropaleontologic study of Maestrichtian (upper Cretaceous) fossils in the lower part of the Pedro Luro Formation which was formerly assigned to the Paleocene (Zambrano and Urien, 1970, Kaasschieter, 1965; Ewing et al., 1963). These sediments which are from wells drilled on the continental shelf are of neritic type, rich in calcareous layers, which alternate with greenish gray or dark gray shales and greenish sandstone. In the Salado basin, the Chilcas Formation of Paleocene and Eocene age is confirmed by micropaleontologic research. Contrary to the conclusions of earlier studies, the upper parts of this unit may reach up into lower Oligocene, a period which as been found to be represented in offshore drillings (Malumian, 1970).

The deposition of younger Tertiary sediments was formerly thought to begin in the Miocene (Table 18). However, in the lower part of the Barranca Final Formation, fossils of probable upper Oligocene age have been found, and upper Oligocene deposits are also reported in the Salado and other basins from both surface and subsurface studies. This means that the sedimentary break during the Oligocene is reduced to the middle part of the period. In the Colorado basin, the Miocene, Pliocene, and Quaternary are represented by marine paralic deposition. On the other hand, the Miocene and post-Miocene in the Salado basin is represented by marine neritic sediments.

Tectonics of the Basins

The post-Cretaceou tectonic pattern of the Salado and Colorado basins is very similar. These basins were formed as a result of post-Jurassic fracturing. Pre-upper Jurassic units cropping out in the area, or present in the subsurface, are composed of igneous and metamorphic rocks together with indurated sediments which, due to consolidation, have acquired the accoustic properties of true basement rocks. In the Salado basin, the presence of basalts (Table 18 and fig. 30) was detected by wells. They lie between the continental Cretaceous sediments and the basement, in a similar way as those reported by Jones (1956) in the Canelones Graben.

The tectonic features of these Atlantic basins are controlled by vertical movements of basement blocks along normal faults; major transcurrent faults may also occur here with a predominant E-W trend. The tensional faults may be parallel, transverse, or, less frequently, oblique to the main depositional axis, and there is a tendency towards E-W, NE-SW, and NW-SE directions.

The inception of faulting probably occurred between middle and younger Jurassic time. The faults were intermittently reactivated throughout Cretaceous time. From Maestrichtian (upper Cretaceous) time onwards, the sedimentary fill absorbed most of the faulting stresses, and few faults were able to fracture the Tertiary cover. However, the basins were subjected to repeated marine transgressions and regressions during the Cenozoic.

De Rezende (1972) suggests that the Salado and Colorado basins belong to the Southern Rifting event (fig. 28) of continental separation between South America and Africa. Thus, both the Salado and Colorado basin are regarded as being aulacogens (fig. 3) and both contain deep sedimentary deposits (fig. 4) with normal faults and associated basaltic intrustions.

6.5. Magnetic, Gravity Anomalies and Correlation (fig. 9, 10, 11, 16)

Generally speaking, magnetic minima and gravity maxima are associated with aulacogens which have a thin crust, a thick cover of sedimentary rocks and which may be sites of high heat flow. This is true for the Takutu, Amazon, Colorado, and Salado basins. In the Takutu rift valley, a magnetic low occurs (C1 in fig. 9) which may extend southeastward to the Amazon basin. The Bouguer gravity anomalies also show a trend of gravity maxima (T1 in fig. 10) in the area of Takutu rift valley. Furthermore, the trend of the gracity maxima is NE-SW which is the same as the trend of the rift valley. In the Amazon basin, a magnetic minima (C2, C3 in fig. 9) occurs throughout most of the entire area. This basin separates the Guyana Shield to the north from the Central Brazilian Shield to south, both areas of high positive anomalies. Both Bouguer and Free-Air gravity maxima (B, B1, B2 in fig. 10, 11) also occur which coincide very well with the trend of the Amazon basin. In the southern part of the South-American Platform and the northern boundary of the patagonian Platform, a large magnetic minima (D2 in fig. 9) and gravity maxima (C in fig. 10, D in fig. 11) are associated with the Salado aulacogen (or so-called Argentina aulacogen) (fig. 3) where two big rivers-Rio Parana and Rio Salado appear. Both the magnetic and gravity anomalies along the Salado aulacogen have the same SE-NW trend.

Several different correlations between the anomalies and the grabens (or aulacogens) that do not follow the general rule of an associated magnetic low and gravity high are also observed in South America. For example, the Reconcavo basin (or aulacogen) (basin 8 in fig. 4) is characterized by a positive magnetic anomaly (A2 in fig. 9) and an poorly-defined regional gravity minimum (A6 in fig. 10, 11). A large amount of metamorphic and volcanic intrusive rock occurs around the Reconcavo basin, and an underlying thick continental crust probably is the main reason for this inverse correlation. Secondly, the Rio Orinoco trough (fig. 3) is associated with moderately high magnetic anomalies (northern part of B1 in fig. 9) and poorly-defined positive gravity anomalies.

Located at the middle of two highly elevated areas (Caribbean Mountain System to the north and Guyana Shield to the south), the Rio Orinoco trough contains Cenozoic sedimentary rock of relative low elevation. The rather indistinct positive gravity anomalies suggest that the area should be underlain by a relatively thin crust. The positive magnetic anomalies in the trough may be influenced by the larger magnetic high that occurs the northwest portion of the Guyana Shield. The third example is the Colorado basin (basin 15, fig. 4) which is characterized by an anomaly trend (T1, fig. 9 and 11) of a moderate magnetic high and gravity low. This anomaly trend has the same direction with the axes of Colorado basin and is probably associated with a deep geologic structural trend.

The grabens in the Andes are usually very narrow and small so that no well-defined magnetic and gravity anomalies is associated with them.

CHAPTER 7
CONCLUSIONS

The correlation between geophysical data, which includes magnetic, Bouguer gravity, and Free-Air gravity anomalies, and the known geologic features is generally good over the entire continent of South America. Correlations are noted between magnetic and gravity anomalies and tectonic provinces, continental rift zones, orogenic fold belts, metallogenic zones, volcanism, grabens, and aulacogens.

Based on origin, age, and structural development, three extensive tectonic provinces can be recognized in South America.

(1) South American Platform. It is the oldest province and contains the only know Archean rocks of the continent. The basement of the platform is exposed in three major shields-Guyana, Central Brazilian, and Atlantic Shield. All of these shields contain thick Precambrian metamorphic sequences and a wide variety of volcanic and intrusive rocks and are characterized by positive magnetic (fig. 32) and Free-Air gravity anomalies (fig. 33). An exception is the eastern part of the Guyana Shield which corresponds to a well-defined negative Free-Air gravity anomaly.

The sedimentary cover and associated volcanics of the platform, which are of Silurian or younger age, are well developed in the four great synclines-Amazon, Parnaiba, Parana, and Chaco basins. These basins are filled with a thick sequence of non-magnetic and low density sedimentary rocks and are associated with negative magnetic and gravity anomalies (fig. 34, 35). An exception is the Parana basin.

Positive magnetic anomalies occur in the basin which are associated with a thick sequence of Parana basalts. In general, grabens or aulacogens, underlying the large basins (Amazon and the southern part of Chaco basins) or in the shield (Takutu rift valley), are characterized by magnetic minima and gravity maxima (fig. 36, 37). These relations suggest a thin continental crust and a thick cover of sedimentary rocks. These aulacogens may be areas of high heat flow.

A thick continental crust underlies the whole eastern part of the South American Platform which includes the Sao Francisco Craton, the northern part of Parana basin, and the southern part of Parnaiba basin. This is the thickest continental crust exclusive of the Andes. A large Bouguer gravity anomaly low occurs in this region (fig. 10).

(2) Patagonian Platform. This is a young platform with a basement that stabilized during the middle Paleozoic. A volcano-sedimentary cover of Carboniferous or younger age almost completely masks the platform basement. Both magnetic and gravity anomaly patterns show a gradient over the platform. These gradients are apparently associated with variation in elevation and thickness of the continental crust. A subsurface geologic structural trend with a NW direction is characterized by a magnetic high and Free-Air gravity low in the northern boundary of the Patagonian Platform.

(3) The Andean Fold Belt. The Andean Cordillera constitutes the entire western margin of South America with rocks dating from the Precambrian to recent time. It is a region of strong seismicity and volcanism. Both the Bouguer and Free-Air gravity anomalies show a distinct trend that parallels the fold belt (fig. 10, 11), and the tremendous low values of Bouguer gravity anomalies indicate that the thickest continental crust underlies the Andean Fold Belt in South America.

However, the magnetic anomaly trends of the Andes do not parallel the gravity anomaly trends which follow the north-south structural trend of the fold belt (fig. 9).

The metamorphic basement probably plays a major role in this magnetic pattern. The distribution of the positive magnetic anomalies match well with the occurrence of the metamorphic basement. The adjacent deep-sea trench along with two large Cenozoic continental grabens may significantly influence the large magnetic low that occurs at the central part of the Andean Fold Belt.

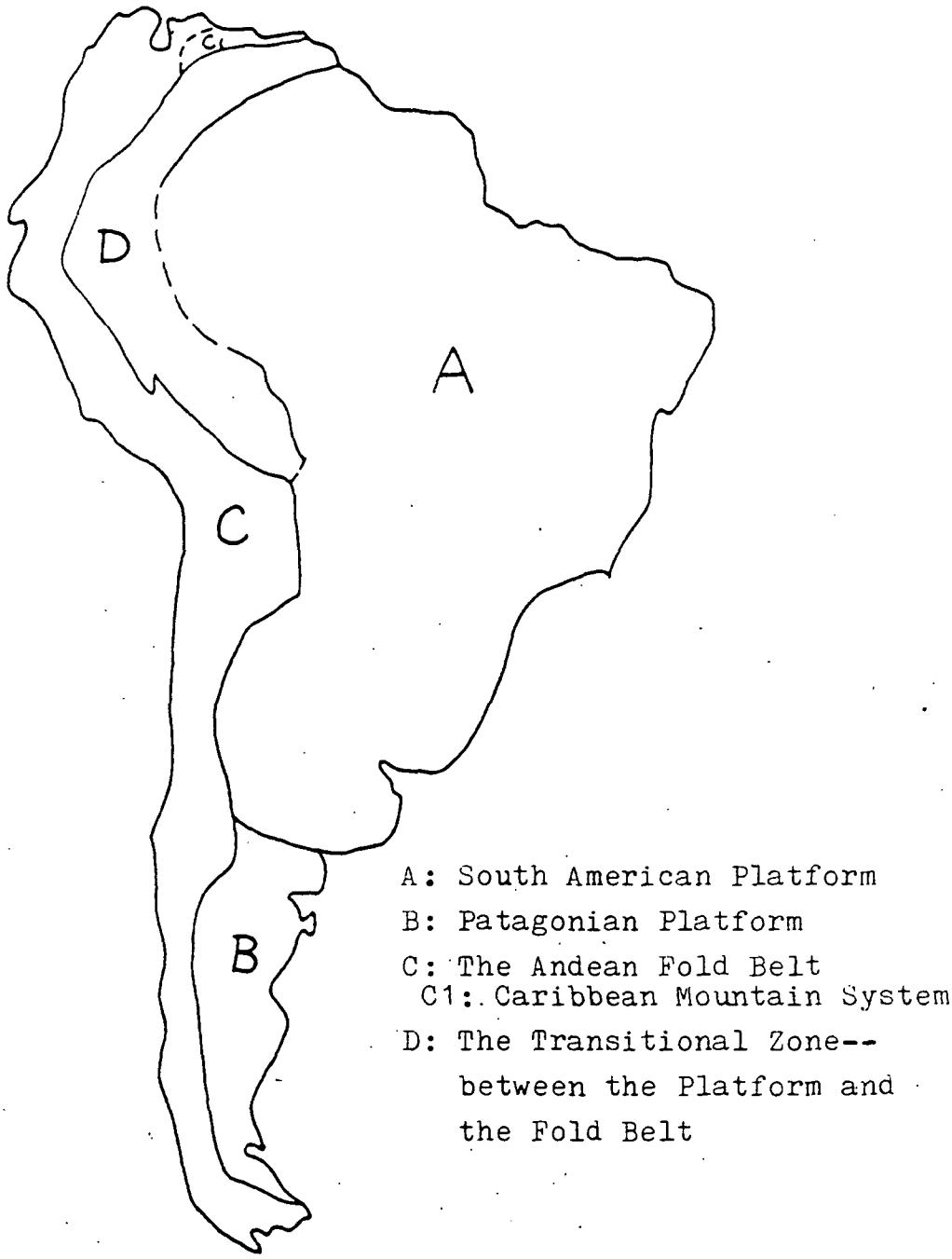

Figure 1: The Tectonic Provinces of South America

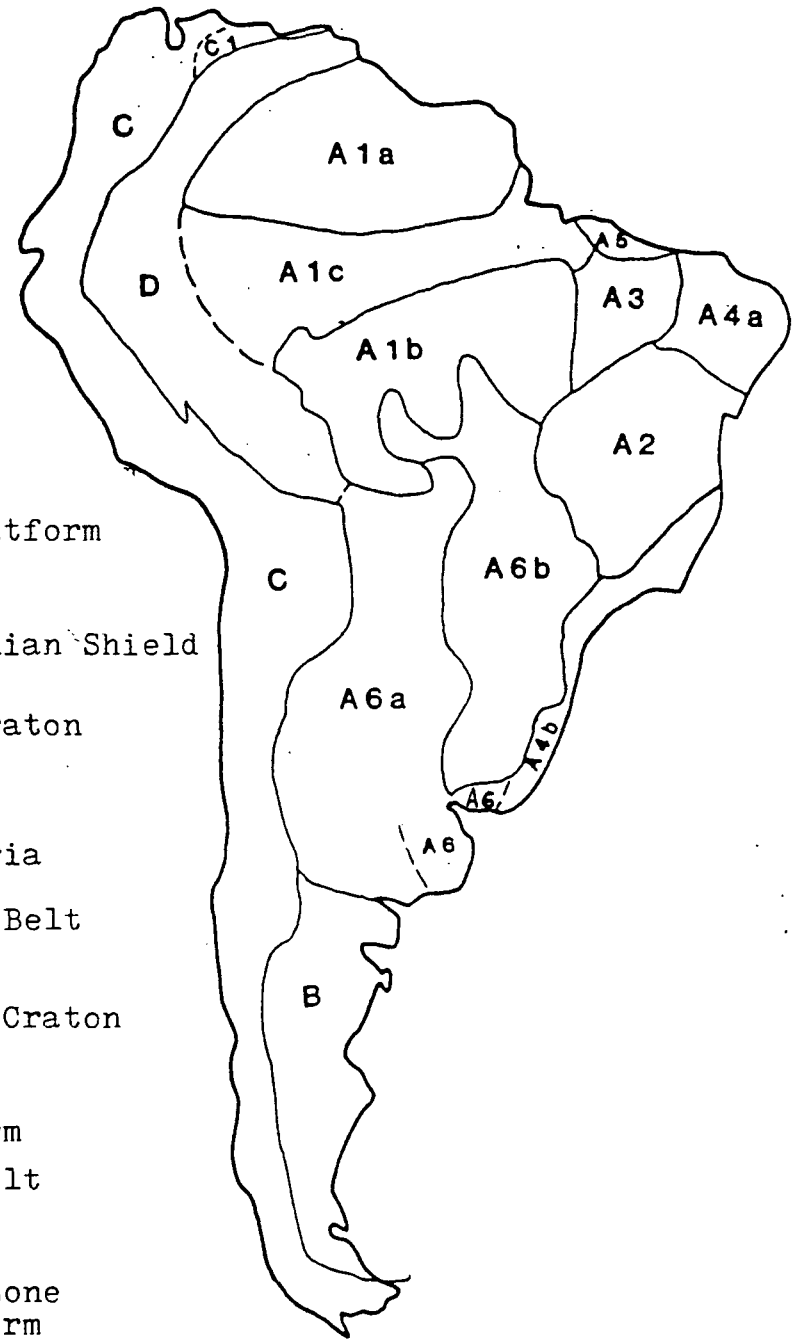

A. South-American Platform

A1. Amazon Craton
- A1a. Guyana Shield
- A1b. Central Brazilian Shield
- A1c. Amazon Basin

A2. Sao Francisco Craton

A3. Parnaiba Basin

A4. Atlantic Shield
- A4a. Caririan-Propria Fold Belt
- A4b. Ribeiran Fold Belt

A5. Sao Luiz Craton

A6. Rio de La Plata Craton
- A6a. Chaco Basin
- A6b. Parana Basin

B. Patagonian Platform

C. The Andean Fold Belt
- C1. The Caribbean Mountain System

D. The Transitional Zone between the Platform and the Fold Belt

Figure 2: The Tectonic Sub-provinces of South America

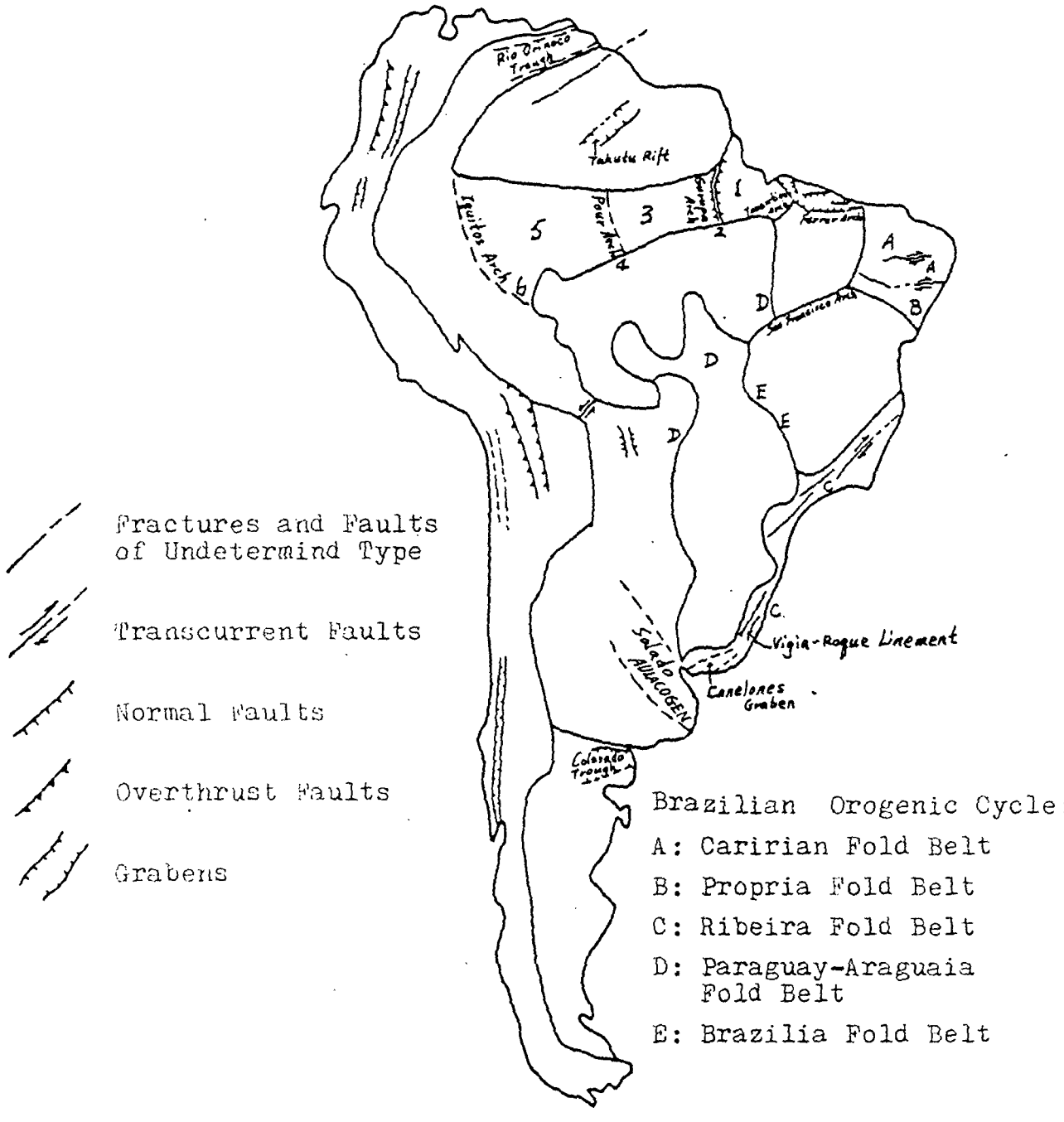

Figure 3: Main Structures of South America

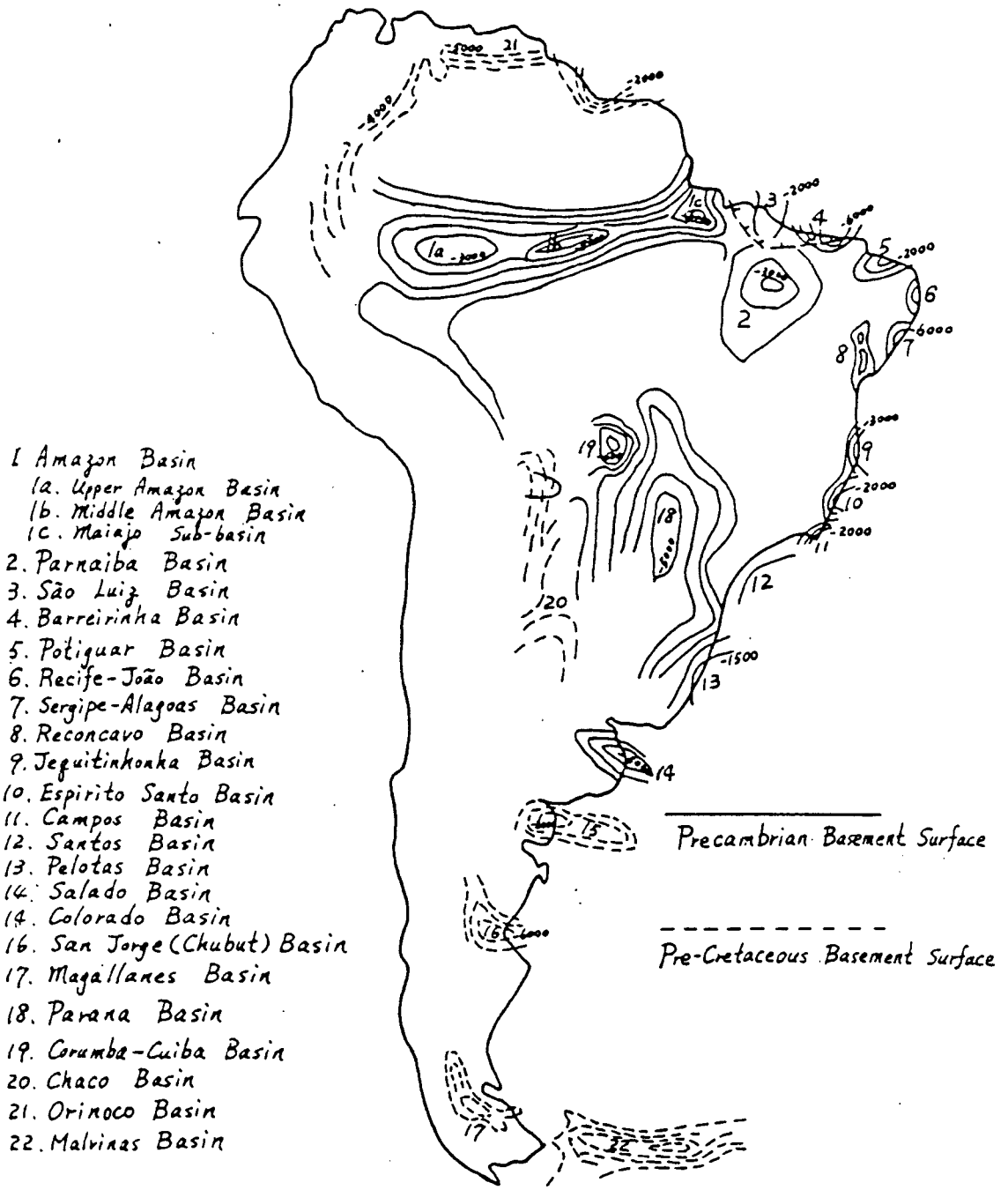

Figure 4: The Basins of South America

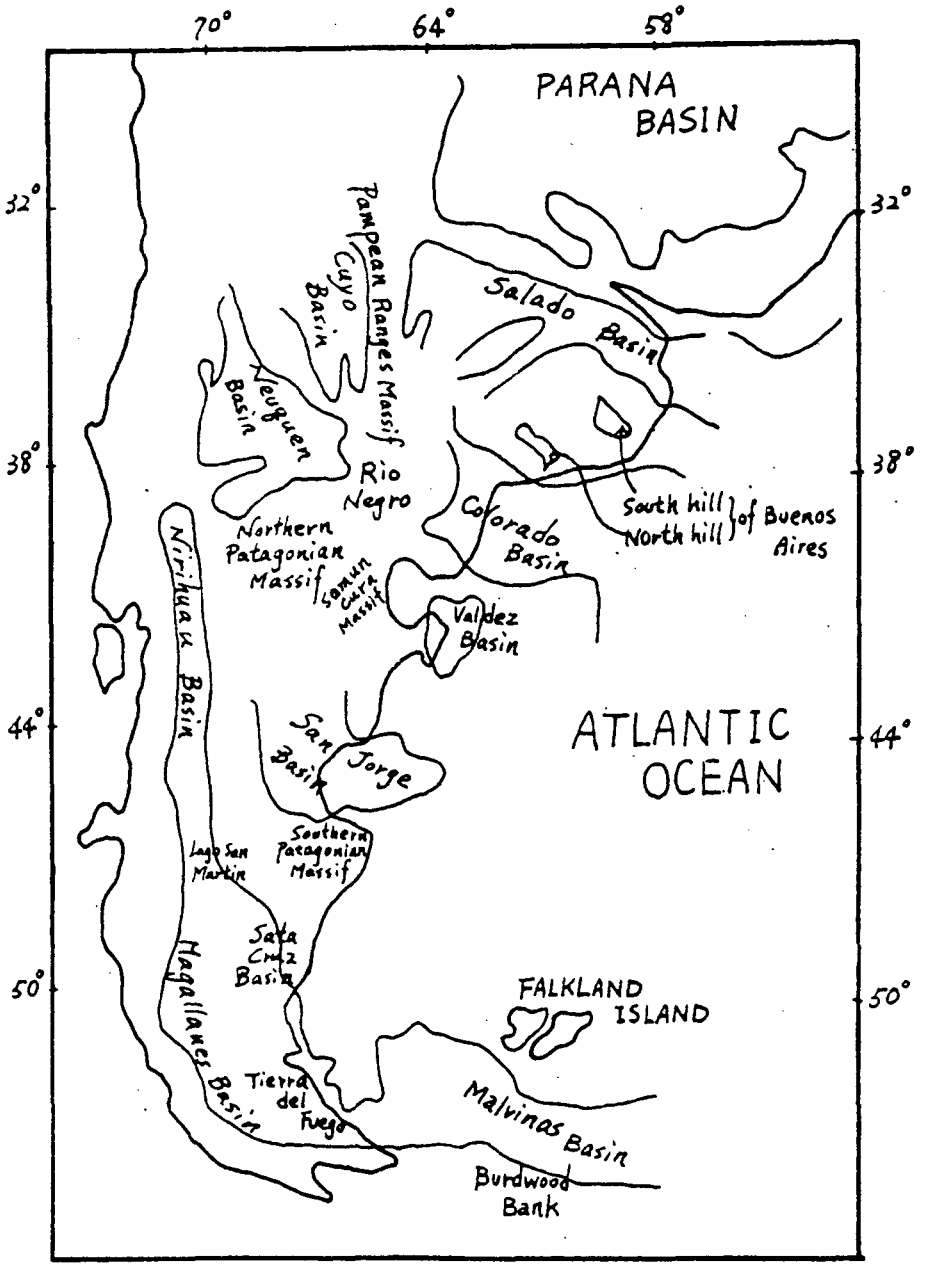

Figure 5: The Principal Geologic Provinces of Patagonian Platform (modified after Zambrano et al., 1970)

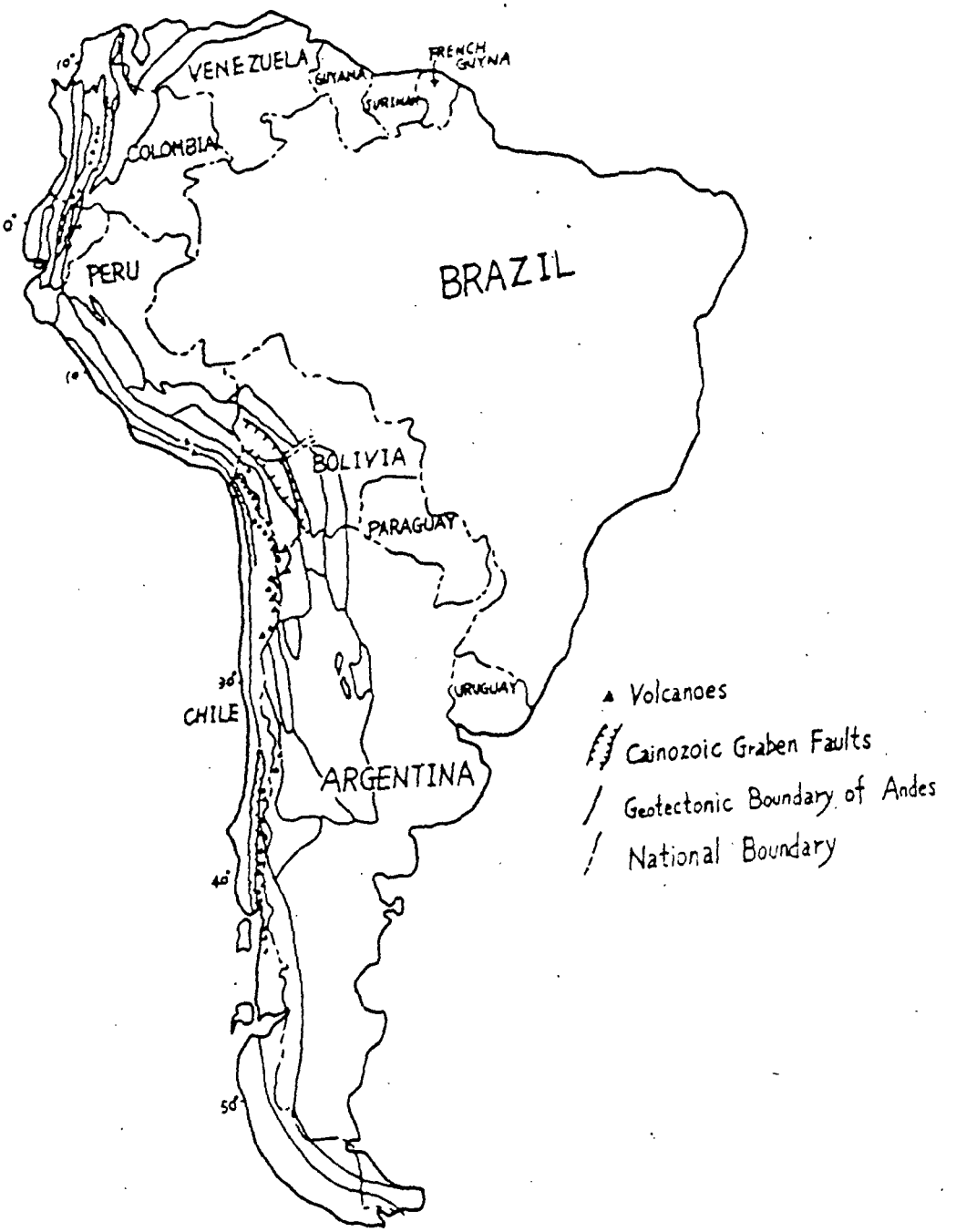

Figure 6: The Andean Orogenic Belt

Figure 7: The Provinces of South America (modified after Harrington, 1962)

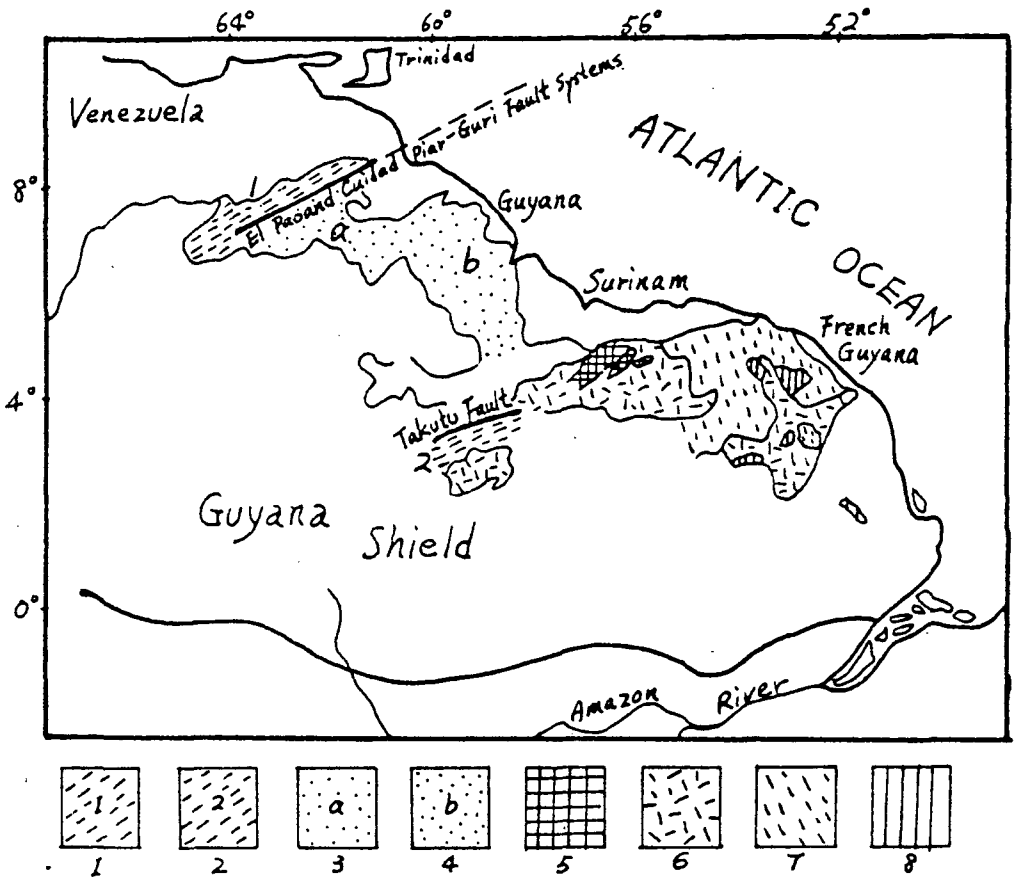

1. Imataca Complex (2700-3400 m.y.)
2. Kanuku Group (Archean)
3. Pastora-Carichapo Assemblage (2000-1800 m.y.)
4. Barama-Mazaruni Assemblage (1900-1800 m.y.)
5. Coeroeni-Falawatra Group (Archean)
6. Trans-Amazonian Granitic Rocks (1900 m.y.)
7. Paramaca-Bonidoro-Lorapu Formation (1900 m.y.)
8. Ile de Cayenne Group (Archean)

Figure 8: The Geological Outline of Guyana Shield (modified after Hurley and Rand, 1973)

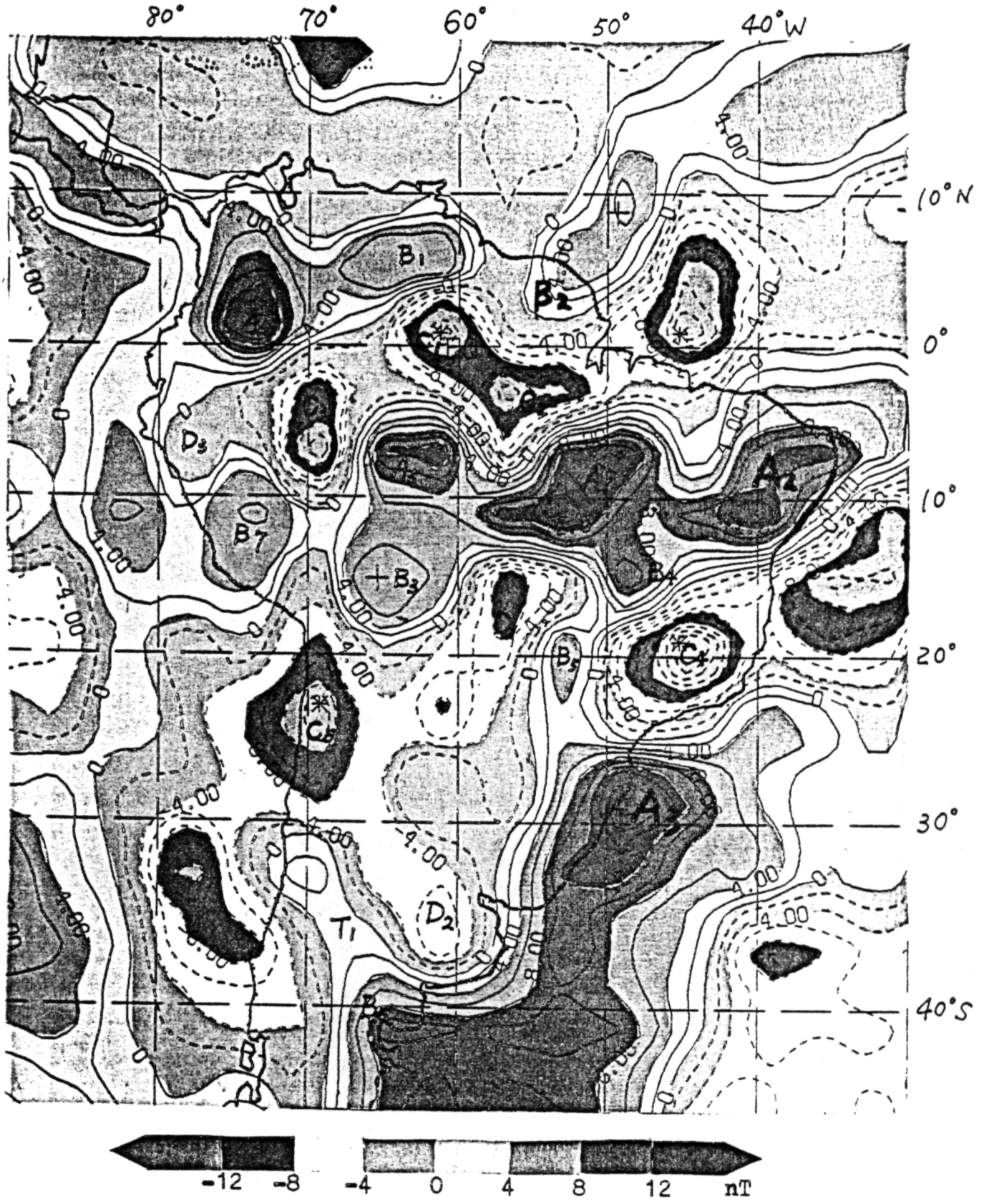

Fig. 9 Magnetic Anomaly Map of South America

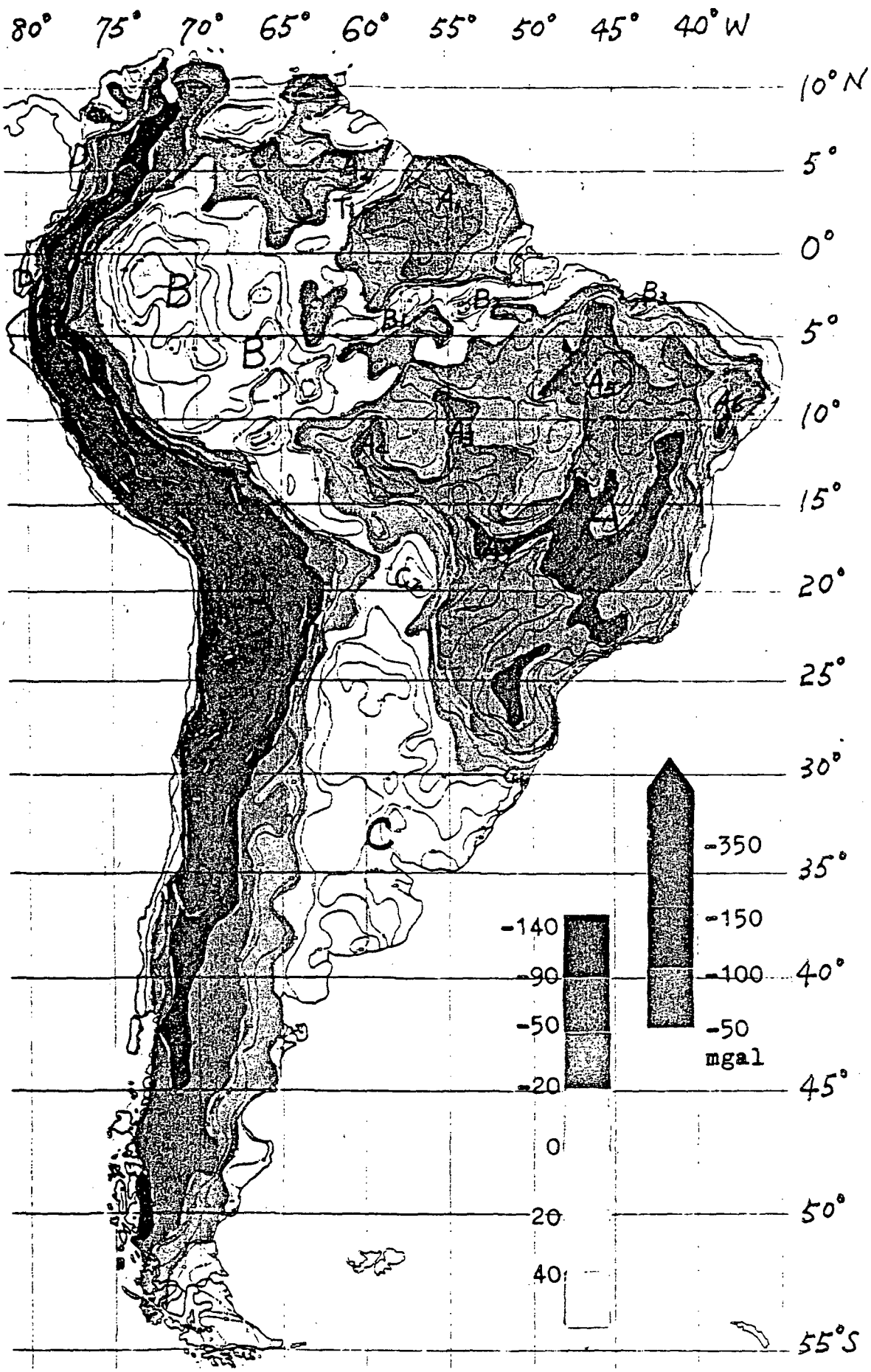

Fig. 10 Bouguer Gravity Anomaly Map of South America
(from Defense Mapping Agency Aerospace Center)

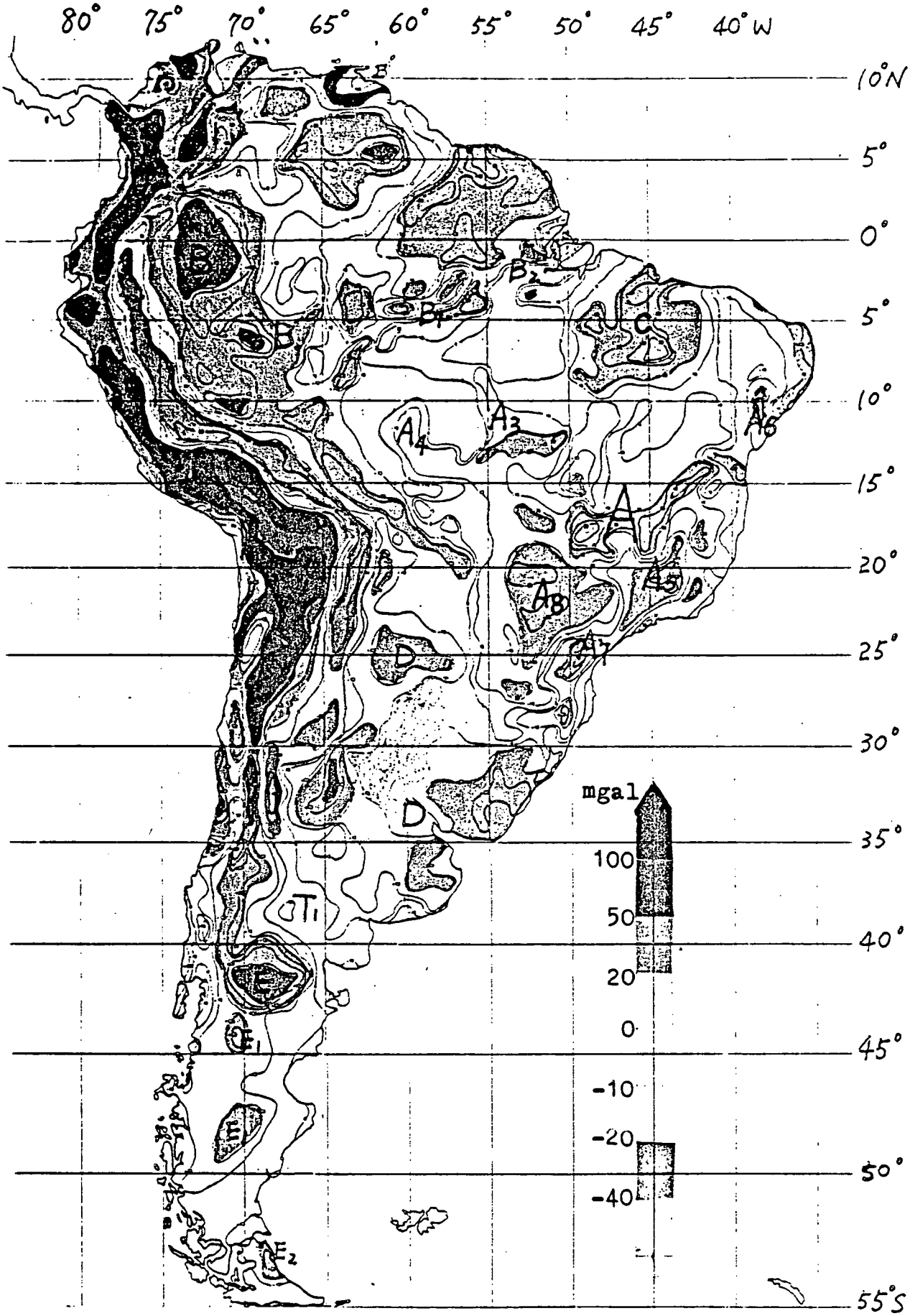

Fig. 11 Free-Air Gravity Amomaly Map of South America (from Defense Mapping Agency Aerospace Center)

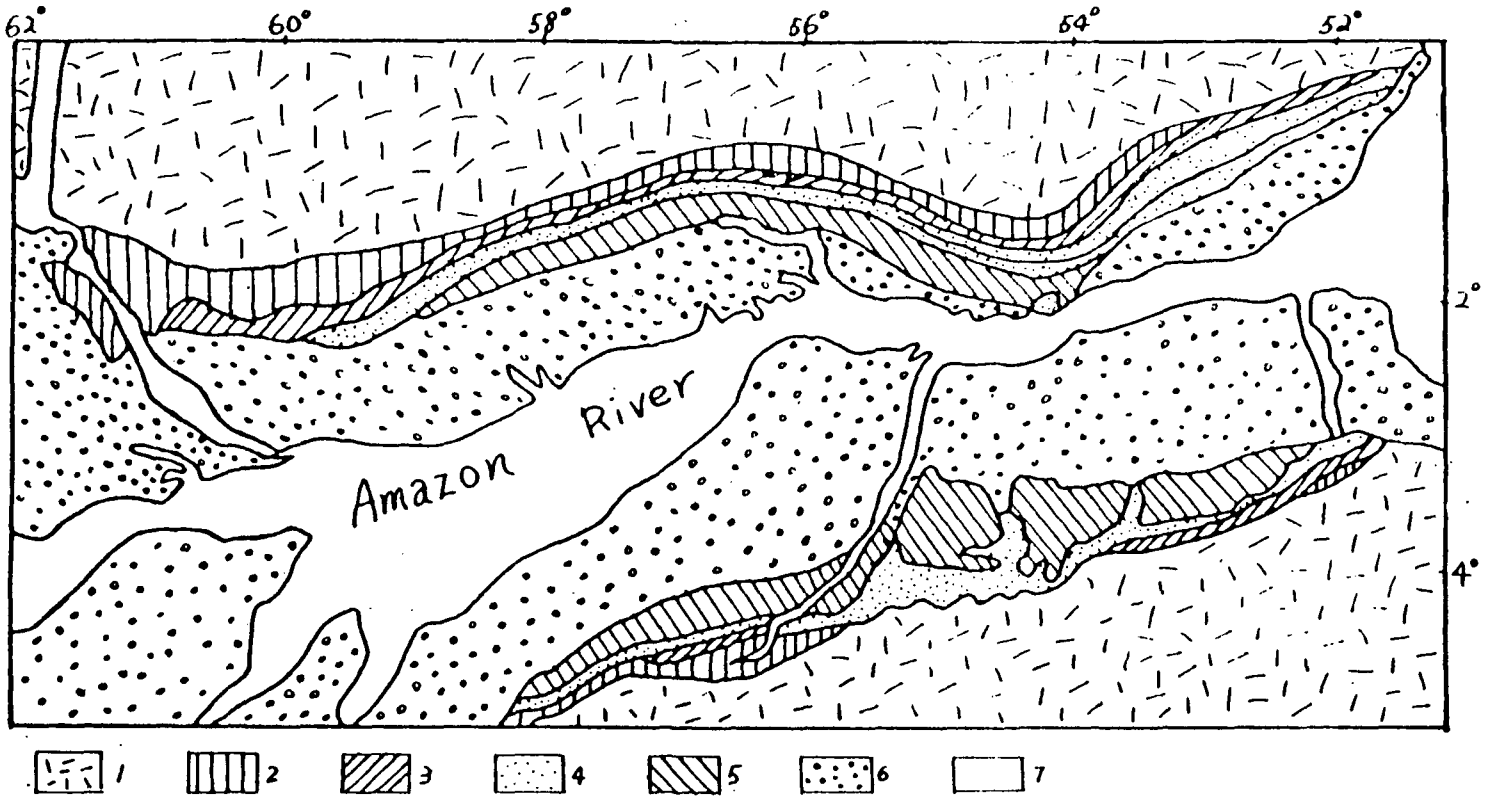

1. Crystalline Basement
2. Uatuma Formation
3. Trombetas Formation
4. Maecuru fm. + Curua fm.
5. Upper Carboniferous
6. Tertiary
7. Quaternary

Figure 12: Geologic Map of the Amazon Basin
(from the geologic map of Brazil, 1960)

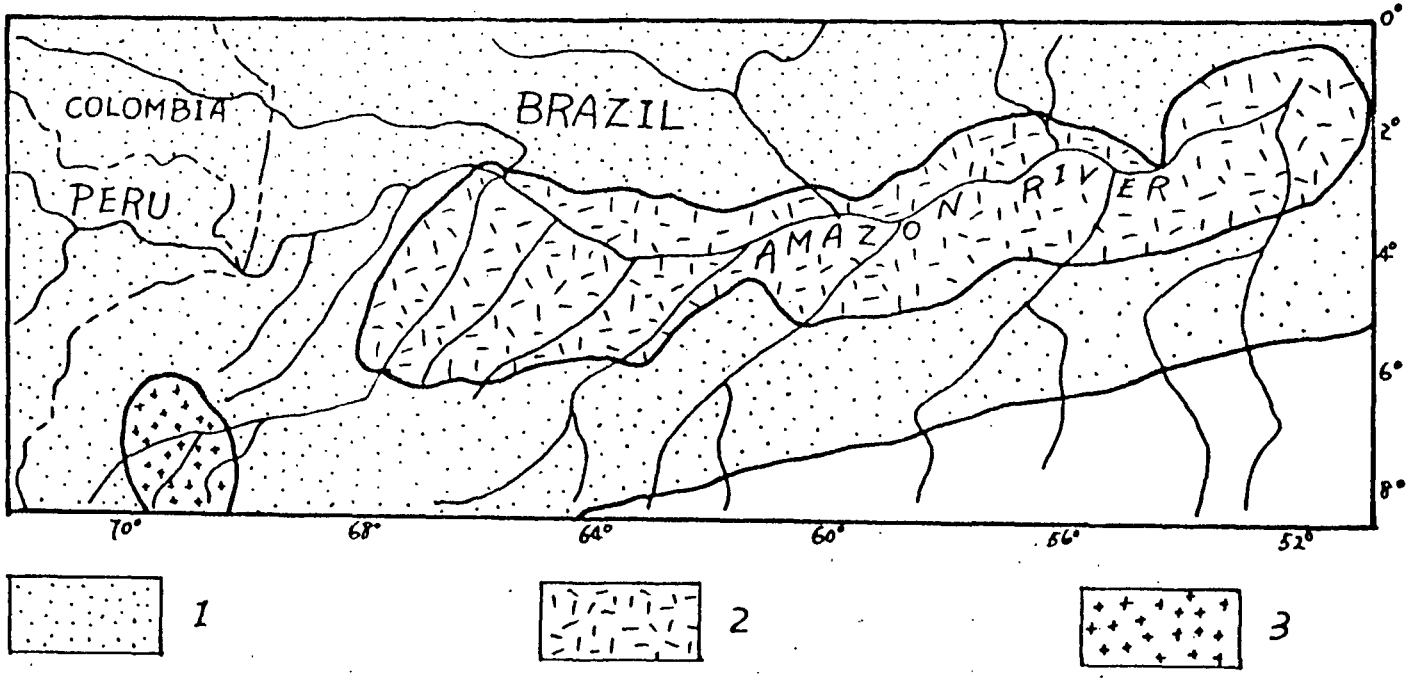

1. Area of dikes
2. Area of dikes and sills
3. Area of dikes and lava flows (data from Petrobras, S.A.)

Figure 13: Area Affected by Volcanism in Amazon Basin (modified after Bigarella, 1973)

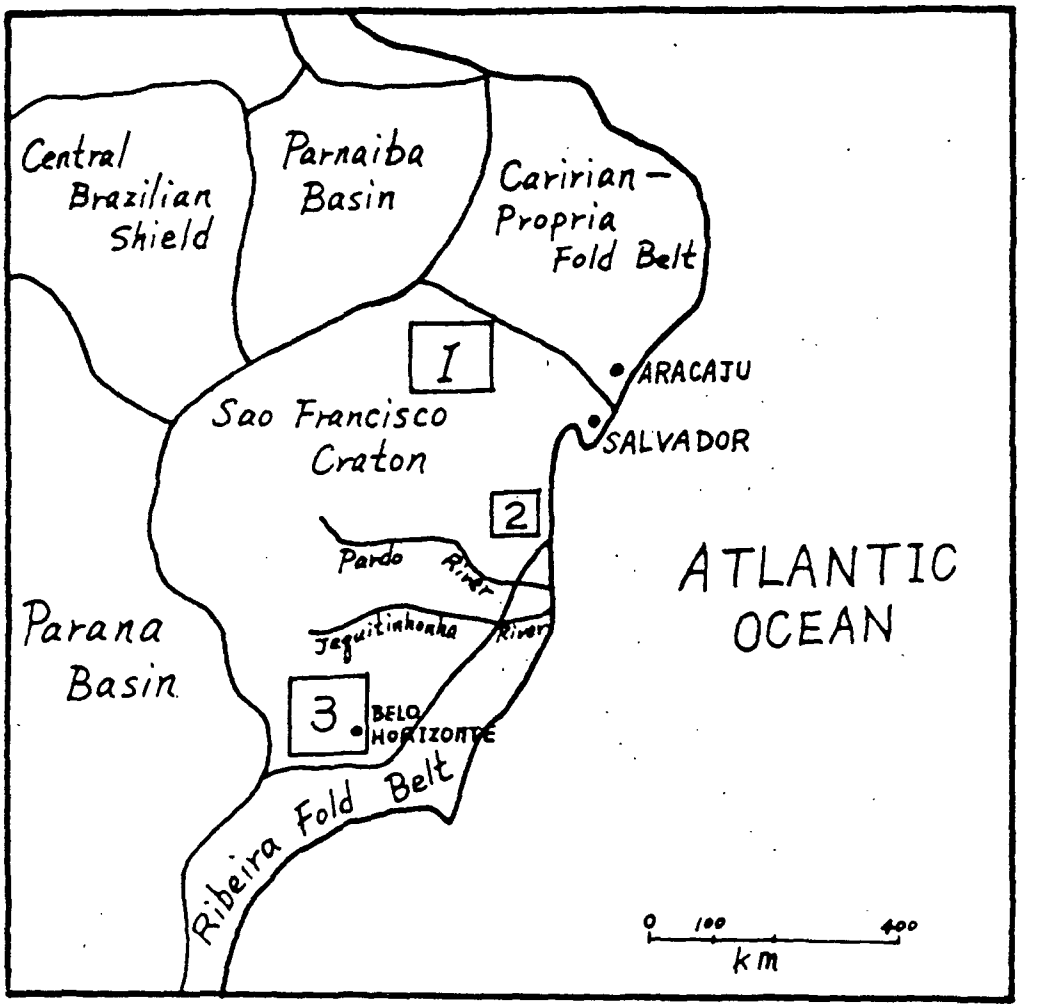

Figure 14: Sao Francisco Craton

Figure 15: The Sataes of Brazil

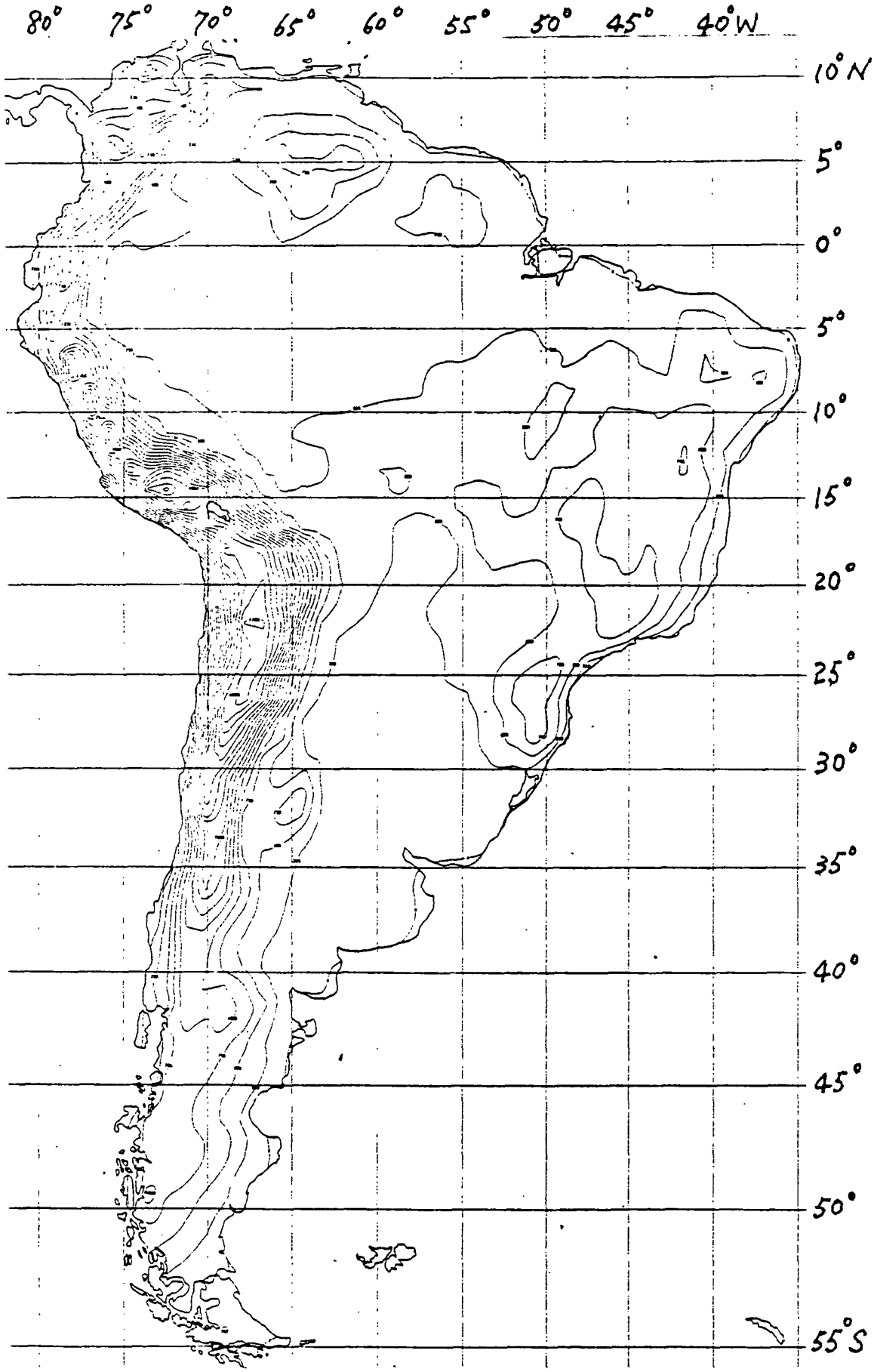

Figure 16: Mean Elevation Map of South America
(from Defense Mapping Agency Aerospace Center)

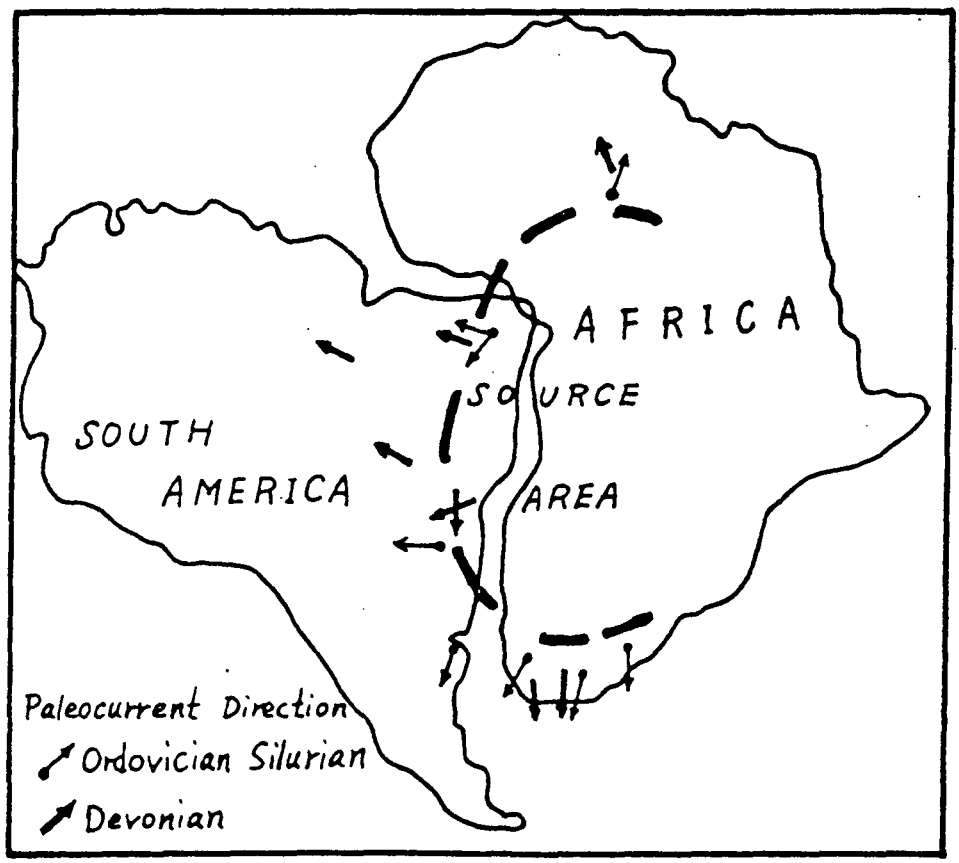

Figure 17: Paleocurrent Direction of South America and Africa (modified from Bigarella, 1970)

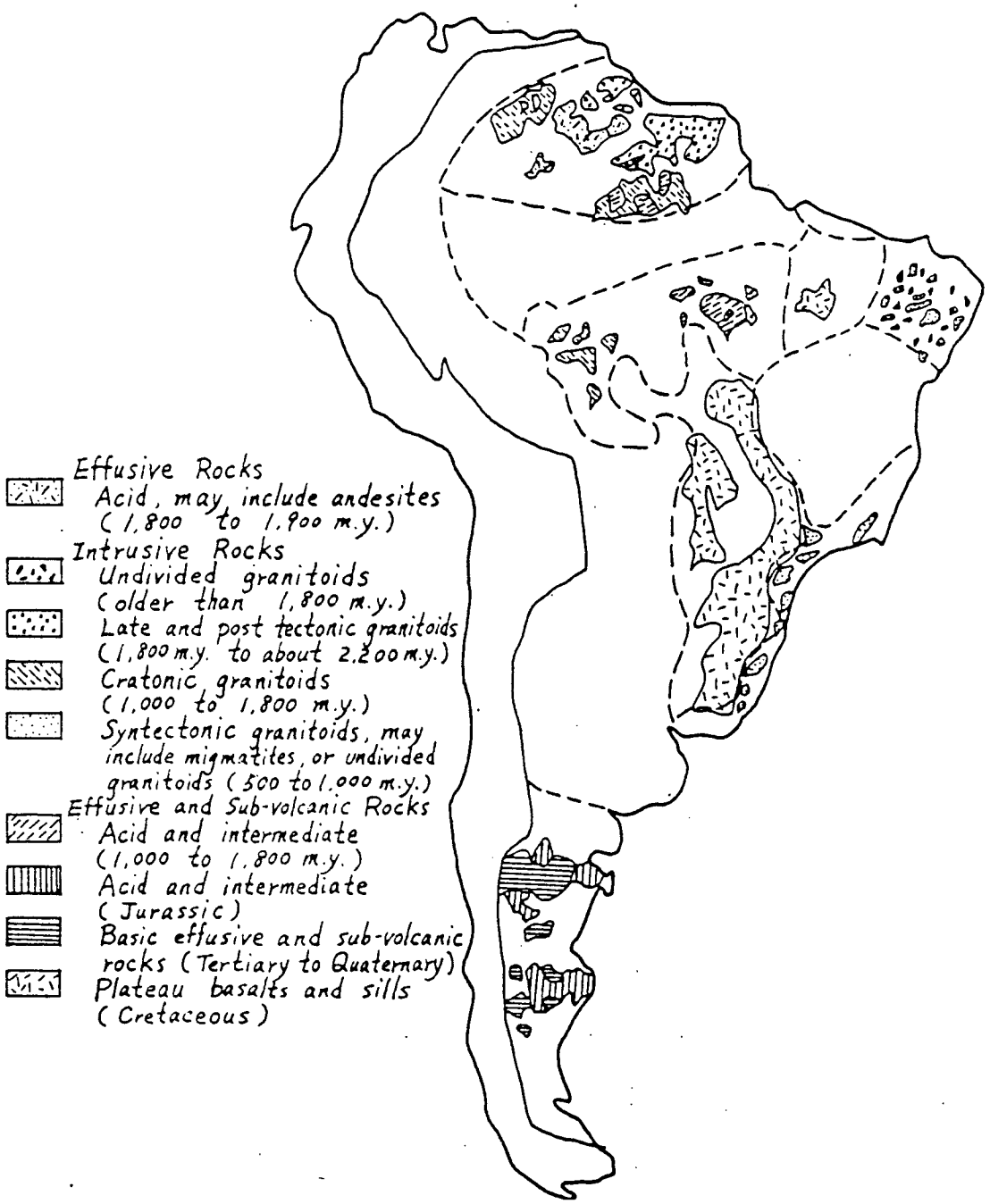

Figure 18: The Volcanics of South America (exclusive of the Andes)

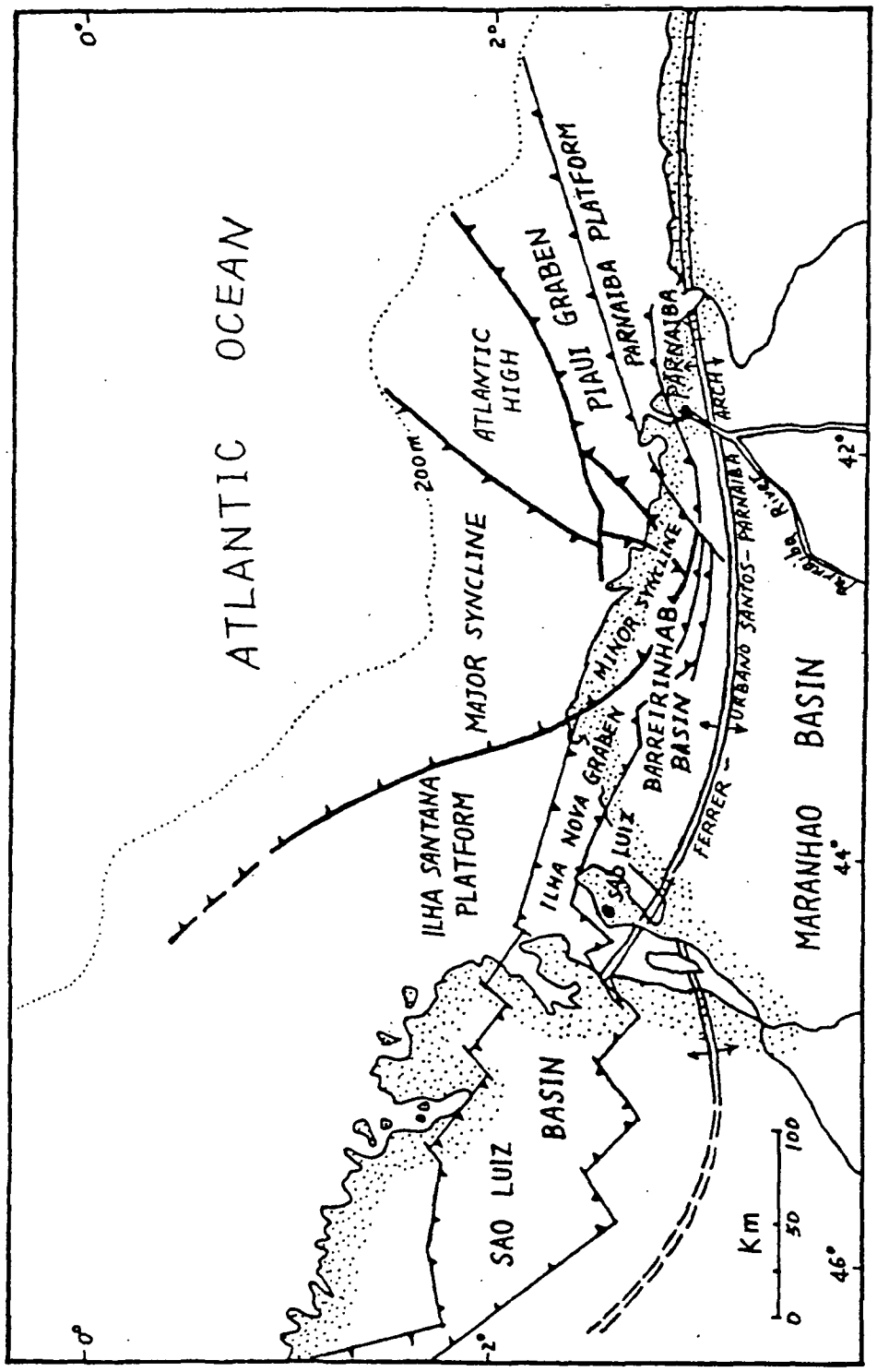

Figure 19: Sao Luiz Craton (modified after Asmus and Ponte, 1973)

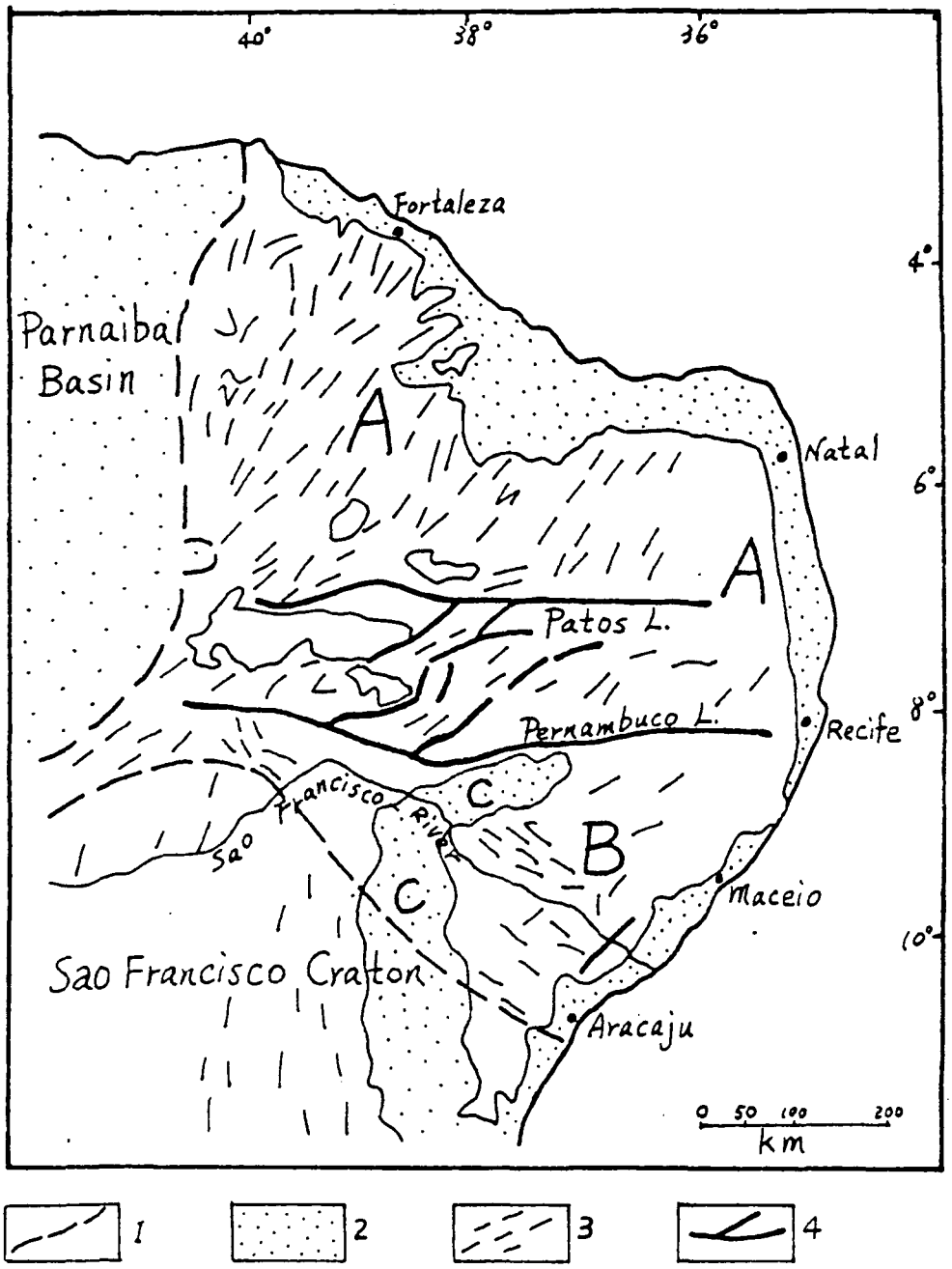

1. Approximate Boundary Between Geotectonic Units
2. Undivided Phanerozoic
3. Structural Trends
4. Faults

Region A: Caririan Fold Belt

Region B: Proprian Fold Belt

Region C: Reconcavo-Tucano Basin

Figure 20: Geotectonic Outline of Caririan-Proprian Fold Belt (modified after de Almeida et al., 1973)

A. Ribeiran Fold Belt
B. Caririan-Proprian Fold Belt
C. Sao Francisco Craton
D. Parana Basin
E. Parnaiba Basin
F. Central Brazilian Shield

Approximate Boundary Between Geotectonic Units

Boundary of States

National Boundary

Figure 21: Geotectonic Outline of South and East Brazil

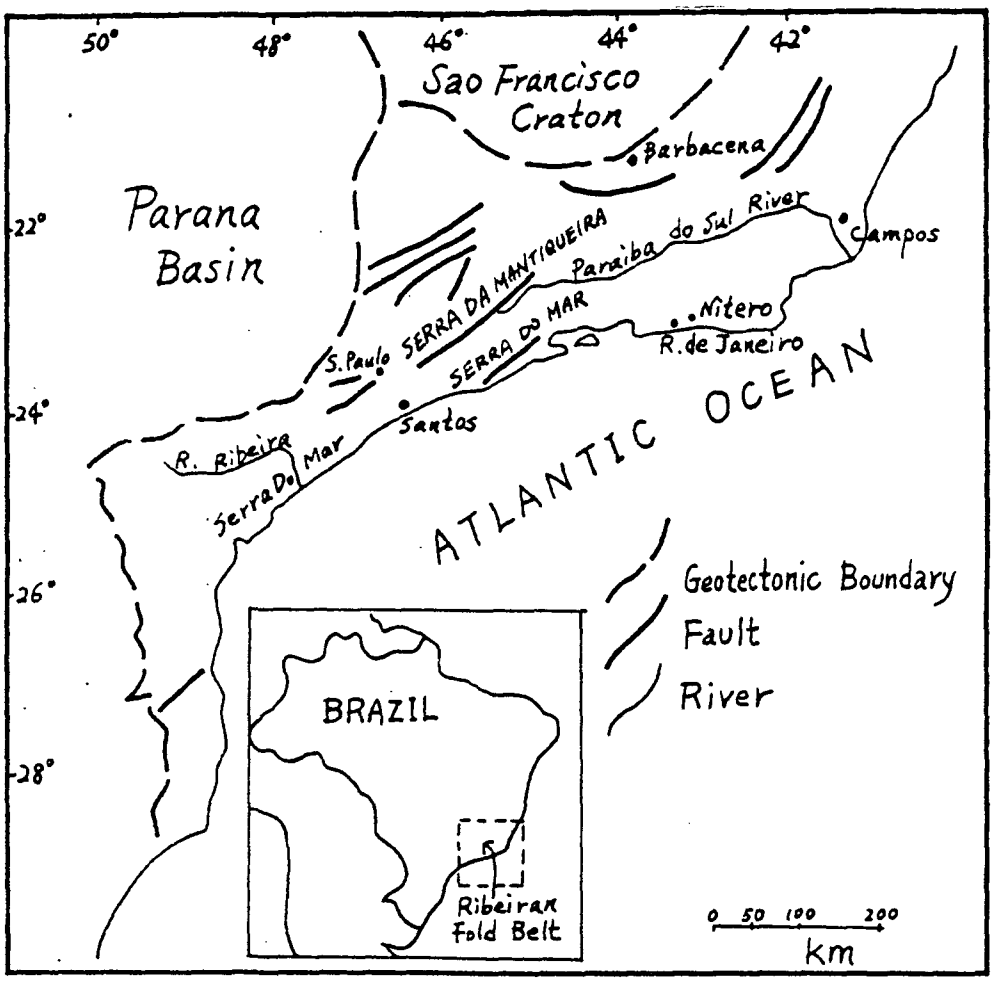

Figure 22: Geotectonic Outline of Ribeiran Fold Belt
(modified after Cordani et al., 1973)

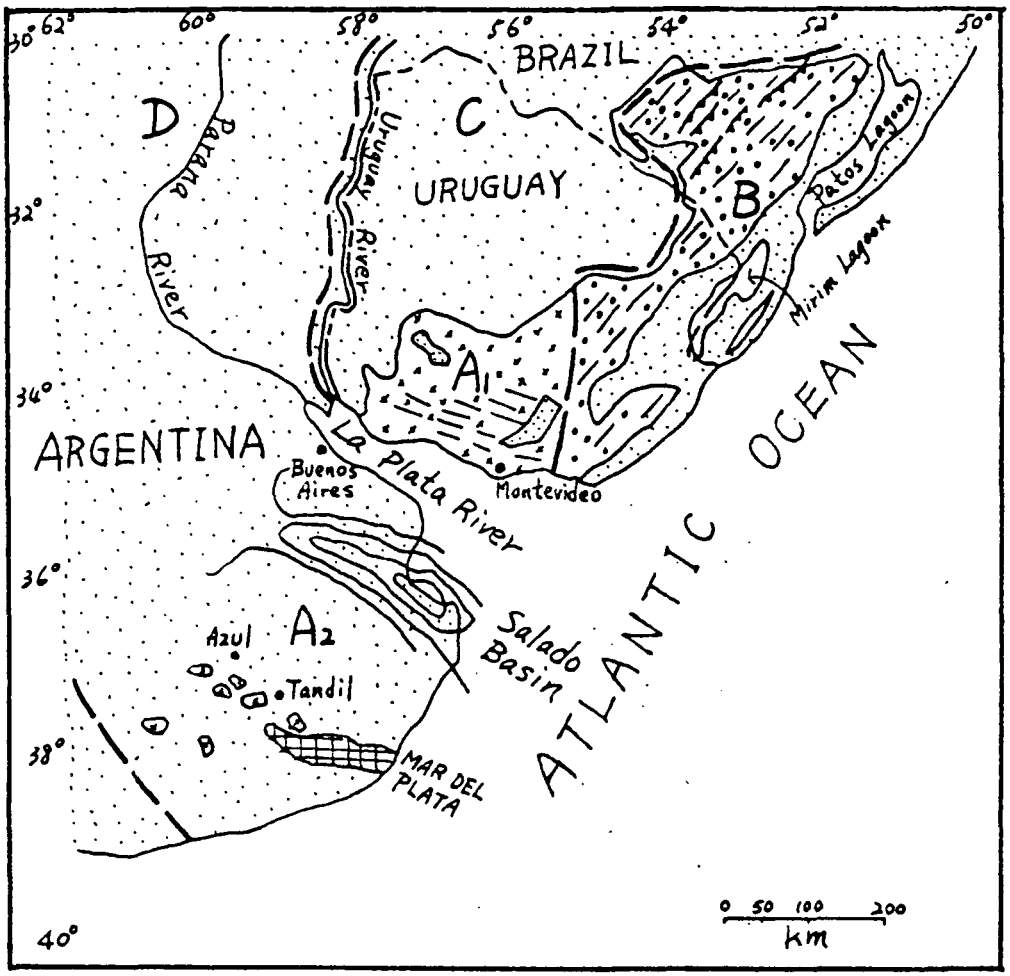

A1,A2: Rio de La Plata Craton
B: Ribeiran Fold Belt
C: Parana Basin
D: Chaco Basin
Geotectonic Boundary
National Boundary
River
Fault
Structural Trend
Undivided Pre-Braziliano to Middle-Precambrian
Upper-Precambrian (Fold Belt)
Eocambrian Sediment
Undivided Phanerozoic

Figure 23: Geological Outline of Rio de La Plata Craton (modified after Amaral et al., 1973)

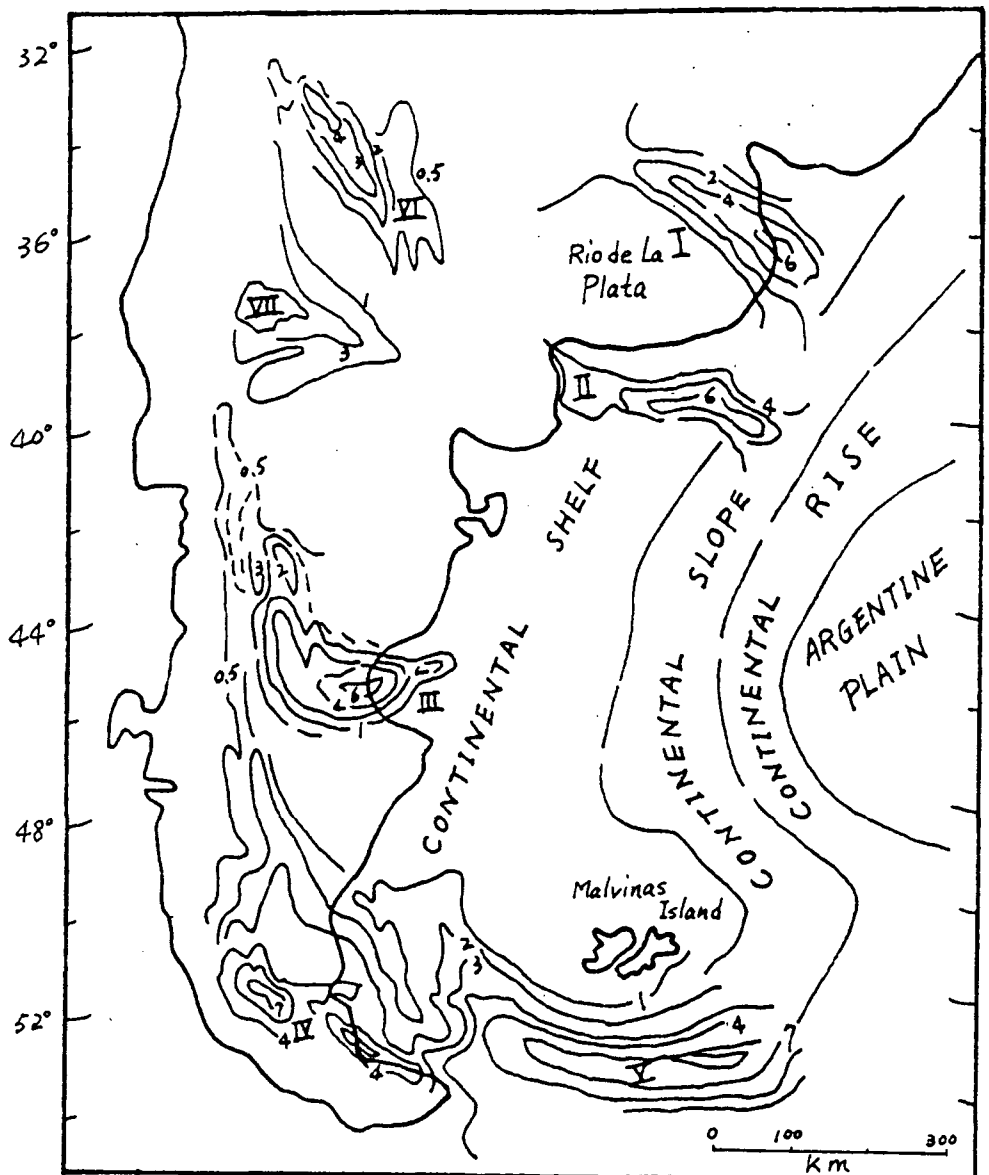

NO.	BASIN	SHAPE	DEPOAXIS	AGE OF SEDIMENTARY FILL	THICK (KM)	TYPE
I	Salado	Triangular	NW–SE	Cret.-Tert.-Quat.	8.5	Transcratonic open to sea
II	Colorado	Trapezoidal (Partly arc)	NW–SE to E–W	Cret.-Tert.-Quat.	7.0	Pericratonic open to sea
III	San Jorge	Oval(arc)	NW–SE to NE–SW	Upper Jur.–Cret. –Tert.-Quat.	6.0	Interneocratonic
IV	Magallanes	Elongated (arc)	NS to EW	Cret.(?)-Tert-Quat.	7.0	Geosyncline
V	Malvinas	Elongated (Partly arc)	NW-SE to EW	Tert.(?)–Quat.	9.5	Geosyncline
VI	Cuyo	Elongated	NW–SE			
VII	Neuquen	Triangular	NW–SE to E–W			

Figure 24: Patagonian Platform and Its Basins
(modified after Zambrano et al., 1970)

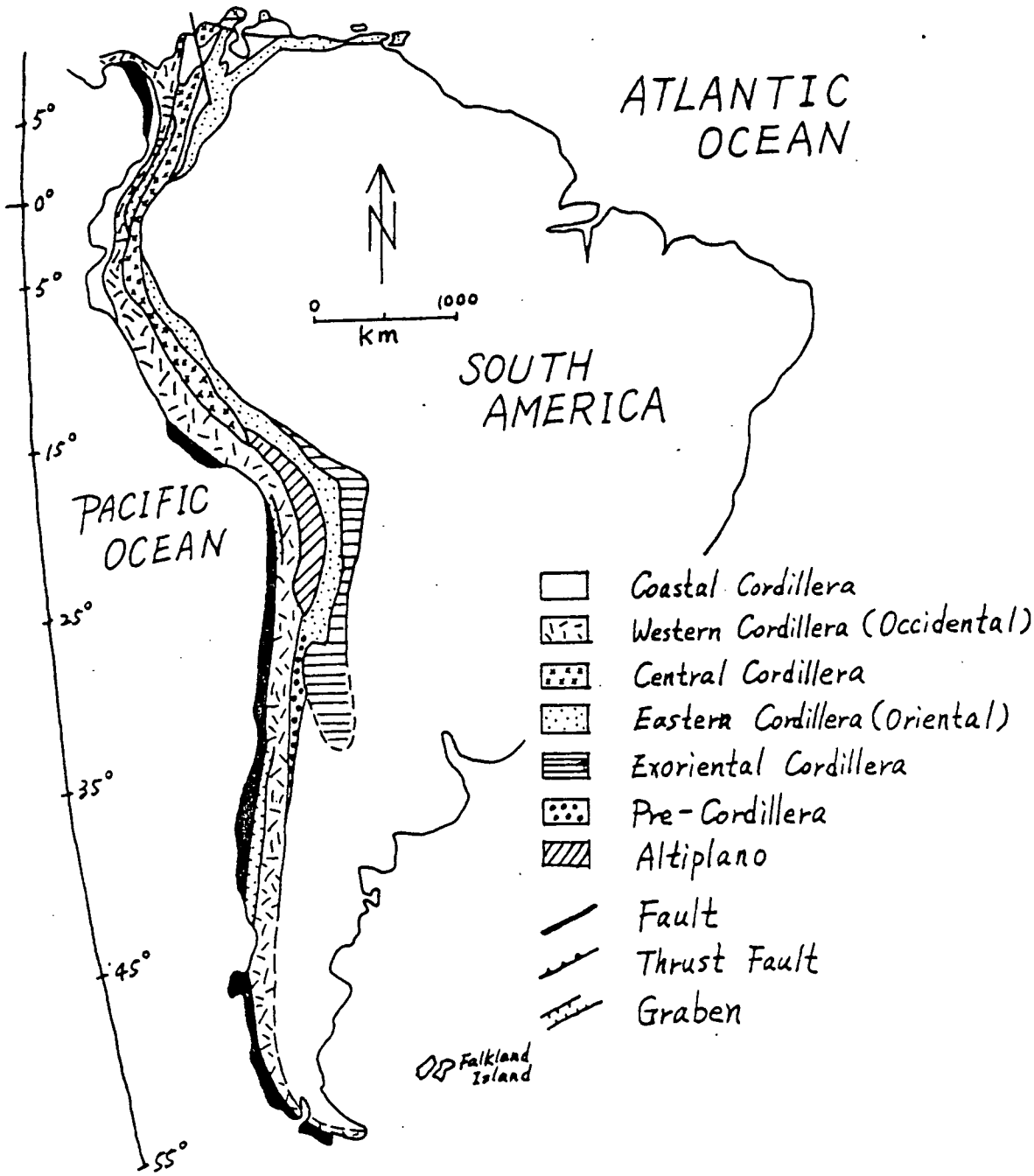

Figure 25: Geological and Tectonic Features of The Andes (modified after Zeil, 1979)

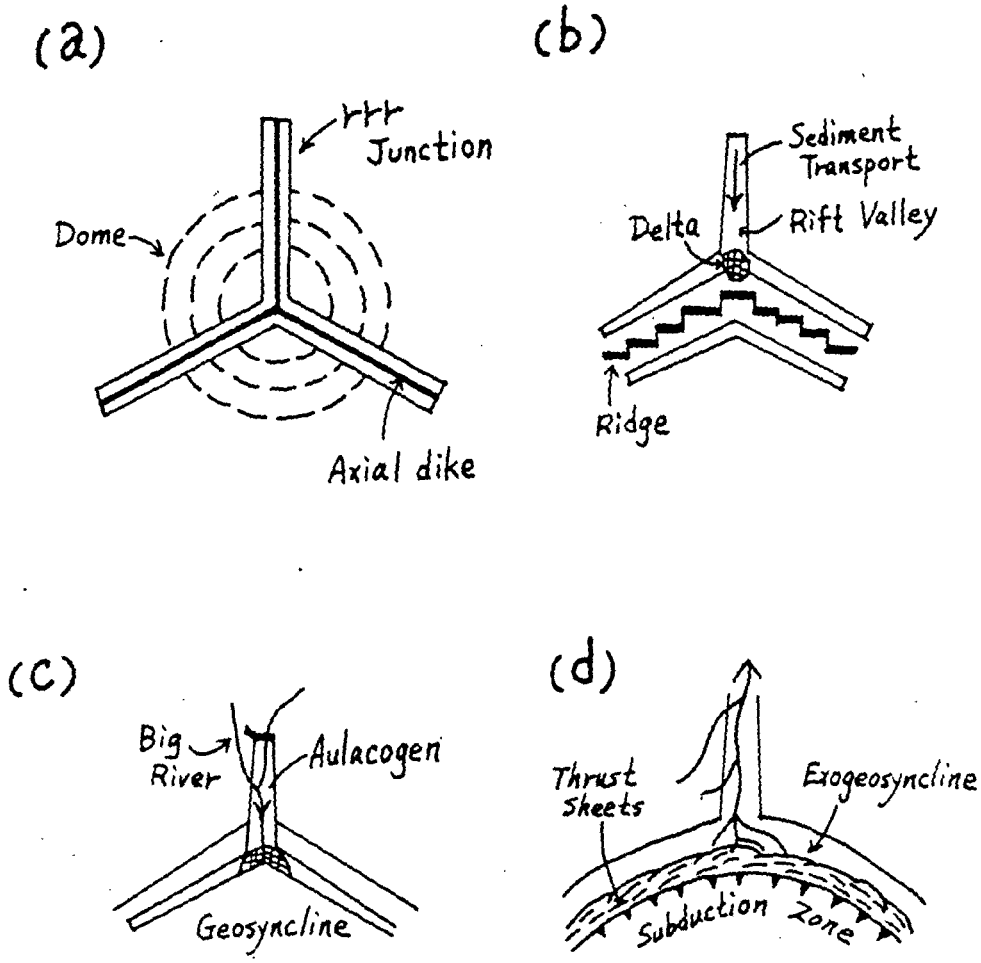

Figure 26: Evolution of Triple Junction, Aulacogen, Mountain Systems, and Big River (modified after Burke and Dewey, 1973a)

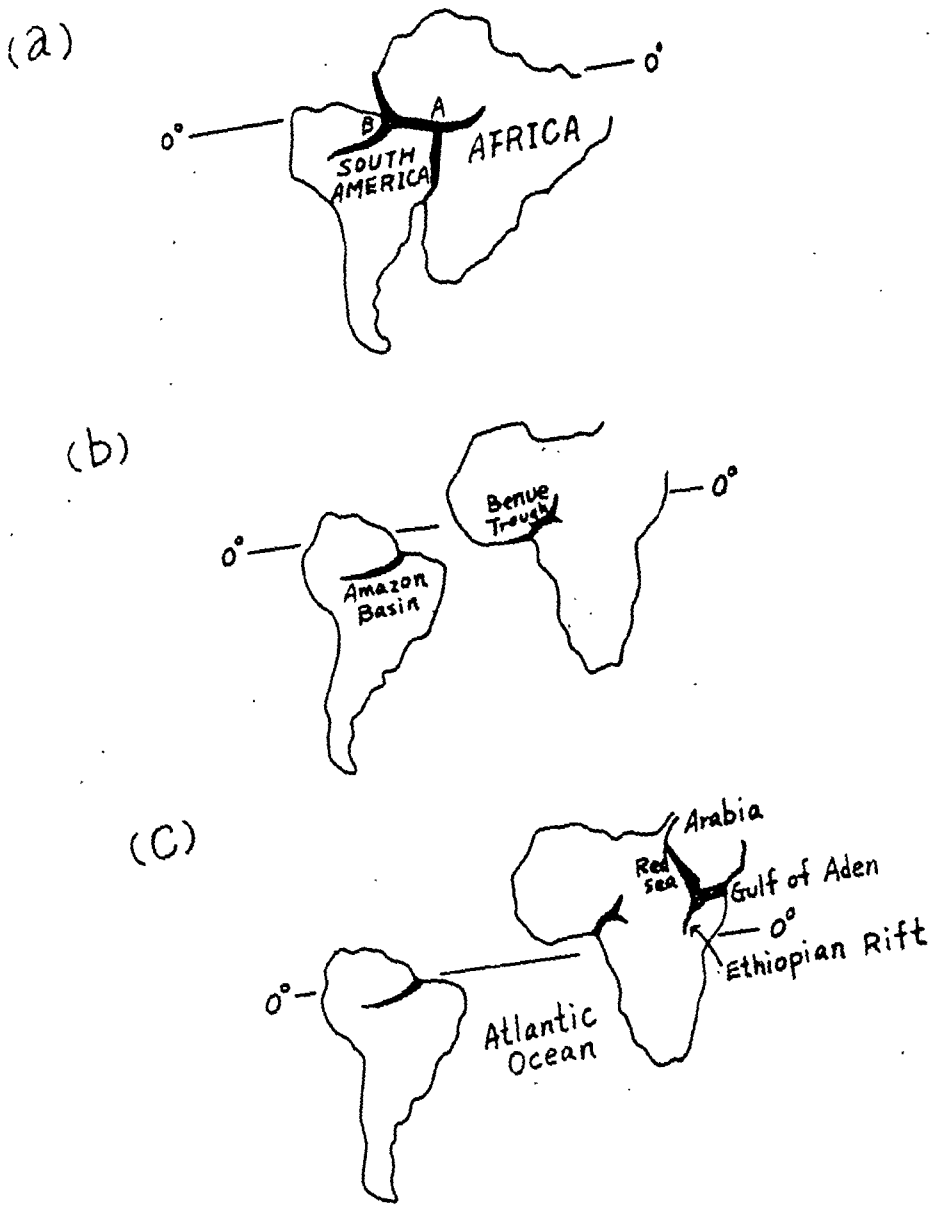

Figure 27: Origin of Amazon Basin and Benue Trough as Rift Arm Abandoned during Continental Rift Separation of Africa and South America in Cretaceous Time (modified after Horrman, Dewey and Burke, 1974)

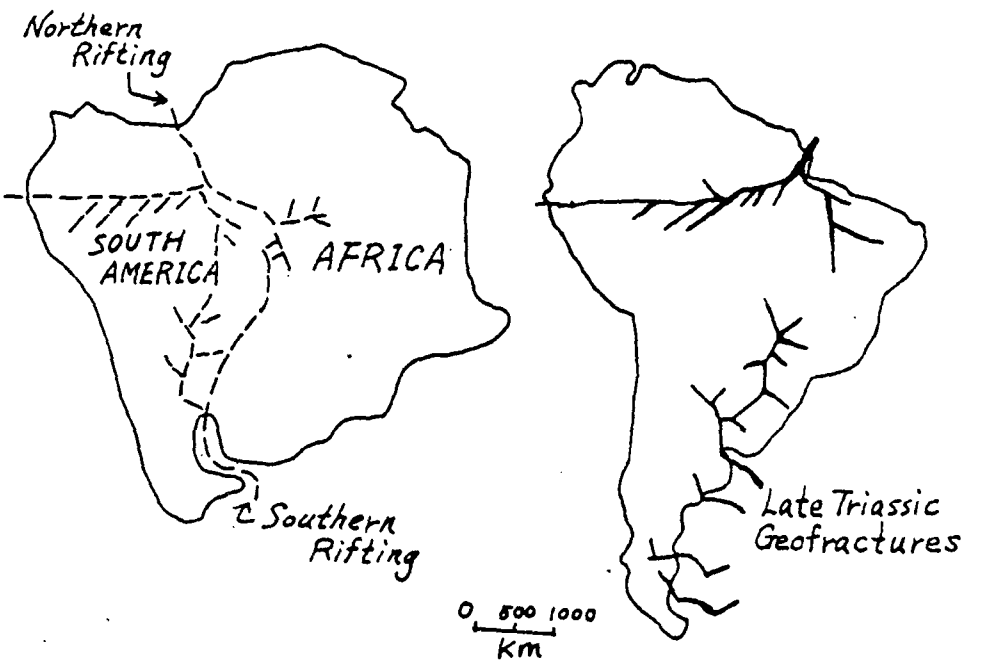

Figure 28: Geofracture System (Related to Continental Separation)
(redrawn from de Rezende 1972)

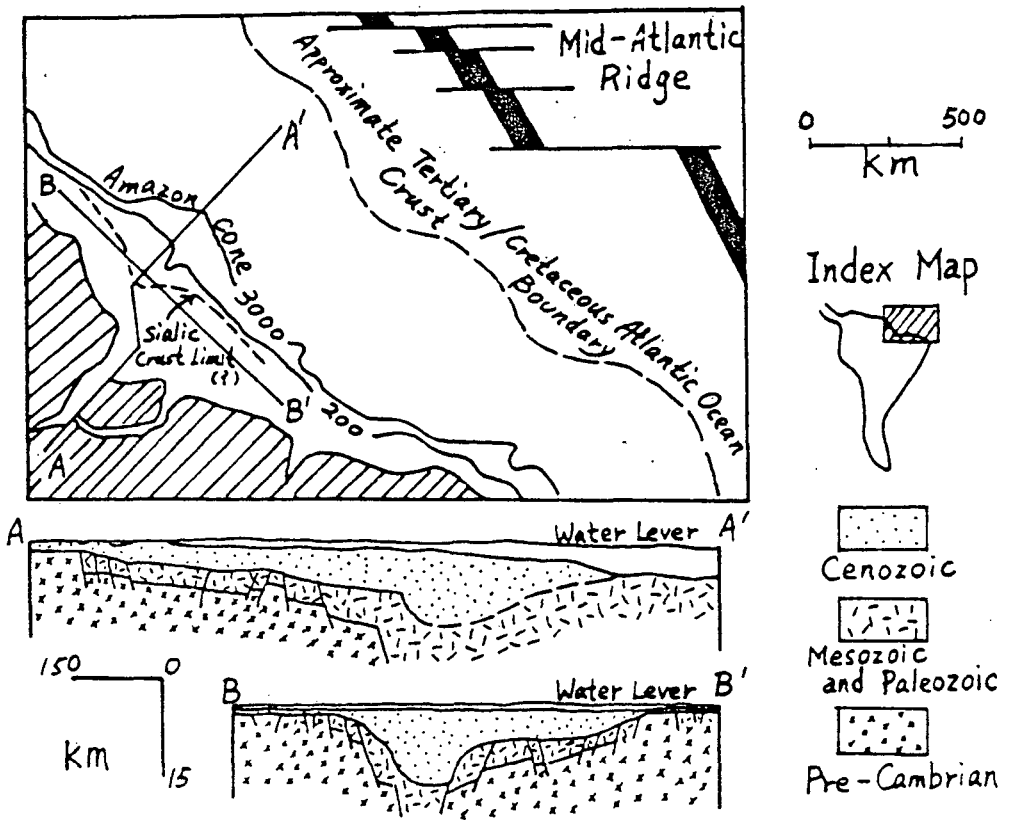

Figure 29: Rift Control on Lower Part of Amazon River
(redrawn from Bacoccoli and Texeira 1973, fig.4)

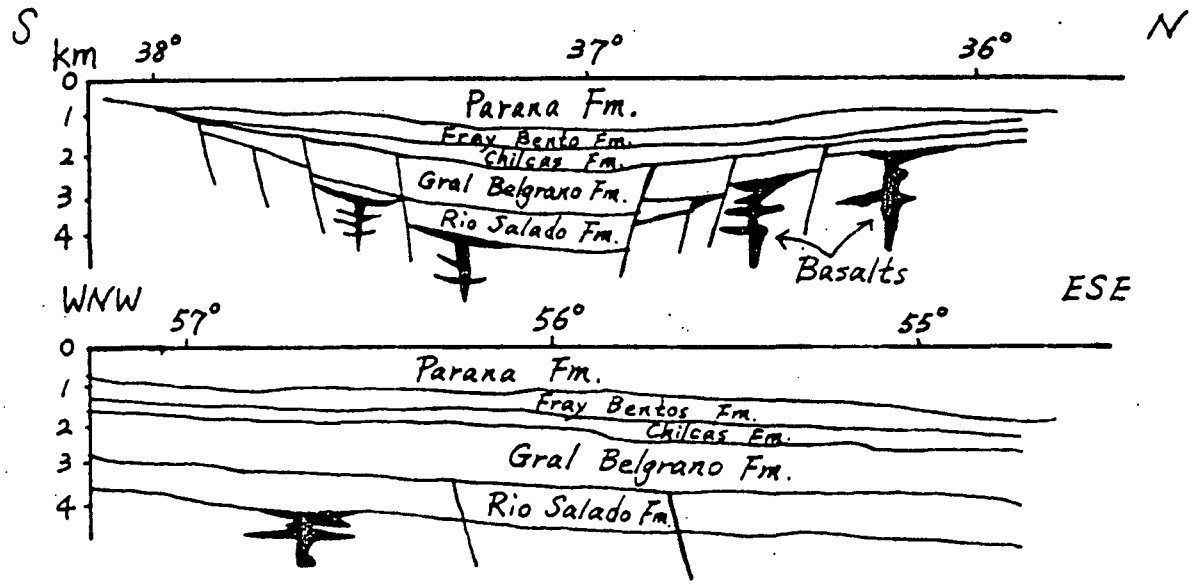

Figure 30: Cross Section of the Salado Basin
(after Urien and Zambrano, 1973)

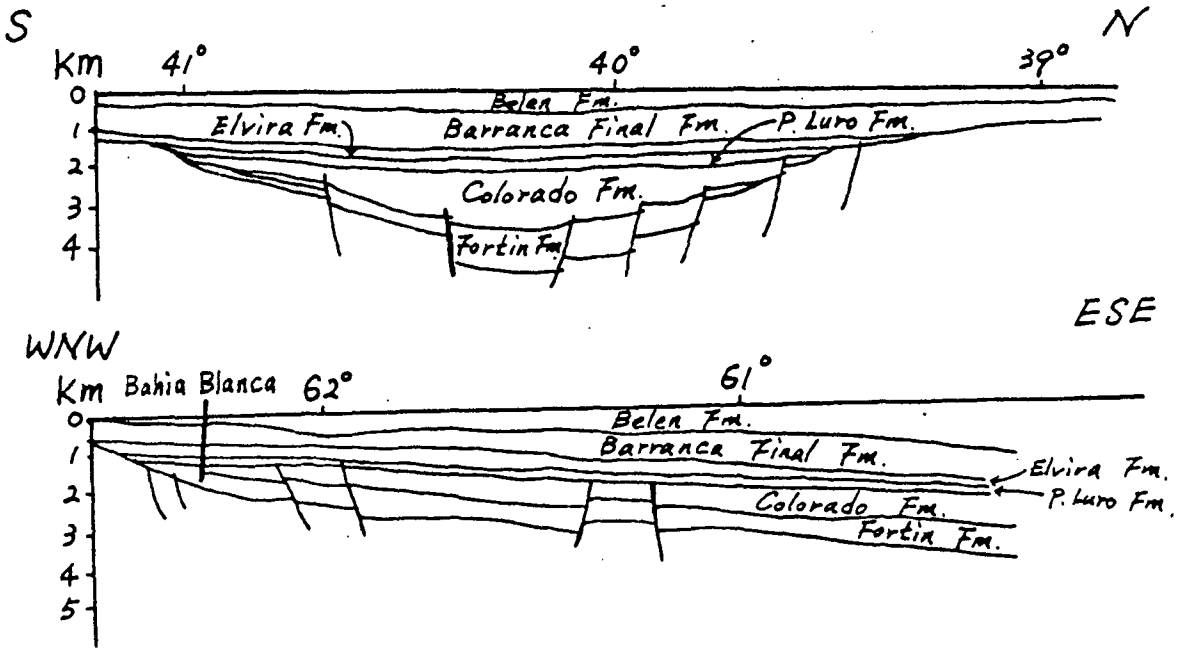

Figure 31: Cross Section of the Colorodo Basin
(after Urien and Zambrano, 1973)

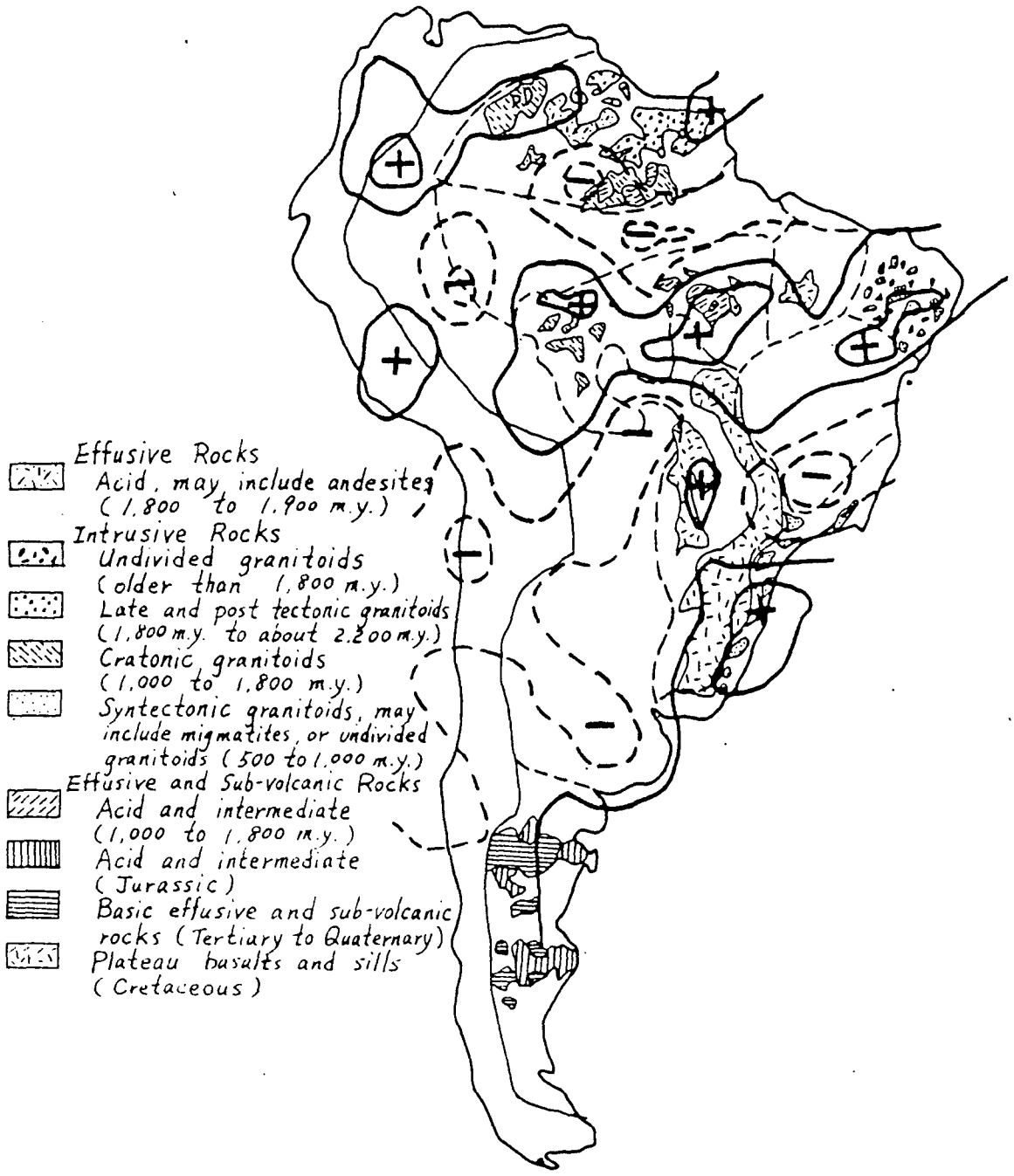

Figure 32: Correlation between the Magnetic Anomalies and Volcanic Rocks of South America

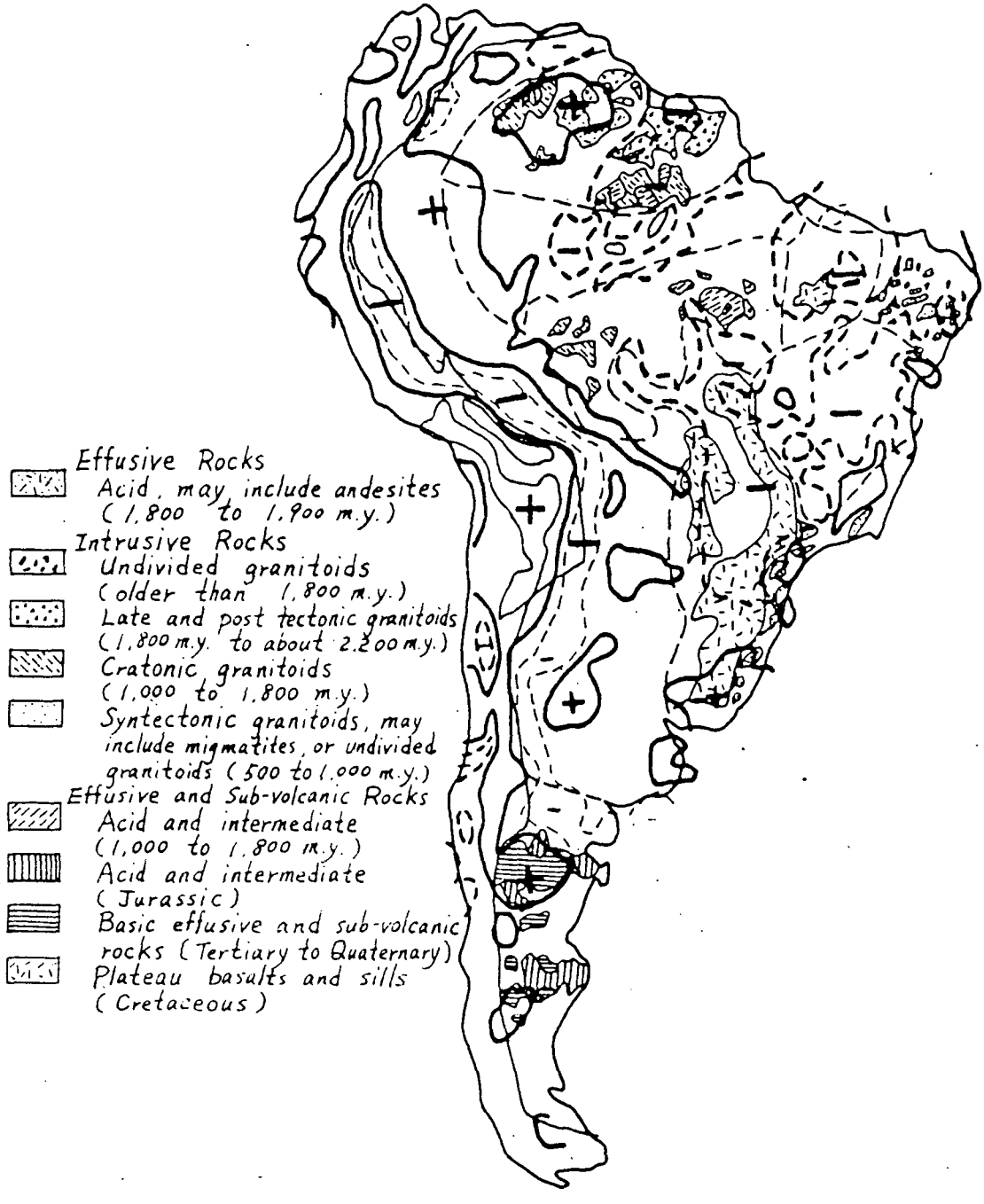

Figure 33: Correlation between the Free-Air Gravity Anomalies and Volcanic Rocks of South America

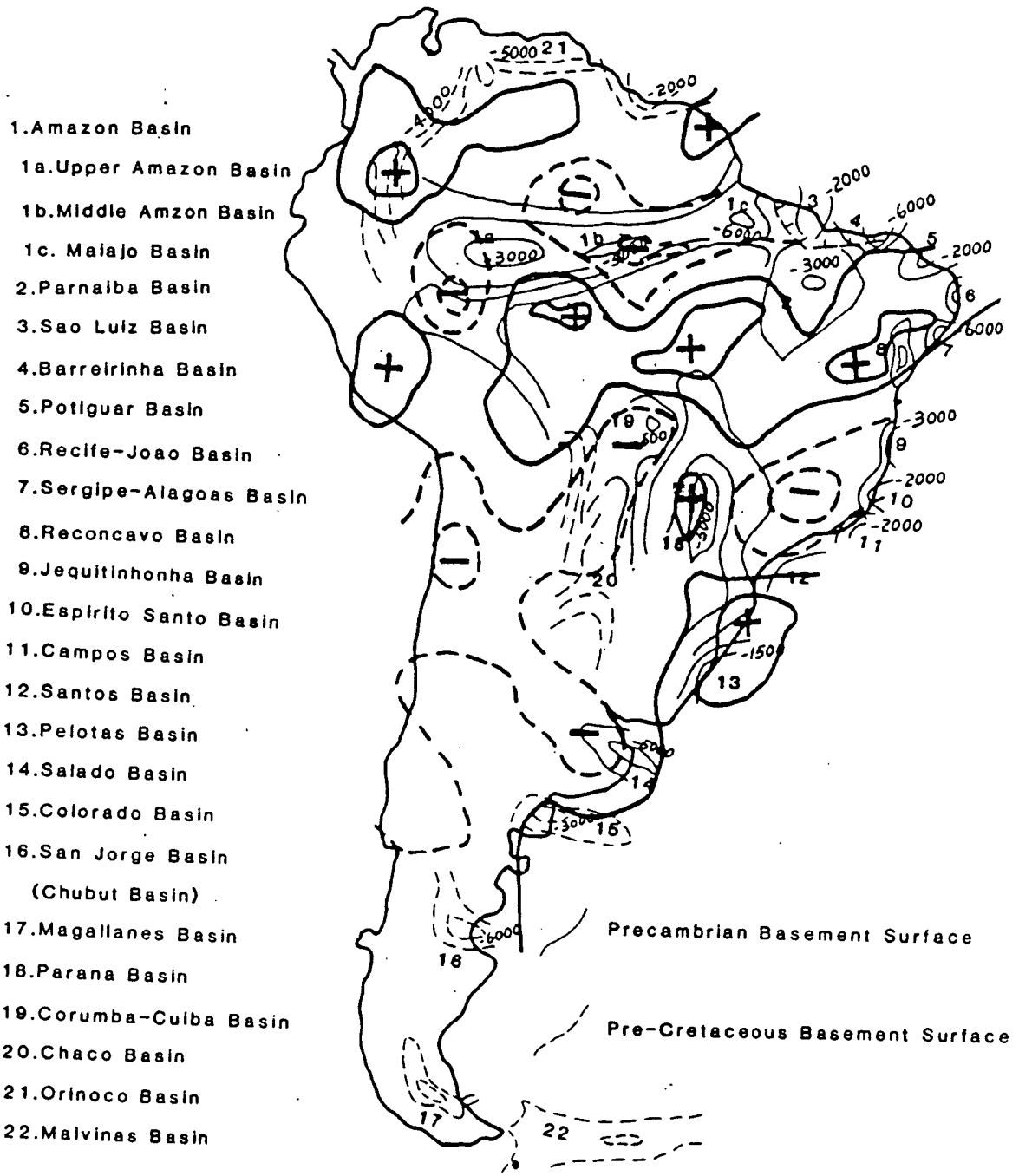

Figure 34: Correlation between Magnetic Anomalies and Major Basins of South America

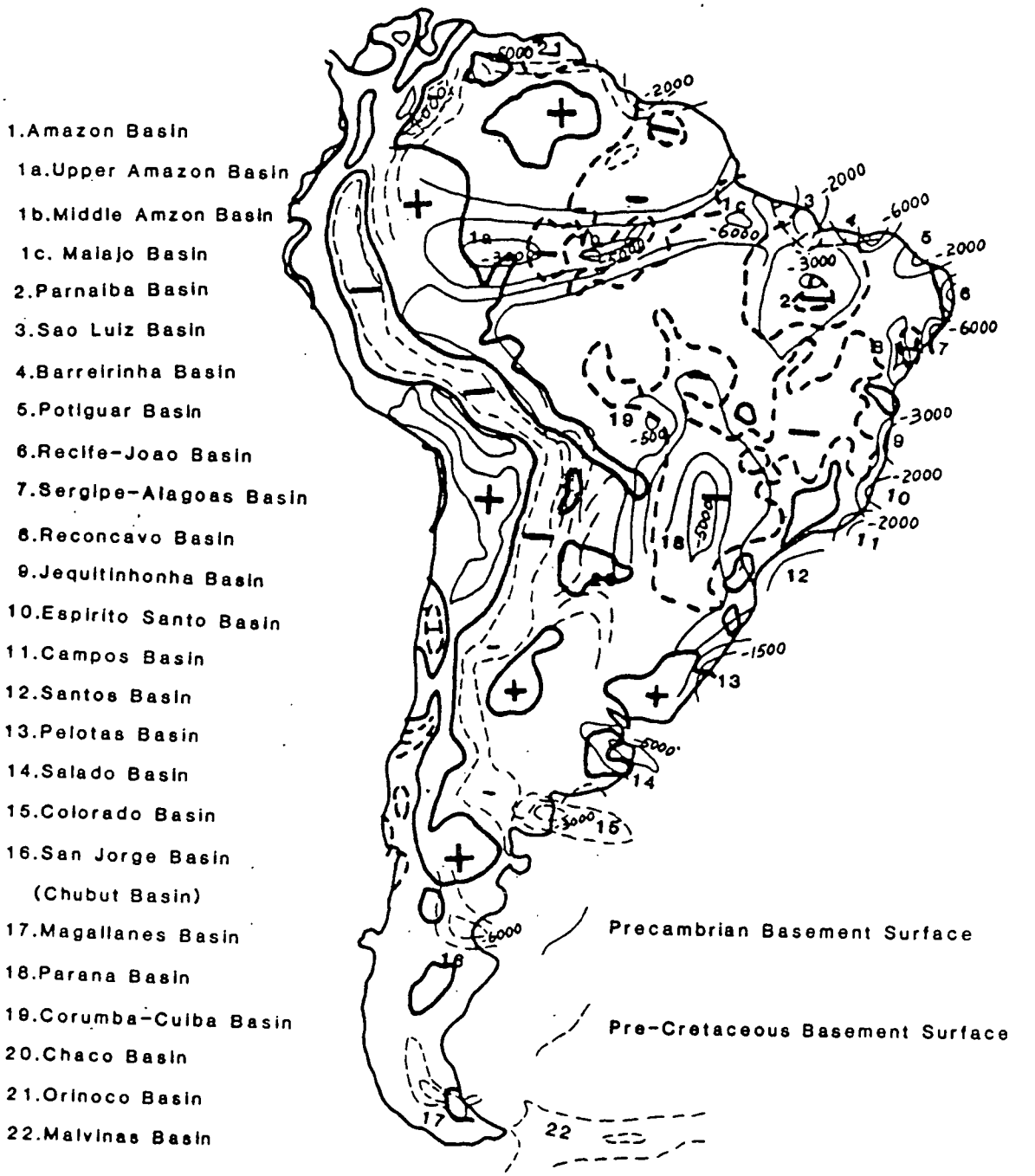

Figure 35: Correlation between the Free-Air Gravity Anomalies and Major Basins of South America

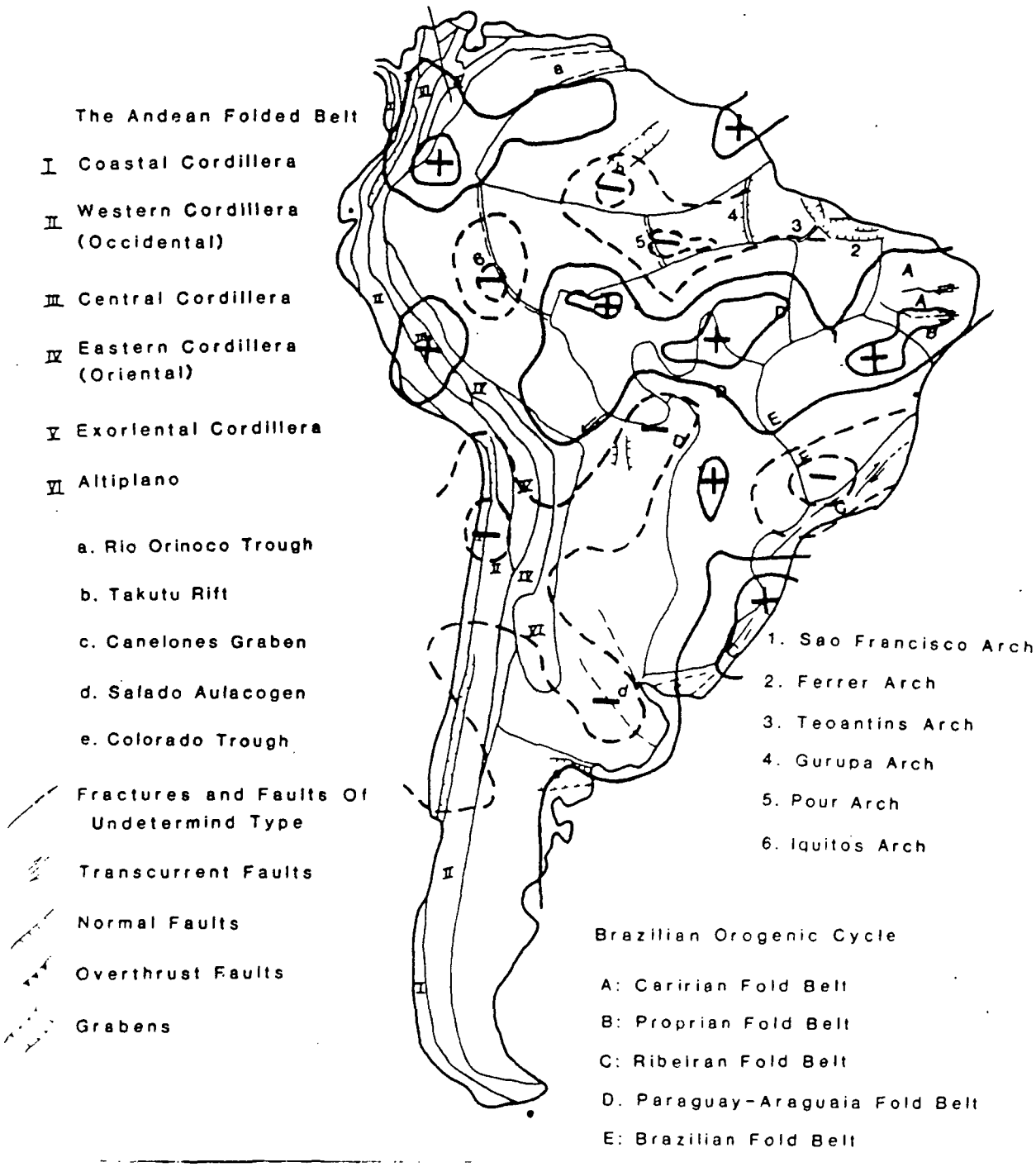

Figure 36: Correlation between the Magnetic Anomalies and Main Structures of South America

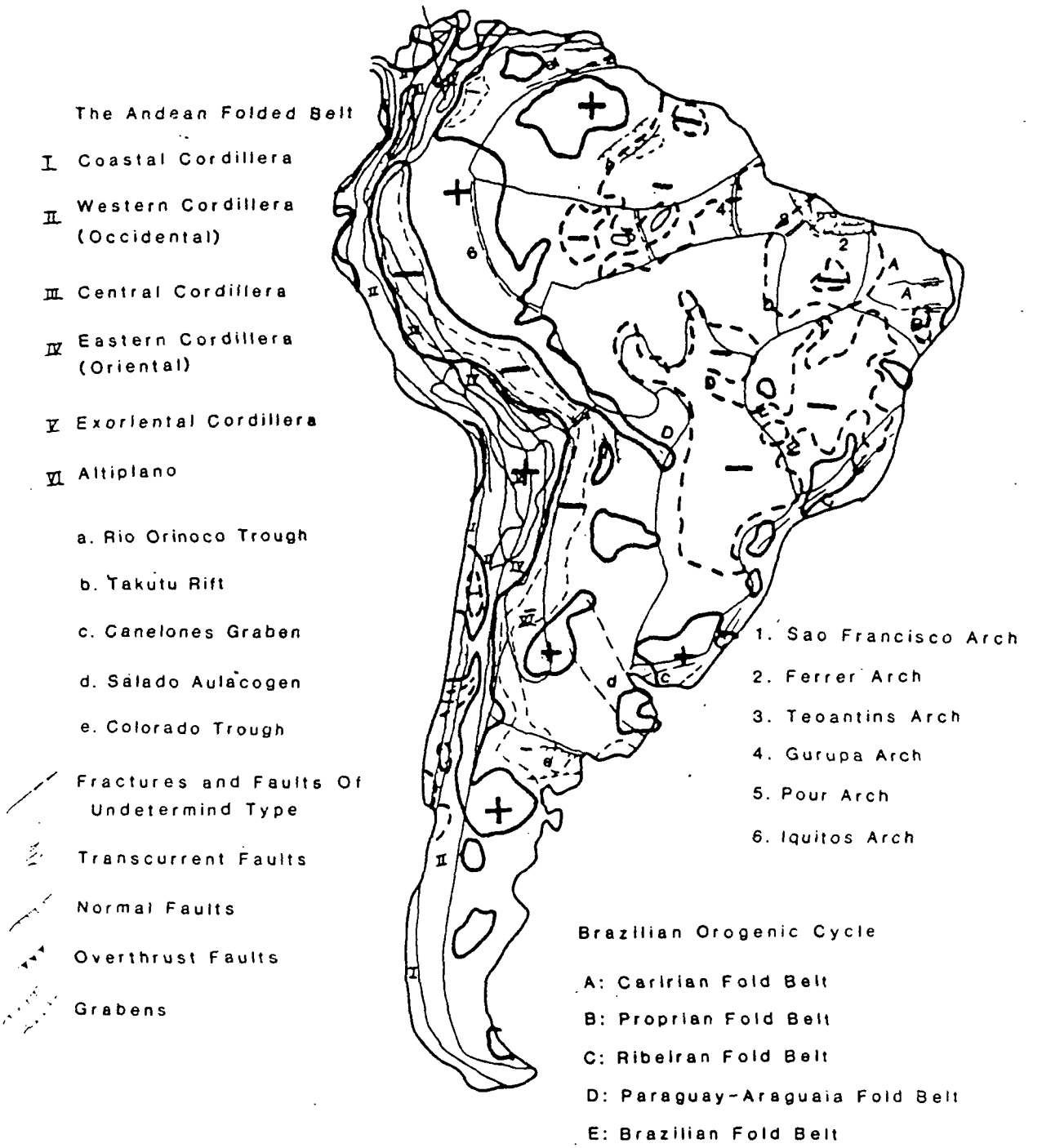

Figure 37: Correlation between the Free-Air Gravity Anomalies and Main Structures of South America

A. Brazilian Orogenic Cycle

450-700 m.y. (Late Proterozoic to Early Paleozoic)

These are several fold belts surrounding old cratonic areas:

(1) Caririan--northeastern Brazil

(2) Proprian--northern Bahia and Sergipe, Brazil

(3) Paraguay-Araguaia--central-western Brazil, and Paraguay

(4) Brazilian--central-southeastern Brazil

(5) Ribeiran--southeastern Atlantic coast of South American Platform

B. Uruacuano Orogenic Cycle

900-1300 m.y. (Middle Proterozoic)

(1) Minas Fold Belt--southern and eastern Minas Gerais Brazil

(2) Araxa Fold Belt--western Minas Gerais and Goian, Brazil

C. Trans-Amazonian Orogenic Cycle

1800-2200 m.y. (Early Proterozoic)

It is best known in the following areas:

(1) Guyana Shield--northern Brazil, Venezuela and the Guyanas

(2) Guapore Craton--northwestern Brazil

(3) Sao Luiz Craton--coastal area of Para and Maranhao Brazil

(4) Sao Francisco Craton--Goias, Minas Gerais, and Bahia, Brazil

(5) Rio de La Plata Craton--southern Uruguay and Buenos Aires Province, Argentina

Table 1: Main Geotectonic Cycles of The South America Platform (after de Almeida et al., 1973)

Unit	Approximate Radiometric Age
Gorotire Formation (?)	1600 m.y.
Rio Fresco Formation	
Vatuma Group	
Cubencranquen Formation (?)	
----------Unconformity----------	
Serra dos Carajas Group	2000 m.y.
----------Unconformity----------	
Undivided basement	more than 3000 m.y.

Table 2: The Stratigraphical Sequence of the Northeastern Portion of the Central Brazil Shield (after Amaral et al., 1973)

Unit (age)		Lithology
After do Chao Formation (Tertiary)		poorly consolidated, sandy, silty, chayey sediments, often with a basal conglomerate. (600 to 1084 m thick) (one of the most important sequences in the world)
----------extensive erosional surface----------		
Cretaceous	Paituna Formation	cross-bedded sandstone (100 to 200 m thick)iintercalated siltstone
	Rio Acre Formation	claystone with many concretions
	Divisor Formation	whitish sandstone, intercalation clays
	Rio Azul Formation	limestone, shale
	Moa Formation	sandstone (1) Upper member (300 m) (2) Capanaua member (100m): basal conglomeratic layer
Jurassic Triassic		Big Gap
----------extensive erosional surface----------		
Sucuruendi Formation (Permian)		micaceous, slightly calcareous sandstone, siltstone, evaporites (no outcrop, 645 m)
Carboniferous	Nova Olinda Formation	clastic deposits, evaporites (1209 m, maximum)
	Itaituba Formation	microcoquinas and calcareous muds (neritic deposits) 150 to 320 m (north), 35 to 400 m (south) limestone, shale, sandstone, siltstone
	Monte Alegre Formation	cross bedding of sandstone (shallow-water marine) limestone, microcoquinas (25 to 300 m)
	(long hiatus, no unconformity)	
	Curua Formation	uniform, dark shales and siltstone (1300 m)
----------Unconformity----------		
Trombetas Formation (Ordovician ? to Silurian)		cross-bedded sandstone, siltstone, shale
----------angular unconformity----------		
Uatuma Formation (Precambrian)		in upper Amazon Basin

Table 3: Stratigraphical Successions in Amazon Basin
(Summarized from Bigarella, 1973)

Unit (radiometric age)	Lithology
Bambui Group (600 20 m.y.)	fine detrital rocks, important limestone beds, Locally stromatolithic.
----------Unconformity----------	
Lavras Group	arenacious rocks (mainly), in part of glacial origin.
(doubtful age, possibly post-Trans-Amazonian)	late upper Precambrian, certainly
----------Unconformity----------	
Jacobina Group (2000 m.y.)	a narrow metasedimentary belt (more than 8000 m thickness), phyllite, quartzite, schists, metaconglomerates, and associated metabasites.
Uaua Group	schists, quartzite, marbles, amphibolites, and several types of paragneisses. amphibolite facies.
----------Unconformity----------	
Caraiba Group (more than 2000 m.y.)	low-maturity metasediments associated with eruptive rocks of basic and ultra-basic character. show extensive migmatization and granitization. granulite facies.

Table 4: Principal Precambrian Formations in the Northern Part of the Sao Francisco Craton (region 1, Fig. 16) (after Cordani et al., 1973)

Unit (radiometric age)	Lithology
Rio Pardo Group	shales, silstones, greywackes,
(600 m.y.)	conglomeratic arkoses, Limestones, dolomites.
----------Unconformity----------	
Basement	gneisses, schists, quaitzites,
(2000 m.y.)	and marbles.

Table 5: The Succession of the Eastern Portion of the Sao Francisco Craton (region 2 in Fig.16) (after Kawashita et al., 1973)

Unit (age)	sedimentary enviroment	maximum thickness (m)	Lithology
Bambui Group (600 20 m.y.)			see Table 4
----------Unconformity----------			
Itacolomi (unknown)	Paralic	2000 ?	quartzite with subordinate
	Molasse ?	1000 ?	phyllites and meta-conglomerates
----------a sharp angular unconformity----------			
Minas Series (more than 1300 m.y.) Piracicaba Group	Eugeosynclinal (flysch)	3000	chlorite schist, phyllite, graywacks, congl, quartzite
	Stable Shelf	685	phyllite, orthoquaitzite, siliceous dolomite.
local erosional unconformity	(blanket)	600	quartzite, phyllite, minor conglomerate, dolomite.

Itabira Group	Stable Shelf	600	Dolomite, minor limestone, dolomitic itabirite phyllite.
	(blanket)	350	Itabirite, iron-formation, minor dolomite and phyllite.
Caraca Group	Stable Shelf	1000	phyllite, Orthoquartzite, conglomerate.
local erosional unconformity-----			minor metachert and iron-formation.
Tamandua Group	Stable Shelf	300	Dolomitic phyllite and iron-formation.
	Paralic Prismatic	1000	Orthoquartzite, conglomerate, grit.
----------Erosional and angular unconformity----------			

continue on next page

Table 6: Stratigraphic Section in the Southern Portion of the Sao Francisco Craton ("Quadrilatero Ferrifero") (region 3 in fig. 16) (modified from Dorr, 1969)

Unit (age)		sedimentary enviroment	maximum thickness (m)	Lithology
Rio das Velhas Series	Maquine Group	Engeosynclinal Molasse	1800	quartz-sericite schists, phyllites, meta-conglomerates, and quartzites.
	-------Local erosional and possibly angular unconformity-------			
	Nova Lima Group	Engeosynclinal (flysch)	4000	subordinate graywackes, quartzites, dolomites, metaconglomerates, cherts, itabirites, metavolcanics.
----------Unconformity----------				
Basement (more than 2700 m.y.)		no basement rocks exposed in the "Quadrilatero Ferrifero" all granitic rocks are intrusive.		

Unit (age)		Sedimentary Environment	Lithology
Bambui Group (?) Eo-Cambrian		transitional (Continental marine)	orthoquartzite and siltstone containing interbeds of shale (called phyllite, but, although at chlorite grade, it lacks a penetrative foliation)
Canastra Group 620-900 m.y. Pre-Cambrian			quartzite, quartz-rich phyllite, pelitic schist (Braun 1970) biotite grade of regional metamorphism
Araxa Group (900-1300 m.y.)	Upper unit	deep marine	quite pelitic, muscovite-biotite-plagioclase-quartz schist (most common), garnet-chlorite-biotite-quartz schist (fairly abundant)
	Middle unit		more psammitic, interbedded quartzite (quartz and turbidites) and muscovite-quartz schist
	Lowermost unit		consists primarily of muscovite-biotite-plagioclase-quartz schist, some micaceous quartzite

Table 7: Stratigraphic Section in Serra de Caldas, Goias (modified from Drake, 1980)

	Unit (age)	Lithology
	Itapecuru Formation (lower Tertiary)	sandstone, siltstone, shale
Cretaceous	Codo Formation	black shale (220 m)
	Corda Formation	yellow sandstone, no fossil
	Basalts 127 m.y.	175 m thick (maximum)
	Sambaiba Formation (Jurassic)	sandstone (400 m), no fossil
	Pastos Bons Formation (Triassic)	white sandstone (70 m), shale, thin limestone (lenses of opal)
	----------great erosional unconformity----------	
Permian	Motuca Formation	shale sandstone, anhydrite, limestone
	Pedra de Fogo Formation	chert, petrified wood (40 cm)
Carboniferous	Piaui Formation	(1) upper: shale, sandstone, anhydrite, dolormite limestone (250 m) (2) lower: sandstone, shale (170 m)
	----------Unconformity----------	
	Poti Formation	carbonaceous sandstone, siltstone (300 m), coal
Devonian	Longa Formation	black shale, sandstone, more than 120 m
	Cabecas Formation	sandstone, siltstone, rare shale, 300 to 400 m
	Pimenteira Formation (Silurian)	Pico member Itaim member (150 m)
	Serra Grande Formation (Ordovician ? to Silurian)	sandstone, conglomerate, 200 m (average)
	----------Unconformity----------	
	Jaibara Formation (Ceara Group) (Precambrian)	

Table 8: Stratigraphic Successions in Parnaiba Basin (summarized from Bigarella, 1973)

Unit	Approximate age (radiometric)	characters
Paleozoic or Younger sedimentary rocks		
Gurupi Group	550-600 m.y.	schists, phyllites, quartzites and itabirites folded with northwest strikes.
----------Unconformity----------		
Basement	2000 m.y.	

Table 9: Principal Successions in Sao Luiz Basin
(modified after Bigarella, 1973)

Age	Geological Characters of the Formation
Quaternary	A predominantly eolian sedimentation in the onshore part covering it with a thin but widespread blanket of sand.
Miocene	A miocene transgression completely covered the basin and extended beyond its limits, flooding also the Sao Luiz basin and the northern part of the Maranhao Paleozoic basin to deposit carbonates and clastics.
Middle Cretaceous	The Ferrer-Urbano Santos-Parnaiba arch subsided
--Upper Cretaceous	The carbonate deposition of the Caju Group of upper Albian through Campanian age.
(Cenomanian-Campanian)	Both shelf limestones and reef complexes were developed.
Lower Cretaceous --Middle Cretaceous (Aptian-Albian)	A marine invasion took place during Aptian time. An Albian marine transgression extended beyond the limits of the basin flooding the northern part of the Paleozoic Maranhao basin to the south of the Ferrer-Parnaiba arch. The western part of this arch supplies clastic materials of the Canarias Group. An upper Albian regression exposed portions of the area to erosion prior to the beginning of the next cycle.
The lowermost Cretaceous (120-130 m.y.)	is marked by widespread basic volcanism (Wealdian)
The basement	is heterogeneous consisting of Precambrian crystalline rocks. Paleozoic-Lower Mesozoic sediments, and lower-most Cretaceous basic volcanics.

Table 10: Principal Sequences in Barreirinhas Basin
(modified after Asmus and Ponte, 1973)

Unit Appoximate radiometric age	Lithology
Jaibaras Group (500 m.y.)	affected by granitic and granodioritic plutonic intrusions. rhyolites, andesites, basalts.
----------Unconformity----------	
Caico Group (2000 m.y.)	Undifferentiated Precambrian
----------Unconformity----------	
Basement (unknown)	Undifferentiated Precambrian

Table 11: Principal Sequences in the Caririan Fold Area (modified from de Almeida et al., 1973)

Unit, Approximate radiometric age	Lithology
Estancia Group (on the platform)	
600 m.y.	
Jua and Acaua Formation (within the geosyncline)	
----------Unconformity----------	
Vaza Barris Group, more than 600 m.y.	eugeosynclinal zone (basic volcanic products are associated with pelites, metagraywackes, in part conglomeratic, sandstones, and limestone).
//////////thrust contact//////////	
Miaba Formation (and Canudos Formation)	age unknown, miogeosynclinal zone
Basement	more than 2000 m.y. (up to 2530 m.y.) undifferentiated Precambrian and middle Precambrian

Table 12: Principal Formations in the Propria Fold Belt (modified from Amaral et al., 1973)

Unit (Approximate radiometric age)	Lithology
Serra dos Orgaos Series, (550-600 m.y.)	migmatites granitic gneisses
----------Unconformity----------	
Paraiba-Desengano Series, (2000 m.y.)	Paragneisses, metagraywackes, metaarkoses with subordinate quartzites mica schists.

Table 13: Successions in the Paraiba do Sul and Ribeira Fold Belt, near Rio de Janeiro (region 1 in Fig. 21) (modified from Cordani et al., 1973)

Unit (Approximate radiometric age)	Lithology
Castro and Itajai Group Camarinha and Guaratubinha Formations (Cambro-Ordovician,500 m.y.)	detritic sediments of molassic nature, volcanic rocks of andesite-rhyolite character.
----------Unconformity----------	
Sao Roque, Acungui and Brusque Groups (650 m.y.)	phyllites, schists, quartzites, dolomites, limestones with suborinate metaconglomerates, metaarkoes, metagraywackes, and itabirites.
----------Unconformity----------	
Basement (more than 1200 m.y.)	undifferentiated Precambrian

Table 14: Sequences in the Ribeira Fold Belt, in Sao Paulo, Parana, and Santa Catarina States. (region 2 in Fig. 21) (modified from Kawashita et al., 1973)

Unit and Approximate radiometric age	Lithology
Camaqua Group	continental detrtic sedi-ments.
---Unconformity--- Cambro-Ordovician	Lavas, pyroclastic rocks of andesitic, rhyolitic and
Bom Jardim Group (500 m.y.)	dacitic composition. granite and granodiorite intrusion.
----------Unconformity----------	
Porongos Group (650 m.y.)	phyllites, schists, quarızites, limestones, metaconglomerates, metagraywackes, metaarkoses, rhyolitic, andesitic or pyroclastic metavolcanics.
Cambai Formation	gneisses, amphibolites, and marbles with associated mig-matization and granitization.
----------Unconformity----------	
Zncantadas Formation (Probably 2,000 m.y.)	hornblende and biolite gneisses partially migmatized

Table 15: Successions in Riberia Fold Belt, in the state of Rio Grande do Sul (region 3 in Fig. 21) (modified from de Almeida et al., 1973)

Unit and Approximate radiometric age	Lithology
Sierra de Animas Piedras de Afilar (500 30 m.y.)	trachytes, syenites, rhyolites Sandstone, quartzites, limestones
----------Unconformity----------	
Lavalleja Group (600 m.y.)	phyllites, schists, quartzites, marbles basic metavolcanic rocks.
----------Unconformity----------	
Basement (including Montevideo Formation, 2000 m.y.)	

Table 16: Successions of the Rio de La Plata Craton in Uruguay (region A1 in Fig. 23) (modified from Cordani et al., 1973)

Unit and Approximate Radiometric Age	Lithology
La Tinta Group (possibly 600 m.y.)	sandstones, quartzites, limestones, dolomites, fine-grained detrital sediments.
----------Unconformity----------	
Basement (around 2000 m.y.)	gneissic complex of metasedimentary origin amphibolites, mica-schists, phyllites, quartzites, migmatites, granites, granodiorites, tonalites, diorites.

Table 17: Successions of the Rio de La Plata Craton in the Province of Buenos Aires, Argentina (region A2 in Fig. 23) (modified from Kawashita et al., 1973)

m.y.	age		Basins	
			Salado	Colorado
	Quaternary			
	Tertiary	Pliocene	Parana Formation	Belen Formation
26		Miocene	Fray Bentos Formation	Bca. Final Formation
38		Oligocene		
54		Eocene		
65		Paleocene	Chilcas Formation	Elvira Formation P. Luro Formation
85	Cretaceous	Upple	G. Belgrano Formation	Colorado Formation
100			R. Salado Formation	Fortin Formation
112		Middle		
136		Lower	Basalts	
			Diabases	Paleozoic Basement
			Precambrian Basement	

Table 18: Stratigraphic Columns of Salado and Colorado Basins (modified from Urien and Zambrano, 1973)

REFERENCES

Aldrich, L.T., Hart, S.R., Tilton, G.R., Davis, G.L., Rama, S.N.I., Steiger. R., Richards. J.R., and Gerken, J.S., 1964, Isotope geology, in: Ann. Rept. Director, Dept Terrestrial Magnetism, Carnegie Inst. Washington Yearbook, v.63, p.328-340.

Almaraz, J.S., 1967, Determinacoes K-Ar na regiao do curso medio do rio Tocantins: Bol. Soc. Bras. Geologia, v.16, no.1, p.121-126.

Almaraz, J.S., and Cordani, U.G., 1969, Delimitacao entre procambrianas ao longo do rio Gurupi, Norte do Brasil: XXIII Cong. Bras. Geologia-Res. Conf. Comun., Bol. Esp. no.1, p.89, (abst.).

Almeida, F.F.M. de, 1964, Os fundamentos geologicos, in: Brasil a Terra e o Homem, Azevedo, A., ed., Sao Paulo, Cia Edit. Nac., p.55-120.

Almeida, F.F.M. de, 1967, Origem e evolucao da plataforma Brasileira: Div. Geol. Mineralogia, Min. Minas Energia. Bol. no.241, p.36.

Almeida, F.F.M. de, 1968, Precambrian geology of Northeastern Brazil and Western Africa and the theory of continental drift: Proc. of the Symposium on the granites of West Africa, Unesco Nat. Res. Research VIII. p.151-162.

Almeida, F.F.M. de, Amaral, G., cordani. U.G., and Kawashita, k., 1973, The Precambrian evolution of the South America cratonic margin south of the Amazon River, in Nairn, A.E.M., and Stehli, F.G., eds., The ocean basins and margins, v.1, The South Atlantic: New York, Plenum Press, p.411-446.

Almeida, F.F.M. de, and Black. R. 1968, Geological comparison of Northeastern South America and Western Africa: An. Acad. Bras. Cienc., v.40 (supl). p.317-319.

Almeida, F.F.M. de Leonardos O.H.Jr., and Valenca, J., 1971, Review on granitic rocks of Northeast South America.

International Union of Geological Sciences, 41 p. Haarlem.

Almeida, F.F.M. de, Melcher, G.G., Cordani, U.G., Kawashita, K., and Vandoros, P., 1968, Radiometric age determinations from Northern Brazil: Soc. Bras. Geologia. v.17, no.1, p.3-14.

Amaral, G., 1970, Precambrian Evolution of the Brazilian Amazon Region. (abs): 1st Latin American Geological Congress, Lima Peru.

Asmus, H.E. and Ponte, F.C., 1973, The Brazilian marginal basins, in Nairn, A.E.M., and Stehli, F.G., eds., The ocean basins and margins, v.1, The South Atlantic: New York, Plenum Press, p.87-132.

Barbosa, A.L.M., Grossi Sad, J.H., Torres, N., and Mello, M.T.V. de, 1966, Description of the preliminary geologic map of the Middle Rio Doce, Internat. Field Inst., Brazil, Guidebook: Am. Geol. Inst., p.III-1.

Barbosa, Octavio, 1955, Guia das excursoes do IX Congresso da Socidade Brasileira de Geologia: Soc. Brasileira Geologia Noticiario 3.

Barbosa O., 1966, Tectonica do Nordeste: Soc. Bras. Geologia, XX Congr. Bras. Geologia, Nucleo Rio de Janeiro, Public., v.1 p.68-72.

Barron, C.N., 1962, The geology of the South Savannos Degree Square: Bull. Geol. Surv. Br. Guiana, v.33.

Barruol, J., 1961, Le Bonidoro en Guyane Francaise: Proc. Fifth Inter-Guiana Geol. Conf., Georgetown, 1959, p.57-67.

Bellizzia, C.M. and Bellizzia, A., 1956, Imataca Series, in Stratigraphic lexicon of Venezuela: Ministero Minas Hidrocarburas, Spec. Publ. 1, p.254-256.

Berbert, C.O., 1970, General geology of the basic-ultrabasic complexes of Goias: Cong. Brasileiro Geologia, 24th. Brasilia, 1970, Bol. Especial 1, p.24-28.

Bigarella, J.J., 1964, Paleogeographic and paleoclimatologic features of the Southern Brazilian Devonian, in: Problems in Paleoclimatology Nairn, A.E.M., ed., London, Wiley, p.293-303.

Bigarella, J.J., 1973, Geology of the Amazon and Parnaiba basins, in Nairn, A.E.M. and Stehli, F.G., eds., The ocean basins and margins, v.1, The South Atlantic: New York, Plenum Press, p.25-79.

Bigarella, J.J., Mabesoone, J.M., Lins, C.J.C., and Mota Fo., F.O., 1965, Palaeogeographical features of the Serra Grande and Pimenteira formations (Parnaiba Basin, Brazil): Palaeogeography, Palaeoclimatol., Palaeoecol. v.1, p.259-296.

Bigarella, J.J. and Salamuni, R., 1967a, Some palaeogeographic features of the Brazilian Devonian, in: Problems in Brazilian Devonian Geology: Bol. Par. Geocien., Bigarella, J.J., ed., no.21/22.

Bigarella, J.J. and Salamuni, R., 1967b, Some palaeogeographic and palaeotectonic features of the Parana Basin, in: Problems in Brazilian Gondwana Geology, Bigarella, J.J., Becker, R.D., and Pinto, I.D. eds., Impr. Univ. Fed. Parana.

Bischoff, G.O., 1963, Zur Geologic des Amazonbeckens: Geol. Jb., v.80, p.771-794.

Bonorino, F.G., 1950, Algunos problemas geologicos de las Sierras Pampeanas: Assoc. Geol. Argentina, V.

Bonorino, F.G., 1954, Geologia de las Sierras Bayas, partido de Olavarria, Provincia de Buenos Aires: Lab. Ens. Mater-Invest. Tecnol. Min. Obras Publicas. Serie II, no.55, p.4-37.

Bossi, J., 1966, Geologia del Uruguay: Univ. de la Republica, Dep. Publ., Col. Cein., v.2, p.464.

Bossi, J. and Fernadez, A., 1963, Evidencias de diferenciacion magmatica hacia dl final del Gondwana uruguayo: Bol. Univ. Parana, Geol., v.9, p.1-20.

Bossi, J., Fernandez, A., and Elizade, G., 1965, Predevoniano en el Uruguay: Univ. de la Republica, Fac. Agronomia. v.78, p.84.

Bouman, Q.C., Mesner, J.C., and Padden, M., 1960, Amazonas Basin study: Petrobras, Int. Rep. DEPEX, no.12.

Braun, O.P.G., 1970a, The economic significance of the Caldas Novas greenschist: Cong. Brasileiro Geologia. 24th, Brasilia, 1970, Bol. Especial 1, p.134-135.

-----1970b, Geologia da area de Caldas Novas, Ipamerie

Arredores, no Estado de Goias: Cong. Brasileiro Geologia, 24th. Brasilia. 1970, Bol. Especial 1, p.205-207.

Brail Departmento Nacional da Producao Mineral, 1971, Mapa geologic do Brasil: Rio de Janeiro. scale 1: 5,000,000.

Burke, K. and Dewey, J.F. (1973a). Plume-generated triple junctions: key indicators in applying plate tectonics to old rocks. J. Geol., 81, 406-433.

Burke, K., Dessauvagie, T.F.J. and Whiteman, A.J. (1971). Opening of the Gulf of Guinea and geological history of the Benue Depression and Niger delta. Nature Phys. Sci., 233. 51-55.

Caminos, R. (1972): Cordillera Frontal.-In: Geologia Regional Argentina, LEANZA, A.F. (Ed.), 305-343.

Caorsi, J.H. and Goni, J.C., 1958, Geologia uruguaya: Inst. Geol. Uruguaya, v.37, p.73.

Case, J.E. and McDonald, W.D. 1973, Regional gravity anomalies and crustal structure in Northern Colombia: Bull. geol. Soc. Amer. 84, 2905-2916.

Case, J.E., Barnes, J., Paris, G., Gonzalez, H.I. and Vina, A., 1973, Trans-Andean geophysical profile, Southern Colombia: Bull. geol. Soc. Amer. 84, 2895-2904.

Case, J.E., Duran, L.G., Alfonso Lopez, P. & Morre, W.R. (1971): Tectonic investigations in western Colombia and eastern Panama. -Bull. geol. Soc. Amer., 82, 2685-2712.

Cazeneuve, H., 1967, Edades isotopicas del basamento de la provincia de Buenos Aires: Ameghiniana, v. V, no.1, p.3-10.

Choubert, B., 1964, Ages absolus du Precambrian guyanais: Compt. Rend. Acad. Sci. Paris, v.258, p.631-634.

Choubert, B., 1965, Etat actuel de nos connaissances sur la geologie de la Guyane francaise: Bull. Soc. Geol. France, v.7, p.129-135.

Choubert, G., 1970. Note au sujet des granites du Nord-Est bresilien: Chronique Mines Recherche Miniere, no.397, p.291-297.

Coleman, R.G., and Irwin, W.P., 1974, Ophiolites and ancient continental margins, in Burk. C.A., and Drake. C.L., eds.,

The geology of continental margins: New York, Springer-Verlag, p.921-931.

Cordani, U.G., 1968, Esboso da Geocronologia Precambriana da America do Sul: An. Acad. Bras. Cien., v.40, Suplemento, p.47-51.

Cordani, U.G. and Bittencourt, I., 1967, Determinacoes de idade potassio-argonic em rochas do Grupo Acungui: Anais XXI Congr. Bras. Geologia, p.218-233.

Cordani, U.G., and Vandoros, P., 1967, Basaltic rocks of the Parana Basin, in Problems in Brazilian Gondwana Geology, First Int. Symposium Gondwana Stratigraphy and Paleontology, Curitiba, p.208-231.

Cordani, U.G., Melcher, G.C., and Almeida, F.F.M. de, 1968, Outline of the Precambrian geochsonology of South America: Can. J. Earth Sci., v.5, p.629-632.

Cordani, V., 1969, Idade do vulcanismo no Oceano Atlantico Sul: Bol. Fac. Fil. Cie. Letr. U.S.P. (em impressao).

Corvalan, J. & Munizaga, F. (1972): Edades radiometricas de rocas intrusivas y metamorficas de la Hoja Valparaiso, San Antonio. -IIG Bol., 28, 40p.

De Boer, N.P., 1964, Report on the geology of Northern Brazil: Petrobras, DEPEX, Internal Report 2020.

De Boer, N.P., 1966, The testonic framework and history of the sedimentary basins of Northern Brazil: Anais VI Conferencia Geologica das Guianas D.N.P.M., D.G.M., Avulso 41, p.78-83.

Delhal, J., Ledent, D., and Cordani, U.G., 1969, Ages Pb/U, Sr/Rb et Ar/K des formations metamorphiques et granitiques du Sud-Est du Bresil: Etats de Rio de Janeiro et de Minas Gerais. Annal. Soc. Geol. Belgique, v.92, p.271-283.

De Loczy, L., 1966, Contribuicao a paleogeografia e historia do desenvolvimento geologico da Bacia do Amazonas: D.N.P.M. Div. Geol. Min., Bol. 223.

De Rezende, W.M., 1972, Post Paleozoic geotectonics of South America related to plate tectonics and continental drift: Sociedade Brasileira de Geologia, Anais do XXVI, Congresso

Brasileiro de Geologia, p.205-210.

Dorr. J.V.N., 2d, 1969, Physiographic, stratigraphic, and structural development of the Quadrilatero Ferrifero, Minas Gerais, Brazil: U.S. Geol. Survey, Prof. Paper 641-A, p.110.

Dorr. J.V.N., 2d, Gair, J.E., Pomerene, J.B., and Rynearson, G.A., 1957, Revisao da estratigrafia pre-cambriana do Quadrilatero Ferrifero: Dept. Nac. Prod. Mineral, Div. Fom. Prod. Mineral, Avuiso 81, p.31.

Dragicevic, M. (1970): Carta gravimetrica de los Andes meridionales e interpretacion de las anomalias de gravedad de Chile Central. Publ. Depart. Geofis. Geodes. Univ. Chile, 93, 42p.

Dyer, R.C., 1970, Apresentacao preliminar da geologia da folha "Brasilia": Cong. Brasileiro Geologia, 24th, Brasilia, 1970, Bol. Especial 1, p.214-216.

Ebert, H., 1957, Beitrag zur Gliederung des Prakambriums in Minas Gerais: Geol. Rundschau, v.45, p.471-519.

Ebert, H., 1962, Baustil und Regionalmetamorphose in prakambrischen Grundgebirge Brasiliens: Tschermaks miner. und petrog. Mitt., v.8, p.49-81.

Ebert, H., 1966, A divisao estratigrafica e tectonica da Precambriano no Rio Grande do Norte e Paraiba: Eng. Min. Metal., v.43, p.37-38.

Ebert, H., 1967, Observacoes sobre a subdivisao estratigrafica e a idade do Pre-Cambriano no Nordeste brasileiro: Eng. Min. Metal., v.46, p.111-113.

Ebert, H., 1968, Ocorrencias da facies granulitica no sul de Minas Gerais e em areas adjacentes em dependencia da estrutur orogenica; hipoteses sobres sua origem: Anais Acad. Bras. Cien., v.40, (supl.), p.215-229.

Ebert, H., 1970, The Precambrian geology of the "Borborema" belt (States of Paraiba and Rio Grande do Norte; northeastern Brazil) and the origin of its mineral provinces: Geol. Rundschau, v.58, p.1291-1326.

Ebert, H., and Brochini, M.F., 1968, Estudos estratigrafcos e geocronologicos no Escudo Cristalino Brasileiro: Cien. Cultura, v.20, p.621-625.

Ewing, M., Ludwig, W.J., and Ewing, J., 1963, Geophysical investigations in the submerged Argentine coastal plain Part 1, Buenos Aires to Peninsula Valdes: Geol. Soc. Amer. Bull. v.74, no.3, p.275-292.

Ferreira, E.O., 1972, Carta tectonica do Brazil (Tectonic map of Brazil): Brazil Dept. Nac. Producao Mineral Bol. 1, 19 p. (Portuguese), 14 p. (English), col. geol. map, scale 1:5,000,000.

Fisher, R.L. (1974): Pacific-type continental margins. -In: The geology of continental margins, C.A. Burk & C.L. Drake (Ed.), 25-41.

Frutos, J., 1980. Andean metallogeny related to the tectonic and petrologic evolution of the Cordillera. Some remarkable points. 90th Birthday Paul Ramdohr Jubileum Volume. Springer, Heidelberg.

Fuck, R.A., Marini, O.J., and Trein, E., 1967, Contribuicao ao estrdo das rochas graniticas fo estado do Parana: Bol. Paran. Geocien., nos. 23 to 25, p.183-219.

Gansser, Augusto, 1974, The ophiolitic melange, a world-wide problem on Tethyan examples: Eclogae Geol. Helvetiae, v.67, no.3, p.479-507.

Goni, J.C., 1961, O rapakivi de Lavras, jazidas metaliferas associadas, Lavras do Sul, Rio Grande do Sul, Esc. Geologia, v.7, p.1-107.

Goni, J.C., 1962, Origine des roches ultrabasiques et serpentineuses du precambrien de Rio Grande do Sul (Bresil). Mode de gisement et mineralisations: Univ. Rio Grande do Sul, Esc. Geologia, v.12, p.7-91.

Gonzalez-Bonorino. F. (1967): Nuevos datos de edad absoluta del basamento cristalino de la Cordil-lera de la Costa Chile central. -Chile Univ., Fac. Cienc. Fis. Mat., Dep. Geol. Ser. Comun., 1, 7p.
- (1970): Series metamorficas del basamento cristalino de la Cordillera de la Costa, Chile Central. -Depart. Geol. Univ. Chile, 32, 68p.
- (1971): Metamorphism of the crystalline basement of central Chile. -J. Petrol., 12, 149-175.

Goossens, P.J. & Rose, W.I. JR. (1973): Chemical composition and

age determination of tholeiitic rocks in the basic igneous complex, Ecuador. -Bull. geol. Soc. Amer., 84, 1043-1052.

Grabert, H., 1971, Die Prae-Andine Drainage des Amazonas Stromsystems: Muenster Forsch. Geol. Palaeontol., no.20-21, p.51-60.

Halpern, M., 1968, Ages of Antartic and Argentine rocks bearing on continental drift: Earth Planet. Sci. Letters, v.5, p.159-167.

Halpern, M. and Linares, E., 1970, Edad rubidio-estroncio de las rocas graniticas del basamento cristalino del area de Olavarria, Pcia. de Bs. As., rep. Arg: Rev. Asoc. Geol. Argentina, v.25, no.3, p.303-307.

Halpern, M., Linares, E., and Latorre, C.O., 1970, Estudio preliminar por el metodo Estroncio-rubidio de rocas metamorficas y graniticas de la provincia de San Luis, Rep. Arg.: Rev. Asoc. Geol. Argentina, v.25, no.3, p.293-302.

Harrington, H.J., 1962, Paleogeographic development of South America: Am. Assoc. Petr. Geol., Bull. v.46, no.10, p.1773-1814.

Harrington, H.J., 1970, Sierras Australes de Bs. As. Rep. Argentina: Cadena Aulacogenica, Rev. Asoc. Geol. Argentina, v.25, no.2, p.151-180.

Hart, S.R., Krogh, T.E., Davids, G.L. and Munizaga, F., 1965, A geochronological approach to the continental drift hypothesis: Carnegie Inst. Washington Year Book 65.

Hasui, Y. and Almeida, F.F.M. de. 1970, Geocronologia do Centro-Oeste brasileiro: Bol. Soc. Bras. Geologia, v.19, p.5-26.

Hasui, Y., Penalva, F., and Hennies, W.T., 1969. Geologia do Grupo Sao Roque: Anais XXIII Cong. Bras. Geologia, p.101-134.

Hennies, W.T., Hasui, Y., and Penalva, F. 1967, O falhamento transcorrente de Taxaquara: Anais XXI Cong. Bras. Geologia, p.156-168.

Herbert, H.J. (1977): Die Grunschiefer der Ost-Kordillere Ecuadors und ihr metamorpher Rahmen. -183 p., Diss. Univ. Tubingen.
- (1977): Petrochemie und-Ausgangsmaterial von Grunschiefern aus der E-Kordillere Ecuadors. -Fortschr. Miner., 55, 1, 45-46.

Herz, 1970, Gneissic and igneous rocks of the Quadrilatero Ferrifero, Minas Gerais, Brazil: U.S. Geol. Survey, Prof. Paper 641-B, p.58.

Humphrey, F.L. and Allard, G.O., 1968, The Propria geosyncline, a newly recognized precambrian tectonic province in the Brazilian Shield: XXIII Intern. Geol. Cong., v.4, p.123-139.

Hunus, V. and Vanek, J., 1978. Morphology of the Andean Wadati-Benioff zone andesitic volcanism, and tectonic features of the Nazca plate. Tectonophysics, 44: 65-77.

Hurley, P.M., 1968, Variations in Isotropic Abundances of Sr, Ca, and Ar and Related Topics: Sixteenth Annual Progress Report to the U.S. Atomic Energy Commission, Contract At (30-1)-1381.

Hurley, P.M., 1970, Variations in Isotropic Abundances of Sr, Ca, and Ar and Related Topics: Eighteenth Annual Progress Report to the U.S. Atomic Energy Commission, M.I.T. Contract At (30-1)-1381.

Hurley, P.M. and Rand, J.R., 1973, Outline of Precambrian chronology in lands bordering the South Atlantic, Exclusive of Brazil, in Nairn, A.E.M. and Stehli, F.G., eds., The ocean basins and margins, v.1, The South Atlantic: New York, Plenum Press, p.391-406.

Hurley, P.M., Almeida, F.F.M. de, Melcher, G.C., Cordani, U.G., Rand, J.R., Kawashita, K., Vandoros, P., Pinson W.H., Jr., and Fairbairn, H.W., 1967, Test of continental drift by comparison of radiometric ages: Science, v.157, p.495-500.

Issler, R.S., Burger, C., Jr., and Roisenberg, A., 1967, Coronito da Area de Mata Grande, Mon. de Sao Sepe, Est. do Rio Grande do Sul: An. XXI Cong. Bras. Geol., p.182-197.

Jones, G., 1956, Memoria explicativa y mapa geologico de la mitad oriental del Departamento de Canelones: Inst. Geol. Uruguay, v.34.

Jones, G., 1956, Some deep Mesozoic Basins recently discovered in Southern Uruguay, Twentieth International Geologica Congress, Section 11, p.53-72, Mexico.

Kaasschieter, J.P.H., 1965, Geologia de la Cuenca del Colorado: Actas de las 2 das. J. Geol. Argentinas, v.3, p.251-271.

Kalliokoski, J., 1965, Geology of north-central Guyana Shield, Venezuela: Bull. Geol. Soc. Am., v.76, p.1027-1050.

Kegel, W., 1953, Contribuicao para o estudo do Devoniano da Bacia do Parnaiba: D.P.N.M. Div. Geol. Min., Bol. 141.

Kegel, W., 1956, As inconformidades na Bacia do Parnaiba e zonas adjacentes: D.N.P.M. Div. Geol. Min., Bol. 160, p.59.

Kegel, W., 1965, A estrutura geologica do Nordeste do Brazil: Div. Geol. Mineral, Min. Minas Energia, no.227, p.47.

Ledent, D., and Pasteels, P., 1968, Determination de l'age des roches postectoniques du sud-est du Bresil: Annal. Soc. Geol. Belgique, v.91, p.305-309.

Leinz, V., 1949, Pequenas notas geologicas e petrograficas sobre O Territorio do Amapa: Bol. Mus. Nac. Geol. 7.

Lesta, P.J., 1968, Estratigrafia de la Cuenca del Golfo de San Jorge: Actas de las 3 das. J. Geol. Argentinas, v.1, p.251-190.

Linares, E. and Latorre, C.O., 1969, Edades Potasio Argon y Plomo Alfa de rocas graniticas de la Pcias. de Cordoba y San Luis: IV J. Geol. Argentinas (in press), Mendoza.

Longacre, M.B., 1981, Satellite magnetic investigation of South America (M.S. Thesis): Purdue University, West lafayette, Indiana, 57 p.

Ludwig, G., 1964, Divisao estratigrafico -faciologica do Paleozoico do Bacia Amazonica: Petrobras. Cenap. Mon. I.

Ludwig, W.J., Ewing, J.I., and Ewing, M., 1968, Structure of the Argentine continental margin: AAPG Bull., v.52, no.12, p.2337-2368.

Malumian, N., 1969, Foraminiferos del Cretacico Superior y Terciario del subsuelo de la Pcia. de Santa Cruz, Argentina: Ameghiniana Rev. de la Asoc. Paleont. Argentina, v.5, no.6, p.191-277.

Malumian, N., 1970, Biostratigrafia del Terciario Marino del subsuelo de la Pcia. de Buenos Aires (Argentina): jAmeghiniana, Rev. Asoc. Paleont. Argentina, v.7, no.2, p.173-204.

Marini, O.J., Trein, E., and Fuck, R.A., 1967, O Grupo Acungui no

Estado do Parana: Bol. Paranaense de Geoc., no.23 to 25, p.43-103.

McConnell, R.B., 1958, Provisional stratigraphic table for British Guiana. A: Rept. Geol. Surv. Br. Guiana, 1957.

McConnell, R.B., 1969, The relationship between fundamental fault zones in continental crust and the axes of Atlantic spreading: Bull. Geol. Soc. Am., v.80.

McConnell, R.B., and Williams, E., 1969, Distribution and provisional correlation of the Precambrian of the Gruiana Shield. Paper presented at the 8th Guiana Geol. Conf., Georgetown, Guyana.

McConnell, R.B., Williams, E., Cannon, R.T., and Snelling, N.J., 1964, A new interpretation of the geology of British Guiana: Nature, v.204, p.115-118.

Melfi, A.J., Bittencourt, I., and Cordani, U.G., 1965, Reconhecimento fotogeologico de parte do Grupo Acungui: Bragantia, v.24, p.447-474.

Melo, O., 1960, Estratigrafia da Bacia Amazonica: Petrobras, Relatorio DEPEX, 2072.

Mesner, J.C. and Wooldridge, L.C.P., 1964a, Maranhao Paleozoic Basin and Cretaceous Coastal Basins, North Brazil: Am. Assoc. Petr. Geol., v.48 (9), p.1475-1512.

Mesner, J.C. and Wooldridge, L.C.P., 1964b, Estratigrafia das bacias paleozoica e cretacea do Maranhao: Bol. Tecn. Petrobrds, v.7, no.2, p.137-164 (translation and condensation by Carlos Walter Marinho Campos).

Meunier, A., 1964, Succession stratigraphique et passages lateraux dus ar metamorphisme de la serie Ceara, Antecambrien du Nord-Est bresilien: C.R. Acad. Sci. Paris, v.259, p.3796-3799.

Miller, H. (1967a): Zur jungen Tekronik in der Hochkordillere Nordchiles. -N. Jb. Geol. Palaont., Mh., 9536-544.
- (1967b): Kritische Betrachtungen zum geologischen Zusammenhang zwischen den chilenischen Anden und der Westantarktis.
- Geol. Rdsch., 56, 2643-656.
- (1970a): Das Problem des hypothetischen,"Pazifischen Kontinentes", gesehen von der chilenichen Pazifikkuste.
-Geol. Rdsch., 59, 3927-938.

- (1970b): Vergleichende Strdien an pramesozoischen Gesteinen Chiles unter besonderer Beruck-sichtigung ihrer Kleintektonik. - Geotekt, Forsch., 36, 64p.

Morales, L.G., 1960, Geologia geral e possibilidades petroliferas da Bacia Amazonica no Brazil: Bol. Inst. Bras. Petr., v.1, no. 2, p.2-13.

Moura, P., 1936, Rio Gurupy: Brazil, Serv. Geol. Mineralogico, v.78, p.1-44.

Munizaga, F., Aguirre, I & Herve, F. (1973): Rb/Sr ages of rocks from the Chilean metamorphic basement. -Earth planet. Sci. Lett., 18, 87-92.

Muratori, A., Fuck, R., and Bigarella, J.J., 1967, Contribucao ao estudo da Formacao Camarinha: Bol. Paran. Geocien., nos. 23 to 25, p.221-235.

Nairn, A.E.M. and Stehli, F.G., 1973, The ocean basins and margins, V.I., The South Atlantic: New York, Plenum Press.

Nwachukwu, S.O. (1972). The tectonic evolution of the southern portion of the Benue Trough, Nigeria. Geol. Mag., 109,411-419.

Olade, M.A. (1975). Evolution of Nigeria's Benue Trough (aulacogen): a tectonic model. Geol. Mag., 112, 575-583.

Pedreira, A.J., Souto, P.G., and Azevedo, H., 1969, Metassedimentos do Grupo Rio Pardo, Bahia, Brazil: Anais do XXIII Cong. Bras. Geologia, p.87-89.

Picada, R.S., 1968, Os sistemas de falhas da parte central do escudo sul-Riograndense: evolucao dos conhecimentos e proposicao de problemas: Anais XXII Cong. Bras. Geologia, p.247-253.

Posadas, V.G. and Kalliokoski, J., 1967, Rb-Sr ages of the Encrucijada granite intrusive in the Imataca Complex, Venezuela: Earth Planet. Sci. Letters, v.2, p.210-214.

Potter, Paul Edwin, 1978, Significane and origin of big rivers, The Journal of Geology, v.86, no.1, p.13-33.

Priem, H.N.A., Boelrijk, N.A.I.M., Hebeda, E.H., Verschure, R.H., and Verdurmen, E.A. Th., 1968, Isotopic age determinations

on Surinam rocks, 4. Ages of basement rocks in north-western Surinam and the Roraima tuff at Tafelberg: Geolen. Mijn., v.47, p.191-196.

Priem, H.N.A., Boelrijk, N.A.I.M., Hebeda, E.H., and Verschure, R.H., 1967, Isotopic age determinations on Surinam rocks, 2: Geol. en Mijn., v.46, p.26-30.

Priem, H.N.A., Boelrijk, N.A.I.M., Hebeda, E.H., Verschure, R.H., and Szumlas, F., 1967, Isotopic age determinations on a biotite grancdiorite and a biotite-hornblende diorite in the coastal area west of Accra, Ghana: Geol. en Mijn., v.46, p.208-210.

Priem, H.N.A., Boelrijk, N.A.I.M., Verschure, R.H., and Hebeda, E.H., 1966, Isotopic age determinations on Surinam rocks, 1: Geol. en Mijn., v.45, p.16-19.

Quartino, B.J. and Fabre, J.F.V., 1967, Geologia y petrologia del basamento de Tandil y Barker, provincia de Buenos Aires: Rev. Assoc. Geol. Argentina, v.XXII, n.3.

Reeves, R.G., 1966, Geology and mineral resources of the Monlevade and Rio Piracicaba quadrangles, Minas Gerais, Brazil: U.S. Geol. Survey, Prof. Paper 341-E, 58p.

Rezende, W.M. de, 1966, Bacia do Amazonas, estrdos dos processos de intrusoes e de magmas basicos: Belem, Petrobras, Dexpro, Renor. Depex Rel. 2485.

Ribeiro, M., Bocchi, P.R., Figueiredo, P.M., and Tessari, R.I., 1966, Geologia da quadricula de Cacapava do Sul: Div. Fom Prod. Mineral. Min. Minas Energia, v.127,200 p.

Ritzwoller, M.H. and Bentley, C.R., 1982, MAGSAT studies over high southern latitudes, 4th. annual conference on the NASA geodynamics program (abstracts). p.107.

Rosier, G.F., 1965, Pesquisas geologicas na parte oriental do Rio de Janeiro e na parte vizinha do Estado de Minas Gerais: Div. Geol. Mineralogia. Min. Minas Energia, v.222, p.40.

Salamuni, R. and Bigarella, J.J., 1967, The Pre-Gondwana Basement, in: Problems in Brazilian Gondwana Geology, Bigarella, J.J., Becker, R.D., and Pinto, I.D., eds., Impr. Univ. Fed. Parana, p.3-24.

Santos, E.J., 1971, As feicoes estruturais da folha Arcoverde. Pernambuco e o mecanismo dos falhamentos da "zona transversal": Miner. Metal., v.LIII, p.35-40.

Shepard, F.P., 1963 Submarine, geology, 2nd ed.: Harper & Row, New York, p.557.

Short, K.C. and Steenken, W.F., 1962, A reconnaissance of the Guyana Shield from Guasipati to the Rio Aro, Venezuela: Bol. Inform. Assoc. Venezolana Geol. Min. Petr., v.5, p.189-221.

Singh, S., 1966, Geology and petrography of part of the Guyana Shield in the South Savanna-Rewa area of southern Guyana: Bull. Geol. Surv. Br. Guyana, v.37, 127 p.

Snelling, N.J., 1965, The geochronology of British Guiana. Report 65.3 (typescript), Age determination unit: Overseas Geological Surveys, London.

Snelling, N. and McConnell, R.B., 1966, the geocronology of Guyana: 7th Inter-Guiana Geol. Conference, Paramaribo.

Snelling, N.J. and Berrange, J.P., 1969, The geochronology of Guyana, 2. Results obtained in the period 1966-1969: Paper presented at the 8th Guiana Geol. Conf., Georgetown (Guyana), August, 1969.

Snelling, N.J. and McConnell, R.B., 1969, The geochronology of Guyana: Geo. Mijn., v.48, p.201-213.

Spooner, C.M., Berrange, J.P., and Fairbairn, H.W., 1971, Rb-Sr whole-rock age of the Kanuku Complex, Guyana: Bull. Geol. Soc. Amer., v.82, p.207-210.

Stauder, W., 1975, Subduction of the Nazca Plate under Peru as evidenced by focal mechanisms and by seismicity. J. Geophys. Res., 80: 1053-1064.

Steinmann, G. (1929): Geologie von Peru. -448 p., Heidelberg.

Sternberg, H.O'R., 1950, Vales tectonicos na planicie Amazonica?: Rev. Bras. Geogr., v.12 (4), p.513-533.

Stipanicic, P., 1967, Consideraciones sobra las edades de algunas fases magmaticas del Neopaleozoico y Mesozoico: Rev. Asoc. Geol. Argentina, v.22, no.2, p.101-133.

Stipanicic, P.N. and Linares, E., 1969, Edades radiometricas determinadas para la Republica Argentina y su significado geologico: Bol. Acad. Nac. Cien., v.XLVIII, p.51-96.

Stipanicic, P.N., Rodrigo, F., Baulies. O.L., and Martinez, C.G., 1968, Las formaciones presenonianas en el denominado -"Macizo" -Norpatagonico y regiones adyacentes: Rev. Asoc. Geol. Argentina, v.XXIII.

Tectonic map of South America, 1978: The Geological Society of America.

Tessari, R.I. and Picada, R.S., 1966, Geologia da quadricula de Encruzilhada do Sul. Rio Grande do Sul, Brazil: Div. Fom. Prod. Mineral, Min. Minas Energia, v.124, p.147.

Trein, E. and Fuck, R.A., 1967, O Grupo Castro: Bol. Paran. Geocien., nos.23 to 25, p.257-305.

Turner, J.C.M. -(1972): Puna. -In: Geologia Regional Argentina, LEANZA, A.F. (Ed.), 91-116.
-(1972): Cordillera Oriental. -In: Geologia Regional Argentina, LEANZA, A.F. (Ed.), 117-142.

Umpierre, M. and Haplern, M., 1971, Edades estroncio-rubidio en rocas cristalinas del sur de Uruguay: Rev. Asoc. Geol. Argentina, v.XXVI, p.133-151.

Urien, C.M. and Zambrano, J.J, 1973, The geology of the basins of the Argentine continental margin and Malvines Platean, in Nairn, A.E.M., and Stehli, F.G., eds., The ocean basins and margins, v.1, The South Atlantic: New York, Plenum Press, p.135-166.

Vandoros, P. and Coutinho, J.M.V., 1966, Estudos geologicos e geocronologicos da area de Sao Goncalo, Paraiba: Bol. Soc. Bras. Geologia, v.15, p.15-26.

Vollbrecht, K., 1964, Die Diabas vorkommen des Amazonas Gebietes und das Problem des Intrusions mechanismus: Geol. Rdsch., v.53, p.686-706.

Walther, K., 1927, Consideraciones sobre los restos de un elemento estructural aun desconocido del Uruguay y el Brazil mas meridional: Bol. Acad. Nac. Ciencia, v.XXX, p.346-381.

Walther, K., 1948, El basamento cristalino de Montevideo, Inst. Geol. Uruguay: v.33.

Williams, E., Cannon, R.Y., and McConnel, R.B., 1967, The folded Precambrian of northern Guyana related to the geology of the Guiana Shield, with age dates by N.J. Snelling: Geol. Surv. Guyana, Records, v.5, p.60.

Williams, Harold, 1977, Ophiolitic melange and its significance in the Fleur de Lys Supergroup, northern Appalachians: Canadian Jour. Earth Sci., v.14, no.5, p.987-1003.

Windley, B.F., 1977, The evolving continents, John Wiley and Sons, New York, 385 p.

Woollard, G.P., and Strange, W.E., 1969, The prediction of gravity, in Gravity Anomalies: Unsurveyed Arcs, Am. Geophys. Union Monogr. 9, 96.

Zambrano, J.J. and Urien. C.M., 1970, Geological outline of the basin in southern Argentina and their continuation of the Atlantic shore: J. Geophys. Res., v.75, no.8, p.1363-1396.

Zeil, W., 1979, The Andes (A geological review), Gebruder Borntraeger, Berlin-Stuttgart, 259 p.

APPENDIX B

A Crustal Structure Study of South America

A CRUSTAL STRUCTURE STUDY OF SOUTH AMERICA

by

Kevin Scott Renbarger, B.S.

THESIS

Presented to the Faculty of the Graduate School of

The University of Texas at El Paso

in Partial Fulfillment

of the Requirements

for the Degree of

MASTER OF SCIENCE, GEOPHYSICS

THE UNIVERSITY OF TEXAS AT EL PASO

May, 1984

ABSTRACT

The regional crustal structure of South America has been investigated by combining a comprehensive analysis of surface wave dispersion along two station paths involving WWSSN seismograph stations and previous geophysical studies. The major results of this study were depicted by constructing a contour map of crustal thickness. Average values for seismic velocities in the crust and upper mantle were also calculated. These results were compared to maps of regional gravity anomalies, satellite (MAGSAT) magnetic anomalies, and major tectonic features. Several interesting correlations and relationships were discovered.

TABLE OF CONTENTS

LIST OF TABLES

LIST OF FIGURES

INTRODUCTION

South America is characterized by a wide variety of strongly contrasting geological and tectonic features. The bulk of the continent is made up of a broad, nearly aseismic stable platform whose Precambrian basement is exposed in large crystalline shields. The eastern edge of this cratonic area, which borders the South Atlantic, forms a passive or trailing plate margin, penetrated by several failed rifts. In sharp contrast, the western edge of the craton is separated from the Pacific ocean by a complex and tectonically active mobile belt which finds its modern expression in a mountain range of spectacular morphology. Strong contemporary seismicity and volcanism occur in parts of the range. The western edge of the South American plate, which carries the continent, is presently overriding the Nazca plate of the East Pacific to form an active or convergent plate margin.

These varied tectonic features are all expressions of South America's imperfectly known crustal and upper mantle structure. Geophysical investigations designed to shed light on the lithospheric structure of South America, however, are hampered by the extensive jungle and rugged terrain which limits access to the interior. Detailed geophysical surveys have been performed only in isolated

parts of the Andes Mountains and across certain profiles of the Peru-Chile trench. With the exception of a recent heat flow study of a portion of the Atlantic shield (Vitroello, 1978), the rest of the continent has been subjected to only very general studies. None of this work has been integrated into a comprehensive view of the continent's crustal structure.

The only set of geophysical data that provides uniform coverage of the South American continent and surrounding oceanic areas are the satellite scalar magnetic anomaly data gathered by the MAGSAT orbital magnetic field survey in 1979-1980. These data were reduced to radial polarization by the South American MAGSAT group (Hinze et al., 1982) to facilitate comparison with the major tectonic features of South America. A free-air gravity map complementing the magnetic data was also compiled as part of this investigation (Longacre, 1981). The purpose of the present study is to continue the MAGSAT investigation by searching for correlations between these previously measured potential field anomalies and the general crustal structure of South America.

Because so few geophysical investigations have been made over the stable eastern platform of South America, the major part of this study consisted of determining variations in the average crustal thickness of the South American platform. This was done by measuring fundamental mode

Rayleigh wave dispersion between nine pairs of South American WWSSN seismograph stations and inverting the measurements to obtain average shear wave velocity-depth models across the platform. Additional models were derived from the Rayleigh wave dispersion data measured by Sherburne (1974) over eastern South America. Both sets of models were interpreted in terms of average crustal thickness and average crustal shear wave velocity, and the results were combined with the results of crustal modeling in the Andean cordillera, reported in the literature, to construct a generalized crustal structure map of the South American continent. This map forms the basis for making comparisons between the potential field anomalies mapped as part of the MAGSAT project and the underlying structure of South America.

GENERAL GEOLOGIC AND TECTONIC SETTING

The South American continent can be divided into three broad tectonic provinces based on important differences in origin, age, and tectonic development. These provinces are the South American platform, the Patagonian platform, and the Andean cordillera.

South American Platform

The oldest, and by far the largest, of the three provinces is the South American platform (Fig. 1). This stable platform forms the bulk of the South American continent, including all the terrain east of the Andes Mountains and north of approximately latitude 35° south. It has a complex, dominantly crystalline Precambrian basement which is unconformably overlain in places by a cover of sedimentary and volcanic rocks that developed from the Silurian onward.

Precambrian Basement

The basement of the South American platform is exposed in three major shields--the Guyana shield, the Central Brazilian shield, and the Atlantic shield--as well as in several smaller isolated massifs (Cordani et al., 1973; de Almeida, 1978). The simplified tectonic map of

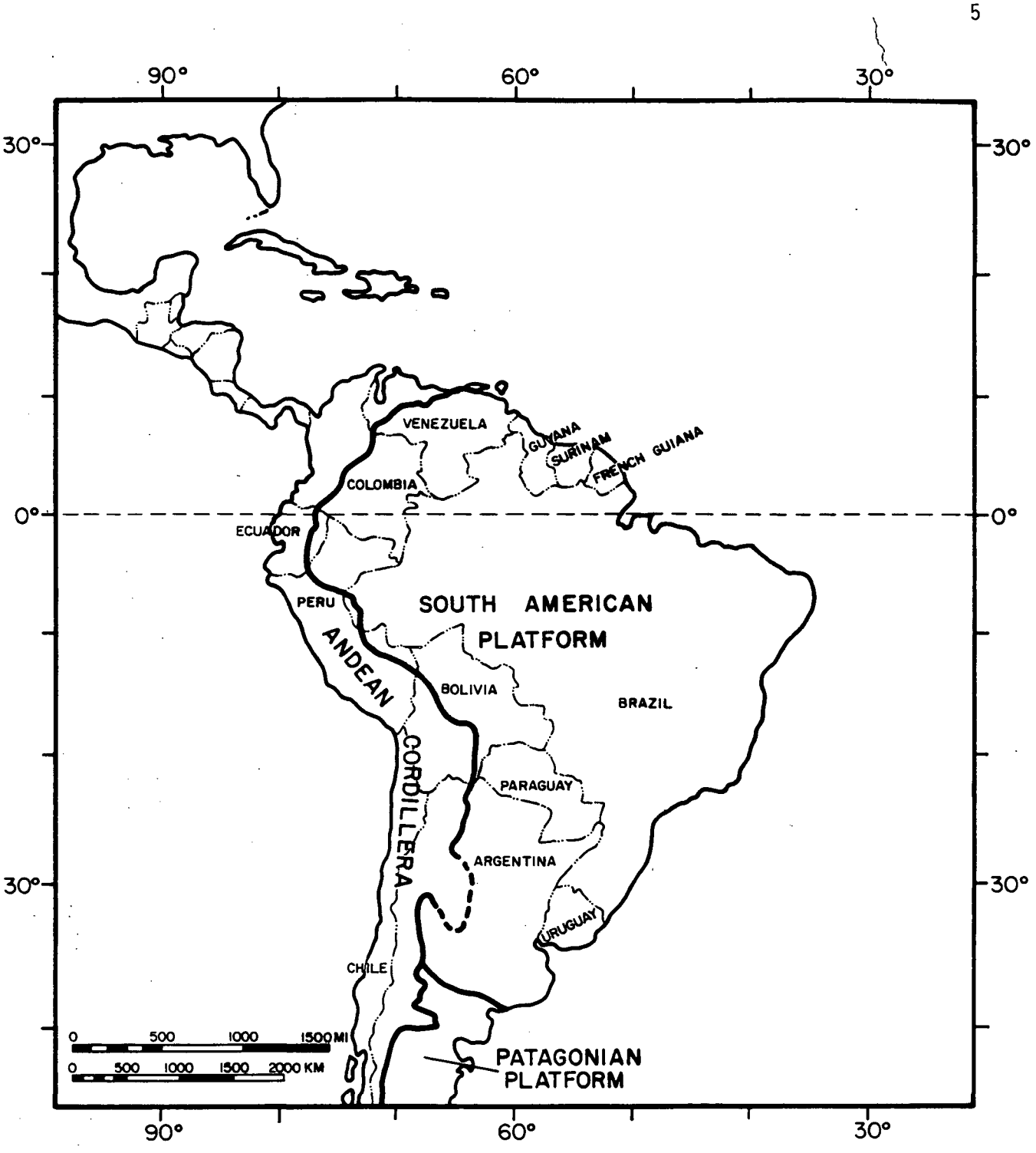

Figure 1. Major tectonic provinces of South America.

South America in Figure 2, modified after de Almeida (1978), shows the location of these shields, and gives the approximate positions of the Precambrian cratonic areas and the superimposed Phanerozoic intracratonic basins.

The Precambrian evolution of the South American platform can be roughly inferred from the radiometric ages and disposition of the rocks exposed in the three shields. Most of the radiometric dates fall into two distinct ranges, corresponding to two widespread tectonic events (Cordani et al. 1973; de Almeida, 1978). The first of these events, the Trans-Amazonian orogenic cycle, occurred between 2,200 and 1,800 million years ago, and represents a time of extensive continental remobilization that affected the entire South American platform. Rocks either formed or strongly affected by this cycle can be found within the large cratonic areas of South America, which stabilized after the deformation ceased, or within relic blocks which crop out occasionally in the younger Precambrian metamorphic belts.

The cratonic areas are separated from each other by remobilized metamorphic belts which formed during the Brazilian orogenic cycle over the late Precambrian-early Paleozoic, between 700 and 450 million years ago. The fact that rocks of Trans-Amazonian and even older ages are found within the Brazilian metamorphic belts indicates that the belts developed over preexisting continental crust.

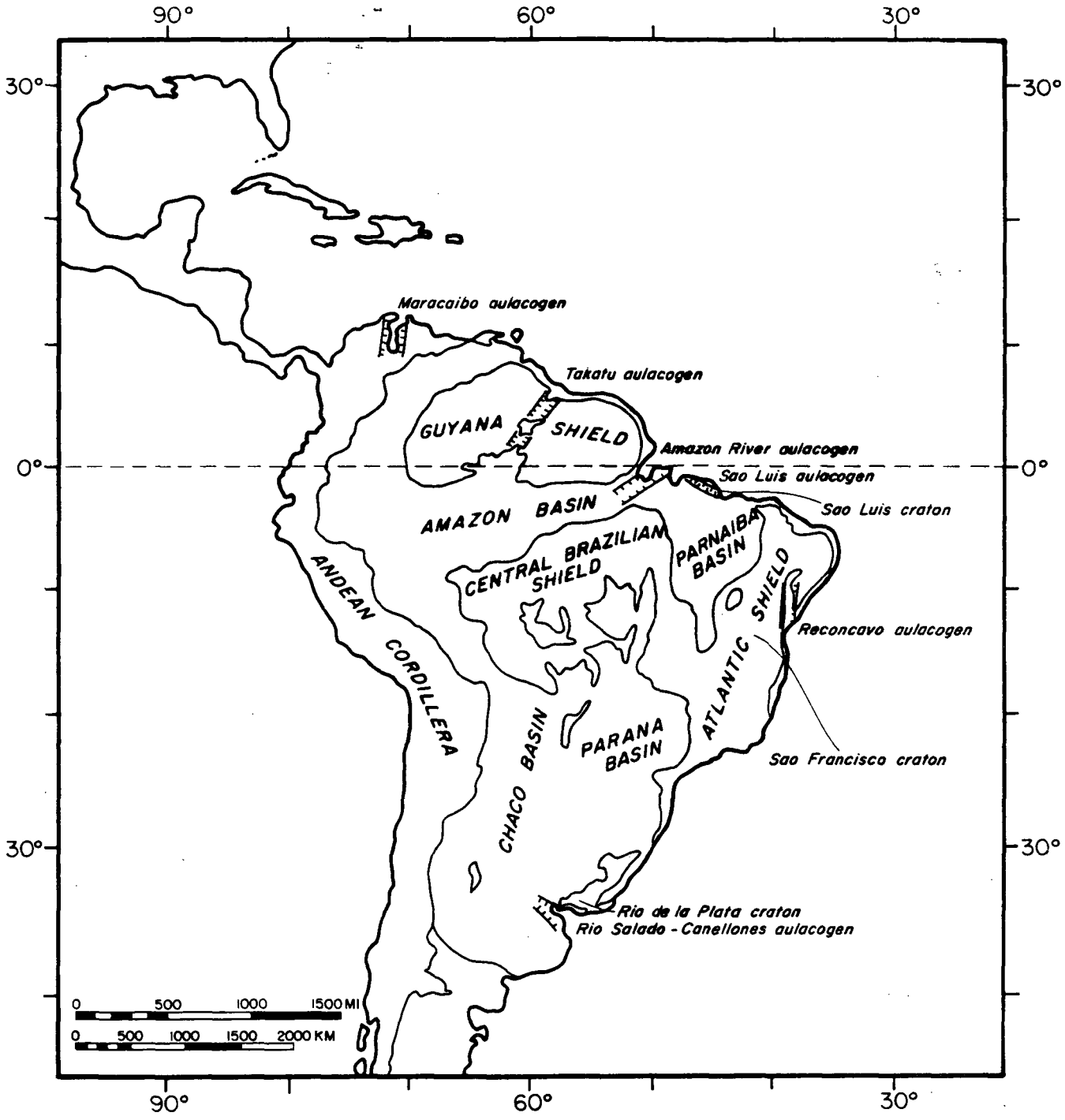

Figure 2. Simplified tectonic map of South America, after de Almeida (1978).

Four stable cratonic areas (or continental nucleii) have been recognized in the South American platform (Cordani et al. 1973). The largest of these regions, covering an area of around 4.5 million square kilometers, includes the Guyana shield, the basement of the Amazon basin, and the Guapore craton just south of the Amazon basin. In a few isolated regions of this cratonic area, rocks of granulitic facies yield radiometric ages as great as 3400 m.y.b.p. (de Almeida, 1978). Such areas represent relics of continental nucleii still older than the Trans-Amazonian. In eastern Brazil, the Atlantic shield exposes the Sao Francisco craton, which outcrops over an area of around one million square kilometers. The Sao Luis craton, located along the northern coast of Brazil southeast of the Amazon river mouth, and the Rio de la Plata craton, surrounding the La Plata river in Uruguay and northern Argentina are two smaller cratons also exposed by the Atlantic shield. Figure 2 shows the locations of these areas. Rock types common to each of these regions include granulites and anorthosites, quartz monzonites, granodiorites, diorites, banded gneisses, migmatites, garnet-quartzite schists, muscovite schists, amphibolites, iron formations, and low-grade metasediments and metavolcanics (de Almeida et al. 1973; Leonardos and Fyfe, 1974).

These rigid blocks of continental crust acted as platforms for the major tectonic remobilization which

occurred during the late Precambrian Brazilian cycle. The peripheral mobile belts which developed during this cycle are characterized by geosynclinal sedimentation, folding and thrusting, and extensive metamorphism. The principal geotectonic units of the Brazilian cycle are the Caririan fold belt and the Sergipe geosyncline in northeastern Brazil, the Ribeira fold belt which crops out along the Atlantic coast of Brazil and Uruguay, and the Brasilia and Paraguay-Araguia fold belts in the central part of the continent (Cordoni et al. 1973). Rock types common to the metamorphic belts include mica schists, gneisses, phyllites, quartz diorites, syenites, quartzites, dolomites, metagraywackes and metavolcanics, granulites, and migmatites preserved from older events (de Almeida et al. 1973; Leonardos and Fyfe, 1974).

Although each of these belts was strongly affected by the events of the Brazilian orogenic cycle, a succession of older radiometric dates measured from the rocks indicates that the belts were zones of weakness repeatedly affected by tectonism subsequent to the Trans-Amazonian cycle and prior to the Brazilian cycle (Vitroello, 1978). The belts stabilized after the Brazilian cycle, with a transitional stage from Precambrian tectonic events to platformal conditions that persisted in places into the Ordovician (de Almeida, 1970).

Phanerozoic Basins

The sedimentary and volcanic cover which unconformably overlies the Precambrian basement is principally developed in the four great intracratonic basins of the Parana, the Chaco, the Parnaiba, and the Amazon (Fig. 2). An extensive blanket of sediments also covers the zone of transition from the Andean cordillera to the shields. The intracratonic basins formed through the gentle subsidence and normal faulting associated with intermittant epeirogenic movements of the basement throughout the Paleozoic. Subsidence and sedimentation began during the Silurian. The Silurian and Devonian sediments deposited in the basins are almost exclusively marine. The sediments deposited during the Carboniferous show a mixed marine-continental character, and Permian and Triassic sediments are predominantly continental.

The Parana basin is a large oval basin whose location, south of the Central Brazilian shield and west of the Sao Francisco craton, was apparently controlled by the position of Precambrian structures. The basin contains over 5,000 meters of sediment in its center. The oldest of these deposits are marine sediments laid down in the Devonian. Continental glaciation deposits interfinger with marine sediments in the upper Carboniferous, and extensive continental sediments characterize the Permian and upper Triassic. The widespread plateau basalts and sills which

accumulated along the edges of the basin during the late Mesozoic and early Cenozoic, in response to a period of tectonic reactivation, are particularly notable (de Almeida, 1978, 1970).

The Parnaiba basin, located southeast of the Amazon River mouth, is situated on the Precambrian metamorphic belt separating the Guapore craton from the Sao Francisco and Sao Luis cratons. Sediments in this basin reach thicknesses in excess of 3,000 meters, with approximately 2,500 meters being detrital sediments of Paleozoic age (de Almeida, 1978, 1970).

The Amazon basin is a long trough-like basin which separates the Guyana shield from the Central Brazilian shield. The basin may have developed over a fracture zone which separates and offsets these two cratonic areas (de Almeida, 1970; de Loczy, 1970), or it may have had its origin in Paleozoic rifting (Burke, 1978). Over 5,000 meters of sediments are deposited in places in the Amazon basin, with more than 3,000 meters of these resulting from marine transgressions which occured during the middle Paleozoic. Continental red beds characterize the late Paleozoic. To the west, at the transition between the Amazon basin and the Andean cordillera, Mesozoic and Cenozoic sediments are much more abundant, ranging in maximum thickness from 5,000 meters in the northern Orinoco trough to 10,000 meters in the basins adjoining the Andean

cordillera. Basaltic dikes and sills, intruded during the Triassic, are also abundant in the basin (de Almeida, 1978, 1970).

The Chaco basin, which actually developed as a pericratonic basin at the Andean border of the South American platform, covers the southern and southwestern part of the platform. It is a broad shallow basin containing a maximum of around 2,500 meters of mostly Devonian and Triassic sediments. A major tectonic boundary hidden beneath the southern rim of the basin and the Cenozoic platform associated with the Andean cordillera separates the South American platform from the younger Patagonian platform to the south (de Almeida, 1978, 1970).

Tectonic Reactivation

A strong tectonic reactivation occurred across the South American platform toward the end of the Mesozoic, culminating in the rifting of the South American continent from the African continent and the opening of the South Atlantic oceans. This reactivation can be divided roughly into three phases (de Almeida, 1970). The first phase, which occurred between the late Jurassic and the early Cretaceous, was characterized by intense tholeiitic basalt and alkaline volcanism, along with extensive faulting and fault reactivation. Large volumes of tholeiitic basalts were extruded over the platform or intruded as dikes and sills within the basins. Large scale structures and high

angle faults were reactivated within all four of the intracratonic basins, and in places fault-block mountains began forming. New faulted basins also began forming, particularly near the present coastline, but they received only continental sediments at this stage.

During the second phase, which lasted from the middle Cretaceous to the Eocene, basaltic volcanism ceased. Alkaline volcanism continued, however, and some granites were intruded in northeastern Brazil. At this time the sea transgressed into the marginal faulted basins and thick marine sedimentary sequences were deposited. Several small sedimentary basins along the coasts of northern Argentina, Brazil, the Guianas, and Venezuela which exhibit graben complexes formed at rifting are known (Burke, 1973). Some of these basins contain a total of more than 5,000 meters of sediments. The sedimentation in all of the basins occurred under active tectonic conditions, as shown by the numerous unconformities, rapid facies changes, and thick interspersed conglomerate formations. Burke (1973) has further identified six of these marginal basins--the Rio Salado-Canellones, Reconcavo, Sao Luis, the Amazon basin mouth, Takatu, and the Maracabo basins--as failed rifts or aulocogens which partially penetrate the South American platform.

The alkaline volcanism which occurred within the Riberira and Brasilia Precambrian fold belts of Brazil and

eastern Paraguay is further evidence of a strong thermal disturbance associated with the tectonic reactivation. Some 50 centers of alkaline and alkaline-ultrabasic volcanism, with a few associated carbonatite and kimberlite intrusions, are known, all dating from the end of the Jurassic to the Eocene (de Almeida, 1978).

The last, post-Eocene phase of the reactivation, consisted of a slow abating of tectonic activity and a gradual restabilization of the South American platform.

Patagonian Platform

The Patagonian platform forms the remainder of the tectonically stable part of the South America. It occupies the southeastern tip of the continent, south of approximately latitude 35° South, and east of the Andean cordillera, extending eastward offshore as Argentina's broad continental shelf (Fig. 1).

Basement

The basement of the Patagonian platform stabilized during the late Paleozoic. The limited number of basement outcrops and occasional deep drill holes which penetrate the basement reveal both metamorphosed and unmetamorphosed rocks ranging in age from the late Precambrian to the middle Paleozoic. The history of the basement's evolution is very poorly known due to a widespread cover of sediments and basic volcanics which has accumulated since the

Carboniferous. The cover is deformed locally near the Andes (de Almeida, 1978).

Basins

The basins characterizing the Patagonian platform are mostly small marginal faulted basins created during the late Jurassic tectonic reactivation that accompanied the rifting of the South American continent from the African continent. The Colorado basin, located in the northeastern extremity of the platform, may contain more than 6,000 meters of sediment. Most of the basin is still covered by the Atlantic ocean. The San Jorge basins have been identified as failed rifts or aulacogens by Burke (1978). The southern end of the Patagonian platform carries the Magellan basin and the offshore Malvinas basin, both of which parallel the eastward curve of the Southern Andes. The Magellan basin is filled with more than 5,000 meters of mostly marine sediments deposited from the Cretaceous through the Tertiary. The sediments in the southwestern sides of both of these basins are folded and bordered by a long thrust fault, due to the influence of Andean tectonics (de Almeida, 1978).

The maximum subsidence in each of these marginal basins occurred during the Cretaceous. The formation of the basins was contemporaneous with those marginal basins formed along the South American platform during its tectonic

reactivation, and both sets of basins are related to the opening of the South Atlantic ocean.

Andean Cordillera

Both the South American platform and the Patagonian platform are bounded to the west by the 9,000 kilometer long Andean cordillera, a complex and tectonically active mobile belt which makes up the entire western margin of South America. A sub-Recent to Recent episode of block uplift and volcanism along the Andean cordillera has created a continous mountain chain which superficially appears to be the result of a single orogeny. The cordillera has actually evolved in a series of irregularly superimposed orogenies and episodes of sedimentation which began during the late Precambrian. The belt has exhibited mobility throughout its entire history. Furthermore, the geologic history of the belt differs greatly from one part of the cordillera to another.

Gansser (1973) divided the Andean cordillera into three segments: the Southern or Patagonian Andes, the Central or Chilean-Peruvian Andes, and the Northern or Colombian-Venezuelan Andes. He further divided the Central Andes into a southern and northern section of the intersection of the aseismic oceanic Nazca ridge with the cordillera. Each of these segments differs notably from the others in overall crustal composition, structural style, and

degree of seismicity and volcanism. A map showing the location of the Central and Northern Andes, together with their internal divisions, is provided in Figure 3.

The following geological discussion is primarily based on the review of Gansser (1973).

Southern Andes

The Southern Andes stretch from the southern tip of the South American continent, where the cordillera turns eastward to merge with the Scotia arc, north to approximately latitude 47° South, where the active oceanic Chilean ridge intersects the continent. The most distinctive characteristic of this segment of the Andes is a central belt of upper Jurassic and Cretaceous ophiolites (oceanic crust), mostly metamorphosed to greenschists, with associated oceanic sediments. In places these rocks are cut by granitic to dioritic batholiths of late Cretaceous to late Miocene age. The Pacific border, west of this belt is made up of widespread granitic to dioritic batholiths intruded during the late Cretaceous. A belt of slightly metamorphosed upper Paleozoic sediments is exposed along the Pacific coast between latitudes 53°South and 48°South.

Quaternary to Recent volcanism is scarce in the Southern Andes, and earthquakes are uncommon. This contrasts sharply with the extensive volcanism and strong modern seismicity of the central Andean cordillera.

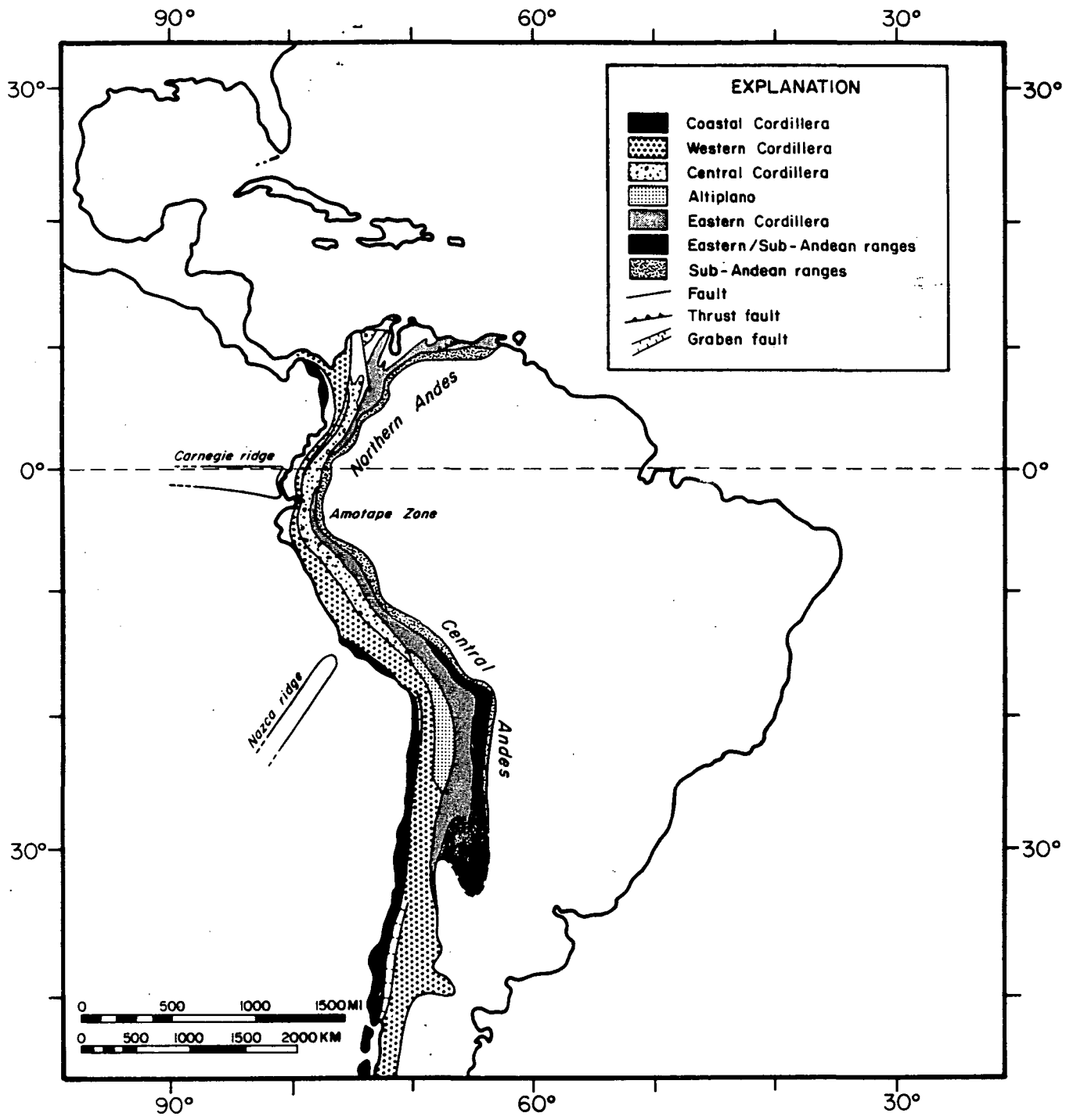

Figure 3. The Andean cordillera: Northern and Central Andes (after Zeil, 1979).

Central Andes

The Central Andes extend from the Gulf of Penas in Chile, where the Chilean ridge intersects the continent, to the Amotape range at the Peru-Ecuador border near latitude 5° South. The regular north-south trend of the Central Andes from the Gulf of Penas northward is interrupted at the Chile-Peru border, where the cordillera makes an abrupt northward bend. This deviation is due to the position of the large cratonic mass of the northern South American platform.

Although some geological and structural differences on either side of the intersection of the Nazca ridge with the continent justify a secondary division of the Central Andes, the cordillera as a whole is geologically simpler than either the Northern or Southern Andes. Three basic geological/morphological units can be distinguished along its length. These are the Coastal cordillera, bordering the Pacific, a central High cordillera, also called the Western cordillera, and the Eastern Sub-Andean ranges, which adjoin the stable cratonic areas.

The Coastal cordillera consits mainly of sharply folded and steeply faulted pre-Mesozoic metamorphic rocks unconformably overlain by a much more gently deformed Mesozoic and Cenozoic cover. The strongly compressed and metamorphosed pre-Devonian rocks of the Coastal cordillera exhibit a distinct northwesterly trend that is not parallel

to the north-south trend of the southern part of the Central Andes. Some of the older rocks of this belt may be as old as the Precambrian. The Mesozoic cover of the cordillera is dominated by an enormous volume of Jurassic and Cretaceous volcanic rocks. However, there are no clear indications of tholeiitic basalt, ultrabasics, glaucophane schist, flysch, or radiolarites (Zeil, 1979). The cover is deformed by gentle flexure and block faulting, in sharp contrast with the intense compressional deformation of the pre-Mesozoic rocks. Widespread and irregularly distributed granitic, granodioritic, and tonalitic batholiths, mostly of late Jurassic to middle Cretaceous age, intrude the belt.

The Coastal cordillera of the Central Andes ends abruptly at the Pracas Peninsula near Nazca, Peru, where the Nazca ridge intersects the continent.

The High cordillera forms the central geological/ morphological unit of the central Andes over most of its length. The southern part of the High cordillera consists mostly of Mesozoic sediments and volcanics intruded in places by Mesozoic plutons. Volcanics dominate the Cretaceous rocks, and numerous Quaternary to Recent volcanos occur in the range. The northern part of the High cordillera is almost completely covered by Plio-Pleistocene sheet flows and stratovolcanos. The structural style of this cordillera as a whole is characterized by large scale

flexuring and block faulting which decreases in intensity from west to east.

The High cordillera merges with the Altiplano of the Chile-Argentina-Bolivia border area in that region where the Andean cordillera widens dramatically and changes its trend from north-south to northwest. The high plateaus are covered by an enormous pile of Pliocene to Quaternary volcanics which is block faulted along steep north-northeasterly (pre-Pliocene) and north-northwesterly (post-Pliocene) faults. The Altiplano narrows north of the northwestward bend of the Central Andes, and the High cordillera of Bolivia and Chile becomes the Western cordillera of Peru, which borders the Pacific ocean. This change coincides with the disappearance of the Coastal cordillera. A nearly continuous belt of Cretaceous batholiths is intruded along the coast within this new coastal range. Tertiary volcanics are widespread, but Quaternary volcanism disappears. Further inland, in Peru, a narrow Central cordillera develops out of the plateau region, characterized by a sharply folded Cretaceous section intruded by granitic to granodioritic plutons.

The Eastern cordillera and the Sub-Andean ranges form a belt bordering the stable platforms of South America along the entire length of the Central Andes. The Sub-Andean ranges are wide and particularly well developed in the Argentine Andes, where they expose great thicknesses of

marine and continental sediments deposited from the Carboniferous onward. These ranges merge northward with Eastern cordillera of Bolivia. The Eastern cordillera is distinguished by narrow, tightly folded anticlines cored with Paleozoic sediments, separated by broader synclines containing Mesozoic and Tertiary sediments. Steep eastward-directed thrust faults cut the belt. These structures all show a distinct easterly vergence which increases in intensity to the east.

The Eastern cordillera bends to the northwest at approximately latitude 18° South with the rest of the Central Andes and continues northwestward across Peru to approximately latitude 5° South, where it terminates against the Amotape zone. The range narrows somewhat north of the bend. A zone of eastward-directed thrust faults develops along the eastern border of the mountains, and Mesozoic plutons, which were absent south of the bend, are intruded into the western half of the range. The Precambrian and lower Peleozoic rocks of the Eastern cordillera here are sharply folded and are overlain by a less deformed cover of upper Paleozoic and Mesozoic rocks.

Northern Andes

The Northern Andes extend from approximately latitude 5° South, near the Peru-Chile border, north-northeastward up to a widely splayed termination at the northern end of the South American continent. Most of the Andean cordillera

turns east here to merge with the Caribbean Andes and the Caribbean island arc complex. A narrow western branch of the mountains continues northward and passes into the Central American ranges.

The geological differences between the Central and Northern Andes are the most striking of any geologic change along the Andean cordillera. The change occurs along the Amotape zone, which coincides with the intersection of the oceanic Carnegie ridge with the continent. The Amotape zone contains several uplifts that expose old eastward to northeastward-striking gneisses and schists intruded by granites. Upper Carboniferous sediments are exposed in parts of the zone. Both the Central and Northern Andes border the Amotape zone with abnormal strikes.

Four cordilleras are clearly and independently developed in the Northern Andes: the Coastal cordillera, the Western cordillera, the Central cordillera, and the Eastern cordillera. The Coastal cordillera of the Northern Andes consists of a series of east-west and northwestward-trending coastal ranges composed of ophiolites and pelagic sediments. These oceanic rocks, of Cenozoic to early Tertiary age, differ greatly from the continental basement rocks which make up the Coastal cordillera of the Central Andes. The northern Coastal cordillera is traceable as a geologic unit as far north as Panama, where it forms the southwestern side of the Panama Andes.

The Western cordillera of the Northern Andes is separated from the Coastal cordillera in Ecuador by a Mio-Pliocene sediment-filled basin floored by basic volcanics. The cordillera itself is composed of thick, slightly metamorphosed pelitic rocks with interspersed basic volcanics, all of Cretaceous age. In places, upper Cretaceous and younger batholiths pierce folded Cretaceous phyllites. In Columbia and eastern Panama, the Western cordillera is composed mainly of thick phyllitic to schistose pelites of late Jurassic to Cretaceous age, together with basic volcanic intercalations and some large ultramafic bodies.

The eastern border of the Western cordillera in Ecuador is formed by the Quito graben, which is filled with late Tertiary continental sediments and Quaternary tuffs. A young volcanic belt lying along fractures in alignment with the Quito graben forms the eastern border of the range in Colombia. The entire eastern border of the Western cordillera is an important tectonic boundary which separates a belt of oceanic crust from thicker continental crust to the east.

The sedimentary facies, the distribution of basic and ultrabasic rocks, and the regional metamorphism of the northern ranges of Venezuela and Trinidad are strikingly similar to that of the Western cordillera of Ecuador and Colombia. An apparent connection exists in the northernmost

tip of the Sierra Nevada de Santa Marta of Colombia-Venezuela, through which similar rocks, offset by the Santa Marta fault zone, can be traced.

Steep east-west trending fault zones showing strike-slip movement border the northern ranges of Venezuela and Trinidad on both their northern and southern sides. The southern fault zone separates the crystalline masses of the northern ranges from an interior range of greenschist metavolcanics and Cretaceous oceanic sediments thrust in from the north. Further east, these oceanic rocks swing northeast to disappear into the Caribbean, and the interior ranges change in composition to unmetamorphosed sediments of a platform-type facies.

The Central cordillera of the Northern Andes is composed mainly of a belt of crystalline metamorphic rocks. Precambrian basement rocks are hidden under a cover of slightly metamorphosed Ordovician sediments, and numerous large young plutons aligned with the late Mesozoic Andean batholiths intrude the belt. These rocks are divided from the ophiolitic rocks of the Western cordillera by a sharp tectonic boundary to the west; platform-type Cretaceous limestones overlap the crystalline rocks in the east and blur the eastern boundary of the cordillera.

The north-northwestward-trending Santa Marta fault zone displaces the entire Central cordillera northward as the separate block of the Sierra Nevada de Santa Marta.

This block represents the northernmost part of the Central cordillera.

The Eastern cordillera of the Northern Andes lies between the Central cordillera and the Guyana shield. The pre-Mesozoic rocks of the Central cordillera apparently connect with the pre-Mesozoic rocks of the Eastern cordillera and eventually pinch out against the Precambrian rocks of the Guyana shield. The thin Paleozoic sedimentary veneer covering the Central cordillera, however, expands into a thick sedimentary sequence in the Eastern cordillera. Precambrian rocks and lower Paleozoic sediments, occasionally intruded by granites, are frequently exposed in the uplifted ranges. The lower Paleozoic mostly consists of a pelitic facies several kilometers thick that is slightly metamorphosed in places. There is ample evidence for a pre-Devonian orogeny.

Although volcanic rocks are common at the base of the Mesozoic, Cretaceous marine sediments laid down by a major transgression make up the most widespread rocks of the Eastern cordillera. Some basins contain Cretaceous marine sediments 17 kilometers thick. The marine sediments thin eastward toward the Guyana shield, where they grade into the veneer of quartz sandstones that cover the western part of the craton.

Tectonic Development

The Andean Cordillera has developed along the western margin of South America in apparent response to the subduction of oceanic lithosphere beneath the moving South American plate. Currently the Nazca plate is being subducted beneath western South America, and there are some complex plate interactions with the Cocos and Caribbean plates occurring in northern South America. The continent has also been influenced by interaction with the Antarctic plate in the south. The presence of Benioff zones beneath parts of the Andean cordillera, the position of the Peru-Chile trench, the initiation of extensive magmatic activity in the Triassic with its subsequent eastward migration and the concurrent development and deformation of a wedge of sediments and volcanics have made the cordillera (particularly the Central Andes), the classic example of a marginal orogeny due to the consumption of an oceanic plate beneath a continental plate (Dewey and Bird, 1970; James, 1971, 1973). However, as more and more geological and geophysical data about the Andean cordillera are collected, it is becoming clear that a simple model of orogeny cannot be applied to the entire cordillera. A uniform Benioff zone has not developed beneath the entire cordillera; the various zones which have been discerned vary in dip, and seem to indicate the subducting Nazca plate has split into unconnected tongues (Barazangi and Isacks, 1976). Only the

modern distribution of seismicity (and volcanism) is known, and any projection back into geologic time is very tentative (Gansser, 1973; Zeil, 1979). Furthermore, the relationship between more or less continuous oceanic plate consumption and episodic orogeny is still unclear.

The pre-Mesozoic history of the Central and Southern Andes also presents difficulties. The highly compressed, obliquely-striking Precambrian and Paleozoic substructure of the Coastal cordillera, which is overlain by an only mildly deformed volcanic cover, crops out along the Pacific coast and contains no oceanic rocks. This conflicts with the distribution of rocks predicted by a simple pacific-type convergent plate margin model.

Except for the Eastern cordillera of the Central Andes and the zone immediately landward of the Peru-Chile trench, the predominant tectonic style of the Andean cordillera since the Triassic has been vertical uplift and block faulting (Zeil, 1979). When this observation is combined with the tremendous amount of igneous activity that has occurred in the central parts of the cordillera, it points to a general regime of uplift and extension rather than compression. Many compressional features of the Andes can be explained as the result of batholith emplacement and gravity tectonics (Meyers, 1975; Dennis, 1982).

Recently, the possibility that the accretion of allochthonous terranes may have played a role in the

formation of the Andes has received some attention. Ben-Avraham et al. (1981) have suggested that oceanic plateaus--extinct island arcs, submerged continental fragments, seamount clusters, or hot spot traces--may have collided with the South American continent and been incorporated into the continent's margin in the past. Unlike the more thoroughly studied North American cordillera, the Andean cordillera is not known in sufficient geological detail to confirm the presence of embedded terranes. The unusual crust of the western part of the Northern Andes is considered a possible example, however. At present, both the Nazca ridge and the Juan Fernandes ridge, which are aseismic oceanic ridges of thick basalt cumulates, are colliding with the South American continent. Nur and Ban-Avraham (1981) have suggested that the attempt to consume these thick-rooted, bouyant ridges has interrupted subduction in places along the margin of South America, causing the gaps in volcanism and seismicity which characterize parts of the Andean cordillera.

Jordan et al. (1983) have published an even more recent study which links lateral tectonic segmentation along the Central Andes (between latitudes 5° South and 40° South) to segmentation of the subducting Nazca plate. The Nazca plate segments are defined by major variations in the dip of the Benioff zone, inferred from the spatial distribution of intermmediate depth earthquakes. From west to east, post-

Oligocene Andean tectonics above nearly flat-subducting segments are characterized by a constant topographic rise from the Pacific coast to the crest of the Andes, insignificant volcanism, a narrow belt of eastward-migrating possibly thin-skinned shortening, and Plio-Pleistocene uplift of crystalline basement along reverse faults. Above steeply dipping (30°) segments, post-Oligocence Andean tectonics are characterized by a fault-bounded longitudinal valley east of coastal mountains, on active belt of andestitic volcanism, an elevated high plateau, a high, inactive thrust belt, and an active eastward-migrating thin-skinned thrust belt. No deformation of the South American plate (i.e., basement involvement) occurs east of the eastern limit of Benioff zone seismicity, although thin-skinned thrust belts have migrated outward beyong this limit. Crustal seismicity above flat-subducting segments is distributed across the cordillera, while crustal seismicity above steeply-dipping segments is limited to the active thrust belts.

Although these authors emphasize the importance of the influence of Nazca plate sementation on the segmentation of central Andean tectonics, they also mention the potential effect that pre-existing structures in the South American plate have had in controlling Andean tectonics and possibly even the position of the Nazca plate segments. The authors further note a relationship between the early Cenozoic

tetonics of western North America and the post-Oligocene to Holocene tectonics of the Central Andes.

PREVIOUS GEOPHYSICAL INVESTIGATIONS

Relatively few detailed geophysical investigations have been made over the South American continent, compared with the work done over the other continents of the world. The majority of South American studies have concentrated on the impressive Andean cordillera and adjacent oceanic areas in attempts to understand the structures and tectonic processes associated with a currently active orogenic belt. The continent's stable platform and shield areas have in contrast received relatively little attention. The only set of geophysical data that provides uniform coverge of the South American continent and surrounding oceanic areas are satellite scalar magnetic anomaly data recently collected by NASA's MAGSAT orbital magnetic field survey (Hinze et al., 1982). Before discussing the results of an analysis of these datas, however, it will be useful to give a general survey of earlier geophysical investigations relevant to the lithospheric structure of South America.

Lithospheric Thickness

Many investigators have used the earthquakes distributed along the Andean subduction zone to estimate the thickness of the South American lithosphere. The lithosphere is defined to be the relatively rigid lid or

outer layer of the earth, involving the crust and part of the upper mantle, that overlies a zone of less rigid mantle called the asthenosphere. The asthenosphere is characterized by slightly lower seismic velocities, and much lower Q (a measure of the efficiency of seismic wave propagation) and viscosity than the lithosphere.

Based on the scatter of earthquake foci throughout the wedge of crust and mantle overlying the subducted Nazca plate, James (1971) suggested that a 200 to 300 kilometer-thick lithosphere underlies central western South America. In contrast, Barazangi and Isacks (1976, 1978) determined the position of four inclined seismic zones beneath western South America, and after identifying them with the location of the descending Nazca plate, suggested that the shallow (10°) dip of the plate beneath northern and central Peru and central Chile constrained the lithospheric thickness of western South America to approximately 130 kilometers. James (1978), however, emphasized that the spatial distribution of earthquakes foci beneath central Peru is confined to small active clusters, rather than being spread along a plane, and that apart from a single isolated intermediate cluster, there is little evidence for a shallow seismic zone beneath the continent. He also mentioned geological and geochemical observations which show that the undersaturated alkalic rocks of eastern Peru were probably associated with a subducted slab at a depth of 300 to 400

kilometers (implying a 30° dip) as recently as 5 m.y.b.p. Sack and Snoke (1978) reemphasized the diffuse character of the seismicity beneath central Peru. They also reported a set of observations of the ScSp phase. (an S-wave reflected from the core and converted to a P wave at a discontinuity within the upper mantle) from deep focus events that suggest the Nazca plate has a dip of approximately 30° beneath central Peru.

Further evidence for a thick lithosphere beneath western South America comes from the anelasticity studies of Sacks and Okada (1974) and Sacks (1977). These investigators found lithospheric-type Q values (low elastic attenuation) down to about 350 kilometers beneath western South America, and a low-Q zone coinciding with a seismic zone between depths of 350 to 500 kilometers. Sacks and Snoke (1977) inferred the existence of an approximately horizontal interface under western and central-southern South America at a depth of around 400 kilometers, based on the positions of S to P wave conversions (the sp phase) below the continent. The polarity of the converted phase indicated a velocity reversal below the interface, and the investigators interpreted the discontinuity as the lithosphere-asthenosphere boundry.

A study relating the lateral segmentation of the tectonics of the Central Andes to differently dipping segments of the subducting Nazca plate has been published

recently by Jordan et al. (1983). The correlations put forth by these authors depend upon the existence of two oceanic segments being subducted at 30° and two segments being subducted nearly horizontally beneath the South American plate. These segments were defined by variations in the dip of the Benioff zone inferred from the spatial distribution of intermediate-depth earthquakes. The tectonic segmentaion observed in the Andean cordillera appears to be valid; the conflict between the existence of shallow-dipping oceanic plate segments and the evidence for thick lithosphere presented earlier was not mentioned. A very recent high-resolution study of the Benioff zone beneath southern Peru (Boyd et al. 1983) seems to confirm the existence of a sharp change in dip in the Nazca plate below this part of western South America. The earthquake data gathered by these researchers from a local seismic network indicates that the Benioff zone dips at a nearly constant 30° beneath southernmost Peru while dipping at 30° and leveling off a 100 kilometers depth to become nearly horizontal further to the north. Plate deformation appears to be continuous across the transition.

The results of a surface wave dispersion study conducted by Sherburne (1975) support the possibility that a thick lithosphere exists beneath the South American platform east of the Andean cordillera. After examining the phase and group velocity dispesion of both Love and Rayleigh waves

along several paths across the South American platform (Fig. 12) Sherburne was unable to identify any pronounced low velocity zone within the mantle, and he concluded that the entire region is laterally uniform and structurally similar to other shield areas to depths of at least 400 kilometers. The dispersion characteristics of the South American platform were most similiar to those observed over the South African shield, indicating a strong structural similarity between the two regions. These results are in agreement with the earlier work of Molnar and Oliver (1969), who found that shear waves propagate very efficiently (implying high Q) below both the Guyana and Central Brazilian shields. These investigators based their findings on the low attenuation of the seismic phase Sn (a short-period shear wave channeled through the uppermost part of the mantle) observed along several paths emanating from an earthquake which ocurred between the Guyana shield and the Amazon basin.

The Brazilian heat flow study of Vitroello (1978) forms an important counterpart to the seismic studies conducted over the South American platform. Vitroello measured the heat flow and heat generation at 19 sites in eastern and central Brazil, sampling the Brazilian portion of the Atlantic shield and part of the Parana basin. The sites were chosen to investigate the influence of three major tectonothermal events: the consolidation of the

cratons formed during the mid-Precambrian Trans-Amazonian orogenic cycle, the formation of the metamorphic belts during the late-Precambrian Brazilian orogenic cycle, and the tectonic reactivation and Cretaceous magmatism associated with the opening of the South Atlantic ocean. Vitroello's results indicate a progressive decrease in heat flow with age of the last thermal event. He measured an average heat flow of 42 mW m^{-2} in the Sao Francisco craton, which is typical of shield areas, a slightly higher heat flow of around 55 mW m^{-2} in the Brazilian metamorphic belts, and a notably higher heat flow of about 79 mW m^{-2} in the Parana basin. Such differences imply differences in temperature of a few hundred degrees Celsius in the lower crust and upper mantle below the three provinces. The heat flow contributed by deep sources beneath all three provinces (the reduced heat flow) measured approximately 28 mW m^{-2}.

Vitroello concluded that the Brazilian Coastal Shield (the Atlantic shield) represents a typical stable shield exhibiting low heat flow and heat production, with a subsolidus geotherm extending deep into the mantle. Taking into account the limited seismic data, this low temperature regime probably extends below most of the South American platform. Since residual heat is observable in provinces as old as 500 to 600 m.y.b.p., he further concluded that the conductive cooling of a thermal disturbance in the platform must extend to a depth of at least 400 kilometers. When

this observation is combined with the observation that the heat flow varies with the age of the province, it suggests that the subcontinental crust and upper mantle below the South American platform has retained its structural integrity to a depth of around 400 kilometers for more than 500 million years.

Andean Crustal Structure

Although the Andean cordillera has attracted a relatively large amount of geological and geophysical attention compared to the rest of the South American continent, the details of its substructure remain poorly understood. With the exception of studies designed to determine the position and continuity of the subducted Nazca plate, the majority of the Andean geophysical investigations have been concerned with the crustal structure of the cordillera.

The earliest attempts to determine the thickness of the crust supporting the Andes took advantage of large-scale blasting in two open-pit copper mines in southern Peru and northern Chile (Aldrich et at. 1958; Tatel and Tuve, 1958). Investigators from the Carnegie Institution of Washington recorded the resulting reflected and refracted seismic waves along several profiles radiating outward from the two pits along the western flank of the Central Andes. No arrivals of any kind were obtained beyond approximately 200 kilometers along profiles running east-west,

perpendicular to the cordillera. This was attributed to extreme attenuation within the crust. Profiles running parallel to the cordillera in Peru yielded a depth to the M-discontinuity of 34 to 36 kilometers (possibly reaching 46 kilometers), assuming a two-layer structure for the crust. In northern Chile, profiles running parallel to the cordillera yielded a 46 kilometer crust, again assuming a two-layer structure. There were fainter signs of an interface at 56 kilometers below Chile. Woollard (1960) reinterpreted this data and tentatively inferred a crustal thickness of around 65 kilometers below the Western cordillera (High cordillera) of the Central Andes, with a steep dip in the M-discontinuity of approximately 18° from west to east. Slightly north of this area, Cisternas (1961) conducted a simple Rayleigh wave dispersion study along two short, single station paths in the Andes to Huancayo, Peru, and concluded that the local crustal thickness was on the order of 50 kilometers.

Lomnitz (1962) discussed the crustal structure of the Chilean Andes in terms of the physiography, seismicity, gravity anomalies, and geologic evolution of Chile. He constructed a north-south gravity profile and theoretical crustal section along the center line of Chile between latitudes 18° South and 41° South, calculating crustal thickness with a rough empirical formula justified by the sparse data. On this basis he concluded that the crust

reaches a thickness of about 70 kilometers beneath the Puna block (the southern Altiplano) at the borders of Chile, Argentina, and Bolivia. The crust thins southward. Lomnitz also provided a simple transcontinental crustal profile, based on gravity anomalies, from Valparaiso, Chile, to Mar del Plata, Argentina, extending offshore at both coasts.

A model of the crustal structure beneath the Peru-Chile trench off the coast of Peru was derived by Fisher and Raitt (1962) using offshore refraction methods. Their model shows oceanic crust thickening from about 11 kilometers below the Pacific basin to nearly 17 kilometers beneath the trench. Ludwig, Ewing, and Ewing (1965) presented the results of 22 offshore seismic retraction profiles made in the Magellan Straits, over continental crust. At the northern end of one profile, running approximately north-south at longitude 71° West, these investigators measured a depth to the M-discontinuity of 29.6 kilometers, increasing steadily to the south to 34.8 kilometers. The velocity of P-waves in the mantle measured 7.95 km/sec.

Based on an analysis of the spectra of teleseismic P-waves, Fernandez and Carcaga (1968) estimated the thickness of the crust beneath La Paz, Bolivia to be 64.6 $\pm$ 7.8 kilometers, with a P-wave velocity in the mantle of 8.1 km/sec and in the crust of 6.76 km/sec.

Dragicevic (1970) constructed an extensive Bouguer gravity anomaly map of the southern Central Andes between

latitude 14° South and latitude 40° South. Dragicevic also constructed two simple profiles of the crust across the central and southern Central Andes at latitude 20° South and latitude 33° South using a density of 2.84 g/cm^3 for the crust and 3.27 g/cm^3 for the mantle. His results confirm the presence of a deep, low density root beneath the mountains that thins to the south.

By determining the hypocenters of a group of earthquakes beneath Santiago, Chile, and then minimizing the difference between arrivals predicted by a simple model and observed arrivals, Chuaqui (1973) inferred the presence of a dipping interface whose position and slope agrees with the crust-mantle interface derived from Dragicevic's gravity modeling at that latitude. Chuaqui also obtained a mantle P-wave velocity of 8.1 km/sec and a crustal P-wave velocity of 6.1 km/sec.

The results of two surface wave dispersion studies conducted in the Andean cordillera were reported in 1970 and 1971. Leeds and Knopoff (1970) measured Rayleigh wave phase velocity dispersion between Quito, Ecuador and Bogota, Colombia for two earthquakes and inferred an average crustal thickness of 60 kilometers between the two stations. They concluded that if any low-velocity zone existed, it was either poorly developed, or extremely deep. An analysis of the phase velocity dispersion of Love waves between Peldehue, Peru, and Antafagasta, Chile for one earthquake

yielded a thinner crust of 40 to 45 kilometers. Shear wave velocities in the mantle here were slightly higher than those measured in the north.

James (1971) made a much more extensive study of the crust and upper mantle strudture beneath southern Peru, eastern Bolivia, and northern Chile using both Rayleigh and Love wave phase and group velocity dispersion between several western South American seismograph stations. The paths are shown on the map in Figure 4. James inverted his dispersion measurements and assembled the resulting models to obtain a three-dimensional crustal model of the middle Central Andes. His final model shows the crust varying in thickness from a maximum of slightly over 70 kilometers beneath the Western cordillera and the western side of the Altiplano, to 30 kilometers along the Pacific coast, to 11 kilometers beneath the Pacific basin. In the east, the crust thins to 50-55 kilometers beneath the Eastern cordillera. It also appears to thin both north and south of the Altiplano to around 55-60 kilometers. The average P- and S-wave velocities within this part of the crust are around 6.2 km/sec. and 3.45 km/sec, respectively, which are somewhat lower than average crustal values. James found no significant low-velocity zone in the upper 150 kilometers of the mantle beneath the Central Andes. Below the Pacific ocean, however, a substantial low-velocity zone ranging in

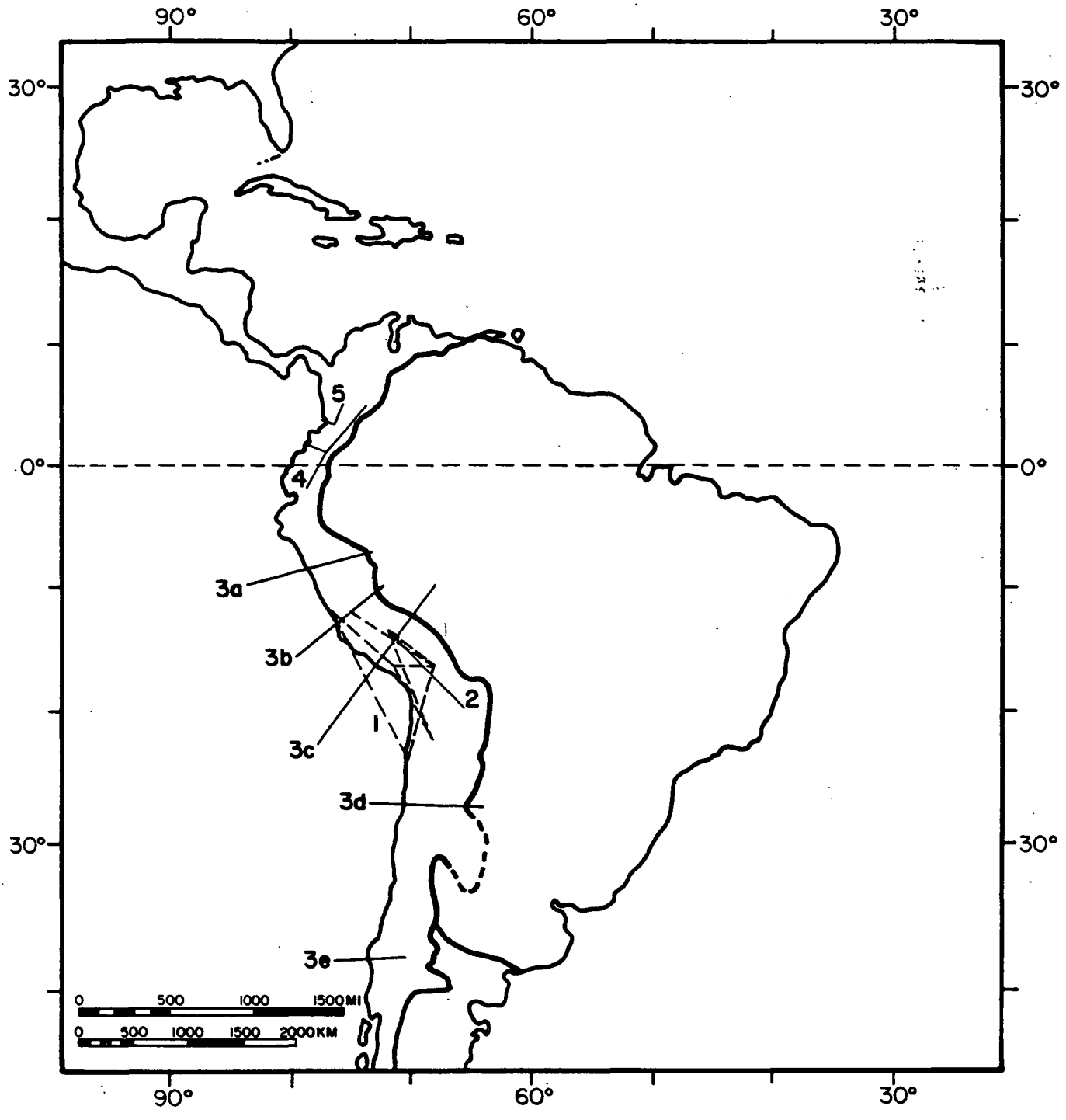

Figure 4. Previous geophysical investigations in the Andean cordillera. (1) James (1971); (2) Ocola and Meyer (1972); (3) Couch et al. (1981); (4) Ocola et al. (1975); (5) Mooney et al. (1979).

depth from 50-60 kilometers to more than 200 kilometers was necessary to satisfy the dispersion data.

A second program of reconnaissance explosion seismology was carried out by the Carnegie Institution of Washington over the Peru-Bolivia altiplano in 1968 (Fig. 4). The data taken from this program, originally interpreted by Ocola, Meyer, and Aldrich (1970), was reinterpreted by Ocola and Meyer (1972) using ray-tracing in a spherical earth to fit the arrival times and relative amplitudes observed on the record sections. These investigators reconfirmed an earlier-derived model having three major refractors: a sedimentary-metamorphic layer 4-9 kilometers thick, characterized by P-wave velocities of 4.5-4.9 km/sec; a "granitic" layer reaching depths of 26-30 kilometers, characterized by P-wave velocities of 6.0-6.1 km/sec; and a "gabbroic" layer bottoming out of 68-70 kilometers, characterized by P-wave velocities of 6.8 to 6.9 km/sec. However, in order to account for relatively large amptitude secondary arrivals, two new low-velocity zones within the crust below the Altiplano were modeled. A shallow low-velocity zone beneath Peru was positioned between depths of 9 and 12 kilometers, separating materials of 6.0 km/sec velocity from those of 6.1 km/sec velocity. A deeper, somewhat thicker low-velocity zone was placed between 30 and 40 kilometers beneath Bolivia, and between 36 and 46 kilometers beneath Peru. This layer was sandwiched

between 6.8 km/sec and 6.9 km/sec velocity material. These low-velocity zones were tentatively related to the magmatic activity which characterizes the Central Andes.

Ocola and Meyer (1973) later published two crustal models along profiles from the Pacific basin to the Brazilian shield for southern Peru and northern Chile. These models were designed to satisfy both the previously collected seismic data and the major features of the Andean and Peru-Chile trench gravity anomalies. Their crustal sections show in general an approximately 10 kilometers thick sedimentary-metamorphic layer characterized by a P-wave velocity of 4.5 km/sec beneath the Altiplano, above a second layer characterized by a P-wave velocities ranging from 5.7 km/sec to 6.1 km/sec. This second layer is thickest under the Altiplano and pinches out near the Peru-Chile trench. A third layer, also deepest and thickest beneath the Altiplano, lies below these two layers, and has a P-wave vewlocities ranging from 6.8 km/sec to 7.0 km/sec. The total crustal thickness is about 12 kilometers beneath the Pacific basin, increasing rapidly to 76 kilometers beneath the Altiplano, and thinning more slowly to approximately 40 kilometers beneath the Brazilian shield.

The most recent, and by far the most detailed set of crustal profiles across the continental margin and Andean cordillera of Peru and Chile has been published by Couch et al. (1981). The location of their profiles is shown in

Figure 4; the crustal profiles themselves are reproduced in Figure 5 through Figure 9. These models were derived by two-dimensional modeling of the continental margin gravity anomalies, constrained by bathymetric, topographic, seismic refraction, and magnetic data. The investigators used empirical relations between seismic velocity and density, together with mapped surface geology, to choose the modeled layer densities. They also assumed a standard mass column of 70 kilometers, with no lateral variations in density below 70 kilometer depth.

Northern Andean Crustal Structure

Since 1971, the Northern Andes (Ecuador, Columbia, Venezuela) have received a comparatively large amount of geophysical attention. Such interest has been spurred by several factors. Unlike the simpler tectonics of the central and southern parts of the Andean cordillera, the tectonics of the Northern Andes reflects the complex interaction of the Guyana shield, the Nazca and Cocos plates of the Pacific, and the Caribbean plate. The western two ranges of the Northern Andes are characterized by an oceanic suite of thick, late Mesozoic tholeiitic volcanics, with associated pelitic sediments, which contrasts strongly with the more typically continental rocks of the eastern two ranges. This geology is very much different from the geology of the Central and Southern Andes. The Northern Andes are also distinguished by an irregular distribution of

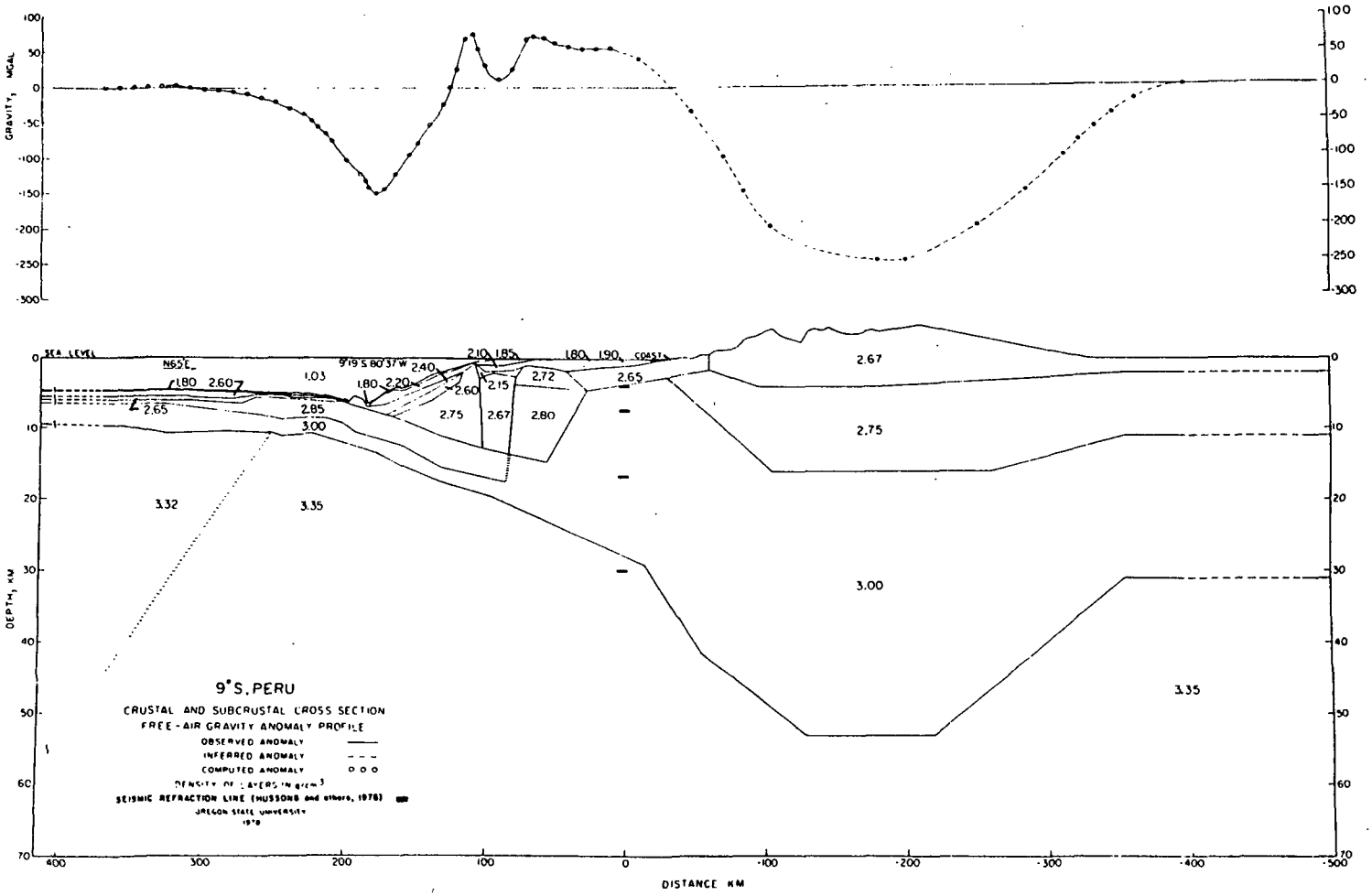

Figure 5. Crustal and subcrustal cross section of the continental margin of Peru at lat 9° S. The vertical exaggeration is 5:1. From Cough et al. (1981) (corresponds to line 3a, Fig. 4).

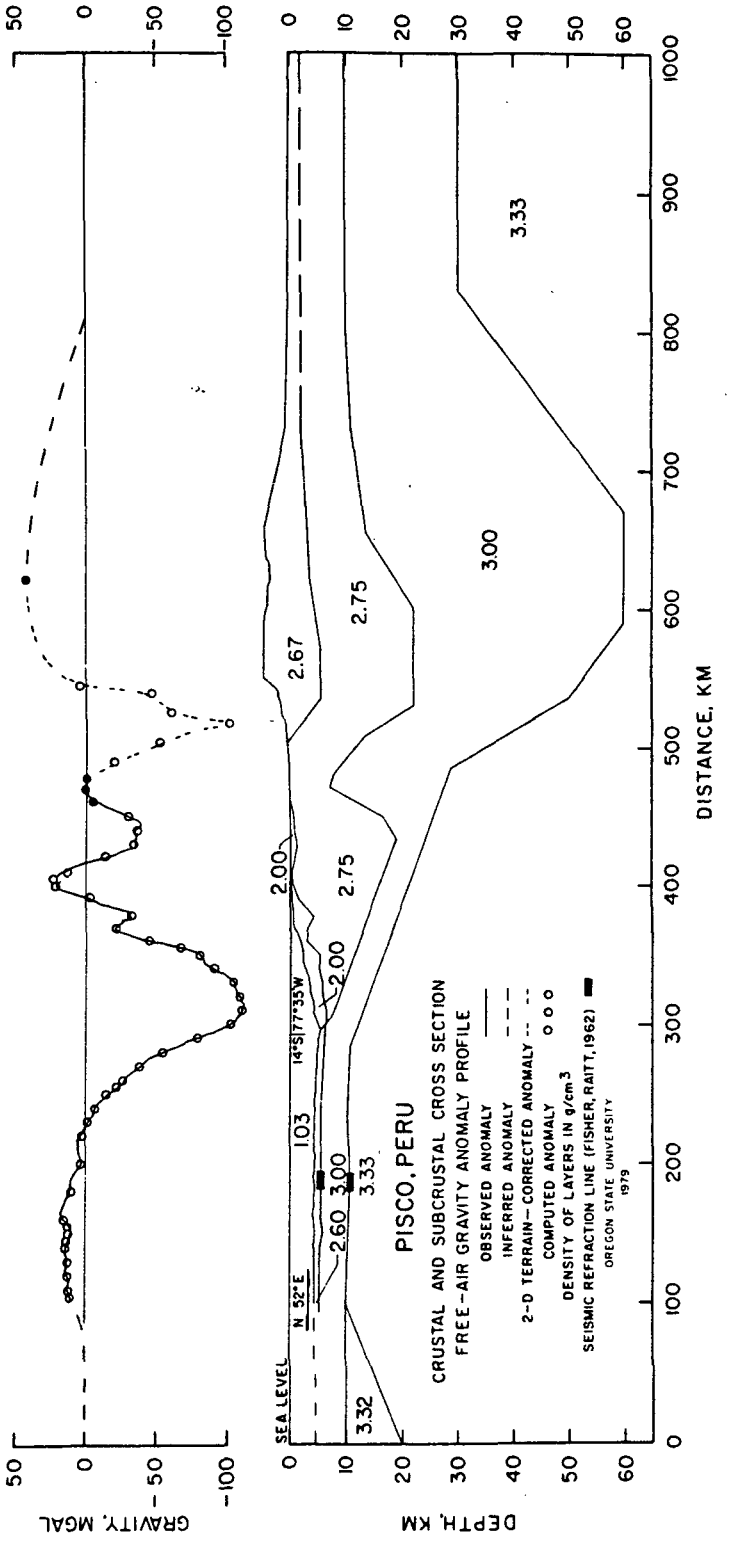

Figure 6. Pisco, Peru, crustal and subcrustal cross section. The vertical exaggeration is 4:1. From Couch et al. (1981)(corresponds to line 3b, Fig. 4).

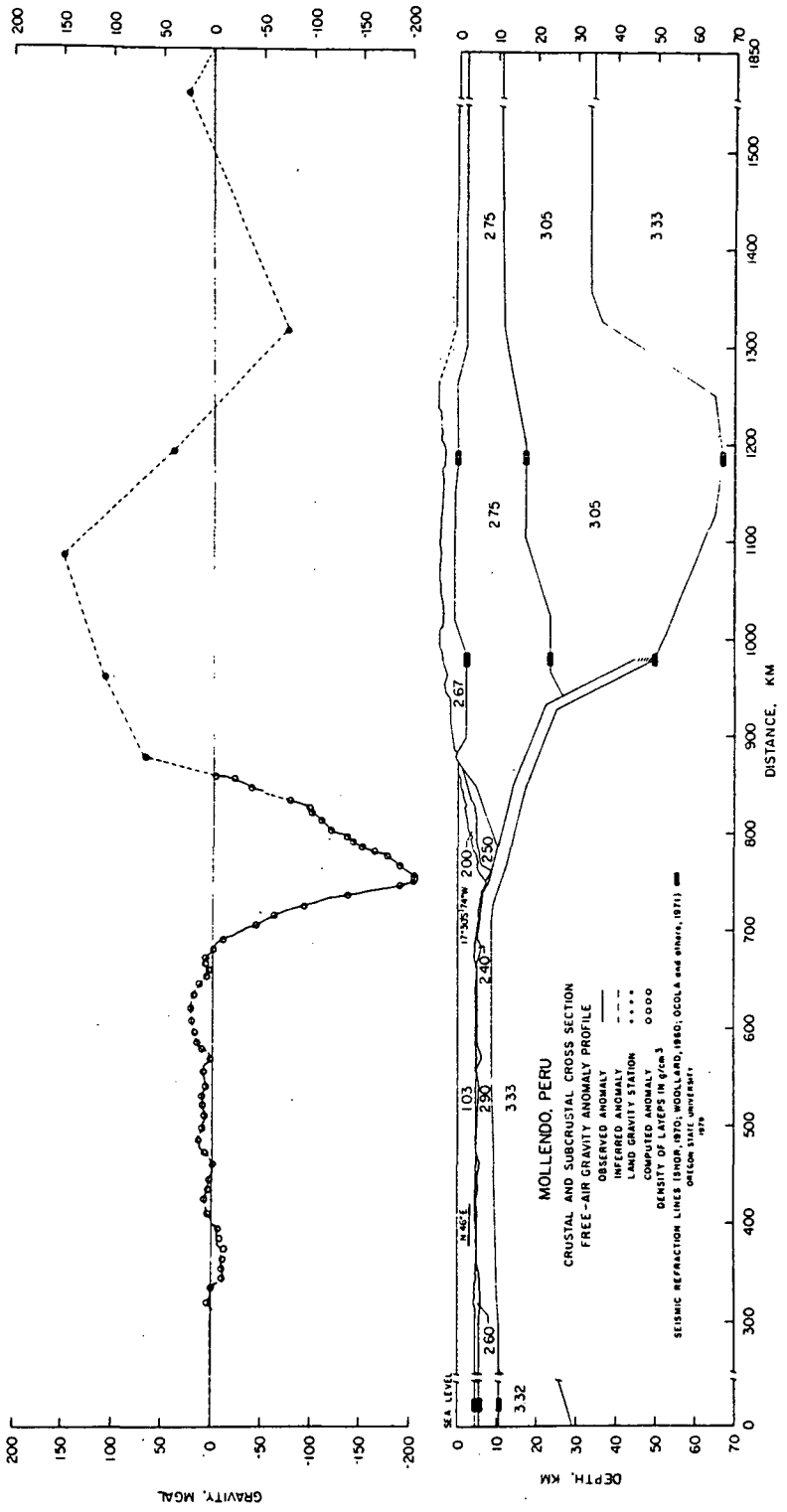

Figure 7. Mollendo, Peru, crustal and subcrustal cross section. The vertical exaggeration is 4:1. From Couch et al. (1981)(corresponds to line 3c, Fig. 4).

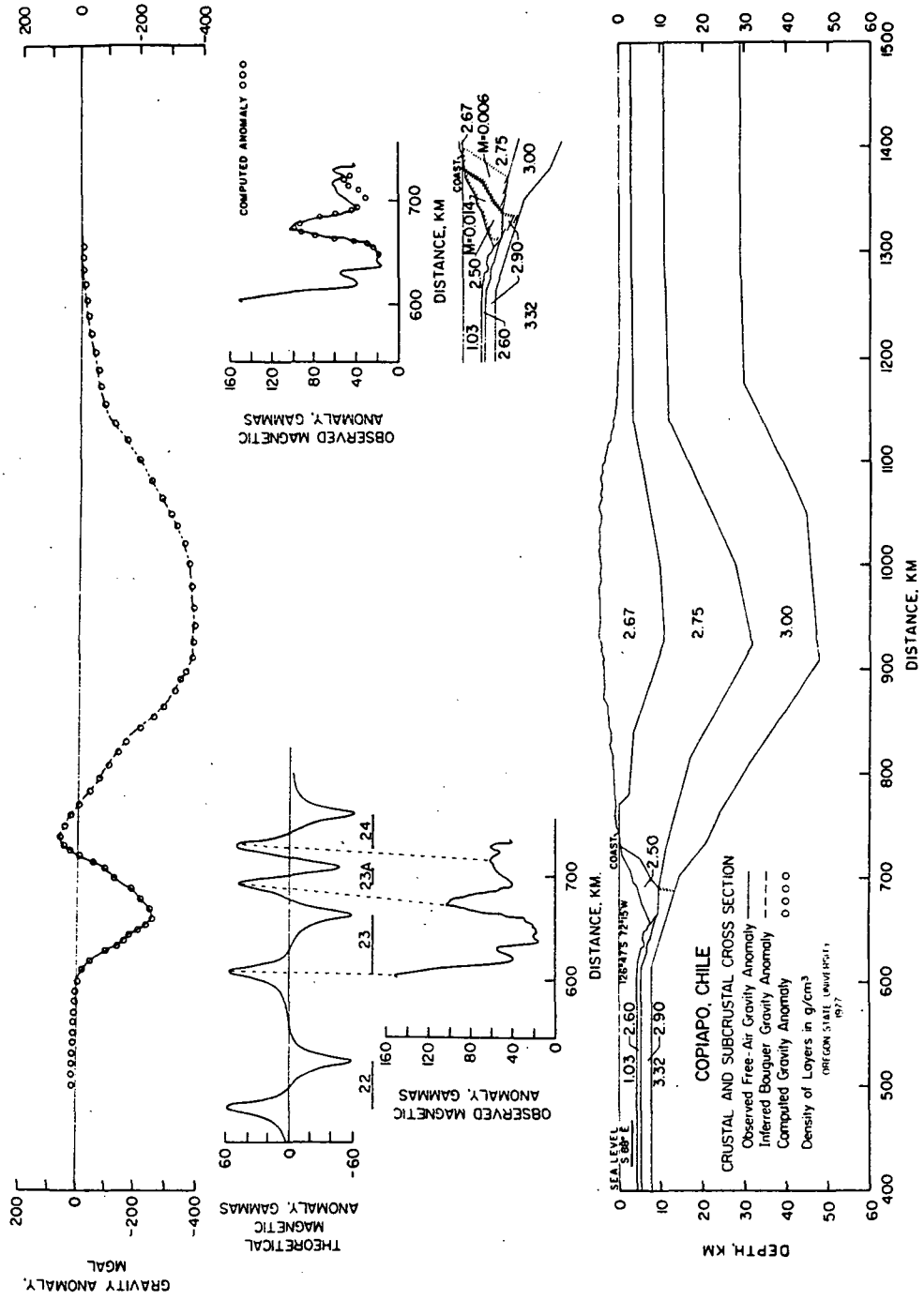

Figure 8. Copiapó, Chile, crustal and subcrustal cross section and two possible interpretations of the observed magnetic anomalies. The vertical exaggeration is 4:1. From Couch et al. (1981)(corresponds to line 3d, Fig. 4).

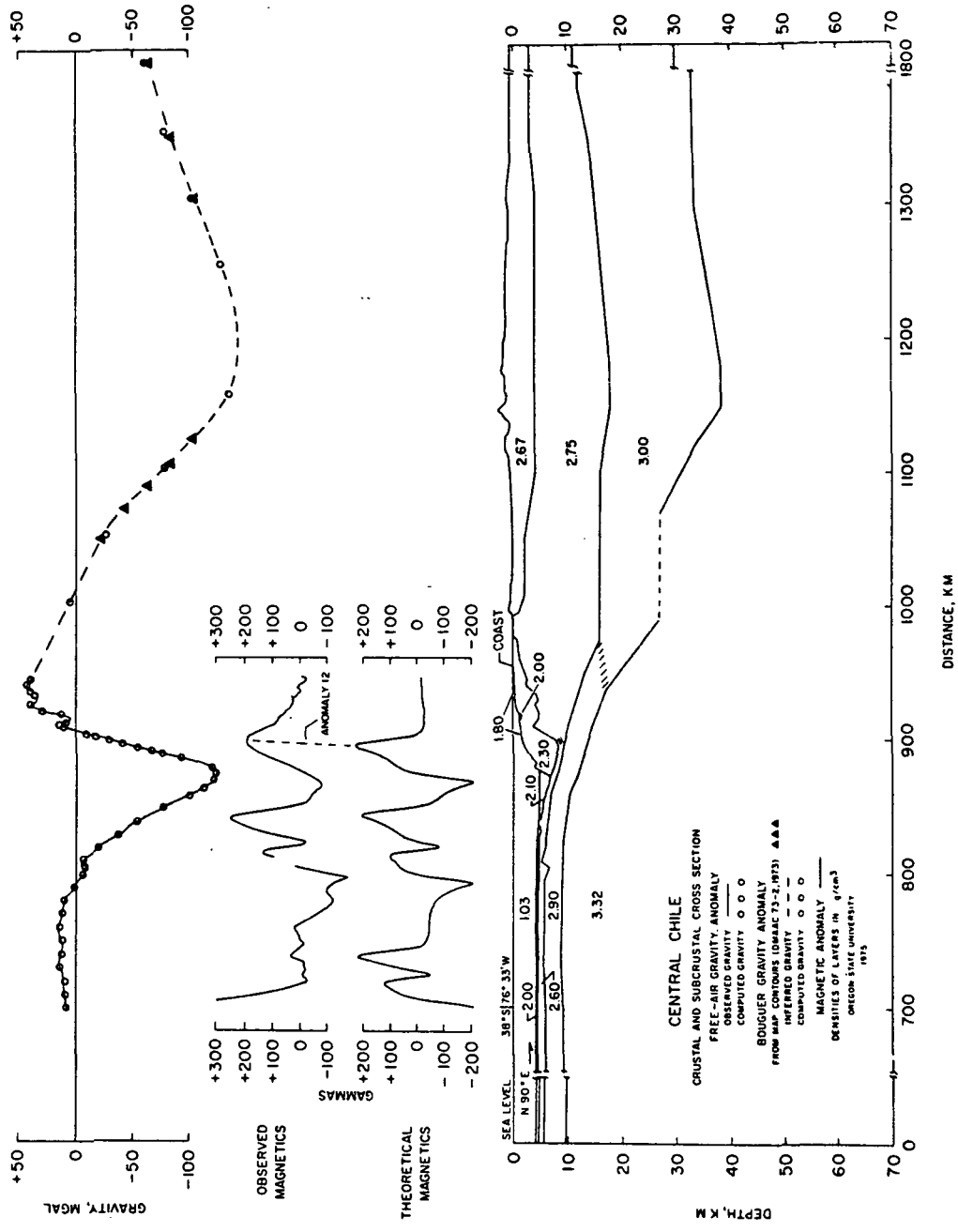

Figure 9. Central Chile crustal and subcrustal cross section. The vertical exaggeration is 4:1. From Couch et al. (1981) (corresponds to line 3e, Fig. 4).

earthquake foci which makes it impossible to identify a uniform Benioff zone. There are almost no deep focus earthquakes (Zeil, 1979). All of these factors suggest the presence of an unusual substructure which must differ from the substructure of the rest of the cordillera.

Case et al. (1971) published a synthesis of the geological and geophysical information available for western Colombia and eastern Panama. The investigators also conducted a gravity and vertical intensity magnetic survey over northwestern and central Colombia to supplement previously collected geophysical data. These measurements revealed a Bouguer anomaly range of a few hundred mgals across the Andean ranges. Once corrections were made for low density Tertiary basin fill, nearly the entire strip of land between the Pacific coast and the Western cordillera of Colombia (the so-called Mesozoic eugeosyncline) was discovered to be characterized by strongly positive Bouguer anomalies. A particularly high ridge of gravity values ranging to +95 mgals (the West Colombian high) parallels the western flank of the Western cordillera, running nearly the entire length of Colombia and extending into southern Ecuador. A complex regional pattern of anomalies exists east of this high, characterized by the distinctive lows of the Central cordillera and its adjacent basins. Case et al. concluded that the eastern margin of the West Colombian high marks the boundary between a thin, dense, probably oceanic

crust flooring westernmost Colombia and thicker continental crust to the east. The high itself is caused by a long narrow belt of dense uplifted rock which the authors interpret as either an oceanic ridge or an island arc complex which was overridden by the Mesozoic eugeosyncline in Tertiary time. Continental crust extends eastward from the eastern flank of the high and supports the Central cordillera of the Northern Andes and adjacent basins. These authors also provided a crustal profile extending from the Pacific eastward across the Central cordillera which shows the thickness of the crust increasing from 16 kilometers beneath the Pacific ocean to around 30 to 35 kilometers beneath the Central cordillera.

Case and MacDonald (1973) later extended the gravity and magnetic survey to include northern Colombia. The survey principally covered the triangular fault-bounded Santa Marta uplift and the Guajira Peninsula of extreme northern Colombia. The Santa Marta uplift, an offset and topographically high section of the Western cordillera, is characterized by a large positive Bouguer anomaly which reach a maximum value of more than 130 mgals in the northwestern corner of the massif. Except for the Tertiary sedimentary basins, much of the Guajira Peninsula is also characterized by positive Bouguer anomalies. The investigators concluded that although these high values may partially be due to dense metamorphic rocks, they indicate

the continental crust of extreme northern Colombia is very thin, and that dense lower crustal or mantle material is unusually close to the surface. The Santa Marta uplift in particular is strongly out of isostatic equilibrium. The total crustal thickness of the massif may only be 15 kilometers. In light of these observations, the investigators suggest that the continental crust of the Santa Marta uplift and the Guajira Peninsula has overridden the adjacent crust and upper mantle of the Caribbean.

In the same year, Case et al. (1973) published the results of a 300 kilometer-long geophysical profile across the Andes of southwestern Colombia. This profile was parallel to the Colombia-Ecuador border and extended from the Pacific coast to the Putamayo basin east of the Andean cordillera. The general pattern of gravity anomalies along this profile is very similar to that measured in the earlier Colombian gravity survey of Case et al. (1971). Bouguer anomalies range from -80 mgals near the Pacific coast over the Tertiary Bolivar trough, to a high of +75 mgals along the western flank of the Western cordillera. This high represents the southern extension of the West Colombian high, and the authors again ascribe it to a raised block of mafic or ultramafic crust just beneath the eastern side of the Bolivar trough and the western edge of the Mesozoic eugeosyncline. From this high the gravity values decrease steadily eastward to a minimum of -220 mgals over the

Colombian altiplano and the Central cordillera. The authors interpret this steep gradient as the reflection of a deep-seated zone separating oceanic crust underlying western coastal Colombia from thicker continental crust beneath the bulk of the Andean cordillera. Case et al. (1973) also constructed a crustal profile, based on gravity modeling, which shows the transition from mafic crust in the west to continental crust in the east. The large negative Bouguer anomaly over the Colombian altiplano and the Central cordillera suggest a maximum crustal root thickness of around 45 kilometers for this section of the Northern Andes.

The geophysical data provided by these gravity and magnetic surveys have been supplemented recently by two important seismic refractions studies carried out in the Northern Andes. Ocola et al. (1975) reported the findings of a seismic refraction survey made along the axis of the regional gravity low of the altiplano of Colombia and Ecuador. The refraction line extended roughly from Bogota through Quito into central Ecuador along two branches radiating from a southwestern Colombian lake shot point (Fig. 4). Synthetic record sections, generated by the reflectivity methods of Fuchs and Muller (1971), were constructed by trial and error modeling of the velocity-depth structure below the line. The best fits between the observed and synthetic data were obtained from models containing P-wave low-velocity zones. In general,

both the Colombia and the Ecuador branches showed upper crustal refractors with apparent velocities less than 6.4 km/sec, lower crustal refractors with apparent velocities ranging from 6.4 km/sec to 7.5 km/sec, and a crust-upper mantle transition zone with apparent velocities greater than 7.5 km/sec. Both branches also show similarly placed, well developed low-velocity zones. The total crustal thickness beneath the axis of the gravity low measured 66 kilometers. This is in sharp disagreement with the crustal thickness of 30 to 45 kilometers derived by Case et al. (1971, 1973), but it does agree with the crustal thickness of 60 kilometers inferred from Rayleigh wave dispersion between Bogota and Quito by Leeds and Knopoff (1971).

The results of a pair of seismic refraction/wide-angle reflection studies made over the Western cordillera of Colombia were reported by Mooney et al. (1979). Data were taken from two profiles extending both north-northeast (parallel to the strike of the cordillera) and west-northwest (perpendicular to strike) from a shot point in a quarry on the eastern flank of the Western cordillera (Fig. 4). The investigators applied a technique of travel-time and relative amplitude modeling of both P- and S- wave first arrivals to obtain velocity-depth profiles of the upper crust. Best results were obtained from models having velocity gradients, rather than distinct layers. Two alternative lower crustal models, one with low-velocity

zones and one without, were obtained for the north-northeasterly striking line by modeling reflected arrivals. In this case, somewhat better agreement was obtained by using low-velocity zones.

The total crustal thickness beneath the Western cordillera measured either 26.5 kilometers or 29 kilometers, depending on the choice of lower crustal model. The seismic velocities measured in the upper crust are unusually high. P-wave velocities increase from 4.5 km/sec at the surface to 6.7 km/sec at a depth of 6 kilometers, reaching 7.0 km/sec at a depth of 11 kilometers. S-wave velocities increase from 2.5 km/sec at the surface to 4.0 km/sec at 11 kilometers. Such velocities are more typical of oceanic crust than continental crust, and the investigators combined this observation with the associated positive Bouguer anomaly and geological evidence to conclude the upper crust of the Western cordillera consists of igneous oceanic rocks of Cretaceous age. An intra-crustal boundary exists at a depth of 19 kilometers to 21 kilometers. The velocity structure of the lower crust, derived from the reflection data, is ambiguous. Depending on the choice of models, the lower crust could consist entirely of oceanic rocks, or could contain an upper 15 kilometer layer of oceanic rock overlying continental rock.

THEORETICAL BACKGROUND

The geophysical technique used in this study to determine variations in the average crustal thickness of the South American platform was fundamental mode Rayleigh wave dispersion analysis. The following sections provide the theoretical background and justification for the use of this technique.

Rayleigh Wave Dispersion

In 1885 Lord Rayleigh investigated the behavior of elastic waves which propagate along the plane free surface of a homogeneous elastic half-space, in rough analogy to water waves traveling over deep water (Rayleigh, 1885). Rayleigh demonstrated that such a medium can support a particular type of harmonic surface wave (now called a Rayleigh wave) which travels with a slightly lower velocity than shear waves traveling in the same medium. Points on the surface of the medium move in vertically polarized, retrograde elliptical orbits with the passage of this wave; no motion transverse to the direction of wave propagation occurs at all. The amplitude of the orbital motion of points within the medium is greatest at the free surface and decays exponentially with distance from the surface. The rate of amplitude decay with depth is proportional to the

wavelength, so that waves with long wavelengths penetrate deeper into the medium than waves with shorter wavelength.

Rayleigh waves are guided along the free surface of the medium in which they propagate, and therefore spread cylindrically in two dimensions rather than spherically in three dimensions. They consequently form an increasingly dominanant part of the vertical surface motion of the earth at greater and greater distances from an earthquake source, as Rayleigh predicted. Unlike the case investigated by Rayleigh, however, the earth is not a flat, homogeneous elastic medium. Since the velocity of seismic waves in the earth generally increases with depth, Rayleigh waves of long wavelength and correspondingly deeper penetration travel faster than waves of shorter wavelength. Figure 10 shows a train of Rayleigh waves excited by an earthquake along the Mid-Atlantic ridge recorded initially at Natal, Brazil, 1,260 kilometers from the epicenter. The second seismogram, beginning 18 minutes later, shows the same Rayleigh wave train recorded in line with the source at La Paz, Bolivia, 3,817 kilometers from Natal. The gradual separation of wave components of different wavelengths that occurs as the wave train crosses the South American Platform is very well displayed. This phenomenon is known as dispersion.

Group and Phase Velocity

Let the function f(t) describe a fundamental mode Rayleigh wave recorded by a station at a distance r and

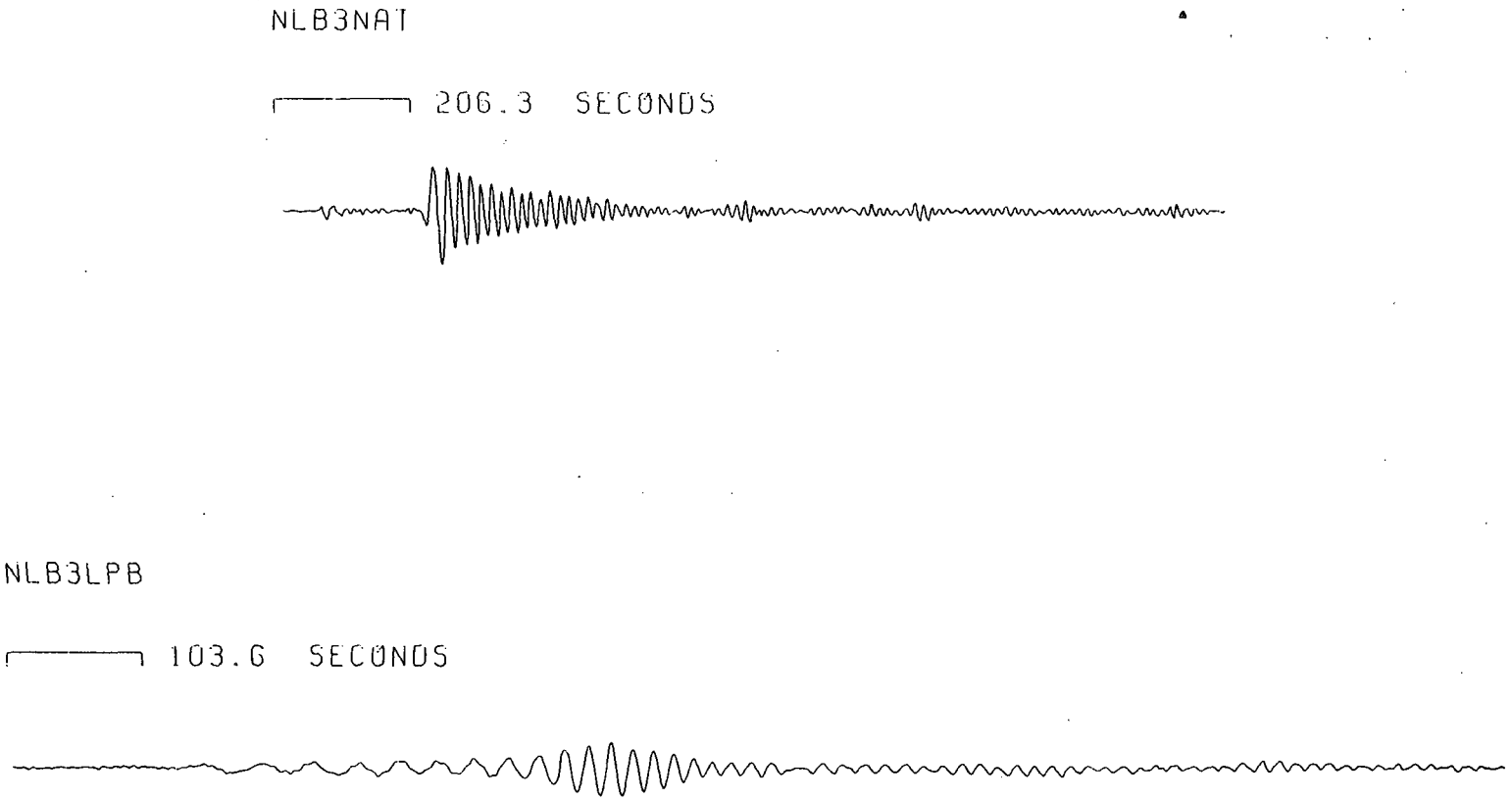

Figure 10. Seismograms recorded at Natal, Brazil (top) and La Paz, Bolivia (bottom) for the event NLB3. Station separation is 3,817 kilometers.

azimuth θ from the epicenter of an earthquake. The Fourier transform of this function gives the spectrum of the Rayleigh wave in terms of its amplitude A and phase ϕ:

$$F(\omega) = A(r, \theta, \omega) \cdot e^{i\phi(r, \theta, \omega)}$$

The variable ω (= $2\pi/T$, T = wave period) represents the frequency of the wave.

The techniques used in this study extract some of the information contained in Rayleigh wave velocity dispersion. For Rayleigh waves of a given mode, it is possible to attribute the time delay due to wave propagation between two stations to the phase difference between the spectra of the waves recorded at each station. (Given the time delay and the distance between the two stations, wave velocities can be calculated.) The information carried by changes in amplitude of the Rayleigh waves with time is ignored.

The waveform of a Rayleigh wave recorded at a station is a function of the earthquake mechanism and the instrumental response of the seismometer as well as a function of the elastic properties of the medium over which the wave has traveled. The two-station method used in this study, which measures the velocity dispersion between two stations with matched instuments, eliminates the effects of both earthquake source phase shift and the instrumental phase shift, and considers only the phase shift due to wave

propagation between the stations. If the terms describing the source and instrumental phase shifts are dropped, the inverse Fourier transform of $F(\omega)$ can be written:

$$f(t) = \frac{1}{2\pi} \int_0^\infty A(r, \theta, \omega) \cdot \exp [i(\omega t - kr)] \, d\omega,$$

where k is the wavenumber ($= 2\pi/\lambda$, λ = wavelength). This equation approximately describes a single-mode Rayleigh wave prpagating in time.

Consider a single sinuoidal component of this wave, of frequency ω_0. Surfaces of constant phase, such as the crest or trough of a wave, move with a velocity which can be found by setting the phase term of this equation equal to a constant:

$$\omega_0 t - k(\omega_0) r = \text{constant}$$

Differentiating with respect to distance r yields

$$\omega_0 \frac{dt}{dr} - k(\omega_0) = 0$$

giving the <u>phase velocity</u>

$$c(\omega_0) = \frac{dr}{dt} = \frac{\omega_0}{k(\omega_0)} .$$

If the phase velocity of each of the sinusoidal components of the Rayleigh wave is the same, as is true in a homogeneous elastic medium, the components move together, and a given waveform will not change shape as it propagates across the medium. Furthermore, the velocity of the various

components will be identical to the group velocity--the speed at which the entire wave train or packet travels. (The group velocity is generally associated with the rate of wave energy transport.) However, in a medium composed of layers whose elastic properties vary with depth, the phase velocity does depend on the wave period, and the various sinusoidal components sort themselves out in time and with distance. As a result the Rayleigh wave train spreads out and changes shape, or disperses, as it travels. In the earth, where seismic velocities generally increase with depth, individual wavefronts actually move faster than the spreading packet of Rayleigh waves which carries them. Wave crests appear at the back of the Rayleigh wave train and move forward to disappear at the front of the train, making it necessary to distinguish between the group velocity and the phase velocity.

A group velocity can be associated with each frequency component ω_0 of a Rayleigh wave by evaluating the equation of the wave in the vicinity of ω_0:

$$f(t)_{\omega_0} = \int_{\omega_0 - \varepsilon}^{\omega_0 + \varepsilon} A\,(r, \theta, \omega) \cdot \exp[i(\omega t - kr)]\, d\omega \,.$$

This function is largest (i.e. wave energy is maximized) when all the waves within the narrow band of frequencies $[\omega_0 - \varepsilon, \omega_0 + \varepsilon]$ are in phase, or when

$$\frac{d}{d\omega} (\omega t - kr)_{\omega = \omega_0} = 0 \,.$$

This yields the group travel time

$$t_{gr} = \frac{dk(\omega)}{d\omega}\bigg|_{\omega = \omega_o} \cdot r$$

and finally the group velocity

$$U(\omega_o) = \frac{r}{t_{gr}} = \frac{d\omega}{dj(\omega)}\bigg|_{\omega = \omega_o}$$ (Dziewonski and Hales, 1972).

An equation uniquely relating the group velocity to the phase velocity can be derived by differentiating the phase velocity $c = \omega/k(\omega)$ with respect to the wavenumber $k(\omega)$:

$$\frac{dc}{dk(\omega)} = \frac{d}{dk(\omega)}\left(\frac{\omega}{k(\omega)}\right)$$

$$\frac{dc}{dk(\omega)} = -\frac{\omega}{k^2(\omega)} + \frac{1}{k(\omega)}\frac{d\omega}{dk(\omega)} .$$

Upon rearrangement this becomes

$$\frac{d\omega}{dk(\omega)} = \frac{\omega}{k(\omega)} + k(\omega)\frac{dc}{dk(\omega)}$$

or

$$U(\omega) = c(\omega) + k(\omega)\frac{dc(\omega)}{dk(\omega)} .$$

This equation shows that as long as the phase velocity does not depend on the wavelength, $dc(\omega)/dk(\omega) = 0$, and the group velocity is identical to the phase velocity. The group velocity will differ from the phase velocity, however, if any dispersion occurs.

Utility

Rayleigh wave velocity dispersion is most sensitive to changes in the distribution of shear wave velocity with depth in the earth (Brune and Dorman 1963; Der et al. 1970). This dependency makes it possible to use dispersion measurements to model the average shear wave velocity distribution with depth between appropriately chosen pairs of seismograph stations. Modeling proceeds by choosing an initial model of velocity distribution, computing the phase and group velocity dispersion which this model would generate, comparing the computed dispersion with the actual observed dispersion, and then repeatedly modifying the velocity distribution model until a satisfactory fit between the computed and observed dispersion is obtained. The long wavelengths of the surface waves which disperse blur the details of earth structure both laterally and vertically, justifying only average models. Because of this, it is important to restrict the choice of wave travel paths to a single geologic province if possible.

The shear wave velocity models derived in this way complement the models of compressional wave velocity distribution obtained by refraction profiling. Furthermore, low seismic velocity zones, which are difficult to detect by conventional refraction and reflection methods, show up well in models derived through dispersion measurements. Rayleigh wave trains are easily discerned on the long-period vertical

component seismometers operated by the World-Wide Standard Seismograph Network (WWSSN). The seismograms are inexpensive and relatively easy to obtain; the digital analysis techniques necessary to measure group and phase velocity dispersion and generate models are already established. The paths connecting WWSSN station pairs provide a network of remote geophysical coverage that is often difficult to obtain otherwise. All of these advantages combine to make Rayleigh wave dispersion analysis an ideal technique for studying the lithopheric structure of an area as large and inaccesible as the interior of South America.

DATA ANALYSIS

In this study, the procedure used for obtaining models of the shear wave velocity distribution with depth below the South American platform can be divided into three general steps. The first step involved chosing a set of Rayleigh wave data that would provide suitable coverage of the South American platform. The second step involved measuring the fundamental mode group and phase velocity dispersion that these datas display. The final step involved inverting the dispersion measurements to obtain shear wave velocity-depth models.

Data Selection

The locations of the South American members of the WWSSN stations chosen for use in this study are shown in Figure 11. The latitudes, longitudes, and elevations of these stations are given in Table 1. With the exception of the Brasilia station, each of these stations lies near the perimeter of the South American platform, and the paths connecting them provide general coverage of the stable cratonic portion of South America. These paths are also shown in Figure 11. Figure 12 shows the South American two-station paths along which Sherburne (1974) measured Rayleigh wave phase velocity dispersion. His results have also been

Table 1

Latitude, Longitude, and Elevation of Seismograph Stations Used in This Study

Code	Station Name	Latitude	Longitude	Elevation
BDF	Brasilia	15° 39' 50" S	47° 54' 12" W	1,260 m
BOG	Bogota	4° 37' 23" N	74° 03' 54" W	2,658 m
CAR	Caracas	10° 30' 24" N	66° 55' 39" W	1,035 m
LPA	La Plata	34° 54' 32" S	57° 55' 55" W	14 m
LPB	La Paz	16° 31' 58" S	68° 05' 54" W	3,292 m
NAT	Natal	5° 07' 00" S	35° 02' 00" W	10 m
TRN	Trinidad	10° 38' 56" N	61° 24' 10" W	24 m
QUI	Quito	0° 12' 05" S	78° 30' 02" W	2,837 m

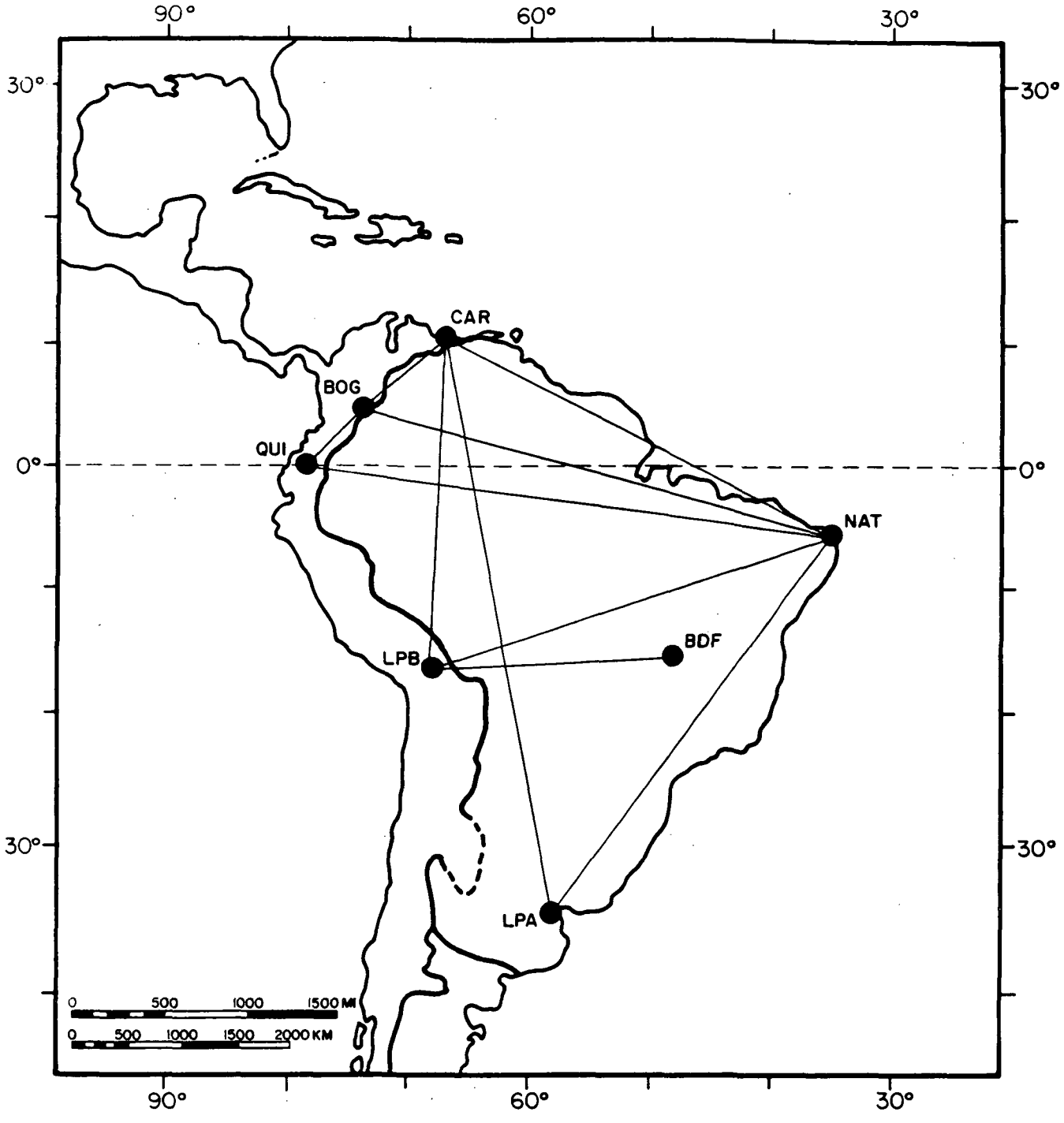

Figure 11. Locations of WWSSN seismograph stations used in this study and the paths over which Rayleigh wave dispersion measurements were made.

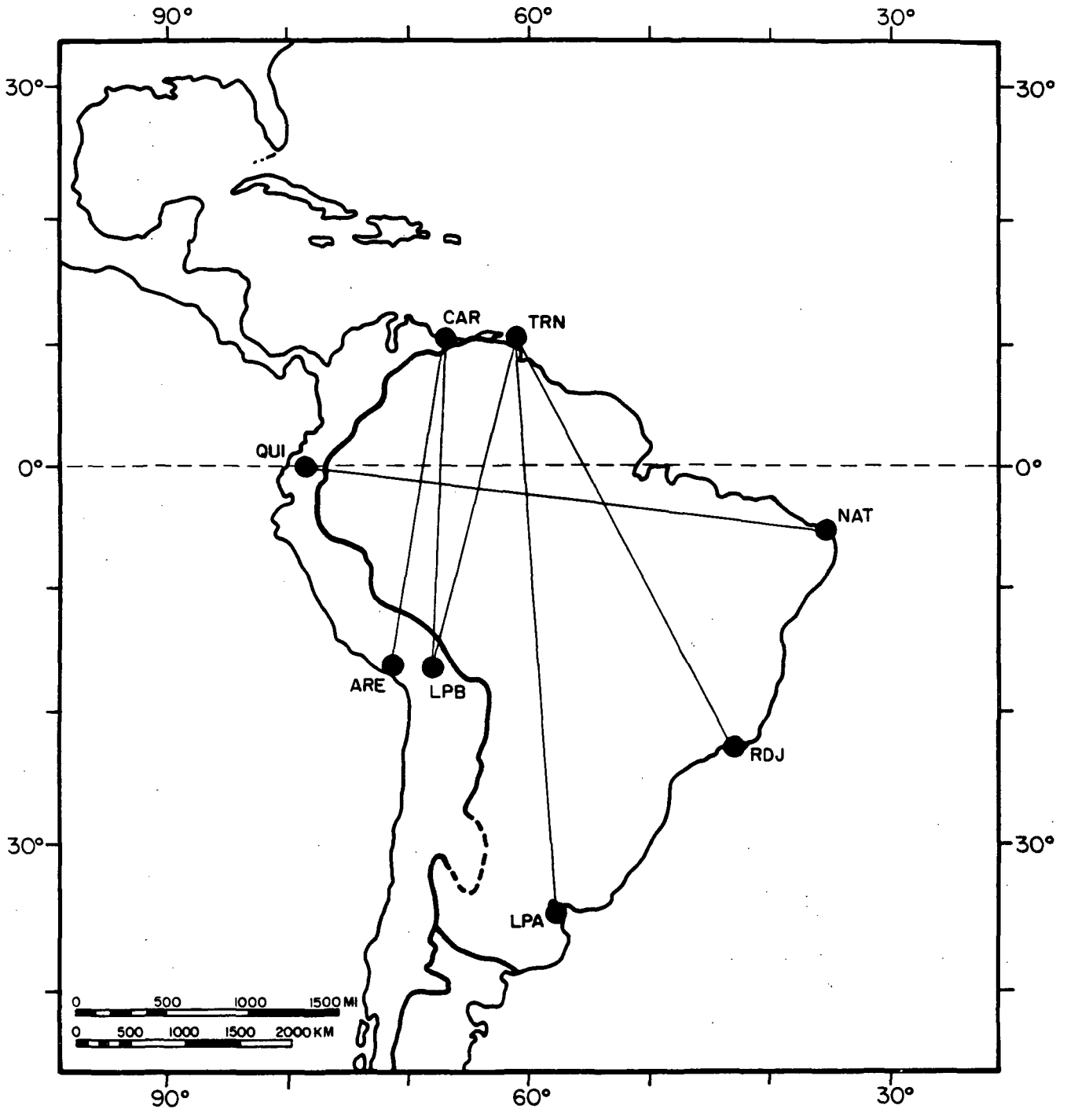

Figure 12. Paths over which Sherburne (1974) made Rayleigh wave dispersion measurements.

inverted to provide additional shear wave velocity models across the platform.

Barring lateral refactions, a given point on the wavefront of a surface wave describes a great circle as the wave spreads over the earth's surface. To obtain suitable Rayleigh wave data, the great circle path connecting each station pair was projected into an area of known seismicity and a Marsden square computer search of the seismicity tapes provided by the National Geophysical and Solar-Terrestrial Data Center, NOAA, was performed around the intersection of the projected path and the active area. Each search generated a list of earthquake epicenters, origin times, magnitudes, and depths to focus. The computer searches were limited to earthquakes recorded sine 1965. Visual inspection of the actual records was further limited to events with magnitudes greater than five on the Richter scale. The long-period vertical component seismogram recorded at each station of a given station pair was then examined for clear, noise-free Rayleigh wave trains that would be suitable for digitization.

Once a useable earthquake was located, the great circle distance and azimuth from the epicenter to each station of the station pair was computed. This was done first, to assure the azimuth of the event actually lies within a few degrees of the great circle path connecting the station pair, and second, to establish the distances that

would later be needed for wave velocity determinations. A list of the earthquakes chosen for each station pair, with their origin times, distances, and azimuths, is provided in Table 2.

The peaks, troughs, and inflection points of each seismogram were digitized by hand on a tablet digitizer. Using the interpolation technique of Wiggins (1976), the irregularly sampled seismograms were digitally reconstructed by first fitting a piecewise-continuous cubic curve to the digitized points, and then resampling the curve at a rate of one sample per second. The reconstructed seismograms were also plotted and visually compared to the original paper records to insure the accuracy of the interpolation routine. The seismograms shown in Figure 10 are taken from a series of these plots.

Dispersion Analysis

The digital processing technique used to measure the group velocity dispersion between the earthquake epicenter and the stations in this study was the moving window technique of Landisman et al. (1969). In this method, the range of wave periods over which the dispersion will be measured is specified. For each period of interest, a computing routine defines a rectangular time window whose length is proportional to the product of the period and a fixed window factor. This window then moves across the digitized seismogram in a series of time steps which

Table 2

Data for Earthquakes Used in This Study

Brasilia-La Paz

Event	Date	Time	Latitude	Longitude
BZB1	6-14-77	21:39:35.2	14.120° S	14.433° W

Station	Epicenter-Station Distance	Azimuth
BDF	3,598.77 km	262.971°
LPB	5,747.64 km	259.974°

Natal-Quito

Event	Date	Time	Latitude	Longitude
SNQ1	3-20-66	01:42:49.9	0.600° N	30.200° E

Station	Epicenter-Station Distance	Azimuth
NAT	7,271.79 km	264.134°
QUI	12,087.00 km	269.991°

Event	Date	Time	Latitude	Longitude
SNQ2	2- 5-67	18:55:47.1	5.500° S	11.400° W

Station	Epicenter-Station Distance	Azimuth
NAT	2,616.94 km	269.812°
QUI	7,471.10 km	272.088°

Natal-Bogota

Event	Date	Time	Latitude	Longitude
NBG1	5-13-68	21:04:13.0	12.975° S	14.721° W

Station	Epicenter-Station Distance	Azimuth
NAT	2,391.84 km	289.439°
BOG	6,835.43 km	282.584°

Table 2 (continued)

Natal-Bogota (continued)

Event	Date	Time	Latitude	Longitude
NBG	11-29-70	06:01:18.7	11.681° S	14.087° W

Station	Epicenter-Station Distance	Azimuth
NAT	2,414.32 km	285.737°
BOG	6,872.71 km	281.700°

Event	Date	Time	Latitude	Longitude
NBG3	9- 9-73	08:32:14.8	7.112° S	12.841° W

Station	Epicenter-Station Distance	Azimuth
NAT	2,463.38 km	273.878°
BDG	6,916.57 km	279.005°

Event	Date	Time	Latitude	Longitude
NBG4	2-25-74	01:32:17.3	11.518° S	13.302° W

Station	Epicenter-Station Distance	Azimuth
NAT	2,492.14 km	284.696°
BOG	6,952.93 km	281.379°

Event	Date	Time	Latitude	Longitude
NBG5	2-27-74	04:28:30.3	11.604° S	13.406° W

Station	Epicenter-Station Distance	Azimuth
NAT	2,483.62 km	284.981°
BOG	6,943.70 km	281.453°

Table 2 (continued)

Caracas-Quito

Event	Date	Time	Latitude	Longitude
CQI1	11-16-65	15:24:43.0	31.000° N	41.500° W

Station	Epicenter-Station Distance	Azimuth
CAR	3,467.31 km	234.645°
QUI	5,208.68 km	235.587°

Natal-Caracas

Event	Date	Time	Latitude	Longitude
NCA1	5-13-68	21:04:13.0	12.975° S	14.721° W

Station	Epicenter-Station Distance	Azimuth
NAT	2,391.84 km	289.439°
CAR	6,319.63 km	291.813°

Event	Date	Time	Latitude	Longitude
NCA2	11- 5-75	16:55:24.4	14.305° S	13.397° W

Station	Epicenter-Station Distance	Azimuth
NAT	2,577.03 km	291.063°
CAR	6,507.25 km	291.975°

Natal-La Paz

Event	Date	Time	Latitude	Longitude
NLB1	9- 1-68	04:48:52.2	0.995° S	24.512° W

Station	Epicenter-Station Distance	Azimuth
NAT	1,253.58 km	248.488°
LPB	5,071.52 km	247.733°

Table 2 (continued)

Natal-La Paz (continued)

Event	Date	Time	Latitude	Longitude
NLB3	4- 7-70	15:36:19.2	0.273° S	24.763° W

Station	Epicenter-Station Distance	Azimuth
NAT	1,259.65 km	244.698°
LPB	5,076.45 km	246.994°

Event	Date	Time	Latitude	Longitude
NLB5	8-22-73	22:15:17.3	0.598° N	25.347° W

Station	Epicenter-Station Distance	Azimuth
NAT	1,247.27 km	239.488°
LPB	5,055.27 km	245.986°

La Plata-Natal

Event	Date	Time	Latitude	Longitude
LAN1	5- 2-73	13:39:45.4	48.908° S	75.840° W

Station	Epicenter-Station Distance	Azimuth
LPA	2,140.84 km	50.033°
NAT	6,189.72 km	52.026°

Event	Date	Time	Latitude	Longitude
LAN2	8-11-75	08:36:44.8	45.756° S	75.471° W

Station	Epicenter-Station Distance	Azimuth
LPA	1,909.46 km	57.024°
NAT	5,955.10 km	53.431°

Table 2 (continued)

La Paz Caracas

Event	Date	Time	Latitude	Longitude
LPC2	9-26-67	11:11:23.7	33.600° S	70.500° W

Station	Epicenter-Station Distance	Azimuth
LPB	1,904.89 km	7.844°
CAR	4,891.46 km	5.061°

Event	Date	Time	Latitude	Longitude
LPC4	7-31-71	22:08:48.0	32.362° S	71.533° W

Station	Epicenter-Station Distance	Azimuth
LPB	1,786.23 km	11.987 °
CAR	4,764.77 km	6.667°

Event	Date	Time	Latitude	Longitude
LPC6	12-29-72	04:51:01.6	30.556° S	71.021° W

Station	Epicenter-Station Distance	Azimuth
LPB	1,580.33 km	11.491°
CAR	4,560.39 km	6.140°

Event	Date	Time	Latitude	Longitude
LPC7	7-16-76	15:59:32.3	31.523° S	71.305° W

Station	Epicenter-Station Distance	Azimuth
LPB	1,690.78 km	11.806°
CAR	4,669.90 km	6.441°

Table 2 (continued)

Caracas-La Plata

Event	Date	Time	Latitude	Longitude
SCL1	9- 4-63	13:32:12.3	71.300° N	73:100° W

Station	Epicenter-Station Distance	Azimuth
CAR	6,767.84 km	173.049°
LPA	11,837.70 km	167.042°

Natal-La Plata

Event	Date	Time	Latitude	Longitude
NLA3	1-13-74	21:31:39.4	3.663° N	31.569° W

Station	Epicenter-Station Distance	Azimuth
NAT	1,043.27 km	201.666°
LPA	5,078.45 km	210.677°

correspond to a series of constant increments in group velocity. At each step in time, the seismogram is multiplied by the window, yielding a truncated fragment of data centered on the group velocity of interest. The fragment is then mutiplied, or modulated, by a symmetrical $\cos^2$ function. This modulation gives greatest weight to that portion of the seismogram fragment which corresponds to the group arrival. It also reduces the prominent side lobes which would otherwise appear in the frequency domain when such a sharply truncated signal is Fourier analyzed. The routine next evaluates the Fourier transform of the modulated fragment and returns an instantaneous spectral amplitude, which is normalized to 100 decibels. For each period, a set of these amplitudes, one for each of the increments of group velocity examined, is produced. These steps are then repeated for each period in the specified period range. As each amplitude is printed as a function of period and group velocity, a two-dimensional numerical display in matrix form is generated. These data are contoured, and a group velocity dispersion curve is drawn along the crest of the contoured values.

Increasing the window length in proportion to increasing wave period is done to keep the frequency resolution relatively constant across the range of periods. A window length of three times the period of interest provided good results in this study. Figure 13

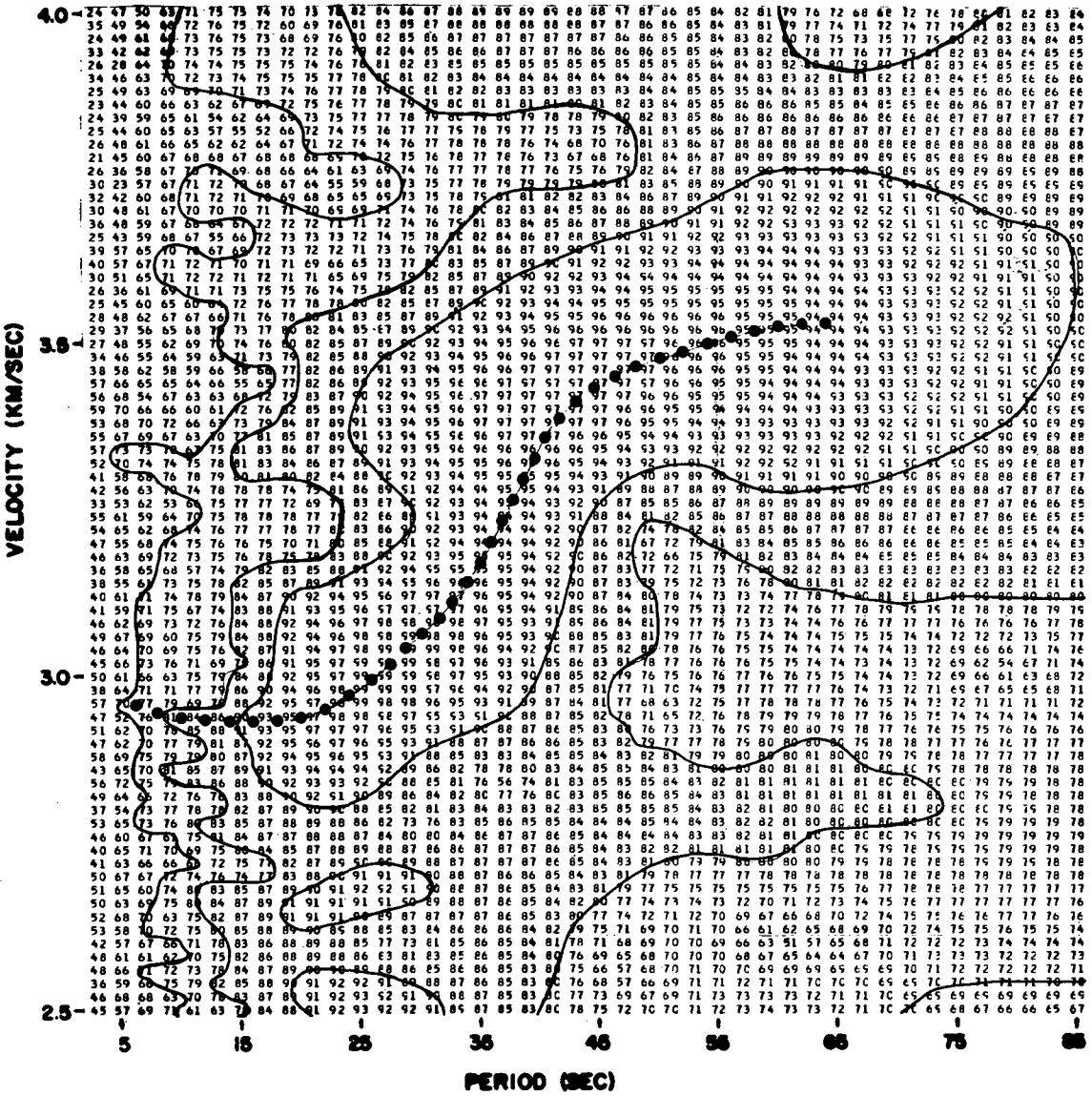

Figure 13. Sample computer output for the moving window analysis. Group velocity determinations are shown by dots.

presents a sample computer output of the moving window analysis with group velocity determinations shown by dots.

Once the group velocity dispersion from the earthquake epicenter to the first and second stations of a station pair is determined, the group velocity dispersion along the path connecting the two stations is obtained by simply computing the range of group delays between the two stations, and dividing the delays into the intrastation distance.

The cross-multiplication technique of Bloch and Hales (1968) was used to determine the phase velocity dispersion between each pair of stations. In order to apply this technique, it is necessary to know the range of group arrival times of the fundamental mode Rayleigh wave periods for both stations. This information is taken from the group velocity dispersion curves obtained previously by moving window analysis. Once these times are known, a computing routine is employed that windows both digitized seismogram, centering each window at the group arrival time of the period of interest. Windowing suppresses those portions of the seismograms outside the interval of expected arrival of the fundamental mode group, eliminating higher mode interference and none-least-time path arrivals.

As in the moving window technique of Landisman et al. (1969), a symmetric, variable length $\cos^2$ function is used to window the digitized seismograms. In this case, a window

length five times each period of interest produced good results. Both seismogram fragments are narrow band-pass filtered for the appropriate period to obtain two essentially single frequency waves separated by a phase shift. Two-thirds of a wavelength of one of the filtered seismograms is then cross-multiplied with the trace of the second filtered seismogram over a range of time shifts. Each time shift corresponds to an increment in phase velocity. The results of the point-by-point cross multiplication at each time shift are summed and normalized, and printed as an amplitude at the appropriate period and phase velocity in a matrix format identical to that used for group velocity analysis. These amplitudes reach a normalized maximum of 99 decibels when the two filtered seismogram fragments are perfectly in phase. When the waves are 180° out of phase, a minimum of -99 decibels is printed.

As the two filtered waves are time shifted with respect to each other, the waves alternately go in and out of phase several times. This causes a series of semi-parallel amplitude bands to be printed on the period-phase velocity diagram. The appropriate phase velocity dispersion curve is chosen by picking the maximum values that lie along the crest of the band which displays reasonable phase velocities at long periods. Figure 14 illustrates the results of a cross-multiplication analysis.

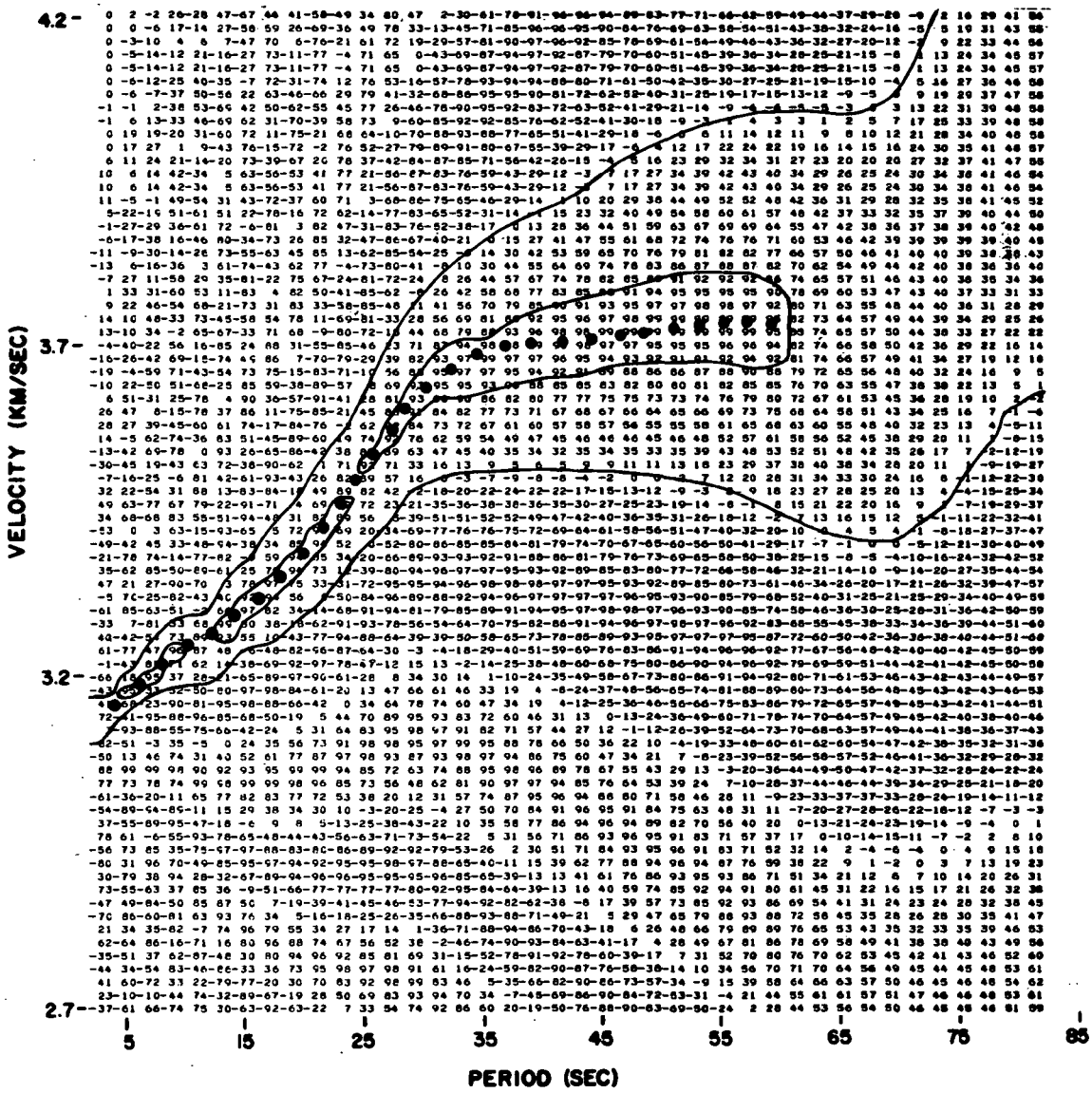

Figure 14. Sample computer output of the cross-multiplication technique. Phase velocity determinations are shown by dots.

For each two-station paths, anywhere from one to five seismic events were analyzed for group and phase velocity dispersion by the preceeding methods. To obtain a single representative group and phase velocity dispersion curve over each path, a least-squares fit to the two respective groups of data was computed. This procedure yielded two data sets for each two-station path examined in the study: (1) group velocities for a period range of approximately 11 to 91 seconds, at 2-second intervals, and (2) corresponding phase velocities for approximately the same period range. (The Rayleigh wave trains analyzed in the investigation rarely allowed the resolution of phase velocities at periods less than 25 seconds.) These dispersion curves are shown in Figures 15 through 37. The two-station phase velocity dispersion curves obtained by Sherburne (1974) are shown in Figure 38 through 43. The single station velocity dispersion data, the calculated interstation group velocity dispersion data, and the interstation phase velocity dispersion data measured over each two-station path for each event are tabulated in Appendix A. The least-squares fitted group and phase velocity dispersion data are also included here. The two-station phase velocity dispersion data obtained by Sherburne are tabulated in Appendix B.

Dispersion Inversion

The final step in the procedure of analyzing Rayleigh wave dispersion data is to use the dispersion measurements

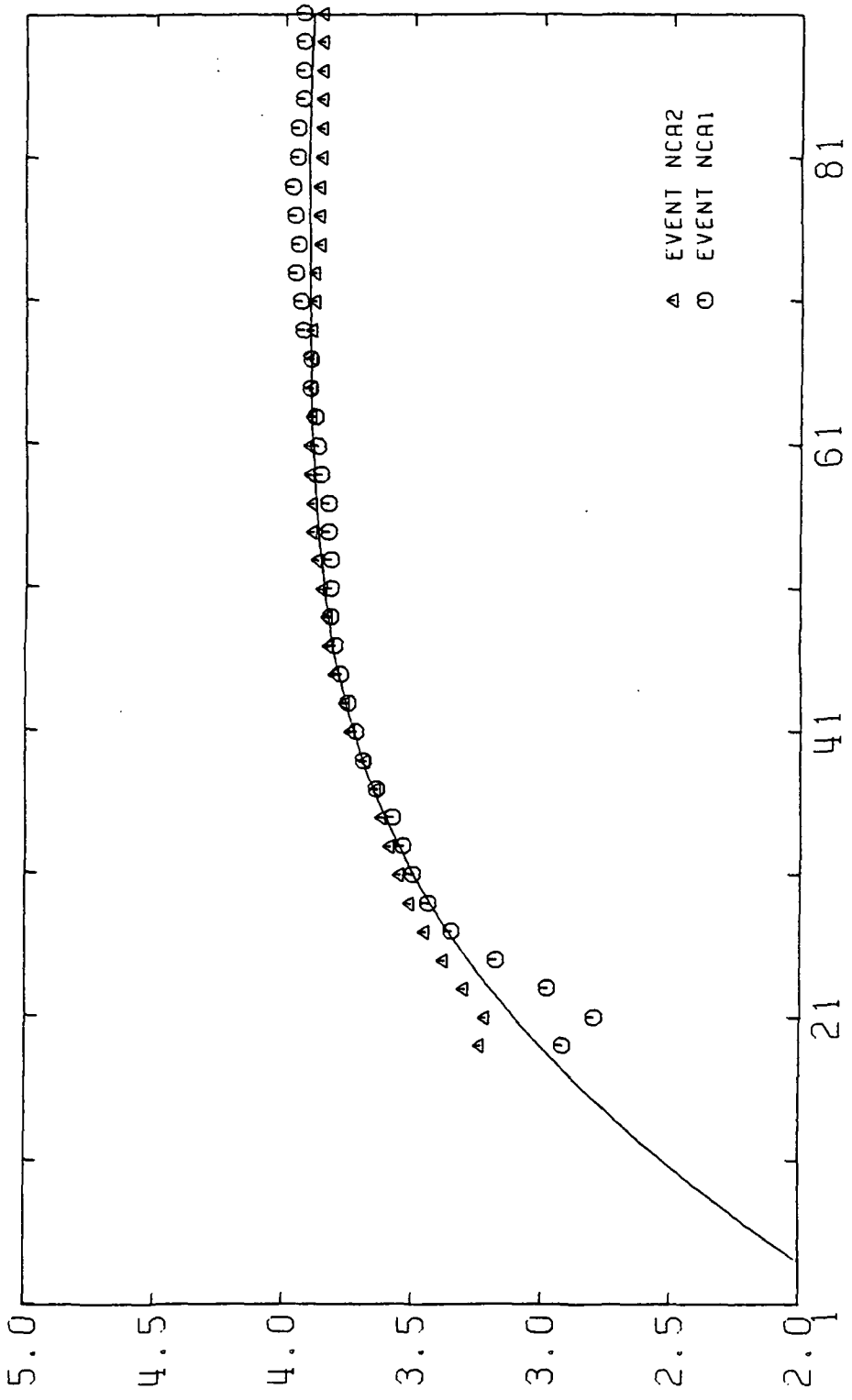
GROUP VELOCITY DISPERSION NCA NATAL-CARACAS
EVENT NCA2
EVENT NCA1
5.0
4.5
4.0
3.5
3.0
2.5
2.0
1
21
41
61
81

Figure 15

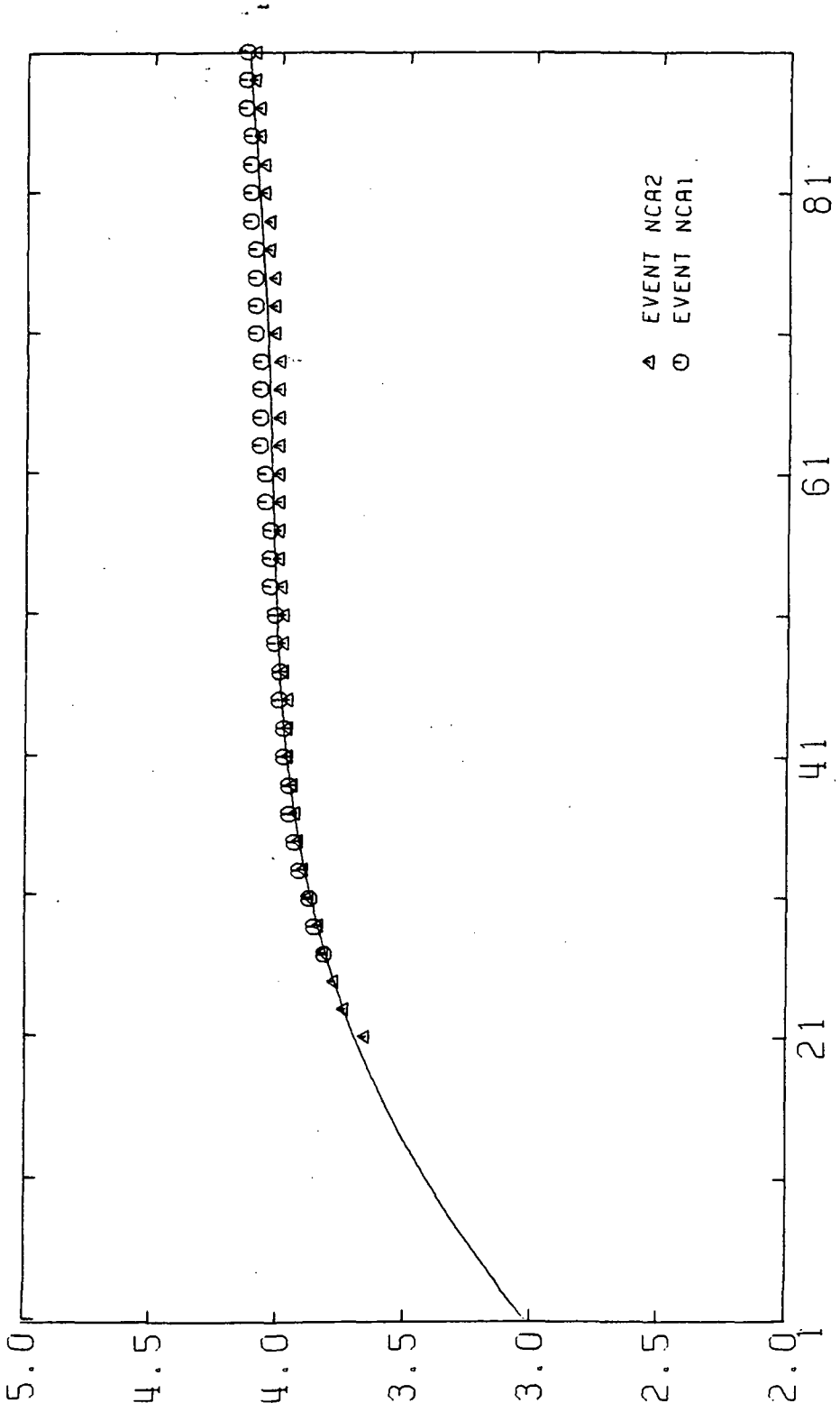
PHASE VELOCITY DISPERSION NCA NATAL-CARACAS
EVENT NCA2
EVENT NCA1
5.0
4.5
4.0
3.5
3.0
2.5
2.0
1
21
41
61
81

Figure 16

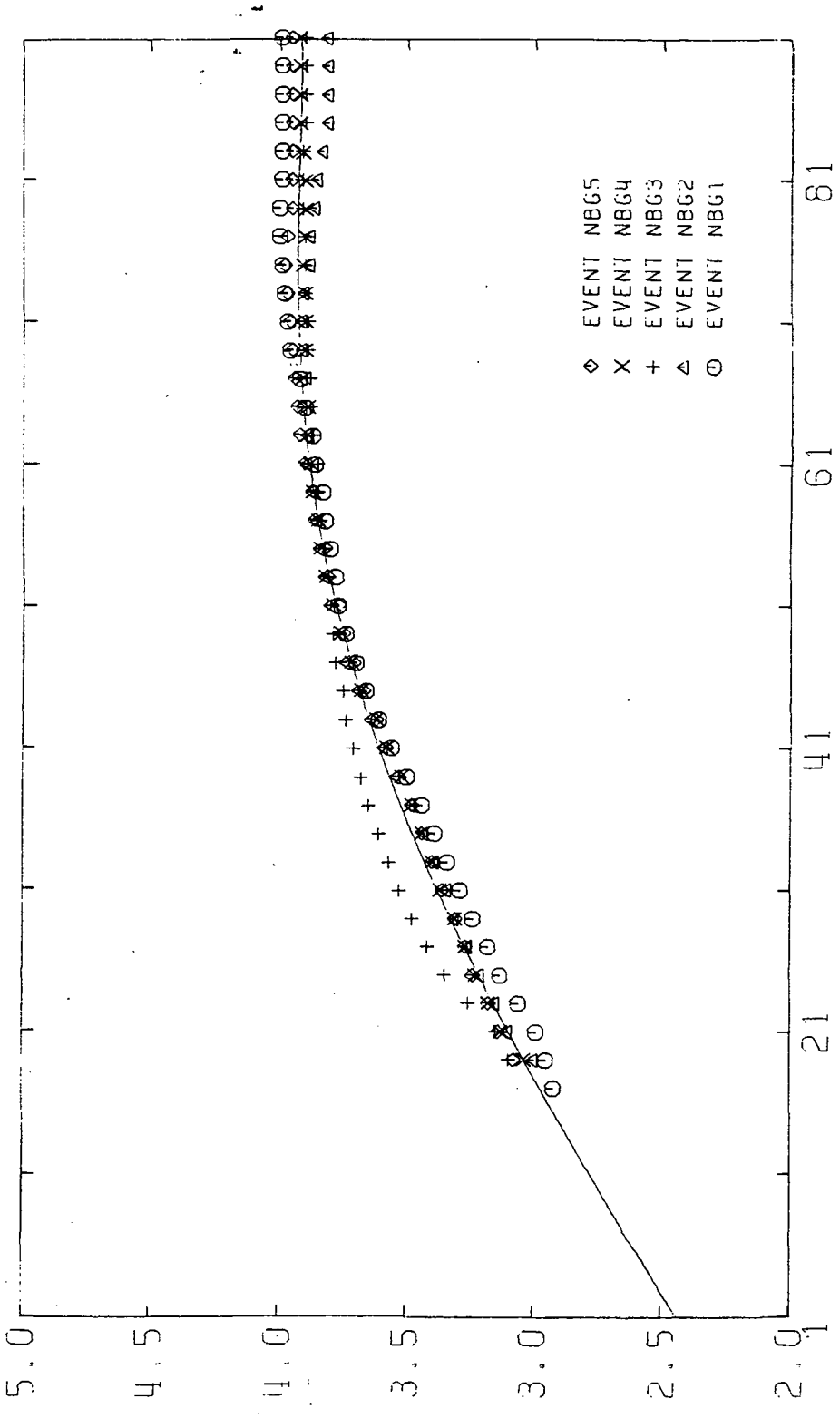
GROUP VELOCITY DISPERSION NBG NATAL$_{1,1}$-BOGOTA
EVENT NBG5
EVENT NBG4
EVENT NBG3
EVENT NBG2
EVENT NBG1
1
21
41
61
81
5.0
4.5
4.0
3.5
3.0
2.5
2.0

Figure 17

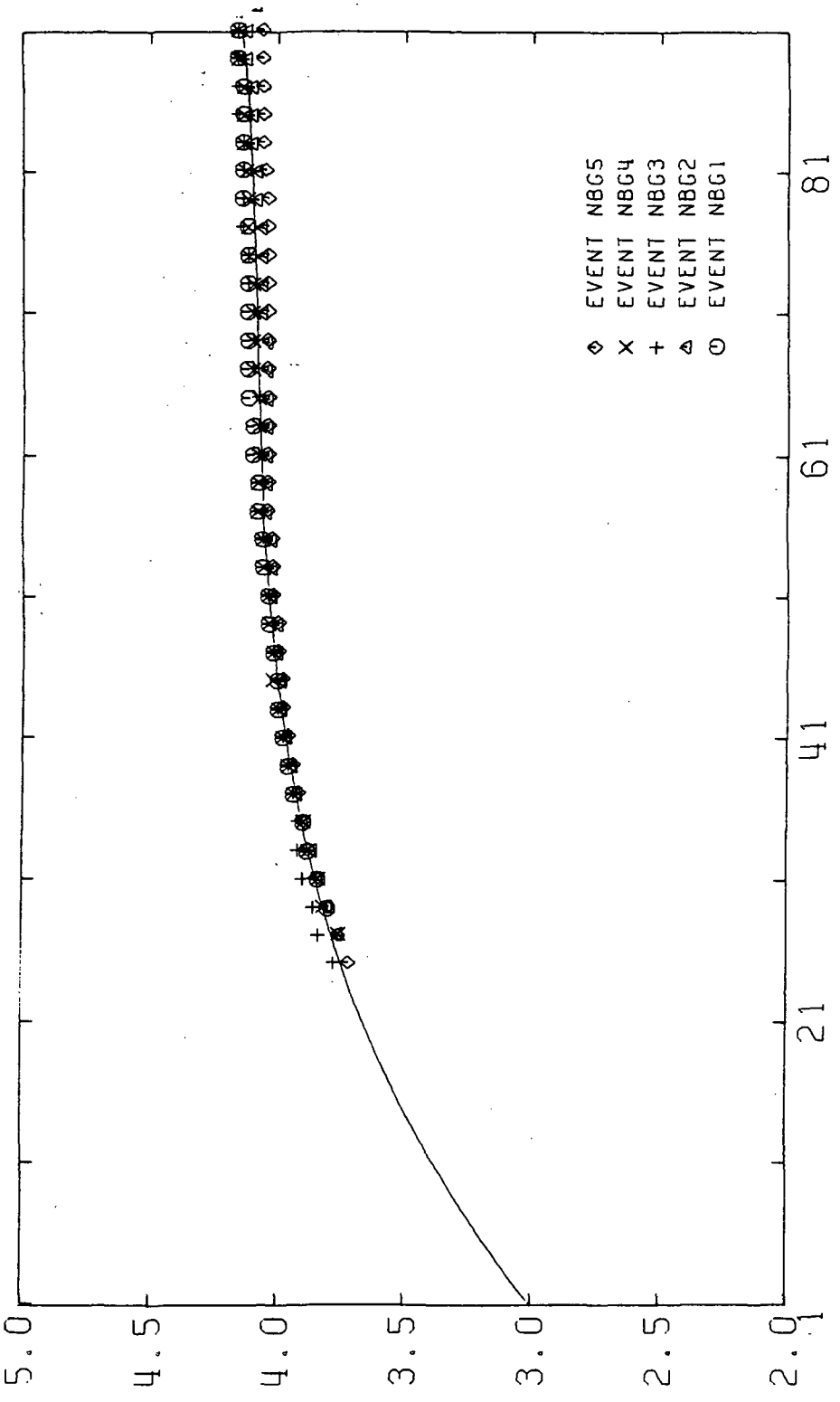
PHASE VELOCITY DISPERSION NBG NATAL-BOGOTA
EVENT NBG5
EVENT NBG4
EVENT NBG3
EVENT NBG2
EVENT NBG1
5.0
4.5
4.0
3.5
3.0
2.5
2.0
1
21
41
61
81

Figure 18

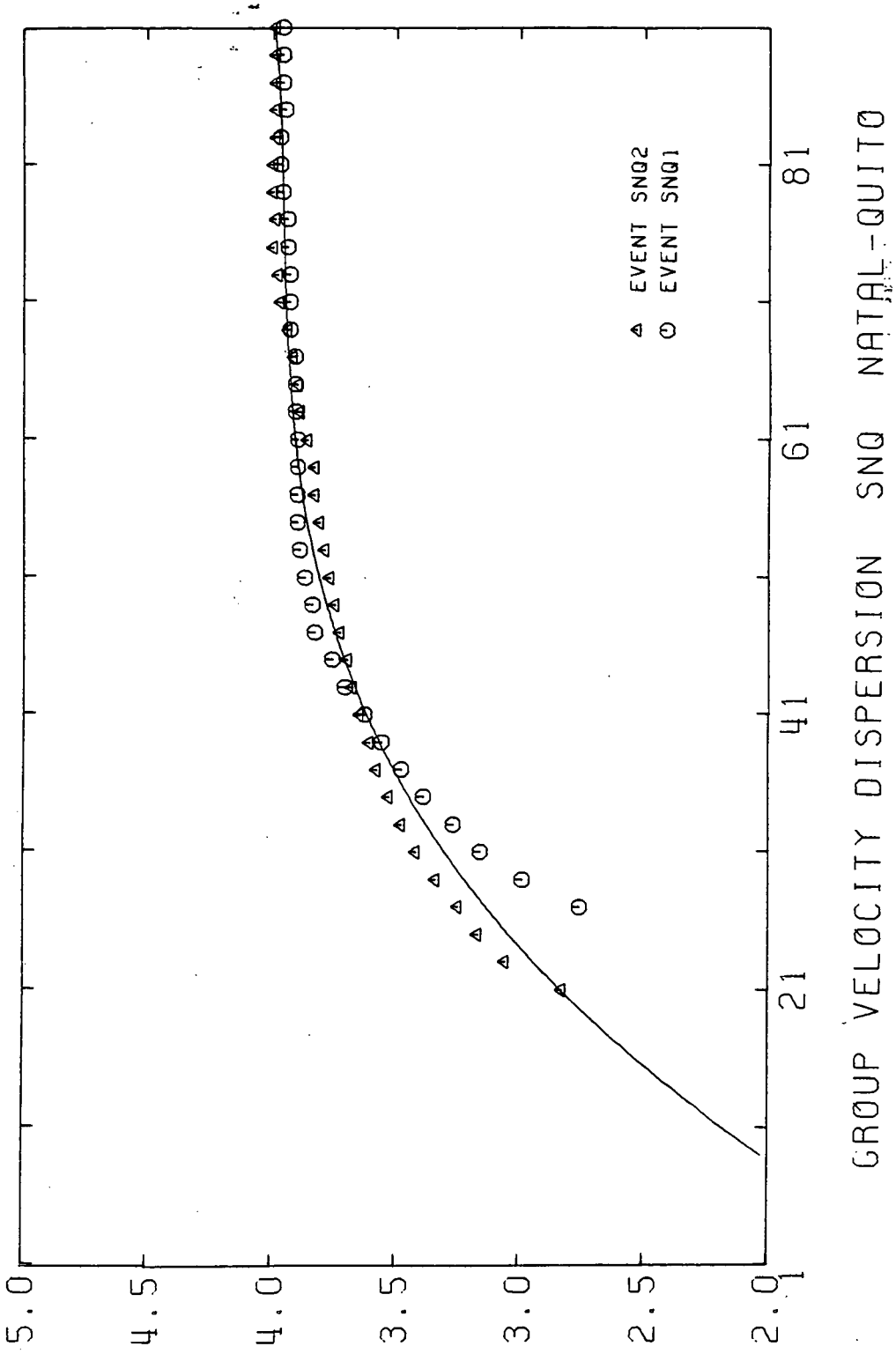
GROUP VELOCITY DISPERSION SNQ NATAL-QUITO
EVENT SNQ2
EVENT SNQ1
5.0
4.5
4.0
3.5
3.0
2.5
2.0
1
21
41
61
81

Figure 19

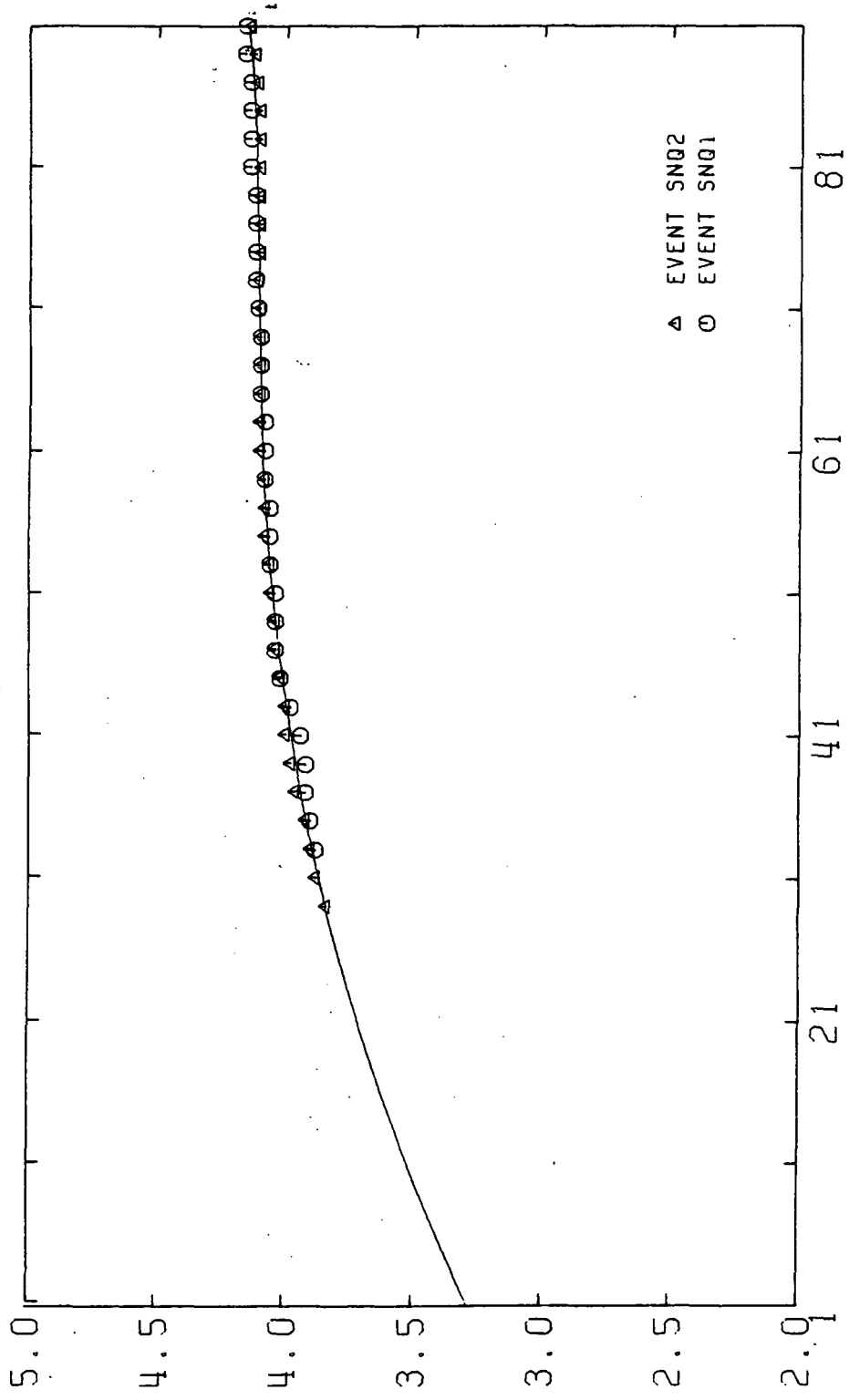
PHASE VELOCITY DISPERSION SNQ NATAL-QUITO
EVENT SNQ2
EVENT SNQ1
5.0
4.5
4.0
3.5
3.0
2.5
2.0
1
21
41
61
81

Figure 20

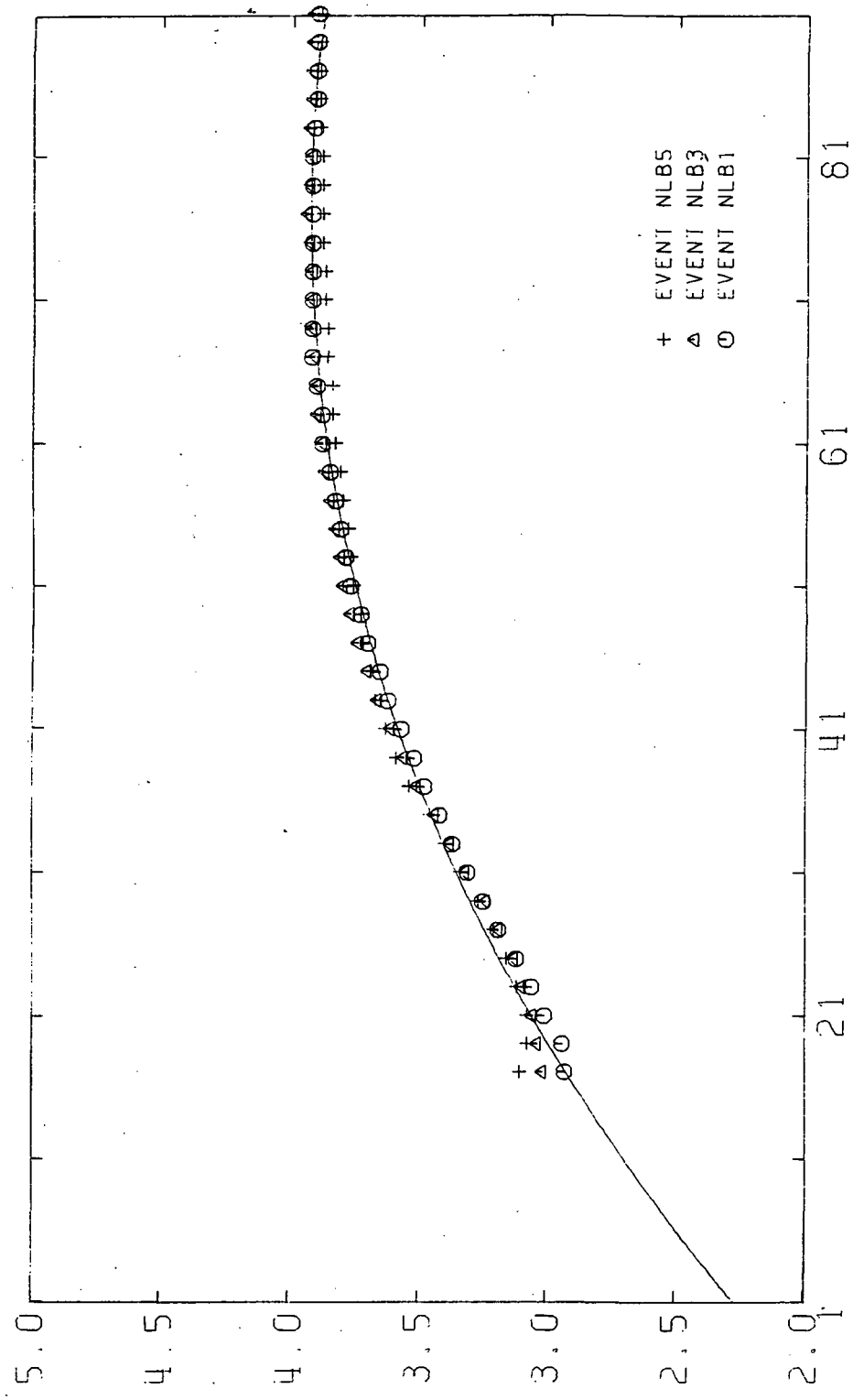
GROUP VELOCITY DISPERSION NLB NATAL-LAPAZ
+ EVENT NLB5
Δ EVENT NLB3
⊖ EVENT NLB1
5.0
4.5
4.0
3.5
3.0
2.5
2.0
1
21
41
61
81

Figure 21

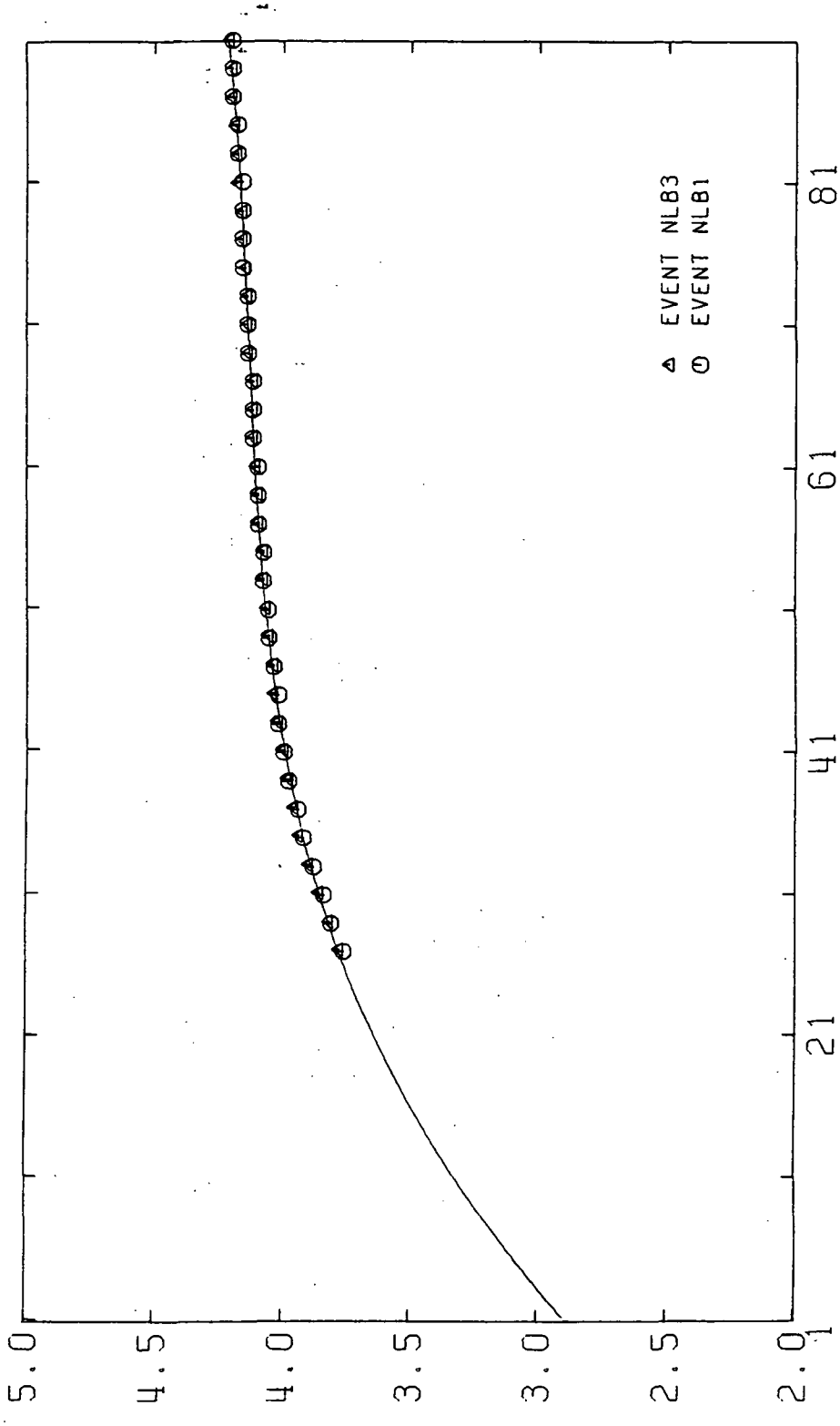
PHASE VELOCITY DISPERSION NLB NATAL-LAPAZ
EVENT NLB3
EVENT NLB1
5.0
4.5
4.0
3.5
3.0
2.5
2.0
1
21
41
61
81

Figure 22

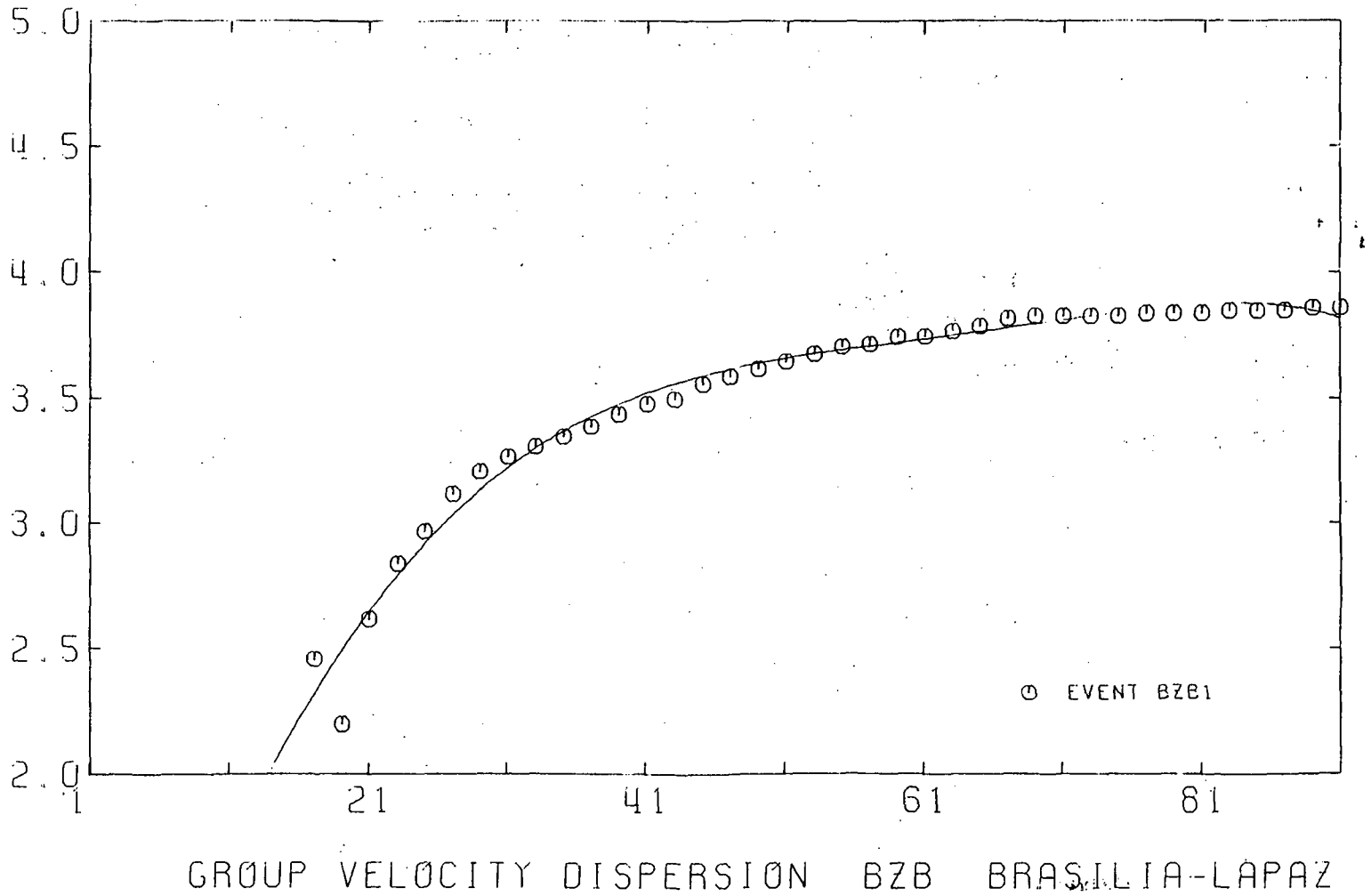
5.0
4.5
4.0
3.5
3.0
2.5
2.0
1
21
41
61
81
EVENT BZB1
GROUP VELOCITY DISPERSION BZB BRASILIA-LAPAZ

Figure 23

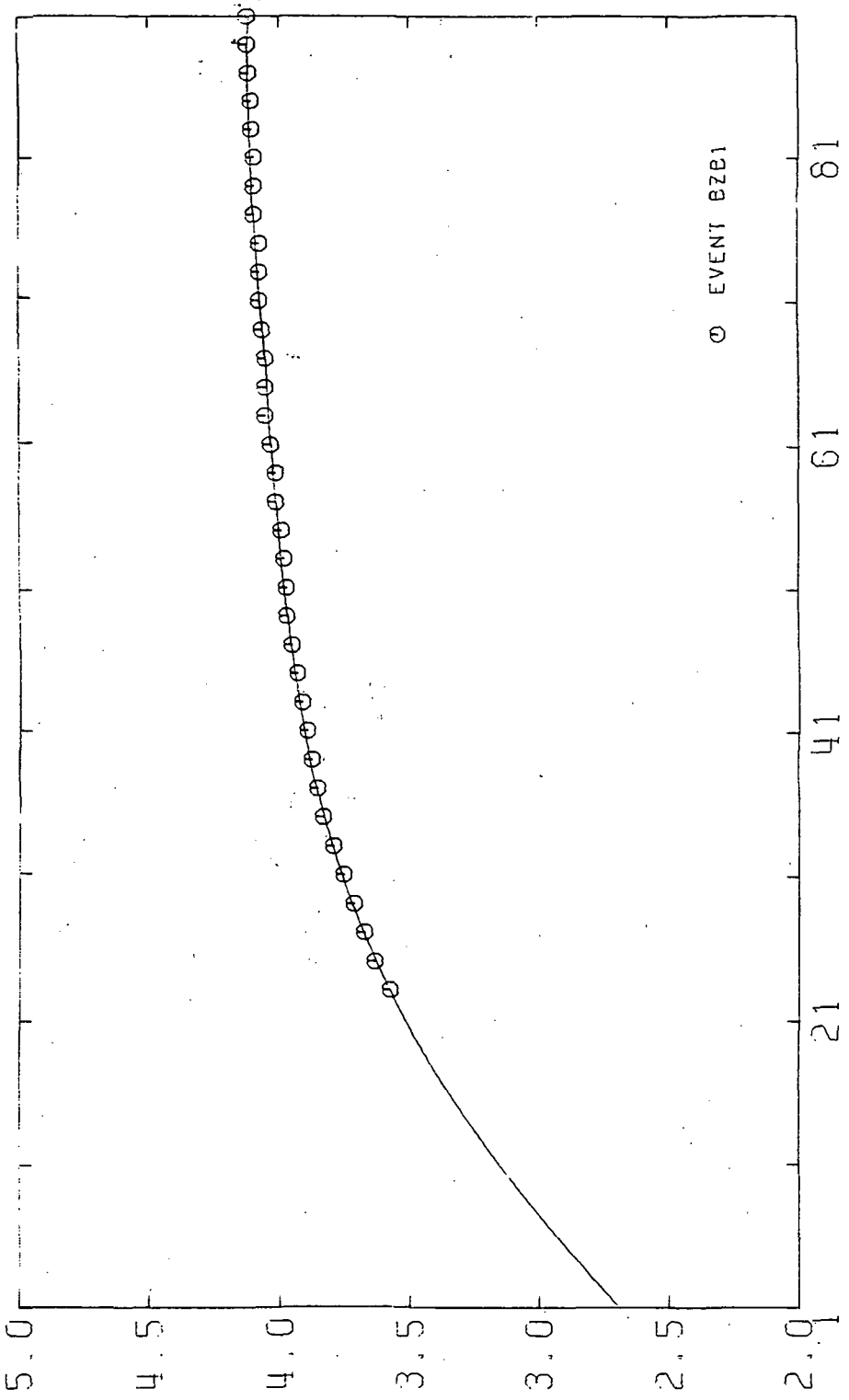
PHASE VELOCITY DISPERSION BZB BRASILIA-LAPAZ
Ø EVENT BZB1
5.0
4.5
4.0
3.5
3.0
2.5
2.0
1
21
41
61
81

Figure 24

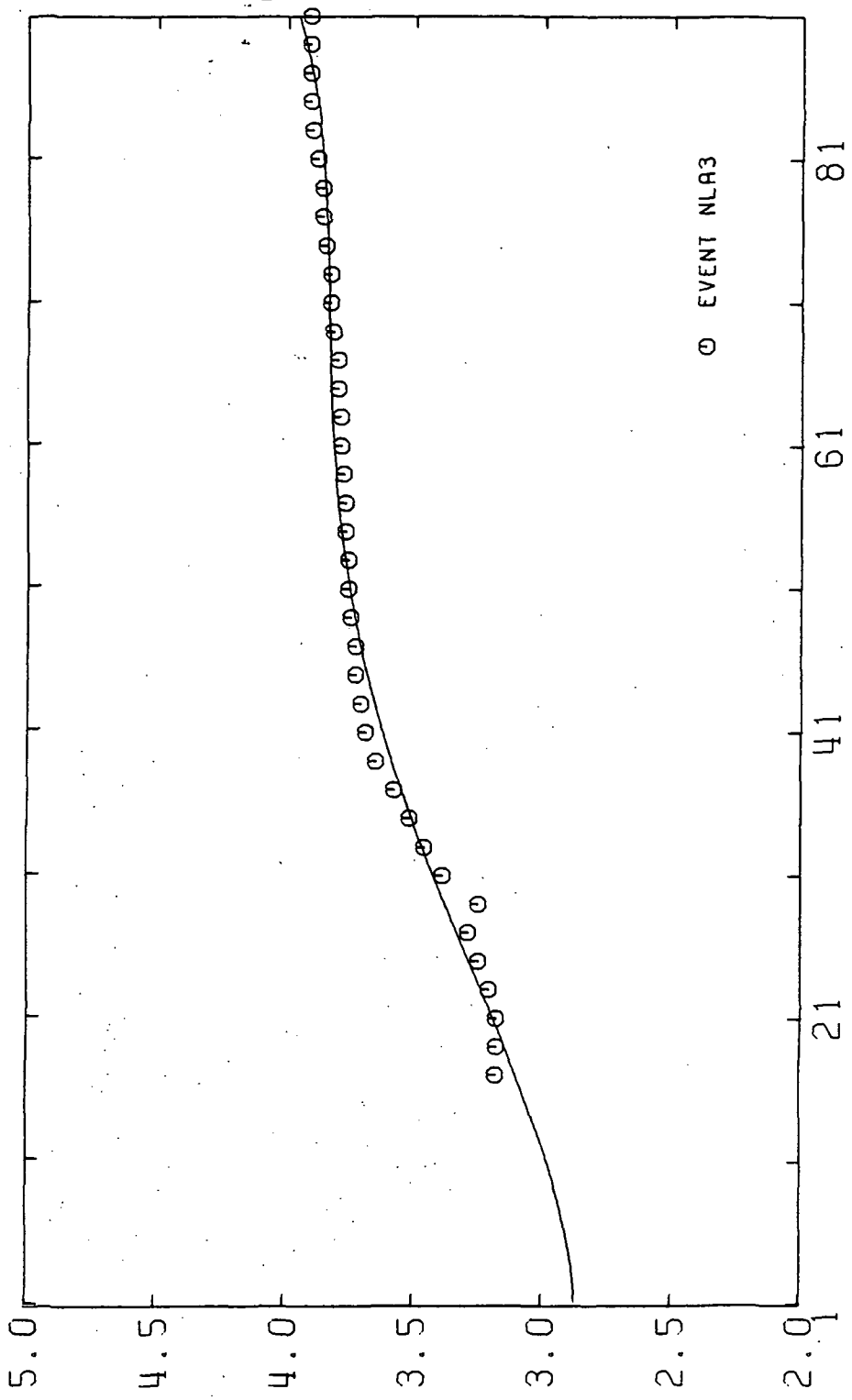
GROUP VELOCITY DISPERSION NLA NATAL-LAPLATA
EVENT NLA3
5.0
4.5
4.0
3.5
3.0
2.5
2.0
1
21
41
61
81

Figure 25

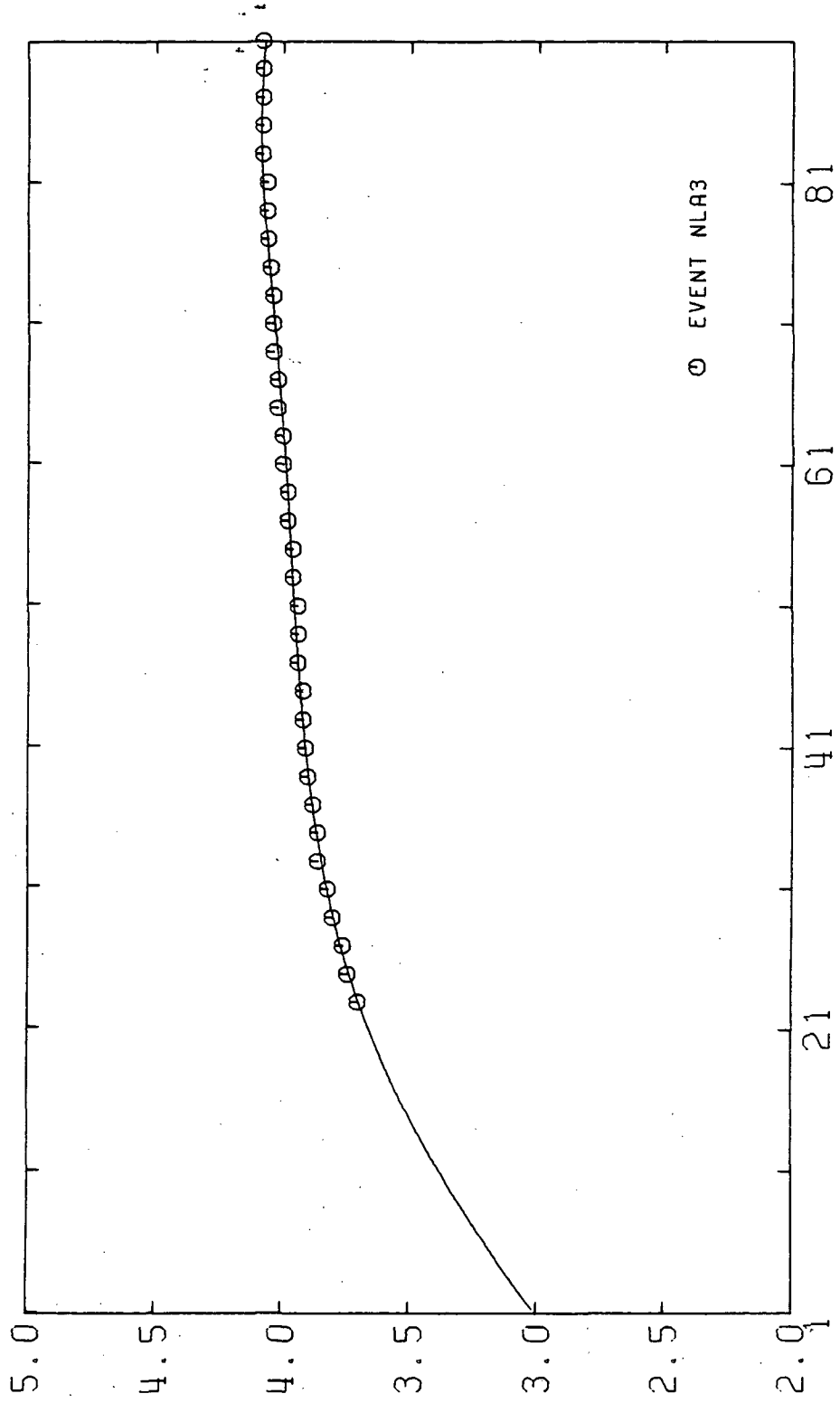
PHASE VELOCITY DISPERSION NLA NATAL-LAPLATA
EVENT NLA3
5.0
4.5
4.0
3.5
3.0
2.5
2.0
1
21
41
61
81

Figure 26

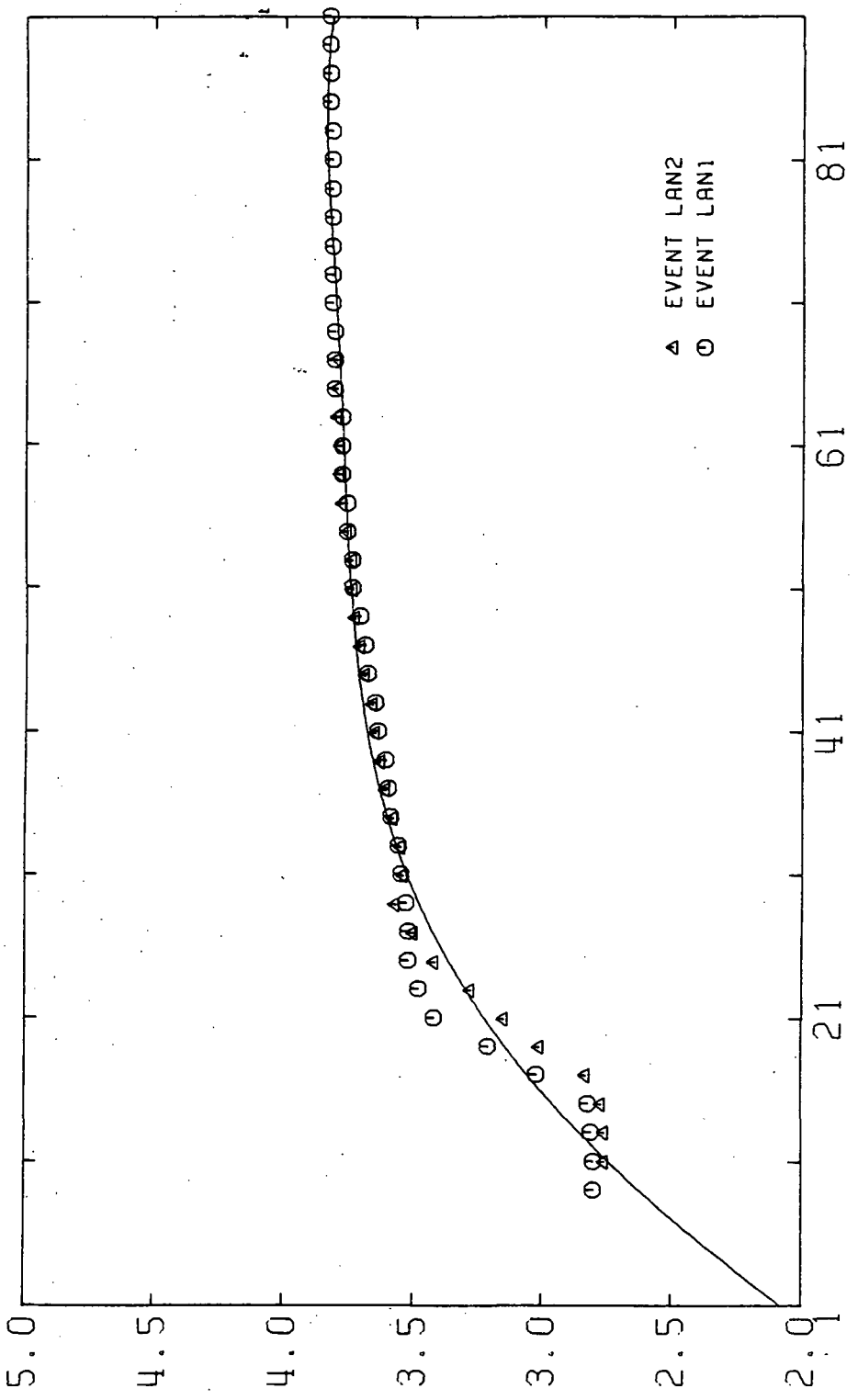
GROUP VELOCITY DISPERSION LAN LAPLATA-NATAL
EVENT LAN2
EVENT LAN1
5.0
4.5
4.0
3.5
3.0
2.5
2.0
1
21
41
61
81

Figure 27

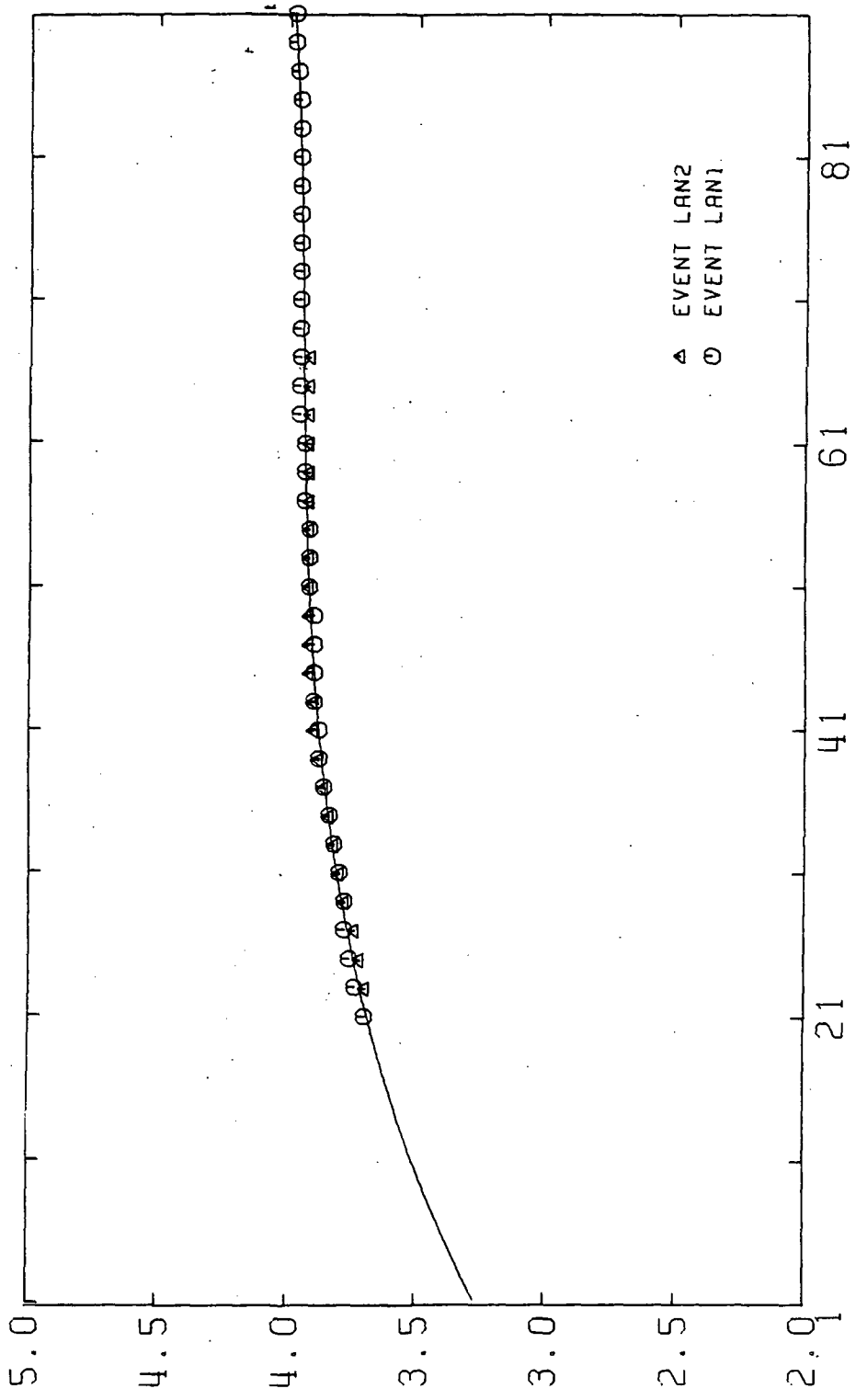
PHASE VELOCITY DISPERSION LAN LAPLATA-NATAL
EVENT LAN2
EVENT LAN1
5.0
4.5
4.0
3.5
3.0
2.5
2.0
1
21
41
61
81

Figure 28

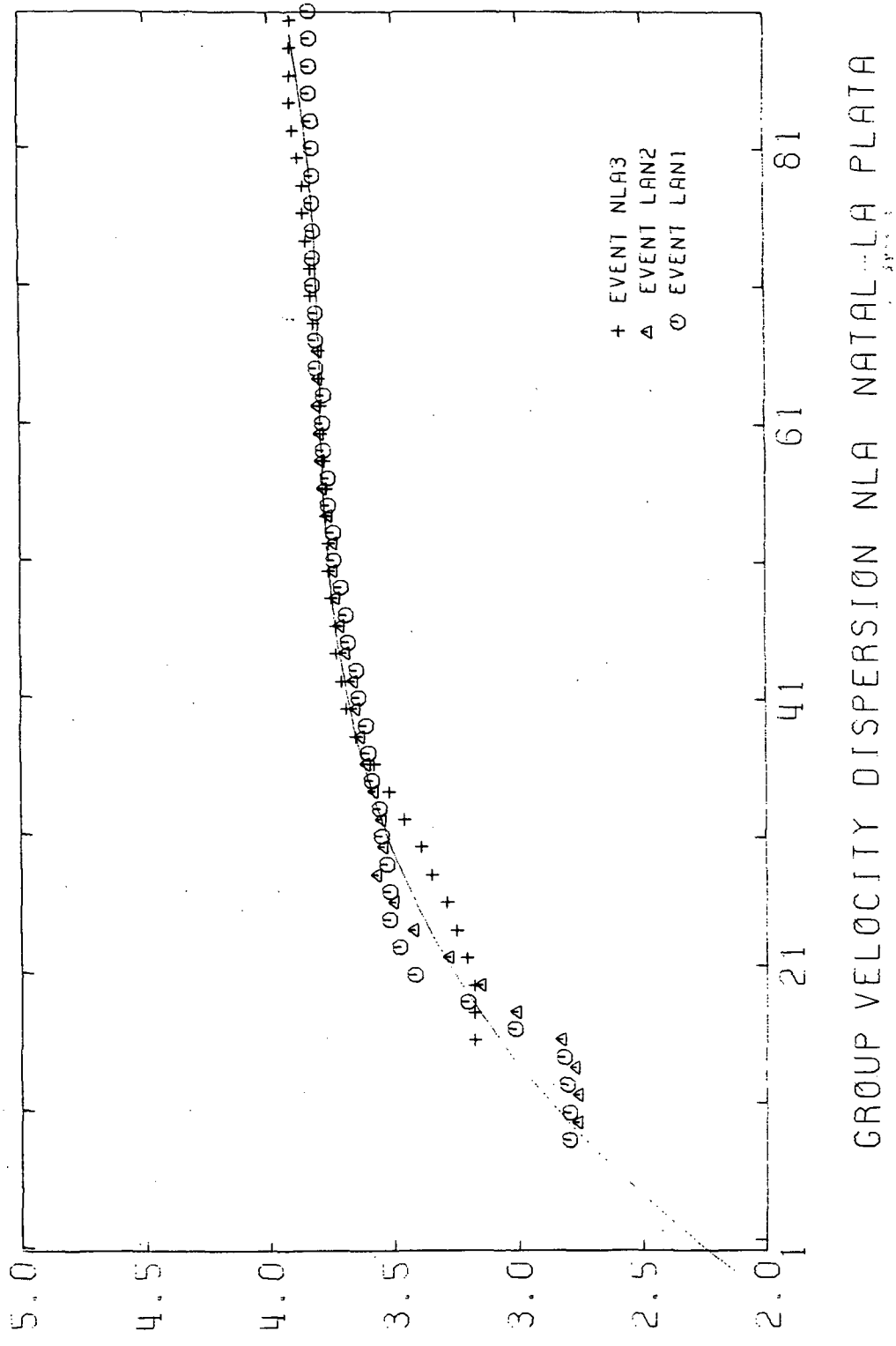
GROUP VELOCITY DISPERSION NLA NATAL-LA PLATA
+ EVENT NLA3
Δ EVENT LAN2
Ø EVENT LAN1
5.0
4.5
4.0
3.5
3.0
2.5
2.0
1
21
41
61
81

Figure 29

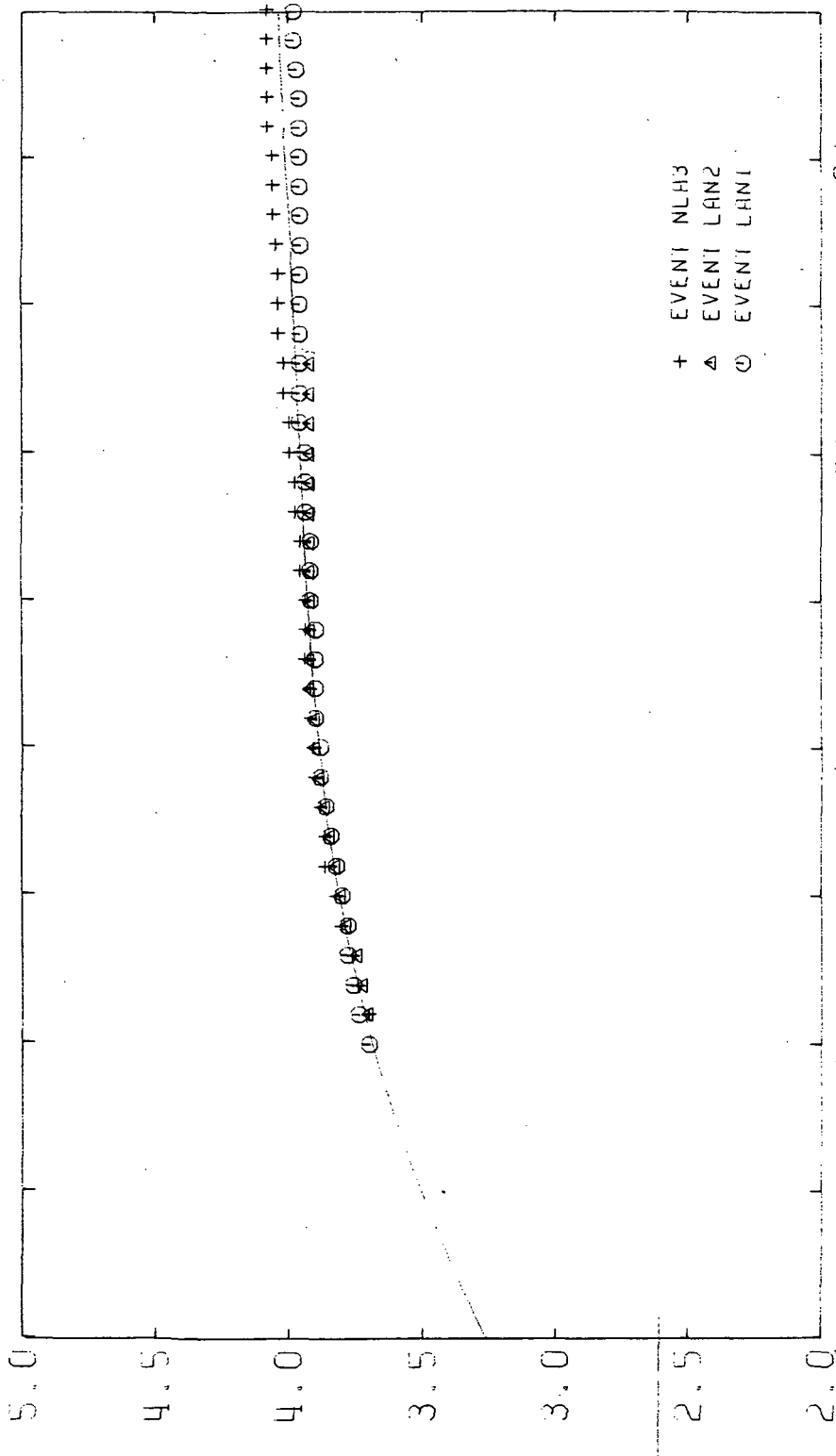
PHASE VELOCITY DISPERSION NLA NHIAL-LH PLATA
+ EVENT NLH3
Δ EVENT LAN2
○ EVENT LAN1
5.0
4.5
4.0
3.5
3.0
2.5
2.0
1
21
41
61
81

Figure 30

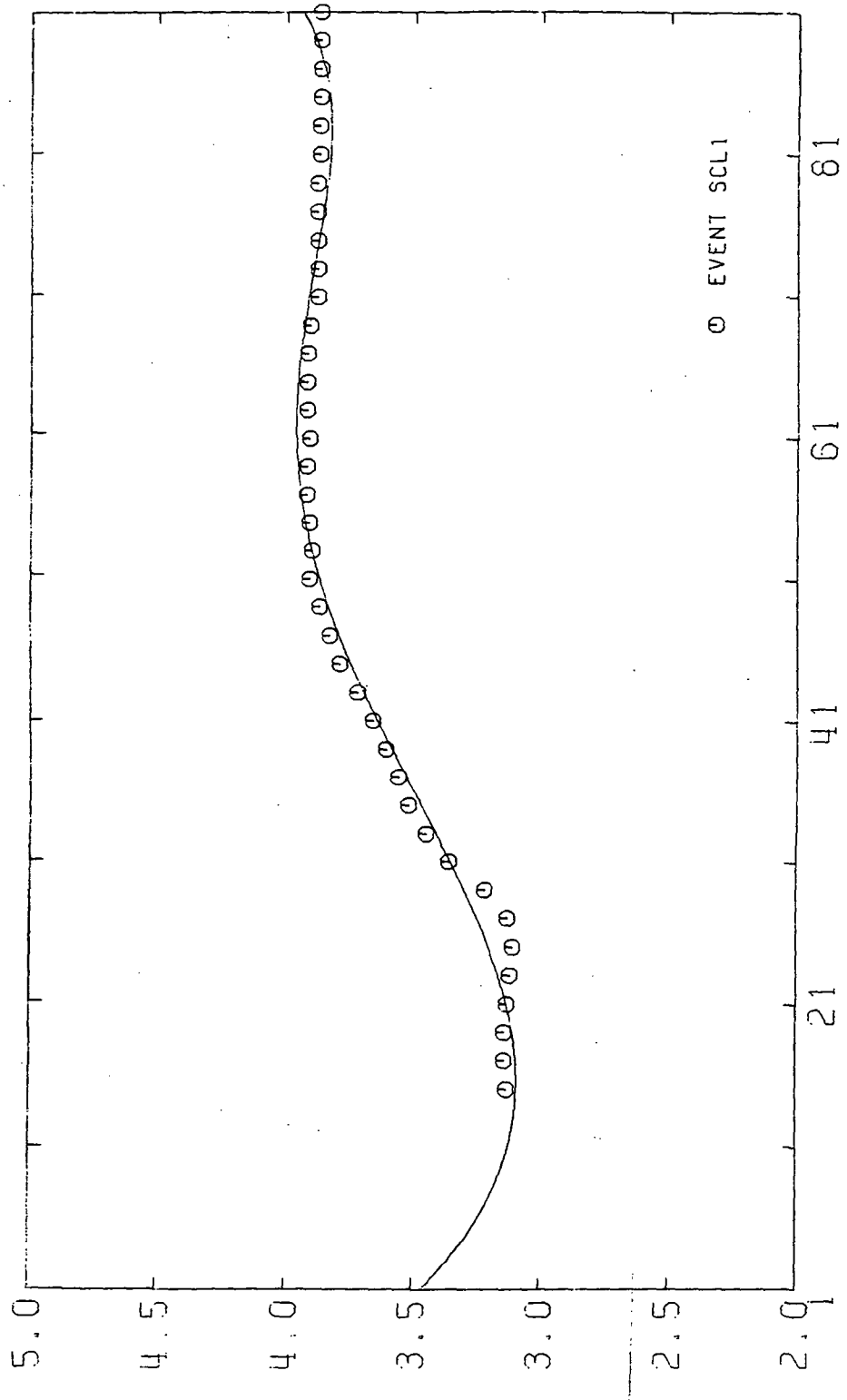
GROUP VELOCITY DISPERSION SCL CARACAS-LAPLATA
EVENT SCL1
5.0
4.5
4.0
3.5
3.0
2.5
2.0
1
21
41
61
81

Figure 31

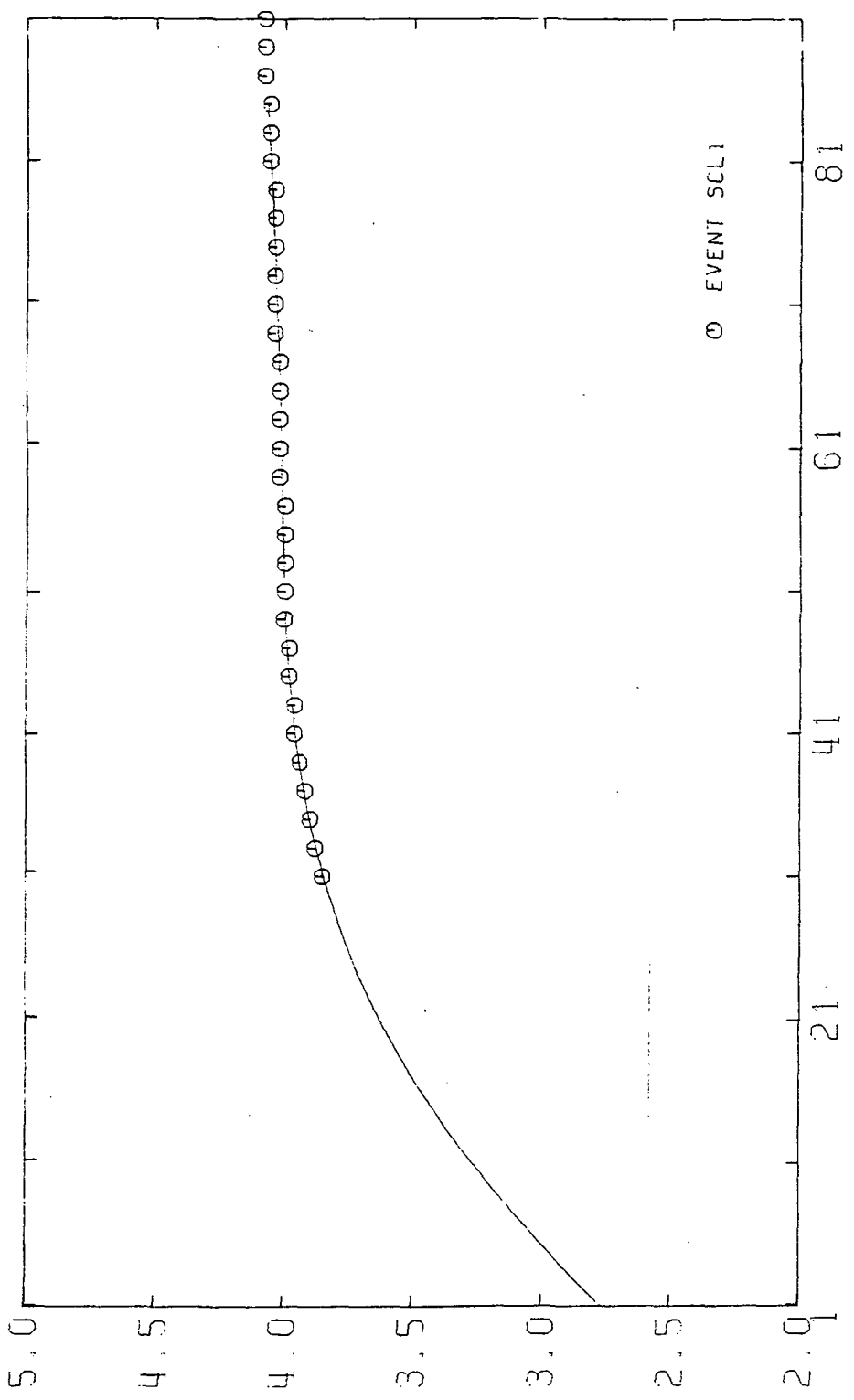
PHASE VELOCITY DISPERSION SCL CARACAS-LAPLATA
EVENT SCL1
5.0
4.5
4.0
3.5
3.0
2.5
2.0
1
21
41
61
81

Figure 32

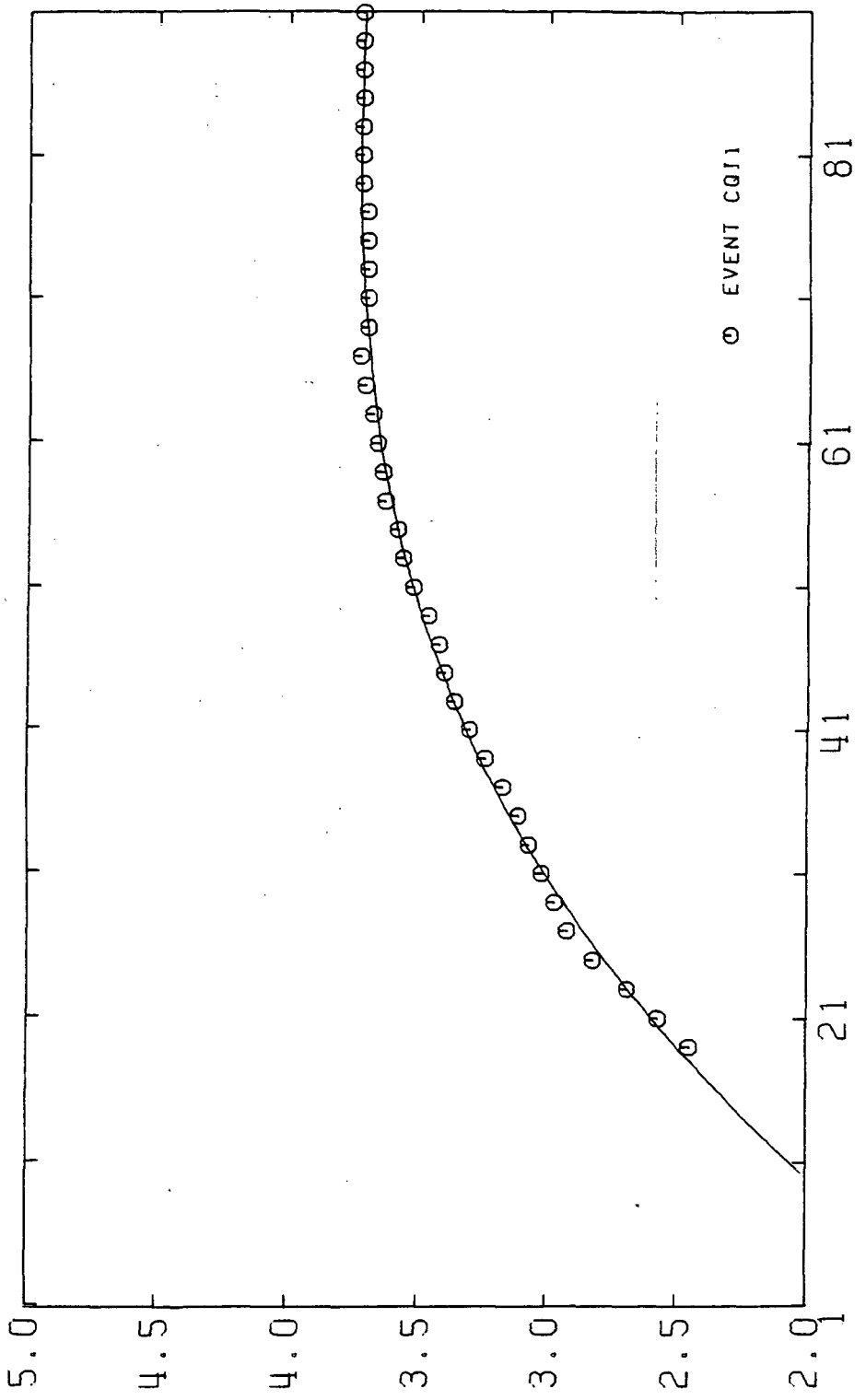
GROUP VELOCITY DISPERSION CQI CARACAS-QUITO
EVENT CQI1
5.0
4.5
4.0
3.5
3.0
2.5
2.0
1
21
41
61
81

Figure 33

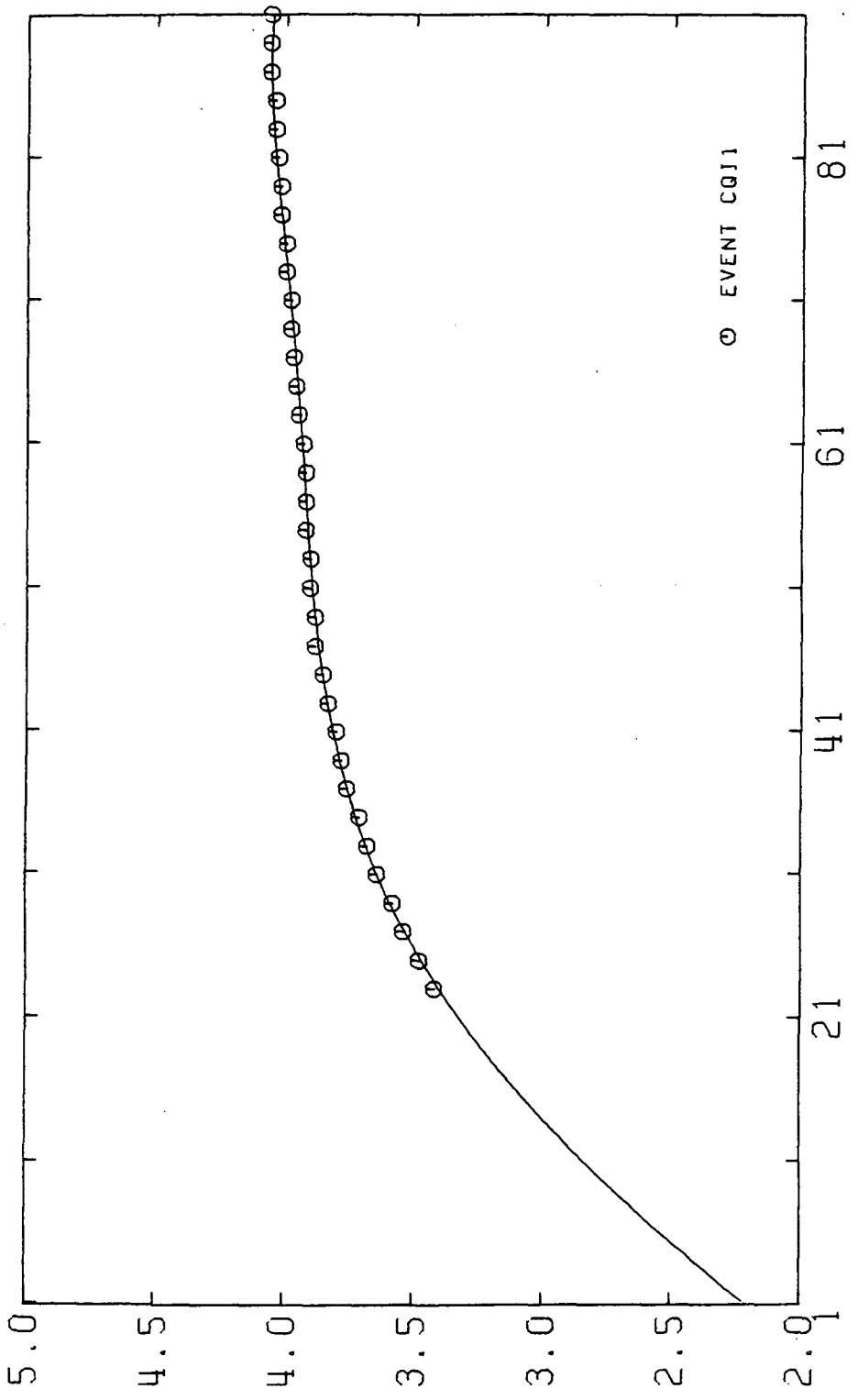
PHASE VELOCITY DISPERSION CQI CARACAS-QUITO
EVENT CQI1
5.0
4.5
4.0
3.5
3.0
2.5
2.0
1
21
41
61
81

Figure 34

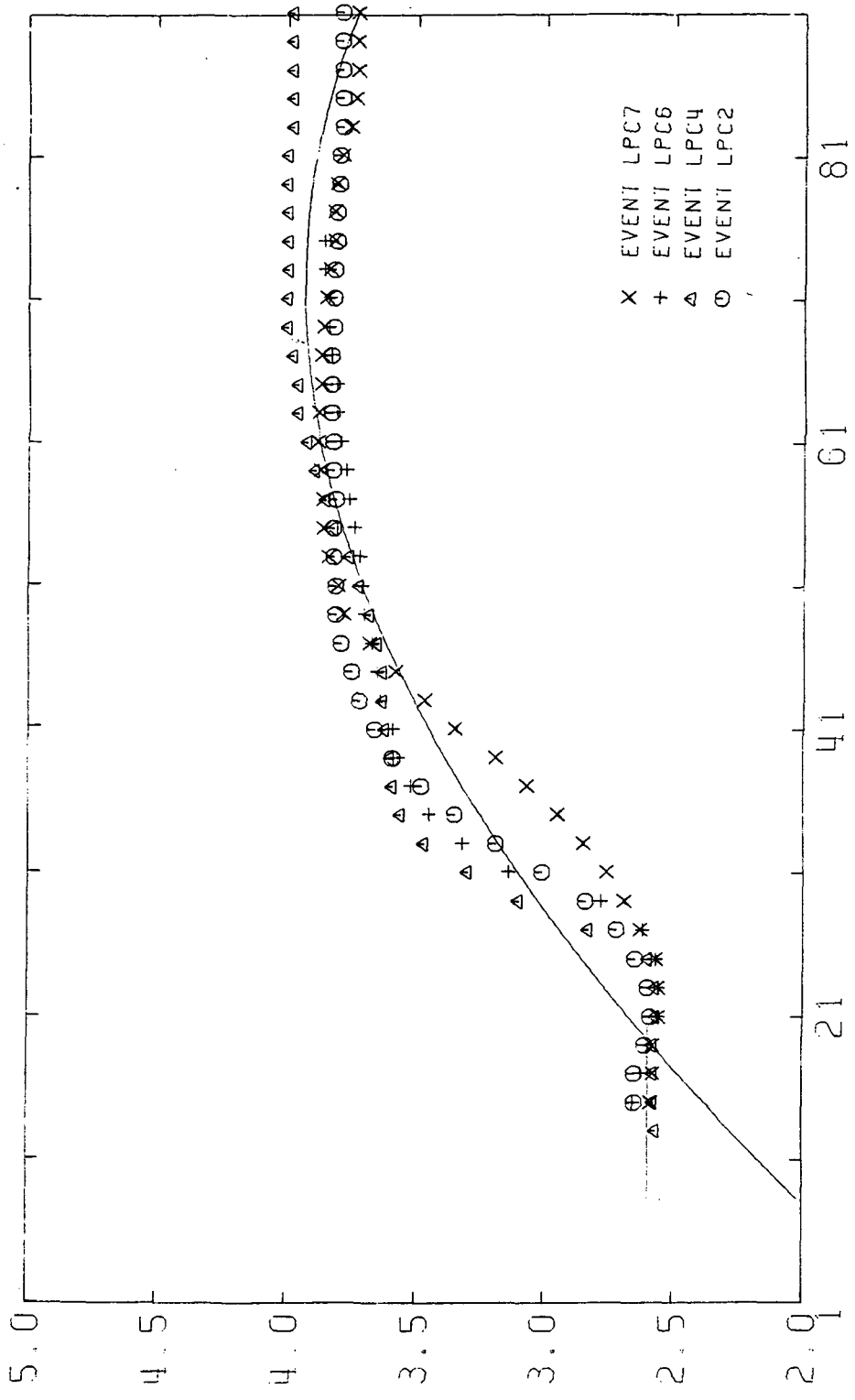
GROUP VELOCITY DISPERSION LPC LAPAZ-CARACAS
EVENT LPC7
EVENT LPC6
EVENT LPC4
EVENT LPC2
5.0
4.5
4.0
3.5
3.0
2.5
2.0
1
21
41
61
81

Figure 35

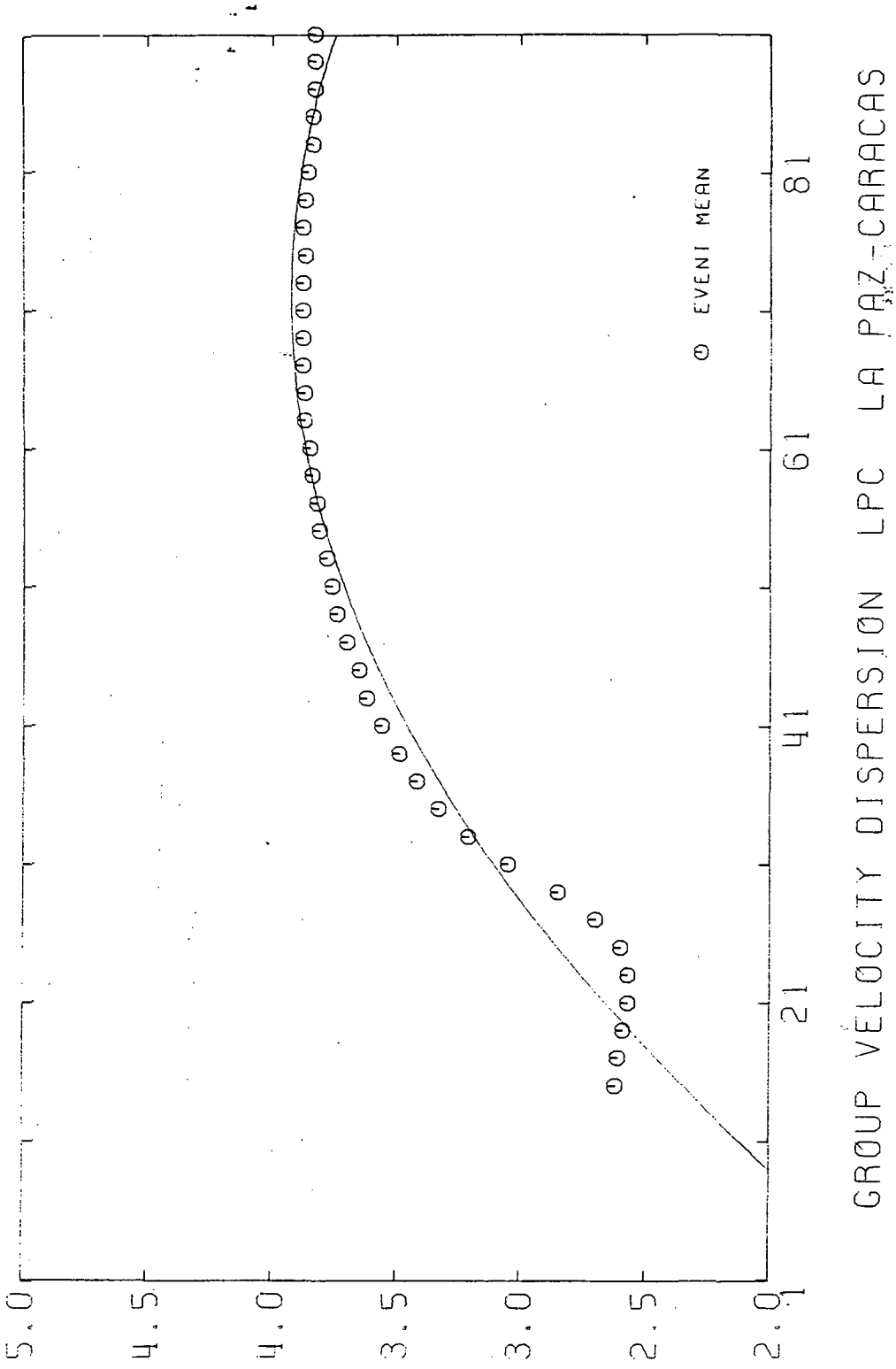
GROUP VELOCITY DISPERSION LPC LA PAZ-CARACAS
EVENI MEAN
5.0
4.5
4.0
3.5
3.0
2.5
2.0
1
21
41
61
81

Figure 36

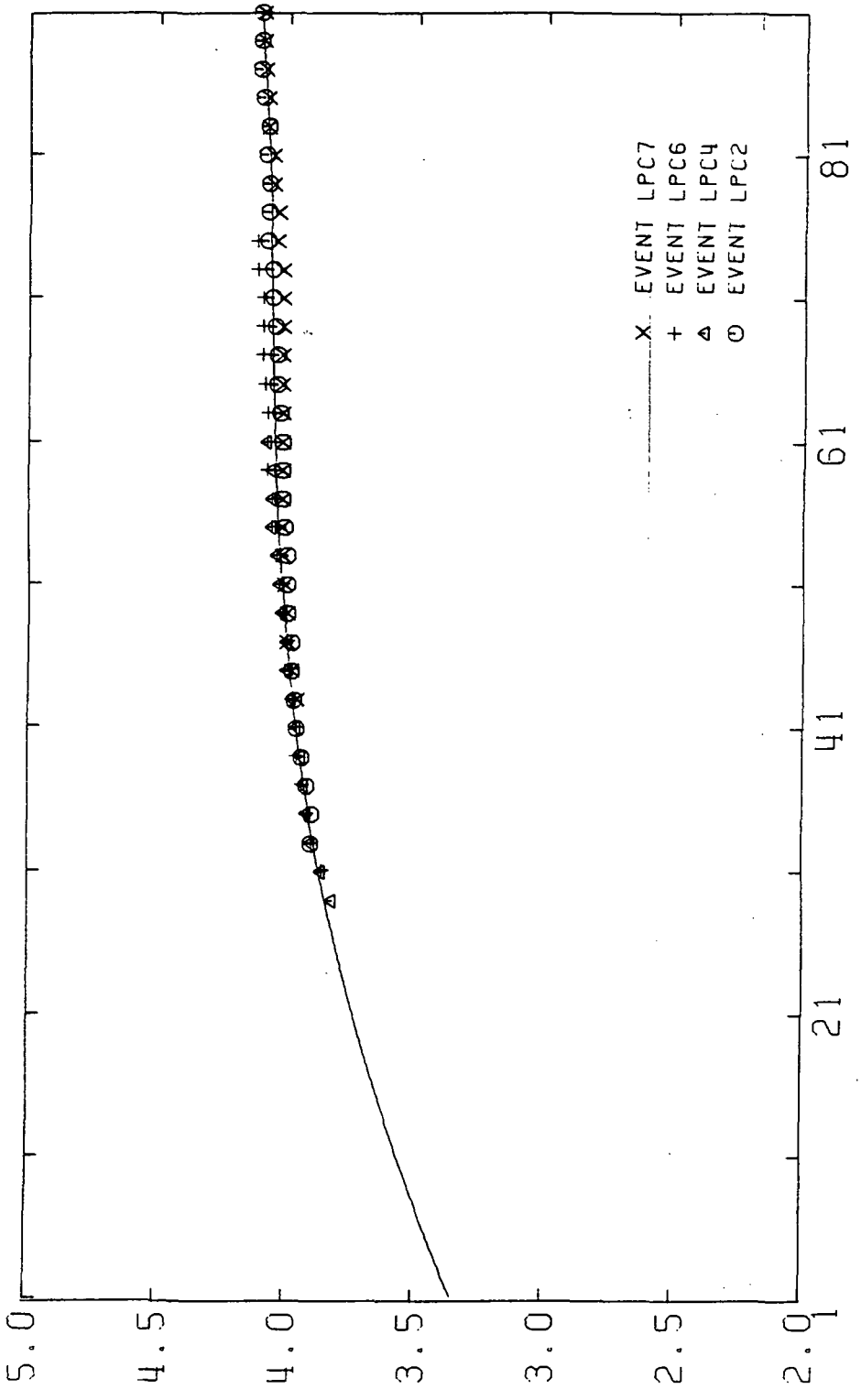
PHASE VELOCITY DISPERSION LPC LAPAZ-CARACAS
X EVENT LPC7
+ EVENT LPC6
Δ EVENT LPC4
O EVENT LPC2
5.0
4.5
4.0
3.5
3.0
2.5
2.0
1
21
41
61
81

Figure 37

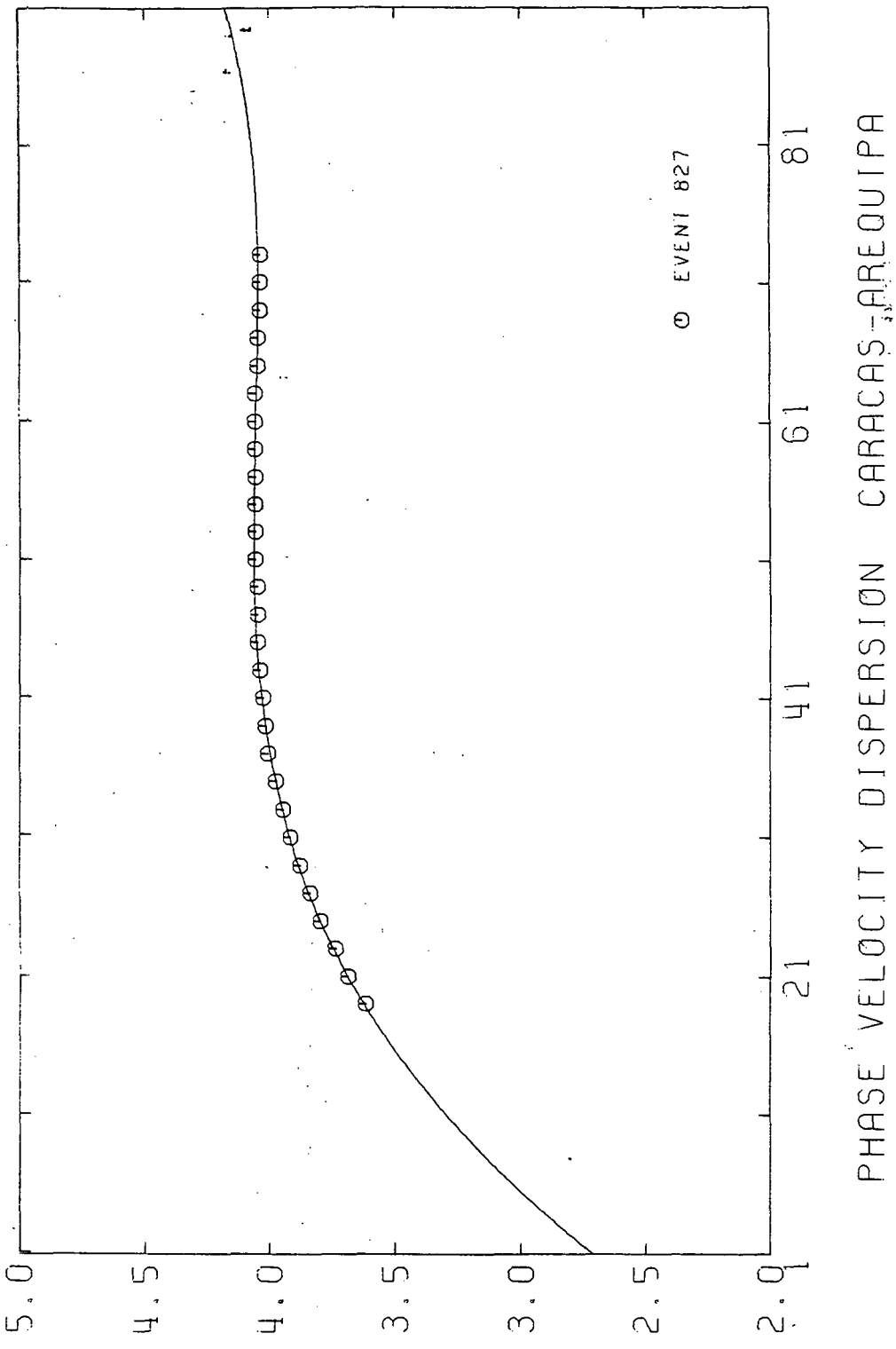
PHASE VELOCITY DISPERSION CARACAS-AREQUIPA
EVENT 827
5.0
4.5
4.0
3.5
3.0
2.5
2.0
1
21
41
61
81

Figure 38

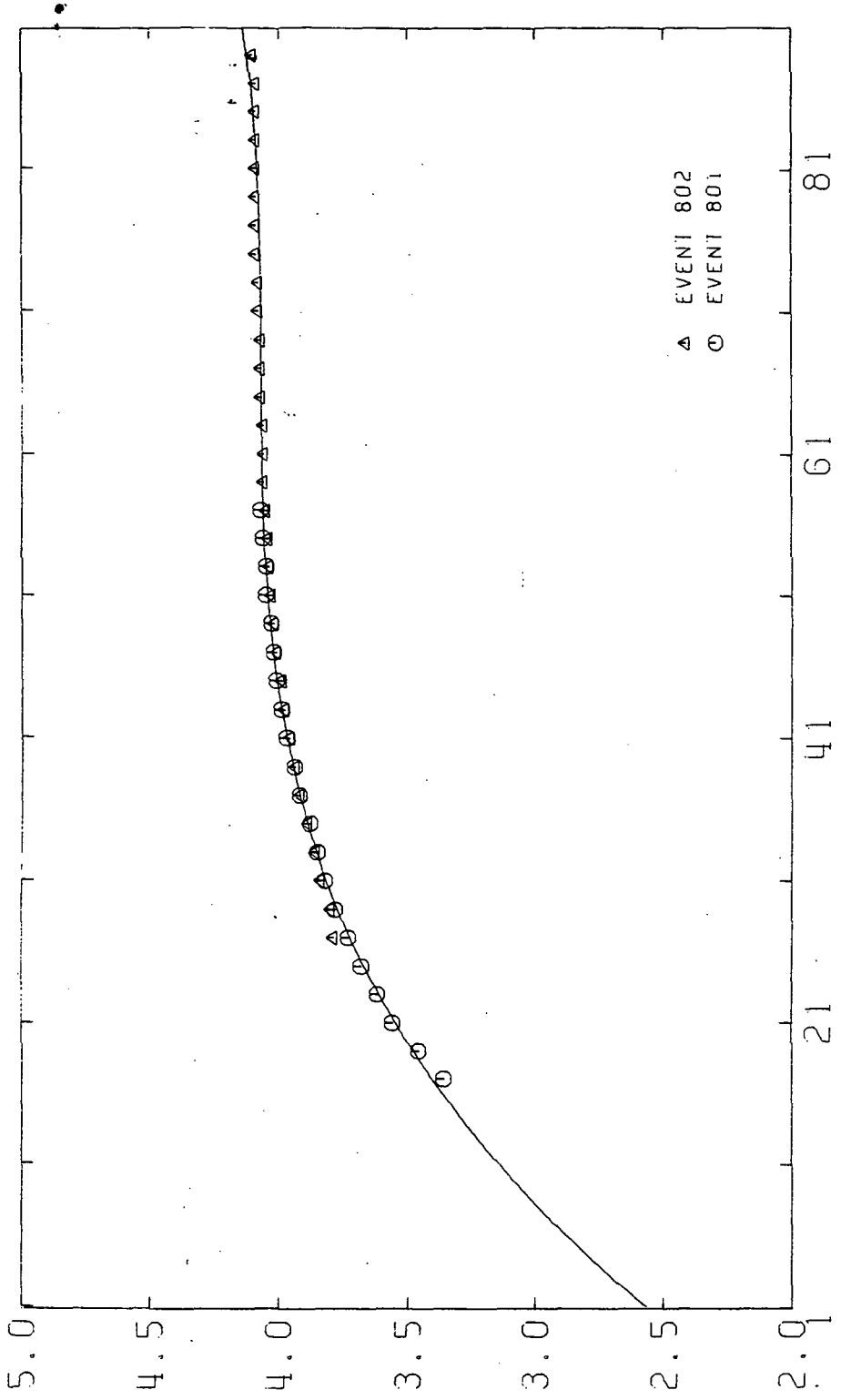
PHASE VELOCITY DISPERSION CARACAS-LA PAZ
EVENT 802
EVENT 801
5.0
4.5
4.0
3.5
3.0
2.5
2.0
1
21
41
61
81

Figure 39

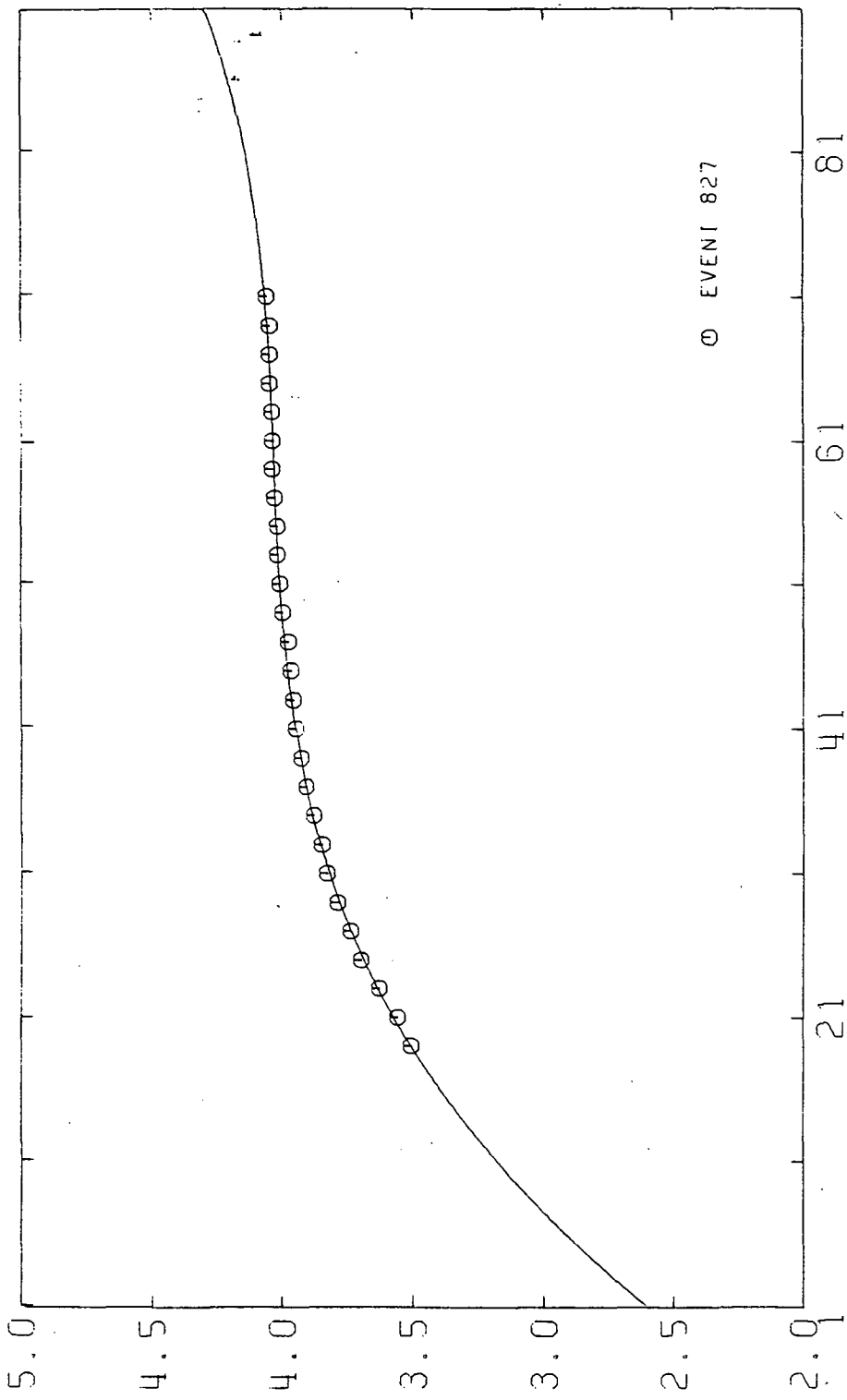
PHASE VELOCITY DISPERSION TRINIDAD-LA PAZ
EVEN1 827
5.0
4.5
4.0
3.5
3.0
2.5
2.0
1
21
41
61
81

Figure 40

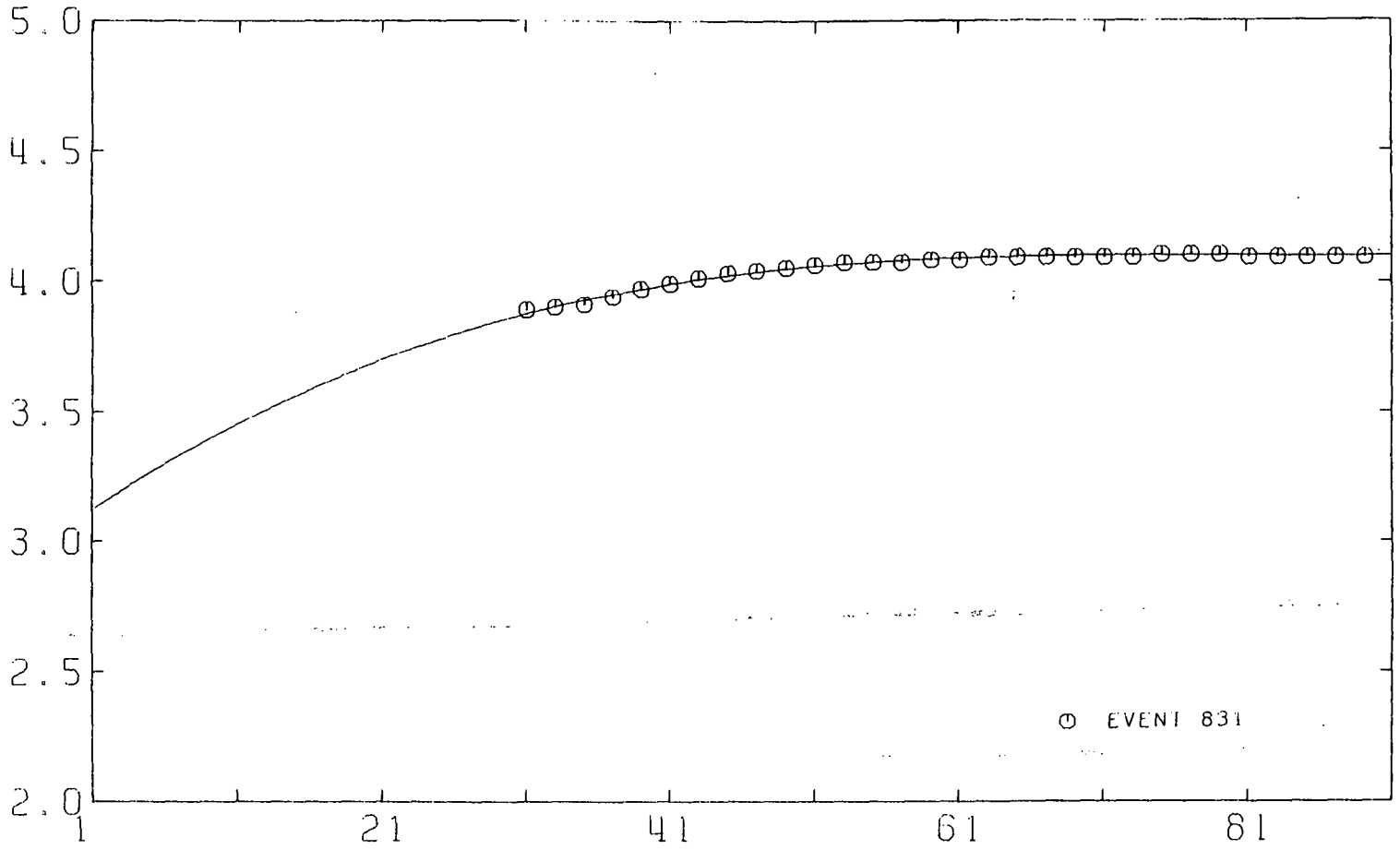
5.0
4.5
4.0
3.5
3.0
2.5
2.0
1
21
41
61
81
EVENT 831
PHASE VELOCITY DISPERSION TRINIDAD-RIO DE JANEIRO

Figure 41

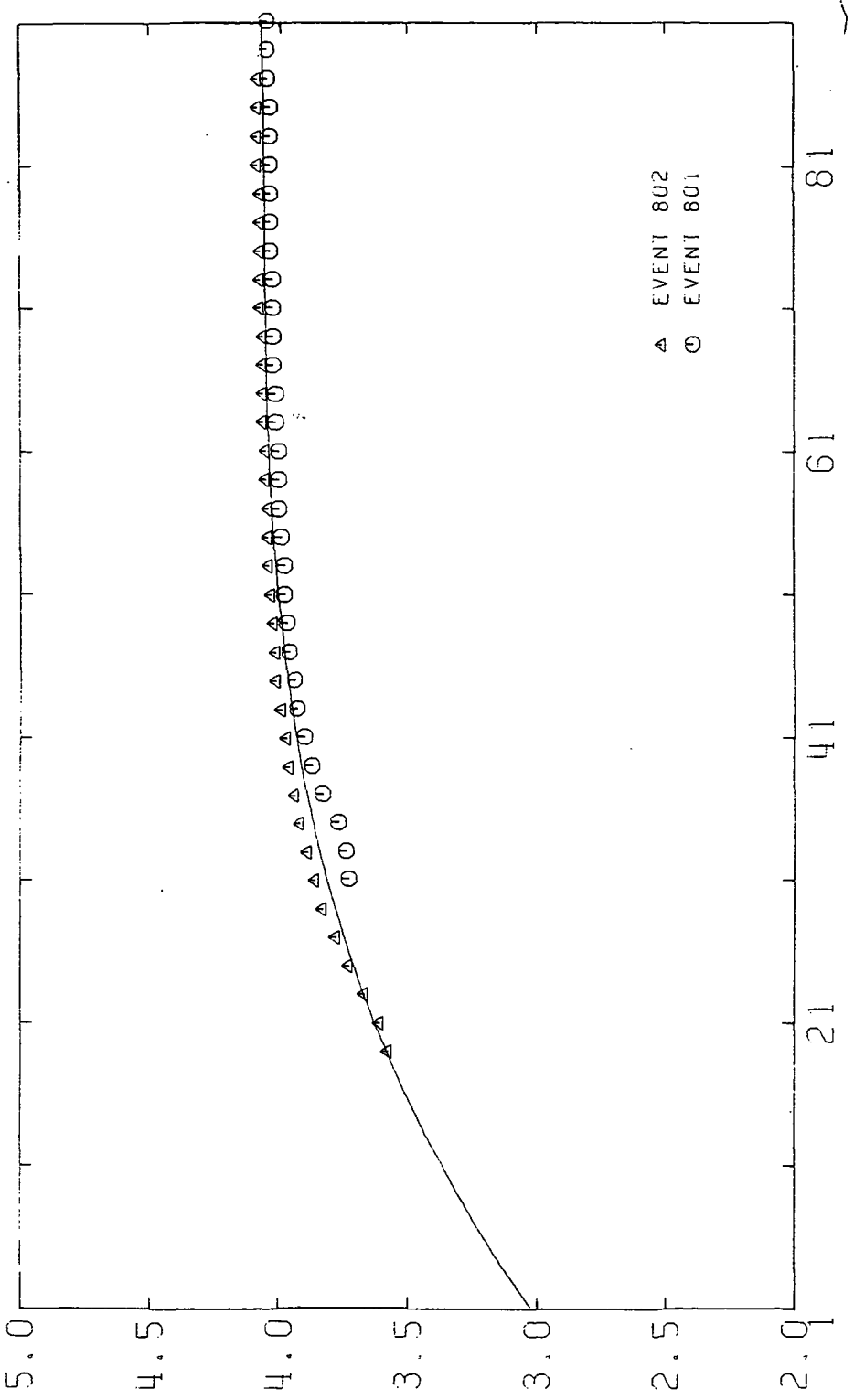
PHASE VELOCITY DISPERSION TRINIDAD-LA PLATA
EVENT 802
EVENT 801
5.0
4.5
4.0
3.5
3.0
2.5
2.0
1
21
41
61
81

Figure 42

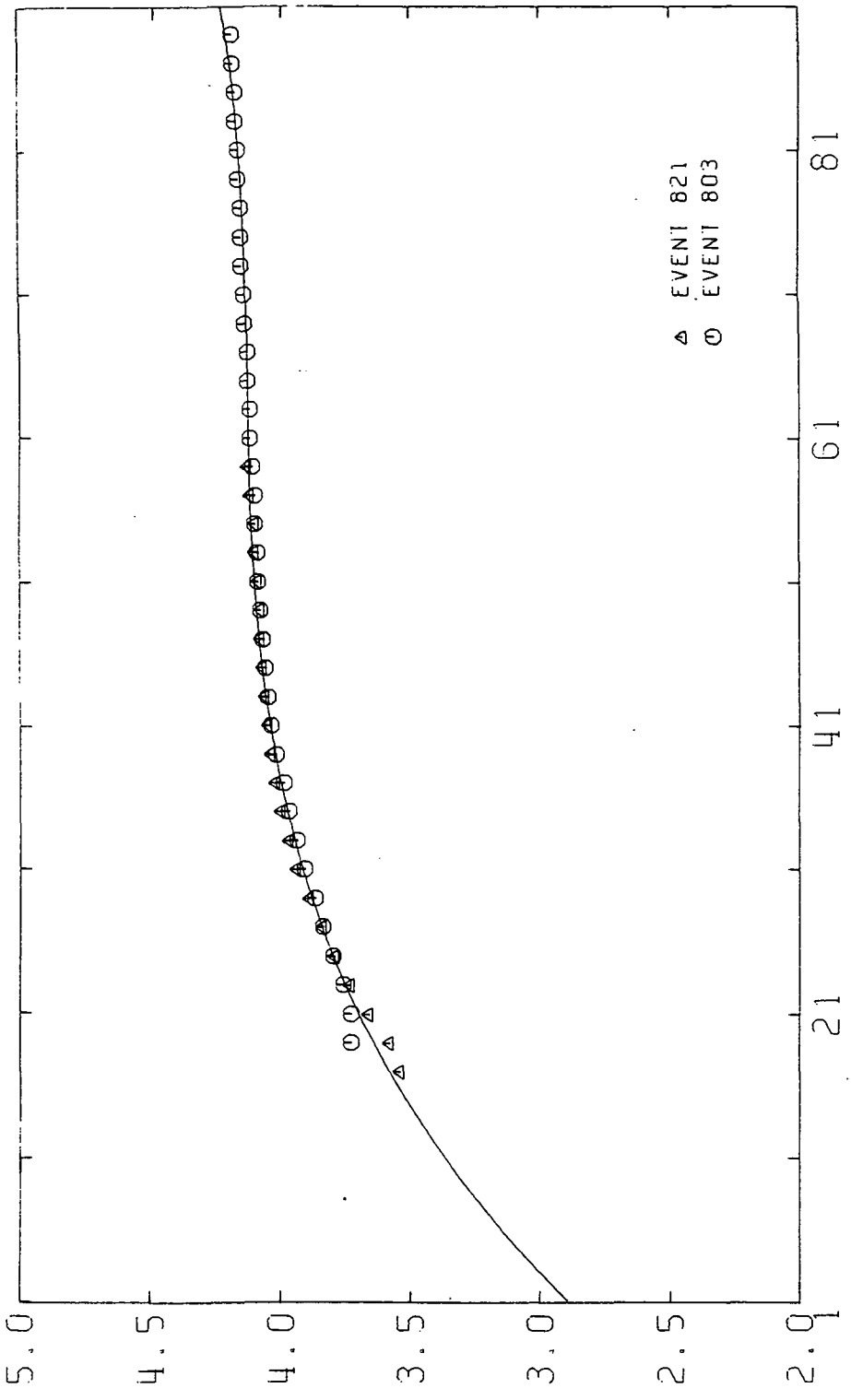
PHASE VELOCITY DISPERSION NATAL-QUITO
EVENT 821
EVENT 803
5.0
4.5
4.0
3.5
3.0
2.5
2.0
1
21
41
61
81

Figure 43

to derive earth models whose parameters can be related to actual geologic structures. In order to do this, it is first necessary to have available a means of computing a range of theoretical group and phase velocity dispersion values from an appropriate earth model. Such a model should be able to represent the variation of elastic properties with depth that can be expected to exist within the earth. Once a method of solving this so-called "forward problem" is established, it is then necessary to have a consistent means of modifying the earth model to bring the theoretical dispersion values it produces into correspondence with the values actually observed. The process of determining a model whose properties match a given set of observations is called inversion.

Forward Problem

Thomson (1950) and Haskell (1953) derived a matrix method of calculating the phase and group velocity dispersion of surface waves propagated across a stack of homogeneous elastic layers overlying a homogeneous half-space. Their method evaluates the wavenumbers $k_0(\omega_n)$, $K_1(\omega_n)$, $k_2(\omega_n)$, . . . $k_m(\omega_n)$ that characterize the fundamental and higher modes of surface waves propagating in a horizontal direction across the multiple layers. This is done by progressively solving the boundry conditions (appropriate to either Rayleigh or Love waves) that exist within the stack of layers in such a way that the general

equation of motion for elastic media is satisfied over a range of frequencies ω_n. Once the corresponding range of wavenumbers k_n for a single mode is determined, the range of phase velocities $c_n = \omega_n/k_n$ for that mode immediately follows. The range of group velocities U_n can then be calculated from this information. By specifying the material properties of the various homogeneous layers (models parameters of thickness, Poisson's ratio, compressional wave velocity, shear wave velocity, and density), a large variety of seismic velocity distributions within the earth can be approximated.

Inverse Problem

The relationship between a set of M model parameters, x_j, and N observables, y_i, can be written as a linear system of equations:

$$yi = \sum_{j=1}^{M} F_{ij} x_j \qquad i = 1, N .$$

In this study, this system of equations would represent the Haskell-Thomson relationship between the layered model and the predicted dispersion values. The inverse problem involves finding a set of model parameters, x_j, which will generate a set of predicted data, y_i, that agrees as closely as required with the actual data. These model parameters are further constrained to be reasonable earth-like values. A standard means of dealing with problems of this nature is to write the relationship between model parameters

and observables as a system of simultaneous linear equations, and then solve for the desired x_j. The Haskell-Thomson relationship is not linear in the model parameters. It can be linearly approximated, however, by expanding the relationship in a Taylor series about some initial model, x_o, and ignoring second and higher order terms:

$$y_i \simeq \sum F_{ij} x_o + \sum_{j=1}^{M} \frac{\partial F_{ij}}{\partial x}_{oj} (x_j - x_o)$$

$$(+ \text{ higher order terms}) .$$

This can be written in vector form as

$$y = y_o + A(x - x_o)$$

or

$$\Delta y = A \Delta x .$$

(Here lower case letters represent vectors, and upper case letters represent matrices.) In the last equation Δy represents an N-length vector containing the differences between the actual data y and the model-predicted data y_o, A represents an NxM matrix of partial derivatives of the function F_{ij} evaluated at the initial model parameters x_o, and Δx represents an M-length vector containing the differences between a desired set of model parameters x and the initial model parameters x_o. Once this linear approximation has been made, the inverse problem becomes

finding a vector Δx which minimizes the difference (or "error").

$$\varepsilon = A\Delta x - \Delta y \ .$$

Assuming that the number of data values N is greater than the number of model parameters M, the solution for Δx which minimizes the squared error $\varepsilon^T\varepsilon$ is given by

$$\Delta x = (A^TA)^{-1} A^T \Delta y \quad \text{(Jackson, 1972)} \ .$$

The solution obtained in this way satisfies the least squares fit criterion, but it can display on large range of values. The method used in this study to constrain Δx to smoother, more simple solutions was to simultaneously require the minimization of first order differences between adjacent solution elements (i.e., minimize the first derivative of the solution). Mathematically, adding the smoothness criterion involves minimizing the quantity

$$[(1 - \beta)\varepsilon^T\varepsilon + \beta \sum_{k=2}^{M} (x_{k-1} - x_k)^2] \qquad \beta\varepsilon[0,1]$$

to give a constrained solution of the form:

$$\Delta x = [(1 - \beta) A^TA + \beta(K^TK)]^{-1}(1 - \beta) A^T \Delta y \ ,$$

where

$$K^TK = \begin{vmatrix} 1 & -1 & 0 & 0 \ldots \\ -1 & 2 & -1 & 0 \ldots \\ 0 & -1 & 2 & 0 \ldots \\ 0 & 0 & -1 & 2 \ldots \\ \cdot & & & \\ \cdot & & & \\ \cdot & & & \end{vmatrix}$$

(Twomey, 1977; Russell, 1980).

Once Δx is known, the desired model parameters x follow by adding the changes Δx to the initial model parameters x_0:

$$\Delta x = x - x_0 \ ;$$

$$x = x_0 + \Delta x \ .$$

The predicted observations generated by the model, x, are computed and compared to the actual data. If the difference, Δy, is still unacceptably large, the entire process can be repeated, using x as a new initial model. Assuming the changes Δx are sufficiently small, and given a reasonable starting model, this process generally converges.

Resolution

The general statement of the linearized forward problem is

$$\Delta y = A\Delta x \ .$$

Again assuming that N is greater than M, the NxM matrix, A, can be decomposed into its constituent eigenvectors and eigenvalues in order to vacilitate finding its inverse as follows:

$$A = U\Lambda V^T ,$$

where U represents an NxM orthogonal matrix of data eigenvectors, V represents an MxN orthogonal matrix of model eigenvectors, and Λ represents an MxM diagonal matrix of eigenvalues. This is called the principal axis decomposition of A. The general linear inverse of A in this form is

$$A^{-1} = H = V\Lambda^{-1}U^T \quad \text{(Lanczos, 1961)} .$$

Once this inverse is known, a particular solution Δx_p is given by operating on the data vector Δy:

$$H\Delta y = HA\Delta x$$

$$\Delta x_p = V\Lambda^{-1}U^T U\Lambda V^T \Delta x$$

$$\Delta x_p = VV^T \Delta x$$

The final equation of this set shows that the solution obtained, Δx_p, is actually a product of the true solution Δx and the matrix VV^T. For mathematically underdetermined systems (in which there are less eigenvalues (in Λ) than either model parameters M or data values N), the matrix VV^T

is often called the resolution matrix R. An individual model parameter in the particular solution Δx_p, for example, the k^{th} parameter, can be interpreted as the result of a convolution of the k^{th} row of R with the solution vector Δx. If R is an identity matrix, the k^{th} parameter of Δx_p will exactly equal the k^{th} model parameter in Δx. The full solution Δx_p will be unique, and each model parameter in Δx_p will be perfectly resolved. If R has non-zero elements scattered along its rows, however, the k^{th} paramter in Δx_p will be a weighted sum of several model paramters in Δx, and the individual model parameters in Δx_p will no longer be perfectly resolved. The extent to which R approaches the identity matrix is a measure of the resolution that the data Δy allows (Jackson, 1972). Since a surface wave of period T propagating over a layered medium is in general influenced by the elastic properties of a wide range of layers, it cannot carry unique information about just one layer. Waves whose periods are similar will carry overlapping or redundant information. Furthermore, the limited range of periods investigated may carry little or no information about, say, very shallow or very deep layers. Error in the measurements compounds these problems. These shortcomings show up as scatter in the resolution matrix, and limited layer resolution in the final earth model.

Model Interpretation

A 21-layer model of the upper 100 kilometers of the earth was used as the starting model in each inversion. The model consisted of an upper two-kilometer-thick layer, assigned an initial shear wave velocity of 2.4 km/s (representing an average sedimentary platform cover), followed by 17 four-kilometer-thick layers and three 10-kilometer-thick layers, each assigned on initial shear wave velocity of 4.0 km/s. A total thickness of 100 kilometers was chosen as the approximate depth range over which Rayleigh waves of period 10-90 seconds are sensitive. Only the model parameter of shear velocity was allowed to vary in the data inversion. The thickness of each layer was kept constant. A Poisson's ratio of 0.25 was assumed for the crust and upper mantle, and compressional wave velocities for the individual layers were calculated from the derived shear velocities and Poisson's ratio. Densities for the layers were calculated from the Nafe-Drake relationship between density and compressional wave velocity and Birch's law (Birch, 1964).

In theory, no more information should be given by simultaneously inverting group velocity dispersion data with phase velocity dispersion data than is given by inverting phase velocity data alone. This is because the group velocity can be uniquely derived from the phase velocity (see earlier discussion). However, since group velocities

are determined independently of phase velocities in this study, the errors the measurements contain should be somewhat different, and the group velocities will act as semi-independent information. The group velocity dispersion may also be influenced in a slightly different manner or degree by the model parameters than is the phase velocity, and including group velocities in the inversion may increase the definition of the earth model. For this reason group velocity dispersion data was inverted together with phase velocity data whenever both sets of data were available.

It is unrealistic to assume that long-period Rayleigh waves are sufficiently sensitive to changes in shear wave velocity with depth to resolve individual four-kilometer-thick layers in the earth (Der et al., 1970). Assigning a relatively large number of thin layers is a means of allowing the inversion to determine ranges of changing shear velocities with depth. Since the shear velocities characterizing adjacent layers are averaged, models consisting of numerous layers cannot show abrupt changes between well-defined zones of constant velocity. Instead, major structural divisions, such as the M-discontinuity, show up as zones of changing velocity, and cannot be resolved better than within perhaps ± four kilometers. (Both layer thicknesses and shear wave velocities can be allowed to vary simultaneously during inversion, but by doing this, no estimates of the degree of uncertainty in

shear velocities in a given layer can be made [Russell, 1980].)

In this study, a graphical display of the increasing uncertainty in shear wave velocity that occurs with increasing depth resolution in the layered model was generated by the edgehog method (Jackson, 1973). Jackson presented a method of finding both the maximum and minimum contributions from the k^{th} model eigenvector which, when added to an optimum model, generate a pair of extreme or marginal models that just barely satisfy both the least squares fit and smoothness criteria mentioned earlier. A series of these models are generated by separately adding the contributions from the first, second, third, etc. model eigenvector to the optimum model, and plotting the results. The edge models generated by contributions from the first model eigenvector show the extent to which the entire shear wave velocity-depth curve may be either increased or decreased without violating either the least squares fit or smoothness criteria. The edge models generated from contributions from the second model eigenvector indicate the extent to which the shear velocity in the upper part of the model may be increased if the velocity in the lower part of the model is decreased (or vice versa) while still honoring the data. These particular edge models form narrow envelopes about the optimum model. As the order of the eigenvectors used to generate the edge

models is increased, the edge models form wider and wider spreading envelopes pinched together at smaller and smaller intervals. According to Jackson, the degree of layer resolution is related to the thickness of the individual envelopes, and the degree of uncertainty in shear velocity is related to the spread in velocity across an individual envelope. In a sense, each edge model pair spans the range of potential shear velocity-depth models that can satisfy the data, using the specified number of model eigenvectors. Figures 44a and 44b show the optimum model and three sets of edge model pairs, corresponding to contributions from the third, fourth, and fifth model eigenvectors, for the two-station path TRN-LPB. The pattern of increasing envelope width (increasing uncertainty) with increasing envelope number (increasing layer resolution) can be clearly seen. The edge models which show the maximum acceptable uncertainty in shear velocity in a given model can provide subjective aid in choosing the position of major layer boundaries, such as the M-discontinuity between the crust and upper mantle. Each of the optimum shear wave velocity-depth models reported in this study is shown together with the edge model pair which displays the maximum acceptable uncertainty in shear velocity.

Finally, it is important to remember that the models obtained by measuring and inverting Rayleigh wave dispersion between two stations represent broad lateral averages of the

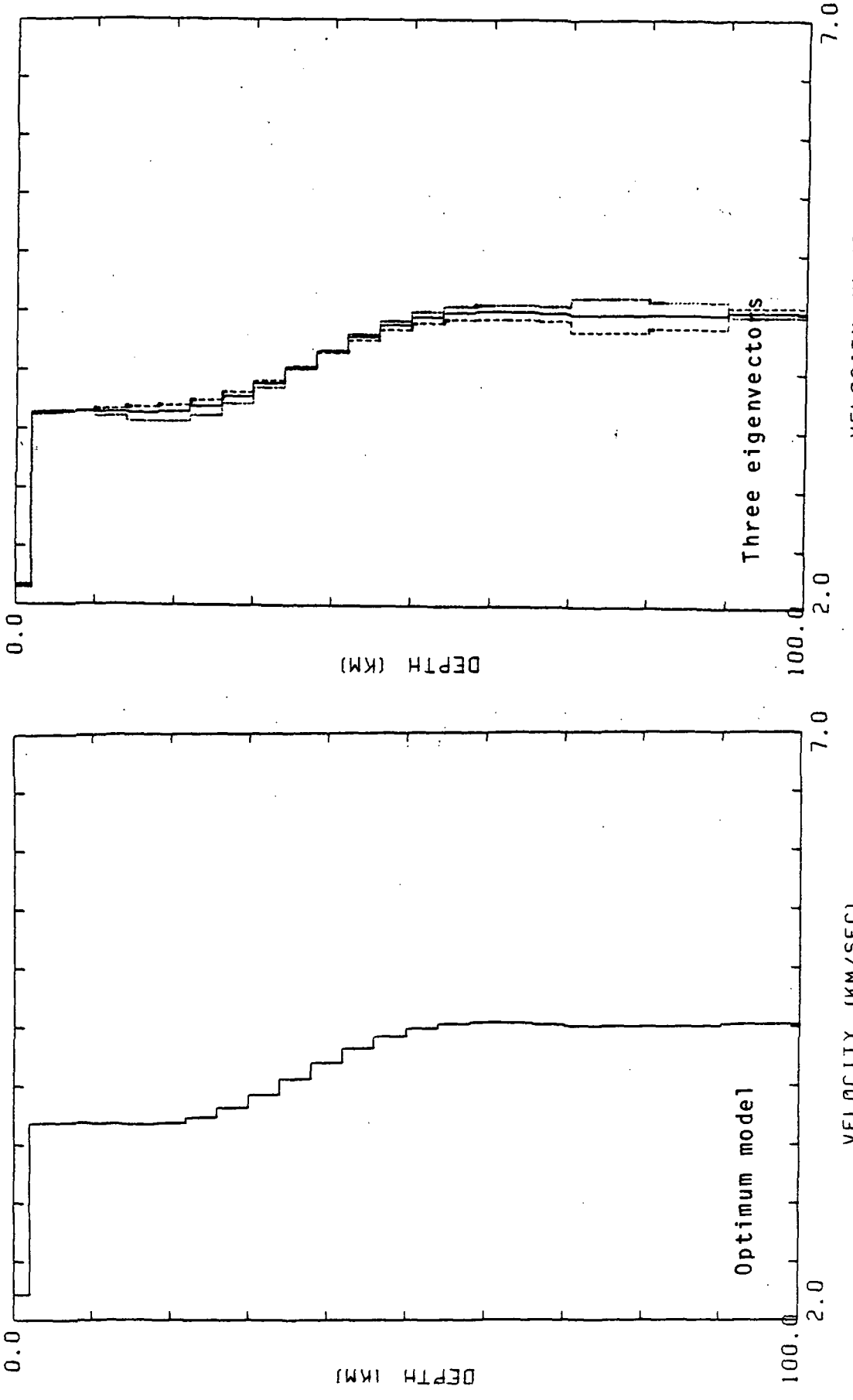

Figure 44a. Examples of the edgehog inversion results for the path TRN-LPB.

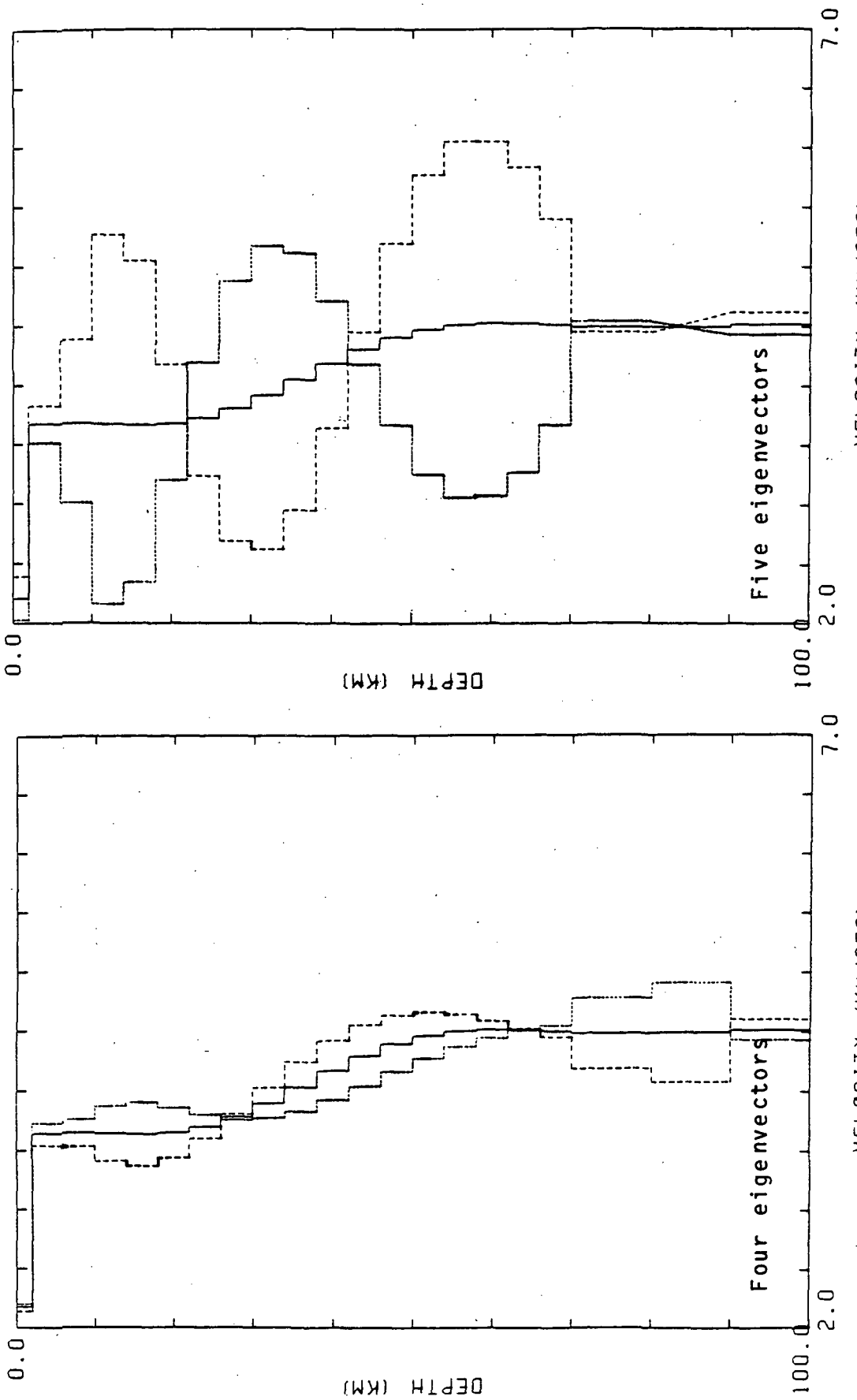

Figure 44b. Examples of the edgehog inversion results for the path TRN-LPB.

crustal structure between the stations, as well as vertical averages. The dispersion measured between two stations is influenced by all the variations in elastic properties in the earth along the path, but only one model can be derived from the measurements.

RESULTS

The two-station paths over which shear wave velocity-depth models were derived in this study may be initially combined into four groups for the purposes of comparison and discussion. The first group ("Northern platform") includes three paths which cross the northern quarter of the South American platform. These three paths radiate in a west-northwesterly direction from Natal to Caracas, Bogota, and Quito. The second group ("Southern platform") includes three paths which cross the central and southeastern portions of the South American platform. Two of these paths extend in a southwesterly direction from Natal to La Paz and La Plata, and one extends due west from Brasilia to La Paz. The third group ("Central platform") includes three paths which cross the length of the South American platform from north to south. Two of thes paths extend from Trinidad south-southeastward to La Plata and Rio de Janeiro, and one extends southeastward from Caracas to La Plata. The fourth group ("Northwestern platform") includes four paths which cross the northwestern lobe of the South American platform. Three of these paths radiate south to southwestward from Caracas to Quito, Arequipa, and La Paz. One path extends from Trinidad to La Paz.

All of these paths are shown in Figures 11 and 12. Taken together, the 13 paths provide general coverage of nearly the entire South American platform. Since all but one of the seismograph stations lie on the perimeter of the platform, the paths connecting the stations are long and usually traverse more than one cratonic area or intracratonic/pericratonic basin. This leads to an unavoidable averaging over potentially different types or thicknesses of crust. Nevertheless, if sufficiently broad differences in crustal structure exist beneath the platform, the shear velocity-depth models should reflect it.

Northern Platform

The path NAT-CAR lies along nearly the entire northeastern coast of South America, extending 3,931 kilometers from Natal, Brazil, to Caracas, Venezuela. Part of the path lies on the continental shelf off the northern coast of Brazil. The path regains land just north of the Amazon River mouth, near the Brazil-French Guiana border, and crosses French Guiana, Surinam, northern Guyana, and northeastern Venezuela. Over its length, the path NAT-CAR crosses the extreme northern end of the Atlantic shield, the offshore extensions (?) of the Parnaiba basin, the Sao Luis craton, and the Amazon River basin, the entire northern side of the Guyana shield, and a deep foreland/marginal faulted basin between the Guyana shield and the Eastern cordillera of northeasten Venezuela. Of all the paths investigated in

this study, NAT-CAR lies closest to the passive Atlantic margin of South America. It intersects both the Amazon River and the Takatu aulacogens, and it may be influenced by the crust under other marginal faulted basins along the coast.

The shear wave velocity-depth model computed for this path, based on inverting both group and phase velocity dispersion data for two events, suggests a crustal thickness of 38 ± 4 kilometers (Fig. 45). The optimum model shows a nearly constant velocity gradient to a depth of approximately 55 kilometers, and the M-discontinuity is poorly defined. The edge models associated with the fourth model eigenvector aid in defining the crust-upper mantle transition. The average crustal shear wave velocity, taken from the optimum model, ranges from 3.80 to 3.89 km/s, which corresponds to an average compressional wave velocity range of 6.58 to 6.74 km/s and an average density range of 2.86 to 2.91 g/cm^3. (In all cases, Poisson's ratio was assumed to have a value of 0.25 throughout the crust and upper mantle.) The optimum model also shows a slight low velocity channel in the uppermost mantle (between 60 and 90 kilometers depth) which is probably not real, based on the results of other shield-area seismic investigations. A low velocity zone occurring at varying depths below 60 kilometers is present to one degree or another in nearly all the velocity-depth models computed in this study. A

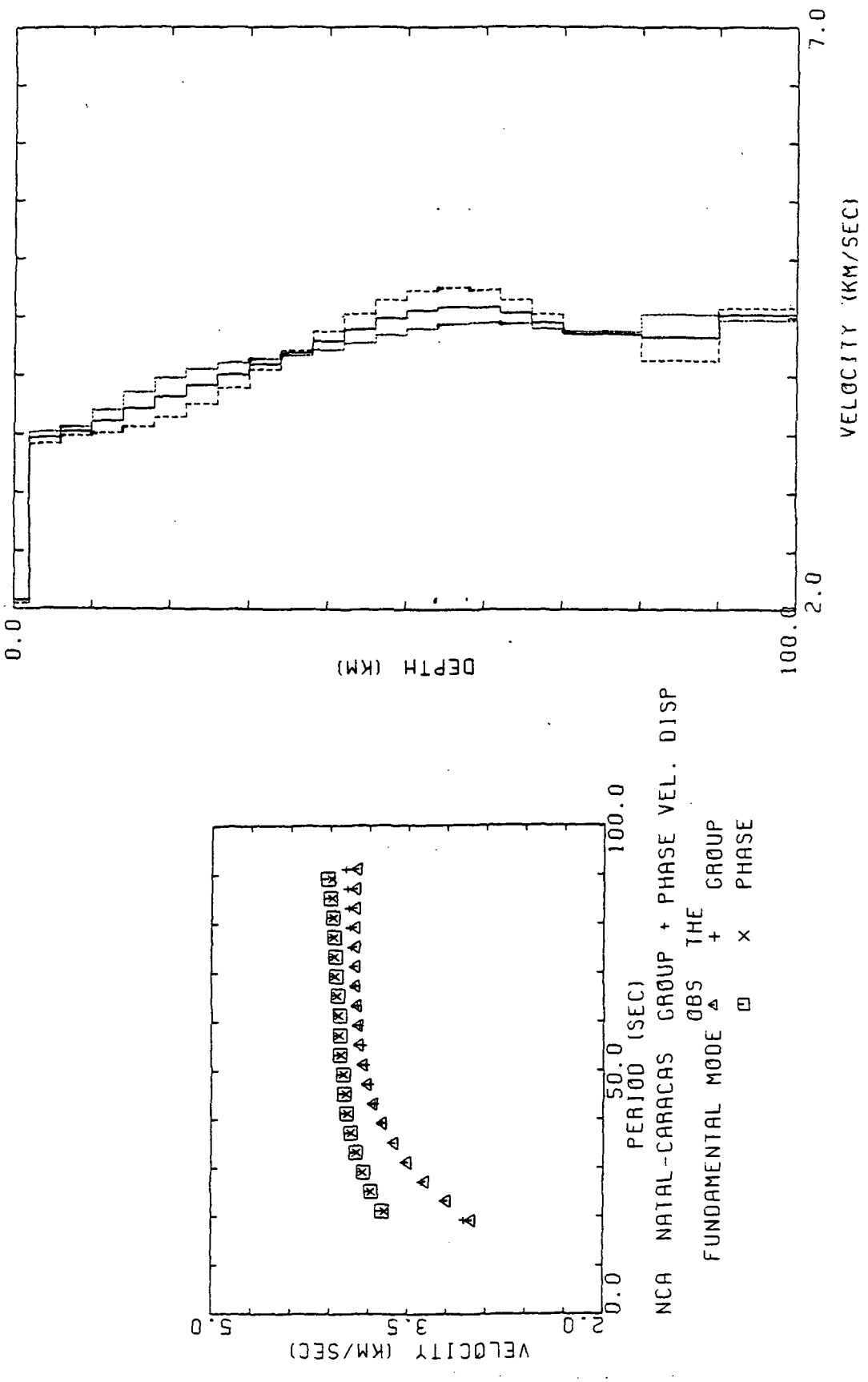

Figure 45. Inversion results for the path NAT-CAR.

complementary high velocity zone often occurs immediately above the low velocity zone, exaggerating its appearance. This pattern of unrealistically high/unrealistically low shear wave velocities in the uppermost mantle is more pronounced in models where both group and phase velocity data have been inverted together than in models derived from inverting phase velocities alone. It is mostly a result of the decrease in resolution with increasing depth.

The path NAT-BOG, extending 4,466 kilometers from Natal, Brazil, to Bogota, Colombia, crosses the length of northernmost Brazil, grazes the southern tip of Venezuela, and cuts into half of central Colombia. Over its length, this path crosses the extreme northern end of the Atlantic shield, the northern end of the Parnaiba basin, the deep easternmost end of the Amazon basin, the length of the southern Guyana shield, and the platform cover/foreland basin between the shield and the Eastern cordillera of Colombia.

The shear wave velocity-depth model computed for the path NAT-BOG, based on inverting both group and phase velocity dispersion data for five events, suggests a crustal thickness of 46 $\pm$ 4 kilometers (Fig. 46). The optimum model shows a distinct increase in the velocity-depth gradient of this depth, and the edge models associated with the fifth model eigenvector reflect this increase. The average crustal shear wave velocity ranges from 3.84 to 3.90 km/s,

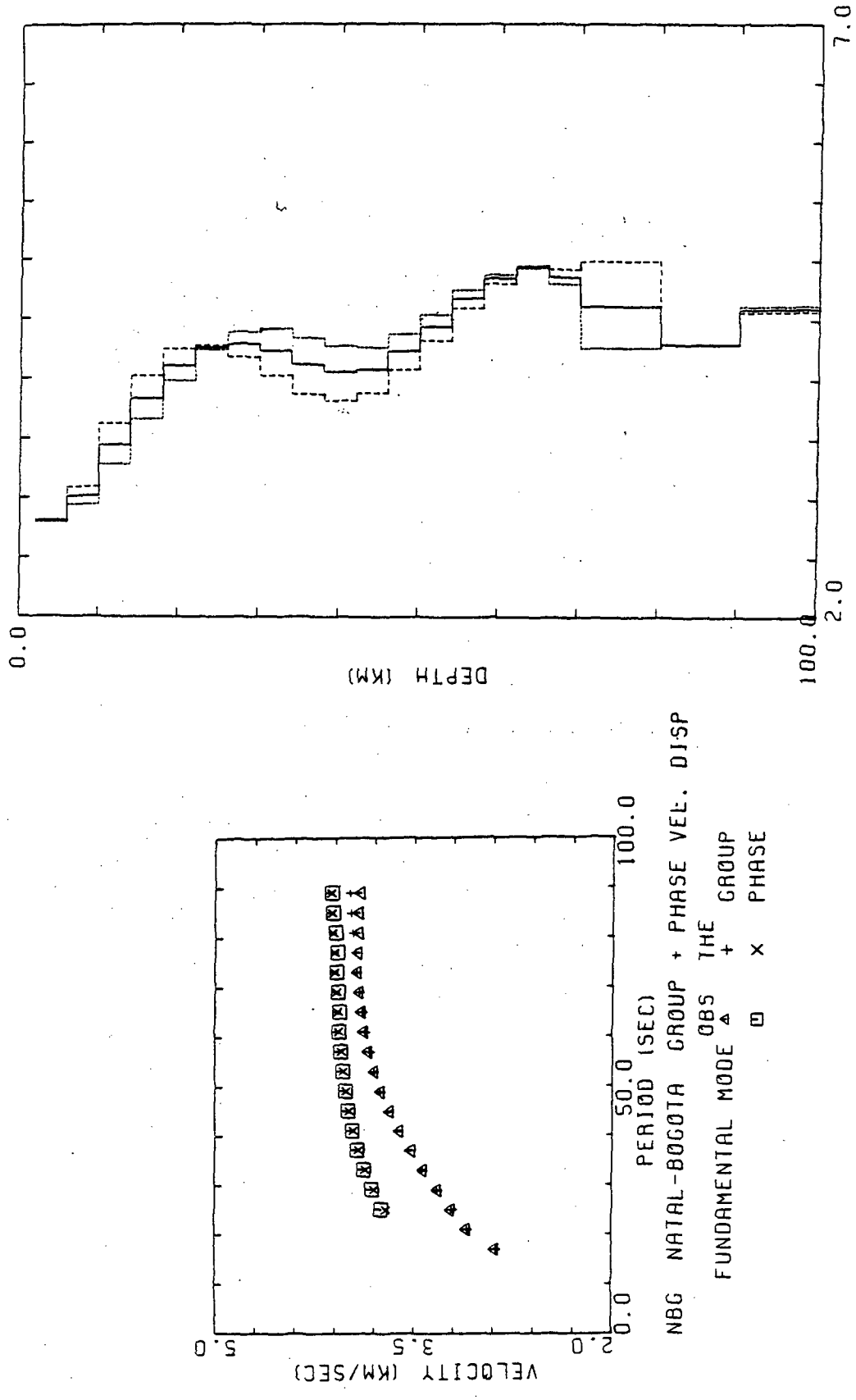

Figure 46. Inversion results for the path NAT-BOG.

which corresponds to an average compressional wave velocity range of 6.66 to 6.76 km/s and an average density range of 2.91 to 2.93 g/cm^3. The average upper mantle shear velocity, down to 100 kilometers, is 4.60 km/s, corresponding to an average compressional wave velocity of 7.97 km/s and an average mantle density of 3.30 g/cm^3. These mantle parameters must be treated with caution, due to the rather pronounced low velocity zone below 80 kilometers required by the inversion. However, at these depths, average velocities are probably more reliable than velocities of individual layers.

The path NAT-QUI, extending 4,857 kilometers from Natal, Brazil, to Quito, Ecuador, crosses all of northern Brazil, southern Colombia, and part of northern Ecuador. After crossing the extreme northern end of the Atlantic shield and the northern edge of the Parnaiba basin, this path cuts across nearly the entire length of the Amazon basin, skirting the Central Brazilian shield to the southeast and the Guyana shield to the northwest. It also crosses the extensive platform cover and broad foreland basin that lies between the western end of the Amazon basin and the curve of the Andean cordillera through Colombia, Ecuador, and Peru. A very small portion of the path cuts the Eastern cordillera of Ecuador.

Two shear wave velocity-depth models were computed for this path. One model (Fig. 47) was derived from

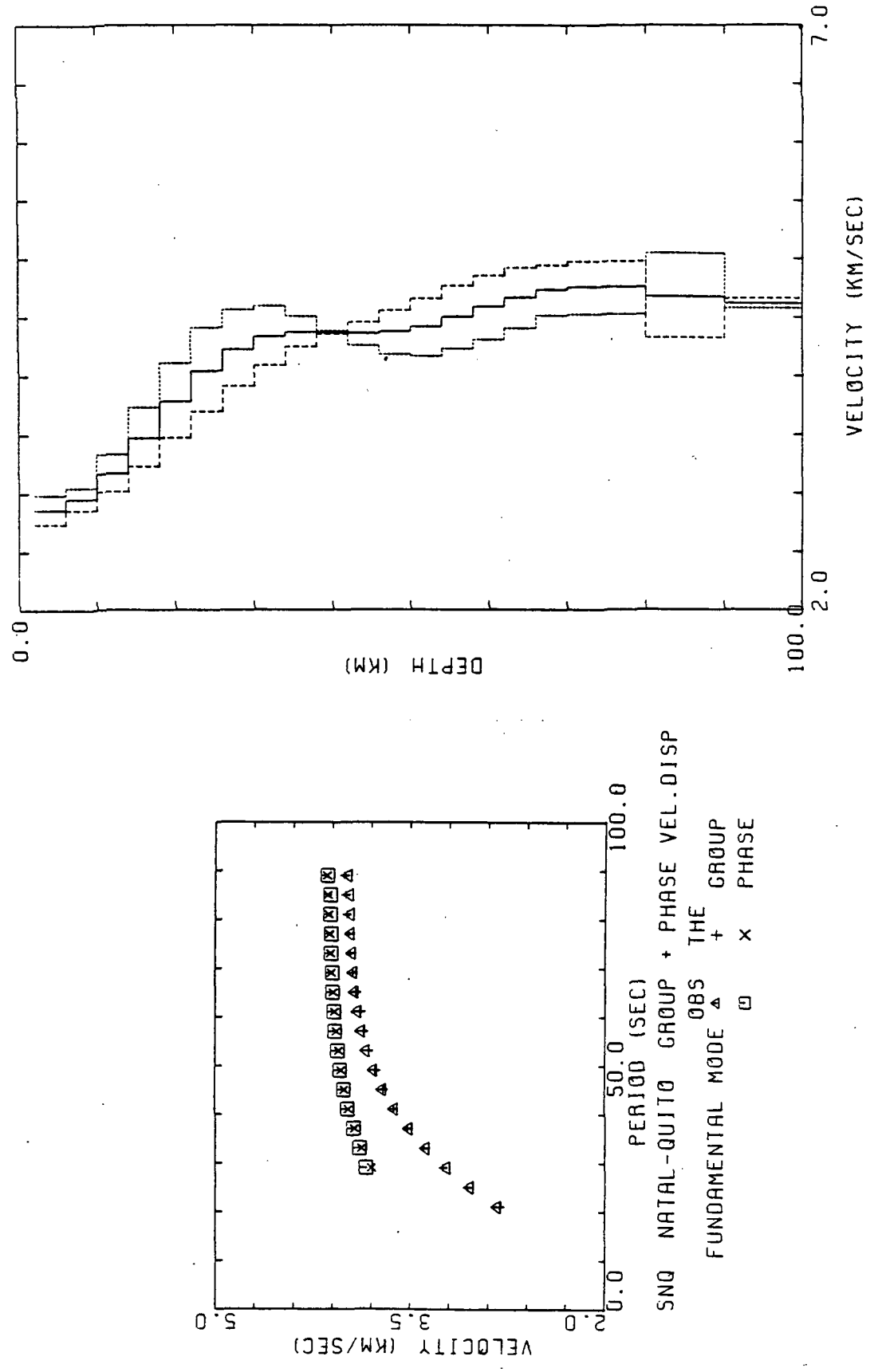

Figure 47. Inversion results for the path NAT-QUI.

inverting both group and phase velocity dispersion data (obtained in this study) for two events, and the other (Fig. 48) was derived from inverting only phase velocity dispersion data (taken from Sherburne [1974]), also for two events. The optimum models agree remarkably well between depths of 50 to 100 kilometers; differences above 50 kilometers are due to the inclusion of group velocity data in the first inversion and an extended short period range of phase velocity data in the second inversion. The crustal thickness estimated from the data obtained in this study is 50 ± 4 kilometers (Fig. 47). The optimum model shows a distinct increase in shear velocity at this depth, following a roughly 20-kilometer-thick zone of constant shear wave velocity. The average crustal shear wave velocity ranges from 3.81 to 3.90 km/s, corresponding to an average compressional wave velocity of 6.60 to 6.76 km/s and an average density range of 2.90 to 2.94 g/cm^3. The optimum upper mantle velocity-depth model (from 50 to 100 kilometers) appears reasonable, yielding an average upper mantle shear velocity of 4.64 km/s. This corresponds to an average compressional wave velocity of 8.04 km/s, and an average density of 3.32 g/cm^3.

The M-discontinuity is less easily defined in the velocity-depth model computed from Sherburne's phase velocity dispersion data. The optimum model suggests a slightly shallower crust approximately 46 ± 4 kilometers

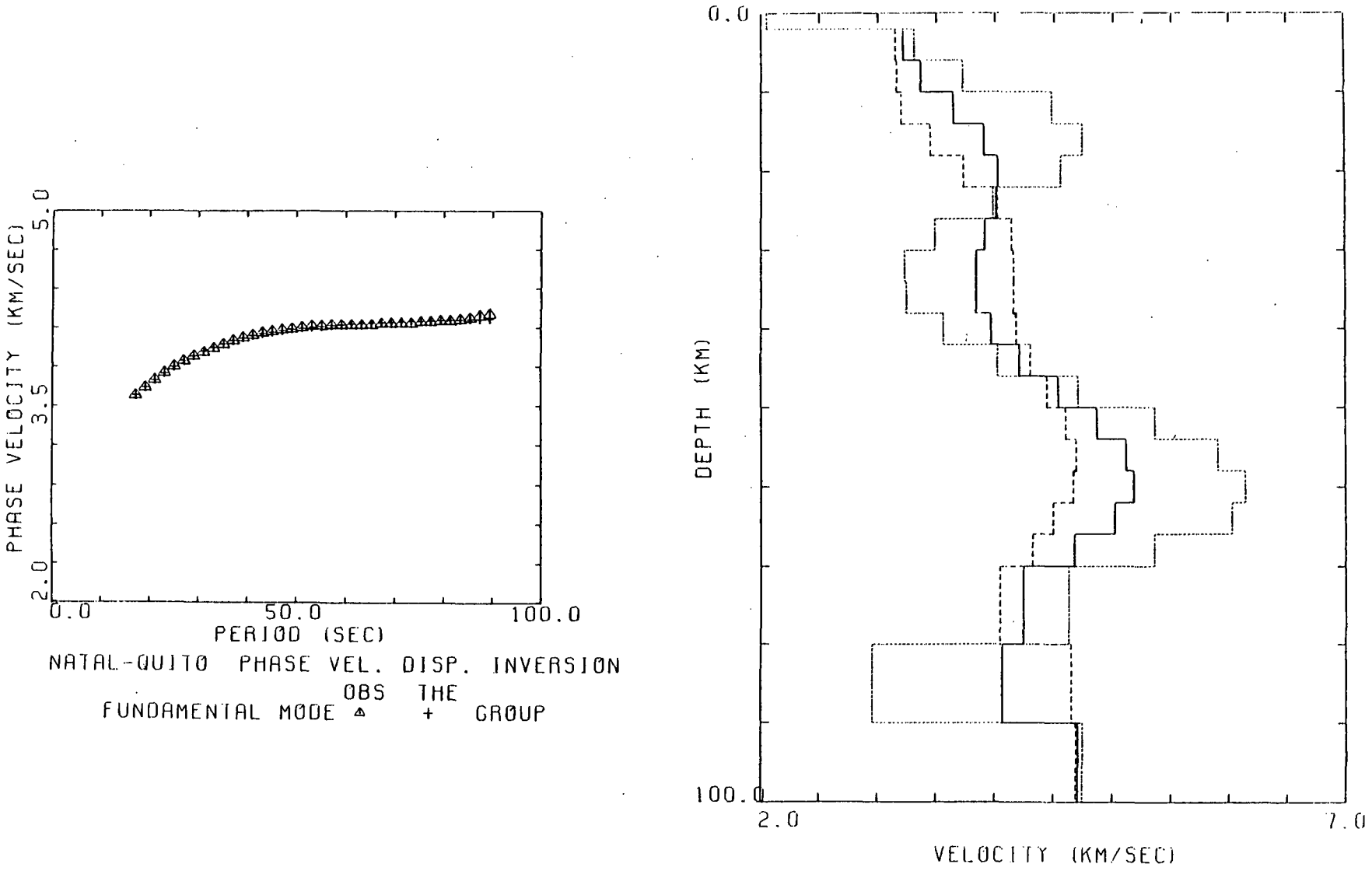

Figure 48. Inversion results for the path NAT-QUI using data from Sherburne (1974).

thick (Fig. 48); this pick supported by one of the edge models associated with the fourth model eigenvector. The average crustal shear wave velocity ranges from 3.92 to 3.98 km/s (slightly higher than the previous range of values) with a corresponding average compressional wave velocity range of 6.80 to 6.90 km/s and a density range of 2.93 to 2.96 g/cm^3. The average upper mantle shear velocity estimated from this model is 4.59 km/s (slightly lower than the previous estimate), yielding an average compressional wave velocity of 7.96 km/s and an average density of 3.30 g/cm^3.

Southern Platform

The path NAT-LPB essentially bisects the South American platform from east to west, extending 3,818 kilometers from Natal, Brazil, to La Paz, Bolivia. The path crosses all of central Brazil and nearly all of central Bolivia. Over its length, the path NAT-LPB crosses the northern Atlantic shield, the southern end of the Parnaiba basin, the entire length of the south-central Central Brazilian shield, a narrow segment of the foreland basin separating the shield from the Andean cordillera, and the thrust belt of the Eastern cordillera of Bolivia. Overall, this path represents a nearly pure shield path.

The shear wave velocity-depth model computed for this path was based on inverting both group and phase velocity dispersion data for three events. Only two sets of phase

velocity data were used because the third set (event NLB5) was consistently and anomalously high. No explanation could be found for these high values. The optimum model suggests a crustal thickness of 42 ± 4 kilometers, based on the position of a sharp increase in shear velocity (Fig. 49); this pick is enforced by the more reasonable of the two edge models associated with the fifth model eigenvector. The average crustal shear velocity ranges from 3.76 to 3.82 km/s, which corresponds to an average compressional wave velocity range of 6.51 to 6.62 km/s and an average density range of 2.85 to 2.88 g/cm^3. The velocity distribution with depth in the upper mantle shown by this model is very irregular (displaying the high/low pattern mentioned earlier), but the averaged mantle shear velocity, which is 4.59 km/s, is reasonable. This corresponds to an average compressional wave velocity of 7.96 km/s and an average density of 3.30 g/cm^3.

The path BDF-LPB, extending 2,160 kilometers from Brasilia, Brazil, to La Paz, Bolivia, crosses a portion of central Brazil and most of central Bolivia. This path crosses the length of the southernmost side of the Central Brazilian shield, a narrow segment of the foreland basin separating the shield from the Andean cordillera, and the thrust belt of the Eastern cordillera of Bolivia. The larger part of this path lies over the shield.

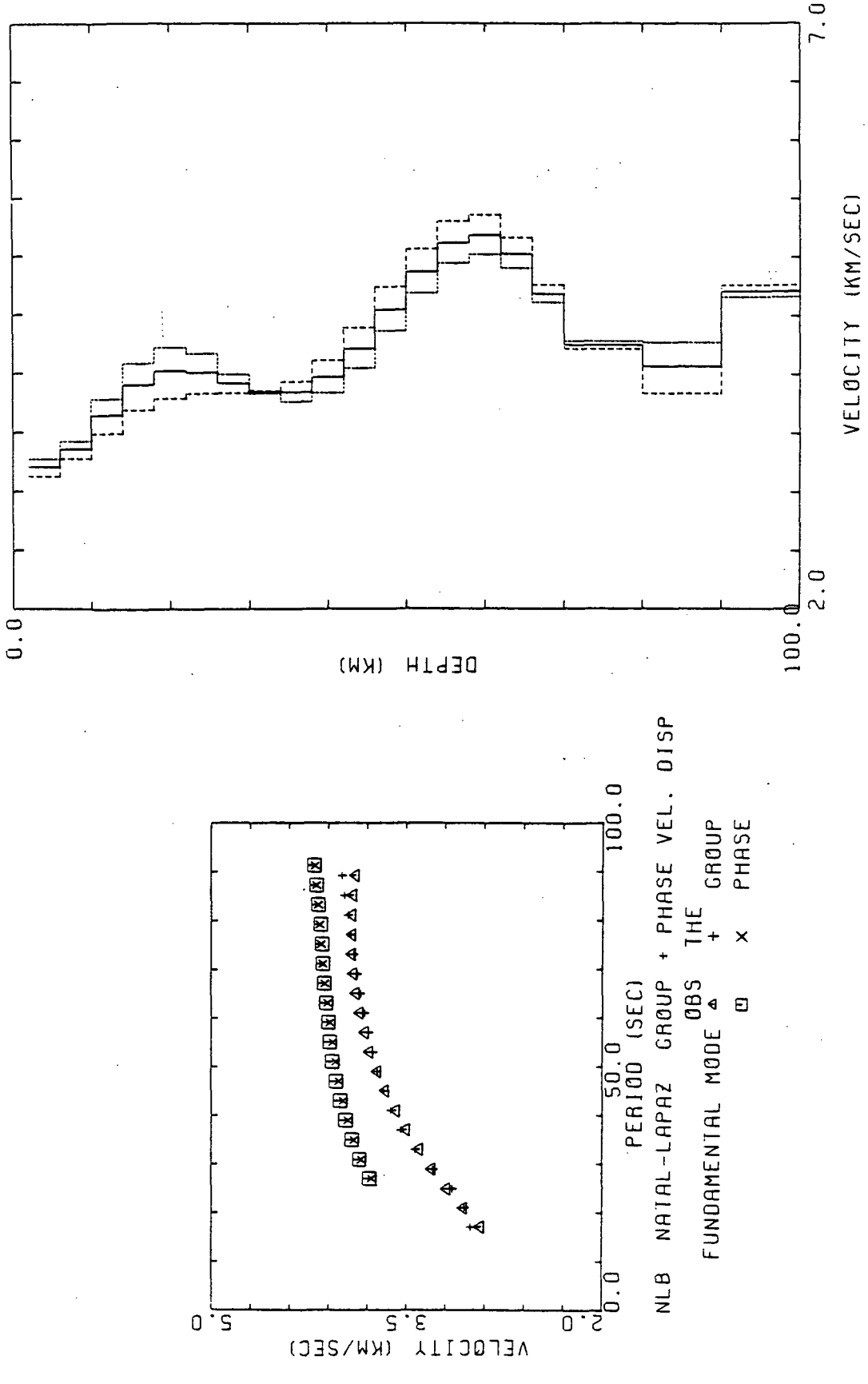

Figure 49. Inversion results for the path NAT-LPB.

The shear wave velocity-depth model computed for this path, based on inverting both group and phase velocity dispersion data for one event, suggests a crustal thickness of 44 ± 4 kilometers (Fig. 50). The velocity gradient of the optimum model shows no dramatic changes to a depth of around 60 kilometers, and the position of the M-discontinuity is hard to estimate. The pick is based on a vague increase in the shear velocity gradient; the edge models provide little support. Assuming the crust-mantle transition does occur at around 44 kilometers depth, the average crustal shear wave velocity ranges from 3.65 to 3.78 km/s, which corresponds to an average compressional wave velocity range of 6.33 to 6.55 km/s and an average density range of 2.82 to 2.88 g/cm^3. The average upper mantle shear velocity, down to a depth of 100 kilometers, is 4.50 km/s. This corresponds to an average compressional wave velocity of 7.78 km/s, and an average density of 3.24 g/cm^3.

The path NAT-LPA extends 4,051 kilometers from Natal, Brazil to La Plata, Argentina, parallel to the entire southeastern coast of Brazil. The path also crosses central Paraguay. The path NAT-LPA crosses the entire length of the Atlantic shield, cutting the Sao Francisco craton, the southeastern side of the Parana basin, and the Rio de la Plata craton.

The shear wave velocity-depth model computed for this path was based on inverting both group and phase velocity

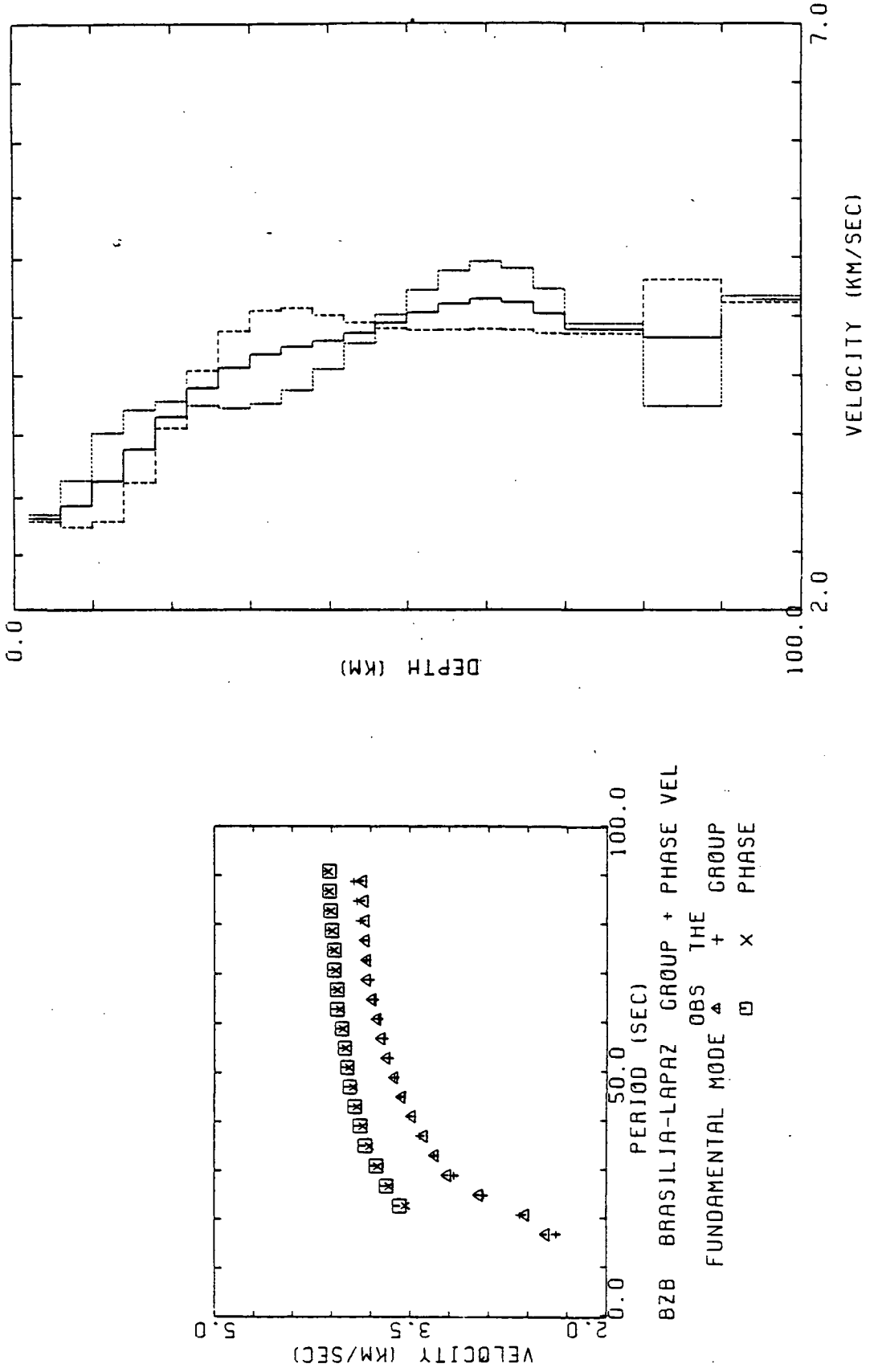

Figure 50. Inversion results for the path BDF-LPB.

dispersion data for three events. Two of these events occurred beneath the southern Central Andes and arrived at the two stations from the southwest, after traversing purely continental paths (LPA-NAT); one event occurred along the Mid-Atlantic ridge and arrived at the stations from the northeast, after traversing oceanic and mixed paths, respectively (NAT-LPA). These two cases were also inverted separately to check for possible differences. The model for NAT-LPA (Fig. 51) suggests a crustal thickness of 38 ± 4 kilometers, which is slightly thinner than the crustal thickness of 42 ± 4 kilometers suggested by the model for LPA-NAT (Fig. 52). The optimum LPA-NAT model also displays a more reasonable distribution of shear velocity with depth in the crust (and to a lesser extent in the mantle) than does the optimum NAT-LPA model. Long-period group and phase velocities are both slightly higher over the path NAT-LPA. However, it is important to remember that only one event provides the data for the path NAT-LPA, while the data for LPA-NAT is based on two events. Figure 27 shows the smoothing effect which fitting the observed dispersion curves to two events has had, particularly with the shorter period group velocities (which would otherwise show two fairly sharp breaks at around 15 and 25 seconds). Because of the differences in the amount and ranges of data for the north-south and south-north traverses, it is impossible to

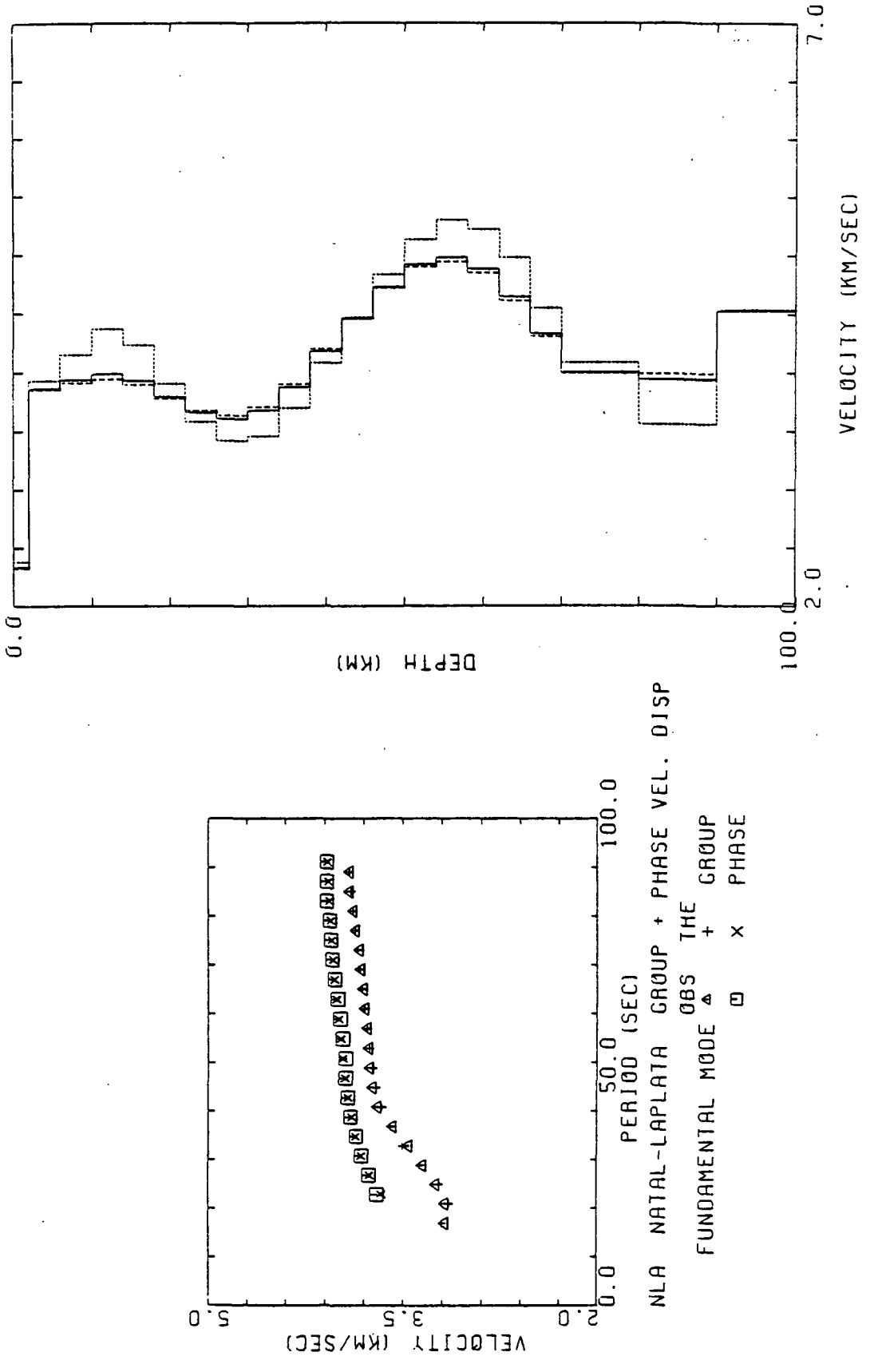

Figure 51. Inversion results for the path NAT-LPA.

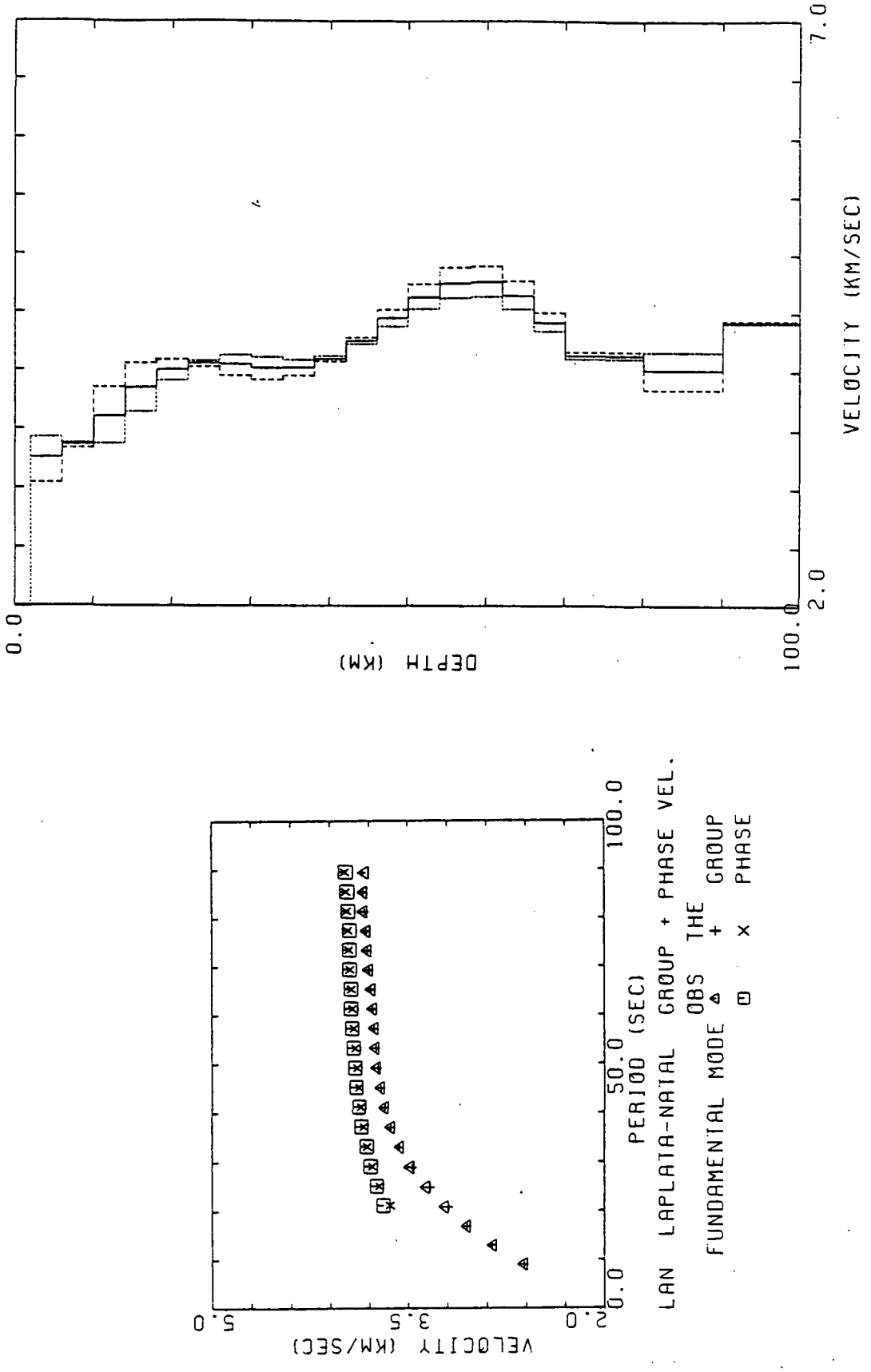

Figure 52. Inversion results for the path LPA-NAT.

determine whether problems with lateral refraction have occurred at the continental crust/oceanic crust interface.

The combined optimum model (Fig. 53) suggests a crustal thickness of 42 ± 4 kilometers. This pick is based on the position of a distinct increase in shear velocity, following a roughly 16-kilometer-thick zone of nearly constant velocity. This pick is supported by the edge models associated with the sixth model eigenvector, which reflect this zone of change. The average crustal shear wave velocity ranges from 3.83 to 3.90 km/s, which corresponds to an average compressional wave velocity range of 6.64 to 6.76 km/s and an average density range of 2.88 to 2.92 g/cm^3. The upper mantle shear wave velocity distribution with depth is irregular, displaying the same rapid increase, then rapid decrease pattern over 40 to 90 kilometers depth that the NAT-LPB model displays. The average shear wave velocity from the M-discontinuity down to 100 kilometers is 4.40 km/s, which corresponds to an average compressional wave velocity of 7.63 km/s and an average density of 3.19 g/cm^3

Central Platform

The path CAR-LPA, which extends 5,111 kilometers from Caracas, Venezuela, to La Plata, Argentina, crosses central Venezuela, western Brazil, eastern Bolivia, eastern Paraguay, and northern Argentina. Along its length, the path crosses the foreland basin of northwestern Venezuela, the western lobe of the Guyana shield, the wide western end

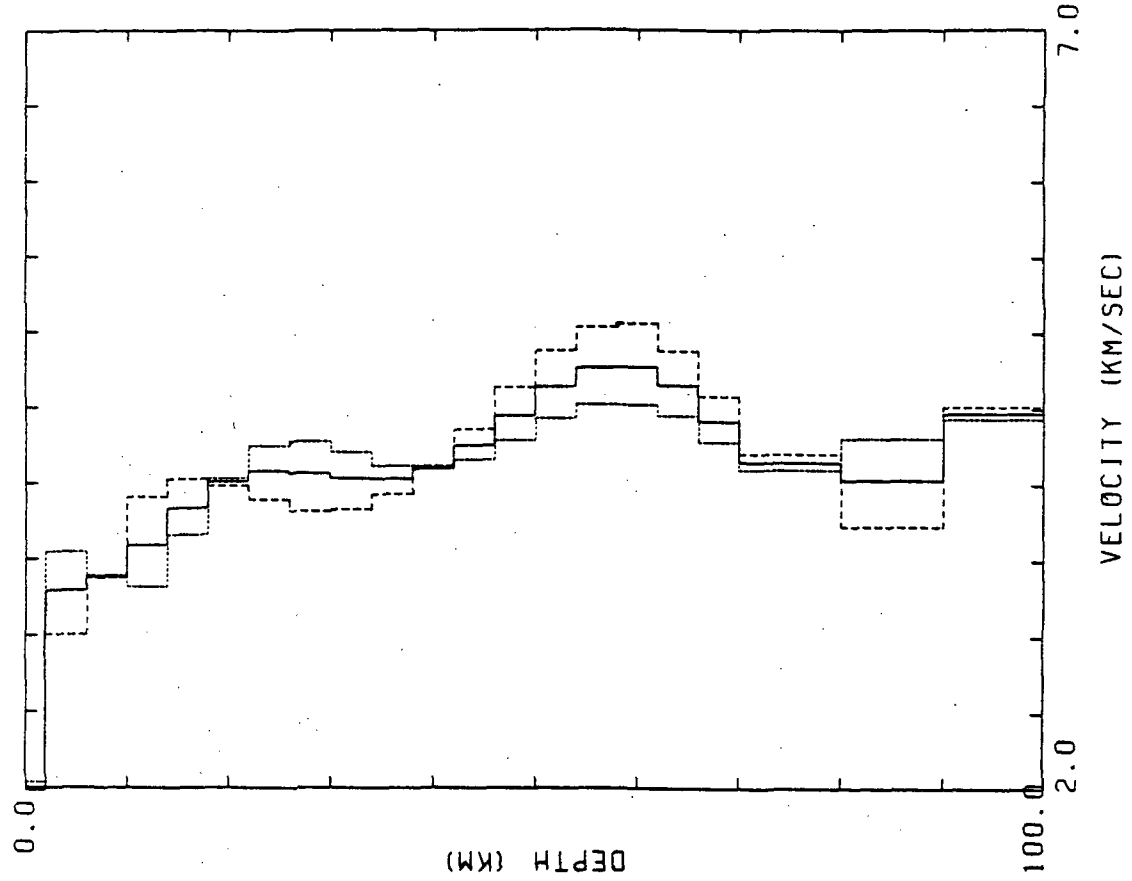

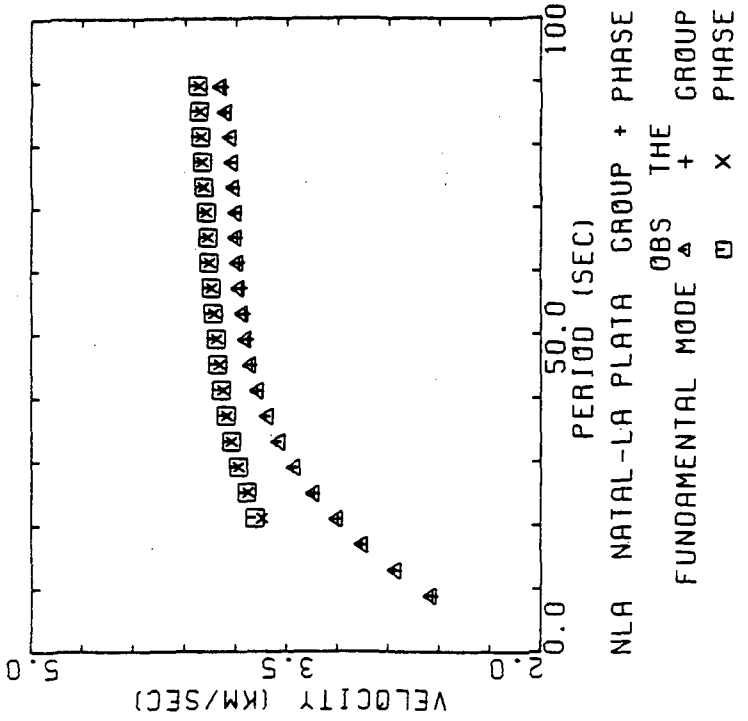

Figure 53. Combined inversion results for paths NAT-LPA and LPA-NAT.

of the Amazon basin, the western side of the Central Brazilian shield, and the entire north-south length of the Chaco basin.

The shear wave velocity-depth model computed for the path CAR-LPA, based on the inversion of both group and phase velocity dispersion data for one event, suggests a crustal thickness of 42 ± 4 kilometers (Fig. 54). This is almost the only useful piece of information this particular model provides. The group velocity dispersion curve displays a range of unusually high values across periods 50 to 70 seconds. In addition, the inversion routine was unable to fit the short period "tail" of the group velocity dispersion curve (Fig. 54). The optimum model displays a prominent (and unlikely) low velocity zone in the lower crust; the model also displays an exaggerated high velocity zone (greatest at 60 kilometers depth) followed by a low velocity zone (greatest at 85 kilometers depth) in the upper mantle. The average crustal shear wave velocity, computed from the optimum model, ranges from 3.76 to 3.80 km/s. This corresponds to an average compressional wave velocity range of 6.52 to 6.58 km/s, and an average density range of 2.85 to 2.87 g/cm^3. The average upper mantle seismic velocities and density were not computed.

The path TRN-LPA, extending from the island of Trinidad to La Plata, Argentina, crosses extreme eastern Venezuela, west-central Brazil, central Paraguay, and

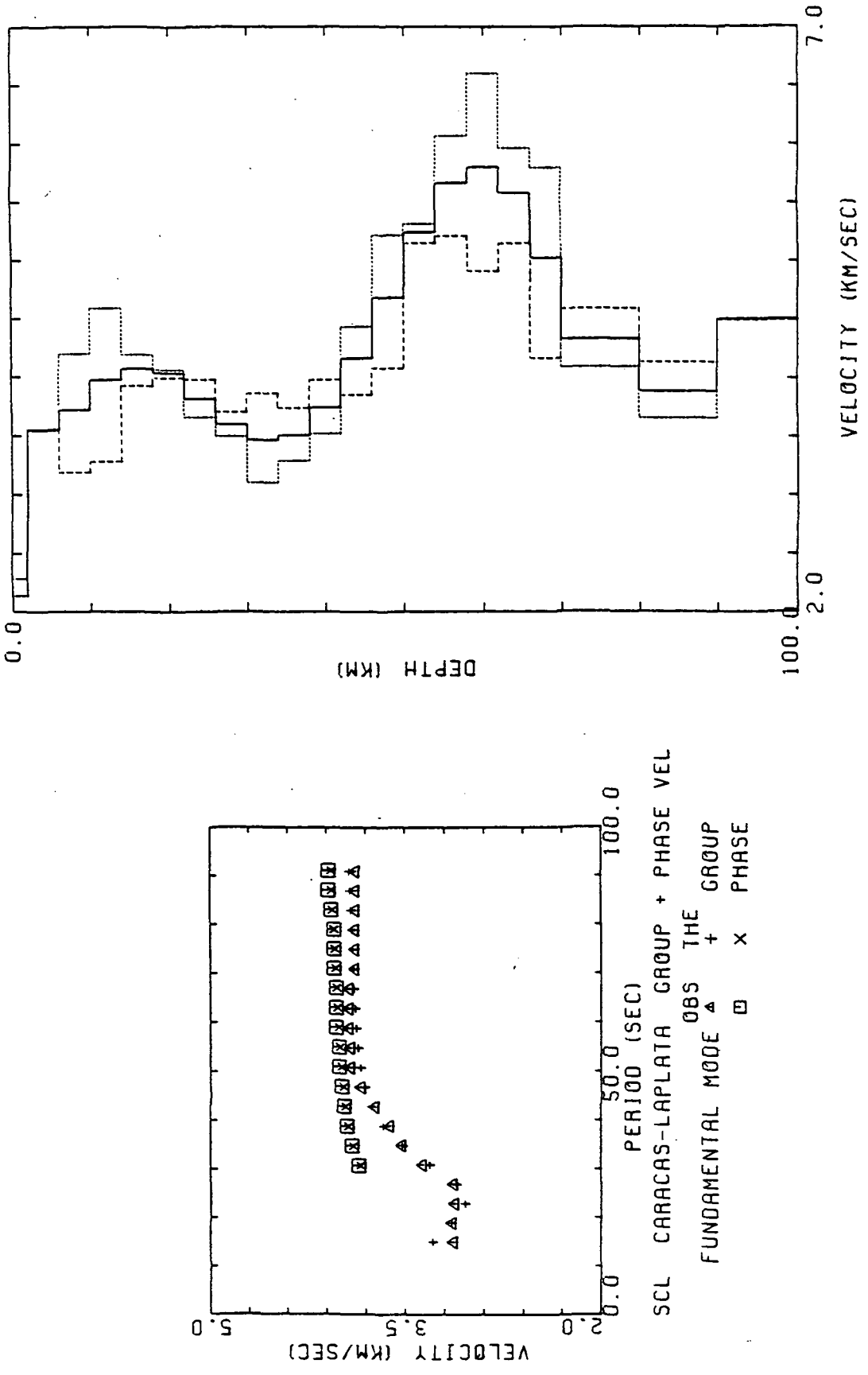

Figure 54. Inversion results for the path CAR-LPA.

northwestern Argentina. Along its length, the path TRN-LPA crosses the central Guyana shield, the central Amazon basin, the west-central Central Brazilian shield, and the Chaco basin. Like the path CAR-LPA, this path represents a long, average South American platform path.

The shear wave velocity-depth model, which was computed from phase velocity dispersion data measured by Sherburne (1974) for two events, suggests a crustal thickness of 42 ± 4 kilometers (Fig. 55). The optimum model shows a zone of increasing shear velocity at this depth, following a relatively thick zone (35 kilometers) of nearly constant shear wave velocity in the crust. One of the edge models associated with the fourth eigenvector vaguely supports this pick, but the transition is not very well defined. The average crustal shear wave velocity range given by the optimum model is 3.90 to 3.92 km/s, which corresponds to an average compressional velocity range of 6.75 to 6.79 km/s and an average density range of 2.91 to 2.92 g/cm^3. The average upper mantle shear wave velocity down to a depth of 100 kilometers is 4.43 km/s. This corresponds to an average compressional wave velocity of 7.68 km/s and an average mantle density of 3.20 g/cm^3.

The path TRN-RDJ, which extends from the island of Trinidad to Rio de Janeiro, Brazil, cuts across Guyana and all of central Brazil. Along its length, this path crosses the eastern lobe of the Guyana shield, the eastern Amazon

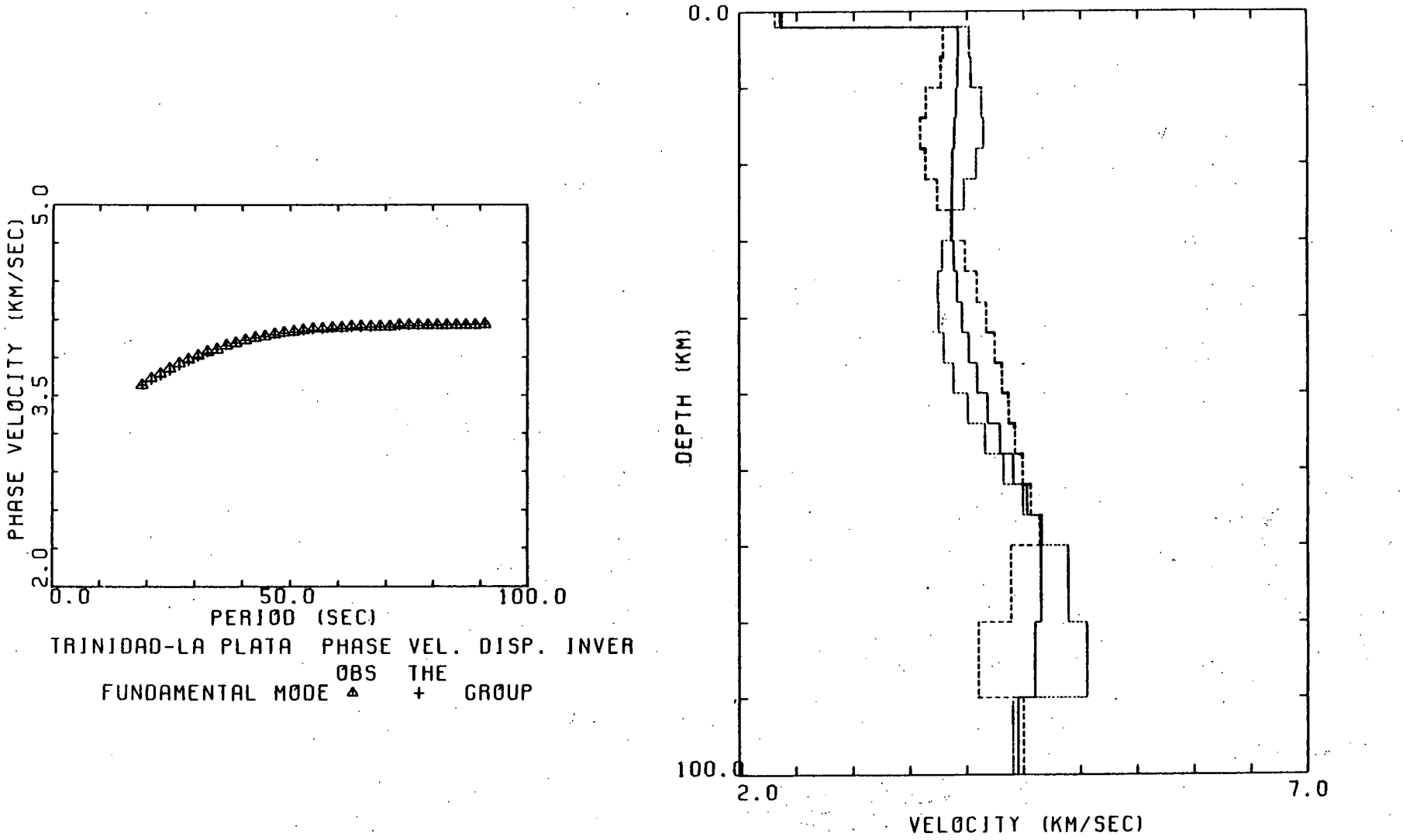

Figure 55. Inversion results for the path TRN-LPA using data from Sherburne (1974).

basin, the eastern Central Brazilian shield, and the central Atlantic shield. This path crosses almost pure shield structures.

The shear wave velocity-depth model computed for this path, based on inverting phase velocity dispersion data measured by Sherburne (1974) for one event, suggests a crustal thickness of 42 ± 4 kilometers (Fig. 56). The phase velocity dispersion measurements start at a period of 31 seconds, however, and the crust-mantle transition is hard to define. The optimum model shows a zone of increasing shear velocity at this depth, following a relatively thick zone (35 kilometers) of constant to slightly decreasing shear velocity. The overall distribution of shear velocity with depth is very similar to the path TRN-LPA discussed previously, although the average crustal shear velocity is somewhat higher. (Since the phase velocity measurements inverted to obtain the model TRN-RDJ start at a period of 31 seconds, this average is probably not well determined.) The average crustal shear wave velocity ranges around 3.99 km/s; this corresponds to an average compressional wave velocity range of 6.90 to 6.92 km/s and an average density of 2.96 g/cm^3. The average upper mantle shear wave velocity, down to a depth of 100 kilometers, is 4.48 km/s. This corresponds to an average compressional wave velocity of 7.77 km/s, and an average density of 3.23 g/cm^3.

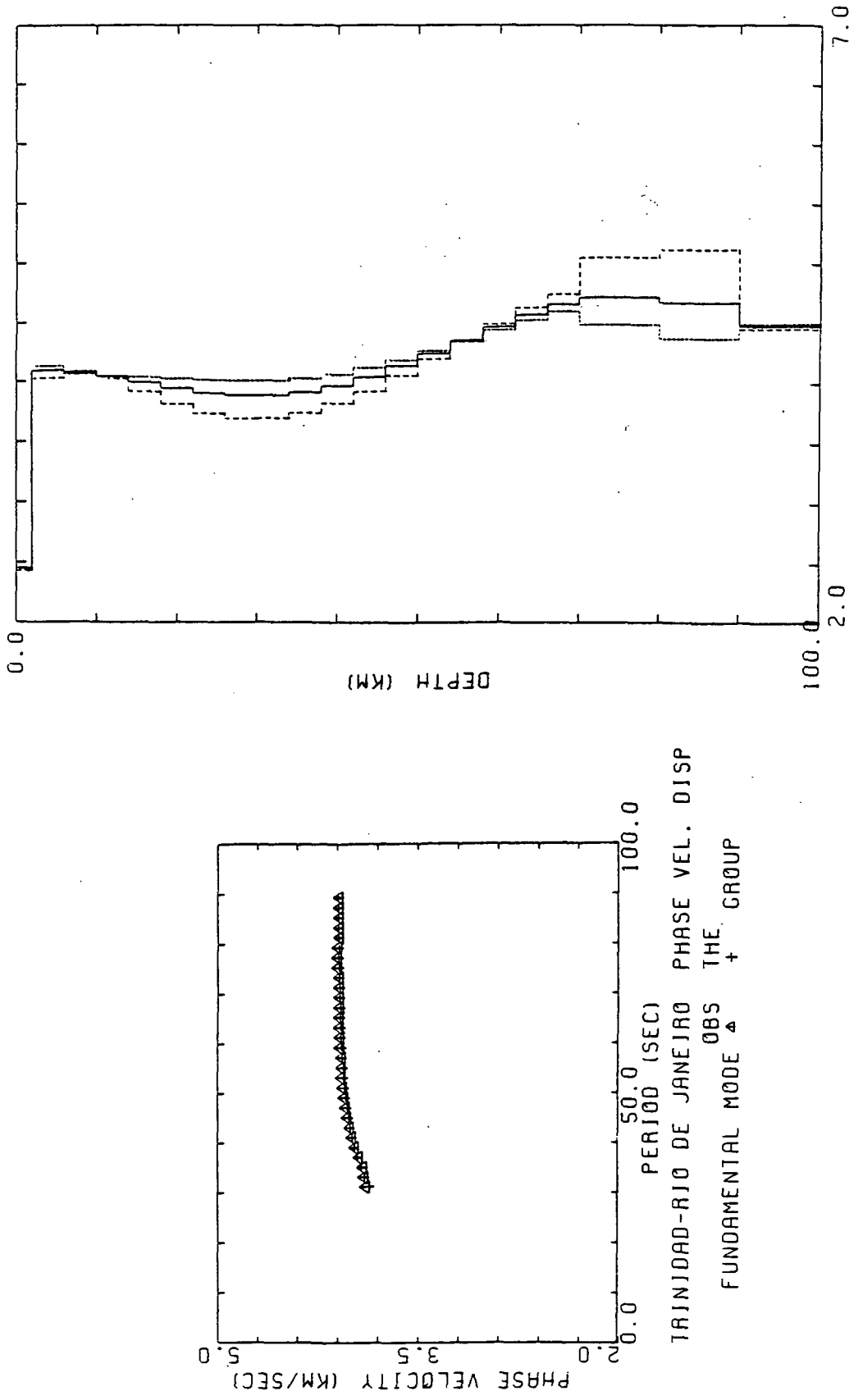

Figure 56. Inversion results for the path TRN-RDJ using data from Sherburne (1974).

Northwestern Platform

The path CAR-QUI, unlike the other paths investigated in this study, is primarily a sub-Andean to Andean path. It extends 1,742 kilometers from Caracas, Venezuela, to Quito, Ecuador, crossing northwestern Venezuela, central to southwestern Colombia, and northern Ecuador. This path crosses the foreland basins of northwestern Venezuela and northern Colombia, and cuts obliquely into the Eastern cordillera of Colombia and the Central cordillera of Ecuador.

The shear wave velocity-depth model computed for this path, based on inverting both group and phase velocity dispersion data for one event, suggests a crustal thickness of 48 ± 4 kilometers (Fig. 57). The optimum model shows a distinct increase in shear velocity at this depth. Both the optimum model and the associated edge models show an irregular and unlikely velocity distribution with depth, particularly in the upper mantle. In addition, the phase velocity dispersion predicted by the model does not match the observed phase velocity dispersion data very well at periods between 20 and 50 seconds. The average crustal shear wave velocity computed from the optimum model ranges from 3.54 to 3.76 km/s, which corresponds to an average compressional wave velocity range of 6.14 to 6.36 km/s and an average density range of 2.77 to 2.83 g/cm^3. The average shear wave velocity from the chosen M-discontinuity down to

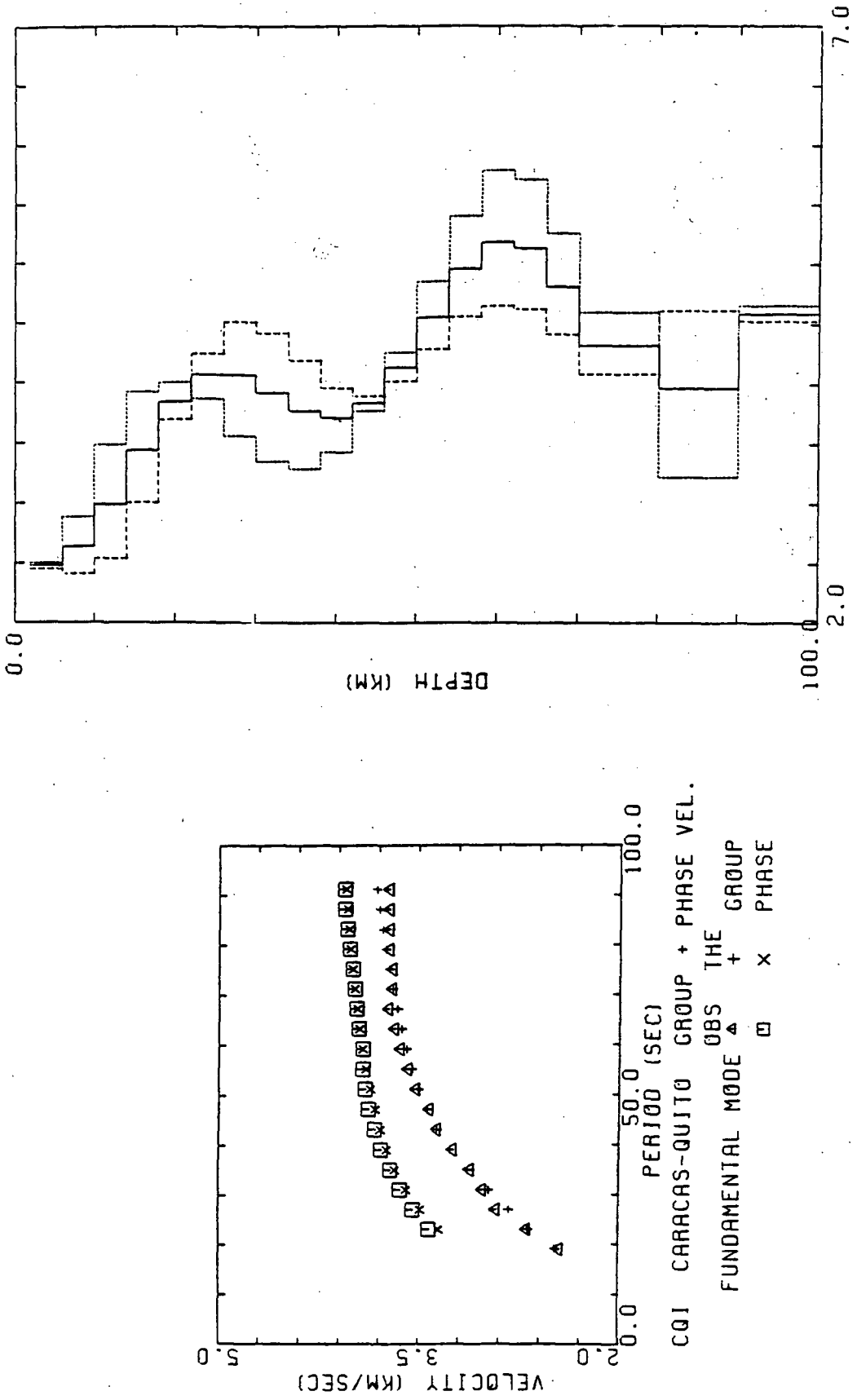

Figure 57. Inversion results for the path CAR-QUI.

100 kilometers is 4.56 km/s which corresponds to an average comrpessional wave velocity of 7.87 km/s and an average density of 3.28 g/cm^3.

The path CAR-ARE extends from Caracas, Venezuela, to Arequipa, Peru, crossing central Venezuela, eastern Colombia, westernmost Brazil, and nearly all of southern Peru. Over its length, this path crosses the foreland basin/platform cover of northern Venezuela, the westernmost lobe of the Guyana shield, the extensive platform cover that merges with the western end of the Amazon basin in western Brazil (the transition zone), and nearly the entire Andean cordillera of southern Peru.

The shear wave velocity-depth model computed for this path, based on inverting phase velocity dispersion data measured by Sherburne (1974) for one event, suggests a crustal thickness of 34 ± 4 kilometers. The optimum model shows a zone of increasing shear velocity at this depth, beneath a nearly 30-kilometer thick zone of almost constant shear velocity. This transition is roughly bracketed by the edge models associated with the fourth model eigenvector. The average crustal shear wave velocity ranges from 3.87 to 3.90 km/s, which corresponds to an average compressional wave velocity range of 6.71 to 6.75 km/s and an average density range of 2.90 to 2.91 g/cm^3. The upper mantle velocity-depth model shows the beginning of a pronounced low velocity zone below 80 kilometers, but as with the other

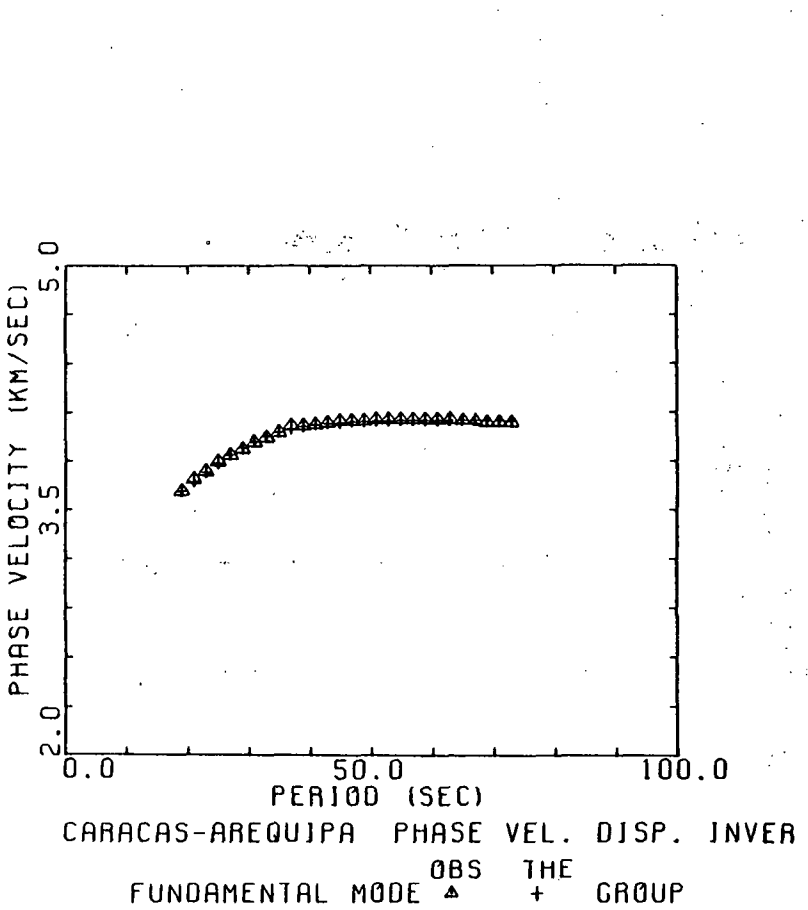

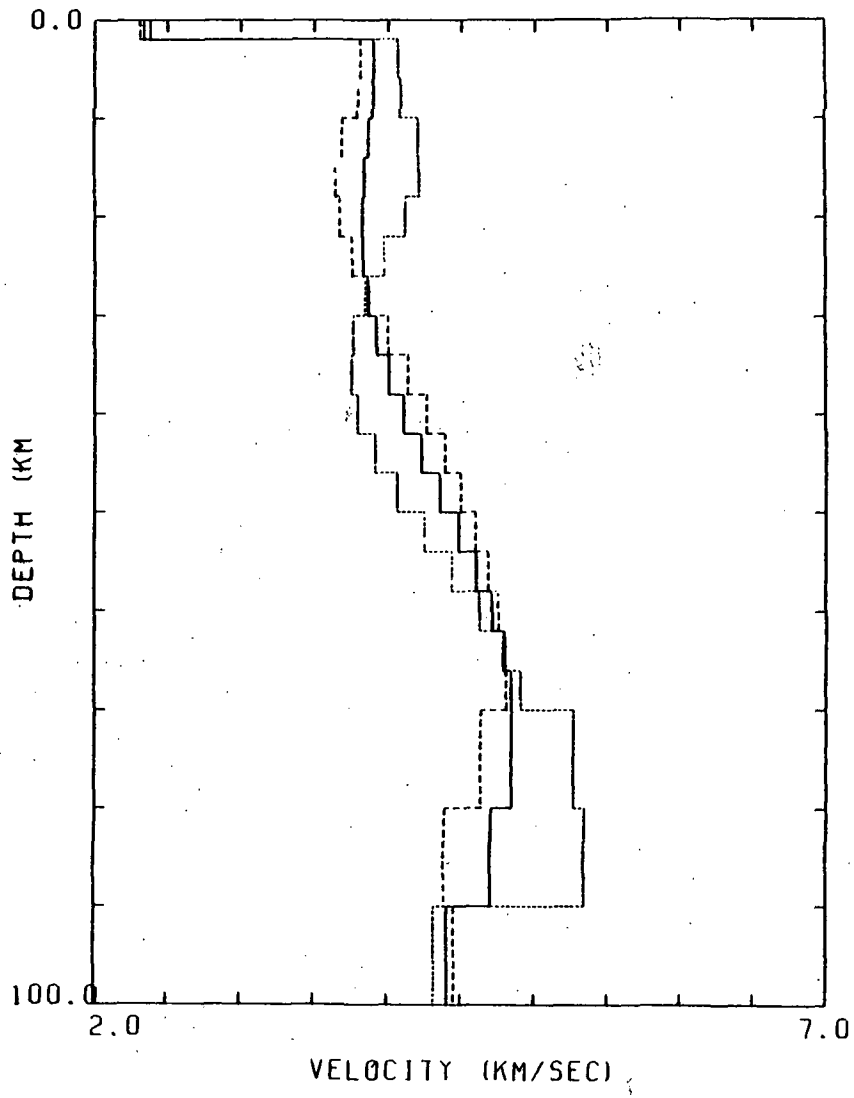

Figure 58. Inversion results for the path CAR-ARE using data from Sherburne (1974).

models derived in this study, the reality of the zone is questionable. The average upper mantle shear wave velocity to a depth of 100 kilometers is 4.57 km/s. This corresponds to an average compressional wave velocity of 7.87 km/s, and an average density of 3.27 g/cm^3.

The path TRN-LPB extends from the island of Trinidad to La Paz, Bolivia, intersecting easternmost Venezuela, western Brazil, and northwestern Bolivia. The path crosses the central part of the Guyana shield (in the western lobe), the western Amazon basin, and the platform cover, foreland basin, and Eastern cordillera of northwestern Bolivia.

The shear wave velocity-depth model representing this path was obtained by inverting the phase velocity dispersion data measured by Sherburne (1974) for one event (Fig. 59). The range of periods only extends to 71 seconds. The optimum model, which shows a broad zone of increasing shear velocity separating an upper and lower region of nearly constant shear velocity, suggests a crustal thickness of 38 ± 4 kilometers. This pick is roughly bracketed by the edge models associated with the fourth model eigenvector. The average crustal shear velocity ranges from 3.72 to 3.80 km/s, which corresponds to an average compressional wave velocity range of 6.45 to 6.59 km/s and an average density range of 2.83 to 2.87 g/cm^3. The upper mantle velocity, averaged from the chosen M-discontinuity to a depth of 100 kilometers, is 4.53 km/s. This corresponds to an average

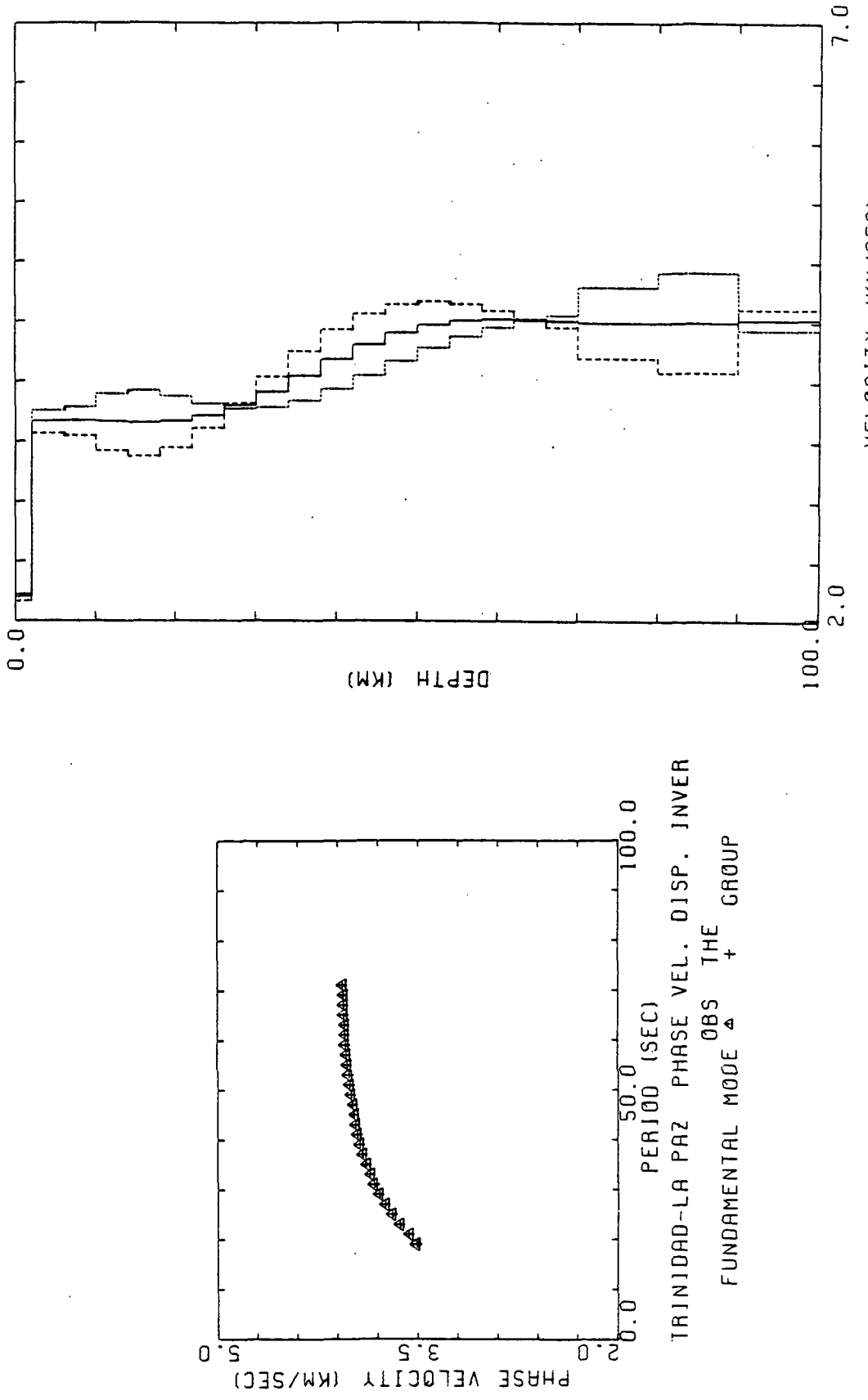

Figure 59. Inversion results for the path TRN-LPA using data from Sherburne (1974).

compressional wave velocity of 7.73 km/s, and an average density of 3.22 g/cm^3.

The path CAR-LPB extends 2,990 kilometers from Caracas, Venezuela, to La Paz, Bolivia, crossing central Venezuela, western Brazil, and northwestern Bolivia. This path crosses the foreland basin of northern Venezuela, the western lobe of the Guyana shield, the broad western end of the Amazon basin, the platform cover/foreland basin of western Brazil and northwestern Bolivia, and the Eastern cordillera of northwestern Bolivia.

Three shear wave velocity-depth models were computed for this line. One model was based on inverting both group and phase velocity dispersion data measured in this study for four events originating south of La Paz (Fig. 60). The second model was based on inverting only the phase velocity dispersion data of this same set (Fig. 61). The third model was based on inverting the phase velocity dispersion data measured by Sherburne (1974) for two events originating north of Caracas (Fig. 62).

The first model suggests a crustal thickness of 38 ± 4 kilometers. The optimum model, and both of the edge models associated with the fifth model eigenvector, show an extremely sharp increase in shear velocity across this depth range. Both the optimum model and the associated edge models show an irregular distribution of shear velocity with depth, particularly in the upper mantle, where there is a

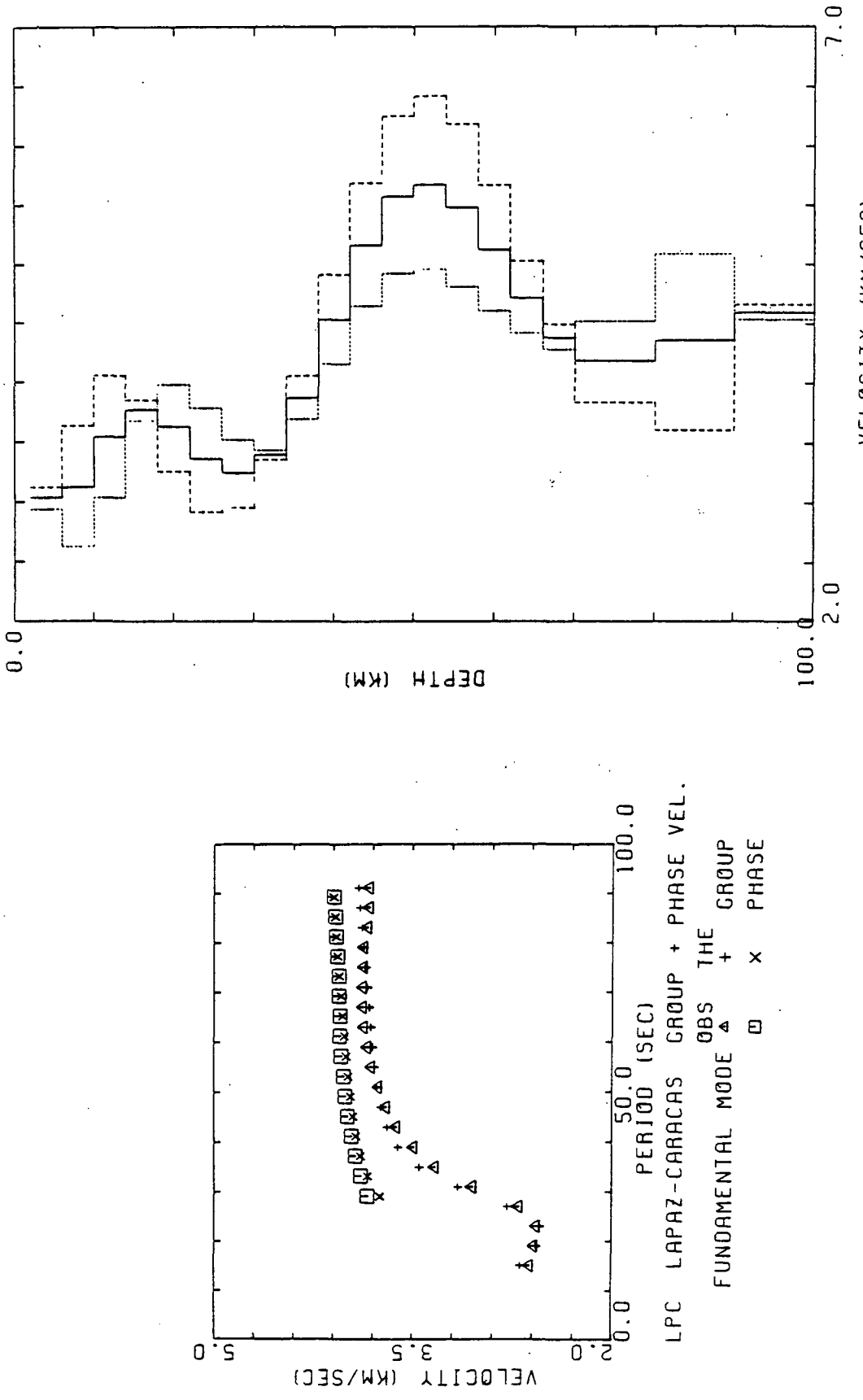

Figure 60. Inversion results for the path LPB-CAR.

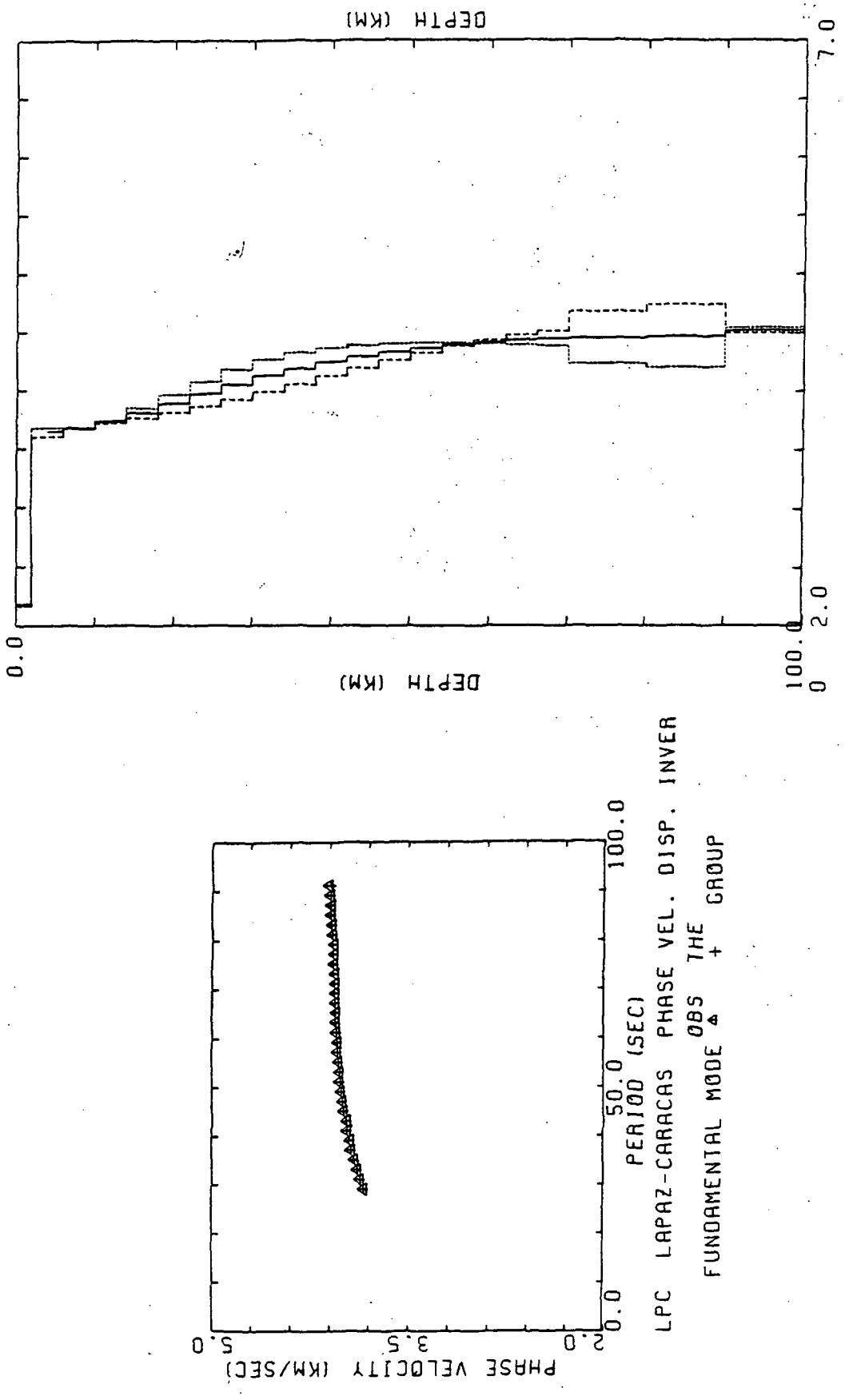

Figure 61. Inversion results for the path LPB-CAR using phase velocity data only.

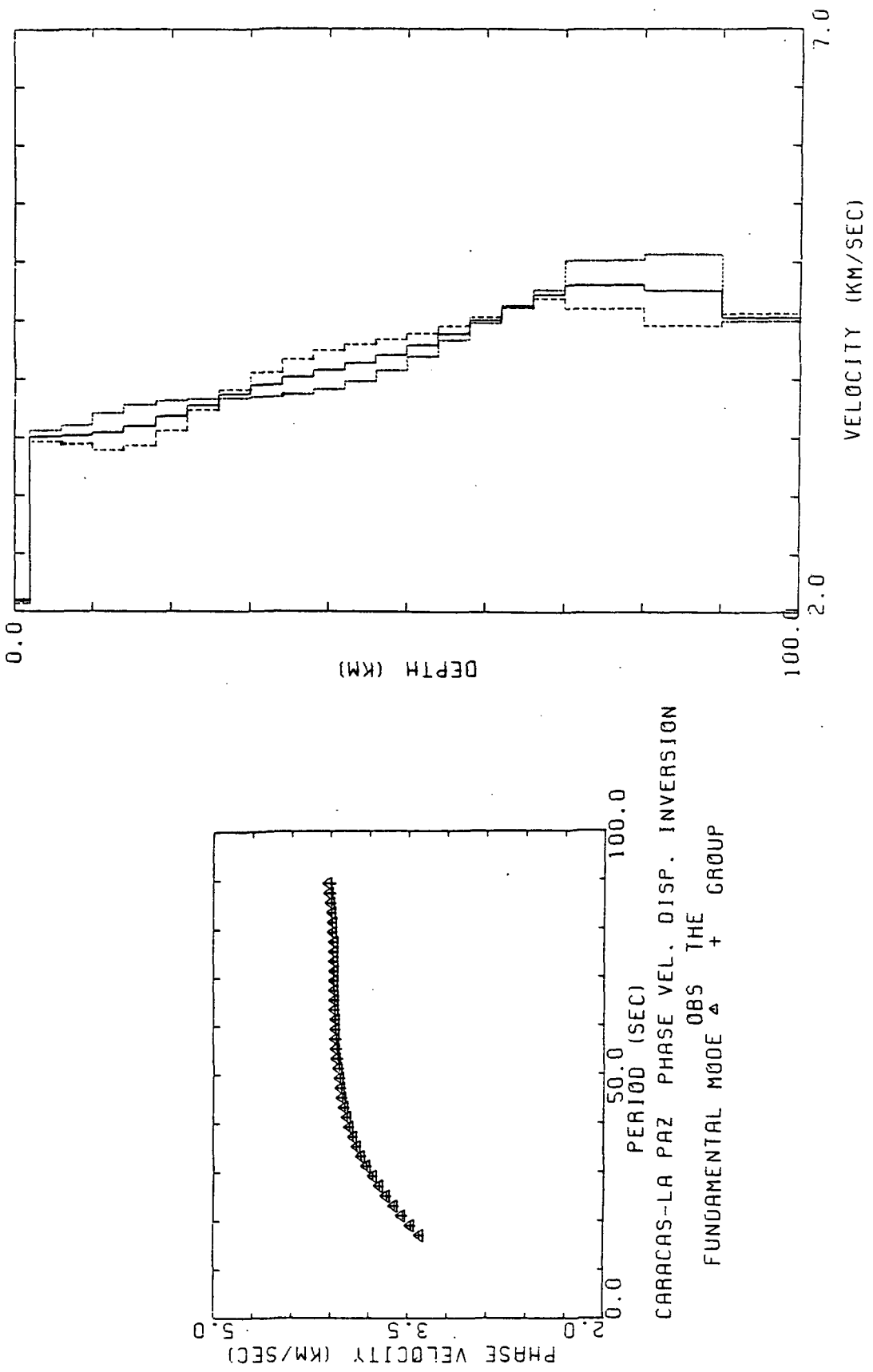

Figure 62. Inversion results for the path CAR-LPB.

zone of extremely high shear velocities centered at approximately 50 kilometers depth. There is also a low velocity zone between 70 and 90 kilometers depth. It should be noted that the group velocity curve inverted to obtain this model represents the mean of measurements from four events, rather than a third or fifth order least-squares fit (Fig. 36). None of the attempts to fit a least squares curve to the four sets of measurements led to a satisfactory represenation. The group velocity dispersion predicted by the model match the observed group velocity dispersion fairly well, but the match between the predicted phase velocity dispersion and the observed phase velocity dispersion is poor at periods less than 60 seconds.

The average crustal shear wave velocity, computed from the optimum model, ranges from 3.40 to 3.56 km/s. This corresponds to an average compressional wave velocity range of 5.88 to 6.16 km/s, and an average density range of 2.82 to 2.85 g/cm^3.

The second model (Fig. 61), which is the result of inverting only the phase velocity dispersion data of this set, is dramatically different from the first model. It is a much smoother model, showing a slightly increasing velocity gradient to a depth of approximately 28 kilometers, followed by a slightly decreasing velocity gradient to a depth of at least 100 kilometers. Although the phase velocity dispersion predicted by this model agrees extremely

well with the observed data, the range of data does not extend to periods shorter than 29 seconds, and it is almost impossible to see the crust-mantle transition in this model. If the transition depth chosen from the first model is assumed, the average shear wave velocity in the upper mantle is 4.52 km/s, which corresponds to an average compressional wave velocity of 7.83 km/s, and an average density of 3.25 km/s.

The phase velocity dispersion measured by Sherburne (1974) for the path CAR-LPB covers a slightly greater period range than the phase velocity dispersion measured in this study, starting at a period of 17 seconds rather than 29 seconds. The shear wave velocity-depth model computed from Sherburne's data (Fig. 62) shows somewhat more variability than the second model described above, but the transition from crust to mantle is still hard to define. The optimum model vaguely suggests a crustal thickness of 38 ± 4 kilometers, a pick which is supported by one of the edge models associated with the fourth model eigenvector. The average crustal shear velocity ranges from 3.70 to 3.77 km/s. This corresponds to an average compressional wave velocity range of 6.41 to 6.54 km/s and an average density of 2.82 to 2.85 g/cm^3. The average upper mantle shear wave velocity from the optimum model is 4.51 km/s, which corresponds to an average compressional wave velocity of 7.82 km/s and an average density of 3.25 g/cm^3. These three

values are nearly identical to the average upper mantle velocities and density obtained by inverting the phase velocity dispersion data measured in this study.

Table 3 summarizes the crustal thicknesses, average crustal seismic velocities and densities, and average upper mantle seismic velocities and densities obtained for each two-station path described in this section. The final model parameters generated by each inversion (corresponding to the shear wave velocity-depth models of Figures 45-62) are listed in Appendix C.

The average crustal parameters obtained by analyzing and interpreting Rayleigh wave dispersion observations across the South American platform are meant to form an addition (admittedly a very generalized addition) to the better known crustal parameters of the northern and central Andean cordillera. A preliminary crustal structure map of continental South America, constructed by integrating the crustal models of the South American platform obtained in this study with the crustal structure models of the Andean cordillera reported in the literature, is shown in Figure 63.

Table 3

Summary of Earth Models Obtained from Inversion Results

Natal-Caracas

Crustal thickness 38 ± 4 km

	S-Velocity (km/s)	P-Velocity (km/s)	Density (g/cm^3)
Crust	3.85	6.66	2.88
Upper Mantle	-	-	-

Natal-Bogota

Crustal thickness 46 ± 4 km

	S-Velocity (km/s)	P-Velocity (km/s)	Density (g/cm^3)
Crust	3.87	6.71	2.91
Upper Mantle	4.60	7.97	3.30

Natal-Quito

Crustal thickness 50 ± 4 km

	S-Velocity (km/s)	P-Velocity (km/s)	Density (g/cm^3)
Crust	3.86	6.68	2.92
Upper Mantle	4.64	8.04	3.32

Natal-Quito (Sherburne)

Crustal thickness 46 ± 4 km

	S-Velocity (km/s)	P-Velocity (km/s)	Density (g/cm^3)
Crust	3.95	6.85	2.94
Upper Mantle	4.59	7.96	3.30

Table 3 (continued)

Natal-La Paz

Crustal thickness 42 ± 4 km

	S-Velocity (km/s)	P-Velocity (km/s)	Density (g/cm^3)
Crust	3.79	6.66	2.86
Upper Mantle	4.59	7.96	3.30

Brasilia-La Paz

Crustal thickness 44 ± 4 km

	S-Velocity (km/s)	P-Velocity (km/s)	Density (g/cm^3)
Crust	3.72	6.44	2.85
Upper Mantle	4.50	7.78	3.24

Natal-La Plata

Crustal thickness 42 ± 4 km

	S-Velocity (km/s)	P-Velocity (km/s)	Density (g/cm^3)
Crust	3.86	6.70	2.90
Upper Mantle	4.40	7.63	3.19

Caracas-La Plata

Crustal thickness 42 ± 4 km

	S-Velocity (km/s)	P-Velocity (km/s)	Density (g/cm^3)
Crust	3.78	6.55	2.86
Upper Mantle	-	-	-

Table 3 (continued)

Trinidad-La Plata (Sherburne)

Crustal thickness 42 ± 4 km

	S-Velocity (km/s)	P-Velocity (km/s)	Density (g/cm^3)
Crust	3.91	6.77	2.91
Upper Mantle	4.43	7.68	3.20

Trinidad-Rio de Janiero (Sherburne)

Crustal thickness 42 ± 4 km

	S-Velocity (km/s)	P-Velocity (km/s)	Density (g/cm^3)
Crust	3.99	6.91	2.96
Upper Mantle	4.48	7.77	3.23

Caracas-Quito

Crustal thickness 48 ± 4 km

	S-Velocity (km/s)	P-Velocity (km/s)	Density (g/cm^3)
Crust	3.65	6.25	2.80
Upper Mantle	4.56	7.87	3.28

Caracas-Arequipa (Sherburne)

Crustal thickness 34 ± 4 km

	S-Velocity (km/s)	P-Velocity (km/s)	Density (g/cm^3)
Crust	3.88	6.73	2.90
Upper Mantle	4.57	7.87	3.27

Table 3 (continued)

Trinidad-La Paz (Sherburne)

Crustal thickness 38 ± 4 km

	S-Velocity (km/s)	P-Velocity (km/s)	Density (g/cm^3)
Crust	3.76	6.52	2.85
Upper Mantle	4.53	7.83	3.25

Caracas-La Paz

Crustal thickness 38 ± 4 km

	S-Velocity (km/s)	P-Velocity (km/s)	Density (g/cm^3)
Crust	3.48	5.97	2.84
Upper Mantle	4.52	7.83	3.25

Caracas-La Paz (Sherburne)

Crustal thickness 38 ± 4 km

	S-Velocity (km/s)	P-Velocity (km/s)	Density (g/cm^3)
Crust	3.74	6.47	2.84
Upper Mantle	4.51	7.82	3.25

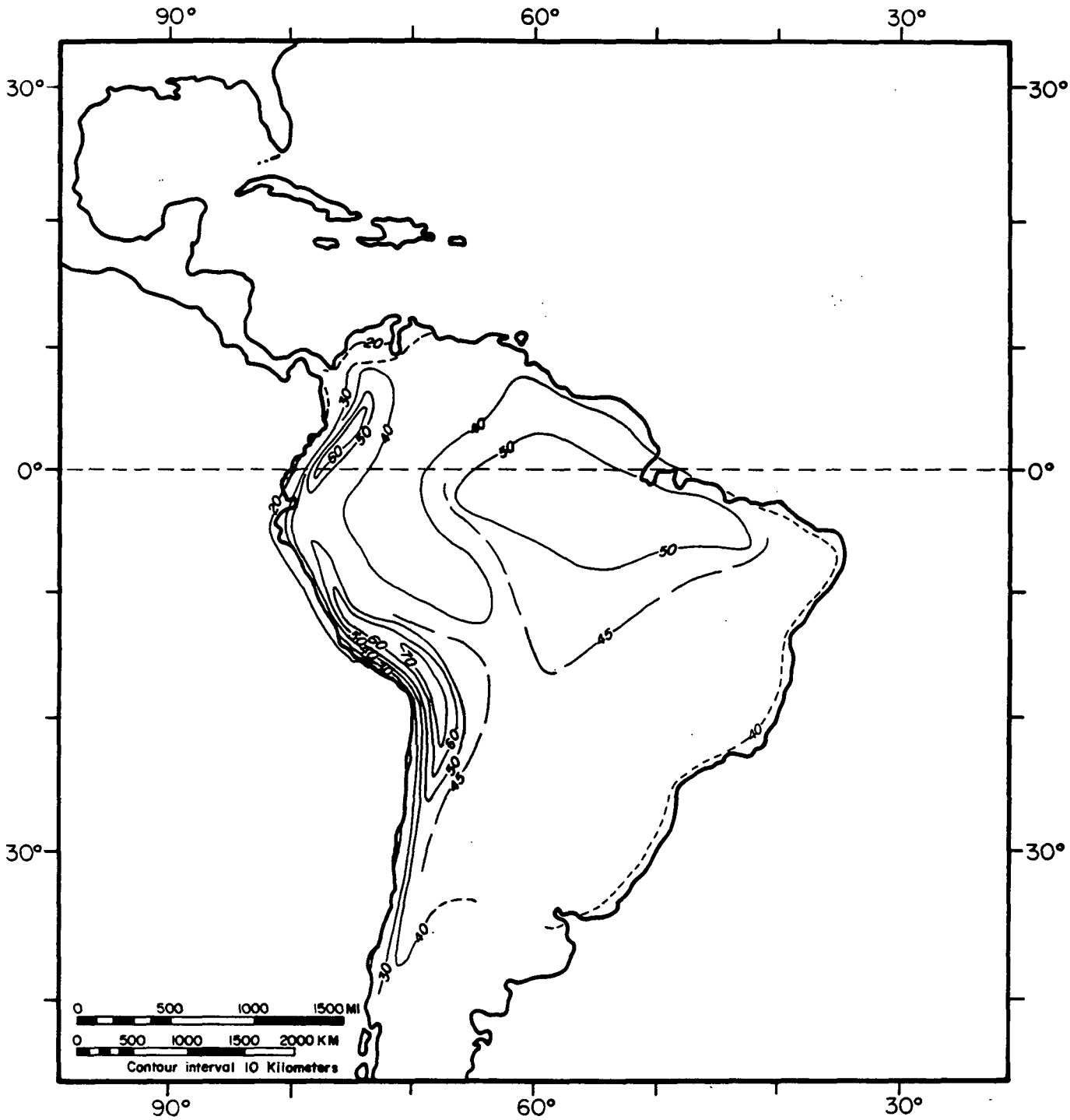

Figure 63. Contour map of crustal thickness values.

SOUTH AMERICAN MAGSAT PROJECT DATA

The only set of geophysical data that provides uniform coverage of the South American continent and surrounding oceanic areas are the satellite scalar magnetic anomaly data gathered during the recent MAGSAT mission (October 30, 1979 to June 11, 1980). In a study performed by the South American MAGSAT group (W. J. Hinze, R. R. B. von Frese, M. B. Longacre, L. W. Braile, E. G. Lidiak, and G. R. Keller) 2°-averaged magnetic anomaly values derived from the MAGSAT data set were compiled for the South American continent and surrounding oceanic areas. After removing the geomagnetic core field component from these data, the values were reduced to radial polarization (as sensed at 350 kilometer elevation) to allow a comparison with the major tectonic features of the continent (Longacre, 1981; Hinze et al., 1982). Figure 64 shows the projection of these magnetic anomaly data on the generalized tectonic map of South America. The investigation also spurred the compilation of a surface 1°-gridded free-air gravity anomaly map of the same region, using gravity data gathered from diverse sources. The continental gravity data in particular were obtained by digitizing the free-air gravity map of South America provided by the Defense Mapping Agency Aerospace Center (Longacre, 1981). It must be cautioned

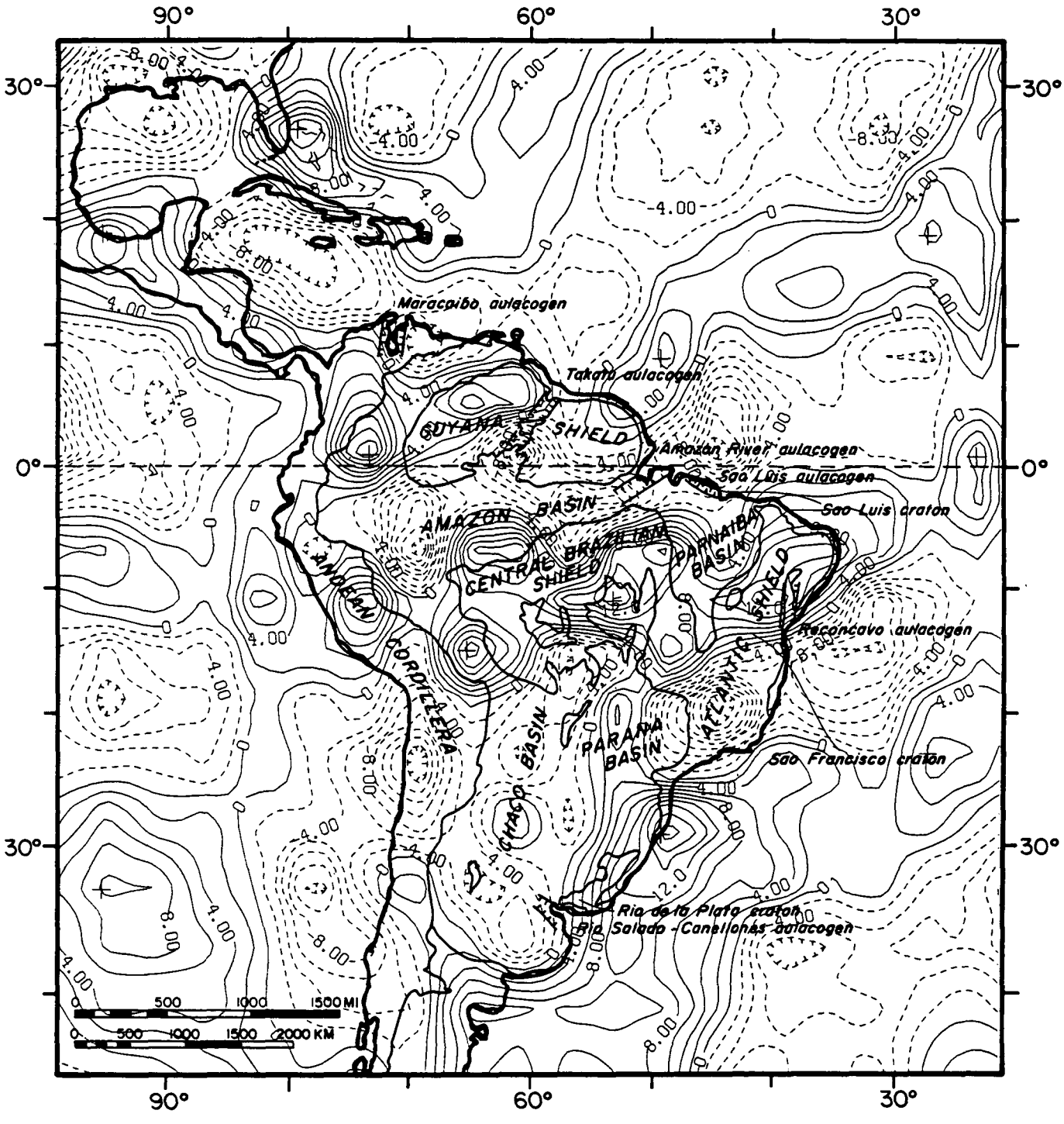

Figure 64. Equivalent point source field approximation of 2^0-averaged scalar MAGSAT magnetic anomaly data differentially reduced to radial polarization at 350 km elevation. Contour interval is 2nT. Modified from Hinze et al. (1982).

that predicted values are incorporated in the DMAAC map due to lack of gravity control over many areas of South America. These gravity data were long-wavelength-pass filtered (wavelengths greater than 8°) at the surface to enhance longer wavelength components, and then upward continued to satellite elevations in order to allow a comparison with the satellite magnetic anomalies (Longacre, 1981). Figure 65 shows the projection of the filtered (but not upward continued) gravity anomaly data on the generalized tectonic map of South America.

Many of the regional tectonic features of the South American continent show some degree of correlation with the long-wavelength potential field anomalies (Longacre, 1981; Yuan, 1983). A concise discussion of the extent to which these anomalies correspond to known tectonic features, together with some remarks on their geologic significance, may be found in Hinze et al. (1982). The primary purpose of constructing a crustal structure map of South America is to allow further comparisons to be made between the MAGSAT and gravity anomalies and the underlying structure of South America.

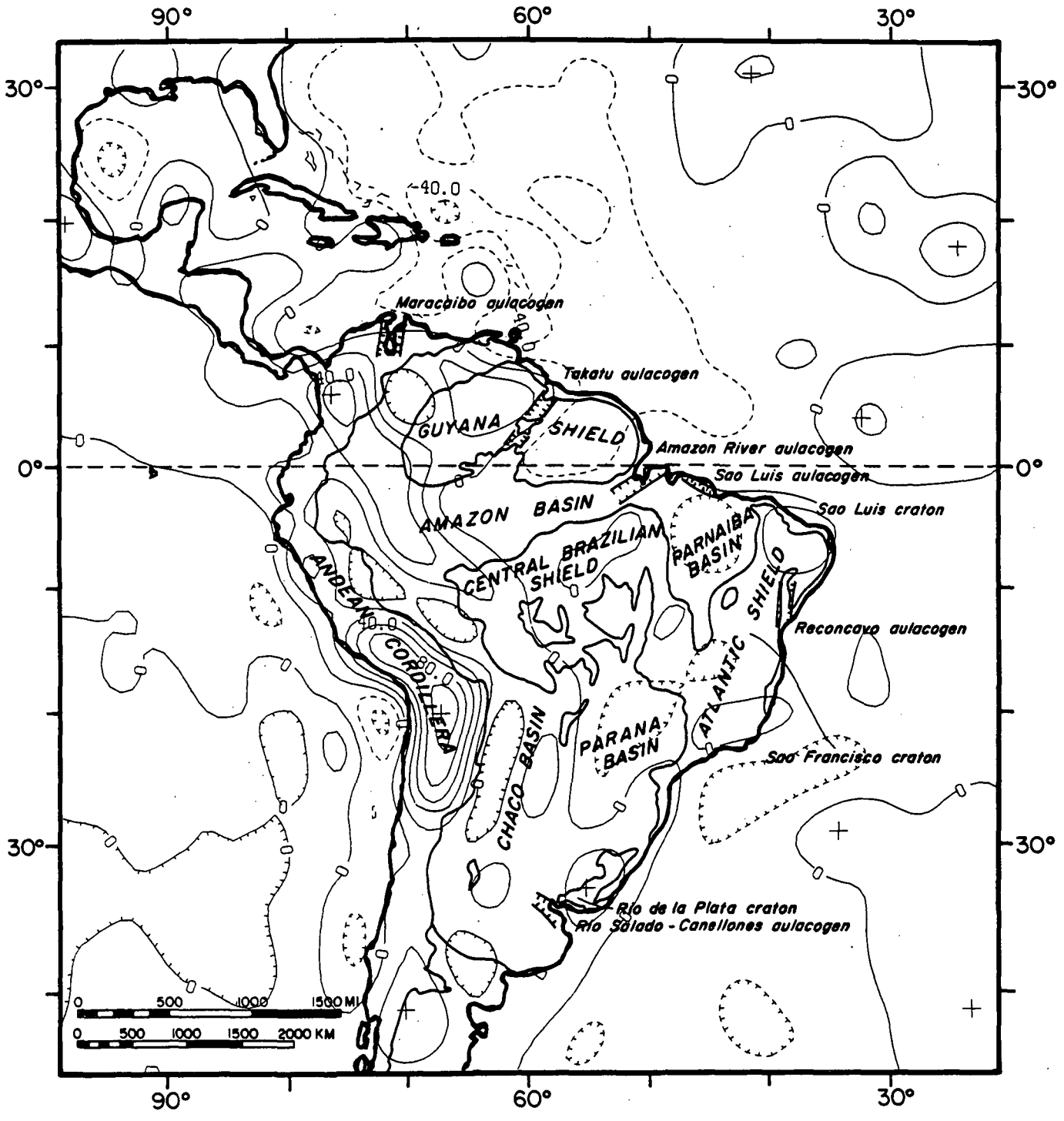

Figure 65. Long-wavelength-pass ($\lambda \geq 8^{a}$) filtered, surface free-air gravity anomaly map of South America and adjacent areas. Contour interval is 20 mgals. Modified from Hinze et al. (1982).

DISCUSSION

The average crustal thickness of the central and northern Andean cordillera is moderately well constrained due to the number of geophysical surveys which have been conducted over the range (e.g., Fig. 4). The most notable feature of the Andean cordillera is the thick crescent-shaped crustal root beneath the Central Andes, between latitudes 6° South and 26° South (Fig. 65). This root reaches depths greater than 70 kilometers beneath the Altiplano of northwestern Bolivia and southern Peru (Fig. 63). A second keel-shaped region of thick crust (greater than 50 kilometers thick) is present beneath the Northern Andes of western Colombia and northern Ecuador, according to seismic evidence (Ocola et al., 1975; Leeds and Knopoff, 1972). These two regions of thick crust incidentally correspond to the two most heavily studied portions of the Andean cordillera, and it is possible that the gap of thinner crust between them (between latitudes 2° South and 6° South) is due to the lack of geophysical control. Certainly the pattern of crustal thickness in northern Colombia (around latitude 6° North) is not well constrained by geophysical data.

The pattern of filtered free-air gravity anomalies over the Andean cordillera is dominated by the arc-shaped

gravity high between latitudes 11° South and 29° South (Fig. 65). The mean elevation of the Andean cordillera is greatest between latitudes 11° South and 32° South (Yuan, 1983), and the gravity high is probably directly related to the topography. The gravity high also corresponds closely to the crescent of thick crust beneath the mid-Central Andes. In a sense, this correlation is not surprising, since the estimated crustal structure of this region is based heavily on gravity modeling. Nevertheless, those thicknesses are supported by seismic evidence (James, 1971; Ocola and Meyer, 1972). The gravity high over northern Colombia, at approximately latitude 6° North, is less easily related to topographic relief, since the average elevation of the cordillera decreases more or less steadily north of latitude 15° South. Considering the relatively low mean elevation of the Northern Andes, it is surprising that the underlying crust should be so thick. (Overcompensated topography is normally characterized by negative free-air gravity anomalies.) The high could be related to the shallow strip of dense oceanic crust beneath western Colombia, along the Pacific coast (Mooney et al., 1979; Case and McDonald, 1973). Only a slightly positive (20 mgal) average free-air gravity anomaly characterizes the Andean cordillera between latitudes 3° North and 6° South. The average free-air gravity anomaly over the cordillera south of latitude 30° South is near zero.

The pattern of magnetic anomalies over the Andean cordillera is discontinuous and shows no consistent correlation with either the variable crustal thickness beneath the cordillera or the associated pattern of gravity anomalies (Fig. 64). A region of negative magnetic values, between latitudes 15° South and 30° South, corresponds to a certain extent with the dominant free-air gravity high of the mid-Central Andes. Also, the prominent magnetic high centered over south-central Colombia (not over the Northern Andes) may partially be related to the dense oceanic crust of western Colombia. Neither of these correlations is very spectacular.

Finally, there is a notable correlation between the north-south width of the central Andean free-air gravity high and the lateral boundaries of a large, steeply-dipping segment of the Nazca plate beneath South America proposed by Jordan et al. (1983). The two adjacent segments of the Nazca plate are postulated to dip much more shallowly. The magnetic anomalies show no strong correlation with this proposed lateral segmentation.

The two-station paths which cross the central and southeastern portions of the South American platform (NAT-LPB, NAT-LPA, BDF-LPB) are widely spaced and give only very general coverage of this broad area (Fig. 11). The two-station paths which cross the South American platform from north to south (CAR-LPA, TRN-LPA, and TRN-RDJ) yield models

averaged over nearly the entire eastern continent, and add little independent information about the central and southern platform. The models derived from the paths NAT-LPB, NAT-LPA, and BDF-LPB indicate that this region of the South American platform is characterized by a crust of fairly uniform thickness (around 42 kilometers thick). The crust may thicken slightly to the northwest, although the evidence, based primarily on the path BDF-LPB, is slight. It must be cautioned that none of these three lines sample the large section of platform crust covered by the Chaco basin (Fig. 2). The models derived from the north-south paths CAR-LPA, TRN-LPBA, and TRN-RDJ (two of which do cross the Chaco basin) do not contradict the suggested regional crustal thickness of around 42 kilometers.

The pattern of free-air gravity anomalies over the central and southern South American platform is not distinguished by any notable highs or lows (Fig. 65). Both the Parnaiba basin and the Parana basin are characterized by semicircular, slightly negative (approximately -20 mgals) gravity anomalies; the broad, shallow Chaco basin has no distinctly associated negative anomaly, although a large elongated low (approximately -20 mgals) occurs over the western side of the basin, parallel to the Andean cordillera. The slight positive anomalies which occur over the Chaco basin may be related to a shallowing of the basement. The Central Brazilian shield and the Atlantic

shield are characterized by near zero to slightly positive free-air gravity anomalies. A regional free-air gravity anomaly near zero, such as that characterizing this area, is considered evidence for isostatic equilibrium.

The pattern of regional magnetic anomalies over the central and southern South American platform is much more distinctive than the pattern of gravity anomalies (Fig. 64). The most prominent feature of the magnetic anomaly map in the region is the pinched trend of positive anomalies between latitudes 3° South and 19° South, which extends across the entire continent from east to west. A branch of this trend of positive anomalies appears to extend down the northeast coast of Brazil to Argentina. This branch is nearly obscured, however, by an enormous negative magnetic anomaly (-18 nT) at latitude 20° South, near the Brazilian coast, in the middle of the Atlantic shield. The broad southern region of the Chaco basin and the western Parana basin is characterized by an irregular alternating pattern of slight positive and negative (mostly negative) magnetic anomalies.

In general, the shield areas are characterized by positive magnetic anomalies, as noted by Hinze et al. (1982). These positive anomalies for the most part blur over the western side of the Parana basin and the central and southern parts of the Parnaiba basin. In view of this, the intense negative magnetic anomaly in the middle of the

Atlantic shield is difficult to explain. The anomaly extends over a region including the southern end of the Sao Francisco craton, the late Precambrian Ribeira and Brasilia fold belts, and the eastern side of the Parana basin. The Parana basin and the Ribeira and Brasilia fold belts were strongly affected by the tectonic reactivation of the South American platform associated with the opening of the Atlantic Ocean (de Almeida, 1970). Large volumes of tholeiitic basalts were extruded from tensional fractures along the rim of the Parana basin, and extensive alkalic volcanism occurred within the Ribeira and Brasilia fold belts north and east of the Prana basin. The igneous activity that occurred within the Parnaiba basin was more limited (Vitroello, 1978). Perhaps the negative anomaly that occurs over this part of the Atlantic shield is related to this major thermotectonic event. Unfortunately, the two-station path NAT-LPA which crosses the Atlantic shield is too long to be much affected by this anomalous region. Both the model computed for the two-station path NAT-LPA and the model computed for the two-station path NAT-LPB, of comparable length, suggest crustal thicknesses of approximately 42 kilometers, in spite of the fact that their respective pairs of dispersion curves are noticeably different (Figs. 49 and 53). The path NAT-LPB lies completely within the major east-west trending positive magnetic anomaly associated with the northern Atlantic and

Central Brazilian shield; the long-period phase velocities measured across this line are the highest recorded along any path in this study. Nevertheless, the average crustal shear wave velocities computed from the model NAT-LPA range from 3.83 to 3.90 km/s, which is slightly higher than the range of crustal shear wave velocities computed from the model NAT-LPB of 3.78 to 3.88 km/s. However, it is not clear whether these slightly higher crustal velocities are related to the anomalous region.

The three two-station paths which cross the South American platform from north to south (CAR-LPA, TRN-LPA, and TRN-RDJ) all yield models which suggest (without great definition) an average crustal thickness of approximately 42 kilometers. These models represent averages over nearly the entire South American platform. Crustal thicknesses in this range are common beneath shields and stable platforms (Bott, 1982). The three two-station paths which provide coverage of the northern quarter of the South American platform (NAT-CAR, NAT-BOG, and NAT-QUI), however, yield models which suggest that a large region of somewhat thicker crust (greater than 50 kilometers) underlies a large portion of northern Brazil (Fig. 63). The western extent of this zone of thickened crust is determined by the crustal models computed from dispersion measurements over the northwestern platform (CAR-ARE, CAR-LPB, and TRN-LPB), which require a broad, arc-shaped region of crust somewhat thinner than

average (slightly less than 35 kilometers) beneath central Venezuela, eastern Colombia, northeastern Peru, westernmost Brazil, and extreme northern Bolivia (Fig. 63).

The pattern of filtered free-air gravity anomalies over the northeastern part of the South American platform is a continuation of the pattern of slightly positive to slightly negative (± 20 mgals) gravity anomalies that characterizes the central and southern parts of the platform (Fig. 65). A distinctive pair of gravity anomalies exists over the western and eastern lobes of the Guyana shield. The western lobe is characterized by a teardrop-shaped gravity high (20 mgals) which extends partially over the transitional zone between the shield and the Northern Andes. The eastern lobe correlates closely with a tongue-shaped gravity low (-20 mgals) which merges with a regional gravity low over the adjacent Atlantic Ocean. The division between the high and low corresponds well with the Takatu aulacogen which divides the shield.

The Amazon basin has no distinct correlative gravity low, unlike the other intracratonic basins of the South American platform. The free-air gravity anomaly associated with the eastern and central Amazon basin, which is just slightly less than zero, extends as far west as longitude 67° West. The western end of the Amazon basin, however, is covered by a prominent northwestward-trending gravity high which reaches values of 40 mgals. This high ridge stretches

southeastward from the 60 mgal high over northwestern Colombia across the broad, low-lying transition zone between the upper Amazon basin and the Andean cordillera, to the northestern corner of the Central Brazilian shield, at approximately latitude 5° South. A series of elongated gravity lows, associated with the foreland basins of the Andean cordillera (Wilcox, 1977), occur west of this ridge, between latitudes 3° South and 15° South.

The pattern of magnetic anomalies over the northern South American platform is dominated by an east-west trending series of interconnected negative magnetic anomalies that nearly crosses the continent (Fig. 64). These anomalies cover much of the Amazon basin and extend into the central part of the transition zone between the upper Amazon basin and the Andean cordillera. The northernmost magnetic low of this series is centered near the intersection of the trend of the Takatu aulacogen with the Amazon basin; this anomaly covers much of the southern side of the Guyana shield (particularly the eastern lobe). The major western magnetic low covers most of the central part of the upper Amazon transition zone. This anomaly lies directly over the free-air gravity high that characterizes the transition zone. Northwest of this negative, however, is a very prominent positive magnetic anomaly, centered over south-central Colombia, that also lies directly over the free-air gravity high. This positive anomaly spreads both

northward, to cover all of the Colombian Andes, and northeastward, to merge with the positive anomaly that lies over the northern side of the western lobe of the Guyana shield.

Although the model NAT-CAR (over the northeastern coast) suggets a fairly standard crustal thickness of around 38 kilometers, the two models NAT-BOG and NAT-QUI, which cross the southern Guyana shield and the Amazon basin, indicate that thicker crust has been traversed. These two models yield average crustal thicknesses of around 46 to 50 kilometers. The average crustal shear wave velocities computed from these two models is also somewhat high for continental crust, falling somewhere in the range of 3.81 to 3.95 km/s. Since the two-station paths crossing the northwestern portion of the South American platform indicate that it is a region of somewhat thinner than average crust, the zone of thick crust suggested by the models NAT-BOG and NAT-QUI must be confined to the area of northern Brazil (Fig. 63).

Much of the path lengths of NAT-BOG and NAT-QUI are confined to the negative magnetic anomaly associated with the eastern Amazon basin and the split Guyana shield, indicating that there may be some relationship between the zone of thickened crust and the magnetic anomaly. Burke (1978) has suggested that the Amazon basin is a Paleozoic rift. Perhaps the area of thick dense crust and the eastern

pattern of negative magnetic anomalies is a reflection of either this tectonic activity, or the tectonic reactivation associated with the later rifting of South America from Africa.

The occurrence of both a negative magnetic anomaly and a (slight) negative free-air gravity anomaly over the eastern lobe of the Guyana shield is unusual, considering the usual trend of magnetic and gravity anomalies over the other shield areas of South America (Figs. 64 and 65). These relations seem to indicate that some difference exists in the crust beneath the two lobes of the Guyana shield. The model NAT-BOG requires the extension of thick crust beneath at least half of the eastern lobe of the Guyana shield. Perhaps the difference in crustal properties beneath the northern cratonic area of South America influenced the position of the Takatu aulacogen.

The models computed from the two-station paths which cross the northwestern portion of the South American platform suggest that a zone of relatively thin crust (less than 35 kilometers thick) must underlie part of this area. This zone has been mapped in as a large curving tongue of shallow crust roughly parallel to the northwestern coast of South America and the crescent of thick crust beneath the Andean cordillera (Fig. 63). The zone is not well defined, however, because the paths which cross this area are mixed, and none of them cross the westernmost side of the

transition zone. The average crustal shear wave velocities computed from models crossing this region are not consistent. The most representative range of average crustal shear wave velocities, computed from the model CAR-LPB (inverting phase velocity dispersion data alone) is 3.70 to 3.77 km/s. This range of velocities is lower than average crustal velocities measured in other parts of the South American platform. Since most of the models crossing this region were derived from inverting phase velocities alone, the upper mantle shear wave velocity distribution with depth was sufficiently stable to pick a range of average upper mantle shear velocities of 4.51 to 4.57 km/s. This is a slightly lower range of velocities than the average upper mantle shear wave velocity picked from the model NAT-QUI of 4.59 km/s (inverting phase velocity dispersion data alone). In this region the large negative magnetic anomaly does not seem to be associated with thickened crust. An arc of thin crust is consistent with the presence of the high free-air gravity anomaly over the upper Amazon transition zone, however, particularly in view of the low, flatlying topography of the transitional area. It would be very interesting to have a heat flow measurement over the central part of this area, to see if the magnetic anomaly is related to a thermal disturbance beneath the crust.

SUMMARY AND CONCLUSIONS

The crustal thickness map of South America constructed in this study is based on very general data. The long-period, long-path Rayleigh wave dispersion analysis used to establish the crustal structure beneath the South American platform averages over potentially significant differences in the crust and upper mantle of the platform, and the crustal models of the Andean cordillera, which have been derived by different investigators using a variety of geophysical methods, give only a preliminary outline of the crustal structure beneath the cordillera. The crustal shear wave velocities measured over the South American platform are also the result of averaging over large, potentially different sections of crust. The potential field anomalies mapped as apart of the MAGSAT project provide more uniform and more detailed geophysical coverage of the South American continent, but these data are also of an averaged and preliminary nature. Furthermore, magnetic and gravitational field measurements are sensitive to lithological variations in the crust (and upper mantle) which are not necessarily related to either the crustal thickness or the tectonic features of South America. Nevertheless, some interesting relationships exist between the variations in crustal thickness and average crustal shear velocity, the magnetic

and free-air gravity anomalies, and the major tectonic features of South America.

A relatively narrow belt of thick crust is present beneath the trend of the Andean cordillera along the western coast of South America. This belt thins gradually southward beneath the Central Andes, and rather abruptly northward beneath the Northern Andes. The crust thickens dramatically beneath the bend in the mid-Central Andes at latitude 18° South, reaching thicknesses greater than 70 kilometers. The crust also thickens beneath the Northern Andes of western Colombia. Except for an intense arc-shaped free-air gravity high over the bend in the Central Andes, neither the pattern of filtered free-air gravity anomalies nor the pattern of magnetic anomalies show a consistent correlation with either the trend of the Andean cordillera or the pattern of crustal thickness. The large free-air gravity high over the Central Andes is probably related to the high mean elevation of the cordillera in this region, which in turn is related to the thick crustal root that supports the cordillera. An interesting correlation also exists between the extent of this gravity high and the boundaries of a large, steeply dipping segment of the Nazca plate beneath South America proposed by Jordan et al. (1983). The smaller free-air gravity high over the mid-Northern Andes does not seem to be related either to the elevation of the cordillera or the presence of a crustal root. The anomaly may, however, be

caused by the zone of dense, shallow oceanic crust that lies between the Central Cordillera and the Pacific coast of Colombia.

2. The central and southern portion of the South American platform is undistinguished by any notable variations in crustal thickness. The average thickness of the crust throughout this region is approximately 42 kilometers, which is typical of stable platform and shield areas; the crust may thicken slightly to the north. (The crust beneath the Chaco basin and surrounding areas has not been sampled adequately, however.) The average regional crustal shear wave velocity falls within a range of 3.65 to 3.70 km/s. The pattern of filtered free-air gravity anomalies across the central and southern platform is characterized by slight lows (-20 mgals) over the basins, and near-zero anomalies to slight highs (20 mgals) over the exposed shields. These ranges indicate that the entire region is broadly in isostatic equilibrium, as would be expected in a large area of uniformly thick crust. Strongly positive magnetic anomalies occur over the Central Brazilian shield and over the northern and southern Atlantic shield; an intense negative magnetic anomaly occurs over the central Atlantic shield. The southern portion of the platform is characterized by an irregular pattern of slighly negative magnetic anomalies. The pattern of magnetic anomalies over the southern and central South American platform does not

seem to be associated with variations in crustal thickness, but may instead be a function of either the exposure of basement rocks in shields across the platform, or of lithological variations within the crust of the platform. The intense magnetic anomaly over the central Atlantic shield may, for instance, be attributable to thermotectonic reactivation of the crust prior to or during the rifting of South America from Africa.

3. Two major trends in crustal thickness dominate the crustal structure of the northern South American platform. An east-west trending zone of thickened crust (slightly thicker than 50 kilometers) exists beneath nearly all of northern Brazil. This zone of crust is characterized by average crustal shear wave velocities of at least 3.81 to 3.95 km/s, which implies that in addition to being thick, the crust here is more dense than average. The northwestern lobe of the South American platform is underlain by a hook-shaped zone of thinned crust (slightly thinner than 35 kilometers) that roughly parallels the curve of the Andean cordillera. The average crustal shear wave velocity in this region is poorly defined, but probably falls within the range of 3.70 to 3.77 km/s. The pattern of filtered free-air gravity anomalies over the northeastern platform is very similar to that of the central and southern platform. However, unlike the other intracratonic basins of the South American platform, the Amazon basin is not characterized by

a distinct gravity low. The slight negative anomaly which lies over the eastern lobe of the Guyana shield is also unusual. A distinctive pair of interconnected magnetic lows covers part of the northeastern platform. One of these anomalies is centered over the eastern Amazon basin and extends out into the Atlantic ocean; the other is centered over the intersection of the trend of the Takatu aulacogen with the central Amazon basin and cuts across much of the southern Guyana shield (particularly the eastern lobe). The area covered by these negative magnetic anomalies corresponds with the zone of thickened crust beneath northern Brazil, suggesting that some relationship may exist between the two features. Perhaps the zone of thickened crust (and low elevation) represents a subsided rift cushion.

A ridge-like free-air gravity high (greater than 40 mgals) covers much of the low-lying, sediment-covered transition zone between the Andean cordillera and the Amazon basin and Guyana shield, over the northwestern South American platform. The western lobe of the Guyana shield is also characterized by a slight free-air gravity high. These anomalies could be a reflection of the zone of thinned crust mapped beneath the area. A distinctive negative magnetic anomaly lies over the central part of the transition zone, at the intersection of the trend of the Amazon basin with the Andean cordillera. The relationship of this anomaly to

the zone of thinned crust is not clear. The magnetic anomaly could be due to the extensive sedimentary cover of the region, to a fundamental lithological difference in the crust, or to remnant thermal activity.

APPENDIX A

DISPERSION DATA FOR PATHS INVESTIGATED IN THIS STUDY

Natal-Caracas: Event NCA 1

Period (Sec)	Group Vel. Natal	Group Vel. Caracas	Inter. Group Vel.	Inter. Phase Vel.
19	3.36	2.82	2.92	
21	3.67	3.08	2.80	
23	3.83	3.25	2.98	
25	3.89	3.42	3.18	
27	3.93	3.55	3.35	3.82
29	3.96	3.62	3.44	3.86
31	3.98	3.67	3.50	3.88
33	3.99	3.70	3.54	3.92
35	4.00	3.73	3.58	3.94
37	4.00	3.77	3.64	3.96
39	4.00	3.80	3.69	3.96
41	4.00	3.82	3.72	3.98
43	4.00	3.84	3.75	3.98
45	3.99	3.86	3.78	4.00
47	3.99	3.87	3.80	4.00
49	3.98	3.88	3.82	4.02
51	3.98	3.88	3.82	4.02
53	3.98	3.88	3.82	4.04
55	3.97	3.88	3.83	4.04
57	3.96	3.88	3.83	4.04
59	3.94	3.89	3.65	4.06
61	3.92	3.89	3.87	4.06
63	3.90	3.89	3.88	4.08
65	3.87	3.89	3.90	4.08
67	3.84	3.88	3.90	4.08
69	3.80	3.88	3.93	4.08
71	3.78	3.88	3.94	4.10
73	3.75	3.88	3.96	4.10
75	3.74	3.87	3.95	4.10
77	3.73	3.87	3.96	4.10
79	3.72	3.87	3.97	4.12
81	3.72	3.86	3.95	4.12
83	3.71	3.86	3.95	4.12
85	3.72	3.85	3.93	4.12
87	3.72	3.85	3.93	4.14
89	3.72	3.85	3.93	4.14
91	3.71	3.85	3.93	4.14

Natal-Caracas: Event NCA 2

Period (Sec)	Group Vel. Natal	Group Vel. Caracas	Inter. Group Vel.	Inter. Phase Vel.
19	3.26	3.25	3.24	
21	3.68	3.39	3.22	3.66
23	3.83	3.49	3.30	3.74
25	3.90	3.57	3.38	3.78
27	3.94	3.63	3.45	3.82
29	3.97	3.68	3.51	3.84
31	3.98	3.71	3.55	3.88
33	3.99	3.74	3.59	3.90
35	4.00	3.76	3.62	3.92
37	4.01	3.78	3.64	3.93
39	4.00	3.80	3.68	3.94
41	4.98	3.83	3.74	3.96
43	3.97	3.84	3.76	3.96
45	3.95	3.86	3.80	3.96
47	3.94	3.87	3.82	3.98
49	3.93	3.87	3.83	3.98
51	3.92	3.88	3.85	3.98
53	3.92	3.89	3.87	3.99
55	3.92	3.90	3.89	4.00
57	3.92	3.90	3.89	4.00
59	3.92	3.91	3.90	4.00
61	3.92	3.91	3.90	4.00
63	3.90	3.90	3.89	4.00
65	3.91	3.90	3.89	4.00
67	3.91	3.90	3.89	4.00
69	3.91	3.90	3.89	4.00
71	3.91	3.89	3.88	4.02
73	3.91	3.89	3.88	4.02
75	3.91	3.88	3.86	4.02
77	3.91	3.88	3.86	4.04
79	3.91	3.88	3.86	4.04
81	3.92	3.88	3.85	4.06
83	3.92	3.88	3.85	4.06
85	3.92	3.88	3.85	4.08
87	3.92	3.88	3.85	4.08
89	3.92	3.88	3.85	4.10
91	3.92	3.88	3.85	4.10

Natal-Bogota: Event NBG 1

Period (Sec)	Group Vel. Natal	Group Vel. Bogota	Inter. Group Vel.	Inter. Phase Vel.
17	2.98	2.94	2.92	
19	3.36	3.08	2.95	
21	3.67	3.20	2 99	
23	3.83	3.29	3.06	
25	3.89	3.36	3.13	
27	3.93	3.41	3.18	
29	3.96	3.46	3.24	3.80
31	3.98	3.50	3.29	3.84
33	3.99	3.54	3.34	3.88
35	4.00	3.58	3.39	3.90
37	4.00	3.62	3.44	3.94
39	4.00	3.66	3.50	3.96
41	4.00	3.70	3.56	3.98
43	4.00	3.74	3.61	4.00
45	3.99	3.77	3.66	4.00
47	3.99	3.80	3.70	4.02
49	3.98	3.82	3.74	4.04
51	3.98	3.84	3.77	4.04
53	3.98	3.85	3.78	4.06
55	3.97	3.86	3.80	4.06
57	3.96	3.87	3.82	4.08
59	3.94	3.87	3.83	4.08
61	3.92	3.88	3.86	4.10
63	3.90	3.88	3.87	4.10
65	3.87	3.89	3.90	4.12
67	3.84	3.89	3.92	4.12
69	3.80	3.90	3.96	4.12
71	3.78	3.90	3.97	4.12
73	3.75	3.90	3.98	4.12
75	3.74	3.90	3.99	4.12
77	3.73	3.90	4.00	4.12
79	3.72	3.90	4.00	4.14
81	3.72	3.89	3.99	4.14
83	3.72	3.89	3.99	4.14
85	3.72	3.88	3.99	4.14
87	3.72	3.88	3.99	4.14
89	3.72	3.88	3.99	4.16
91	3.72	3.88	3.99	4.16

Natal-Bogota: Event NBG 2

Period (Sec)	Group Vel. Natal	Group Vel. Bogota	Inter. Group Vel.	Inter. Phase Vel.
19	3.36	3.12	3.00	
21	3.68	3.28	3.10	
23	3.80	3.35	3.15	
25	3.85	3.41	3.21	
27	3.89	3.46	3.26	3.76
29	3.92	3.50	3.31	3.80
31	3.94	3.53	3.34	3.84
33	3.96	3.57	3.39	3.86
35	3.96	3.60	3.43	3.90
37	3.97	3.64	3.48	3.92
39	3.96	3.68	3.54	3.94
41	3.96	3.71	3.59	3.96
43	3.96	3.75	3.64	3.98
45	3.95	3.78	3.69	3.98
47	3.94	3.81	3.74	4.00
49	3.93	3.82	3.76	4.00
51	3.92	3.84	3.80	4.02
53	3.91	3.85	3.82	4.02
55	3.90	3.86	3.84	4.02
57	3.90	3.87	3.85	4.04
59	3.89	3.88	3.87	4.04
61	3.89	3.89	3.89	4.04
63	3.89	3.89	3.89	4.04
65	3.88	3.90	3.91	4.04
67	3.88	3.90	3.91	4.04
69	3.88	3.90	3.91	4.04
71	3.88	3.90	3.91	4.06
73	3.88	3.89	3.90	4.06
75	3.88	3.88	3.88	4.06
77	3.88	3.88	3.88	4.06
79	3.88	3.87	3.86	4.08
81	3.88	3.86	3.85	4.08
83	3.88	3.85	3.83	4.10
85	3.89	3.84	3.81	4.10
87	3.89	3.84	3.81	4.10
89	3.89	3.84	3.81	4.12
91	3.89	3.84	3.81	4.12

Natal-Bogota: Event NBG 3

Period (Sec)	Group Vel. Natal	Group Vel. Bogota	Inter. Group Vel.	Inter. Phase Vel.
19	3.21	3.14	3.10	
21	3.68	3.31	3.15	
23	3.79	3.43	3.26	
25	3.84	3.51	3.35	3.78
27	3.87	3.57	3.42	3.84
29	3.90	3.62	3.48	3.86
31	3.92	3.66	3.53	3.90
33	3.93	3.69	3.57	3.92
35	3.94	3.72	3.61	3.92
37	3.94	3.75	3.65	3.94
39	3.95	3.77	3.68	3.96
41	3.95	3.79	3.71	3.98
43	3.95	3.81	3.74	4.00
45	3.95	3.82	3.75	4.00
47	3.95	3.84	3.78	4.02
49	3.94	3.84	3.79	4.02
51	3.94	3.85	3.80	4.04
53	3.94	3.86	3.82	4.04
55	3.93	3.86	3.82	4.06
57	3.92	3.87	3.84	4.06
59	3.90	3.87	3.85	4.06
61	3.90	3.87	3.85	4.08
63	3.89	3.88	3.87	4.08
65	3.88	3.88	3.88	4.08
67	3.87	3.88	3.88	4.10
69	3.86	3.88	3.89	4.10
71	3.86	3.88	3.89	4.10
73	3.85	3.88	3.90	4.12
75	3.85	3.88	3.90	4.12
77	3.84	3.88	3.90	4.14
79	3.83	3.88	3.91	4.14
81	3.82	3.88	3.91	4.14
83	3.81	3.88	3.91	4.14
85	3.81	3.87	3.90	4.16
87	3.81	3.87	3.90	4.16
89	3.81	3.87	3.90	4.16
91	3.81	3.87	3.90	4.16

Natal-Bogota: Event NBG 4

Period (Sec)	Group Vel. Natal	Group Vel. Bogota	Inter. Group Vel.	Inter. Phase Vel.
19	3.30	3.13	3.04	
21	3.62	3.29	3.13	
23	3.77	3.37	3.18	
25	3.85	3.43	3.23	
27	3.93	3.48	3.27	3.76
29	3.97	3.52	3.31	3.82
31	3.99	3.57	3.37	3.84
33	4.01	3.60	3.40	3.88
35	4.02	3.63	3.44	3.90
37	4.04	3.66	3.48	3.94
39	4.04	3.69	3.52	3.96
41	4.04	3.73	3.58	3.98
43	4.04	3.76	3.62	4.00
45	4.03	3.80	3.68	4.02
47	4.01	3.82	3.72	4.02
49	3.98	3.84	3.76	4.04
51	3.96	3.85	3.79	4.04
53	3.93	3.86	3.82	4.06
55	3.90	3.86	3.84	4.06
57	3.87	3.86	3.85	4.08
59	3.84	3.86	3.87	4.08
61	3.82	3.86	3.88	4.08
63	3.80	3.86	3.89	4.08
65	3.78	3.85	3.89	4.08
67	3.75	3.85	3.91	4.10
69	3.73	3.84	3.90	4.10
71	3.71	3.83	3.90	4.10
73	3.69	3.82	3.90	4.10
75	3.67	3.82	3.91	4.12
77	3.66	3.81	3.90	4.12
79	3.64	3.80	3.90	4.12
81	3.63	3.80	3.90	4.13
83	3.62	3.80	3.91	4.14
85	3.61	3.80	3.92	4.14
87	3.61	3.80	3.92	4.14
89	3.61	3.80	3.92	4.16
91	3.61	3.80	3.92	4.16

Natal-Bogota: Event NBG 5

Period (Sec)	Group Vel. Natal	Group Vel. Bogota	Inter. Group Vel.	Inter. Phase Vel.
19	3.38	3.18	3.08	
21	3.66	3.31	3.14	
23	3.82	3.38	3.18	
25	3.88	3.44	3.34	3.72
27	3.93	3.48	3.27	3.76
29	3.96	3.52	3.31	3.80
31	3.98	3.56	3.36	3.84
33	3.99	3.59	3.40	3.88
35	4.00	3.62	3.44	3.90
37	4.00	3.65	3.48	3.92
39	4.01	3.69	3.53	3.94
41	4.01	3.72	3.58	3.96
43	4.01	3.75	3.62	3.98
45	4.00	3.78	3.67	3.98
47	4.00	3.81	3.71	4.00
49	3.99	3.83	3.75	4.00
51	3.98	3.84	3.77	4.02
53	3.96	3.86	3.81	4.02
55	3.94	3.86	3.82	4.02
57	3.92	3.88	3.86	4.04
59	3.90	3.88	3.87	4.04
61	3.88	3.89	3.90	4.04
63	3.86	3.90	3.92	4.04
65	3.84	3.90	3.93	4.04
67	3.83	3.90	3.94	4.04
69	3.81	3.90	3.95	4.04
71	3.80	3.90	3.96	4.04
73	3.78	3.90	3.97	4.04
75	3.77	3.90	3.98	4.04
77	3.76	3.89	3.97	4.04
79	3.76	3.88	3.95	4.04
81	3.76	3.88	3.95	4.05
83	3.76	3.88	3.95	4.06
85	3.76	3.88	3.95	4.06
87	3.76	3.88	3.95	4.06
89	3.76	3.88	3.95	4.06
91	3.76	3.88	3.95	4.06

Natal-Quito: Event SNQ 1

Period (Sec)	Group Vel. Natal	Group Vel. Quito	Inter. Group Vel.	Inter. Phase Vel.
27	3.71	3.26	2.76	
29	3.76	3.41	2.99	
31	3.79	3.51	3.16	
33	3.82	3.58	3.27	3.88
35	3.83	3.64	3.39	3.90
37	3.84	3.69	3.48	3.92
39	3.85	3.73	3.56	3.92
41	3.85	3.76	3.63	3.94
43	3.86	3.80	3.71	3.98
45	3.86	3.82	3.76	4.02
47	3.86	3.85	3.83	4.04
49	3.87	3.86	3.84	4.04
51	3.87	3.87	3.87	4.04
53	3.87	3.88	3.89	4.06
55	3.87	3.88	3.90	4.06
57	3.87	3.88	3.90	4.06
59	3.87	3.88	3.90	4.08
61	3.87	3.88	3.90	4.08
63	3.86	3.88	3.91	4.08
65	3.86	3.88	3.91	4.10
67	3.86	3.88	3.91	4.10
69	3.85	3.88	3.93	4.10
71	3.85	3.88	3.93	4.11
73	3.85	3.88	3.93	4.12
75	3.84	3.88	3.94	4.12
77	3.84	3.88	3.94	4.12
79	3.83	3.88	3.96	4.12
81	3.82	3.88	3.97	4.14
83	3.82	3.88	3.97	4.14
85	3.82	3.87	3.95	4.14
87	3.83	3.88	3.96	4.14
89	3.83	3.88	3.96	4.16
91	3.83	3.88	3.96	4.16

Natal-Quito: Event SNQ 2

Period (Sec)	Group Vel. Natal	Group Vel. Quito	Inter. Group Vel.	Inter. Phase Vel.
21	3.68	3.08	2.83	
23	3.79	3.28	3.06	
25	3.85	3.38	3.17	
27	3.89	3.45	3.25	
29	3.91	3.52	3.34	3.84
31	3.93	3.58	3.42	3.88
33	3.94	3.63	3.48	3.90
35	3.95	3.67	3.53	3.92
37	3.95	3.70	3.58	3.96
39	3.95	3.72	3.61	3.98
41	3.95	3.75	3.65	4.00
43	3.95	3.77	3.68	4.00
45	3.94	3.78	3.70	4.02
47	3.94	3.80	3.73	4.04
49	3.93	3.81	3.75	4.04
51	3.92	3.82	3.77	4.06
53	3.91	3.83	3.79	4.06
55	3.90	3.84	3.81	4.08
57	3.89	3.85	3.83	4.08
59	3.88	3.85	3.83	4.08
61	3.86	3.86	3.86	4.10
63	3.84	3.87	3.89	4.10
65	3.82	3.87	3.90	4.10
67	3.80	3.88	3.92	4.10
69	3.78	3.88	3.94	4.10
71	3.75	3.89	3.97	4.10
73	3.73	3.89	3.98	4.11
75	3.72	3.90	4.00	4.10
77	3.71	3.89	3.99	4.10
79	3.70	3.89	4.00	4.10
81	3.70	3.89	4.00	4.10
83	3.69	3.88	3.99	4.10
85	3.69	3.88	3.99	4.10
87	3.69	3.88	3.99	4.11
89	3.69	3.88	3.99	4.12
91	3.69	3.88	3.99	4.14

Natal-La Paz: Event NLB 1

Period (Sec)	Group Vel. Natal	Group Vel. La Paz	Inter. Group Vel.	Inter. Phase Vel.
17	3.02	2.90	2.93	
19	3.38	3.04	2.94	
21	3.53	3.12	3.01	
23	3.61	3.18	3.06	
25	3.66	3.24	3.12	
27	3.70	3.30	3.19	3.76
29	3.74	3.36	3.25	3.81
31	3.76	3.41	3.31	3.84
33	3.78	3.46	3.37	3.88
35	3.78	3.50	3.42	3.92
37	3.79	3.55	3.48	3.94
39	3.79	3.58	3.52	3.98
41	3.79	3.62	3.57	4.00
43	3.78	3.66	3.62	4.02
45	3.78	3.68	3.65	4.02
47	3.77	3.72	3.70	4.04
49	3.76	3.74	3.73	4.06
51	3.74	3.76	3.77	4.06
53	3.74	3.78	3.79	4.08
55	3.73	3.79	3.81	4.08
57	3.72	3.80	3.83	4.10
59	3.72	3.82	3.85	4.10
61	3.71	3.84	3.88	4.10
63	3.71	3.84	3.88	4.12
65	3.70	3.85	3.90	4.12
67	3.70	3.86	3.92	4.12
69	3.70	3.86	3.92	4.14
71	3.70	3.86	3.92	4.14
73	3.69	3.86	3.92	4.14
75	3.69	3.86	3.92	4.16
77	3.69	3.86	3.92	4.16
79	3.68	3.86	3.92	4.16
81	3.68	3.86	3.92	4.16
83	3.68	3.85	3.91	4.18
85	3.68	3.84	3.90	4.18
87	3.68	3.84	3.90	4.20
89	3.68	3.84	3.90	4.20
91	3.68	3.84	3.90	4.20

Natal-La Paz: Event NBG 4

Period (Sec)	Group Vel. Natal	Group Vel. La Paz	Inter. Group Vel.	Inter. Phase Vel.
17	3.10	3.04	3.02	
19	3.37	3.12	3.04	
21	3.49	3.16	3.06	
23	3.56	3.20	3.10	
25	3.62	3.24	3.13	
27	3.65	3.29	3.19	3.78
29	3.67	3.34	3.24	3.82
31	3.68	3.40	3.32	3.86
33	3.68	3.45	3.38	3.90
35	3.68	3.50	3.44	3.94
37	3.68	3.55	3.51	3.96
39	3.68	3.59	3.56	3.98
41	3.68	3.63	3.61	4.00
43	3.67	3.66	3.66	4.02
45	3.67	3.69	3.70	4.04
47	3.66	3.72	3.74	4.04
49	3.65	3.74	3.77	4.06
51	3.64	3.76	3.80	4.07
53	3.64	3.77	3.81	4.08
55	3.63	3.78	3.83	4.08
57	3.62	3.79	3.85	4.10
59	3.60	3.80	3.87	4.10
61	3.58	3.80	3.88	4.11
63	3.57	3.81	3.90	4.12
65	3.55	3.81	3.90	4.12
67	3.53	3.81	3.91	4.12
69	3.52	3.81	3.92	4.14
71	3.50	3.81	3.92	4.14
73	3.48	3.80	3.92	4.14
75	3.46	3.80	3.93	4.15
77	3.44	3.80	3.94	4.16
79	3.42	3.79	3.93	4.16
81	3.40	3.78	3.92	4.18
83	3.39	3.78	3.93	4.18
85	3.38	3.77	3.92	4.19
87	3.38	3.77	3.92	4.20
89	3.38	3.77	3.92	4.20
91	3.38	3.77	3.92	4.21

Natal-La Paz: Event NLB 5

Period (Sec)	Group Vel. Natal	Group Vel. La Paz	Inter. Group Vel.	Inter. Phase Vel.
17	3.14	3.12	3.11	
19	3.40	3.15	3.08	
21	3.52	3.18	3.08	
23	3.58	3.22	3.12	
25	3.62	3.26	3.16	
27	3.64	3.31	3.21	3.80
29	3.66	3.36	3.27	3.84
31	3.67	3.41	3.34	3.89
33	3.68	3.46	3.40	3.94
35	3.68	3.51	3.46	3.96
37	3.68	3.57	3.54	3.98
39	3.68	3.61	3.59	4.00
41	3.68	3.64	3.63	4.04
43	3.68	3.67	3.67	4.06
45	3.68	3.69	3.69	4.06
47	3.68	3.71	3.72	4.08
49	3.68	3.72	3.73	4.10
51	3.67	3.74	3.76	4.12
53	3.66	3.74	3.77	4.14
55	3.66	3.75	3.78	4.14
57	3.65	3.76	3.80	4.16
59	3.64	3.77	3.81	4.16
61	3.63	3.78	3.83	4.18
63	3.62	3.78	3.84	4.20
65	3.61	3.78	3.84	4.20
67	3.60	3.79	3.86	4.22
69	3.58	3.79	3.86	4.22
71	3.57	3.79	3.87	4.24
73	3.56	3.79	3.87	4.26
75	3.55	3.79	3.88	4.26
77	3.54	3.79	3.88	4.28
79	3.54	3.79	3.88	4.29
81	3.53	3.79	3.88	4.30
83	3.52	3.79	3.89	4.32
85	3.52	3.79	3.89	4.32
87	3.52	3.79	3.89	4.34
89	3.52	3.79	3.89	4.34
91	3.52	3.79	3.89	4.36

Brazilia-La Paz: Event BZB 1

Period (Sec)	Group Vel. Brasilia	Group Vel. La Paz	Inter. Group Vel.	Inter. Phase Vel.
17	2.90	2.72	2.46	
19	3.44	2.84	2.20	
21	3.56	3.14	2.62	
23	3.63	3.29	2.84	3.58
25	3.68	3.38	2.97	3.64
27	3.72	3.47	3.12	3.68
29	3.75	3.53	3.21	3.72
31	3.78	3.57	3.27	3.76
33	3.80	3.60	3.31	3.80
35	3.82	3.63	3.35	3.84
37	3.84	3.66	3.39	3.86
39	3.86	3.69	3.44	3.88
41	3.88	3.72	3.48	3.90
43	3.90	3.74	3.50	3.92
45	3.91	3.77	3.56	3.94
47	3.92	3.79	3.59	3.96
49	3.93	3.81	3.62	3.98
51	3.93	3.82	3.65	3.98
53	3.94	3.84	3.68	3.99
55	3.94	3.85	3.71	4.00
57	3.93	3.85	3.72	4.02
59	3.93	3.86	3.75	4.02
61	3.93	3.86	3.75	4.04
63	3.93	3.87	3.77	4.06
65	3.92	3.87	3.79	4.06
67	3.92	3.87	3.82	4.06
69	3.92	3.86	3.83	4.07
71	3.92	3.86	3.81	4.08
73	3.92	3.86	3.83	4.08
75	3.92	3.86	3.83	4.08
77	3.92	3.85	3.84	4.10
79	3.92	3.85	3.84	4.10
81	3.91	3.84	3.84	4.10
83	3.90	3.84	3.85	4.11
85	3.90	3.84	3.85	4.11
87	3.90	3.84	3.85	4.12
89	3.89	3.84	3.86	4.12
91	3.89	3.84	3.86	4.12

La Plata-Natal: Event LAN 1

Period (Sec)	Group Vel. La Plata	Group Vel. Natal	Inter. Group Vel.	Inter. Phase Vel.
9	2.80	2.80	2.80	
11	2.80	2.80	2.80	
13	2.81	2.81	2.81	
15	2.84	2.93	2.82	
17	2.90	2.98	3.02	
19	2.96	3.12	3.21	
21	3.04	3.28	3.42	3.70
23	3.15	3.36	3.48	3.74
25	3.24	3.42	3.52	3.76
27	3.30	3.44	3.52	3.78
29	3.33	3.46	3.53	3.78
31	3.35	3.48	3.55	3.80
33	3.36	3.49	3.56	3.82
35	3.37	3.51	3.59	3.84
37	3.37	3.52	3.60	3.85
39	3.38	3.53	3.61	3.88
41	3.37	3.54	3.64	3.88
43	3.37	3.55	3.65	3.90
45	3.36	3.56	3.68	3.90
47	3.36	3.57	3.69	3.90
49	3.36	3.58	3.71	3.92
51	3.34	3.59	3.74	3.92
53	3.34	3.59	3.74	3.92
55	3.33	3.60	3.76	3.94
57	3.33	3.60	3.76	3.94
59	3.32	3.61	3.78	3.94
61	3.32	3.61	3.78	3.96
63	3.32	3.61	3.78	3.96
65	3.31	3.62	3.81	3.96
67	3.31	3.62	3.81	3.96
69	3.31	3.62	3.81	3.96
71	3.30	3.62	3.82	3.96
73	3.30	3.62	3.82	3.96
75	3.30	3.62	3.82	3.96
77	3.30	3.62	3.82	3.96
79	3.29	3.62	3.82	3.96
81	3.29	3.62	3.82	3.96
83	3.29	3.62	3.82	3.96
85	3.28	3.62	3.83	3.96
87	3.28	3.62	3.83	3.97
89	3.28	3.62	3.83	3.98
91	3.28	3.62	3.83	3.98

La Plata-Natal: Event LAN 2

Period (Sec)	Group Vel. La Plata	Group Vel. Natal	Inter. Group Vel.	Inter. Phase Vel.
11	2.89	2.80	2.76	
13	2.89	2.80	2.76	
15	2.90	2.81	2.77	
17	2.92	2.86	2.83	
19	2.94	2.99	3.01	
21	2.97	3.09	3.15	
23	3.01	3.19	3.28	3.70
25	3.05	3.29	3.42	3.72
27	3.10	3.36	3.50	3.74
29	3.17	3.43	3.57	3.78
31	3.32	3.47	3.54	3.80
33	3.42	3.51	3.55	3.82
35	3.49	3.55	3.58	3.84
37	3.54	3.59	3.61	3.86
39	3.59	3.62	3.63	3.88
41	3.64	3.65	3.65	3.90
43	3.69	3.67	3.66	3.90
45	3.73	3.70	3.69	3.92
47	3.77	3.73	3.71	3.92
49	3.80	3.75	3.73	3.92
51	3.83	3.77	3.74	3.92
53	3.86	3.78	3.74	3.92
55	3.88	3.80	3.76	3.92
57	3.91	3.82	3.78	3.92
59	3.92	3.83	3.79	3.92
61	3.94	3.84	3.79	3.92
63	3.96	3.85	3.80	3.92
65	3.98	3.86	3.80	3.92
67	4.00	3.86	3.80	3.92

Natal-La Plata: Event NLA 3

Period (Sec)	Group Vel. Natal	Group Vel. La Plata	Inter. Group Vel.	Inter. Phase Vel.
17	3.12	3.17	3.18	
19	3.27	3.20	3.18	
21	3.45	3.23	3.18	
23	3.52	3.27	3.21	3.70
25	3.56	3.31	3.25	3.74
27	3.59	3.35	3.29	3.76
29	3.61	3.40	3.35	3.80
31	3.63	3.44	3.39	3.82
33	3.63	3.39	3.46	3.86
35	3.62	3.54	3.52	3.86
37	3.61	3.59	3.58	3.88
39	3.60	3.64	3.65	3.90
41	3.58	3.67	3.69	3.91
43	3.56	3.68	3.71	3.92
45	3.55	3.69	3.73	3.92
47	3.53	3.69	3.73	3.94
49	3.51	3.70	3.75	3.94
51	3.49	3.70	3.76	3.94
53	3.47	3.70	3.76	3.96
55	3.46	3.70	3.77	3.96
57	3.44	3.70	3.77	3.98
59	3.42	3.70	3.78	3.98
61	3.40	3.70	3.79	4.00
63	3.38	3.70	3.79	4.00
65	3.37	3.70	3.80	4.02
67	3.35	3.70	3.80	4.02
69	3.33	3.71	3.82	4.04
71	3.32	3.71	3.83	4.04
73	3.30	3.71	3.83	4.04
75	3.28	3.72	3.85	4.05
77	3.27	3.72	3.86	4.06
79	3.25	3.72	3.86	4.06
81	3.24	3.73	3.88	4.06
83	3.22	3.74	3.90	4.08
85	3.21	3.74	3.91	4.08
87	3.21	3.74	3.91	4.08
89	3.21	3.75	3.92	4.08
91	3.21	3.75	3.92	4.08

Caracas-La Plata: Event SCL 1

Period (Sec)	Group Vel. Caracas	Group Vel. La Plata	Inter. Group Vel.	Inter. Phase Vel.
15	3.31	3.23	3.13	
17	3.32	3.24	3.14	
19	3.32	3.24	3.14	
21	3.33	3.24	3.13	
23	3.34	3.24	3.12	
25	3.36	3.25	3.11	
27	3.40	3.28	3.13	
29	3.47	3.36	3.22	
31	3.56	3.47	3.36	3.85
33	3.63	3.55	3.45	3.88
35	3.68	3.61	3.52	3.90
37	3.72	3.65	3.56	3.92
39	3.75	3.69	3.61	3.94
41	3.77	3.72	3.66	3.96
43	3.79	3.76	3.72	3.96
45	3.81	3.80	3.79	3.98
47	3.83	3.83	3.83	3.98
49	3.85	3.86	3.87	4.00
51	3.86	3.88	3.91	4.00
53	3.88	3.89	3.90	4.00
55	3.89	3.90	3.91	4.00
57	3.90	3.91	3.92	4.00
59	3.90	3.91	3.92	4.02
61	3.91	3.91	3.91	4.02
63	3.92	3.92	3.92	4.02
65	3.92	3.92	3.92	4.02
67	3.92	3.92	3.92	4.02
69	3.93	3.92	3.91	4.04
71	3.93	3.91	3.88	4.04
73	3.93	3.91	3.88	4.04
75	3.93	3.91	3.88	4.04
77	3.93	3.91	3.88	4.04
79	3.93	3.91	3.88	4.04
81	3.92	3.90	3.87	4.06
83	3.92	3.90	3.87	4.06
85	3.92	3.90	3.87	4.06
87	3.92	3.90	3.87	4.08
89	3.92	3.90	3.87	4.08
91	3.92	3.90	3.87	4.08

Caracas-Quito: Event CQI 1

Period (Sec)	Group Vel. Caracas	Group Vel. Quito	Inter. Group Vel.	Inter. Phase Vel.
19	3.16	2.88	2.45	
21	3.42	3.08	2.57	
23	3.65	3.26	2.69	3.42
25	3.70	3.35	2.82	3.48
27	3.74	3.42	2.92	3.54
29	3.77	3.46	2.97	3.58
31	3.80	3.50	3.02	3.64
33	3.92	3.53	3.07	3.68
35	3.84	3.56	3.11	3.71
37	3.86	3.60	3.17	3.76
39	3.88	3.64	3.24	3.78
41	3.89	3.67	3.30	3.80
43	3.89	3.70	3.36	3.83
45	3.89	3.71	3.40	3.85
47	3.89	3.72	3.42	3.88
49	3.88	3.73	3.46	3.88
51	3.86	3.74	3.52	3.90
53	3.85	3.75	3.56	3.90
55	3.84	3.75	3.58	3.92
57	3.83	3.76	3.63	3.92
59	3.82	3.76	3.64	3.92
61	3.81	3.76	3.66	3.93
63	3.80	3.76	3.68	3.95
65	3.80	3.77	3.71	3.96
67	3.79	3.77	3.73	3.97
69	3.79	3.76	3.70	3.98
71	3.79	3.76	3.70	3.98
73	3.79	3.76	3.70	4.00
75	3.79	3.76	3.70	4.00
77	3.79	3.76	3.70	4.02
79	3.78	3.76	3.72	4.02
81	3.78	3.76	3.72	4.03
83	3.78	3.76	3.72	4.04
85	3.78	3.76	3.72	4.04
87	3.78	3.76	3.72	4.06
89	3.78	3.76	3.72	4.06
91	3.78	3.76	3.72	4.06

La Paz-Caracas: Event LPC 2

Period (Sec)	Group Vel. La Paz	Group Vel. Caracas	Inter. Group Vel.	Inter. Phase Vel.
15	2.90	2.73	2.65	
17	2.90	2.73	2.65	
19	2.95	2.72	2.61	
21	3.01	2.72	2.59	
23	3.09	2.75	2.60	
25	3.14	2.80	2.65	
27	3.19	2.87	2.72	
29	3.22	2.96	2.84	
31	3.25	3.09	3.01	
33	3.27	3.22	3.19	3.90
35	3.30	3.33	3.35	3.90
37	3.33	3.43	3.48	3.92
39	3.36	3.51	3.59	3.94
41	3.38	3.56	3.66	3.96
43	3.40	3.60	3.72	3.97
45	3.42	3.63	3.75	3.98
47	3.44	3.66	3.79	3.98
49	3.46	3.68	3.81	4.00
51	3.48	3.69	3.81	4.00
53	3.50	3.70	3.82	4.00
55	3.52	3.71	3.82	4.01
57	3.54	3.71	3.81	4.02
59	3.55	3.72	3.82	4.02
61	3.55	3.72	3.82	4.02
63	3.56	3.73	3.83	4.03
65	3.56	3.73	3.83	4.04
67	3.56	3.73	3.83	4.04
69	3.57	3.73	3.82	4.05
71	3.57	3.73	3.82	4.06
73	3.57	3.73	3.82	4.06
75	3.58	3.73	3.81	4.08
77	3.58	3.73	3.81	4.08
79	3.58	3.73	3.80	4.08
81	3.58	3.72	3.80	4.09
83	3.59	3.72	3.79	4.08
85	3.59	3.72	3.79	4.10
87	3.59	3.72	3.79	4.11
89	3.59	3.72	3.79	4.11
91	3.59	3.72	3.79	4.11

La Paz-Caracas: Event LPC 4

Period (Sec)	Group Vel. La Paz	Group Vel. Caracas	Inter. Group Vel.	Inter. Phase Vel.
13	2.89	2.68	2.57	
15	2.90	2.69	2.58	
17	2.90	2.69	2.58	
19	2.92	2.70	2.58	
21	2.97	2.71	2.57	
23	3.04	2.73	2.57	
25	3.10	2.77	2.60	
27	3.15	2.94	2.83	
29	3.20	3.14	3.10	3.82
31	3.25	3.28	3.30	3.86
33	3.29	3.40	3.47	3.90
35	3.33	3.47	3.56	3.92
37	3.36	3.50	3.59	3.93
39	3.39	3.52	3.60	3.94
41	3.42	3.54	3.62	3.96
43	3.45	3.56	3.63	3.98
45	3.46	3.57	3.63	4.00
47	3.50	3.59	3.65	4.00
49	3.52	3.62	3.68	4.02
51	3.53	3.65	3.72	4.03
53	3.55	3.68	3.76	4.04
55	3.56	3.72	3.82	4.06
57	3.57	3.74	3.85	4.06
59	3.58	3.77	3.89	4.06
61	3.58	3.79	3.92	4.08
63	3.58	3.81	3.96	
65	3.60	3.82	3.96	
67	3.60	3.83	3.98	
69	3.60	3.84	4.00	
71	3.60	3.84	4.00	
73	3.60	3.84	4.00	
75	3.60	3.84	4.00	
77	3.60	3.84	4.00	
79	3.60	3.84	4.00	
81	3.60	3.84	4.00	
83	3.60	3.83	3.98	
85	3.60	3.83	3.98	
87	3.60	3.83	3.98	
89	3.60	3.83	3.98	
91	3.60	3.83	3.98	

La Paz-Caracas: Event LPC 6

Period (Sec)	Group Vel. La Paz	Group Vel. Caracas	Inter. Group Vel.	Inter. Phase Vel.
15	2.66	2.66	2.66	
17	2.71	2.66	2.63	
19	2.82	2.67	2.60	
21	2.93	2.68	3.56	
23	3.00	2.70	3.56	
25	3.06	2.72	3.57	
27	3.11	2.77	3.62	
29	3.15	2.90	3.78	
31	3.20	3.16	3.14	3.86
33	4.24	3.29	3.32	3.90
35	4.28	3.39	3.45	3.92
37	4.32	3.45	3.52	3.94
39	4.35	3.49	3.57	3.96
41	4.39	3.52	3.59	3.96
43	4.42	3.56	3.64	3.98
45	4.45	3.58	3.65	3.98
47	4.48	3.60	3.67	4.00
49	3.51	3.63	3.70	4.02
51	3.54	3.65	3.71	4.02
53	3.57	3.67	3.72	4.04
55	3.60	3.69	3.74	4.06
57	3.62	3.71	3.76	4.06
59	3.65	3.73	3.77	4.08
61	3.67	3.75	3.79	4.08
63	3.70	3.77	3.81	4.08
65	3.72	3.78	3.81	4.09
67	3.74	3.80	3.83	4.10
69	3.76	3.81	3.84	4.10
71	3.78	3.82	3.84	4.10
73	3.80	3.84	3.86	4.12
75	3.83	3.85	3.86	4.12

La Paz-Caracas: Event LPC 7

Period (Sec)	Group Vel. La Paz	Group Vel. Caracas	Inter. Group Vel.	Inter. Phase Vel.
15	2.92	2.70	2.59	
17	2.93	2.70	2.58	
19	2.94	2.70	2.58	
21	2.98	2.70	2.56	
23	3.02	2.71	2.56	
25	3.06	2.73	2.57	
27	3.09	2.78	2.63	
29	3.12	2.83	2.69	
31	3.15	2.89	2.76	
33	3.18	2.96	2.85	
35	3.21	3.04	2.95	
37	3.24	3.13	3.07	
39	3.27	3.22	3.19	
41	3.30	3.33	3.35	
43	3.34	3.42	3.47	3.96
45	3.37	3.50	3.58	3.98
47	3.41	3.58	3.68	4.00
49	3.44	3.65	3.78	4.00
51	3.48	3.68	3.80	4.01
53	3.50	3.71	3.84	4.02
55	3.52	3.73	3.86	4.02
57	3.54	3.74	3.86	4.02
59	3.55	3.75	3.87	4.02
61	3.56	3.76	3.88	4.02
63	3.57	3.76	3.88	4.02
65	3.58	3.76	3.87	4.02
67	3.58	3.76	3.87	4.02
69	3.59	3.76	3.86	4.02
71	3.59	3.75	3.85	4.02
73	3.60	3.75	3.84	4.02
75	3.60	3.74	3.82	4.04
77	3.60	3.74	3.82	4.04
79	3.60	3.73	3.81	4.06
81	3.60	3.72	3.79	4.06
83	3.60	3.70	3.76	4.08
85	3.61	3.69	3.74	4.08
87	3.61	3.69	3.74	4.09
89	3.61	3.69	3.74	4.10
91	3.61	3.69	3.74	4.10

APPENDIX B

PHASE VELOCITY DISPERSION DATA FROM SHERBURNE (1974)

Natal-Quito: Event 803

Period (Sec)	Inter. Phase Vel.
19	3.73
21	3.73
23	3.76
25	3.80
27	3.84
29	3.87
31	3.91
33	3.94
35	3.97
37	3.99
39	4.02
41	4.04
43	4.05
45	4.06
47	4.07
49	4.08
51	4.09
53	4.09
55	4.10
57	4.10
59	4.11
61	4.12
63	4.12
65	4.13
67	4.13
69	4.14
71	4.17
73	4.15
75	4.15
77	4.15
79	4.16
81	4.16
83	4.17
85	4.17
87	4.18
89	4.18

Natal-Quito: Event 821

Period (Sec)	Inter. Phase Vel.
17	3.54
19	3.58
21	3.66
23	3.73
25	3.79
27	3.84
29	3.89
31	3.94
33	3.97
35	4.00
37	4.02
39	4.04
41	4.05
43	4.06
45	4.07
47	4.08
49	4.08
51	4.09
53	4.10
55	4.10
57	4.12
59	4.13

Trinidad-La Plata: Event 801

Period (Sec)	Inter. Phase Vel.
31	3.73
33	3.74
35	3.77
37	3.83
39	3.87
41	3.90
43	3.93
45	3.94
47	3.96
49	3.97
51	3.98
53	3.98
55	3.99
57	4.00
59	4.00
61	4.00
63	4.01
65	4.01
67	4.02
69	4.02
71	4.02
73	4.02
75	4.03
77	4.03
79	4.03
81	4.03
83	4.03
85	4.03
87	4.04
89	4.04
91	4.04

Trinidad-La Plata: Event 802

Period (Sec)	Inter. Phase Vel.
19	3.58
21	3.61
23	3.67
25	3.73
27	3.78
29	3.83
31	3.86
33	3.89
35	3.92
37	3.94
39	3.96
41	3.97
43	3.99
45	4.01
47	4.01
49	4.02
51	4.03
53	4.04
55	4.04
57	4.04
59	4.05
61	4.05
63	4.06
65	4.06
67	4.06
69	4.06
71	4.07
73	4.07
75	4.07
77	4.07
79	4.07
81	4.08
83	4.08
85	4.08
87	4.08

Trinidad-Rio de Janairo Event 831

Period (Sec)	Inter. Phase Vel.
31	3.89
33	3.90
35	3.91
37	3.94
39	3.97
41	3.99
43	4.01
45	4.03
47	4.04
49	4.05
51	4.06
53	4.07
55	4.07
57	4.07
59	4.08
61	4.08
63	4.09
65	4.09
67	4.09
69	4.09
71	4.09
73	4.09
75	4.10
77	4.10
79	4.10
81	4.09
83	4.09
85	4.09
87	4.09
89	4.09

Caracas-Arequipa: Event 827

Period (Sec)	Inter. Phase Vel.
19	3.62
21	3.69
23	3.74
25	3.80
27	3.84
29	3.88
31	3.92
33	3.95
35	3.98
37	4.01
39	4.02
41	4.03
43	4.04
45	4.05
47	4.05
49	4.05
51	4.06
53	4.06
55	4.06
57	4.06
59	4.06
61	4.06
63	4.06
65	4.05
67	4.05
69	4.04
71	4.04
73	4.04

Caracas-La Paz: Event 801

Period (Sec)	Inter. Phase Vel.
17	3.36
19	3.46
21	3.56
23	3.62
25	3.68
27	3.73
29	3.78
31	3.82
33	3.85
35	3.88
37	3.92
39	3.94
41	3.97
43	3.99
45	4.01
47	4.02
49	4.03
51	4.05
53	4.05
55	4.06
57	4.07

Caracas-La Paz: Event 802

Period (Sec)	Inter. Phase Vel.
27	3.79
29	3.80
31	3.84
33	3.86
35	3.89
37	3.92
39	3.94
41	3.96
43	3.98
45	3.99
47	4.01
49	4.02
51	4.03
53	4.04
55	4.04
57	4.05
59	4.06
61	4.06
63	4.06
65	4.07
67	4.07
69	4.07
71	4.08
73	4.08
75	4.09
77	4.09
79	4.09
81	4.09
83	4.09
85	4.09
87	4.09
89	4.10

Trinidad-La Paz: Event 827

Period (Sec)	Inter. Phase Vel.
19	3.51
21	3.56
23	3.63
25	3.70
27	3.74
29	3.79
31	3.83
33	3.85
35	3.88
37	3.91
39	3.93
41	3.95
43	3.96
45	3.97
47	3.98
49	4.00
51	4.01
53	4.02
55	4.02
57	4.03
59	4.04
61	4.04
63	4.04
65	4.05
67	4.05
69	4.05
71	4.06

APPENDIX C

EARTH MODELS OBTAINED IN THIS STUDY

Natal-Caracas Optimum Model Group and Phase Velocity Dispersion Inversion

Thickness	S-Velocity	P-Velocity	Density
2.0	2.10	3.64	2.25
4.0	3.50	6.07	2.72
4.0	3.55	6.16	2.75
4.0	3.64	6.31	2.79
4.0	3.74	6.48	2.84
4.0	3.84	6.66	2.89
4.0	3.94	6.82	2.93
4.0	4.03	6.98	2.98
4.0	4.12	7.14	3.02
4.0	4.22	7.30	3.08
4.0	4.32	7.48	3.13
4.0	4.42	7.65	3.19
4.0	4.51	7.81	3.25
4.0	4.58	7.93	3.29
4.0	4.61	7.98	3.30
4.0	4.60	7.97	3.30
4.0	4.55	7.88	3.27
4.0	4.46	7.73	3.22
10.0	4.37	7.57	3.16
10.0	4.34	7.51	3.14
10.0	4.53	7.84	3.26

Natal-Bogota Optimum Model Group and Phase Velocity Dispersion Inversion

Thickness	S-Velocity	P-Velocity	Density
2.0	1.72	2.97	2.14
4.0	2.83	4.91	2.48
4.0	3.04	5.27	2.55
4.0	3.47	6.01	2.70
4.0	3.86	6.69	2.90
4.0	4.14	7.18	3.04
4.0	4.30	7.44	3.12
4.0	4.32	7.49	3.14
4.0	4.26	7.38	3.10
4.0	4.14	7.18	3.04
4.0	4.08	7.07	3.00
4.0	4.10	7.11	3.02
4.0	4.26	7.38	3.10
4.0	4.46	7.73	3.22
4.0	4.70	8.14	3.36
4.0	4.86	8.43	3.46
4.0	4.96	8.59	3.52
4.0	4.88	8.44	3.47
10.0	4.63	8.02	3.32
10.0	4.31	7.46	3.13
10.0	4.60	7.97	3.30

Natal-Quito Optimum Model Group and Phase Velocity Dispersion Inversion

Thickness	S-Velocity	P-Velocity	Density
2.0	1.71	2.96	2.14
4.0	2.86	4.95	2.49
4.0	2.95	5.11	2.52
4.0	3.17	5.49	2.60
4.0	3.47	6.01	2.70
4.0	3.78	6.55	2.86
4.0	4.04	7.00	2.98
4.0	4.23	7.32	3.08
4.0	4.33	7.51	3.14
4.0	4.38	7.58	3.17
4.0	4.37	7.57	3.16
4.0	4.36	7.55	3.16
4.0	4.38	7.58	3.17
4.0	4.42	7.66	3.19
4.0	4.50	7.80	3.24
4.0	4.59	7.95	3.29
4.0	4.67	8.09	3.34
4.0	4.73	8.20	3.38
10.0	4.76	8.24	3.40
10.0	4.67	8.10	3.34
10.0	4.62	8.01	3.31

Natal-Quito[a] Optimum Model Phase Velocity Dispersion Inversion

Thickness	S-Velocity	P-Velocity	Density
2.0	2.13	3.70	2.26
4.0	3.56	6.16	2.75
4.0	3.60	6.24	2.77
4.0	3.71	6.42	2.82
4.0	3.83	6.63	2.88
4.0	3.94	6.83	2.94
4.0	4.03	6.99	2.98
4.0	4.09	7.09	3.01
4.0	4.13	7.16	3.03
4.0	4.16	7.21	3.05
4.0	4.19	7.26	3.06
4.0	4.24	7.35	3.09
4.0	4.31	7.47	3.13
4.0	4.40	7.63	3.18
4.0	4.50	7.80	3.24
4.0	4.60	7.97	3.30
4.0	4.67	8.10	3.34
4.0	4.71	8.16	3.37
10.0	4.72	8.17	3.37
10.0	4.64	8.04	3.32
10.0	4.60	7.97	3.30

[a]Data from Sherburne (1974).

Natal-LaPaz Optimum Model Group and Phase Velocity Dispersion Inversion

Thickness	S-Velocity	P-Velocity	Density
2.0	1.94	3.37	2.21
4.0	3.22	5.58	2.62
4.0	3.37	5.84	2.67
4.0	3.66	6.34	2.80
4.0	3.92	6.78	2.92
4.0	4.03	6.98	2.98
4.0	4.02	6.96	2.97
4.0	3.93	6.80	2.93
4.0	3.85	6.67	2.89
4.0	3.85	6.67	2.89
4.0	3.98	6.89	2.95
4.0	4.22	7.31	3.08
4.0	4.55	7.88	3.27
4.0	4.87	8.44	3.47
4.0	5.12	8.87	3.62
4.0	5.18	8.98	3.65
4.0	5.03	8.70	3.56
4.0	4.68	8.11	3.35
10.0	4.25	7.36	3.10
10.0	4.06	7.04	2.99
10.0	4.71	8.16	3.37

Brasilia-La Paz Optimum Model Group and Phase Velocity Dispersion Inversion

Thickness	S-Velocity	P-Velocity	Density
2.0	1.67	2.90	2.13
4.0	2.79	4.84	2.46
4.0	2.90	5.03	2.50
4.0	3.11	5.39	2.58
4.0	3.38	5.86	2.67
4.0	3.66	6.34	2.80
4.0	3.90	6.76	2.92
4.0	4.07	7.05	3.00
4.0	4.18	7.25	3.06
4.0	4.25	7.36	3.09
4.0	4.30	7.44	3.12
4.0	4.36	7.55	3.16
4.0	4.44	7.70	3.21
4.0	4.53	7.85	3.26
4.0	4.61	7.98	3.30
4.0	4.65	8.05	3.33
4.0	4.62	8.00	3.31
4.0	4.52	7.83	3.25
10.0	4.39	7.60	3.17
10.0	4.32	7.48	3.13
10.0	4.64	8.04	3.32

Natal-La Plata Optimum Model Group and Phase Velocity Dispersion Inversion

Thickness	S-Velocity	P-Velocity	Density
2.0	2.33	4.04	2.32
4.0	3.87	6.70	2.90
4.0	3.95	6.84	2.94
4.0	3.99	6.92	2.96
4.0	3.93	6.82	2.93
4.0	3.79	6.57	2.87
4.0	3.66	6.34	2.80
4.0	3.61	6.25	2.787
4.0	3.68	6.38	2.81
4.0	3.88	6.72	2.91
4.0	4.19	7.26	3.06
4.0	4.47	7.74	3.22
4.0	4.74	8.20	3.38
4.0	4.93	8.54	3.50
4.0	4.98	8.64	3.54
4.0	4.89	8.47	3.48
4.0	4.65	8.06	3.33
4.0	4.33	7.50	3.14
10.0	4.00	6.94	2.96
10.0	3.94	6.83	2.94
10.0	4.53	7.85	3.26

La Plata-Natal Optimum Model Group and Phase Velocity Dispersion Inversion

Thickness	S-Velocity	P-Velocity	Density
2.0	1.97	3.41	2.22
4.0	3.28	5.68	2.64
4.0	3.39	5.87	2.67
4.0	3.63	6.29	2.79
4.0	3.87	6.71	2.90
4.0	4.03	6.98	2.97
4.0	4.08	7.07	3.00
4.0	4.07	7.05	3.00
4.0	4.04	7.00	2.98
4.0	4.04	7.00	2.98
4.0	4.12	7.13	3.02
4.0	4.27	7.40	3.11
4.0	4.46	7.73	3.22
4.0	4.65	8.05	3.33
4.0	4.76	8.25	3.40
4.0	4.77	8.27	3.41
4.0	4.65	8.06	3.33
4.0	4.42	7.66	3.19
10.0	4.14	7.16	3.03
10.0	4.01	6.95	2.97
10.0	4.42	7.66	3.20

Natal-La Plata[a] Optimum Model Group and Phase Velocity Dispersion Inversion

Thickness	S-Velocity	P-Velocity	Density
2.0	2.00	3.47	2.22
4.0	3.32	5.75	2.65
4.0	3.41	5.90	2.68
4.0	3.62	6.27	2.78
4.0	3.86	6.68	2.90
4.0	4.03	6.99	2.98
4.0	4.10	7.10	3.01
4.0	4.08	7.07	3.00
4.0	4.05	7.01	2.98
4.0	4.04	7.01	2.98
4.0	4.12	7.14	3.02
4.0	4.26	7.39	3.10
4.0	4.46	7.73	3.22
4.0	4.65	8.06	3.33
4.0	4.77	8.27	3.41
4.0	4.78	8.28	3.41
4.0	4.65	8.06	3.33
4.0	4.42	7.65	3.19
10.0	4.14	7.18	3.04
10.0	4.03	6.98	2.97
10.0	4.47	7.74	3.22

[a]Representative model (3 events).

Caracas-La Plata Optimum Model Group and Phase Velocity Dispersion Inversion

Thickness	S-Velocity	P-Velocity	Density
2.0	2.15	3.73	2.27
4.0	3.57	6.18	2.76
4.0	3.74	6.48	2.84
4.0	3.99	6.91	2.96
4.0	4.08	7.08	3.00
4.0	4.05	7.02	2.98
4.0	3.83	6.63	2.88
4.0	3.61	6.26	2.78
4.0	3.48	6.03	2.71
4.0	3.52	6.10	2.73
4.0	3.76	6.51	2.85
4.0	4.17	7.23	3.05
4.0	4.69	8.12	3.35
4.0	5.25	9.10	3.70
4.0	5.68	9.83	3.99
4.0	5.81	10.07	4.10
4.0	5.58	9.68	3.93
4.0	5.02	8.70	3.56
10.0	4.33	7.50	3.14
10.0	3.89	6.73	2.91
10.0	4.51	7.81	3.24

Trinidad-La Plata[a] Optimum Model Phase Velocity Dispersion Inversion

Thickness	S-Velocity	P-Velocity	Density
2.0	2.36	4.08	2.33
4.0	3.93	6.81	2.93
4.0	3.92	6.79	2.93
4.0	3.91	6.77	2.92
4.0	3.89	6.74	2.91
4.0	3.88	6.72	2.90
4.0	3.87	6.70	2.90
4.0	3.87	6.71	2.90
4.0	3.89	6.73	2.91
4.0	3.92	6.78	2.92
4.0	3.96	6.86	2.94
4.0	4.02	6.96	2.97
4.0	4.10	7.10	3.01
4.0	4.19	7.26	3.06
4.0	4.30	7.44	3.12
4.0	4.41	7.64	3.19
4.0	4.53	7.85	3.26
4.0	4.66	8.07	3.33
10.0	4.66	8.06	3.33
10.0	4.60	7.97	3.30
10.0	4.45	7.71	3.21

[a]Data from Sherburne (1974).

Trinidad-Rio de Janeiro[a] Optimum Model Phase Velocity Dispersion Inversion

Thickness	S-Velocity	P-Velocity	Density
2.0	2.47	4.27	2.36
4.0	4.11	7.12	3.02
4.0	4.09	7.09	3.01
4.0	4.06	7.03	2.99
4.0	4.01	6.94	2.96
4.0	3.96	6.85	2.94
4.0	3.92	6.79	2.92
4.0	3.90	6.75	2.92
4.0	3.90	6.76	2.92
4.0	3.93	6.81	2.93
4.0	3.98	6.90	2.95
4.0	4.06	7.03	2.99
4.0	4.15	7.18	3.04
4.0	4.25	7.36	3.10
4.0	4.36	7.56	3.16
4.0	4.47	7.75	3.22
4.0	4.58	7.93	3.28
4.0	4.66	8.07	3.34
10.0	4.72	8.18	3.37
10.0	4.68	8.10	3.34
10.0	4.48	7.76	3.23

[a]Data from Sherburne (1974).

Caracas-Quito Optimum Model Group and Phase Velocity Dispersion Inversion

Thickness	S-Velocity	P-Velocity	Density
2.0	1.50	2.60	2.07
4.0	2.50	4.33	2.37
4.0	2.66	4.61	2.41
4.0	3.01	5.21	2.54
4.0	3.46	6.00	2.70
4.0	3.87	6.70	2.90
4.0	4.09	7.08	3.01
4.0	4.09	7.08	3.00
4.0	3.94	6.82	2.93
4.0	3.78	6.56	2.86
4.0	3.73	6.46	2.84
4.0	3.85	6.68	2.90
4.0	4.15	7.18	3.04
4.0	4.57	7.91	3.28
4.0	4.96	8.60	3.52
4.0	5.19	8.99	3.66
4.0	5.14	8.90	3.63
4.0	4.81	8.33	3.43
10.0	4.32	7.48	3.14
10.0	3.97	6.87	2.95
10.0	4.58	7.94	3.29

Caracas-Arequipa[a] Optimum Model Phase Velocity Dispersioin Inversion

Thickness	S-Velocity	P-Velocity	Density
2.0	2.35	4.07	2.33
4.0	3.92	6.79	2.92
4.0	3.91	6.77	2.92
4.0	3.88	6.72	2.91
4.0	3.85	6.68	2.90
4.0	3.84	6.65	2.89
4.0	3.84	6.66	2.89
4.0	3.87	6.71	2.90
4.0	3.93	6.81	2.93
4.0	4.02	6.96	2.97
4.0	4.12	7.14	3.02
4.0	4.24	7.34	3.09
4.0	4.36	7.56	3.16
4.0	4.49	7.78	3.23
4.0	4.61	7.78	3.23
4.0	4.72	8.17	3.37
4.0	4.80	8.32	3.42
4.0	4.85	8.40	3.45
10.0	4.85	8.40	3.46
10.0	4.71	8.15	3.36
10.0	4.41	7.63	3.18

[a]Data from Sherburne (1974).

Trinidad-La Paz[a] Optimum Model Phase Velocity Dispersion Data

Thickness	S-Velocity	P-Velocity	Density
2.0	2.20	3.82	2.29
4.0	3.67	6.36	2.81
4.0	3.68	6.37	2.81
4.0	3.67	6.36	2.81
4.0	3.66	6.34	2.80
4.0	3.67	6.36	2.81
4.0	3.72	6.44	2.83
4.0	3.80	6.59	2.87
4.0	3.92	6.79	2.92
4.0	4.05	7.02	2.98
4.0	4.19	7.25	3.06
4.0	4.31	7.46	3.13
4.0	4.41	7.64	3.18
4.0	4.48	7.75	3.22
4.0	4.51	7.82	3.25
4.0	4.52	7.84	3.25
4.0	4.52	7.83	3.25
4.0	4.51	7.81	3.24
10.0	4.49	7.78	3.24
10.0	4.50	7.79	3.24
10.0	4.52	7.82	3.25

[a]Data from Sherburne (1974).

La Paz-Caracas Optimum Model Group and Phase Velocity Dispersion Inverstion

Thickness	S-Velocity	P-Velocity	Density
2.0	1.78	3.09	2.16
4.0	3.05	5.28	2.56
4.0	3.13	5.43	2.58
4.0	3.55	6.15	2.74
4.0	3.78	6.54	2.86
4.0	3.64	6.30	2.79
4.0	3.37	5.83	2.67
4.0	3.25	5.63	2.62
4.0	3.40	5.89	2.68
4.0	3.88	6.72	2.91
4.0	4.53	7.85	3.26
4.0	5.16	8.94	3.64
4.0	5.58	9.66	3.92
4.0	5.67	9.83	3.98
4.0	5.48	9.49	3.86
4.0	5.12	8.87	3.62
4.0	4.71	8.16	3.37
4.0	4.38	7.58	3.17
10.0	4.18	7.25	3.06
10.0	4.36	7.56	3.16
10.0	4.60	7.96	3.30

La Paz-Caracas[a] Optimum Model Phase Velocity Dispersion Inversion

Thickness	S-Velocity	P-Velocity	Density
2.0	2.12	3.67	2.26
4.0	3.54	6.13	2.74
4.0	3.54	6.14	2.79
4.0	3.57	6.18	2.75
4.0	3.62	6.27	2.78
4.0	3.70	6.41	2.82
4.0	3.80	6.58	2.87
4.0	3.89	6.73	2.91
4.0	3.96	6.87	2.94
4.0	4.03	6.98	2.98
4.0	4.09	7.08	3.01
4.0	4.15	7.19	3.04
4.0	4.22	7.30	3.08
4.0	4.30	7.44	3.12
4.0	4.40	7.62	3.18
4.0	4.51	7.81	3.24
4.0	4.62	8.01	3.31
4.0	4.73	8.19	3.38
10.0	4.81	8.33	3.43
10.0	4.76	8.24	3.40
10.0	4.53	7.85	3.26

[a]Data from Sherburne (1974).

La Paz-Caracas Optimum Model Phase Velocity[a] Dispersion Inversion

Thickness	S-Velocity	P-Velocity	Density
2.0	2.20	3.81	2.29
4.0	3.67	6.36	2.81
4.0	3.70	6.40	2.82
4.0	3.75	6.50	2.85
4.0	3.82	6.62	2.88
4.0	3.90	6.76	2.92
4.0	3.99	6.90	2.96
4.0	4.07	7.04	2.99
4.0	4.14	7.17	3.04
4.0	4.20	7.28	3.07
4.0	4.26	7.37	3.10
4.0	4.30	7.45	3.12
4.0	4.34	7.52	3.15
4.0	4.38	7.58	3.17
4.0	4.40	7.63	3.18
4.0	4.43	7.67	3.20
4.0	4.44	7.69	3.20
4.0	4.45	7.71	3.21
10.0	4.46	7.72	3.22
10.0	4.47	7.75	3.22
10.0	4.52	7.83	3.25

[a]Group velocity dispersion data omitted.

REFERENCES

Aldrich, L. T., 1958, The Earth's crust, in Carnegie Institution of Washington Yearbook, 1957-1958.

Barazangi, M., and Isacks, B. L., 1976, Spatial distribution of earthquakes and subduction of the Nazca Plate beneath South America: Geology, v. 4, p. 686-692.

Barazangi, M., and Isacks, B. L., 1978, Subduction of the Nazca plate beneath South America: Evidence from spatial distribution of earthquakes (abstract): EOS, Transactions, American Geophysical Union, v. 59, p. 382.

Ben-Avraham, Z., Nur, A., Jones, D., and Cox., A., 1981, Continental accretion: From oceanic plateaus to allochthonous terranes: Science, v. 213, p. 47-54.

Birch, F., 1964, Density and composition of mantle and core: Journal of Geophysical Research, v. 69, p. 4377-4388.

Bloch, S., and A. L. Hales, 1968, New techniques for the determination of surface wave phase velocities: Seismological Society of America Bulletin, v. 58, p. 1021-1034.

Bott, M. H. P., 1982, The Interior of the Earth: Its structure, constitution and evolution, 2nd ed., Elsevier, London, 403 p.

Boyd, T. M., Snoke, J. A., Sacks, I. S., and A. Rodriguez B., 1983, High-resolution study of the Benioff zone beneath southern Peru (abstract): EOS, Transactions, American Geophysical Union, v. 64, p. 311.

Brune, J., and J. Dorman, 1963, Seismic waves and earth structure in the Canadian Shield: Seismological Society of America Bulletin, v. 53, p. 167-209.

Burke, K., Delano, L., Dewey, J. F., Edelstein, A., Kidd, W. S. F., Nelson, K. D., Sengor, A. M. C., and J. Stroup, 1978, Rifts and sutures of the world: NASA Report, NASA Contract No. NAS5-24094, 238 p.

Case, J. E., Duran, S., Lopez, A. R., and Moore, W. R., 1971, Tectonic investigations in western Colombia and estern Panama: Geological Society of America Bulletin, v. 82, p. 2685-2712.

Case, J. E., Barnes, J., Paris Q., G., Gonzalez I., H., and Vina, A., 1973, Trans-Andean geophysical profile, southern Colombia: Geological Society of America Bulletin, v. 84, p. 2895-2904.

Case, J. E., and MacDonald, W. D., 1973, Regional gravity anomalies and crustal structure in northern Colombia: Geological Society of America Bulletin, v. 84, p. 2905-2916.

Chuoqui, L., 1973, A simple model of the crust and upper mantle in central Chile: Seismological Society of America Bulletin, v. 63, p. 819-825.

Cisternos, A., 1961, Crustal structure of the Andes from Rayleigh wave dispersion: Seismological Society of America Bulletin, v. 51, p. 381-388.

Cordani, U. G., Gilberto, A., and Kawashita, K., 1973, The Precambrian evolution of South America: Geologische Rundschau, v. 62, p. 309-317.

Couch, R., Whitsett, R. M., Huehn, B., and Briceno-Guarape, L., 1981, Structures of the continental margin of Peru and Chile, in Kulm, L. D., Dymond, J., Dasch, E. J., and Hussong, D. M., eds., Nazca Plate: Crustal Formation and Andean Convergence: Geological Society of America Memoir 154, p. 703-726.

de Almeida, F. F. G., 19970, Structural evolution of the Brazilian platform, in Symposium on the Results of Upper Mantle Investigation with Emphasis on Latin America: International Upper Mantle Project Scientific Report No. 37-II, Buenos Aires, p. 431-442.

de Almeida, F. F. M., Amaral, G., Cordani, U. G., and Kawashita, K., 1973, The Precambrian evolution of the South American cratonic margin south of the Amazon river, in Nairn, A. E. M., and Stehli, F. G., eds., The Ocean Basins and Margins, v. 1, Plenum Publishing Corp., New York, p. 411-446.

de Almeida, F. F. G., 1978, Explanatory note: Tectonic Map of South America: Geological Society of America Map and Chart Series MC-32, scale 1:5,000,000.

de Loczy, L., 1970, Role of transcurrent faulting in South American tectonic framework: American Association of Petroleum Geologists Bulletin, v. 54, p. 2111-2119.

Dennis, J. G., 1982, in Dennis, J. G., ed., Orogeny: Benchmark Paper in Geology, v. 62, Hutchinson Ross Publishing Co., Stroudsburg, Pennsylvania, 579 p.

Der, Z., Masse, R., and Landisman, M., 1970, Effects of observational errors on the resolution of surface waves at intermediate distances: Journal of Geophysical Research, v. 75, p. 3399-3409.

Dewey, J. F., and Bird, J. M., 1970, Mountain belts and the new global tectonics: Journal of Geophysical Research, v. 75, p. 2625-2647.

Dragicevic, M., 1970, Carta gravimetrica de los Andes meridionales e interpretacion de las anomalias de gravedad de Chile Central: Publ. Depart. Geofis. Geodes., Universidad de Chile, v. 93, 42 p.

Dziewonski, A. M., and A. L. Hales, 1972, Numerical analysis of dispersed seismic waves: Methods in Computational Physics, v. 11, p. 39-85.

Fernandez, L. M., and Carega, J., 1968, The thickness of the crust in central United States and La Paz, Bolivia, from the spectrum of longitudinal seismic waves: Seismological Society of America Bulletin, v. 58, p. 711-741.

Fisher, R. L., and Raitt, R. W., 1962, Topography and structure of the Peru-Chile trench: Deep-Sea Research, v. 9, p. 423-443.

Gansser, A., 1973, Facts and theories on the Andes: Journal of the Geological Society of London, v. 129, p. 93-131.

Haskell, N. S., 1953, The dispersion of surface waves on multi-layered media: Seismological Society of America Bulletin, v. 43, p. 17-34.

Hinze, W. J., von Frese, R. R. B., Longacre, M. B., and L. W. Braile, Regional magnetic and gravity anomalies of South America: Geophysical Research Letters, v. 9, p. 314-317.

Jackson, D. D., 1972, Interpretation of inaccurate, insufficient, and inconsistent data: Geophysical Journal of the Royal Astronomical Society, v. 28, p. 97-109.

Jackson, D. D., 1973, Marginal solutions to quasi-linear inverse problems in geophysics: the edgehog method: Geophysical Journal of the Royal Astronomical Society, v. 35, p. 121-136.

James, D. E., 1971, Andean crustal and upper mantle structure: Journal of Geophysical Research, v. 76, p. 3246-3271.

James, D. E., 1971, Plate tectonic model for the evolution of the central Andes: Geological Society of America Bulletin, v. 82, p. 3325-3346.

James, D. E., 1973, The evolution of the Andes: Scientific American, v. 229., p. 60-69.

James, D. E., 1978, Dip of Nazca plate beneath central Peru (abstract): EOS, Transactions, American Geophysical Union, v. 59, p. 383.

Jordan, T. E., Isacks, B. L., Allmendinger, R. W., Brewer, J. A., Ramos, V. A., and J. A. Clifford, 1983, Andean tectonics related to geometry of subducted Nazca plate: Geological Society of America Bulletin, v. 94, p. 341-361.

Landisman, M., Dziewonski, A., and Y. Sato, 1969, Recent improvements in the analysis of surface wave observations: Geophysical Journal of the Royal Astronomical Society, v. 17, p. 369-403.

Leeds, A. R., and Knopoff, L., 1970, Surface wave dispersion in the Andes, in Symposium on the Results of Upper Mantle Investigation with Emphasis on Latin America: International Upper Mantle Project Scientific Report No. 37-II, Buenos Aires, p. 205-210.

Leonardos, O. H., and Fyfe, W. S., 1974, Ultrametamorphism and melting of a continental margin: the Rio de Janeiro region, Brazil: Contributions to Mineralogy and Petrology, v. 46, p. 201-214.

Lomnitz, C., 1962, On Andean structure: Journal of Geophysical Research, v. 67, p. 351-363.

Ludwig, W. J., Ewing, J. I., and Ewing, M., 1965, Seismic refraction measurements in the Magellan Straits: Journal of Geophysical Research, v. 70, p. 1855-1876.

Molnar, P., and Oliver, J., 1969, Lateral variations of attenuation in the upper mantle and discontinuities in the lithosphere: Journal of Geophysical Research, v. 74, p. 2648-2682.

Mooney, W. D., Meyer, R. P., Laurence, J. P., Meyer, H., and Ramirez, J. E., 1979, Seismic refraction studies of the Western Cordillera, Colombia: Seismological Society of America Bulletin, v. 69, p. 1745-1761.

Myers, J. S., 1975, Vertical crustal movements of the Andes in Peru: Nature, v. 254, p. 672-674.

Nur, A., and Ben-Avraham, Z., 1981, Volcanic gaps and the consumption of aseismic ridges in South America, in Kulm, L. D., Dymond, J., Dasch, E. J., and Hussong, D. M., eds., Nazca plate--Crustal Formation and Andean Convergence: Geological Society of America Memoir 154, p. 729-740.

Ocola, L. C., Meyer, R. P., and Aldrich, L. T., 1970, Gross crustal structure under the Peru-Bolivia Altoplano from 1968 explosion studies, in Symposium on the Results of Upper Mantle Investigation with Emphasis on Latin America: International Upper Mantle Project Scientific Report No. 37-II, Buenos Aires, p. 233-243.

Ocola, L. C., and Meyer, R. P., 1972, Crustal low-velocity zones under the Peru-Bolivia Altoplano: Geophysical Journal of the Royal Astronomical Society, v. 30, p. 199-209.

Ocola, L. C., and Meyer, R. P., 1973, Crustal structure from the Pacific basin to the Brazilian shield between 12° and 30° South latitude: Geological Society of America Bulletin, v. 84, p. 1681-1695.

Ocola, L. C., Aldrich, L. T., Gettrust, J. F., Meyer, R. P., and Ramirez, J. E., 1975, Project Narino I: Crustal structure under southern Colombian-northern Ecuador Andes from seismic refraction data: Seismological Society of America Bulletin, v. 65, p. 1681-1695.

Rayleigh, Lord, 1885, On waves propagated along the plane surface of an elastic solid: Proceedings of the London Mathematical Society, v. 17, p. 4-11.

Russell, D. R., 1980, Constrained inversion techniques applied to surface wave analysis (M.S. thesis): University of Texas El Paso, 76 p.

Sacks, I. S., 1977, Interrelationships between volcanism, seismicity, and anelasticity in western South America: Tectonophysics, v. 37, p. 131-139.

Sacks, I. S., and Okada, H., 1974, A comparison of the anelasticity structure beneath western South America and Japan: Physics of Earth and Planetary Interiors, v. 9, p. 211-219.

Sacks, I. S., and Snoke, J. A., 1977, The use of converted phases to infer the depth of the lithosphere-asthenosphere boundary beneath South America: Journal of Geophysical Research, v. 82, p. 2011-2017.

Sacks, I. S., and Snoke, J. A., 1978, Structure of the South American lithosphere from anelasticity, converted wave, and seismicity observations (abstract): EOS, Transactions, American Geophysical Union, v. 59, p. 383.

Sherburne, R. W., 1975, Crust-mantle structure in continental South America and its relation to sea-floor spreading (Ph.D. thesis): Pennsylvania State University, 145 p.

Tatal, H. E., and Tuve, M. A., 1958, Seismic studies in the Andes: Transactions, American Geophysical Union, v. 39, p. 580.

Thomson, W. T., 1950, Transmission of elastic waves through a stratified solid medium: Journal of Applied Physics, v. 21, p. 89-93.

Twomey, S., 1977, Introduction to the mathematics of inversion in remote sensing and indirect measurements: Elsevier, Amsterdam, 243 p.

Vitroello, I., 1978, Heat flow and radiogenic heat production in Brazil with implications for thermal evolution of continents (Ph.D. thesis): University of Michigan, 145 p.

Wiggins, R. A., 1976, Interpolation of digitized curves: Seismological Society of America Bulletin, v. 66, p. 2077-2081.

Wilcox, L., 1977, Bouguer gravity anomaly of South America, in Geophysics of the Americas: A Symposium of the Geophysics Commission of the Pan American Institute of Geography and History, Ottawa, Canada, September 1976, ed. by J. G. Tanner and M. R. Dence, Energy, Mines and Resources Canada, Earth Physics Branch, Vol. 46, No. 3.

Wollard, G. P., 1960, Seismic crustal studies during the IGY 2, Continental Program (IGY Bulletin 34): Transactions, American Geophysical Union, v. 41, p. 351-355.

Yuan, Ding-Wen, 1983, Relation of MAGSAT and gravity anomalies to the main tectonic provinces of South America (M.S. thesis): University of Pittsburgh, 167 p.

Zeil, W., 1979, The Andes--a geological review: Beitrage zur Regionalen Geologie der Erde, Gebruder Borntraeger, Berlin, 260 p.